Kreith, F.; Boehm, R.F.; et. al. "Heat and Mass Transfer"
Mechanical Engineering Handbook
Ed. Frank Kreith
Boca Raton: CRC Press LLC, 1999

Heat and Mass Transfer

Frank Kreith
University of Colorado

Robert F. Boehm
University of Nevada-Las Vegas

George D. Raithby
University of Waterloo

K. G. T. Hollands
University of Waterloo

N. V. Suryanarayana
Michigan Technological University

Michael F. Modest
Pennsylvania State University

Van P. Carey
University of California at Berkeley

John C. Chen
Lehigh University

Noam Lior
University of Pennsylvania

Ram K. Shah
Delphi Harrison Thermal Systems

Kenneth J. Bell
Oklahoma State University

Robert J. Moffat
Stanford University

Anthony F. Mills
University of California at Los Angeles

Arthur E. Bergles
Rensselaer Polytechnic Institute

Larry W. Swanson
Heat Transfer Research Institute

Vincent W. Antonetti
Poughkeepsie, New York

Thomas F. Irvine, Jr.
State University of New York, Stony Brook

Massimo Capobianchi
State University of New York, Stony Brook

4.1   Conduction Heat Transfer

Robert F. Boehm

Introduction

Conduction heat transfer phenomena are found throughout virtually all of the physical world and the industrial domain. The analytical description of this heat transfer mode is one of the best understood. Some of the bases of understanding of conduction date back to early history. It was recognized that by invoking certain relatively minor simplifications, mathematical solutions resulted directly. Some of these were very easily formulated. What transpired over the years was a very vigorous development of applications to a broad range of processes. Perhaps no single work better summarizes the wealth of these studies than does the book by Carslaw and Jaeger (1959). They gave solutions to a broad range of problems, from topics related to the cooling of the Earth to the current-carrying capacities of wires. The general analyses given there have been applied to a range of modern-day problems, from laser heating to temperature-control systems.

Today conduction heat transfer is still an active area of research and application. A great deal of interest has developed in recent years in topics like contact resistance, where a temperature difference develops between two solids that do not have perfect contact with each other. Additional issues of current interest include non-Fourier conduction, where the processes occur so fast that the equation described below does not apply. Also, the problems related to transport in miniaturized systems are garnering a great deal of interest. Increased interest has also been directed to ways of handling composite materials, where the ability to conduct heat is very directional.

Much of the work in conduction analysis is now accomplished by use of sophisticated computer codes. These tools have given the heat transfer analyst the capability of solving problems in nonhomogenous media, with very complicated geometries, and with very involved boundary conditions. It is still important to understand analytical ways of determining the performance of conducting systems. At the minimum these can be used as calibrations for numerical codes.

Fourier's Law

The basis of conduction heat transfer is **Fourier's Law**. This law involves the idea that the heat flux is proportional to the temperature gradient in any direction *n*. **Thermal conductivity**, *k*, a property of materials that is temperature dependent, is the constant of proportionality.

$$q_k = -kA\frac{\partial T}{\partial n} \tag{4.1.1}$$

In many systems the area *A* is a function of the distance in the direction *n*. One important extension is that this can be combined with the first law of thermodynamics to yield the **heat conduction equation**. For constant thermal conductivity, this is given as

$$\nabla^2 T + \frac{\dot{q}_G}{k} = \frac{1}{\alpha}\frac{\partial T}{\partial t} \tag{4.1.2}$$

In this equation, α is the thermal diffusivity and $\dot{q}_G$ is the internal heat generation per unit volume. Some problems, typically steady-state, one-dimensional formulations where only the heat flux is desired, can be solved simply from Equation (4.1.1). Most conduction analyses are performed with Equation (4.1.2). In the latter, a more general approach, the temperature distribution is found from this equation and appropriate boundary conditions. Then the heat flux, if desired, is found at any location using Equation (4.1.1). Normally, it is the temperature distribution that is of most importance. For example,

it may be desirable to know through analysis if a material will reach some critical temperature, like its melting point. Less frequently the heat flux is desired.

While there are times when it is simply desired to understand what the temperature response of a structure is, the engineer is often faced with a need to increase or decrease heat transfer to some specific level. Examination of the thermal conductivity of materials gives some insight into the range of possibilities that exist through simple conduction.

Of the more common engineering materials, pure copper exhibits one of the higher abilities to conduct heat with a thermal conductivity approaching 400 W/m² K. Aluminum, also considered to be a good conductor, has a thermal conductivity a little over half that of copper. To increase the heat transfer above values possible through simple conduction, more-involved designs are necessary that incorporate a variety of other heat transfer modes like convection and phase change.

Decreasing the heat transfer is accomplished with the use of insulations. A separate discussion of these follows.

Insulations

Insulations are used to decrease heat flow and to decrease surface temperatures. These materials are found in a variety of forms, typically *loose fill*, *batt*, and *rigid*. Even a gas, like air, can be a good insulator if it can be kept from moving when it is heated or cooled. A vacuum is an excellent insulator. Usually, though, the engineering approach to insulation is the addition of a low-conducting material to the surface. While there are many chemical forms, costs, and maximum operating temperatures of common forms of insulations, it seems that when a higher operating temperature is required, many times the thermal conductivity and cost of the insulation will also be higher.

Loose-fill insulations include such materials as milled alumina-silica (maximum operating temperature of 1260°C and thermal conductivities in the range of 0.1 to 0.2 W/m² K) and perlite (maximum operating temperature of 980°C and thermal conductivities in the range of 0.05 to 1.5 W/m² K). Batt-type insulations include one of the more common types — glass fiber. This type of insulation comes in a variety of densities, which, in turn, have a profound affect on the thermal conductivity. Thermal conductivities for glass fiber insulations can range from about 0.03 to 0.06 W/m²K. Rigid insulations show a very wide range of forms and performance characteristics. For example, a rigid insulation in foam form, polyurethane, is very lightweight, shows a very low thermal conductivity (about 0.02 W/m² K), but has a maximum operating temperature only up to about 120°C. Rigid insulations in refractory form show quite different characteristics. For example, high-alumina brick is quite dense, has a thermal conductivity of about 2 W/m² K, but can remain operational to temperatures around 1760°C. Many insulations are characterized in the book edited by Guyer (1989).

Often, commercial insulation systems designed for high-temperature operation use a layered approach. Temperature tolerance may be critical. Perhaps a refractory is applied in the highest temperature region, an intermediate-temperature foam insulation is used in the middle section, and a high-performance, low-temperature insulation is used on the outer side near ambient conditions.

Analyses can be performed including the effects of temperature variations of thermal conductivity. However, the most frequent approach is to assume that the thermal conductivity is constant at some temperature between the two extremes experienced by the insulation.

The Plane Wall at Steady State

Consider steady-state heat transfer in a plane wall of thickness L, but of very large extent in both other directions. The wall has temperature T_1 on one side and T_2 on the other. If the thermal conductivity is considered to be constant, then Equation (4.1.1) can be integrated directly to give the following result:

$$q_k = \frac{kA}{L}\left(T_1 - T_2\right) \tag{4.1.3}$$

This can be used to determine the steady-state heat transfer through slabs.

An electrical circuit analog is widely used in conduction analyses. This is realized by considering the temperature difference to be analogous to a voltage difference, the heat flux to be like current flow, and the remainder of Equation (4.1.3) to be like a thermal resistance. The latter is seen to be

$$R_k = \frac{L}{kA} \tag{4.1.4}$$

Heat transfer through walls made of layers of different types of materials can be easily found by summing the resistances in series or parallel form, as appropriate.

In the design of systems, seldom is a surface temperature specified or known. More often, the surface is in contact with a bulk fluid, whose temperature is known at some distance from the surface. Convection from the surface is then represented by Newton's law of cooling:

$$q = \bar{h}_c A \left(T_s - T_\infty \right) \tag{4.1.5}$$

This equation can also be represented as a temperature difference divided by a thermal resistance, which is $1/\bar{h}_{cA}$. It can be shown that a very low surface resistance, as might be represented by phase change phenomena, has the effect of imposing the fluid temperature directly on the surface. Hence, usually a *known* surface temperature results from a fluid temperature being imposed directly on the surface through a very high heat transfer coefficient. For this reason, in the later results given here, particularly those for transient systems, a convective boundary will be assumed. For steady results this is less important because of the ability to add resistances through the circuit analogy.

Long, Cylindrical Systems at Steady State

For long (*L*) annular systems at steady-state conditions with constant thermal conductivities, the following two equations are the appropriate counterparts to Equations (4.1.3) and (4.1.4). The heat transfer can be expressed as

$$q_k = \frac{2\pi Lk}{\ln\left[r_2/r_1\right]} \left(T_1 - T_2 \right) \tag{4.1.6}$$

Here, r_1 and r_2 represent the radii of annular section. A thermal resistance for this case is as shown below.

$$R_k = \frac{\ln\left[r_2/r_1\right]}{2\pi Lk} \tag{4.1.7}$$

The Overall Heat Transfer Coefficient

The **overall heat transfer coefficient** concept is valuable in several aspects of heat transfer. It involves a modified form of Newton's law of cooling, as noted above, and it is written as

$$Q = \bar{U}A\Delta T \tag{4.1.8}$$

In this formulation $\bar{U}$ is the overall heat transfer coefficient based upon the area *A*. Because the area for heat transfer in a problem can vary (as with a cylindrical geometry), it is important to note that the $\bar{U}$ is dependent upon which area is selected. The overall heat transfer coefficient is usually found from a combination of thermal resistances. Hence, for a common series-combination-circuit analog, the $\bar{U}A$ product is taken as the sum of resistances.

$$\overline{U}A = \frac{1}{\sum\limits_{i=1}^{n} R_i} = \frac{1}{R_{\text{total}}} \tag{4.1.9}$$

To show an example of the use of this concept, consider Figure 4.1.1.
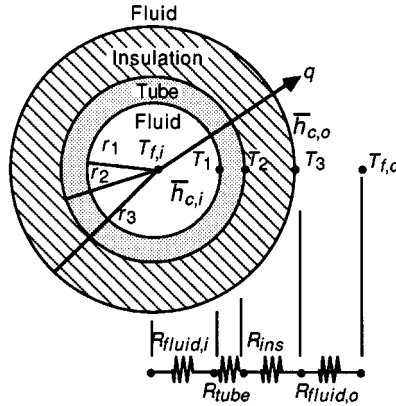

FIGURE 4.1.1. An insulated tube with convective environments on both sides.

For steady-state conditions, the product $\overline{U}A$ remains constant for a given heat transfer and overall temperature difference. This can be written as

$$\overline{U}_1 A_1 = \overline{U}_2 A_2 = \overline{U}_3 A_3 = \overline{U}A \tag{4.1.10}$$

If the inside area, A_1, is chosen as the basis, the overall heat transfer coefficient can then be expressed as

$$\overline{U}_1 = \frac{1}{\dfrac{1}{\overline{h}_{c,i}} + \dfrac{r_1 \ln(r_2/r_1)}{k_{\text{pipe}}} + \dfrac{r_1 \ln(r_3/r_2)}{k_{\text{ins}}} + \dfrac{r_1}{r_3 \overline{h}_{c,o}}} \tag{4.1.11}$$

Critical Thickness of Insulation

Sometimes insulation can cause an increase in heat transfer. This circumstance should be noted in order to apply it when desired and to design around it when an insulating effect is needed. Consider the circumstance shown in Figure 4.1.1. Assume that the temperature is known on the outside of the tube (inside of the insulation). This could be known if the inner heat transfer coefficient is very large and the thermal conductivity of the tube is large. In this case, the inner fluid temperature will be almost the same as the temperature of the inner surface of the insulation. Alternatively, this could be applied to a coating (say an electrical insulation) on the outside of a wire. By forming the expression for the heat transfer in terms of the variables shown in Equation (4.1.11), and examining the change of heat transfer with variations in r_3 (that is, the thickness of insulation) a maximum heat flow can be found. While simple results are given many texts (showing the critical radius as the ratio of the insulation thermal conductivity to the heat transfer coefficient on the outside), Sparrow (1970) has considered a heat transfer coefficient that varies as $\overline{h}_{c,o} \sim r_3^{-m} |T_3 - T_{f,o}|^n$. For this case, it is found that the heat transfer is maximized at

$$r_3 = r_{\text{crit}} = \left[(1-m)/(1+n)\right]\frac{k_{\text{ins}}}{\bar{h}_{c,o}} \tag{4.1.12}$$

By examining the order of magnitudes of m, n, k_{ins}, and $\bar{h}_{c,o}$ the critical radius is found to be often on the order of a *few millimeters*. Hence, additional insulation on small-diameter cylinders such as small-gauge electrical wires could actually increase the heat dissipation. On the other hand, the addition of insulation to large-diameter pipes and ducts will almost always decrease the heat transfer rate.

Internal Heat Generation

The analysis of temperature distributions and the resulting heat transfer in the presence of volume heat sources is required in some circumstances. These include phenomena such as nuclear fission processes, joule heating, and microwave deposition. Consider first a slab of material $2L$ thick but otherwise very large, with internal generation. The outside of the slab is kept at temperature T_1. To find the temperature distribution within the slab, the thermal conductivity is assumed to be constant. Equation (4.1.2) reduces to the following:

$$\frac{d^2T}{dx^2} + \frac{\dot{q}_G}{k} = 0 \tag{4.1.13}$$

Solving this equation by separating variables, integrating twice, and applying boundary conditions gives

$$T(x) - T_1 = \frac{\dot{q}_G L^2}{2k}\left[1 - \left(\frac{x}{L}\right)^2\right] \tag{4.1.14}$$

A similar type of analysis for a long, cylindrical element of radius r_1 gives

$$T(r) - T_1 = \frac{\dot{q}_G r_1^2}{4k}\left[1 - \left(\frac{r}{r_1}\right)^2\right] \tag{4.1.15}$$

Two additional cases will be given. Both involve the situation when the heat generation rate is dependent upon the local temperature in a linear way (defined by a slope β), according to the following relationship:

$$\dot{q}_G = \dot{q}_{G,o}\left[1 + \beta(T - T_o)\right] \tag{4.1.16}$$

For a plane wall of $2L$ thickness and a temperature of T_1 specified on each surface

$$\frac{T(x) - T_o + 1/\beta}{T_1 - T_o + 1/\beta} = \frac{\cos\mu x}{\cos\mu L} \tag{4.1.17}$$

For a similar situation in a long cylinder with a temperature of T_1 specified on the outside radius r_1

$$\frac{T(r) - T_o + 1/\beta}{T_1 - T_o + 1/\beta} = \frac{J_o(\mu r)}{J_o(\mu r_1)} \tag{4.1.18}$$

In Equation (4.1.18), the J_o is the typical notation for the Bessel function. Variations of this function are tabulated in Abramowitz and Stegun (1964). In both cases the following holds:

$$\mu \equiv \sqrt{\frac{\beta \dot{q}_{G,o}}{k}}$$

Fins

Fins are widely used to enhance the heat transfer (usually convective, but it could also be radiative) from a surface. This is particularly true when the surface is in contact with a gas. Fins are used on air-cooled engines, electronic cooling forms, as well as for a number of other applications. Since the heat transfer coefficient tends to be low in gas convection, area is added in the form of fins to the surface to decrease the convective thermal resistance.

The simplest fins to analyze, and which are usually found in practice, can be assumed to be one-dimensional and constant in cross section. In simple terms, to be one-dimensional, the fins have to be long compared with a transverse dimension. Three cases are normally considered for analysis, and these are shown in Figure 4.1.2. They are the insulated tip, the infinitely long fin, and the convecting tip fin.
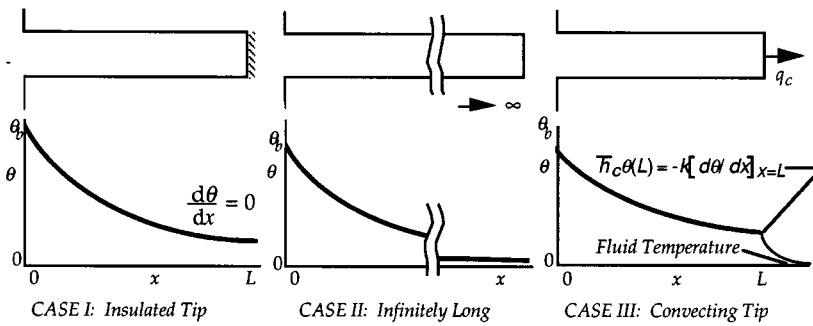
FIGURE 4.1.2. Three typical cases for one-dimensional, constant-cross-section fins are shown.

For Case, I, the solution to the governing equation and the application of the boundary conditions of the known temperature at the base and the insulated tip yields

$$\text{Case I:} \qquad \theta = \theta_b = \frac{\cosh m(L-x)}{\cosh mL} \qquad (4.1.19)$$

For the infinitely long case, the following simple form results:

$$\text{Case II:} \qquad \theta(x) = \theta_b e^{-mx} \qquad (4.1.20)$$

The final case yields the following result:

$$\text{Case III:} \qquad \theta(x) = \theta_b \frac{mL\cosh m(L-x) + \text{Bi}\sinh m(L-x)}{mL\cosh mL + \text{Bi}\sinh mL} \qquad (4.1.21)$$

where

$$\text{Bi} \equiv \bar{h}_c\, L/k$$

In all three of the cases given, the following definitions apply:

$$\theta \equiv T(x) - T_\infty, \quad \theta_b \equiv T(x = 0) - T_\infty, \quad \text{and} \quad m^2 \equiv \frac{\overline{h_c} P}{kA}$$

Here A is the cross section of the fin parallel to the wall; P is the perimeter around that area.

To find the heat removed in any of these cases, the temperature distribution is used in Fourier's law, Equation (4.1.1). For most fins that truly fit the one-dimensional assumption (i.e., long compared with their transverse dimensions), all three equations will yield results that do not differ widely.

Two performance indicators are found in the fin literature. The **fin efficiency** is defined as the ratio of the actual heat transfer to the heat transfer from an ideal fin.

$$\eta \equiv \frac{q_{\text{actual}}}{q_{\text{ideal}}} \tag{4.1.22}$$

The ideal heat transfer is found from convective gain or loss from an area the same size as the fin surface area, all at a temperature T_b. Fin efficiency is normally used to tabulate heat transfer results for various types of fins, including ones with nonconstant area or which do not meet the one-dimensional assumption. An example of the former can be developed from a result given by Arpaci (1966). Consider a straight fin of triangular profile, as shown in Figure 4.1.3. The solution is found in terms of modified Bessel functions of the first kind. Tabulations are given in Abramowitz and Stegun (1964).

$$\eta = \frac{I_1\left(2\tilde{m}L^{1/2}\right)}{\tilde{m}L^{1/2} I_o\left(2\tilde{m}L^{1/2}\right)} \tag{4.1.23}$$

Here, $\tilde{m} \equiv \sqrt{2\overline{h_c}L/kb}$.

The **fin effectiveness**, ε, is defined as the heat transfer from the fin compared with the bare-surface transfer through the same base area.
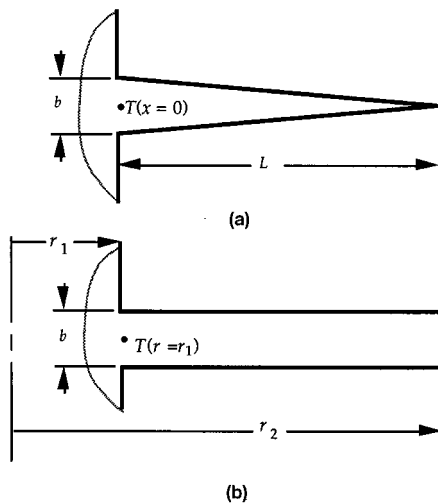

FIGURE 4.1.3. Two examples of fins with a cross-sectional area that varies with distance from the base. (a) Straight triangular fin. (b) Annular fin of constant thickness.

$$\varepsilon = \frac{q_{\text{actual}}}{q_{\text{bare base}}} = \frac{q_f}{\overline{h}_c A(T_b - T_\infty)} \tag{4.1.24}$$

Carslaw and Jaeger (1959) give an expression for the effectiveness of a fin of constant thickness around a tube (see Figure 4.1.3) This is given as ($\tilde{\mu} \equiv \sqrt{2\overline{h}_c/kb}$).

$$\varepsilon = \frac{2}{\tilde{\mu}b} \frac{I_1(\tilde{\mu}r_2)K_1(\tilde{\mu}r_1) - K_1(\tilde{\mu}r_2)I_1(\tilde{\mu}r_1)}{I_o(\tilde{\mu}r_1)K_1(\tilde{\mu}r_2) + K_o(\tilde{\mu}r_1)I_1(\tilde{\mu}r_2)} \tag{4.1.25}$$

Here the notations I and K denote Bessel functions that are given in Abramowitz and Stegun (1964).

Fin effectiveness can be used as one indication whether or not fins should be added. A rule of thumb indicates that if the effectiveness is less than about three, fins should not be added to the surface.

Transient Systems

Negligible Internal Resistance

Consider the transient cooling or heating of a body with surface area A and volume V. This is taking place by convection through a heat transfer coefficient $\overline{h}_c$ to an ambient temperature of T_∞. Assume the thermal resistance to conduction inside the body is significantly less than the thermal resistance to convection (as represented by Newton's law of cooling) on the surface of the body. This ratio is denoted by the **Biot number**, Bi.

$$\text{Bi} = \frac{R_k}{R_c} = \frac{\overline{h}_c(V/A)}{k} \tag{4.1.26}$$

The temperature (which will be uniform throughout the body at any time for this situation) response with time for this system is given by the following relationship. Note that the shape of the body is not important — only the ratio of its volume to its area matters.

$$\frac{T(t) - T_\infty}{T_o - T_\infty} = e^{-\overline{h}_c At/\rho Vc} \tag{4.1.27}$$

Typically, this will hold for the Biot number being less than (about) 0.1.

Bodies with Significant Internal Resistance

When a body is being heated or cooled transiently in a convective environment, but the internal thermal resistance of the body cannot be neglected, the analysis becomes more complicated. Only simple geometries (a symmetrical plane wall, a long cylinder, a composite of geometric intersections of these geometries, or a sphere) with an imposed step change in ambient temperature are addressed here.

The first geometry considered is a large slab of minor dimension $2L$. If the temperature is initially uniform at T_o, and at time 0+ it begins convecting through a heat transfer coefficient to a fluid at T_∞, the temperature response is given by

$$\theta = 2\sum_{n=1}^{\infty}\left(\frac{\sin\lambda_n L}{\lambda_n L + \sin\lambda_n L\cos\lambda_n L}\right)\exp(-\lambda_n^2 L^2\text{Fo})\cos(\lambda_n x) \tag{4.1.28}$$

and the λ_n are the roots of the transcendental equation: $\lambda_n L \tan \lambda_n L = \text{Bi}$. The following definitions hold:

$$\text{Bi} \equiv \frac{\bar{h}_c L}{k} \qquad \text{Fo} \equiv \frac{\alpha t}{L^2} \qquad \theta \equiv \frac{T - T_\infty}{T_o - T_\infty}$$

The second geometry considered is a very long cylinder of diameter $2R$. The temperature response for this situation is

$$\theta = 2\text{Bi} \sum_{n=1}^{\infty} \frac{\exp\left(-\lambda_n^2 R^2 \text{Fo}\right) J_o\left(\lambda_n r\right)}{\left(\lambda_n^2 R^2 + \text{Bi}^2\right) J_o\left(\lambda_n R\right)} \qquad (4.1.29)$$

Now the λ_n are the roots of $\lambda_n R \, J_1(\lambda_n R) + \text{Bi} \, J_o(\lambda_n R) = 0$, and

$$\text{Bi} = \frac{\bar{h}_c R}{k} \qquad \text{Fo} = \frac{\alpha t}{R^2} \qquad \theta = \frac{T - T_\infty}{T_o - T_\infty}$$

The common definition of Bessel's functions applies here.

For the similar situation involving a solid sphere, the following holds:

$$\theta = 2 \sum_{n=1}^{\infty} \frac{\sin\left(\lambda_n R\right) - \lambda_n R \cos\left(\lambda_n R\right)}{\lambda_n R - \sin\left(\lambda_n R\right)\cos\left(\lambda_n R\right)} \exp\left(-\lambda_n^2 R^2 \text{Fo}\right) \frac{\sin\left(\lambda_n r\right)}{\lambda_n r} \qquad (4.1.30)$$

and the λ_n are found as the roots of $\lambda_n R \cos \lambda_n R = (1 - \text{Bi}) \sin \lambda_n R$. Otherwise, the same definitions as were given for the cylinder hold.

Solids that can be envisioned as the geometric intersection of the simple shapes described above can be analyzed with a simple product of the individual-shape solutions. For these cases, the solution is found as the product of the dimensionless temperature functions for each of the simple shapes with appropriate distance variables taken in each solution. This is illustrated as the right-hand diagram in Figure 4.1.4. For example, a very long rod of rectangular cross section can be seen as the intersection of two large plates. A short cylinder represents the intersection of an infinitely long cylinder and a plate. The temperature at any location within the short cylinder is

$$\theta_{2R,2L \, \text{Rod}} = \theta_{\text{Infinite } 2R \, \text{Rod}} \theta_{2L \, \text{Plate}} \qquad (4.1.31)$$

Details of the formulation and solution of the partial differential equations in heat conduction are found in the text by Arpaci (1966).

Finite-Difference Analysis of Conduction

Today, numerical solution of conduction problems is the most-used analysis approach. Two general techniques are applied for this: those based upon finite-difference ideas and those based upon finite-element concepts. General numerical formulations are introduced in other sections of this book. In this section, a special, physical formulation of the finite-difference equations to conduction phenomena is briefly outlined.

Attention is drawn to a one-dimensional slab (very large in two directions compared with the thickness). The slab is divided across the thickness into smaller subslabs, and this is shown in Figure 4.1.5. All subslabs are thickness Δx except for the two boundaries where the thickness is $\Delta x/2$. A characteristic temperature for each slab is assumed to be represented by the temperature at the slab center. Of course, this assumption becomes more accurate as the size of the slab becomes smaller. With
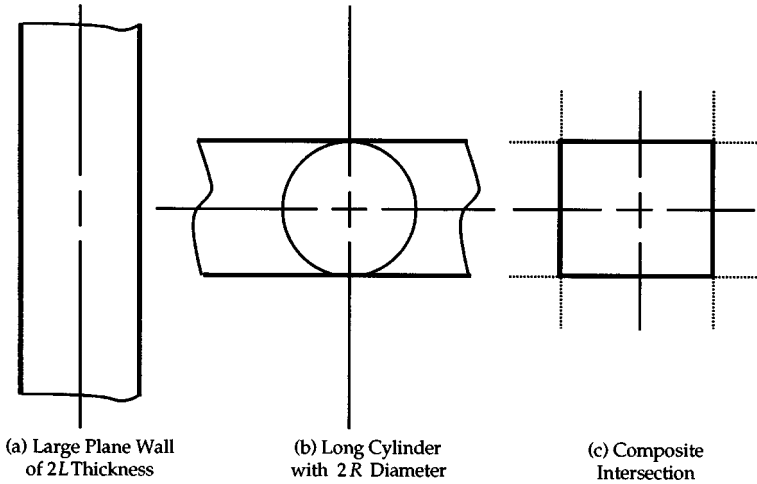
(a) Large Plane Wall
of 2*L* Thickness

(b) Long Cylinder
with 2*R* Diameter

(c) Composite
Intersection

FIGURE 4.1.4. Three types of bodies that can be analyzed with results given in this section. (a) Large plane wall of 2*L* thickness; (b) long cylinder with 2*R* diameter; (c) composite intersection.
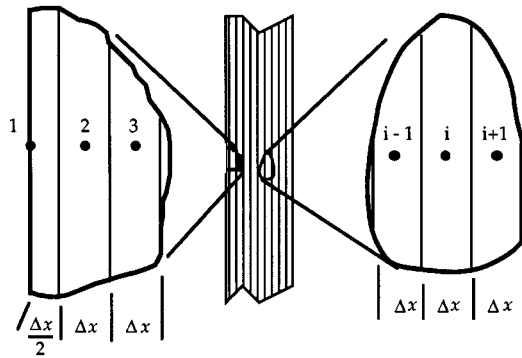
FIGURE 4.1.5. A one-dimensional finite differencing of a slab with a general interior node and one surface node detailed.

the two boundary-node centers located exactly on the boundary, a total of *n* nodes are used (*n* − 2 full nodes and one half node on each of the two boundaries).

In the analysis, a general interior node *i* (this applies to all nodes 2 through *n* − 1) is considered for an overall energy balance. Conduction from node *i* − 1 and from node *i* + 1 as well as any heat generation present is assumed to be energy per unit time flowing into the node. This is then equated to the time rate of change of energy within the node. A backward difference on the time derivative is applied here, and the notation $T_i' \equiv T_i(t + \Delta t)$ is used. The balance gives the following on a per-unit-area basis:

$$\frac{T_{i-1}' - T_i'}{\Delta x / k_-} + \frac{T_{i+1}' - T_i'}{\Delta x / k_+} + \dot{q}_{G,i} \Delta x = \rho \Delta x c_p \frac{T_i' - T_i}{\Delta t} \tag{4.1.32}$$

In this equation different thermal conductivities have been used to allow for possible variations in properties throughout the solid.

The analysis of the boundary nodes will depend upon the nature of the conditions there. For the purposes of illustration, convection will be assumed to be occurring off of the boundary at node 1. A balance similar to Equation (4.1.32) but now for node 1 gives the following:

$$\frac{T_\infty' - T_1'}{1/\overline{h}_c} + \frac{T_2' - T_1'}{\Delta x/k_+} + \dot{q}_{G,1}\frac{\Delta x}{2} = \rho\frac{\Delta x}{2}c_p\frac{T_1' - T_1}{\Delta t} \tag{4.1.33}$$

After all n equations are written, it can be seen that there are n unknowns represented in these equations: the temperature at all nodes. If one or both of the boundary conditions are in terms of a specified temperature, this will decrease the number of equations and unknowns by one or two, respectively. To determine the temperature as a function of time, the time step is arbitrarily set, and all the temperatures are found by simultaneous solution at $t = 0 + \Delta t$. The time is then advanced by Δt and the temperatures are then found again by simultaneous solution.

The finite difference approach just outlined using the backward difference for the time derivative is termed the *implicit* technique, and it results in an $n \times n$ system of linear simultaneous equations. If the forward difference is used for the time derivative, then only one unknown will exist in each equation. This gives rise to what is called an *explicit* or "marching" solution. While this type of system is more straightforward to solve because it deals with only one equation at a time with one unknown, a *stability criterion* must be considered which limits the time step relative to the distance step.

Two- and three-dimensional problems are handled in conceptually the same manner. One-dimensional heat fluxes between adjoining nodes are again considered. Now there are contributions from each of the dimensions represented. Details are outlined in the book by Jaluria and Torrance (1986).

Defining Terms

Biot number: Ratio of the internal (conductive) resistance to the external (convective) resistance from a solid exchanging heat with a fluid.

Fin: Additions of material to a surface to increase area and thus decrease the external thermal resistance from convecting and/or radiating solids.

Fin effectiveness: Ratio of the actual heat transfer from a fin to the heat transfer from the same cross-sectional area of the wall without the fin.

Fin efficiency: Ratio of the actual heat transfer from a fin to the heat transfer from a fin with the same geometry but completely at the base temperature.

Fourier's law: The fundamental law of heat conduction. Relates the local temperature gradient to the local heat flux, both in the same direction.

Heat conduction equation: A partial differential equation in temperature, spatial variables, time, and properties that, when solved with appropriate boundary and initial conditions, describes the variation of temperature in a conducting medium.

Overall heat transfer coefficient: The analogous quantity to the heat transfer coefficient found in convection (Newton's law of cooling) that represents the overall combination of several thermal resistances, both conductive and convective.

Thermal conductivity: The property of a material that relates a temperature gradient to a heat flux. Dependent upon temperature.

References

Abramowitz, M. and Stegun, I. 1964. *Handbook of Mathematical Functions with Formulas, Graphs, and Mathematical Tables*. National Bureau of Standards, Applied Mathematics Series 55.

Arpaci, V. 1966. *Conduction Heat Transfer*, Addison-Wesley, Reading, MA.

Carslaw, H.S. and Jaeger, J.C. 1959. *Conduction of Heat in Solids*, 2nd ed., Oxford University Press, London.

Guyer, E., Ed. 1989. Thermal insulations, in *Handbook of Applied Thermal Design*, McGraw-Hill, New York, Part 3.

Jaluria, Y. and Torrance, K. 1986. *Computational Heat Transfer*, Hemisphere Publishing, New York.

Sparrow, E. 1970. Reexamination and correction of the critical radius for radial heat conduction, *AIChE J.* 16, 1, 149.

Further Information

The references listed above will give the reader an excellent introduction to analytical formulation and solution (Arpaci), material properties (Guyer), and numerical formulation and solution (Jaluria and Torrance). Current developments in conduction heat transfer appear in several publications, including *The Journal of Heat Transfer*, *The International Journal of Heat and Mass Transfer*, and *Numerical Heat Transfer.*

4.2   Convection Heat Transfer

Natural Convection

George D. Raithby and K.G. Terry Hollands

Introduction

Natural convection heat transfer occurs when the convective fluid motion is induced by density differences that are themselves caused by the heating. An example is shown in Figure 4.2.1(A), where a body at surface temperature T_s transfers heat at a rate q to ambient fluid at temperature $T_\infty < T_s$.

$$Nu = qL/\overline{\Delta T}A_S k$$
$$Ra = g\beta\,\overline{\Delta T}\,L^3/\nu\alpha$$
$$Ra^* = g\beta qL^4/A_S\nu\alpha k = NuRa$$

$$L^* = A_S/P$$
$$Nu = qL^*/A_S\Delta T$$
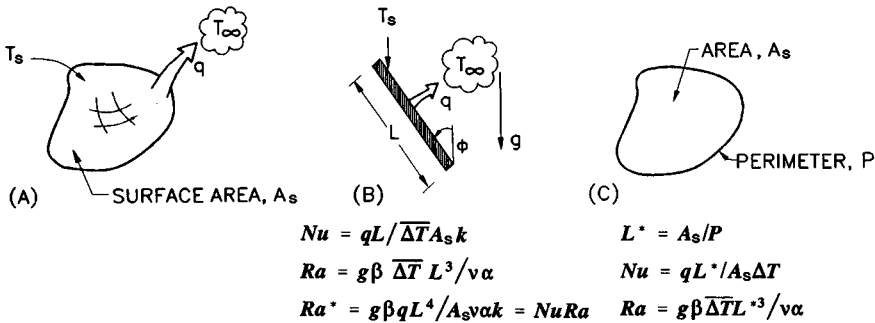$$Ra = g\beta\overline{\Delta T}L^{*3}/\nu\alpha$$

FIGURE 4.2.1 (A) Nomenclature for external heat transfer. (A) General sketch; (B) is for a tilted flat plate, and (C) defines the lengths cal for horizontal surfaces.

In this section, correlations for the average Nusselt number are provided from which the heat transfer rate q from surface area A_s can be estimated. The Nusselt number is defined as

$$\mathrm{Nu} = \frac{\overline{h}_c L}{k} = \frac{qL}{A_s \Delta T\, k} \tag{4.2.1}$$

where $\Delta T = T_s - T_\infty$ is the temperature difference driving the heat transfer. A dimensional analysis leads to the following functional relation:

$$\mathrm{Nu} = f\big(\mathrm{Ra,\ Pr,\ geometric\ shape,\ boundary\ conditions}\big) \tag{4.2.2}$$

For given thermal boundary conditions (e.g., isothermal wall and uniform T_∞), and for a given geometry (e.g., a cube), Equation (4.2.2) states that Nu depends only on the Rayleigh number, Ra, and Prandtl number, Pr. The length scales that appear in Nu and Ra are defined, for each geometry considered, in a separate figure. The fluid properties are generally evaluated at T_f, the average of the wall and ambient temperatures. The exception is that β, the temperature coefficient of volume expansion, is evaluated at T_∞ for external natural convection(Figures 4.2.1 to 4.2.3) in a *gaseous* medium.

The functional dependence on Pr is approximately independent of the geometry, and the following Pr-dependent function will be useful for laminar heat transfer (Churchill and Usagi, 1972):

$$\overline{C}_\ell = 0.671\Big/\left(1 + \left(0.492/\mathrm{Pr}\right)^{9/16}\right)^{4/9} \tag{4.2.3}$$

C_t^V and C_t^H are functions that will be useful for turbulent heat transfer:
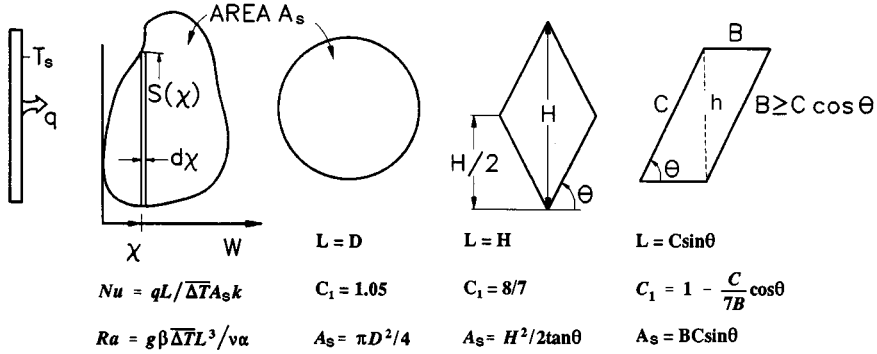
FIGURE 4.2.2 Nomenclature for heat transfer from planar surfaces of different shapes.
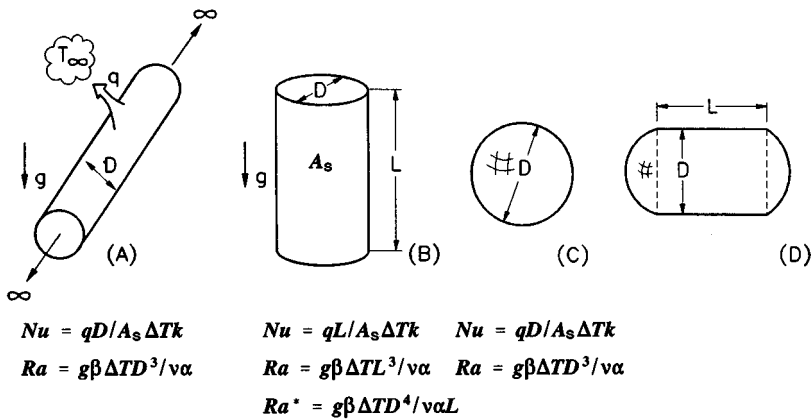
FIGURE 4.2.3 Definitions for computing heat transfer from a long circular cylinder (A), from the lateral surface of a vertical circular cylinder (B), from a sphere (C), and from a compound body (D).

$$C_t^V = 0.13 \mathrm{Pr}^{0.22} \big/ \left(1 + 0.61 \mathrm{Pr}^{0.81}\right)^{0.42} \tag{4.2.4}$$

$$C_t^H = 0.14 \left(\frac{1 + 0.0107 \mathrm{Pr}}{1 + 0.01 \mathrm{Pr}}\right) \tag{4.2.5}$$

The superscripts *V* and *H* refer to the vertical and horizontal surface orientation.

The Nusselt numbers for fully laminar and fully turbulent heat transfer are denoted by Nu_ℓ and Nu_t, respectively. Once obtained, these are blended (Churchill and Usagi, 1972) as follows to obtain the equation for Nu:

$$\mathrm{Nu} = \left(\left(\mathrm{Nu}_\ell\right)^m + \left(\mathrm{Nu}_t\right)^m\right)^{1/m} \tag{4.2.6}$$

The blending parameter *m* depends on the body shape and orientation.

The equation for Nu_ℓ in this section is usually expressed in terms of Nu^T, the Nusselt number that would be valid if the thermal boundary layer were thin. The difference between Nu_ℓ and Nu^T accounts for the effect of the large boundary layer thicknesses encountered in natural convection.

It is assumed that the wall temperature of a body exceeds the ambient fluid temperature ($T_s > T_\infty$). For $T_s < T_\infty$ the same correlations apply with ($T_\infty - T_s$) replacing ($T_s - T_\infty$) for a geometry that is rotated

180° relative to the gravitational vector; for example, the correlations for a horizontal heated upward-facing flat plate applies to a cooled downward-facing flat plate of the same planform.

Correlations for External Natural Convection

This section deals with problems where the body shapes in Figures 4.2.1 to 4.2.3 are heated while immersed in a quiescent fluid. Different *cases* are enumerated below.

1. *Isothermal Vertical ($\phi = 0$) Flat Plate, Figure 4.2.1B.* For heat transfer from a vertical plate (Figure 4.2.1B), for $1 < \mathrm{Ra} < 10^{12}$,

$$\mathrm{Nu}^T = \overline{C}_\ell \mathrm{Ra}^{1/4} \qquad \mathrm{Nu}_\ell = \frac{2.0}{\ln\left(1 + 2.0/\mathrm{Nu}^T\right)} \tag{4.2.7}$$

$$\mathrm{Nu}_t = C_t^V \mathrm{Ra}^{1/3} \Big/ \left(1 + 1.4 \times 10^9 \,\mathrm{Pr}/\mathrm{Ra}\right)$$

$\overline{C}_\ell$ and C_t^V are given by Equations (4.2.3) and (4.2.4). Nu is obtained by substituting Equation (4.2.7) expressions for Nu_ℓ and Nu_t into Equation (4.2.6) with $m = 6$.

2. *Vertical Flat Plate with Uniform Heat Flux, Figure 4.2.1B.* If the plate surface has a constant (known) heat flux, rather than being isothermal, the objective is to calculate the average temperature difference, $\overline{\Delta T}$, between the plate and fluid. For this situation, and for $15 < \mathrm{Ra}^* < 10^5$,

$$\mathrm{Nu}^T = \overline{G}_\ell \left(\mathrm{Ra}^*\right)^{1/5} \qquad \mathrm{Nu}_\ell = \frac{1.83}{\ln\left(1 + 1.83/\mathrm{Nu}^T\right)} \qquad \mathrm{Nu}_t = \left(C_t^V\right)^{3/4}\left(\mathrm{Ra}^*\right)^{1/4} \tag{4.2.8a}$$

$$\overline{G}_\ell = \frac{6}{5}\left(\frac{\mathrm{Pr}}{4 + 9\sqrt{\mathrm{Pr}} + 10\mathrm{Pr}}\right)^{1\;5} \tag{4.2.8b}$$

Ra^* is defined in Figure 4.2.1B and C_t^V is given by Equation (4.2.4). Find Nu by inserting these expressions for Nu_ℓ and Nu_t into Equation (4.2.6) with $m = 6$. The $\overline{G}_\ell$ expression is due to Fujii and Fujii (1976).

3. *Horizontal Upward-Facing ($\phi = 90°$) Plates, Figure 4.2.1C.* For horizontal isothermal surfaces of various platforms, correlations are given in terms of a lengthscale L^* (Goldstein et al., 1973), defined in Figure 4.2.1C. For $\mathrm{Ra} \geq 1$,

$$\mathrm{Nu}^T = 0.835\overline{C}_\ell \mathrm{Ra}^{1/4} \qquad \mathrm{Nu}_\ell = \frac{2.0}{\ln\left(1 + 1.4/\mathrm{Nu}^T\right)} \qquad \mathrm{Nu}_t = C_t^H \mathrm{Ra}^{1/3} \tag{4.2.9}$$

Nu is obtained by substituting Nu_ℓ and Nu_t from Equation 4.2.9 into Equation 4.2.6 with $m = 10$. For non-isothermal surfaces, replace ΔT by $\overline{\Delta T}$.

4. *Horizontal Downward-Facing ($\phi = -90°$) Plates, Figure 4.2.1C.* For horizontal downward-facing plates of various planforms, the main buoyancy force is into the plate so that only a very weak force drives the fluid along the plate; for this reason, only laminar flows have been measured. For this case, the following equation applies for $\mathrm{Ra} < 10^{10}$, $\mathrm{Pr} \geq 0.7$:

$$\mathrm{Nu}^T = H_\ell \mathrm{Ra}^{1/5} \qquad H_\ell = \frac{0.527}{\left[1 + \left(1.9/\mathrm{Pr}\right)^{9/10}\right]^{2/9}} \qquad \mathrm{Nu} = \frac{2.45}{\ln\left(1 + 2.45/\mathrm{Nu}^T\right)} \tag{4.2.10}$$

H_ℓ fits the analysis of Fujii et al. (1973).

5. *Inclined Plates, Downward Facing (–90° ≤ ϕ ≤ 0), Figure 4.2.1B*. First calculate *q* from *Case 1* with *g* replaced by *g* cos ϕ; then calculate *q* from *Case 4* (horizontal plate) with *g* replaced by *g* sin (–ϕ), and use the maximum of these two values of *q*.

6. *Inclined Plates, Upward Facing (0 ≤ ϕ ≤ 90), Figure 4.2.1B*. First calculate *q* from *Case 1* with *g* replaced by *g* cos ϕ; then calculate *q* from *Case 3* with *g* replaced by *g* sin ϕ, and use the maximum of these two values of *q*.

7. *Vertical and Tilted Isothermal Plates of Various Planform, Figure 4.2.2*. The line of constant χ in Figure 4.2.2 is the line of steepest ascent on the plate. Provided all such lines intersect the plate edges just twice, as shown in the figure, the thin-layer (Nu^T) heat transfer can be found by subdividing the body into strips of width Δχ, calculating the heat transfer from each strip, and adding. For laminar flow from an isothermal vertical plate, this results in

$$\mathrm{Nu}^T = C_1 \overline{C}_\ell \mathrm{Ra}^{1/4} \qquad C_1 \equiv \left(\frac{L^{1/4}}{A} \int_0^W S^{3/4} \, d\chi \right) \qquad (4.2.11)$$

Symbols are defined in Figure 4.2.2, along with *L* and calculated C_1 values for some plate shapes. If the plate is vertical, follow the procedure in *Case 1* above (isothermal vertical flat plate) except replace the expression for Nu^T in Equation (4.2.7) by Equation (4.2.11). If the plate is tilted, follow the procedure described in *Case 5* or *6* (as appropriate) but again use Equation (4.2.11) for Nu^T in Equation (4.2.7)

8. *Horizontal Cylinders, Figure 4.2.3A*. For a long, horizontal circular cylinder use the following expressions for Nu_ℓ and Nu_t:

$$\mathrm{Nu}^T = 0.772 \overline{C}_\ell \mathrm{Ra}^{1/4} \qquad \mathrm{Nu}_\ell = \frac{2f}{\left(1 + 2f/\mathrm{Nu}^T\right)} \qquad \mathrm{Nu}_t = \overline{C}_t \mathrm{Ra}^{1/3} \qquad (4.2.12)$$

$\overline{C}_t$ is given in the table below. For Ra > 10^{-2}, *f* = 0.8 can be used, but for 10^{-10} < Ra < 10^{-2} use $f = 1 - 0.13/(\mathrm{Nu}^T)^{0.16}$. To find Nu, the values of Nu_ℓ and Nu_t from Equation (4.2.12) are substituted into Equation (4.2.6) with *m* = 15 (Clemes et al., 1994).

$\overline{C}_t$ **for Various Shapes and Prandtl Numbers**

Pr→	0.01	0.022	0.10	0.71	2.0	6.0	50	100	2000
Horizontal cylinder	0.077	0.81	0.90	0.103	0.108	0.109	0.100	0.097	0.088
Spheres	0.074	0.078	0.088	0.104	0.110	0.111	0.101	0.97	0.086

9. *Vertical Cylinders (ϕ = 90°), Figure 4.2.3B*. For high Ra values and large diameter, the heat transfer from a vertical cylinder approaches that for a vertical flat plate. Let the Nu^T and Nu_ℓ equations for a vertical flat plate of height *L*, Equation (4.2.7), be rewritten here as Nu_p^T and Nu_p, respectively. At smaller Ra and diameter, transverse curvature plays a role which is accounted for in the following equations:

$$\mathrm{Nu}_\ell = \frac{0.9\xi \mathrm{Nu}_p}{\ln\left(1 + 0.9\xi\right)} \qquad \xi = \frac{2L/D}{\mathrm{Nu}_p^T} \qquad (4.2.13)$$

These equations are valid for purely laminar flow. To obtain Nu, blend Equation (4.2.13) for Nu_ℓ with Equation (4.2.7) for Nu_t using Equation (4.2.6) with *m* = 10.

10. *Spheres, Figure 4.2.3C*. For spheres use Equation (4.2.6), with $m = 6$, and with

$$\text{Nu}_\ell = 2 + 0.878\overline{C}_\ell\text{Ra}^{1/4} \quad \text{and} \quad \text{Nu}_t = \overline{C}_t\text{Ra}^{1/3} \tag{4.2.14}$$

The table above contains $\overline{C}_t$ values.

11. *Combined Shapes, Figure 4.2.3D*. For combined shapes, such as the cylinder in Figure 4.2.3D with spherical end caps, calculate the heat transfer from the cylinder of length L (*Case 8*), the heat transfer from a sphere of diameter D (*Case 10*) and add to obtain the total transfer. Other shapes can be treated in a similar manner.

Correlations for Open Cavities

Examples of this class of problem are shown in Figure 4.2.4. Walls partially enclose a fluid region (cavity) where boundary openings permit fluid to enter and leave. Upstream from its point of entry, the fluid is at the ambient temperature, T_∞. Since access of the ambient fluid to the heated surfaces is restricted, some of the heated surface is starved of cool ambient to which heat can be transferred. As the sizes of the boundary openings are increased, the previous class of problems is approached; for example, when the plate spacing in Figure 4.2.4A (*Case 12*) becomes very large, the heat transfer from each vertical surface is given by *Case 1*.
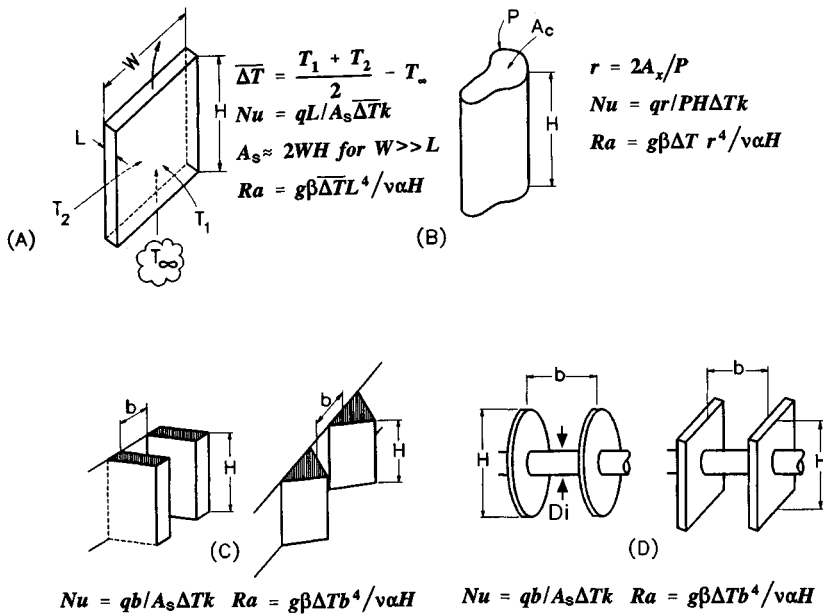

FIGURE 4.2.4 Nomenclature for various open-cavity problems.

12. *Isothermal Vertical Channels, Figure 4.2.4A and B*. Figure 4.2.4A shows an open cavity bounded by vertical walls and open at the top and bottom. The large opposing plates are isothermal, at temperatures T_1 and T_2, respectively, and the spacing between these plates is small. $\overline{\Delta T}$ is the average temperature difference between the plates and T_∞, as shown in Figure 4.2.4A, but T_1 and T_2 must not straddle T_∞. For this case

$$\text{Nu} = \left(\left(\frac{\text{Ra}}{f\text{Re}}\right)^m + \left(C_1\overline{C}_\ell\text{Ra}^{1/4}\right)^m\right)^{1/m} \qquad \text{Ra} \leq 10^5 \tag{4.2.15}$$

where fRe is the product of friction factor and Reynolds number for fully developed flow through, and C_1 is a constant that accounts for the augmentation of heat transfer, relative to a vertical flat plate (*Case 1*), due to the chimney effect. The fRe factor accounts for the cross-sectional shape (Elenbaas, 1942a). Symbols are defined in Figure 4.2.4A and B; in the Nu equation, q is the total heat transferred to the ambient fluid from all heated surfaces.

For the parallel plate channel shown in Figure 4.2.4(A), use f Re = 24, $m = -1.9$, and for gases $C_1 \approx 1.2$. It should be noted, however, that C_1 must approach 1.0 as Pr increases or as the plate spacing increases. For channels of circular cross section (Figure 4.2.4B) fRe - 16, $m = -1.03$, and for gases $C_1 \approx 1.17$. For other cross-sectional shapes like the square (fRe = 14.23), hexagonal (fRe = 15.05), or equilateral triangle (fRe = 13.3), use Equation (4.2.15) with the appropriate fRe, and with $m = -1.5$, and $C_1 \approx 1.2$ for gases.

The heat transfer per unit cross-sectional area, q/A_c, for a given channel length H and temperature difference, passes through a maximum at approximately Ra_{max}, where

$$Ra_{max} = \left(\frac{f \, Re \, C_1 \overline{C}_\ell}{2^{1/m}} \right)^{4/3} \tag{4.2.16}$$

Ra_{max} provides the value of hydraulic radius $r = 2A_c/P$ at this maximum.

13. *Isothermal Triangular Fins, Figure 4.2.4C.* For a large array of triangular fins (Karagiozis et al., 1994) in air, for $0.4 < Ra < 5 \times 10^5$

$$Nu = \overline{C}_\ell Ra^{1/4} \left[1 + \left(\frac{3.26}{Ra^{0.21}} \right)^3 \right]^{-1/3} \qquad 0.4 < Ra < 5 \times 10^5 \tag{4.2.17}$$

In this equation, b is the average fin spacing (Figure 4.2.4C), defined such that bL is the cross-sectional flow area between two adjacent fin surfaces up to the plane of the fin tips. For Ra < 0.4, Equation (4.2.17) underestimates the convective heat transfer. When such fins are mounted horizontally (vertical baseplate, but the fin tips are horizontal), there is a substantial reduction of the convective heat transfer (Karagiozis et al., 1994).

14. *U-Channel Fins, Figure 4.2.4C.* For the fins most often used as heat sinks, there is uncertainty about the heat transfer at low Ra. By using a conservative approximation applying for Ra < 100 (that underestimates the real heat transfer), the following equation may be used:

$$Nu = \left[\left(\frac{Ra}{24} \right)^{-2} + \left(C_1 \overline{C}_\ell Ra \right)^{-2} \right]^{-0.5} \tag{4.2.18}$$

For air C_1 depends on aspect ratio of the fin as follows (Karagiozis, 1991):

$$C_1 = \left[1 + \left(\frac{H}{b} \right), 1.16 \right]_{min} \tag{4.2.19}$$

Equation (4.2.18) agrees well with measurements for Ra > 200, but for smaller Ra it falls well below data because the leading term does not account for heat transfer from the fin edges and for three-dimensional conduction from the entire array.

15. *Circular Fins on a Horizontal Tube, Figure 4.24D.* For heat transfer from an array of circular fins (Edwards and Chaddock, 1963), for $H/D_i = 1.94$, $5 < Ra < 10^4$, and for air,

$$\text{Nu} = 0.125\text{Ra}^{0.55}\left[1 - \exp\left(-\frac{137}{\text{Ra}}\right)\right]^{0.294} \tag{4.2.20}$$

A more general, but also more complex, relation is reported by Raithby and Hollands (1985).

16. *Square Fins on a Horizontal Tube, Figure 4.2.4D*. Heat transfer (Elenbaas, 1942b) from the square fins (excluding the cylinder that connects them) is correlated for gases by

$$\text{Nu} = \left[\left(\text{Ra}^{0.89}/18\right)^m + \left(0.62\text{Ra}^{1/4}\right)^m\right]^{1/m} \quad m = -2.7 \tag{4.2.21}$$

Heat Transfer in Enclosures

This section deals with cavities where the bounding walls are entirely closed, so that no mass can enter or leave the cavity. The fluid motion inside the cavity is driven by natural convection, which enhances the heat transfer among the interior surfaces that bound the cavity.

17. *Extensive Horizontal Layers, Figure 4.2.5A with $\theta = 0°$*. If the heated plate, in a horizontal parallel-plate cavity, is on the top, heat transfer is by conduction alone, so that Nu = 1. For heat transfer from below (Hollands, 1984):

$$\text{Nu} = 1 + \left[1 - \frac{1708}{\text{Ra}}\right]^{\bullet}\left[k_1 + 2\left(\frac{\text{Ra}^{1/3}}{k_2}\right)^{1-\ln\left(\text{Ra}^{1/3}/k_2\right)}\right] + \left[\left(\frac{\text{Ra}}{5830}\right)^{1/3} - 1\right]^{\bullet} \tag{4.2.22}$$

where

$$[x]^{\bullet} = (x,0)_{\max} \quad k_1 = \frac{1.44}{1 + 0.018/\text{Pr} + 0.00136/\text{Pr}^2} \quad k_2 = 75\,\exp\left(1.5\text{Pr}^{-1/2}\right) \tag{4.2.23}$$

The equation has been validated for Ra < 10^{11} for water, Ra < 10^8 for air, and over a smaller Ra range for other fluids. Equation (4.2.22) applies to extensive layers: $W/L \geq 5$. Correlations for nonextensive layers are provided by Raithby and Hollands (1985).
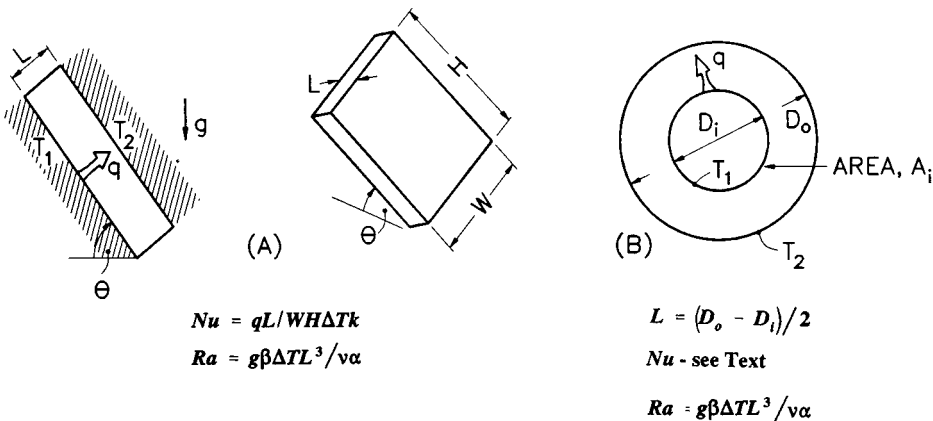

$$Nu = qL/WH\Delta Tk$$
$$Ra = g\beta\Delta TL^3/\nu\alpha$$

$$L = (D_o - D_i)/2$$
$$Nu \text{ - see Text}$$
$$Ra = g\beta\Delta TL^3/\nu\alpha$$

FIGURE 4.2.5 Nomenclature for enclosure problems.

18. *Vertical Layers, Figure 4.2.5(A), with θ = 90°.* W/L > 5. For a vertical, gas-filled (Pr ≈ 0.7) cavity with H/L ≥ 5, the following equation closely fits the data, for example that of Shewen et al. (1996) for $Ra(H/L)^3 \leq 5 \times 10^{10}$ and $H/L \geq 40$.

$$Nu_1 = \left[1 + \left(\frac{0.0665Ra^{1/3}}{1 + \left(\frac{9000}{Ra}\right)^{1.4}}\right)^2\right]^{1/2} \qquad Nu_2 = 0.242\left(Ra\frac{L}{H}\right)^{0.273} \qquad Nu = \left[Nu_1, Nu_2\right]_{max} \quad (4.2.24)$$

For Pr ≥ 4, the following equation is recommended (Seki et al., 1978) for $Ra(H/L)^3 < 4 \times 10^{12}$

$$Nu = \left[1, 0.36Pr^{0.051}\left(\frac{L}{H}\right)^{0.36}Ra^{0.25}, 0.084Pr^{0.051}\left(\frac{L}{H}\right)^{0.1}Ra^{0.3}\right]_{max} \qquad (4.2.25a)$$

and for $Ra (H/L)^3 > 4 \times 10^{12}$

$$Nu = 0.039Ra^{1/3} \qquad (4.2.25b)$$

19. *Tilted Layers, Figure 4.25A, with 0 ≤ θ ≤ 90°,* W/L > 8. For gases (Pr ≈ 0.7), 0 ≤ θ ≤ 60° and Ra ≤ 10⁵ (Hollands et al., 1976), use

$$Nu = 1 + 1.44\left[1 - \frac{1708}{Ra\cos\theta}\right]^{\bullet}\left[1 - \frac{1708(\sin 1.8\theta)^{1.6}}{Ra\cos\theta}\right] + \left[\left(\frac{Ra\cos\theta}{5830}\right)^{1/3} - 1\right]^{\bullet} \qquad (4.2.26)$$

See equation (4.2.23) for definition of [x]°. For 60° ≤ θ ≤ 90° linear interpolation is recommended using Equations (4.2.24) for θ = 90° and (4.2.26) for θ = 60°.

20. *Concentric Cylinders, Figure 4.2.5B.* For heat transfer across the gap between horizontal concentric cylinders, the Nusselt number is defined as $Nu = q' \ln(D_o/D_i)/2\pi\Delta T$ where q' is the heat transfer per unit length of cylinder. For $Ra \leq 8 \times 10^7$, $0.7 \leq Pr \leq 6000$, $1.15 \leq D/D_i \leq 8$ (Raithby and Hollands, 1975)

$$Nu = \left[0.603\overline{C}_{\ell}\frac{\ln\left(D_o/D_i\right)Ra^{1/4}}{\left[\left(L/D_i\right)^{3/5} + \left(L/D_o\right)^{3/5}\right]^{5/4}}, 1\right]_{max} \qquad (4.2.27)$$

For eccentric cylinders, see Raithby and Hollands (1985).

21. *Concentric Spheres, Figure 4.2.5B.* The heat transfer between concentric spheres is given by the following equation (Raithby and Hollands, 1975) for $Ra \leq 6 \times 10^8$, $5 \leq Pr \leq 4000$, $1.25 < D_o/D_i \leq 2.5$,

$$Nu = \frac{qL}{D_iD_ok\Delta T} = \left[1.16\overline{C}_{\ell}\left(\frac{L}{D_i}\right)^{1/4}\frac{Ra^{1/4}}{\left[\left(D_i/D_o\right)^{3/5} + \left(D_o/D_i\right)^{4/5}\right]^{5/4}}, 1\right]_{max} \qquad (4.2.28)$$

For eccentric spheres, see Raithby and Hollands (1985).

Example Calculations

Problem 1: Heat Transfer from Vertical Plate, Figure 4.2.6A. For the vertical isothermal surface in Figure 4.2.6A with $T_s = 40°C$, $H_1 = 1$ m, $H_2 = 1$ m, $W_1 = 1$ m, $W_2 = 1$ m and for an ambient air temperature of $T_\infty = 20°C$ (at 1 atm), find the heat transfer from one side of the plate.
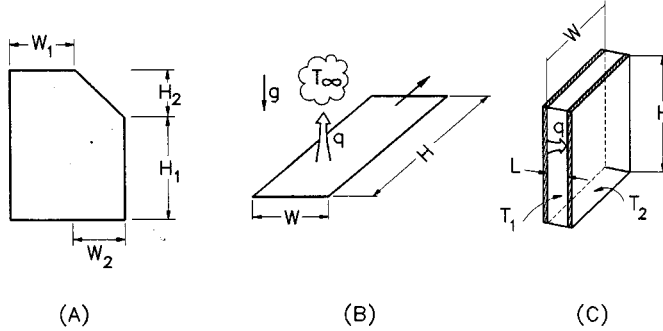

FIGURE 4.2.6 Sketches for example problems.

Properties: At $T_f = (T_w + T_\infty)/2 = 30°C$ and atmospheric pressure for air: $\nu = 1.59 \times 10^{-5}$ m²/sec, Pr = 0.71, k = 0.0263 W/mK. At T_∞, $\beta \approx 1/T_\infty = 1(273 + 20) = 0.00341$ K⁻¹.

Solution: For the geometry shown in Figure 4.2.6A:

$$A_s = (H_1 + H_2)W_1 + \left(H_1 + \frac{H_2}{2}\right)W_2 = 3.5 \text{ m}^2 \quad \text{(plate surface area)}$$

$$\int_0^{W_1 + W_2} S^{3/4} \, d\chi = (H_1 + H_2)^{3/4} W_1 + \frac{4}{7}\frac{W_2}{H_2}\left[(H_1 + H_2)^{7/4} - H_1^{7/4}\right] = 3.03 \text{ m}^{7/4}$$

$$L^{1/4} = (H_1 + H_2)^{1/4} = 1.19 \text{ m}^{1/4} \quad \text{(see comments below)}$$

$$C_1 = \frac{L^{1/4} \int_0^{W_1 + W_2} S^{3/4} \, d\chi}{A_s} = \frac{1.19 \times 3.03}{3.5} = 1.03$$

$$\text{Ra} = \frac{g\beta_\infty L^3 (T_w - T_\infty)}{\nu\alpha} = \frac{9.81 \times 0.00341 \times 2^3 \times (40 - 20)}{1.59 \times 10^{-5} \times 2.25 \times 10^{-5}} = 1.50 \times 10^{10}$$

$\overline{C}_\ell = 0.514$ from Equation (4.2.3); $C_t = C_t^V = 0.103$ from Equation (4.2.4). $\text{Nu}^T = C_1 \overline{C}_\ell \text{Ra}^{1/4} = 185$ from Equation (4.2.11).

$$\left.\begin{aligned}
\text{Nu}_\ell &= \frac{2.0}{\ln(1 + 2.0/\text{Nu}^T)} = 186 \\
\text{Nu}_t &= C_t^V \text{Ra}^{1/3}/(1 + 1.4 \times 10^9 \, \text{Pr}/\text{Ra}) = 238
\end{aligned}\right\} \text{(from Equation (4.2.7))}$$

$$\text{Nu} = \frac{qL}{A\Delta Tk} = \left(\text{Nu}_\ell^6 + \text{Nu}_t^6\right)^{1/6} = 246$$

from Equation (4.2.6) with $m = 6$.

$$q = \frac{A_s \Delta T k \text{Nu}}{\text{L}} = \frac{3.5 \times 20 \times 0.0263 \times 246}{2} = 226W$$

Comments on Problem 1: Since $\text{Nu}_\ell < \text{Nu}_t$, the heat transfer is primarily turbulent. Do not neglect radiation. Had the surface been specified to be at constant heat flux, rather than isothermal, the equations in this section can be used to find the approximate average temperature difference between the plate and fluid.

Problem 2: Heat Transfer from Horizontal Strip, Figure 4.2.6B. Find the rate of heat loss per unit length from a very long strip of width $W = 0.1$ m with a surface temperature of $T_s = 70°C$ in water at $T_\infty = 30°C$.
   Properties: At $T_f = (T_s + T_\infty)1/2 = 50°C$

$$v = 5.35 \times 10^{-7} \text{ m}^2/\text{sec} \qquad \alpha = 1.56 \times 10^{-7} \text{ m}^2/\text{sec} \qquad \text{Pr} = 3.42$$

$$k = 0.645 \text{ W/mK} \qquad \beta = 2.76 \times 10^{-4} \text{ K}^{-1}$$

Solution: This problem corresponds to *Case 3* and Figure 4.2.1C.

$$C_t^H = 0.14$$

from Equation 4.2.5 and $\overline{C}_l = 0.563$ from Equation (4.2.3).

$$L^* = \lim_{H \to \infty} \left(\frac{WH}{2W + 2H} \right) = \frac{W}{2} = 0.05 \text{ m}$$

from Figure 4.2.1C.

$$\text{Ra} = \frac{g\beta\Delta T L^{*3}}{v\alpha} = 1.62 \times 10^8 \qquad \text{Nu}^T = 0.835\overline{C}_l \text{Ra}^{1/4} = 53.5$$

$$\text{Nu}_\ell = \frac{1.4}{\ln\left(1 + 1.4/\text{Nu}^T\right)} = 54.2 \qquad \text{Nu}_t = C_t^H \text{Ra}^{1/3} = 76.3$$

$$\text{Nu} = \frac{q}{WH\Delta T} \frac{L^*}{k} = \left(\text{Nu}_\ell^{10} + \text{Nu}_t^{10} \right)^{0.1} = 76.5$$

$$q/H = \frac{W\Delta T k \text{Nu}}{L^*} = 3950 \text{ W/m-length}$$

Comments: Turbulent heat transfer is dominant. Radiation can be ignored (since it lies in the far infrared region where it is not transmitted by the water).

Problem 3: Heat Loss across a Window Cavity, Figure 4.2.6C. The interior glazing is at temperature $T_1 = 10°C$, the exterior glazing at $T_2 = -10°C$, the window dimensions are $W = 1$ m, $H = 1.7$ m, and the air gap between the glazings is $L = 1$ cm and is at atmospheric pressure. Find the heat flux loss across the window.

Properties: At $\overline{T} = T_1 + T_2/2 = 0°C = 273K$

$$v = 1.35 \times 10^{-5} \text{ m}^2/\text{sec} \qquad \alpha = 1.89 \times 10^{-5} \text{ m}^2/\text{sec} \qquad \text{Pr} = 0.71$$

$$k = 0.024 \text{ W/mK} \qquad \beta = 1/273 = 3.66 \times 10^{-3} \text{ K}^{-1}$$

Solution: The appropriate correlations are given in *Case 18* and by Equation (4.2.24).

$$\text{Ra} = \frac{g\beta(T_1 - T_2)L^3}{v\alpha} = \frac{9.81 \times 3.66 \times 10^{-3} \times 20 \times (0.01)^3}{1.35 \times 10^{-5} \times 1.89 \times 10^{-5}} = 2.81 \times 10^3$$

$$\text{Nu}_1 = \left[1 + \left\{ \frac{0.0665\text{Ra}^{1/3}}{1 + \left(\frac{9000}{\text{Ra}} \right)^{1.4}} \right\}^2 \right]^{1/2} = 1.01$$

$$\text{Nu}_2 = 0.242 \left(\text{Ra}\frac{L}{H} \right)^{0.273} = 0.242 \left(2.81 \times 10^3 \times \frac{0.01}{1.7} \right)^{0.273} = 0.520$$

$$\text{Nu} = \frac{qL}{WH(T_1 - T_2)k} = \left(\text{Nu}_1, \text{Nu}_2 \right)_{\text{max}} = 1.01$$

$$q / WH = \frac{N(T_1 - T_2)k}{L} = \frac{1.01 \times 20 \times 0.24}{0.01} = 48.5 \text{ W/m}^2$$

Comments: For pure conduction across the air layer, Nu = 1.0. For the calculated value of Nu = 1.01, convection must play little role. For standard glass, the heat loss by radiation would be roughly double the natural convection value just calculated.

Special Nomenclature

Note that nomenclature for each geometry considered is provided in the figures that are referred to in the text.

$\overline{C}_\ell$ = function of Prandtl number, Equation (4.2.3)
C_t^V = function of Prandtl number, Equation (4.2.4)
C_t^H = function of Prandtl number, Equation (4.2.5)
$\overline{C}_t$ = surface averaged value of C_t, page 4–38
$\overline{\Delta T}$ = surface averaged value of $T_w - T_\infty$

References

Churchill, S.W. 1983. *Heat Exchanger Design Handbook*, Sections 2.5.7 to 2.5.10, E.V. Schlinder, Ed., Hemisphere Publishing, New York.

Churchill S.W. and Usagi, R. 1972. A general expression for the correlation of rates of transfer and other phenomena, *AIChE J.*, 18, 1121–1128.

Clemes, S.B., Hollands, K.G.T., and Brunger, A.P. 1994. Natural convection heat transfer from horizontal isothermal cylinders, *J. Heat Transfer*, 116, 96–104.

Edwards, J.A. and Chaddock, J.B. 1963. An experimental investigation of the radiation and free-convection heat transfer from a cylindrical disk extended surface, *Trans., ASHRAE*, 69, 313–322.

Elenbaas, W. 1942a. The dissipation of heat by free convection: the inner surface of vertical tubes of different shapes of cross-section, *Physica*, 9(8), 865–874.

Elenbaas, W. 1942b. Heat dissipation of parallel plates by free convection, *Physica*, 9(1), 2–28.

Fujii, T. and Fujii, M. 1976. The dependence of local Nusselt number on Prandtl number in the case of free convection along a vertical surface with uniform heat flux, *Int. J. Heat Mass Transfer*, 19, 121–122.

Fujii, T., Honda, H., and Morioka, I. 1973. A theoretical study of natural convection heat transfer from downward-facing horizontal surface with uniform heat flux, *Int. J. Heat Mass Transfer*, 16, 611–627.

Goldstein, R.J., Sparrow, E.M., and Jones, D.C. 1973. Natural convection mass transfer adjacent to horizontal plates, *Int. J. Heat Mass Transfer*, 16, 1025–1035.

Hollands, K.G.T. 1984. Multi-Prandtl number correlations equations for natural convection in layers and enclosures, *Int. J. Heat Mass Transfer*, 27, 466–468.

Hollands, K.G.T., Unny, T.E., Raithby, G.D., and Konicek, K. 1976. Free convection heat transfer across inclined air layers, *J. Heat Transfer*, 98, 189–193.

Incropera, F.P. and DeWitt, D.P. 1990. *Fundamentals of Heat and Mass Transfer*, 3rd ed., John Wiley & Sons, New York.

Karagiozis, A. 1991. An Investigation of Laminar Free Convection Heat Transfer from Isothermal Finned Surfaces, Ph.D. Thesis, Department of Mechanical Engineering, University of Waterloo.

Karagiozis, A., Raithby, G.D., and Hollands, K.G.T. 1994. Natural convection heat transfer from arrays of isothermal triangular fins in air, *J. Heat Transfer*, 116, 105–111.

Kreith, F. and Bohn, M.S. 1993. *Principles of Heat Transfer.* West Publishing, New York.

Raithby, G.D. and Hollands, K.G.T. 1975. A general method of obtaining approximate solutions to laminar and turbulent free convection problems, in *Advances in Heat Transfer*, Irvine, T.F. and Hartnett, J.P., Eds., Vol. 11, Academic Press, New York, 266–315.

Raithby, G.D. and Hollands, K.G.T. 1985. *Handbook Heat Transfer*, Chap. 6: Natural Convection, Rohsenow, W.M., Hartnett, J.P., and Ganic, E.H., Eds., McGraw-Hill, New York.

Seki, N., Fukusako, S., and Inaba, H. 1978. Heat transfer of natural convection in a rectangular cavity with vertical walls of different temperatures, *Bull. JSME.*, 21(152), 246–253.

Shewan, E., Hollands, K.G.T., and Raithby, G.D. 1996. Heat transfer by natural convection across a vertical air cavity of large aspect ratio, *J. Heat Transfer*, 118, 993–995.

Further Information

There are several excellent heat transfer textbooks that provide fundamental information and correlations for natural convection heat transfer (e.g., Kreith and Bohn, 1993; Incropera and DeWitt, 1990). The correlations in this section closely follow the recommendations of Raithby and Hollands (1985), but that reference considers many more problems. Alternative equations are provided by Churchill (1983).

Forced Convection — External Flows

N.V. Suryanarayana

Introduction

In this section we consider heat transfer between a solid surface and an adjacent fluid which is in motion relative to the solid surface. If the surface temperature is different from that of the fluid, heat is transferred as forced convection. If the bulk motion of the fluid results solely from the difference in temperature of the solid surface and the fluid, the mechanism is natural convection. The velocity and temperature of the fluid far away from the solid surface are the free-stream velocity and free-stream temperature. Both

are usually known or specified. We are then required to find the heat flux from or to the surface with specified surface temperature or the surface temperature if the heat flux is specified. The specified temperature or heat flux either may be uniform or may vary. The convective heat transfer coefficient *h* is defined by

$$q'' = h(T_s - T_\infty) \qquad (4.2.29)$$

In Equation (4.2.29) with the local heat flux, we obtain the local heat transfer coefficient, and with the average heat flux with a uniform surface temperature we get the average heat transfer coefficient. For a specified heat flux the local surface temperature is obtained by employing the local convective heat transfer coefficient.

Many correlations for finding the convective heat transfer coefficient are based on experimental data which have some uncertainty, although the experiments are performed under carefully controlled conditions. The causes of the uncertainty are many. Actual situations rarely conform completely to the experimental situations for which the correlations are applicable. Hence, one should not expect the actual value of the heat transfer coefficient to be within better than ±10% of the predicted value.

Many different correlations to determine the convective heat transfer coefficient have been developed. In this section only one or two correlations are given. For other correlations and more details, refer to the books given in the bibliography at the end of this section.

Flat Plate

With a fluid flowing parallel to a flat plate, changes in velocity and temperature of the fluid are confined to a thin region adjacent to the solid boundary — the boundary layer. Several cases arise:

1. Flows without or with pressure gradient
2. Laminar or turbulent boundary layer
3. Negligible or significant viscous dissipation (effect of frictional heating)
4. $Pr \geq 0.7$ or $Pr \ll 1$

Flows with Zero Pressure Gradient and Negligible Viscous Dissipation

When the free-stream pressure is uniform, the free-stream velocity is also uniform. Whether the boundary layer is laminar or turbulent depends on the Reynolds number Re_x ($\rho U_\infty x/\mu$) and the shape of the solid at entrance. With a sharp edge at the leading edge (Figure 4.2.7) the boundary layer is initially laminar but at some distance downstream there is a transition region where the boundary layer is neither totally laminar nor totally turbulent. Farther downstream of the transition region the boundary layer becomes turbulent. For engineering applications the existence of the transition region is usually neglected and it is assumed that the boundary layer becomes turbulent if the Reynolds number, Re_x, is greater than the critical Reynolds number, Re_{cr}. A typical value of 5×10^5 for the critical Reynolds number is generally accepted, but it can be greater if the free-stream turbulence is low and lower if the free-stream turbulence is high, the surface is rough, or the surface does not have a sharp edge at entrance. If the entrance is blunt, the boundary layer may be turbulent from the leading edge.
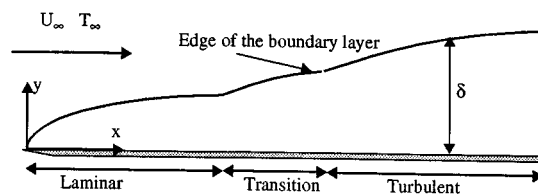

FIGURE 4.2.7 Flow of a fluid over a flat plate with laminar, transition, and turbulent boundary layers.

Temperature Boundary Layer

Analogous to the velocity boundary layer there is a temperature boundary layer adjacent to a heated (or cooled) plate. The temperature of the fluid changes from the surface temperature at the surface to the free-stream temperature at the edge of the temperature boundary layer (Figure 4.2.8).
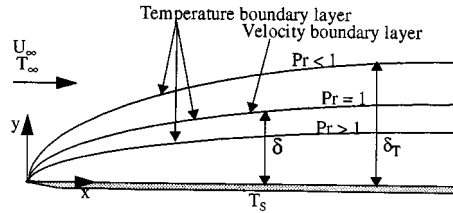

FIGURE 4.2.8 Temperature boundary layer thickness relative to velocity boundary layer thickness.

The velocity boundary layer thickness δ depends on the Reynolds number Re_x. The thermal boundary layer thickness δ_T depends both on Re_x and Pr

$\mathrm{Re}_x < \mathrm{Re}_{cr}$:

$$\frac{\delta}{x} = \frac{5}{\sqrt{\mathrm{Re}_x}} \qquad \mathrm{Pr} > 0.7 \qquad \frac{\delta}{\delta_T} = \mathrm{Pr}^{1/3}$$

$$\mathrm{Pr} \ll 1 \qquad \frac{\delta}{\delta_T} = \mathrm{Pr}^{1/2} \tag{4.2.30}$$

$\mathrm{Re}_{cr} < \mathrm{Re}_x$:

$$\frac{\delta}{x} = \frac{0.37}{\mathrm{Re}_x^{0.2}} \qquad \delta \approx \delta_T \tag{4.2.31}$$

Viscous dissipation and high-speed effects can be neglected if $\mathrm{Pr}^{1/2}\,\mathrm{Ec}/2 \ll 1$. For heat transfer with significant viscous dissipation see the section on flow over flat plate with zero pressure gradient: Effect of High Speed and Viscous Dissipation. The Eckert number Ec is defined as $\mathrm{Ec} = U_\infty^2/C_p(T_s - T_\infty)$.

With a rectangular plate of length L in the direction of the fluid flow the average heat transfer coefficient h_L with uniform surface temperature is given by

$$h_L = \frac{1}{L}\int_0^L h_x\, dx$$

Laminar Boundary Layer *(Re$_x$ < Re$_{cr}$, Re$_L$ < Re$_{cr}$)*: With heating or cooling starting from the leading edge the following correlations are recommended. Note: in all equations evaluate fluid properties at the film temperature defined as the arithmetic mean of the surface and free-stream temperatures unless otherwise stated (Figure 4.2.9).
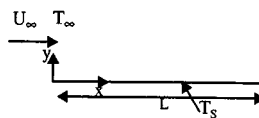

FIGURE 4.2.9 Heated flat plate with heating from the leading edge.

Local Heat Transfer Coefficient (Uniform Surface Temperature)

The Nusselt number based on the local convective heat transfer coefficient is expressed as

$$\mathrm{Nu}_x = f_{\mathrm{Pr}}\mathrm{Re}_x^{1/2} \tag{4.2.32}$$

The classical expression for f_{Pr} is 0.564 $\mathrm{Pr}^{1/2}$ for liquid metals with very low Prandtl numbers, 0.332$\mathrm{Pr}^{1/3}$ for 0.7 < Pr < 50 and 0.339$\mathrm{Pr}^{1/3}$ for very large Prandtl numbers. Correlations valid for all Prandtl numbers developed by Churchill (1976) and Rose (1979) are given below.

$$\mathrm{Nu}_x = \frac{0.3387\mathrm{Re}_x^{1/2}\mathrm{Pr}^{1/3}}{\left[1+\left(\dfrac{0.0468}{\mathrm{Pr}}\right)^{2/3}\right]^{1/4}} \tag{4.2.33}$$

$$\mathrm{Nu}_x = \frac{\mathrm{Re}^{1/2}\mathrm{Pr}^{1/2}}{\left(27.8+75.9\mathrm{Pr}^{0.306}+657\mathrm{Pr}\right)^{1/6}} \tag{4.2.34}$$

In the range 0.001 < Pr < 2000, Equation (4.2.33) is within 1.4% and Equation (4.2.34) is within 0.4% of the exact numerical solution to the boundary layer energy equation.

Average Heat Transfer Coefficient

The average heat transfer coefficient is given by

$$\mathrm{Nu}_L = 2\mathrm{Nu}_{x=L} \tag{4.2.35}$$

From Equation 4.2.35 it is clear that the average heat transfer coefficient over a length L is twice the local heat transfer coefficient at x = L.

Uniform Heat Flux

Local Heat Transfer Coefficient

Churchill and Ozoe (1973) recommend the following single correlation for all Prandtl numbers.

$$\mathrm{Nu}_x = \frac{0.886\mathrm{Re}_x^{1/2}\mathrm{Pr}^{1/2}}{\left[1+\left(\dfrac{\mathrm{Pr}}{0.0207}\right)^{2/3}\right]^{1/4}} \tag{4.2.36}$$

Note that for surfaces with uniform heat flux the local convective heat transfer coefficient is used to determine the local surface temperature. The total heat transfer rate being known, an average heat transfer coefficient is not needed and not defined.

Turbulent Boundary Layer *($Re_x > Re_{cr}$, $Re_L > Re_{cr}$):* For turbulent boundary layers with heating or cooling starting from the leading edge use the following correlations:

Local Heat Transfer Coefficient

$Re_{cr} < Re_x < 10^7$:

$$\mathrm{Nu}_x = 0.0296\mathrm{Re}_x^{4/5}\mathrm{Pr}^{1/3} \tag{4.2.37}$$

$10^7 < Re_x$:

$$\mathrm{Nu}_x = 1.596\mathrm{Re}_x\left(\ln\mathrm{Re}_x\right)^{-2.584}\mathrm{Pr}^{1/3} \tag{4.2.38}$$

Equation (4.2.38) is obtained by applying Colburn's *j* factor in conjunction with the friction factor suggested by Schlicting (1979).

In laminar boundary layers, the convective heat transfer coefficient with uniform heat flux is approximately 36% higher than with uniform surface temperature. With turbulent boundary layers, the difference is very small and *the correlations for the local convective heat transfer coefficient can be used for both uniform surface temperature and uniform heat flux.*

<u>*Average Heat Transfer Coefficient*</u>

If the boundary layer is initially laminar followed by a turbulent boundary layer at $Re_x = Re_{cr}$, the following correlations for $0.7 < Pr < 60$ are suggested:

$Re_{cr} < Re_L < 10^7$:

$$Nu_L = \left[0.664 Re_L^{1/2} + 0.037\left(Re_L^{4/5} - Re_{cr}^{4/5}\right)\right] Pr^{1/3} \tag{4.2.39}$$

If $Re_{cr} < Re_L < 10^7$ and $Re_{cr} = 10^5$, Equation 4.2.39 simplifies to

$$Nu_L = \left(0.037 Re_L^{4/5} - 871\right) Pr^{1/3} \tag{4.2.40}$$

$10^7 < Re_L$ and $Re_{cr} = 5 \times 10^5$:

$$Nu_L = \left[1.963 Re_L \left(\ln Re_L\right)^{-2.584} - 871\right] Pr^{1/3} \tag{4.2.41}$$

Uniform Surface Temperature — Pr > 0.7: Unheated Starting Length

If heating does not start from the leading edge as shown in Figure 4.2.10, the correlations have to be modified. Correlation for the local convective heat transfer coefficient for laminar and turbulent boundary layers are given by Equations (4.2.42) and (4.2.43) (Kays and Crawford, 1993) — the constants in Equations (4.2.42) and (4.2.43) have been modified to be consistent with the friction factors. These correlations are also useful as building blocks for finding the heat transfer rates when the surface temperature varies in a predefined manner. Equations (4.2.44) and (4.2.45), developed by Thomas (1977), provide the average heat transfer coefficients based on Equations (4.2.42) and (4.2.43).
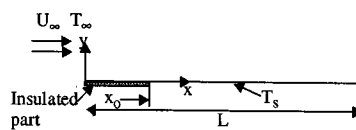

FIGURE 4.2.10 Heated flat plate with unheated starting length.

<u>*Local Convective Heat Transfer Coefficient*</u>

$Re_x < Re_{cr}$:

$$Nu_x = \frac{0.332 Re_x^{1/2} Pr^{1/3}}{\left[1 - \left(\dfrac{x_o}{x}\right)^{3/4}\right]^{1/3}} \tag{4.2.42}$$

$Re_x > Re_{cr}$:

$$Nu_x = \frac{0.0296 Re_x^{4/5} Pr^{3/5}}{\left[1 - \left(\dfrac{x_o}{x}\right)^{9/10}\right]^{1/9}} \tag{4.2.43}$$

Average Heat Transfer Coefficient over the Length $(L - x_o)$

$Re_L < Re_{cr}$:

$$h_{L-x_o} = \frac{0.664 Re_L^{1/2} Pr^{1/3} \left[1 - \left(\dfrac{x_o}{L} \right)^{3/4} \right]^{2/3} k}{L - x_o}$$

$$= 2 \frac{1 - \left(\dfrac{x_o}{L} \right)^{3/4}}{1 - x_o/L} h_{x=L}$$

(4.2.44)

In Equation (4.2.44) evaluate $h_{x=L}$ from Equation (4.2.42).

$Re_{cr} = 0$:

$$h_{L-x_o} = \frac{0.037 Re_L^{4/5} Pr^{3/5} \left[1 - \left(\dfrac{x_o}{L} \right)^{9/10} \right]^{8/9} k}{L - x_o}$$

$$= 1.25 \frac{1 - \left(x_o/L \right)^{9/10}}{1 - x_o/L} h_{x=L}$$

(4.2.45)

In Equation (4.2.45) evaluate $h_{x=L}$ from Equation (4.2.43).

Flat Plate with Prescribed Nonuniform Surface Temperature

The linearity of the energy equation permits the use of Equations (4.2.42) through (4.2.45) for uniform surface temperature with unheated starting length to find the local heat flux and the total heat transfer rate by the principle of superposition when the surface temperature is not uniform. Figure 4.2.11 shows the arbitrarily prescribed surface temperature with a uniform free-stream temperature of the fluid. If the surface temperature is a differentiable function of the coordinate *x*, the local heat flux can be determined by an expression that involves integration (refer to Kays and Crawford, 1993). If the surface temperature can be approximated as a series of step changes in the surface temperature, the resulting expression for the local heat flux and the total heat transfer rate is the summation of simple algebraic expressions. Here the method using such an algebraic simplification is presented.
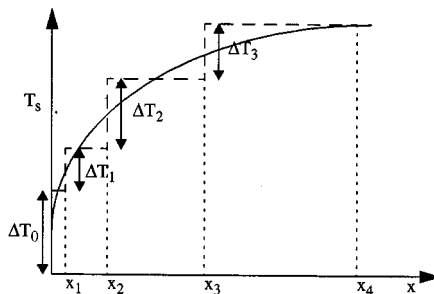

FIGURE 4.2.11 Arbitrary surface temperature approximated as a finite number of step changes.

The local convective heat flux at a distance x from the leading edge is given by

$$q''_x = \sum_1^n h_{xi} \Delta T_{si} \tag{4.2.46}$$

where h_{xi} denotes the local convective heat transfer coefficient at x due to a single step change in the surface temperature ΔT_{si} at location $x_i (x_i < x)$. Referring to Figure 4.2.11, the local convective heat flux at x ($x_3 < x < x_4$) is given by

$$q''_x = h_x(x,0)\Delta T_o + h_x(x,x_1)\Delta T_1 + h_x(x,x_2)\Delta T_2 + h_x(x,x_3)\Delta T_3$$

where $h_x(x, x_1)$ is the local convective heat transfer coefficient at x with heating starting from x_1; the local convective heat transfer is determined from Equation (4.2.42) if the boundary layer is laminar and Equation (4.2.43) if the boundary layer is turbulent from the leading edge. For example, $h_x(x, x_2)$ in the third term is given by

$$\mathrm{Re}_x < \mathrm{Re}_{cr} \qquad h_x(x,x_2) = \frac{0.332\left(\dfrac{\rho U_\infty x}{\mu}\right)^{1/2}\mathrm{Pr}^{1/3}}{\left[1-\left(\dfrac{x_2}{x}\right)^{3/4}\right]^{1/3}}\frac{k}{x}$$

$$\mathrm{Re}_{cr} = 0 \qquad h_x(x,x_2) = \frac{0.0296\left(\dfrac{\rho U_\infty x}{\mu}\right)^{4/5}\mathrm{Pr}^{3/5}}{\left[1-\left(\dfrac{x_2}{x}\right)^{9/10}\right]^{1/9}}\frac{k}{x}$$

The procedure for finding the total heat transfer rate from $x = 0$ to $x = L$ is somewhat similar. Denoting the width of the plate by W,

$$\frac{q}{W} = \sum h_{L-x_i} \Delta T_i (L - x_i) \tag{4.2.47}$$

where h_{L-x_i} is the average heat transfer coefficient over the length $L - x_i$ due to a step change ΔT_i in the surface temperature at x_i. For example, the heat transfer coefficient in the third term in Equation (4.2.47) obtained by replacing x_o by x_2 in Equation (4.2.44) or (4.2.45) depending on whether $\mathrm{Re}_L < \mathrm{Re}_{cr}$ or $\mathrm{Re}_{cr} = 0$.

Flows with Pressure Gradient and Negligible Viscous Dissipation

Although correlations for flat plates are for a semi-infinite fluid medium adjacent to the plate, most applications of practical interest deal with fluid flowing between two plates. If the spacing between the plates is significantly greater than the maximum boundary layer thickness, the medium can be assumed to approach a semi-infinite medium. In such a case if the plates are parallel to each other and if the pressure drop is negligible compared with the absolute pressure, the pressure gradient can be assumed to be negligible. If the plates are nonparallel and if the boundary layer thickness is very much smaller than the spacing between the plates at that location, the medium can still be considered as approaching a semi-infinite medium with a non-negligible pressure gradient. In such flows the free-stream velocity (core velocity outside the boundary layer) is related to the pressure variation by the Bernoulli equation:

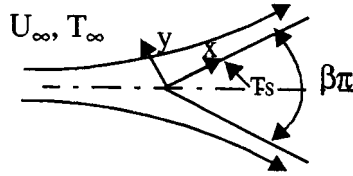$$\frac{p}{\rho} + \frac{U_\infty^2}{2} + zg = \text{constant}$$

FIGURE 4.2.12 Flow over a wedge. $\beta\pi$ is the wedge angle.

Another situation where the free-stream velocity varies in the direction of flow giving rise to a pressure gradient is flow over a wedge. For the family of flows for which the solutions are applicable, the free-stream velocity at the edge of the boundary layer is related to the x-coordinate by a power law, $U_\infty = cx^m$. Flows over semi-infinite wedges (Figure 4.2.12) satisfy that condition. The exponent m is related to the wedge angle $\beta\pi$

$$\beta = \frac{2m}{1+m} \qquad m = \frac{\beta}{2-\beta}$$

With laminar boundary layers, the boundary layer thickness, friction factor, and Nusselt numbers are defined by

$$\frac{\delta}{x} = \frac{c_1}{\sqrt{\text{Re}_x}} \qquad \frac{C_{fx}}{2} = \frac{\tau_w}{\rho U_\infty^2} = \frac{c_2}{\sqrt{\text{Re}_x}} \qquad \text{Nu}_x = c_3 \text{Re}_x^{1/2}$$

The values of c_1, c_2, and c_3 are available in Burmeister (1993). For example, for $\beta = 0.5$ (wedge angle $= 90°$), $m = 1/3$, $c_1 = 3.4$, $c_2 = 0.7575$, and $c_3 = 0.384$ for Pr $= 0.7$, and $c_3 = 0.792$ for Pr $= 5$. Re_x is based on $U_\infty = cx^m$; the free-stream velocity is not uniform.

Uniform Temperature: Flat Plate with Injection or Suction with External Flows of a Fluid Parallel to the Surface

Injection or suction has engineering applications. When the free-stream temperature of the fluid is high, as in gas turbines, a cooling fluid is introduced into the mainstream to cool the surface. If the cooling fluid is introduced at discrete locations (either perpendicular to the surface or at an angle), it is known as film cooling. If a fluid is introduced or withdrawn through a porous medium, it is known as transpiration (Figure 4.2.13). An application of suction is to prevent boundary layer separation (Figure 4.2.13).

Analytical solutions for a laminar boundary layer with transpiration suction or blowing are available if the velocity perpendicular to the surface varies in the following manner:

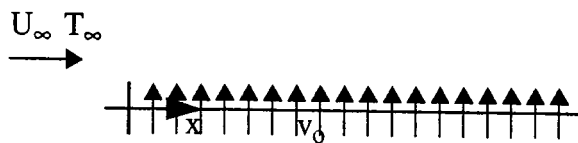$$\mathbf{v}_o = \text{constant } x^{(m-1)/2}$$

FIGURE 4.2.13 Flat plate with transpiration injection.

Solutions are limited to the cases of the injected fluid being at the same temperature as the surface and the injected fluid being the same as the free-stream fluid. Positive values of v_o indicate blowing and negative values indicate suction. Values of $\mathrm{Nu}_x/\mathrm{Re}_x^{1/2}$ for different values of Pr and for different values of blowing or suction parameter are given in Kays and Crawford (1993).

For example, for a laminar boundary layer over a flat plate with a fluid (Pr = 0.7) the value of $\mathrm{Nu}_x/\mathrm{Re}_x^{1/2}$ is 0.722 for $(v_o/U_\infty)\sqrt{\rho U_\infty x/\mu} = -0.75$ (suction) and 0.166 for $(v_o/U_\infty)\sqrt{\rho U_\infty x/\mu} = 0.25$ (blowing). Heat transfer coefficient increases with suction which leads to a thinning of the boundary layer. Blowing increases the boundary layer thickness and decreases the heat transfer coefficient.

For *turbulent boundary layers* Kays and Crawford (1993) suggest the following procedure for finding the friction factor and convective heat transfer coefficient. Define friction blowing parameter B_f and heat transfer blowing parameter B_h as

$$B_f = \frac{\mathbf{v}_o/U_\infty}{C_f/2} \tag{4.2.48}$$

$$B_h = \frac{\mathbf{v}_o/U_\infty}{\mathrm{St}} = \frac{\dot{m}''/G_\infty}{\mathrm{St}} \tag{4.2.49}$$

where

$$
\begin{aligned}
\mathrm{v}_o &= \text{velocity normal to the plate} \\
U_\infty &= \text{free-stream velocity} \\
\dot{m}'' &= \text{mass flux of the injected fluid at the surface } (\rho \mathrm{v}_o) \\
G_\infty &= \text{mass flux in the free stream } (\rho U_\infty) \\
\mathrm{St} &= \text{Stanton number} = \mathrm{Nu}_x/\mathrm{Re}_x\mathrm{Pr} = h/\rho U_\infty c_p
\end{aligned}
$$

The friction factors and Stanton number with and without blowing or suction are related by

$$\frac{C_f}{C_{fo}} = \frac{\ln(1+B_f)}{B_f} \tag{4.2.50}$$

$$\frac{\mathrm{St}}{\mathrm{St}_o} = \frac{\ln(1+B_h)}{B_h} \tag{4.2.51}$$

In Equations (4.2.50) and (4.2.51) C_{fo} and St_o are the friction factor and Stanton number with $\mathrm{v}_o = 0$ (no blowing or suction), and C_f and St are the corresponding quantities with blowing or suction at the same $\mathrm{Re}_x(\rho U_\infty x/\mu)$.

For the more general case of variable free-stream velocity, temperature difference, and transpiration rate, refer to Kays and Crawford (1993).

Flow over Flat Plate with Zero Pressure Gradient: Effect of High-Speed and Viscous Dissipation

In the boundary layer the velocity of the fluid is reduced from U_∞ to zero at the plate leading to a reduction in the kinetic energy of the fluid. Within the boundary layer there is also the work done by viscous forces; the magnitude of the such viscous work is related to the velocity of the fluid, the velocity gradient, and the viscosity of the fluid. The effect of such a reduction in the kinetic energy and the viscous work is to increase the internal energy of the fluid in the boundary layer. The increase in the internal energy may be expected to lead to an increase in the temperature; but because of the heat transfer to the adjacent fluid the actual increase in the internal energy (and the temperature) will be less than the sum of the decrease in the kinetic energy and viscous work transfer; the actual temperature

increase depends on the decrease in the kinetic energy, the viscous work transfer, and the heat transfer from the fluid. The maximum temperature in the fluid with an adiabatic plate is known as the adiabatic wall temperature (which occurs at the wall) and is given by

$$T_{aw} = T_\infty + r\frac{U_\infty^2}{2C_p}$$
(4.2.52)

In Equation (4.2.52) r is the recovery factor and is given by Eckert and Drake (1972).

$$\text{Laminar boundary layer} \quad 0.6 < \text{Pr} < 15 \quad r = \text{Pr}^{1/2}$$

$$\text{Turbulent boundary layer} \qquad\qquad r = \text{Pr}^{1/3}$$

Equation (4.2.52) can be recast as

$$\frac{T_{aw} - T_\infty}{T_s - T_\infty} = \frac{r}{2}\frac{U_\infty^2}{C_p(T_s - T_\infty)}$$
(4.2.53)

From Equation (4.2.53) the maximum increase in the fluid temperature as a fraction of the difference between the plate and free-stream temperatures is given by r Ec/2. With air flowing over a plate at 500 m/sec, the increase in the temperature of the air can be as high as 105°C. With $T_s = 40$°C and $T_\infty = 20$°C, the temperature of the air close to the plate can be higher than the plate temperature. It is thus possible that although the plate temperature is higher than the free-stream temperature, the heat transfer is from the air to the plate. At a Mach number greater than 0.1 for gases, viscous dissipation becomes significant.

The temperature profiles for high-speed flows for different values of T_s are shown in Figure 4.2.14. In high-speed flows, as heat transfer can be to the plate even if the plate temperature is greater than the fluid temperature, the definition of the convective heat transfer coefficient given in Equation (4.2.29) is not adequate. On the other hand, as the heat transfer is always from the plate if $T_s > T_{aw}$, the adiabatic wall temperature is more appropriate as the reference temperature. Thus, in high-speed flows the definition of the convective heat transfer coefficient is given by

$$q'' = h(T_s - T_{aw})$$
(4.2.54)
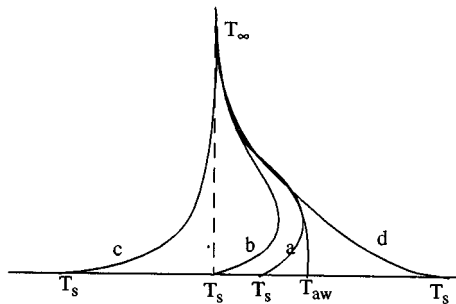
FIGURE 4.2.14 Temperature profiles for high-speed flows: (a) $T_\infty < T_s < T_{aw}$; (b) $T_s = T_\infty$; (c) $T_s \ll T_\infty$; (d) $T_s > T_{aw}$.

Equation (4.2.54) is consistent with Equation (4.2.29) as the adiabatic wall temperature equals the free-stream temperature if the effects of viscous dissipation and reduced kinetic energy in the boundary layer are neglected. With the adiabatic wall temperature as the fluid reference temperature for the definition

of the convective heat transfer coefficient, equations for low speeds can also be used for high-speed flows. Because of the greater variation in the fluid temperature in the boundary layer, the variation of properties due to temperature variation becomes important. It is found that the correlations are best approximated if the properties are evaluated at the reference temperature T^* defined by Eckert (1956):

$$T^* = 0.5(T_s + T_\infty) + 0.22(T_{aw} - T_\infty)$$ (4.2.55)

With properties evaluated at the reference temperature given by Equation (4.2.55), Equation (4.2.56) through (4.2.61) are applicable to high-speed flows with Prandtl numbers less than 15. It should be noted that the adiabatic wall temperatures in the laminar and turbulent regions are different affecting both the temperature at which the properties are evaluated and the temperature difference for determining the local heat flux. Therefore, when the boundary layer is partly laminar and partly turbulent, an average value of the heat transfer coefficient is not defined as the adiabatic wall temperatures in the two regions are different. In such cases the heat transfer rate in each region is determined separately to find the total heat transfer rate.

Evaluate properties at reference temperature given by Equation (4.2.55):

Laminar   Local: $\mathrm{Re}_x < \mathrm{Re}_{cr}$ $\mathrm{Nu}_x = 0.332\mathrm{Re}_x^{1/2}\mathrm{Pr}^{1/3}$ (4.2.56)

               Average: $\mathrm{Re}_L < \mathrm{Re}_{cr}$ $\mathrm{Nu}_L = 0.664\mathrm{Re}_L^{1/2}\mathrm{Pr}^{1/3}$ (4.2.57)

Turbulent   Local: $10^7 > \mathrm{Re}_x > \mathrm{Re}_{cr}$ $\mathrm{Nu}_x = 0.0296\mathrm{Re}_x^{4/5}\mathrm{Pr}^{1/3}$ (4.2.58)

               Local: $10^7 < \mathrm{Re}_x < 10^9$ $\mathrm{Nu}_x = 1.596\mathrm{Re}_x(\ln\mathrm{Re}_x)^{-2.584}\mathrm{Pr}^{1/3}$ (4.2.59)

               Average: $\mathrm{Re}_{cr} = 0$, $\mathrm{Re}_L < 10^7$ $\mathrm{Nu}_L = 0.037\mathrm{Re}_L^{4/5}\mathrm{Pr}^{1/3}$ (4.2.60)

               Average: $\mathrm{Re}_{cr} = 0$, $10^7 < \mathrm{Re}_L < 10^9$ $\mathrm{Nu}_L = 1.967\mathrm{Re}_L(\ln\mathrm{Re}_L)^{-2.584}\mathrm{Pr}^{1/3}$ (4.2.61)

When the temperature variation in the boundary layer is large, such that the assumption of constant specific heat is not justified, Eckert (1956) suggests that the properties be evaluated at a reference temperature corresponding to the specific enthalpy i^* given by

$$i^* = 0.5(i_s + i_\infty) + 0.22(i_s - i_\infty)$$ (4.2.62)

where i is the specific enthalpy of the fluid evaluated at the temperature corresponding to the subscript. Equation (4.2.62) gives the same values as Equation (4.2.55) if C_p is constant or varies linearly with temperature.

At very high speeds the gas temperature may reach levels of temperatures that are sufficient to cause disassociation and chemical reaction; these and other effects need to be taken into account in those cases.

Flow over Cylinders, Spheres, and Other Geometries

Flows over a flat plate and wedges were classified as laminar or turbulent, depending on the Reynolds number, and correlations for the local and average convective heat transfer coefficients were developed. But flows over cylinders (perpendicular to the axis) and spheres are more complex. In general, the flow over cylinders and spheres may have a laminar boundary layer followed by a turbulent boundary layer
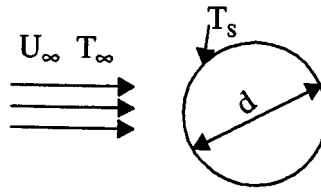
FIGURE 4.2.15 A fluid stream in cross flow over a cylinder.

and a wake region depending on the Reynolds number with the diameter as the characteristic length. Because of the complexity of the flow patterns, only correlations for the average heat transfer coefficients have been developed (Figure 4.2.15).

Cylinders: Use the following correlation proposed by Churchill and Bernstein (1977): $\mathrm{Re}_d \, \mathrm{Pr} > 0.2$. Evaluate properties at $(T_s + T_\infty)/2$:

$$\mathrm{Re}_d > 400,000: \qquad \mathrm{Nu}_d = 0.3 + \frac{0.62\mathrm{Re}_d^{1/2}\mathrm{Pr}^{1/3}}{\left[1+\left(0.4/\mathrm{Pr}\right)^{2/3}\right]^{1/4}}\left[1+\left(\frac{\mathrm{Re}_d}{282,000}\right)^{5/8}\right]^{4/5} \qquad (4.2.63)$$

$$10,000 < \mathrm{Re}_d < 400,000: \ \mathrm{Nu}_d = 0.3 + \frac{0.62\mathrm{Re}_d^{1/2}\mathrm{Pr}^{1/3}}{\left[1+\left(0.4/\mathrm{Pr}\right)^{2/3}\right]^{1/4}}\left[1+\left(\frac{\mathrm{Re}_d}{282,000}\right)^{1/2}\right] \qquad (4.2.64)$$

$$\mathrm{Re}_d < 10,000: \qquad \mathrm{Nu}_d = 0.3 + \frac{0.62\mathrm{Re}_d^{1/2}\mathrm{Pr}^{1/3}}{\left[1+\left(0.4/\mathrm{Pr}\right)^{2/3}\right]^{1/4}} \qquad (4.2.65)$$

For flow of liquid metals, use the following correlation suggested by Ishiguro et al. (1979):

$$1 < \mathrm{Re}_d\mathrm{Pr} < 100 \qquad \mathrm{Nu}_d = 1.125\left(\mathrm{Re}_d\mathrm{Pr}\right)^{0.413} \qquad (4.2.66)$$

For more information on heat transfer with flow over cylinders, refer to Morgan (1975) and Zukauskas (1987).

Spheres: For flows over spheres (Figure 4.2.16) use one of the following two correlations.
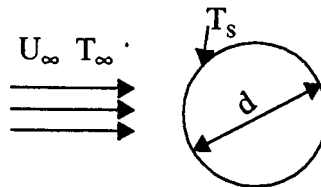

FIGURE 4.2.16 A fluid flowing over a sphere.

  1. Whitaker (1972): Evaluate properties at T_∞ except μ_s at T_s.

$$3.5 < \mathrm{Re}_d < 76,000 \qquad 0.71 < \mathrm{Pr} < 380 \qquad 1 < \mu/\mu_s < 3.2$$

$$\text{Nu}_d = 2.0 + \left(0.4\text{Re}_d^{1/2} + 0.06\text{Re}_d^{2/3}\right)\text{Pr}^{2/5}\left(\frac{\mu}{\mu_s}\right)^{1/4} \tag{4.2.67}$$

2. Achenbach (1978): Evaluate properties at $(T_s + T_\infty)/2$:

$$100 < \text{Re}_d < 2 \times 10^5 \qquad \text{Pr} = 0.71$$

$$\text{Nu}_d = 2 + \left(0.25\text{Re}_d + 3 \times 10^{-4}\,\text{Re}_d^{1.6}\right)^{1/2} \tag{4.2.68}$$

$$4 \times 10^5 < \text{Re}_d < 5 \times 10^6 \qquad \text{Pr} = 0.71$$

$$\text{Nu}_d = 430 + 5 \times 10^{-3}\,\text{Re}_d + 0.25 \times 10^{-9}\,\text{Re}_d^2 - 3.1 \times 10^{-17}\,\text{Re}_d^3 \tag{4.2.69}$$

3. Liquid Metals: From experimental results with liquid sodium, Witte (1968) proposed

$$3.6 \times 10^4 < \text{Re}_d < 1.5 \times 10^5 \qquad \text{Nu}_d = 2 + 0.386\left(\text{Re}_d\text{Pr}\right)^{1/2} \tag{4.2.70}$$

Other Geometries: For geometries other than cylinders and spheres, use Equation (4.2.71) with the characteristic dimensions and values of the constants given in the Table 4.2.1.

$$\text{Nu}_D = c\text{Re}_D^m \tag{4.2.71}$$

Although Equation (4.2.71) is based on experimental data with gases, its use can be extended to fluids with moderate Prandtl numbers by multiplying Equation (4.2.71) by $(\text{Pr}/0.7)^{1/3}$.

Heat Transfer across Tube Banks

When tube banks are used in heat exchangers, the flow over the tubes in the second subsequent rows of tubes is different from the flow over a single tube. Even in the first row the flow is modified by the presence of the neighboring tubes. The extent of modification depends on the spacing between the tubes. If the spacing is very much greater than the diameter of the tubes, correlations for single tubes can be used. Correlations for flow over tube banks when the spacing between tubes in a row and a column is not much greater than the diameter of the tubes have been developed for use in heat-exchanger applications. Two arrangements of the tubes are considered — aligned and staggered as shown in Figure 4.2.17. The nomenclature used in this section is shown in the figure.

For the average convective heat transfer coefficient with tubes at uniform surface temperature, from experimental results, Zukauskas (1987) recommends correlations of the form:

$$\text{Nu}_d = c\left(\frac{a}{b}\right)^p \text{Re}_d^m \text{Pr}^n \left(\frac{\text{Pr}}{\text{Pr}_s}\right)^{0.25} \tag{4.2.72}$$

In Equation (4.2.72) all properties are evaluated at the arithmetic mean of the inlet and exit temperatures of the fluid, except Pr_s which is evaluated at the surface temperature T_s. The values of the constants c, p, m, and n are given in Table 4.2.2 for in-line arrangement and in Table 4.2.3 for staggered arrangement.

TABLE 4.2.1   Values of *c* and *m* in Equation (4.2.71)

Geometry	Re_D	c	m
→ ▢	5000-100 000	0.092	0.675
→ ▢	2500-8000	0.160	0.699
→ ◇	5000-100 000	0.222	0.588
→ ◇	2500-7500	0.261	0.624
→ ⬡	5000-19500	0.144	0.638
	19 500-100 000	0.035	0.782
→ ⬡	5000-100 000	0.138	0.638
→ ⬭	2500-15 000	0.224	0.612
→ ⬮	3000-15 000	0.085	0.804
→ ǀ	4000-15 000	0.205	0.731
Charcteristic dimension is the equivalent circular diameter = Perimeter/π For example, for a square rod with each side a, D = 4a/π			

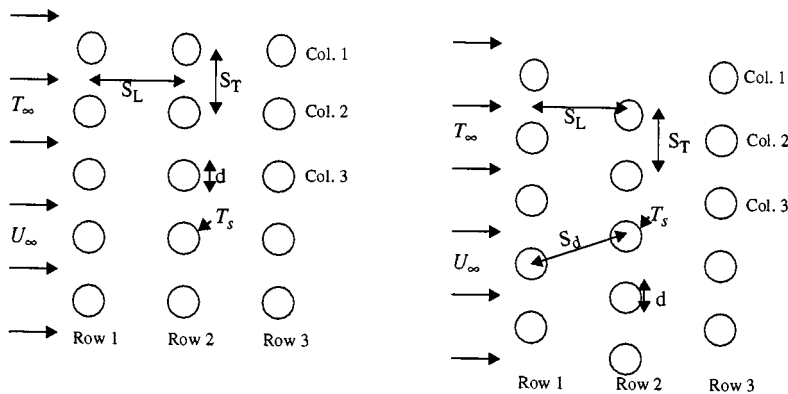From Jakob, 1949. With permission.

FIGURE 4.2.17 Two arrangements of tube banks. In-line or aligned arrangement on the left and staggered arrangement on the right. ($a = S_T/d$; $b = S_L/d$.)

TABLE 4.2.2   In-Line Arrangement — Values of Constants in Equation (4.2.72) ($p = 0$ in all cases)

Re_d	c	m	n
1–100	0.9	0.4	0.36
100–1000	0.52	0.5	0.36
10^3–2×10^5	0.27	0.63	0.36
$2 \times 10^5 - 2 \times 10^6$	0.033	0.8	0.4

TABLE 4.2.3   Staggered Arrangement — Values of Constants in Equation (4.2.72)

Re_d	c	p	m	n
1–500	1.04	0	0.4	0.36
500–1000	0.71	0	0.5	0.36
10^3–2×10^5	0.35	0.2	0.6	0.36
$2 \times 10^5 - 2 \times 10^6$	0.031	0.2	0.8	0.36

In computing Re_d, the maximum average velocity between tubes is used. The maximum velocities for the in-line and staggered arrangements are given by

$$\text{In-line:} \qquad U_{\max} = \frac{U_\infty S_T}{S_T - d} \tag{4.2.73}$$

$$\text{Staggered:} \qquad S_d > \frac{S_T + d}{2} \qquad U_{\max} = \frac{U_\infty S_T}{S_T - d} \tag{4.2.74}$$

$$\text{Staggered:} \qquad S_d < \frac{S_T + d}{2} \qquad U_{\max} = \frac{U_\infty S_T}{2(S_d - d)}$$

$$S_d = \left[S_L^2 + \left(\frac{S_T}{2} \right)^2 \right]^{1/2} \tag{4.2.75}$$

Equation (4.2.72) is for tube banks with 16 or more rows. When there are fewer than 16 rows, the heat transfer coefficient given by Equation (4.2.72) is multiplied by the correction factor c_1 defined by Equation (4.2.76) and given in Table 4.2.4.

$$\frac{h_N}{h_{16}} = c_1 \tag{4.2.76}$$

where

h_N = heat transfer coefficient with N rows (fewer than 16)
h_{16} = heat transfer coefficient with 16 or more rows

TABLE 4.2.4   Correction Factor c_1 to Be Used with Equation (4.2.76)

Tube Arrangement	Number of Rows (N)							
	1	2	3	4	5	7	10	13
In-line	0.70	0.80	0.86	0.90	0.93	0.96	0.98	0.99
Staggered	0.64	0.76	0.84	0.89	0.93	0.96	0.98	0.99

Pressure Drop: With tube banks, pressure drop is a significant factor, as it determines the fan power required to maintain the fluid flow. Zukauskas (1987) recommends that the pressure drop be computed from the relation

$$\Delta p = p_i - p_e = N\chi \frac{\rho U_{max}^2}{2} f \tag{4.2.77}$$

where p_i and p_e are the fluid pressures at inlet and exit of the tube banks. The values of χ and f are presented in Figure 4.2.18A. In Figure 4.2.18A the friction factor f for in-line arrangement is presented for different values of b (S_L/d) for $S_L = S_T$. For values of S_L/S_T other than 1, the correction factor χ is given in the inset for different values of $(a - 1)/(b - 1)$. Similarly, the friction factor for staggered arrangement (for equilateral triangle arrangement) and a correction factor for different values of a/b are also given in Figure 4.2.18b. The value of f is for one row of tubes; the total pressure drop is obtained by multiplying the pressure drop for one row by the number of rows, N.

The temperature of the fluid varies in the direction of flow, and, therefore, the value of the convective heat transfer coefficient (which depends on the temperature-dependent properties of the fluid) also varies in the direction of flow. However, it is common practice to compute the total heat transfer rate with the assumption of uniform convective heat transfer coefficient evaluated at the arithmetic mean of the inlet and exit temperatures of the fluid. With such an assumption of uniform convective heat transfer coefficient, uniform surface temperature and constant specific heat (evaluated at the mean fluid temperature), the inlet and exit fluid temperatures are related by

$$\ln\left(\frac{T_s - T_e}{T_s - T_i}\right) = -\frac{hA_s}{\dot{m}c_p} \tag{4.2.78}$$

The heat transfer rate to the fluid is related by the equation

$$q = \dot{m}c_p\left(T_i - T_e\right) \tag{4.2.79}$$

Example

A heat exchanger with aligned tubes is used to heat 40 kg/sec of atmospheric air from 10 to 50°C with the tube surfaces maintained at 100°C. Details of the heat exchanger are

Diameter of tubes	25 mm
Number of columns	20
Length of each tube	3 m
$S_L = S_T$	75 mm

Determine the number of rows required.

Solution: Average air temperature = $(T_i + T_e)/2 = 30°C$. Properties of atmospheric air (from Suryanarayana, 1995):

$$\rho = 1.165 \text{ kg/m}^3 \qquad c_p = 1007 \text{ J/kg K}$$

$$\mu = 1.865 \times 10^{-5} \text{ Nsec/m}^3 \quad k = 0.0264 \text{ W/mK}$$

$$\text{Pr} = 0.712 \qquad \text{Pr}_s(\text{at } 100°C) = 0.705$$
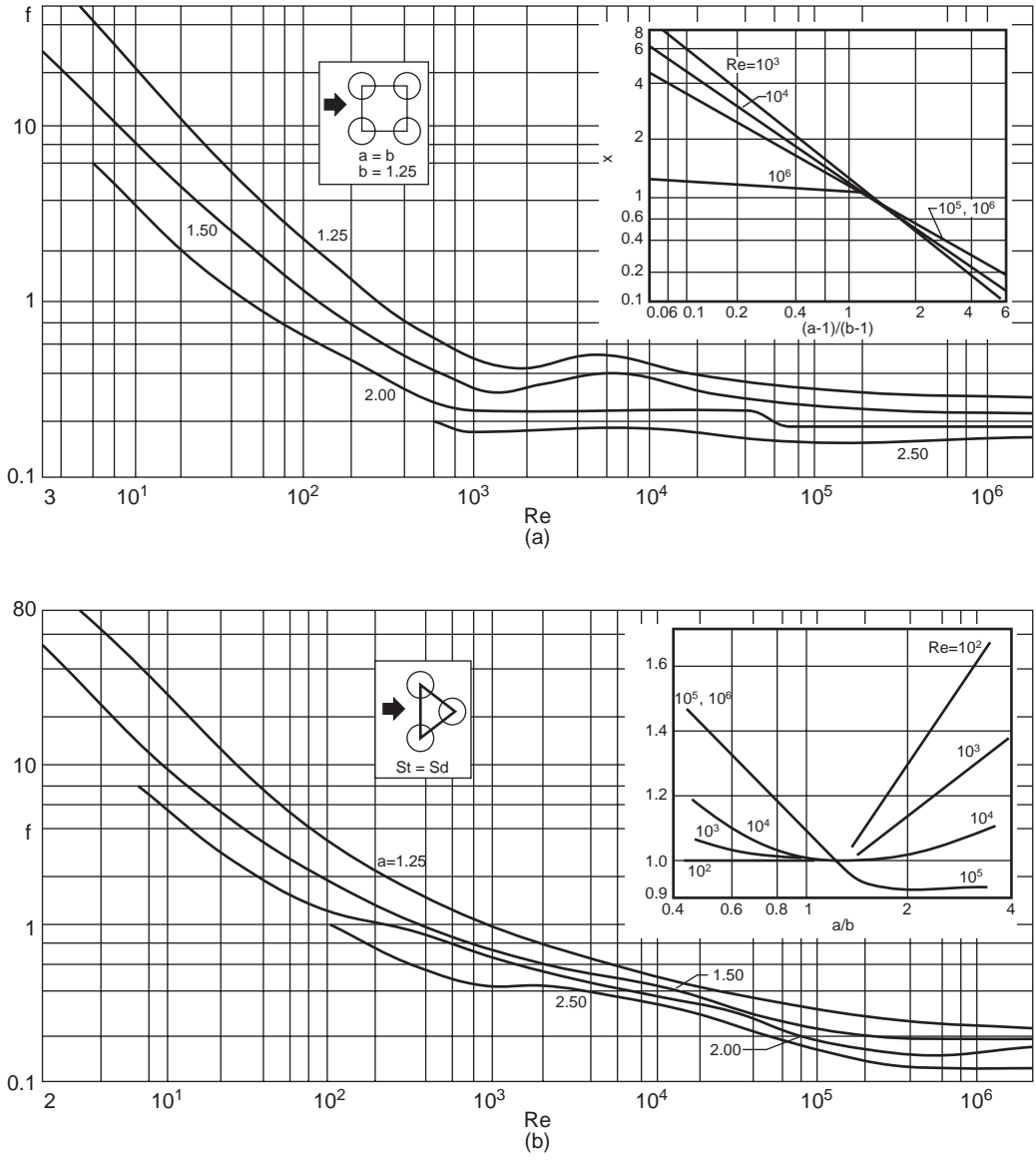
FIGURE 4.2.18 Friction factors for tube banks. (a) In-line arrangement; (b) Staggered arrangement.

To find U_{max} we need the minimum area of cross section for fluid flow (Figure 4.2.19).

$$H = 20 \times 0.075 = 1.5 \text{ m}$$

$$A_{min} = 20(0.075 - 0.025) \times 3 = 3 \text{ m}^2$$

$$U_{max} = \frac{\dot{m}}{\rho A_{min}} = \frac{40}{1.165 \times 3} = 11.44 \text{ m/sec}$$
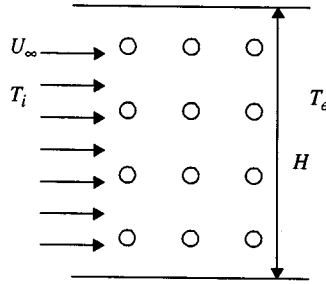
FIGURE 4.2.19 Aligned tube heat exchanger (only a few of the 20 columns and rows are shown).

$$\text{Re}_d = \frac{\rho U_{max} d}{\mu} = \frac{1.165 \times 11.44 \times 0.025}{1.865 \times 10^{-5}} = 17,865$$

With values from Table 4.2.2,

$$\text{Nu}_d = 0.27 \times 17,865^{0.63} \times 0.712^{0.36} \left(\frac{0.712}{0.705}\right)^{0.25} = 114.3$$

$$h = \frac{114.3 \times 0.0264}{0.025} = 120.7 \ \text{W/m}^2 \ \text{K}$$

From Equation 4.2.78,

$$\ln\left(\frac{100 - 50}{100 - 10}\right) = -\frac{120.7 \times A_s}{40 \times 1007} \qquad A_s = \pi \times 0.025 \times 3 \times 20 \times N$$

$$\underline{N = \text{number of rows} = 42}$$

Fan Power: From the first law of thermodynamics (see Chapter 2), the fan power is

$$\dot{W}_F = \dot{m}\left(\frac{p_i}{\rho_i} + \frac{p_e}{\rho_e} + \frac{\mathbf{v}_e^2}{2}\right)$$

p_i and p_e are the pressures at inlet and exit of the heat exchanger and $\mathbf{v}_e$ is the fluid velocity at exit. Assuming constant density evaluated at $(T_i + T_e)/2$ the pressure drop is found from Figure 4.2.18a.

$\text{Re}_p = 17,865$: $\qquad\qquad\qquad a = b = S_T/d = 75/25 = 3$

In Figure 4.2.18, although the friction factor is available for values of b up to 2.5, we will estimate the value of f for $b = 3$. From Figure 4.2.18, $f \approx 0.11$. The correction factor $c = 1$.

$$p_i - p_e = N\chi\frac{\rho U_{max}^2}{2} f = 42 \times 1\frac{1.165 \times 11.44^2}{2} \times 0.11 = 352.2 \ \text{kPa}$$

$$\mathbf{v}_e = \frac{11.44 \times 50}{75} = 7.63 \ \text{m/sec}$$

$$\dot{W}_F = 40\left(352.2 + \frac{7.63^2}{2}\right) = \underline{15,250 \text{ W}}$$

Heat Transfer with Jet Impingement

Jet impingement (Figure 4.2.20) on a heated (or cooled) surface results in high heat transfer rates, and is used in annealing of metals, tempering of glass, cooling of electronic equipment, internal combustion engines, and in a wide variety of industries — textiles, paper, wood, and so on. Usually, the jets are circular, issuing from a round nozzle of diameter *d*, or rectangular, issuing from a slot of width *w*. They may be used singly or in an array. The jets may impinge normally to the heated surface or at an angle. If there is no parallel solid surface close to the heated surface, the jet is said to be free; in the presence of a parallel surface close to the heated surface, the jet is termed confined. In this section only single, free jets (round or rectangular) impinging normally to the heated surface are considered.
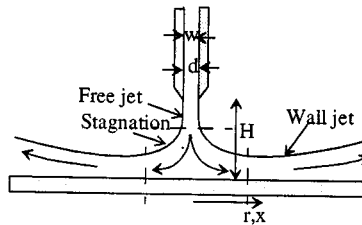

FIGURE 4.2.20 Circular jet of diameter *d* or a rectangular jet of width *w*.

Jets may be submerged with the fluid from the nozzle exiting into a body of a fluid (usually the same fluid), for example, air impinging on a surface surrounded by atmospheric air. In submerged jets entrained fluid (the part of the surrounding fluid dragged by the jet) has a significant effect on the flow and heat transfer characteristics of the jet, but the effect of gravity is usually negligible. In free-surface jets — a liquid jet in an atmosphere of air is a good approximation to a free-surface jet — the entrainment effect is usually negligible, but the effect of gravity may be significant.

A jet is usually divided into three regions, a free-jet region, a stagnation region, and a wall-jet region. In the free-jet region the effect of the target surface on the flow is negligible. In the stagnation region the target surface affects the flow field, and the velocity parallel to the surface increases while the velocity component normal to the surface decreases. At the beginning of the stagnation region, the axial velocity of the fluid is very much greater than the radial component (or the *x*-component) of the velocity. The stagnation region is followed by the wall-jet region where the radial component (or the *x*-component) of the velocity is much greater than the axial velocity.

The heat transfer coefficient is a function of *H/d* (or *H/w*), $\text{Re}_d(\rho v_j d/\mu)$ or $(\rho v_j 2w/\mu)$, and Pr and depends on the region (stagnation or wall jet), whether it is submerged or nonsubmerged and whether the flow adjacent to the plate is laminar or turbulent. Some of the heat transfer correlations suggested by different researchers are given below. All the correlations are for single jets.

Submerged Jets: Single Circular Jets

$$\text{Re}_d = \frac{4\dot{m}}{\pi d \mu} \qquad \text{Nu}_d = \frac{hd}{k} \qquad \dot{m} = \text{mass rate of flow of fluid}$$

Average heat transfer coefficients up to radius r (Martin, 1990):

$$\mathrm{Nu}_d = 2\frac{d}{r}\frac{1-1.1d/r}{1+0.1(H/d-6)d/r}\left[\mathrm{Re}_d\left(1+\frac{\mathrm{Re}_d^{0.55}}{200}\right)\right]^{1/2}\mathrm{Pr}^{0.42} \qquad (4.2.80)$$

Range of validity:

$$2000 \le \mathrm{Re}_d \le 400{,}000 \qquad 2.5 \le r/d \le 7.5 \qquad 2 \le H/d \le 12$$

Local convective heat transfer coefficient at radius r (Webb and Ma, 1995):

$$\mathrm{Nu}_d = 1.29\mathrm{Re}_d^{1/2}\mathrm{Pr}^{0.4}\left\{\left[\frac{\tanh(0.88r/d)}{r/d}\right]^{-8.5}+\left[1.69\left(\frac{r}{d}\right)^{-1.07}\right]^{-17}\right\}^{-1/17} \qquad (4.2.81)$$

Submerged Jets: Single Rectangular Jet

$$\mathrm{Re}_w = \frac{\rho\mathbf{v}_j 2w}{\mu} = \frac{2\dot{m}}{\mu} \qquad \dot{m} = \text{mass rate of flow per unit length of jet}$$

$$\mathrm{Nu}_w = \frac{h2w}{k}$$

Average heat transfer coefficient (Martin, 1990):

$$\mathrm{Nu}_w = \frac{1.53\mathrm{Pr}^{0.42}\mathrm{Re}_w^m}{\dfrac{x}{2w}+\dfrac{H}{2w}+1.39} \qquad (4.2.82)$$

$$m = 0.695 - \left[\frac{x}{2w}+\left(\frac{H}{2w}\right)^{1.33}+3.06\right]^{-1}$$

Free-Surface Jets: Single Circular Jet. Correlations are given in Table 4.2.5 (Liu et al., 1991 and Webb and Ma, 1995).

   For more information on jet impingement heat transfer, refer to Martin (1977) and Webb and Ma (1995) and the references in the two papers.

Bibliography

ASHRAE *Handbook of Fundamentals*, 1993. American Society of Heating, Ventilating and Air Conditioning Engineers, Atlanta, GA.

Hewitt, G.F., Ed. 1990. *Handbook of Heat Exchanger Design*, Hemisphere Publishing, New York.

Incropera, F.P. and Dewitt, D.P. 1990. *Fundamentals of Heat and Mass Transfer*, 3rd ed., John Wiley & Sons, New York.

Kakaç, S., Shah, R.K., and Win Aung, Eds. 1987. *Handbook of Single Phase Convective Heat Transfer*, Wiley-Interscience, New York.

Kreith, F. and Bohn, M.S. 1993. *Principles of Heat Transfer*, 5th ed., PWS, Boston.

Suryanarayana, N.V. 1995. *Engineering Heat Transfer*, PWS, Boston.

TABLE 4.2.5   Correlations for Free-Surface Jets $r_v/d = 0.1773\ \mathrm{Re}_d^{1/3}$

		$\mathbf{Nu}_d$	
	$0.15 \leq \mathrm{Pr} \leq 3$	$0.715\mathrm{Re}_d^{1/2}\mathrm{Pr}^{0.4}$	(4.2.83)
$r/d < 0.787$	$\mathrm{Pr} > 3$	$0.797\mathrm{Re}_d^{1/2}\mathrm{Pr}^{1/3}$	(4.2.84)
$0.787 < r/d < r_v/d$		$0.632\mathrm{Re}_d^{1/2}\mathrm{Pr}^{1/3}\left(\dfrac{d}{r}\right)^{1/2}$	(4.2.85)
$r_v/d < r/d < r_t/d$		$\dfrac{0.407\mathrm{Re}_d^{1/3}\mathrm{Pr}^{1/3}(d/r)^{2/3}}{\left[\dfrac{0.1713}{(r/d)^2}+\dfrac{5.147}{\mathrm{Re}_d}\dfrac{r}{d}\right]^{2/3}\left[\dfrac{(r/d)^2}{2}+C\right]^{1/3}}$	(4.2.86)

where

$$C = -5.051\times10^{-5}\,\mathrm{Re}_d^{2/3}$$

$$\frac{r_t}{d} = \left\{-\frac{s}{2}+\left[\left(\frac{s}{2}\right)^2+\left(\frac{p}{3}\right)^3\right]^{1/2}\right\}^{1/3}$$

$$+\left\{-\frac{s}{2}+\left[\left(\frac{s}{2}\right)^2-\left(\frac{p}{3}\right)^3\right]^{1/2}\right\}^{1/3}$$

$$p = \frac{-2C}{0.2058\mathrm{Pr}-1}\qquad s = \frac{0.00686\mathrm{Re}_d\mathrm{Pr}}{0.2058\mathrm{Pr}-1}$$

$r > r_t$	$\mathrm{Pr} < 4.86$	$\dfrac{0.25}{\dfrac{1}{\mathrm{Re}_d\mathrm{Pr}}\left[1-\left(\dfrac{r_t}{r}\right)^2\right]\left(\dfrac{r}{d}\right)^2+0.13\dfrac{h}{d}+0.0371\dfrac{h_t}{d}}$	(4.2.87)

where $h_t = h$ at r_t and

$$\frac{h}{d} = \frac{0.1713}{r/d}+\frac{5.147}{\mathrm{Re}_d}\left(\frac{r}{d}\right)^2$$

References

Achenbach, E. 1978. *Heat Transfer from Spheres up to Re = 6 × 10⁶*, in *Proc. 6th Int. Heat Transfer Conf.,* Vol. 5, Hemisphere Publishing, Washington, D.C.

Burmeister, L.C. 1993. *Convective Heat Transfer*, Wiley-Interscience, New York.

Churchill, S.W. 1976. A comprehensive correlation equation for forced convection from a flat plate, *AIChE J*. 22(2), 264.

Churchill, S.W. and Bernstein, M. 1977. A correlating equation for forced convection from gases and liquids to a circular cylinder in cross flow, *J. Heat Transfer,* 99, 300.

Churchill, S.W. and Ozoe, H. 1973. Correlations for laminar forced convection with uniform heating in flow over a plate and in developing and fully developed flow in a tube, *J. Heat Transfer,* 18, 78.

Eckert, E.R.G. 1956. Engineering relations for heat transfer and friction in high-velocity laminar and turbulent boundary-layer flow over surfaces with constant pressure and temperature, *Trans. ASME*, 56, 1273.

Eckert, E.R.G. and Drake, M., Jr. 1972. *Analysis of Heat and Mass Transfer*, McGraw-Hill, New York.

Ishiguro, R., Sugiyama, K., and Kumada, T. 1979. Heat transfer around a circular cylinder in a liquid-sodium cross flow, *Int. J. Heat Mass Transfer*, 22, 1041.

Jakob, H., 1949. *Heat Transfer*, John Wiley and Sons, London.

Kays, W.M. and Crawford, M.E. 1993. *Convective Heat and Mass Transfer*, 3rd ed., McGraw-Hill, New York.

Liu, X., Lienhard, v., J.H., and Lombara, J.S. 1991. Convective heat transfer by impingement of circular liquid jets, *J. Heat Transfer*, 113, 571.

Martin, H. 1977. Heat and mass transfer between imping gas jets and solid surfaces, in *Advances in Heat Transfer*, Hartnett, J.P. and Irvine, T.F., Eds., 13, 1, Academic Press, New York.

Martin, H. 1990. Impinging jets, in *Handbook of Heat Exchanger Design*, Hewitt, G.F., Ed., Hemisphere, New York.

Morgan, Vincent T., 1975. The overall convective heat transfer from smooth circular cylinders, in *Advances in Heat Transfer*, Irvine, T.F. and Hartnett, J.P., Eds., 11, 199, Academic Press, New York.

Rose, J.W. 1979. Boundary layer flow on a flat plate, *Int. J. Heat Mass Transfer*, 22, 969.

Schlichting, H. 1979. *Boundary Layer Theory*, 7th ed., McGraw-Hill, New York.

Suryanarayana, N.V. 1995. *Engineering Heat Transfer*, West Publishing, Minneapolis.

Thomas, W.C. 1977. Note on the heat transfer equation for forced-convection flow over a flat plate with an unheated starting length, *Mech. Eng. News* (*ASEE*), 9(1), 19.

Webb, B.W. and Ma, C.F. 1995. Single-phase liquid jet impingement heat transfer, in *Advances in Heat Transfer*, Hartnett, J.P. and Irvine, T.F., Eds., 26, 105, Academic Press, New York.

Witte, L.C. 1968. An experimental study of forced-convection heat transfer from a sphere to liquid sodium, *J. Heat Transfer*, 90, 9.

Zukauskas, A. 1987. Convective heat transfer in cross flow, in *Handbook of Single-Phase Convective Heat Transfer*, Kakaç, S., Shah, R.K., and Win Aung, Eds., Wiley-Interscience, New York.

Forced Convection — Internal Flows

N.V. Suryanarayana

Introduction

Heat transfer to (or from) a fluid flowing inside a tube or duct is termed *internal forced convection*. The fluid flow may be laminar or turbulent. If the Reynolds number based on the average velocity of the fluid and diameter of the tube ($\rho v d/\mu$) is less than 2100 (Reynolds numbers in the range of 2000 to 2300 are cited in different sources), the flow is laminar. If the Reynolds number is greater than 10,000, the flow is turbulent. The flow with a Reynolds number in the range 2100 to 10,000 is considered to be in the transitional regime. With heating or cooling of the fluid, there may or may not be a change in the phase of the fluid. Here, only heat transfer to or from a single-phase fluid is considered.

Fully Developed Velocity and Temperature Profiles. When a fluid enters a tube from a large reservoir, the velocity profile at the entrance is almost uniform as shown in Figure 4.2.21. The fluid in the immediate vicinity of the tube surface is decelerated and the velocity increases from zero at the surface to u_c at a distance δ from the surface; in the region $r = 0$ to $(R - \delta)$ the velocity is uniform. The value of δ increases in the direction of flow and with constant fluid density the value of the uniform velocity u_c increases. At some location downstream, δ reaches its maximum possible value, equal to the radius of the tube, and from that point onward the velocity profile does not change.

The region where δ increases, i.e., where the velocity profile changes, is known as the entrance region or hydrodynamically developing region. The region downstream from the axial location where δ reaches its maximum value and where the velocity profile does not change is the fully developed velocity profile or hydrodynamically fully developed region. Similarly, downstream of the location where heating or cooling of the fluid starts, the temperature profile changes in the direction of flow. But beyond a certain distance the dimensionless temperature profile does not change in the direction of flow. The region where the dimensionless temperature profile changes is the thermally developing region or the thermal entrance region, and the region where the dimensionless temperature profile does not change is the thermally
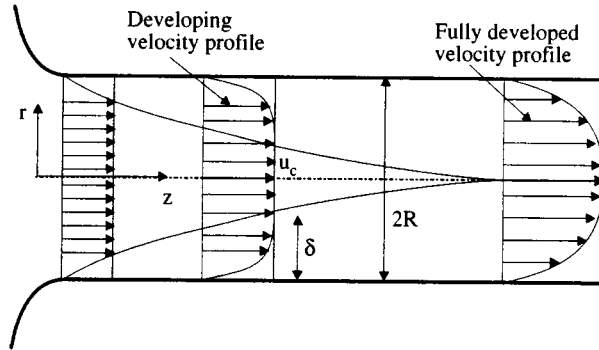
FIGURE 4.2.21 Developing and fully developed velocity profiles.

fully developed region. For simultaneously developing velocity and temperature profiles in laminar flows, the hydrodynamic and thermal entrance lengths are given by

$$\frac{L_e}{d} = 0.0565 \mathrm{Re}_d \tag{4.2.88}$$

$$\frac{L_{e,th}}{d} = 0.053 \mathrm{Re}_d \mathrm{Pr} \qquad \text{Uniform heat flux} \tag{4.2.89}$$

$$\frac{L_{e,th}}{d} = 0.037 \mathrm{RePr} \qquad \text{Uniform surface temperature} \tag{4.2.90}$$

In most engineering applications, with turbulent flows, correlations for fully developed conditions can be used after about 10 diameters from where the heating starts.

Convective Heat Transfer Coefficient and Bulk Temperature. The reference temperature for defining the convective heat transfer coefficient is the bulk temperature T_b and the convective heat flux is given by

$$q'' = h\left(T_s - T_b\right) \tag{4.2.91}$$

The bulk temperature T_b is determined from the relation

$$T_b = \frac{\displaystyle\int_{A_c} \rho v C_p T dA_c}{\displaystyle\int_{A_c} \rho v C_p dA_c} \tag{4.2.92}$$

where A_c is the cross-sectional area perpendicular to the axis of the tube.

If the fluid is drained from the tube at a particular axial location and mixed, the temperature of the mixed fluid is the bulk temperature. It is also know as the mixing cup temperature. With heating or cooling of the fluid the bulk temperature varies in the direction of flow. In some cases we use the term *mean fluid temperature*, T_m, to represent the arithmetic mean of the fluid bulk temperatures at inlet and exit of the tube.

Heat Transfer Correlations

Laminar Flows — Entrance Region. For laminar flows in a tube with uniform surface temperature, in the entrance region the correlation of Sieder and Tate (1936) is

$$\overline{\mathrm{Nu}_d} = 1.86 \left(\frac{\mathrm{Re}_d \mathrm{Pr}}{L/d} \right)^{1/3} \left(\frac{\mu}{\mu_s} \right)^{0.14}$$
(4.2.93)

valid for

$$\frac{L}{d} < \frac{\mathrm{Re}_d \mathrm{Pr}}{8} \left(\frac{\mu}{\mu_s} \right)^{0.42} \qquad 0.48 < \mathrm{Pr} < 16{,}700 \qquad 0.0044 < \frac{\mu}{\mu_s} < 9.75$$

The overbar in the Nusselt number indicates that it is formed with the average heat transfer coefficient over the entire length of the tube. Properties of the fluid are evaluated at the arithmetic mean of the inlet and exit bulk temperatures. In Equation (4.2.93) the heat transfer coefficient was determined from

$$q = \bar{h} \pi dL \left(T_s - \frac{T_{bi} + T_{be}}{2} \right)$$
(4.2.94)

Therefore, to find the total heat transfer rate with $\bar{h}$ from Equation (4.2.93) employ Equation (4.2.94).

Laminar Flows — Fully Developed Velocity and Temperature Profiles. Evaluate properties at the bulk temperature

      Uniform Surface Temperature $\mathrm{Nu}_d = 3.66$ (4.2.95)

      Uniform Surface Heat Flux $\mathrm{Nu}_d = 4.36$ (4.2.96)

Turbulent Flows. If the flow is turbulent, the difference between the correlations with uniform surface temperature and uniform surface heat flux is not significant and the correlations can be used for both cases. For turbulent flows, Gnielinsky (1976, 1990) recommends:
Evaluate properties at the bulk temperature.

$$0.6 < \mathrm{Pr} < 2000 \qquad 2300 < \mathrm{Re}_d < 10^6 \qquad 0 < d/L < 1$$

$$\mathrm{Nu}_d = \frac{(f/2)(\mathrm{Re}_d - 1000)\mathrm{Pr}}{1 + 12.7(f/2)^{1/2}\left(\mathrm{Pr}^{2/3} - 1\right)} \left[1 + \left(\frac{d}{L} \right)^{2/3} \right]$$
(4.2.97)

$$f = \left[1.58\ln(\mathrm{Re}_d) - 3.28 \right]^{-2}$$
(4.2.98)

f = friction factor = $2\tau_w/\rho v^2$.

To reflect the effect of variation of fluid properties with temperature, multiply the Nusselt numbers in Equation (4.2.97) by $(T_b/T_s)^{0.45}$ for gases and $(\mathrm{Pr}/\mathrm{Pr}_s)^{0.11}$ for liquids where the temperatures are absolute, and T and Pr with a subscript s are to be evaluated at the surface temperature. The equations can be used to evaluate the heat transfer coefficient in the developing profile region. To determine the heat

transfer coefficient in the fully developed region set $d/L = 0$. A simpler correlation (fully developed region) is the Dittus–Boelter (1930) equation. Evaluate properties at T_b.

$$0.7 \leq \text{Pr} \leq 160 \qquad \text{Re}_d > 10{,}000 \qquad d/L > 10$$

$$\text{Nu}_d = 0.023 \text{Re}_d^{4/5} \text{Pr}^n \tag{4.2.99}$$

where $n = 0.4$ for heating ($T_s > T_b$) and $n = 0.3$ for cooling ($T_s < T_b$).

For liquid metals with $\text{Pr} \ll 1$ the correlations due to Sleicher and Rouse (1976) are
Uniform surface temperature:

$$\text{Nu}_{d,b} = 4.8 + 0.0156 \text{Re}_{d,f}^{0.85} \text{Pr}_s^{0.93} \tag{4.2.100}$$

Uniform heat flux:

$$\text{Nu}_{d,b} = 6.3 + 0.0167 \text{Re}_{d,f}^{0.85} \text{Pr}_s^{0.93} \tag{4.2.101}$$

Subscripts b, f, and s indicate that the variables are to be evaluated at the bulk temperature, film temperature (arithmetic mean of the bulk and surface temperatures), and surface temperature, respectively.

In the computations of the Nusselt number the properties (evaluated at the bulk temperature) vary in the direction of flow and hence give different values of h at different locations. In many cases a representative average value of the convective heat transfer coefficient is needed. Such an average value can be obtained either by taking the arithmetic average of the convective heat transfer coefficients evaluated at the inlet and exit bulk temperatures or the convective heat transfer coefficient evaluated at the arithmetic mean of the inlet and exit bulk temperatures. If the variation of the convective heat transfer coefficient is large, it may be appropriate to divide the tube into shorter lengths with smaller variation in the bulk temperatures and evaluating the average heat transfer coefficient in each section.

Uniform Surface Temperature — Relation between the Convective Heat Transfer Coefficient and the Total Heat Transfer Rate: With a uniform surface temperature, employing an average value of the convective heat transfer coefficient the local convective heat flux varies in the direction of flow. To relate the convective heat transfer coefficient to the temperatures and the surface area, we have, for the elemental length Δz (Figure 4.2.22).

$$\dot{m} C_p \frac{dT_b}{dz} = h \frac{dA_s}{dz} \left(T_s - T_b \right) \tag{4.2.102}$$
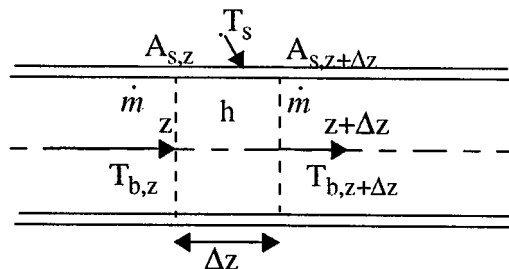

FIGURE 4.2.22 Elemental length of a tube for determining heat transfer rate.

Assuming a suitable average convective heat transfer coefficient over the entire length of the tube, separating the variables, and integrating the equation from $z = 0$ to $z = L$, we obtain

$$\ln\frac{T_s - T_{be}}{T_s - T_{bi}} = -\frac{hA_s}{\dot{m}C_p} \qquad (4.2.103)$$

Equation (4.2.103) gives the exit temperature. For a constant-density fluid or an ideal gas, the heat transfer rate is determined from

$$q = \dot{m}C_p\left(T_{be} - T_{bi}\right) \qquad (4.2.104)$$

Equation (4.2.103) was derived on the basis of uniform convective heat transfer coefficient. However, if the functional relationship between h and T_b is known, Equation (4.2.102) can be integrated by substituting the relationship. The convective heat transfer coefficient variation with T_b for water in two tubes of different diameters for two different flow rates is shown in Figure 4.2.23. From the figure it is clear that h can be very well approximated as a linear function of T. By substituting such a linear function relationship into Equation (4.2.102), it can be shown that

$$\ln\frac{h_i}{h_e}\frac{T_s - T_{be}}{T_s - T_{bi}} = -\frac{h_s A_s}{\dot{m}C_p} \qquad (4.2.105)$$

where h_i, h_e, and h_s are the values of the convective heat transfer coefficient evaluated at bulk temperatures of T_{bi}, T_{be}, and T_s, respectively. Although it has been demonstrated that h varies approximately linearly with the bulk temperature with water as the fluid, the variation of h with air and oil as the fluid is much smaller and is very well approximated by a linear relationship. For other fluids it is suggested that the relationship be verified before employing Equation (4.2.105). [**Note:** It is tempting to determine the heat transfer rate from the relation

$$q = hA_s\frac{\left(T_s - T_{be}\right) + \left(T_s - T_{bi}\right)}{2}$$

Replacing q by Equation (4.2.104) and solving for T_{be} for defined values of the mass flow rate and tube surface area, the second law of thermodynamics will be violated if $hA_s/\dot{m}C_p > 2$. Use of Equation (4.2.103) or (4.2.105) ensures that no violation of the second law occurs however large A_s is.]

Uniform Surface Heat Flux: If the imposed heat flux is known, the total heat transfer rate for a defined length of the tube is also known. From Equation (4.2.104) the exit temperature of the fluid is determined. The fluid temperature at any location in the pipe is known from the heat transfer rate up to that location ($q = q''A_s$) and Equation (4.2.104). The convective heat transfer coefficient is used to find the surface temperature of the tube.

Temperature Variation of the Fluid with Uniform Surface Temperature and Uniform Heat Flux: The fluid temperature variations in the two cases are different. With the assumption of uniform heat transfer coefficient, with a uniform surface temperature the heat flux decreases in the direction of flow leading to a progressively decreasing rate of temperature change in the fluid with axial distance. With uniform heat flux, the surface and fluid temperatures vary linearly except in the entrance region where the higher heat transfer coefficient leads to a smaller difference between the surface and fluid temperatures. The variation of the fluid temperature in the two cases is shown in Figure 4.2.24.

Convective Heat Transfer in Noncircular Tubes

Laminar Flows: The Nusselt numbers for laminar flows have been analytically determined for different noncircular ducts. Some of them can be found in Kakac et al. (1987), Kays and Crawford (1993), and
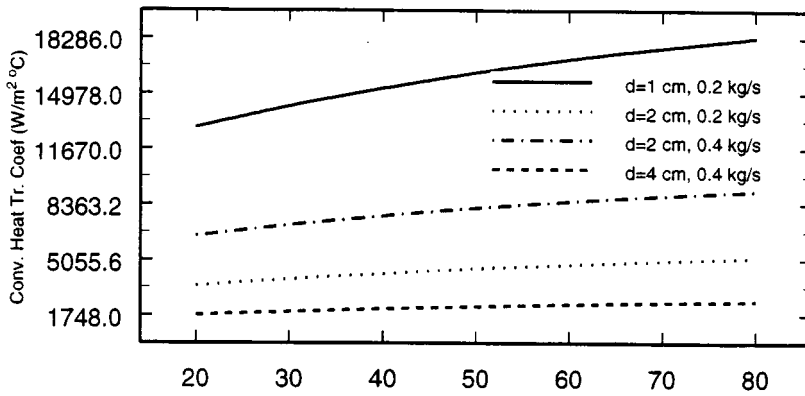
FIGURE 4.2.23 Variation of h with T_b in 1-, 2-, and 4-cm-diameter tubes with water flow rates of 0.2 kg/sec and 0.4 kg/sec with uniform surface temperature.
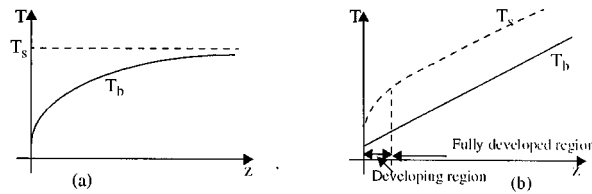

FIGURE 4.2.24 Variation of fluid temperature in a tube with (a) uniform surface temperature and (b) uniform heat flux.

Burmeister (1993). A few of the results are given below. The characteristic length for forming the Reynolds number and Nusselt number is the hydraulic mean diameter defined as

$$d_h = \frac{4 \text{ cross-sectional area}}{\text{wetted perimeter}}$$

Infinite parallel plates: a = spacing between plates, $d_h = 2a$

  Both plates maintained at uniform and equal temperatures: Nu = 7.54
  Both plates with imposed uniform and equal heat fluxes: Nu = 8.24

Rectangular ducts: a = longer side, b = shorter side, $d_h = 2ab/(a + b)$

b/a	1	0.7	0.5	0.25	0.125
Uniform surface temperature	2.98	3.08	3.39	4.44	5.6
Uniform heat flux[*]	3.61	3.73	4.12	5.33	6.49

Equilateral triangle: $d_h = a/3^{1/2}$, a = length of each side

  Uniform surface temperature: Nu = 2.35
  Uniform surface heat flux:[*] Nu = 3.0

Coaxial tubes: With coaxial tubes many different cases arise — each tube maintained at uniform but different temperatures, each tube subjected to uniform but different heat fluxes (an insulated

---

[*] Uniform axial heat flux but circumferentially uniform surface temperature.

surface is a special case of imposed heat flux being zero), or a combinations of uniform surface temperature of one tube and heat flux on the other. The manner in which the heat transfer coefficient is determined for uniform but different heat fluxes on the two tubes is described below. Define:

$$d_h = 2(r_o - r_i) \qquad r^* = r_i/r_o$$

$$q_i'' = h_i(T_i - T_b) \qquad \mathrm{Nu}_i = \frac{h_i d_h}{k} \qquad q_o'' = h_o(T_o - T_b) \qquad \mathrm{Nu}_o = \frac{h_o d_h}{k}$$

$$q_o'' = 0 \qquad \mathrm{Nu}_{ii} = \frac{h_i d_h}{k} \quad \text{and} \quad q_i'' = 0 \qquad \mathrm{Nu}_{oo} = \frac{h_o d_h}{k}$$

Then

$$\mathrm{Nu}_i = \frac{\mathrm{Nu}_{ii}}{1 - \dfrac{q_o''}{q_i''}\theta_i^*} \quad \text{and} \quad \mathrm{Nu}_o = \frac{\mathrm{Nu}_{oo}}{1 - \dfrac{q_i''}{q_o''}\theta_o^*} \qquad (4.2.106)$$

TABLE 4.2.6   Values for Use with Equation (4.2.106)

r^*	Nu_{ii}	Nu_{oo}	θ_i^*	θ_o^*
0.05	17.81	4.792	2.18	0.0294
0.1	11.91	4.834	1.383	0.0562
0.2	8.499	4.883	0.905	0.1041
0.4	6.583	4.979	0.603	0.1823
0.6	5.912	5.099	0.473	0.2455
0.8	5.58	5.24	0.401	0.299
1.0	5.385	5.385	0.346	0.346

Some of the values needed for the computations of Nu_i and Nu_o (taken from Kays and Crawford, 1993) are given in the Table 4.2.6.

For a more detailed information on heat transfer and friction factors for laminar flows in noncircular tubes refer to Kakac et al. (1987).

Turbulent Flows: For noncircular tubes, estimates of the convective heat transfer coefficient can be obtained by employing equations for circular tubes with d_h replacing d in the computations of the Reynolds and Nusselt numbers. To determine the heat transfer coefficients in developing regions and for more-accurate values with turbulent flows in noncircular tubes refer to Kakac et al. (1987) and the references in that book.

Mixed Convection

If the fluid velocity is low, the effect of natural convection becomes significant and the heat transfer rate may be increased or decreased by natural convection. From a review of experimental results, Metais and Eckert (1964) developed maps to delineate the different regimes where one or the other mode is dominant and where both are significant. Figures 4.2.25 and 4.2.26 show the relative significance of natural and forced convection in vertical and horizontal tubes. The maps are applicable for $10^{-2} < \mathrm{Pr}(d/L) < 1$ where d and L are the diameter and the axial length of the tube. The maps show the limits of forced and natural convection regimes. The limits are delineated "in such a way that the actual heat flux under the combined influence of the forces does not deviate by more than 10 percent from the heat flux that
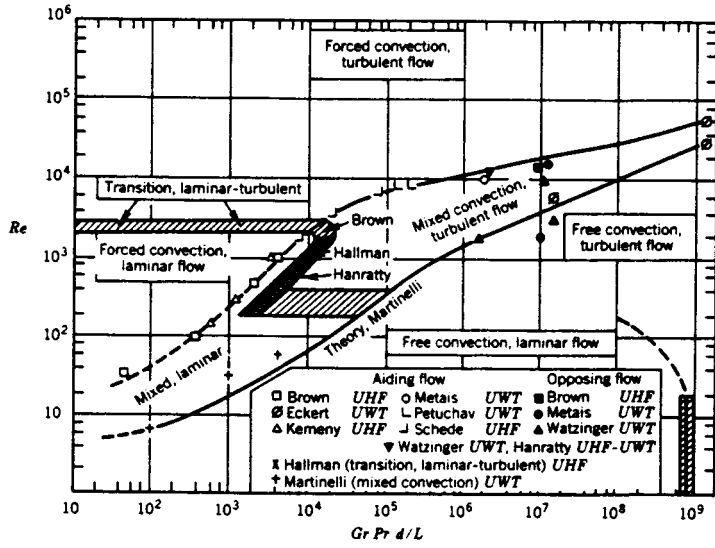
FIGURE 4.2.25 Map delineating forced, mixed, and natural convection — vertical tubes.
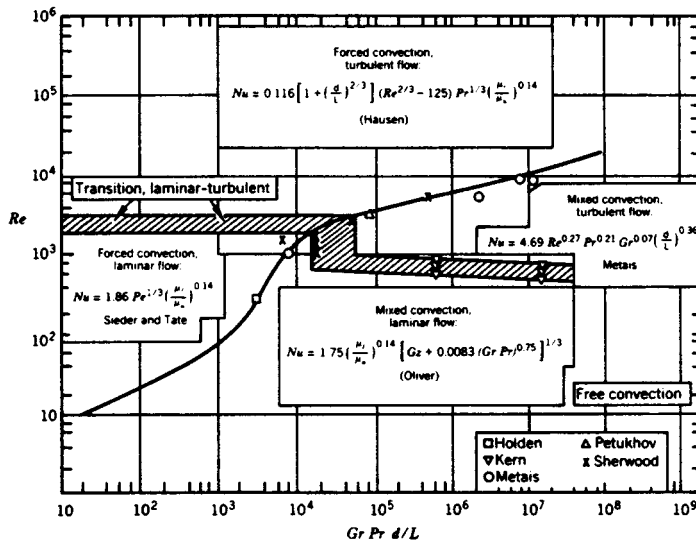
FIGURE 4.2.26 Map delineating forced, mixed, and natural convection — horizontal tubes.

would be caused by the external forces alone or by the body forces alone." The Grashof number is based on the diameter of the tube.

For flows in horizontal tubes, correlations were developed for the mixed convection regime in isothermal tubes by Depew and August (1971) and for uniform heat flux by Morcos and Bergles (1975).

Uniform Surface Temperature. Fully developed velocity profile, developing temperature profile:

$L/d < 28.4$ $25 < Gz < 712$ $0.7 \times 10^5 < Gr < 9.9 \times 10^5$

μ_s = dynamic viscosity, evaluated at the wall temperature

All other properties at the average bulk temperature of the fluid

$$\text{Gz} = \frac{\dot{m}C_p}{kL} \qquad \text{Gr} = g\beta\Delta T \, d^3 / \nu^2$$

$$\text{Nu}_d = 1.75\Big[\text{Gz} + 0.12\big(\text{GzGr}^{1/3}\text{Pr}^{0.36}\big)^{0.88}\Big]^{1/3}\big(\mu_b/\mu_s\big)^{0.14} \tag{4.2.107}$$

Uniform Heat Flux. Properties at $(T_{s+}T_b)/2$: $3 \times 10^4 < \text{Ra} < 10^6$, $4 < \text{Pr} < 175$, $2 < hd^2/(k_w t) < 66$, $k_w =$ tube wall thermal conductivity, $t =$ tube wall thickness.

$$\text{Gr}_d^* = g\beta d^4 \, q_w'' / \big(\nu^2 k\big) \qquad P_w = kd/\big(k_w t\big) \qquad \text{Ra}_d = g\beta\Delta T \, d^3\text{Pr}/\nu^2$$

$$\text{Nu}_d = \left\{ 4.36^2 + \left[0.145\left(\frac{\text{Gr}_d^*\text{Pr}^{1.35}}{P_w^{0.25}} \right)^{0.265} \right]^2 \right\}^{0.5} \tag{4.2.108}$$

In Equation (4.2.107) and (4.2.108) evaluate fluid properties at the arithmetic mean of the bulk and wall temperatures.

Nomenclature

A_s — surface area
d — diameter
d_h — hydraulic mean diameter
f — friction factor
h — convective heat transfer coefficient
k — fluid thermal conductivity
L_e — hydrodynamic entrance length
$L_{e,th}$ — thermal entrance length
Nu_d — Nusselt number
Nu_{ii} — Nusselt number with only inner tube heated
Nu_{oo} — Nusselt number with only outer tube heated
Pr — Prandtl number
q'' — heat flux
q_i'' — heat flux on the inner tube surface
q_o'' — heat flux on the outer tube surface
Re_d — Reynolds number ($\rho vd/\mu$)
T_b — bulk temperature
T_s — surface temperature
v — average fluid velocity
μ — dynamic viscosity
μ_s — dynamic viscosity at surface temperature
ρ — fluid density

References

Burmeister, L.C. 1993. *Convective Heat Transfer*, 2nd ed., Wiley-Interscience, New York.

Depew, C.A. and August, S.E. 1971. Heat transfer due to combined free and forced convection in a horizontal and isothermal tube, *Trans. ASME* 93C, 380.

Dittus, F.W. and Boelter, L.M.K. 1930. Heat transfer in automobile radiators of the tubular type, *Univ. Calif. Pub. Eng.,* 13, 443.

Gnielinsky, V. 1976. New equations for heat and mass transfer in turbulent pipe channel flow, *Int. Chem. Eng.,* 16, 359.

Gnielinsky, V. 1990. Forced convection in ducts, in *Handbook of Heat Exchanger Design*, Hewitt, G.F., Ed., Begell House/Hemisphere, New York.

Kakac, S., Shah, R.K., and Win Aung, Eds. 1987. *Handbook of Single-Phase Convective Heat Transfer*, Wiley-Interscience, New York.

Kays, W.M. and Crawford, M.E. 1993. *Convective Heat and Mass Transfer*, 3rd ed., McGraw-Hill, New York.

Metais, B. and Eckert, E.R.G. 1964. Forced, mixed, and free convection regimes, *Trans. ASME* 86C, 295.

Morcos, S.M. and Bergles, A.E. 1975. Experimental investigation of combined forced and free laminar convection in a horizontal tube, *Trans. ASME* 97C, 212.

Sieder, E.N. and Tate, C.E. 1936. Heat transfer and pressure drop of liquids in tubes, *Ind. Eng. Chem.,* 28, 1429.

Sleicher, C.A. and Rouse, M.W. 1976. A convenient correlation for heat transfer to constant and variable property fluids in turbulent pipe flow, *Int. J. Heat Mass Transfer,* 18, 677.

4.3   Radiation[*]

Michael F. Modest

Nature of Thermal Radiation

All materials continuously emit and absorb radiative energy by lowering or raising their molecular energy levels. This thermal radiative energy may be viewed as consisting of electromagnetic waves or of massless energy parcels, called **photons**. Electromagnetic waves travel through any medium at the speed of light c, which is $c_0 = 2.998 \times 10^8$ m/sec in vacuum and approximately the same in most gases such as air and combustion products. These are characterized by their wavelength λ or frequency ν, which are related by

$$\nu = c/\lambda \tag{4.3.1}$$

The strength and wavelengths of **emission** and **absorption** depend on the temperature and nature of the material.

   The ability of photons to travel unimpeded through vacuum and gases makes thermal radiation the dominant mode of heat transfer in vacuum, low-pressure environments, and outer space applications (due to the near absence of conduction and convection). Its temperature dependence [as given by Equation (4.3.3) below] on the other hand, guarantees that radiative heat transfer is of utmost importance in high-temperature applications (including solar radiation: with the sun being a high-temperature heat source at an effective temperature of $T_{sun} = 5762$ K).

   When an electromagnetic wave traveling through a gas (or vacuum) strikes the surface of a medium, the wave may be partly or totally reflected, and any nonreflected part will penetrate into the medium. If a wave passes through a medium without any attenuation, the material is called **transparent**. A body with partial attenuation is known as **semitransparent**, and a body through which none of the incoming radiation penetrates is called **opaque**. Most gases are rather transparent to radiation (except for narrow spectral regions, called *absorption bands*), while most solids tend to be strong absorbers for most wavelengths, making them opaque over a distance of a few nanometers (electrical conductors, i.e., metals) to a few micrometers (ceramics, semiconductors), or more (dielectrics).

Blackbody Radiation

The total amount of radiative energy emitted from a surface into all directions above it is termed **emissive power**; we distinguish between **spectral** (at a given wavelength λ, per unit wavelength) and total (encompassing all wavelengths) emissive power. The magnitude of emissive power depends on wavelength λ, temperature T, and a surface property, called **emissivity** ε, which relates the ability of a surface to emit radiative energy to that of an ideal surface, which emits the maximum possible energy (at a given wavelength and temperature). Such an ideal surface is known as a "**blackbody**" or "black surface," since it absorbs all incoming radiation; i.e., it reflects no radiation and is, therefore, invisible ("black") to the human eye. The spectral distribution of the emissive power of a black surface is given by **Planck's law**.

$$E_{b\lambda} = \frac{C_1}{\lambda^5 \left[e^{C_2/\lambda T} - 1 \right]}, \qquad C_1 = 3.7419 \times 10^{-16}\ \text{Wm}^2, \qquad C_2 = 14{,}388\ \mu\text{mK} \tag{4.3.2}$$

where C_1 and C_2 are sometimes called Planck function constants. The total emissive power of a blackbody is given by

---

[*]From Modest, M., *Radiative Heat Transfer*, 1993; reproduced with permission of MacGraw-Hill, Inc.

$$E_b = \int_0^\infty E_{b\lambda} \ d\lambda = \sigma T^4, \qquad \sigma = 5.670 \times 10^{-8} \ \text{W/m}^2\text{K}^4 \tag{4.3.3}$$

with σ known as the Stefan–Boltzmann constant. Figure 4.3.1 shows the spectral solar irradiation that impinges on Earth, which closely resembles the spectrum of a blackbody at 5762 K. The general behavior of Planck's law is depicted in Figure 4.3.2, together with the fractional emissive power, $f(\lambda T)$, defined as

$$f(\lambda T) = \frac{1}{E_b} \int_0^\lambda E_{b\lambda}(\lambda, T) \ d\lambda \tag{4.3.4}$$
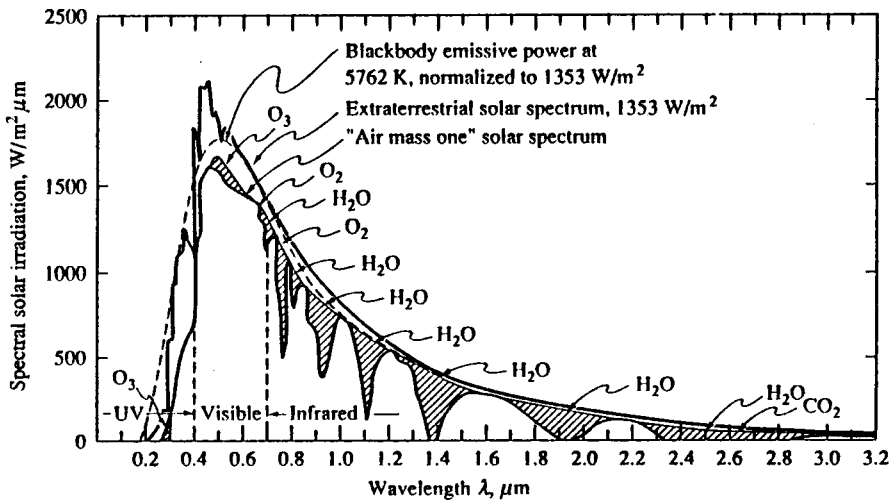

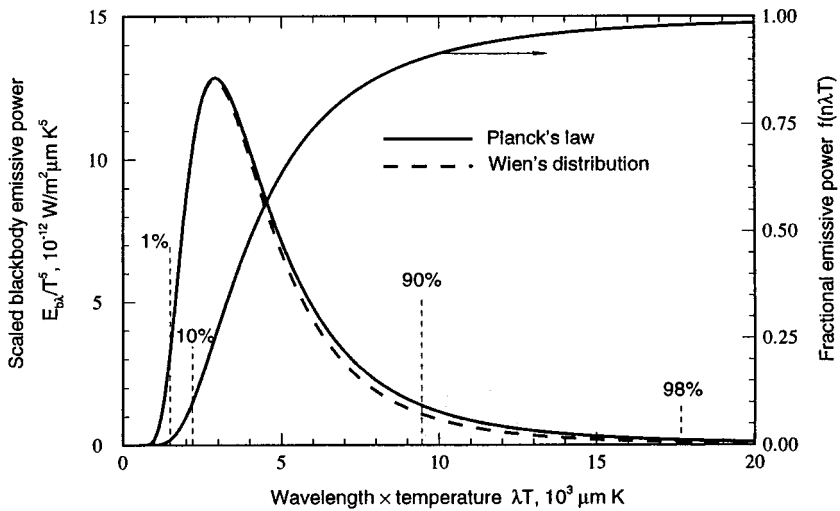**FIGURE 4.3.1** Solar irradiation onto Earth.

FIGURE 4.3.2 Normalized blackbody emissive power spectrum.

Note that 90% of all blackbody emission takes place at wavelengths of $\lambda T > 2200$ µmK and at all wavelengths $\lambda T < 9400$ µmK. This implies that — for typical high-temperature heat transfer applications in the range between 1000 and 2000 K — infrared wavelengths in the range $1 \text{ µm} < \lambda < 10 \text{ µm}$ govern the heat transfer rates. For solar applications shorter wavelengths, down to $\lambda \cong 0.4$ µm are also important. Also shown in Figure 4.3.2 is Wien's law:

$$E_{b\lambda} = \frac{C_1}{\lambda^5} e^{-C_2/\lambda T}$$

(4.3.5)

which approximates Planck's law accurately over the part of the spectrum that is important to heat transfer, and that is easier to manipulate mathematically.

Example 4.3.1

What fraction of total solar emission falls into the visible spectrum (0.4 to 0.7 µm)?

Solution: With a solar temperature of 5762 K it follows that for

$$\lambda_1 = 0.4 \text{ µm}, \qquad \lambda_1 T_{sun} = 0.4 \times 5762 = 2304 \text{ µmK}$$

and for

$$\lambda_2 = 0.7 \text{ µm}, \qquad \lambda_2 T_{sun} = 0.7 \times 5762 = 4033 \text{ µmK}$$

From Figure 4.3.2 we can estimate $f(\lambda_1 T_{sun}) \cong 12\%$ and $f(\lambda_2 T_{sun}) \cong 48\%$. Thus, the visible fraction of sunlight is $48 - 12 \cong 36\%$: with a bandwidth of only 0.3 µm the human eye responds to approximately 36% of all emitted sunlight!

Radiative Exchange between Opaque Surfaces

Radiative Properties of Surfaces

Strictly speaking, the surface of an enclosure wall can only reflect radiative energy and allow a part of it to penetrate into the substrate. A surface cannot absorb or emit photons: attenuation takes place inside the solid, as does emission of radiative energy (with some of the emitted energy escaping through the surface into the enclosure). In practical systems, the thickness of the surface layer over which absorption of **irradiation** from inside the enclosure occurs is very small compared with the overall dimension of an enclosure — usually a few nanometers for metals and a few micrometers for most nonmetals. The same may be said about emission from within the walls that escapes into the enclosure. Thus, in the case of opaque walls it is customary to speak of absorption by and emission from a "surface," although a thin surface layer is implied. Four fundamental radiative properties are defined:

Reflectivity, $\qquad \rho \equiv \dfrac{\text{reflected part of incoming radiation}}{\text{total incoming radiation}}$ (4.3.6a)

Absorptivity, $\qquad \rho \equiv \dfrac{\text{absorbed part of incoming radiation}}{\text{total incoming radiation}}$ (4.3.6b)

Transmissivity, $\qquad \tau \equiv \dfrac{\text{transmitted part of incoming radiation}}{\text{total incoming radiation}}$ (4.3.6c)

Emissivity, $$\varepsilon \equiv \frac{\text{energy emitted from a surface}}{\text{energy emitted by a black surface at same temperature}} \quad (4.3.6d)$$

Since all incoming radiation must be reflected, absorbed, or transmitted, it follows that

$$\rho + \alpha + \tau = 1 \quad (4.37)$$

In most practical applications surface layers are thick enough to be opaque ($\tau = 0$, leading to $\rho + \alpha = 1$. All four properties may be functions of wavelength, temperature, incoming direction (except emissivity), and outgoing direction (except absorptivity).

Directional Behavior. For heat transfer applications, the dependence on incoming direction for absorptivity (as well as ρ and τ) and outgoing direction for emissivity is generally weak and is commonly neglected; i.e., it is assumed that the surface absorbs and emits **diffusely**. Then, for an opaque surface, for any given wavelength

$$\varepsilon_\lambda = \alpha_\lambda = 1 - \rho_\lambda \quad (4.38)$$

Published values of emissivities are generally either "normal emissivities" (the directional value of ε_λ in the direction perpendicular to the surface) or "hemispherical emissivities" (an average value over all outgoing directions). The difference between these two values is often smaller than experimental accuracy and/or repeatability.

Reflected energy (due to a single, distinct incoming direction) may leave the surface into a single direction ("specular" reflection, similar to reflection from a mirror for visible light), or the reflection may spread out over all possible outgoing directions. In the extreme case of equal amounts going into all directions, we talk about "diffuse" reflection. Smooth surfaces (as compared with the wavelength of radiation) tend to be specular reflectors, while rough surfaces tend to be more or less diffusely reflecting. Analysis is vastly simplified if diffuse reflections are assumed. Research has shown that — except for some extreme geometries and irradiation conditions susceptible to beam channeling (irradiated open cavities, channels with large aspect ratios) — radiative heat transfer rates are only weakly affected by the directional distribution of reflections. Therefore, it is common practice to carry out radiative heat transfer calculations assuming only diffuse reflections.

Spectral Dependence. The emissivity of a surface generally varies strongly and in complex ways with wavelength, depending on the material, surface layer composition, and surface structure (roughness). Therefore, unlike bulk material properties (such as thermal conductivity) the surface emissivity may display significant differences between two ostensibly identical samples, and even for one and the same sample measured at different times (due to surface roughness and contamination). Despite these difficulties, surfaces may be loosely grouped into two categories — metals and nonconductors (dielectrics), and some generalizations can be made.

Polished Metals. Smooth, purely metallic surfaces (i.e., without any nonmetallic surface contamination, such as metal oxides) tend to have very low emissivities in the infrared. For many clean metals $\varepsilon_\lambda < 0.1$ for $\lambda > 2$ µm, and spectral as well as temperature dependence are generally well approximated by the proportionality $\varepsilon_\lambda \propto \sqrt{T/\lambda}$ in the infrared. However, for shorter wavelengths ($\lambda < 1$ µm), emissivity values may become quite substantial, and temperature dependence is usually reversed (decreasing, rather than increasing, with temperature). Typical room temperature behavior of several metals is shown in Figure 4.3.3. Caution needs to be exercised when choosing an emissivity value for a metal surface: unless extraordinary care is taken to keep a polished metal clean (i.e., free from oxidation and/or surface contamination), its emissivity may soon become several times the value of the original, polished specimen (for example, consider the formation of aluminum oxide on top of aluminum, Figure 4.3.3).
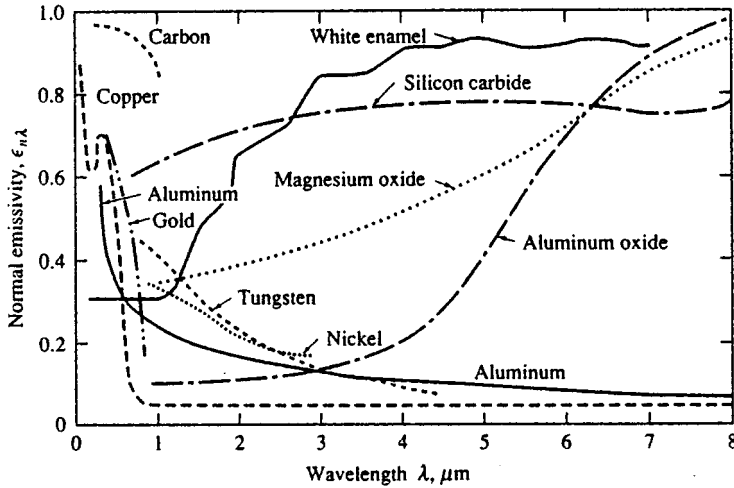
FIGURE 4.3.3 Normal, spectral emissivities for selected materials.

Ceramics and Refractories. Smooth ceramics tend to have fairly constant and intermediate emissivity over the near- to mid-infrared, followed by a sharp increase somewhere between 4 and 10 µm. At short wavelengths these materials display strong decreases in emissivity, so that a number of them may appear white to the human eye even though they are fairly black in the infrared. The temperature dependence of the emissivity of ceramics is rather weak; generally a slight increase with temperature is observed in the infrared. The spectral emissivity of a few ceramics is also shown in Figure 4.3.3.

Other Nonconductors. The behavior of most electrically nonconducting materials is governed by surface structure, nonhomogeneity, dopants, porosity, flaws, surface films, etc. The emissivity may vary irregularly across the spectrum because of various emission bands, influence of flaws, etc., making any generalization impossible. This irregularity may be exploited to obtain surfaces of desired spectral behavior, so-called selective surfaces. Some selective surfaces (as compared with a common steel) are depicted in Figure 4.3.4. For a solar collector it is desirable to have a high spectral emissivity for short wavelengths $\lambda < 2.5$ µm (strong absorption of solar irradiation), and a low value for $\lambda > 2.5$ µm (to minimize re-emission from the collector). The opposite is true for a spacecraft radiator panel used to reject heat into space.

It is clear that (1) values of spectral surface emissivity are subject to great uncertainty and (2) only a relatively small range of infrared wavelengths are of importance. Therefore, it is often assumed that the surfaces are "**gray**", i.e., the emissivity is constant across (the important fraction of) the spectrum, $\varepsilon_\lambda \neq \varepsilon_\lambda(\lambda)$, since this assumption also vastly simplifies analysis. Table 4.3.1 gives a fairly detailed listing of total emissivities of various materials, defined as

$$\varepsilon(T) = \frac{1}{E_b(T)} \int_0^\infty \varepsilon_\lambda(\lambda,T) E_{b\lambda}(T) \, d\lambda \tag{4.3.9}$$

which may be enlisted for a gray analysis.

View Factors

In many engineering applications the exchange of radiative energy between surfaces is virtually unaffected by the medium that separates them. Such (radiatively) *nonparticipating media* include vacuum as well as monatomic and most diatomic gases (including air) at low to moderate temperature levels (i.e., before ionization and dissociation occurs). Examples include spacecraft heat rejection systems, solar collector systems, radiative space heaters, illumination problems, and so on. It is common practice
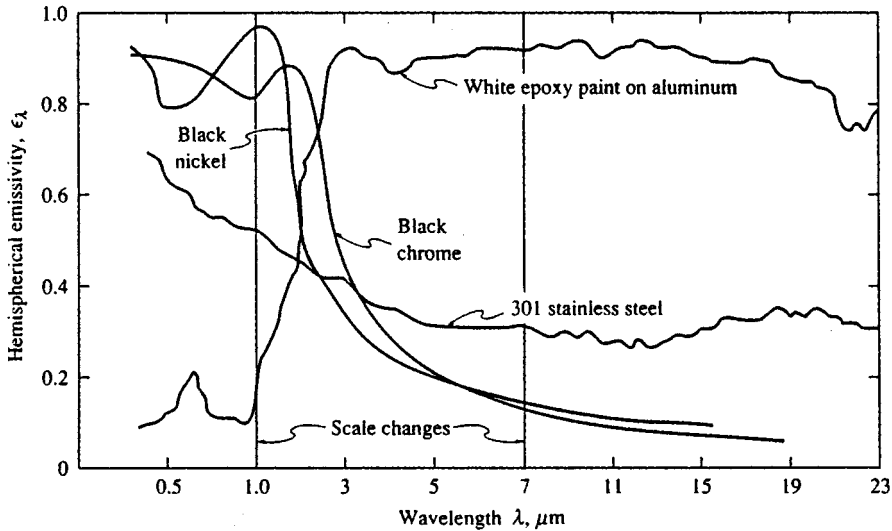
FIGURE 4.3.4 Spectral, hemispherical reflectivities of several spectrally selective surfaces.

to simplify the analysis by making the assumption of an *idealized enclosure* and/or of *ideal surface properties*. The greatest simplification arises if all surfaces are black: for such a situation no reflected radiation needs to be accounted for, and all emitted radiation is diffuse (i.e., the radiative energy leaving a surface does not depend on direction). The next level of difficulty arises if surfaces are assumed to be gray, diffuse emitters (and, thus, absorbers) as well as gray, diffuse reflectors. The vast majority of engineering calculations are limited to such ideal surfaces, since, particularly, the effects of nondiffuse reflections are usually weak (see discussion in previous section).

Thermal radiation is generally a long-range phenomenon. This is *always* the case in the absence of a participating medium, since photons will travel unimpeded from surface to surface. Therefore, performing a thermal radiation analysis for one surface implies that all surfaces, no matter how far removed, that can exchange radiative energy with one another must be considered simultaneously. How much energy any two surfaces exchange depends in part on their size, separation, distance, and orientation, leading to geometric functions known as **view factors**, defined as

$$F_{i-j} = \frac{\text{diffuse energy leaving } A_i \text{ directly toward and intercepted by } A_j}{\text{total diffuse energy leaving } A_i} \tag{4.3.10}$$

In order to make a radiative energy balance we always need to consider an entire *enclosure* rather than and infinitesimal control volume (as is normally done for other modes of heat transfer, i.e., conduction or convection). The enclosure must be closed so that irradiation from all possible directions can be accounted for, and the enclosure surfaces must be *opaque* so that all irradiation is accounted for, for each direction. In practice, an incomplete enclosure may be closed by introducing artificial surfaces. An enclosure may be idealized in two ways, as indicated in Figure 4.3.5: by replacing a complex geometric shape with a few simple surfaces, and by assuming surfaces to be isothermal with constant (i.e., average) heat flux values across them. Obviously, the idealized enclosure approaches the real enclosure for sufficiently small isothermal subsurfaces.

Mathematically, the view factor needs to be determined from a double integral, i.e.,

$$F_{i-j} = \frac{1}{A_i} \int_{A_i} \int_{A_j} \frac{\cos\theta_i \cos\theta_j}{\pi S_{ij}^2} dA_j \, dA_i \tag{4.3.11}$$

TABLE 4.3.1   Total Emissivity and Solar Absorptivity of Selected Surfaces

	Temperature (°C)	Total Normal Emissivity	Extraterrestrial Solar Absorptivity
Alumina, flame-sprayed	–25	0.80	0.28
Aluminum foil			
As received	20	0.04	
Bright dipped	20	0.025	0.10
Aluminum, vacuum-deposited	20	0.025	0.10
Hard-anodized	–25	0.84	0.92
Highly polished plate, 98.3% pure	225–575	0.039–0.057	
Commercial sheet	100	0.09	
Rough polish	100	0.18	
Rough plate	40	0.055–0.07	
Oxidized at 600°C	200–600	0.11–0.19	
Heavily oxidized	95–500	0.20–0.31	
Antimony, polished	35–260	0.28–0.31	
Asbestos	35–370	0.93–0.94	
Beryllium	150	0.18	0.77
	370	0.21	
	600	0.30	
Beryllium, anodized	150	0.90	
	370	0.88	
	600	0.82	
Bismuth, bright	75	0.34	
Black paint			
Parson's optical black	–25	0.95	0.975
Black silicone	–25–750	0.93	0.94
Black epoxy paint	–25	0.89	0.95
Black enamel paint	95–425	0.81–0.80	
Brass, polished	40–315	0.10	
Rolled plate, natural surface	22	0.06	
Dull plate	50–350	0.22	
Oxidized by heating at 600°C	200–600	0.61–0.59	
Carbon, graphitized	100–320	0.76–0.75	
	320–500	0.75–0.71	
Candle soot	95–270	0.952	
Graphite, pressed, filed surface	250–510	0.98	
Chromium, polished	40–1100	0.08–0.36	
Copper, electroplated	20	0.03	0.47
Carefully polished electrolytic copper	80	0.018	
Polished	115	0.023	
Plate heated at 600°C	200–600	0.57	
Cuprous oxide	800–1100	0.66–0.54	
Molten copper	1075–1275	0.16–0.13	
Glass, Pyrex, lead, and soda	260–540	0.95–0.85	
Gypsum	20	0.903	
Gold, pure, highly polished	225–625	0.018–0.035	
Inconel X, oxidized	–25	0.71	0.90
Lead, pure (99.96%), unoxidized	125–225	0.057–0.075	
Gray oxidized	25	0.28	
Oxidized at 150°C	200	0.63	
Magnesium oxide	275–825	0.55–0.20	
	900–1705	0.20	
Magnesium, polished	35–260	0.07–0.13	
Mercury	0–100	0.09–0.12	
Molybdenum, polished	35–260	0.05–0.08	
	540–1370	0.10–0.18	

TABLE 4.3.1 (continued) Total Emissivity and Solar Absorptivity of Selected Surfaces

	Temperature (°C)	Total Normal Emissivity	Extraterrestrial Solar Absorptivity
	2750	0.29	
Nickel, electroplated	20	0.03	0.22
Polished	100	0.072	
Platinum, pure, polished	225–625	0.054–0.104	
Silica, sintered, powdered, fused silica	35	0.84	0.08
Silicon carbide	150–650	0.83–0.96	
Silver, polished, pure	40–625	0.020–0.032	
Stainless steel			
Type 312, heated 300 hr at 260°C	95–425	0.27–0.32	
Type 301 with Armco black oxide	–25	0.75	0.89
Type 410, heated to 700°C in air	35	0.13	0.76
Type 303, sandblasted	95	0.42	0.68
Titanium, 75A	95–425	0.10–0.19	
75A, oxidized 300 hr at 450°C	35–425	0.21–0.25	0.80
Anodized	–25	0.73	0.51
Tungsten, filament, aged	27–3300	0.032–0.35	
Zinc, pure, polished	225–325	0.045–0.053	
Galvanized sheet	100	0.21	
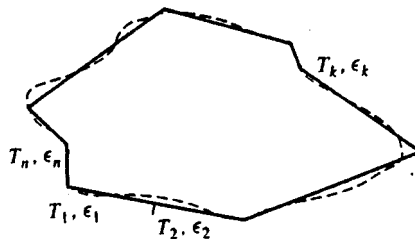
FIGURE 4.3.5 Real and ideal enclosures for radiative transfer calculations.

where θ_i and θ_j are the angles between the surface normals on A_i and A_j, respectively, and the line (of length S_{ij}) connecting two points on the two surfaces. Analytical solutions to Equation (4.3.11) may be found for relatively simple geometries. A few graphical results for important geometries are shown in Figures 4.3.6 to 4.3.8. More-extensive tabulations as well as analytical expressions may be found in textbooks on the subject area (Modest, 1993; Siegel and Howell, 1992) as well as view factor catalogs (Howell, 1982). For nontrivial geometries view factors must be calculated numerically, either (1) by numerical quadrature of the double integral in Equation (4.3.11), or (2) by converting Equation (4.3.11) into a double-line integral, followed by numerical quadrature, or (3) by a Monte Carlo method (statistical sampling and tracing of selected light rays).

View Factor Algebra. For simple geometries analytical values can often be found by expressing the desired view factor in terms of other, known ones. This method is known as *view factor algebra*, by manipulating the two relations,

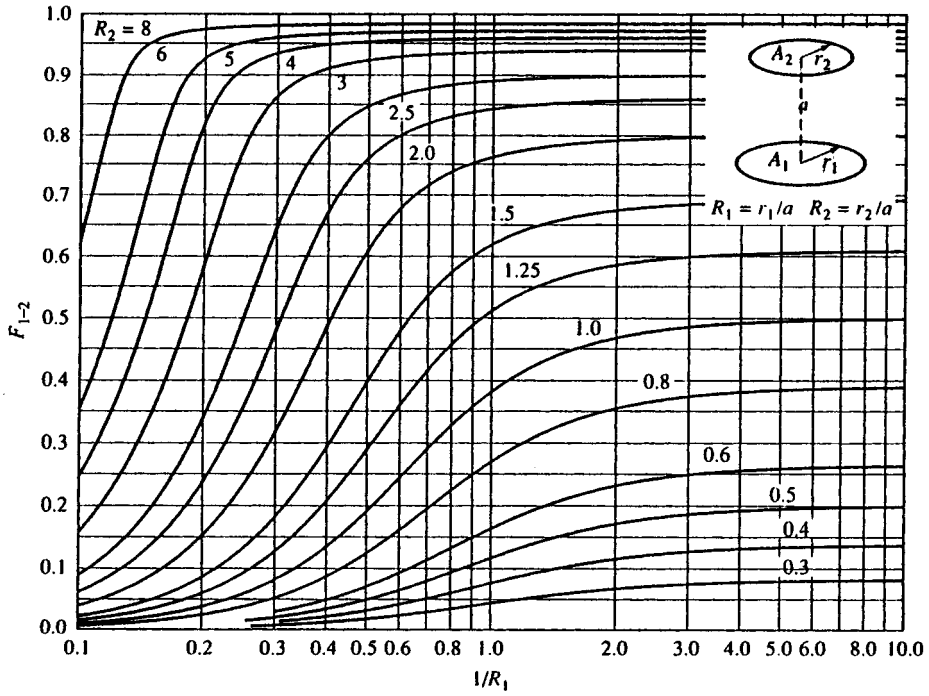*Reciprocity rule:* $\qquad A_i F_{i-j} = A_j F_{j-i}$ $\hfill$ (4.3.12)

FIGURE 4.3.6 View factor between parallel, coaxial disks of unequal radius.
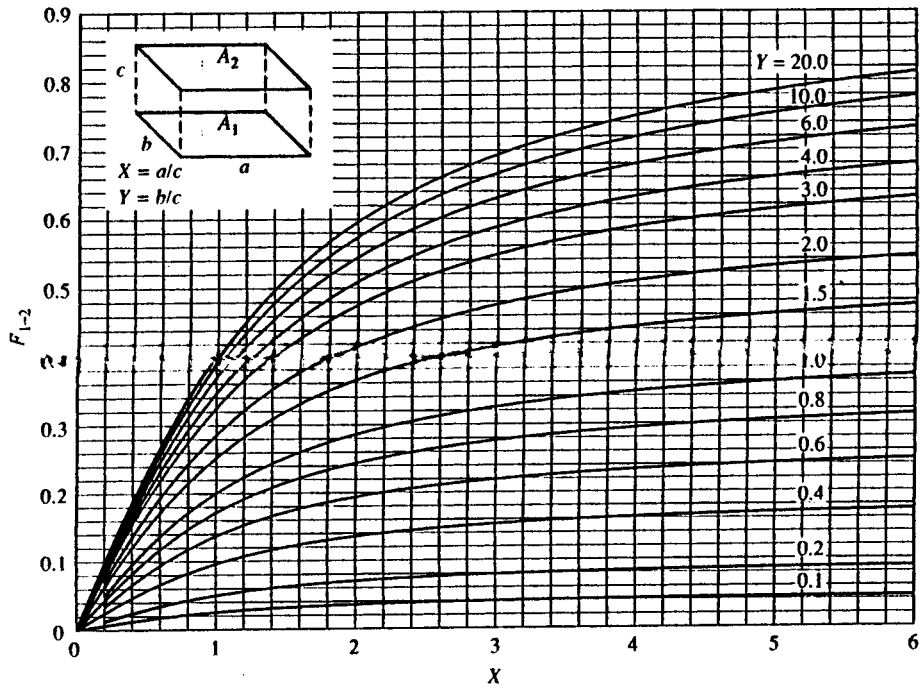
FIGURE 4.3.7 View factor between identical, parallel, directly opposed rectangles.
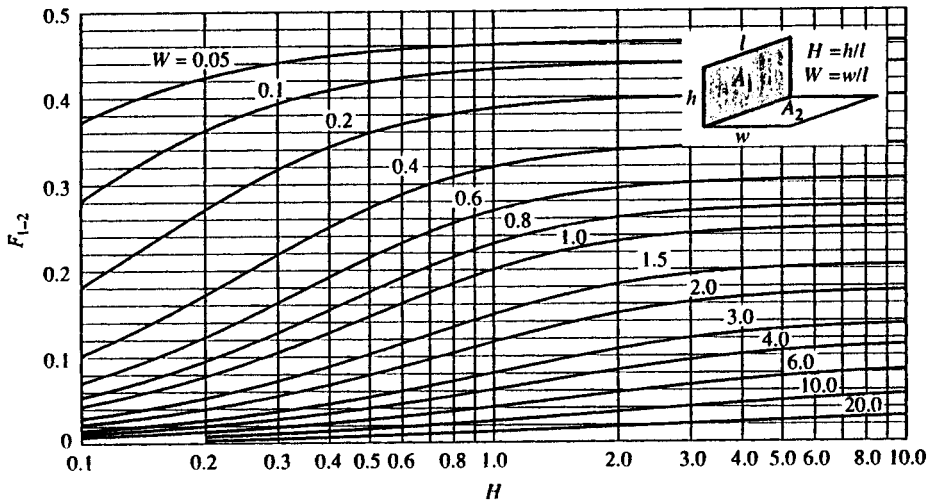
FIGURE 4.3.8 View factor between perpendicular rectangles with common edge.

Summation rule:
$$\sum_{j=1}^{N} F_{i-j} = 1, \qquad i = 1, N \tag{4.3.13}$$

assuming that the (closed) configuration consists of N surfaces. The reciprocity rule follows immediately from Equation (4.3.11), while the summation rule simply states that the fractional energies leaving surface A_i must add up to a whole.

Example 4.3.2

Assuming the view factor for a finite corner, as shown in Figure 4.3.8 is known, determine the view factor F_{3-4}, between the two perpendicular strips as shown in Figure 4.3.9.
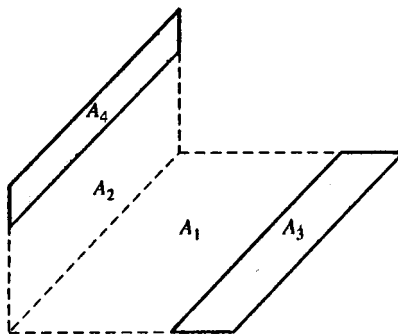
FIGURE 4.3.9 Configuration for Example 4.3.2 (strips on a corner piece).

Solution. From the definition of the view factor, and since the energy traveling to A_4 is the energy going to A_2 and A_4 minus the one going to A_2, it follows that

$$F_{3-4} = F_{3-(2+4)} - F_{3-2}$$

and, using reciprocity,

$$F_{3-4} = \frac{1}{A_3}\Big[\big(A_2 + A_4\big)F_{(2+4)-3} - A_2 F_{2-3}\Big]$$

Similarly, we find

$$F_{3-4} = \frac{A_2 + A_4}{A_3}\Big(F_{(2+4)-(1+3)} - F_{(2+4)-1}\Big) - \frac{A_2}{A_3}\Big(F_{2-(1+3)} - F_{2-1}\Big)$$

All view factors on the right-hand side are corner pieces and, thus, are known from Figure 4.3.8.

Crossed-Strings Method. A special type of view factor algebra may be used to determine all the view factors in long enclosures with constant cross section. The method is called the crossed-strings method since the view factors can be determined experimentally with four pins, a roll of string, and a yardstick. Consider the configuration in Figure 4.3.10, which shows the cross section of an infinitely long enclosure, continuing into and out of the plane of the figure. Repeatedly applying reciprocity and summation rules allows the evaluation of F_{1-2} as

$$F_{1-2} = \frac{\big(A_{bc} + A_{ad}\big) - \big(A_{ac} + A_{bd}\big)}{2A_1} \tag{4.3.14}$$
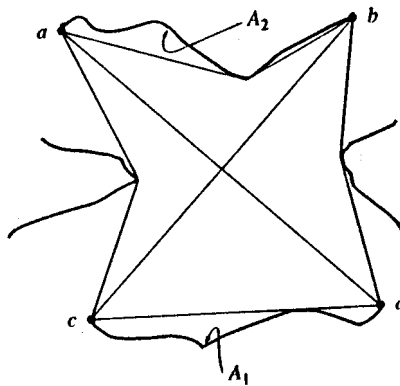
FIGURE 4.3.10 The crossed-strings method for arbitrary two-dimensional configurations.

where A_{ab} is the area (per unit depth) defined by the length of the string between points *a* and *b*, etc. This formula is easily memorized by looking at the configuration between any two surfaces as a generalized "rectangle," consisting of A_1, A_2, and the two sides A_{ac} and A_{bd}. Then

$$F_{1-2} = \frac{\text{diagonals} - \text{sides}}{2 \times \text{originating area}} \tag{4.3.15}$$

Example 4.3.3

Calculate F_{1-2} for the configuration shown in Figure 4.3.11.

Solution. From the figure it is obvious that

$$s_1^2 = \big(c - d\cos\alpha\big)^2 + d^2\sin^2\alpha = c^2 + d^2 - 2cd\cos\alpha$$
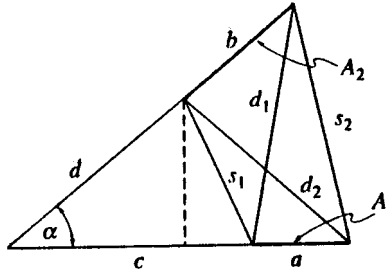
FIGURE 4.3.11 Infinitely long wedge-shaped groove for Example 4.3.3.

Similarly, we have

$$s_2^2 = (a+c)^2 + (b+d)^2 - 2(a+c)(b+d)\cos\alpha$$

$$d_1^2 = (a+c)^2 + d^2 - 2(a+c)d\cos\alpha$$

$$d_2^2 = c^2 + (b+d)^2 - 2c(b+d)\cos\alpha$$

and

$$F_{1-2} = \frac{d_1 + d_2 - (s_1 + s_2)}{2a}$$

Radiative Exchange between Opaque Surfaces (Net Radiation Method)

Consider an enclosure consisting of *N* opaque surfaces. The enclosure is closed, or, if not, no surface external to the surface reflects or emits radiation into the enclosure (i.e., the open configuration may be artificially closed by replacing openings with cold, black surfaces); any external radiation entering the enclosure is dealt with individually for each surface [see Equation (4.3.17) below]. All surfaces are assumed to be gray, and emit and reflect diffusely. Traditionally, the **radiosity** *J* of the surfaces is determined, defined as the total diffuse radiative energy leaving a surface (by emission and reflection),

$$J_i = \varepsilon_1 E_{bi} + \rho_i H_i, \qquad i = 1, N \tag{4.3.16}$$

where H_i is the incoming radiative flux (irradiation) onto surface A_i. This leads to *N* simultaneous equations for the unknown radiosities, specifically,

$$J_i = \varepsilon_i E_{bi} + (1 - \varepsilon_i)\left[\sum_{j=1}^{N} J_i F_{i-j} + H_{oi}\right] \tag{4.3.17a}$$

or

$$J_i = q_i + \sum_{j=1}^{N} J_j F_{i-j} + H_{oi} \tag{4.3.17b}$$

depending on whether surface temperature or surface flux are known on surface A_i. In Equation (4.3.17) H_{oi} is irradiation on surface A_i from outside the enclosure, if any; H_{oi} is always zero for closed configurations, but is useful in the presence of external light sources (such as solar energy, lasers, etc.). The

radiosity neither is a useful quantity to determine, nor is there a need to determine it. Eliminating the radiosities from Equations (4.3.17a) and (4.3.17b) leads to N simultaneous equations in temperature (E_{bi}) and heat flux (q_i):

$$\frac{q_i}{\varepsilon_i} - \sum_{j=1}^{N}\left(\frac{1}{\varepsilon_j} - 1\right)F_{i-j}q_j + H_{oi} = E_{bi} - \sum_{j=1}^{N}F_{i-j}E_{bj} \qquad (4.3.18)$$

Note that no artificial closing surfaces ($j > N$) appear in Equation (4.3.18), since for these surfaces $\varepsilon_j = 1$ and $E_{bj} = 0$. Thus, such closing surfaces may simply be ignored in the analysis.

Since Equation (4.3.18) is a set of N equations, this requires that N values of emissive power E_{bi} and/or flux q_i must be given as boundary conditions, in order to solve for the remaining N unknowns. For computer calculations Equation (4.3.18) may be recast in matrix form

$$\mathbf{C} \cdot \mathbf{q} = \mathbf{A} \cdot \mathbf{e_b} - \mathbf{h_o} \qquad (4.3.19a)$$

where

$$C_{ij} = \frac{\delta_{ij}}{\varepsilon_j} - \left(\frac{1}{\varepsilon_j} - 1\right)F_{i-j} \qquad (4.3.19b)$$

$$A_{ij} = \delta_{ij} - F_{i-j} \qquad (4.3.19c)$$

δ_{ij} is Kronecker's delta, i.e.,

$$\delta_{ij} = \begin{cases} 1 & \text{if } i = j \\ 0 & \text{if } i \neq j \end{cases} \qquad (4.3.20)$$

and $\mathbf{q}$, $\mathbf{e_b}$, and $\mathbf{h_o}$ are vectors of the surface heat fluxes q_i, emissive powers E_{bi}, and external irradiations H_{oi} (if any). For example, if the temperatures are given for all the surfaces, and the heat fluxes are to be determined, Equation (4.3.19) is solved by matrix inversion, and

$$\mathbf{q} = \left(\mathbf{C}^{-1} \cdot \mathbf{A}\right) \cdot \mathbf{e_b} - \left(\mathbf{C}^{-1} \cdot \mathbf{h_o}\right) \qquad (4.3.21)$$

Example 4.3.4

A right-angled groove, consisting of two long black surfaces of width a, is exposed to solar radiation q_{sol} (Figure 4.3.12). The entire groove surface is kept isothermal at temperature T. Determine the net radiative heat transfer rate from the groove.

Solution. We may employ Equation (4.3.19). However, the enclosure is not closed, and we must close it artificially. We note that any radiation leaving the cavity will not come back (barring any reflection from other surfaces nearby). Thus, our artificial surface should be black. We also assume that, with the exception of the (parallel) solar irradiation, no external radiation enters the cavity. Since the solar irradiation is best treated separately through the external irradiation term H_o, our artificial surface is nonemitting. Both criteria are satisfied by covering the groove with a black surface at 0 K (A_3). Even though we now have three surfaces, the last one does not really appear in Equation (4.3.18) (since $E_{b3} = 0$ and $1/\varepsilon_3 - 1 = 0$):
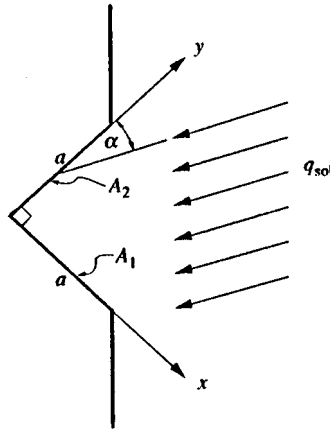
FIGURE 4.3.12 Right-angled groove exposed to solar irradiation, Example 4.3.4.

$$q_1 = E_{b1} - F_{1-2}E_{b2} - H_{o1} = \sigma T^4\left(1 - F_{1-2}\right) - q_{sol}\cos\alpha$$

$$q_2 = E_{b2} - F_{2-1}E_{b1} - H_{o2} = \sigma T^4\left(1 - F_{2-1}\right) - q_{sol}\sin\alpha$$

From the crossed-strings method, Equation (4.3.15), we find

$$F_{1-2} = \frac{a + a - \left(\sqrt{2}a + 0\right)}{2a} = \frac{1}{2}\left(2 - \sqrt{2}\right) = 0.293 = F_{2-1}$$

and

$$Q' = a\left(q_1 + q_2\right) = a\left[\sqrt{2}\sigma T^4 - q_{sol}\left(\cos\alpha + \sin\alpha\right)\right]$$

Example 4.3.5

Consider a very long duct as shown in Figure 4.3.13. The duct is 30×40 cm in cross section, and all surfaces are covered with gray, diffuse surface material. Top and bottom walls are at $T_1 = T_3 = 1000$ K with $\varepsilon_1 = \varepsilon_3 = 0.3$, while the side walls are at $T_2 = T_4 = 600$ K with $\varepsilon_2 = \varepsilon_4 = 0.8$ as shown. Determine the net radiative heat transfer rates for each surface.

FIGURE 4.3.13 Two-dimensional gray, diffuse duct for Example 4.3.5.

Solution. Using Equation (4.3.18) for $i = 1$ and $i = 2$ and noting that $F_{1-2} = F_{1-4}$ and $F_{2-1} = F_{2-3}$,

$$i = 1: \quad \frac{q_1}{\varepsilon_1} - 2\left(\frac{1}{\varepsilon_2} - 1\right)F_{1-2}q_2 - \left(\frac{1}{\varepsilon_1} - 1\right)F_{1-3}q_1 = 2F_{1-2}\left(E_{b1} - E_{b2}\right)$$

$$i = 2: \quad \frac{q_2}{\varepsilon_2} - 2\left(\frac{1}{\varepsilon_1} - 1\right)F_{2-1}q_1 - \left(\frac{1}{\varepsilon_2} - 1\right)F_{2-4}q_2 = 2F_{2-1}\left(E_{b2} - E_{b1}\right)$$

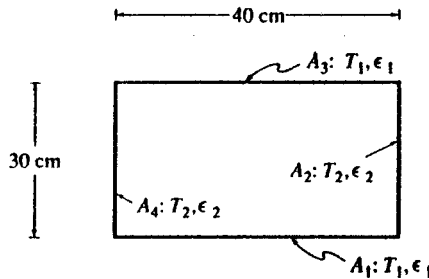The view factors are readily evaluated from the crossed-strings method as $F_{1-2} = {}^1/_4$, $F_{1-3} = 1 - 2F_{1-2} = {}^1/_2$, $F_{2-1} = {}^4/_3 F_{1-2} = {}^1/_3$ and $F_{2-4} = 1 - 2F_{2-1} = {}^1/_3$. Substituting these, as well as emissivity values, into the relations reduces them to the simpler form of

$$\left[\frac{1}{0.3} - \left(\frac{1}{0.3} - 1\right)\frac{1}{2}\right]q_1 - 2\left(\frac{1}{0.8} - 1\right)\frac{1}{4}q_2 = 2 \times \frac{1}{4}\left(E_{b1} - E_{b2}\right)$$

$$-2\left(\frac{1}{0.3} - 1\right)\frac{1}{3}q_1 + \left[\frac{1}{0.8} - \left(\frac{1}{0.8} - 1\right)\right]\frac{1}{3}q_2 = 2 \times \frac{1}{3}\left(E_{b2} - E_{b1}\right)$$

or

$$\frac{13}{6}q_1 - \frac{1}{8}q_2 = \frac{1}{2}\left(E_{b1} - E_{b2}\right)$$

$$-\frac{14}{9}q_1 + \frac{7}{6}q_2 = -\frac{2}{3}\left(E_{b1} - E_{b2}\right)$$

Thus,

$$\left(\frac{13}{6} \times \frac{7}{6} - \frac{14}{9} \times \frac{1}{8}\right)q_1 = \left(\frac{1}{2} \times \frac{7}{6} - \frac{2}{3} \times \frac{1}{8}\right)\left(E_{b1} - E_{b2}\right)$$

$$q_1 = \frac{3}{7} \times \frac{1}{2}\left(E_{b1} - E_{b2}\right) = \frac{3}{14}\sigma\left(T_1^4 - T_2^4\right)$$

and

$$\left(-\frac{1}{8} \times \frac{14}{9} + \frac{7}{6} \times \frac{13}{6}\right)q_2 = \left(\frac{1}{2} \times \frac{14}{9} - \frac{2}{3} \times \frac{13}{6}\right)\left(E_{b1} - E_{b2}\right)$$

$$q_2 = \frac{3}{7} \times \frac{2}{3}\left(E_{b1} - E_{b2}\right) = -\frac{2}{7}\sigma\left(T_1^4 - T_2^4\right)$$

Finally, substituting values for temperatures,

$$Q_1' = 0.4 \text{ m} \times \frac{3}{14} \times 5.670 \times 10^{-8} \; \frac{\text{W}}{\text{m}^2\text{K}^4}\left(1000^4 - 600^4\right) \text{K}^4 = 4230 \text{ W/m}$$

$$Q_2' = -0.3 \text{ m} \times \frac{2}{7} \times 5.670 \times 10^{-8} \ \frac{\text{W}}{\text{m}^2\text{K}^4} \left(1000^4 - 600^4\right) \text{K}^4 = -4230 \text{ W/m}$$

Note that, for conservation of energy, both heat transfer rates must add up to zero.

Small Body Inside Isothermal Enclosure. An especially simple — but important — case occurs if a small, convex body A_1 (i.e., a surface that cannot "see" itself, or $F_{1-1} = 0$) is totally enclosed by an isothermal enclosure A_2. Then, with $N = 2$ and $F_{1-2} = 1$, Equation (4.3.18) reduces to

$$q_1 = \frac{E_{b1} - E_{b2}}{\dfrac{1}{\varepsilon_1} + \dfrac{A_1}{A_2}\left(\dfrac{1}{\varepsilon_2} - 1\right)} = \frac{\sigma\left(T_1^4 - T_2^4\right)}{\dfrac{1}{\varepsilon_1} + \dfrac{A_1}{A_2}\left(\dfrac{1}{\varepsilon_2} - 1\right)} \tag{4.3.22}$$

If the enclosure is large, i.e., $A_1 \ll A_2$, then Equation (4.3.22) simplifies further to

$$q_1 = \varepsilon_1 \sigma\left(T_1^4 - T_2^4\right) \tag{4.3.23}$$

Radiation Shields. If it is desired to minimize radiative heat transfer between two surfaces, it is common practice to place one or more radiation shields between them (usually thin metallic sheets of low emissivity). If two surfaces A_i and A_j are close together, so that $A_i \cong A_j$ and $F_{i-j} \cong 1$, then the radiative exchange between them is, from Equation (4.3.22),

$$q = \frac{E_{bi} - E_{bj}}{R_{ij}}, \qquad R_{ij} = \frac{1}{\varepsilon_i} + \frac{1}{\varepsilon_j} - 1 \tag{4.3.24}$$
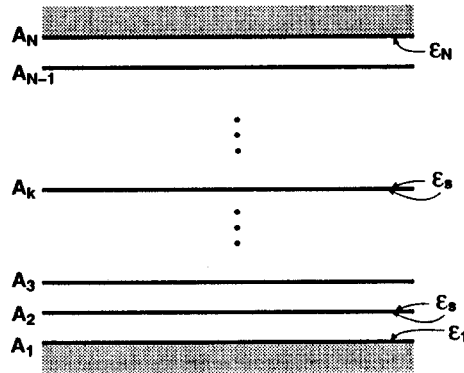
FIGURE 4.3.14 Placement of radiation shields between two large, parallel plates.

where R_{ij} is termed the *radiative resistance*. Equation (4.3.24) is seen to be analogous to an electrical circuit with "current" q and "voltage potential" $E_{bi} - E_{bj}$. Therefore, expressing radiative fluxes in terms of radiative resistances is commonly known as **network analogy**. The network analogy is a very powerful method of solving one-dimensional problems (i.e., whenever only two isothermal surfaces see each other, such as infinite parallel plates, or when one surface totally encloses another). Consider, for example, two large parallel plates, A_1 and A_N, separated by $N - 2$ radiation shields, as shown in Figure 4.3.14. Let each shield have an emissivity ε_S on both sides. Then, by applying Equation (4.3.24) to any two consecutive surfaces and using the fact that q remains constant throughout the gap,

$$q = \frac{E_{b1} - E_{b2}}{R_{12}} = \cdots = \frac{E_{bk-1} - E_{bk}}{R_{k-1,k}} = \cdots = \frac{E_{bN-1} - E_{bN}}{R_{N-1,N}} = \frac{E_{b1} - E_{bN}}{\sum\limits_{j-2}^{N} R_{j-1,j}} \tag{4.3.25}$$

where

$$R_{j-1,j} = \frac{1}{\varepsilon_{j-1}} + \frac{1}{\varepsilon_{j}} - 1 \tag{4.3.26}$$

and, if $\varepsilon_2 = \varepsilon_3 \cdots = \varepsilon_{N-1} = \varepsilon_S$,

$$\sum_{j=2}^{N} R_{j-1,j} = \frac{1}{\varepsilon_1} + \frac{1}{\varepsilon_N} - 1 + (N-2)\left(\frac{2}{\varepsilon_S} - 1\right) \tag{4.3.27}$$

Equations (4.3.24) to (4.3.27) are also valid for concentric cylinders, concentric spheres, and similar configurations, as long as $r_N - r_1 \ll r_1$. Also, the relations are readily extended to shields with nonidentical emissivities.

While the network analogy can (and has been) applied to configurations with more than two surfaces seeing each other, this leads to very complicated circuits (since there is one resistance between any two surfaces). For such problems the network analogy is not recommended, and the net radiation method, Equation (4.3.18), should be employed.

Radiative Exchange within Participating Media

In many high-temperature applications, when radiative heat transfer is important, the medium between surfaces is not transparent, but is "participating," i.e., it absorbs, emits, and (possibly) scatters radiation. In a typical combustion process this interaction results in (1) continuum radiation due to tiny, burning soot particles (of dimension <1 μm) and also due to larger suspended particles, such as coal particles, oil droplets, fly ash; (2) banded radiation in the infrared due to emission and absorption by molecular gaseous combustion products, mostly water vapor and carbon dioxide; and (3) chemiluminescence due to the combustion reaction itself. While chemiluminescence may normally be neglected, particulates as well as gas radiation generally must be accounted for.

Radiative Properties of Molecular Gases

When a photon (or an electromagnetic wave) interacts with a gas molecule, it may be absorbed, raising the energy level of the molecule. Conversely, a gas molecule may spontaneously lower its energy level by the emission of an appropriate photon. This leads to large numbers of narrow spectral lines, which partially overlap and together form so-called vibration-rotation bands. As such, gases tend to be transparent over most of the spectrum, but may be almost opaque over the spectral range of a band. The **absorption coefficient** κ_λ is defined as a measure of how strongly radiation is absorbed or emitted along a path of length, L, leading to the spectral absorptivity and emissivity for this path, or

$$\alpha_\lambda = \varepsilon_\lambda = 1 - e^{-\kappa_\lambda L} \tag{4.3.28}$$

Although gases are distinctly nongray, for simple heat transfer calculations we often need to determine the total emissivity for an isothermal path (compare Equation (4.3.9))

$$\varepsilon = \frac{1}{E_b} \int_0^\infty \left(1 - e^{-\kappa_\lambda L}\right) E_{b\lambda}\left(T_g\right) d\lambda \tag{4.3.29}$$

For a mixture of gases the total emissivity is a function of path length L, gas temperature T_g, partial pressure(s) of the absorbing gas(es) p_a, and total pressure p. For the — in combustion applications most important — mixture of nitrogen with water vapor and/or carbon dioxide, the total emissivity may be calculated from Leckner.[8] First, the individual emissivities for water vapor and carbon dioxide, respectively, are calculated separately from

$$\varepsilon\left(p_a L, p, T_g\right) = \varepsilon_0\left(p_a L, T_g\right)\left(\frac{\varepsilon}{\varepsilon_0}\right)\left(p_a L, p, T_g\right) \tag{4.3.30a}$$

$$\left(\frac{\varepsilon}{\varepsilon_0}\right)\left(p_a L, p, T_g\right) = \left[1 - \frac{(a-1)(1-P_E)}{a+b-1+P_E}\exp\left(-c\left[\log_{10}\frac{(p_a L)_m}{p_a L}\right]^2\right)\right] \tag{4.3.30b}$$

$$\varepsilon_0\left(p_a L, T_g\right) = \exp\left[\sum_{i=0}^{N}\sum_{j=0}^{N} c_{ji}\left(\frac{T_g}{T_0}\right)^j\left(\log_{10}\frac{p_a L}{(p_a L)_0}\right)^i\right] \tag{4.3.30c}$$

Here ε_0 is the total emissivity of a reference state, i.e., for the case of $p = 1$ bar and $p_a \rightarrow 0$ (but $p_a L > 0$), and the correlation constants a, b, c, c_{ji}, P_E $(p_a L)_0$, $(p_a L)_m$, and T_0 are given in Table 4.3.2 for water vapor and carbon dioxide. (For convenience, plots of ε_0 are given in Figures 4.3.15 for CO_2 and 4.3.16 for H_2O.) The total emissivity of a mixture of nitrogen with both water vapor and carbon dioxide is calculated from

$$\varepsilon_{CO_2+H_2O} = \varepsilon_{CO_2} + \varepsilon_{H_2O} - \Delta\varepsilon \tag{4.3.31}$$

TABLE 4.3.2 Correlation Constants for the Determination of the Total Emissivity for Water Vapor and Carbon Dioxide

Gas	Water Vapor			Carbon Dioxide			
M, N	2,2			2,3			
$c_{00} \cdots c_{N1}$	−2.2118	−1.1987	0.035596	−3.9893	2.7669	−2.1081	0.39163
$\vdots \ddots \vdots$	0.85667	0.93048	−0.14391	1.2710	−1.1090	1.0195	−0.21897
$c_{0M} \cdots c_{NM}$	−0.10838	−0.17156	0.045915	−0.23678	0.19731	−0.19544	0.044644
P_E	$(p + 2.56 p_a/\sqrt{t})/p_0$			$(p + 0.28 p_a)/p_0$			
$(p_a L)_m/(p_a L)_0$	$13.2 t^2$			$0.054/t^2, \quad t < 0.7$ $0.225 t^2, \quad t > 0.7$			
a	$2.144, \qquad t < 0.75$ $1.88 - 2.053 \log_{10} t, \quad t > 0.75$			$1 + 0.1/t^{1.45}$			
b	$1.10/t^{1.4}$			0.23			
c	0.5			1.47			

Note: $T_0 = 1000$ K, $p_0 = 1$ bar, $t = T/T_0$, $(p_a L)_0 = 1$ bar cm.

$$\Delta\varepsilon = \left(\frac{\zeta}{10.7 + 101\zeta} - 0.0089\zeta^{10.4}\right)\left(\log_{10}\frac{\left(p_{H_2O} + p_{CO_2}\right)L}{\left(p_a L\right)_0}\right)^{2.76}$$

(4.3.32)

$$\zeta = \frac{p_{H_2O}}{p_{H_2O} + p_{CO_2}}$$

FIGURE 4.3.15 Total emissivity of water vapor at reference state (total gas pressure $p = 1$ bar, partial pressure of H_2O $p_a \to 0$).

where the $\Delta\varepsilon$ compensates for overlap effects between H_2O and CO_2 bands, and the ε_{CO_2} and ε_{H_2O} are calculated from Equation (4.3.30).

If radiation emitted externally to the gas (for example, by emission from an adjacent wall at temperature T_s) travels through the gas, the total amount absorbed by the gas is of interest. This leads to the absorptivity of a gas path at T_g with a source at T_s:

$$\alpha\left(p_a L, p, T_g, T_s\right) = \frac{1}{E_b(T_s)}\int_0^\infty \left(1 - e^{-\kappa_\lambda(T_g)L}\right)E_{b\lambda}(T_s)\, d\lambda$$

(4.3.33)

which for water vapor or carbon dioxide may be estimated from

$$\alpha\left(p_a L, p, T_g, T_s\right) = \left(\frac{T_g}{T_s}\right)^{1/2}\varepsilon\left(p_a L \frac{T_s}{T_g}, p, T_s\right)$$
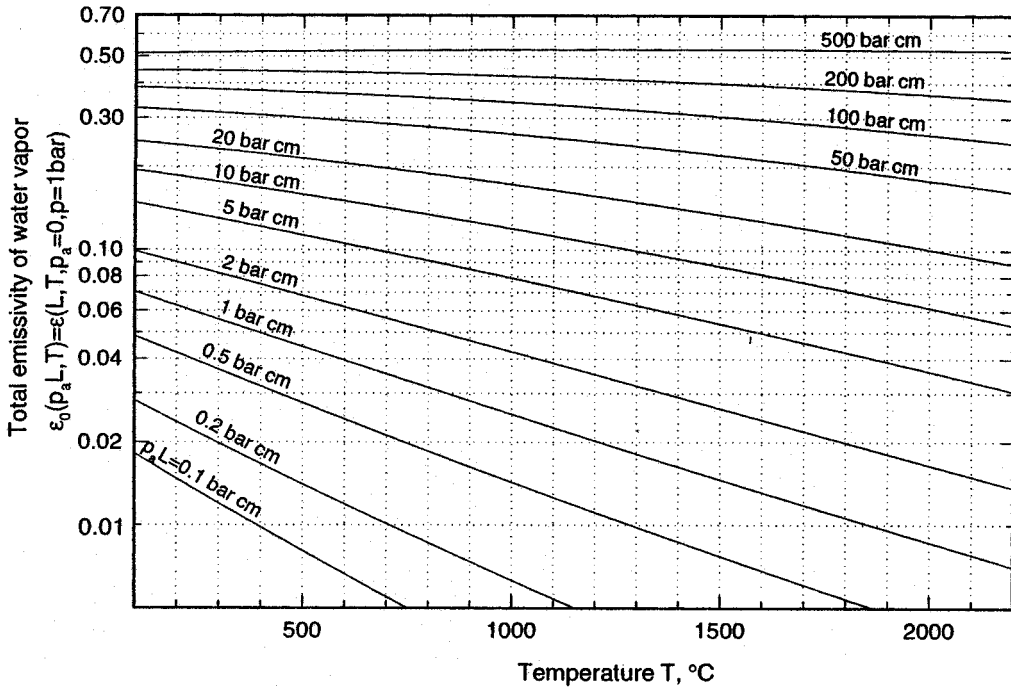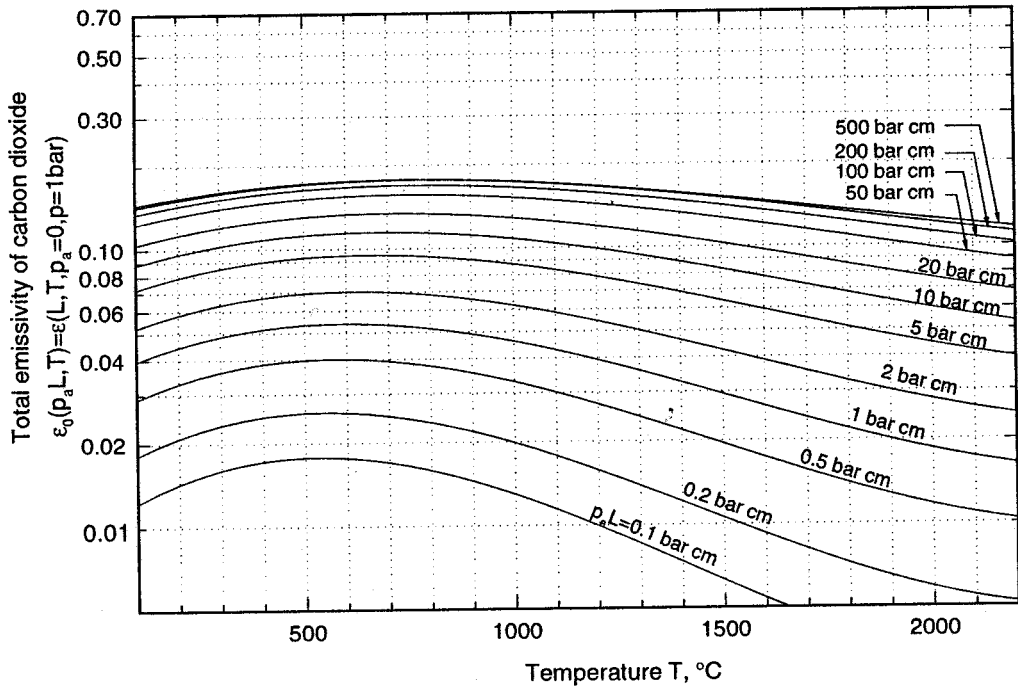
(4.3.34)

FIGURE 4.3.16 Total emissivity of carbon dioxide at reference state (total gas pressure $p = 1$ bar, partial pressure of CO_2 $p_a \rightarrow 0$).

where ε is the emissivity calculated from Equation (4.3.30) evaluated at the temperature of the surface T_s, and using an adjusted pressure path length, $p_a L T_s / T_g$. For mixtures of water vapor and carbon dioxide band overlap is again accounted for by taking

$$\alpha_{CO_2+H_2O} = \alpha_{CO_2} + \alpha_{H_2O} - \Delta\varepsilon \qquad (4.3.35)$$

with $\Delta\varepsilon$ evaluated for a pressure path length of $p_a L T_s / T_g$.

Example 4.3.6

Consider a layer of a gas mixture at 1000 K and 5 bar that consists of 10% carbon dioxide and 70% nitrogen. What is its emissivity for a path length of 1.76 m, and its absorptivity (for the same path) if the layer is irradiated by a source at 1500 K?

Solution. First we calculate the total emissivity of the CO_2 at the reference state ($p = 1$ bar, $p_a \rightarrow 0$). for a length of 1.76 m from Equation (4.3.30c) or Figure 4.3.15. With

$$T_g = 1000 \text{ K} = 727°\text{C} \quad \text{and} \quad p_a L = 0.1 \times 5 \text{ bar} \times 1.76 \text{ m} = 88 \text{ bar cm}$$

one gets, interpolating Figure 4.3.15, $\varepsilon_0 \cong 0.15$. The correction factor in Equation (4.3.30b) is calculated from Table 4.3.2 with $P_E = 5 + 0.28 \times 0.5 = 5.14$, $a = 1.1$, $b = 0.23$, $c = 1.47$, and $(p_a L)_m = 0.225$ bar cm. Thus,

$$\frac{\varepsilon}{\varepsilon_0} = 1 - \frac{0.1 \times (-4.14)}{0.33 + 5.14} \exp\left(-1.47\left(\log_{10}\frac{0.225}{88}\right)^2\right) \cong 1$$

and

$$\varepsilon \cong 0.15$$

To calculate the absorptivity ε_0 must be found for a temperature of

$$T_s = 1500 \text{ K} = 1227°\text{C} \quad \text{and} \quad p_a L \frac{T_s}{T_g} = 88 \times 1500/1000 = 132 \text{ bar cm}$$

From Figure 4.3.15 it follows that $\varepsilon_0 \cong 0.15$ again and, with $\varepsilon/\varepsilon_0$ pretty much unchanged, from Equation (4.3.34),

$$\alpha \cong \left(\frac{1000}{1500}\right)^{1/2} \times 0.15 \times 1.00 = 0.122$$

Radiative Properties of Particle Clouds

Nearly all flames are visible to the human eye and are, therefore, called *luminous* (sending out light). Apparently, there is some radiative emission from within the flame at wavelengths where there are no vibration–rotation bands for any combustion gases. This luminous emission is known today to come from tiny *char* (almost pure carbon) particles, call *soot*, which are generated during the combustion process. The "dirtier" the flame is (i.e., the higher the soot content), the more luminous it is.

Radiative Properties of Soot. Soot particles are produced in fuel-rich flames, or fuel-rich parts of flames, as a result of incomplete combustion of hydrocarbon fuels. As shown by electron microscopy, soot particles are generally small and spherical, ranging in size between approximately 50 and 800 Å (0.005 to 0.08 μm), and up to about 3000 Å in extreme cases. While mostly spherical in shape, soot particles may also appear in agglomerated chunks and even as long agglomerated filaments. It has been determined experimentally in typical diffusion flames of hydrocarbon fuels that the volume percentage of soot generally lies in the range between 10^{-4} to 10^{-6}%.

Since soot particles are very small, they are generally at the same temperature as the flame and, therefore, strongly emit thermal radiation in a continuous spectrum over the infrared region. Experiments have shown that soot emission often is considerably stronger than the emission from the combustion gases.

For a simplified heat transfer analysis it is desirable to use suitably defined mean absorption coefficients and emissivities. If the soot volume fraction f_v is known as well as an appropriate spectral average of the complex index of refraction of the soot, $m = n - ik$, one may approximate the spectral absorption coefficient by (Felske and Tien, 1977).

$$\kappa_\lambda = C_0 \frac{f_v}{\lambda} \qquad C_0 = \frac{36\pi nk}{\left(n^2 - k^2 + 2\right)^2 + 4n^2k^2} \tag{4.3.36}$$

and a total, or spectral-average value may be taken as

$$\kappa_m = 3.72 f_v C_0 T / C_2 \tag{4.3.37}$$

where $C_2 = 1.4388$ mK is the second Planck function constant. Substituting Equation (4.3.37) into Equation (4.3.29) gives a total soot cloud emissivity of

$$\varepsilon(f_v TL) = 1 - e^{-\kappa_m L} = 1 - e^{-3.72 C_0 f_v TL/C_2} \tag{4.3.38}$$

Pulverized Coal and Fly Ash Dispersions. To calculate the radiative properties of arbitrary size distributions of coal and ash particles, one must have knowledge of their complex index of refraction as a function of wavelength and temperature. Data for carbon and different types of coal indicate that its real part, *n*, varies little over the infrared and is relatively insensitive to the type of coal (e.g., anthracite, lignite, bituminous), while the absorptive index, *k*, may vary strongly over the spectrum and from coal to coal. If the number and sizes of particles are known and if a suitable average value for the complex index of refraction can be found, then the spectral absorption coefficient of the dispersion may be estimated by a correlation given by Buckius and Hwang, 1980. Substitution into Equation (4.3.29) can then provide an estimate of the total emissivity. If both soot as well as larger particles are present in the dispersion, the absorption coefficients of all constituents must be added before applying Equation (4.3.29).

Mixtures of Molecular Gases and Particulates. To determine the total emissivity of a mixture it is generally necessary to find the spectral absorption coefficient κ_λ of the mixture (i.e., the sum of the absorption coefficient of all contributors), followed by numerical integration of Equation (4.3.29). However, since the molecular gases tend to absorb only over a small part of the spectrum, to some degree of accuracy

$$\varepsilon_{mix} \cong \varepsilon_{gas} + \varepsilon_{particulates} \tag{4.3.39}$$

Equation (4.3.39) gives an upper estimate since overlap effects result in lower emissivity (compare Equation (4.3.31) for gas mixtures).

Heat Exchange in the Presence of a Participating Medium

The calculation of radiative heat transfer rates through an enclosure filled with a participating medium is a challenging task, to say the least. High-accuracy calculations are rare and a topic of ongoing research. There are, however, several simplistic models available that allow the estimation of radiative heat transfer rates, and relatively accurate calculations for some simple cases.

Diffusion Approximation. A medium through which a photon can only travel a short distance without being absorbed is known as *optically thick*. Mathematically, this implies that $\kappa_\lambda L \gg 1$ for a characteristic dimension *L* across which the temperature does not vary substantially. For such an optically thick, nonscattering medium the spectral radiative flux may be calculated from

$$\mathbf{q}_\lambda = -\frac{4}{3\kappa_\lambda} \nabla E_{b\lambda} \tag{4.3.40}$$

similar to Fourier's diffusion law for heat conduction. Note that a medium may be optically thick at some wavelengths, but thin ($\kappa_\lambda L \ll 1$) at others (e.g., molecular gases!). For a medium that is optically thick for all wavelengths, Equation (4.3.40) may be integrated over the spectrum, yielding the total radiative flux

$$\mathbf{q} = -\frac{4}{3\kappa_R} \nabla E_b = -\frac{4}{3\kappa_R} \nabla\left(\sigma T^4\right) = -\frac{16\sigma T^3}{3\kappa_R} \nabla T \tag{4.3.41}$$

where κ_R is the suitably averaged absorption coefficient, termed the *Rosseland-mean absorption coefficient*. For a cloud of soot particles, $\kappa_R \cong \kappa_m$ from Equation (4.3.37) is a reasonable approximation. Equation (4.3.41) may be rewritten by defining a "radiative conductivity" k_R,

$$\mathbf{q} = -k_R \nabla T \qquad k_R = \frac{16\sigma T^3}{3\kappa_R} \tag{4.3.42}$$

This form shows that the diffusion approximation is mathematically equivalent to conductive heat transfer with a (strongly) temperature-dependent conductivity.

Note: More accurate calculations show that, in the absence of other modes of heat transfer (conduction, convection), there is generally a temperature discontinuity near the boundaries ($T_{surface} \neq T_{adjacent\ medium}$), and, unless boundary conditions that allow such temperature discontinuities are chosen, the diffusion approximation will do very poorly in the vicinity of bounding surfaces.

Example 4.3.7

A soot cloud is contained between two walls at $T_1 = 1000$ K and $T_2 = 2000$ K, spaced 1 m apart. The effective absorption coefficient of the medium is $\kappa_R = 10$ m^{-1} and the effective thermal conductivity is $k_c = 0.1$ W/mK. Estimate the total heat flux between the plates (ignoring convection effects).

Solution. For simplicity we may want to assume a constant total conductivity $k = k_c + k_R$, leading to

$$q = -k\frac{dT}{dx} = k\frac{T_2 - T_1}{L}$$

where k_R must be evaluated at some effective temperature. Choosing, based on its temperature dependence,

$$k_R \cong \frac{8\sigma}{3\kappa_R}\left(T_1^3 + T_2^3\right) = \frac{8 \times 5.670 \times 10^{-8}\ \text{W/m}^2\text{K}^4}{3 \times 10/\text{m}}\left(1000^3 + 2000^3\right)\text{K}^3 = 136\frac{\text{W}}{\text{mK}}$$

gives

$$q = (0.1 + 136)\frac{2000 - 1000}{1}\ \frac{\text{W}}{\text{m}^2} = 136\frac{\text{kW}}{\text{m}^2\text{K}}$$

Note that (1) conduction is negligible in this example and (2) the surface emissivities do not enter the diffusion approximation. While a more accurate answer can be obtained by taking the temperature dependence of k_R into account, the method itself should be understood as a relatively crude approximation.

Mean Beam Length Method. Relatively accurate yet simple heat transfer calculations can be carried out if an isothermal, absorbing–emitting, but not scattering medium is contained in an isothermal, black-walled enclosure. While these conditions are, of course, very restrictive, they are met to some degree by conditions inside furnaces. For such cases the local heat flux on a point of the surface may be calculated from

$$q = \left[1 - \alpha\left(L_m\right)\right]E_{bw} - \varepsilon\left(L_m\right)E_{bg} \tag{4.3.43}$$

where E_{bw} and E_{bg} are blackbody emissive powers for the walls and medium (gas and/or particulates), respectively, and $\alpha(L_m)$ and $\varepsilon(L_m)$ are the total absorptivity and emissivity of the medium for a path length L_m through the medium. The length L_m, known as the average *mean beam length*, is a directional average of the thickness of the medium as seen from the point on the surface. On a spectral basis Equation (4.3.43) is exact, provided the above conditions are met and provided an accurate value of the (spectral) mean beam length is known. It has been shown that spectral dependence of the mean beam length is weak (generally less than ±5% from the mean). Consequently, total radiative heat flux at the

surface may be calculated very accurately from Equation (4.3.43), provided the emissivity and absorptivity of the medium are also known accurately. The mean beam lengths for many important geometries have been calculated and are collected in Table 4.3.3. In this table L_o is known as the geometric mean beam length, which is the mean beam length for the optically thin limit ($\kappa_\lambda \to 0$), and L_m is a spectral average of the mean beam length. For geometries not listed in Table 4.3.3, the mean beam length may be estimated from

$$L_o \cong 4\frac{V}{A} \qquad L_m \cong 0.9L_o \cong 3.6\frac{V}{A} \qquad (4.3.44)$$

TABLE 4.3.3   Mean Beam Lengths for Radiation from a Gas Volume to a Surface on Its Boundary

Geometry of Gas Volume	Characterizing Dimension L	Geometric Mean Beam Length L_0/L	Average Mean Beam Length L_m/L	L_m/L_0
Sphere radiating to its surface	Diameter, L = D	0.67	0.65	0.97
Infinite circular cylinder to bounding surface	Diameter, L = D	1.00	0.94	0.94
Semi-infinite circular cylinder to:	Diameter, L = D			
Element at center of base		1.00	0.90	0.90
Entire base		0.81	0.65	0.80
Circular cylinder (height/diameter = 1) to:	Diameter, L = D			
Element at center of base		0.76	0.71	0.92
Entire surface		0.67	0.60	0.90
Circular cylinder (height/diameter = 2) to:	Diameter, L = D			
Plane base		0.73	0.60	0.82
Concave surface		0.82	0.76	0.93
Entire surface		0.80	0.73	0.91
Circular cylinder (height/diameter = 0.5) to:	Diameter, L = D			
Plane base		0.48	0.43	0.90
Concave surface		0.53	0.46	0.88
Entire surface		0.50	0.45	0.90
Infinite semicircular cylinder to center of plane rectangular face	Radius, L = R	—	1.26	—
Infinite slab to its surface	Slab thickness, L	2.00	1.76	0.88
Cube to a face	Edge L	0.67	0.6	0.90
Rectangular $1 \times 1 \times 4$ parallelepipeds:	Shortest edge, L			
To 1×4 face		0.90	0.82	0.91
To 1×1 face		0.86	0.71	0.83
To all faces		0.89	0.81	0.91

where V is the volume of the participating medium and A is its entire bounding surface area.

Example 4.3.8

An isothermal mixture of 10% CO_2 and 90% nitrogen at 1000 K and 5 bar is contained between two large, parallel, black plates, which are both isothermal at 1500 K. Estimate the net radiative heat loss from the surfaces.

Solution. The heat loss may be calculated from Equation (4.3.43), after determining the mean beam length, followed by evaluation of $\varepsilon(L_m)$ and $\alpha(L_m)$. From Table 4.3.3 it is clear that $L_m = 1.76 \times$ thickness of slab = 1.76 m. It turns out that the necessary $\varepsilon(L_m) = 0.15$ and $\alpha(L_m) = 0.122$ have already been calculated in Example 4.3.6. Thus, the heat flux is immediately calculated from Equation (4.3.43) as

$$q = (1 - 0.122)5.670 \times 10^{-8} \times 1500^4 - 0.15 \times 5.670 \times 10^{-8} \times 1000^4$$

$$= 2.44 \times 10^5 \frac{W}{m^2} = 244 \ kW/m^2$$

Defining Terms

Absorptivity: The ability of a medium to absorb (i.e., trap and convert to other forms of energy) incoming radiation; gives the fraction of incoming radiation that is absorbed by the medium.

Absorption coefficient: The ability of a medium to absorb (i.e., trap and convert to other forms of energy) over a unit path length; the reciprocal of the mean distance a photon travels before being absorbed.

Blackbody: Any material or configuration that absorbs all incoming radiation completely. A blackbody also emits the maximum possible amount of radiation as described by Planck's law.

Diffuse surface: A surface that emits and/or reflects equal amounts of radiative energy (photons) into all directions. Or a surface that absorbs and/or reflects equal amounts of radiation independent of incoming direction.

Emissive power: The rate of radiative energy leaving a surface through emission. The maximum amount of emissive power is emitted by a blackbody with a spectral strength described by Planck's law.

Emissivity: The ability of a medium to emit (i.e., convert internal energy into electromagnetic waves or photons) thermal radiation; gives the fraction of emission as compared with a blackbody.

Gray: A medium whose radiative properties (such as absorptivity, emissivity, reflectivity, absorption coefficient) do not vary with wavelength.

Irradiation: Incoming radiative flux onto a surface from outside it.

Network analogy: Expressing radiative heat exchange between surfaces in terms of an electrical network, with heat flux as "current," differences in emissive power as "potentials," and defining radiative resistances.

Opaque medium: A medium of sufficient thickness that absorbs all nonreflected irradiation; no radiation is transmitted through the medium.

Photon: A massless particle carrying energy in the amount of $h\nu$; the quantum mechanical alternative view of an electromagnetic wave carrying radiative energy.

Planck's law: The law describing the spectral distribution of the radiative energy emitted (emissive power) of a blackbody.

Radiosity: Total radiative flux leaving a surface (diffusely), consisting of emitted as well as reflected radiation.

Reflectivity: The ability of an interface, or of a medium or of a composite with a number of interfaces, to reflect incoming radiation back into the irradiating medium.

Semitransparent: See **transparent**.

Spectral value: The value of a quantity that varies with wavelength at a given wavelength; for dimensional quantities the amount per unit wavelength.

Transmissivity: The ability of a medium to let incoming radiation pass through it; gives the fraction of incoming radiation that is transmitted through the medium.

Transparent: The ability of a medium to let incoming radiation pass through it. A medium that lets all radiation pass through it is called transparent, a medium that only allows a part to pass through it is called **semitransparent**.

View factor: The fraction of diffuse radiant energy leaving one surface that is intercepted by another surface.

References

1. Brewster, M.Q. 1992. *Thermal Radiative Transfer & Properties*, John Wiley & Sons, New York.
2. Buckius, R.O. and Hwang, D.C. 1980. Radiation properties for polydispersions: application to coal, *J. Heat Transfer*, 102, 99–103.
3. Felske, J.D. and Tien, C.L. 1977. The use of the Milne-Eddington absorption coefficient for radiative heat transfer in combustion systems, *J. Heat Transfer*, 99(3), 458–465.
4. Hottel, H.C. and Sarofim, A.F. 1967. *Radiation Transfer*, McGraw-Hill, New York.
5. Howell, J.R. 1982. *Catalog of Radiation Configuration Factors*, McGraw-Hill, New York.
6. Leckner, B. 1972. Spectral and total emissivity of water vapor and carbon dioxide, *Combust. Flame*, 19, 33–48.
7. Modest, M.F. 1993. *Radiative Heat Transfer*, McGraw-Hill, New York.
8. Ozisik, M.N. 1973. *Radiative Transfer and Interactions with Conduction and Convection*, John Wiley & Sons, New York.
9. Siegel, R. and Howell, J.R. 1992. *Thermal Radiation Heat Transfer*, 3rd ed., Hemisphere Publishing, New York.
10. Sparrow, E.M. and Cess, R.D. 1978. *Radiation Heat Transfer*, Hemisphere, New York.

4.4   Phase-Change

Boiling and Condensation

Van P. Carey

Introduction

Liquid-vapor phase-change processes play an important role in many technological applications. The virtually isothermal heat transfer associated with boiling and condensation processes makes their inclusion in power and refrigeration processes highly advantageous from a thermodynamic efficiency standpoint. In addition, the high heat transfer coefficients associated with boiling and condensation have made the use of these processes increasingly attractive in the thermal control of compact devices that have high heat dissipation rates. Applications of this type include the use of boiling heat transfer to cool electronic components in computers and the use of compact evaporators and condensers for thermal control of aircraft avionics and spacecraft environments. Liquid-vapor phase-change processes are also of critical importance to nuclear power plant design, both because they are important in normal operating circumstances and because they dominate many of the accident scenarios that are studied as part of design evaluation.

The heat transfer and fluid flow associated with liquid-vapor phase-change processes are typically among the more complex transport circumstances encountered in engineering applications. These processes have all the complexity of single-phase convective transport, plus additional elements resulting from motion of the interface, nonequilibrium effects, and dynamic interactions between the phases. Due to the highly complex nature of these processes, development of methods to accurately predict the associated heat and mass transfer is often a formidable task.

In this section, commonly used variables not defined in the nomenclature are as follows: q'' = surface heat flux, μ_l = liquid viscosity, μ_v = vapor viscosity, Pr_l = liquid Prandtl number, T_w = wall surface temperature, T_{sat} = saturation temperature, c_{pl} = liquid specific heat, k_v = vapor thermal conductivity, g = gravitational acceleration, and x = mass quality.

Boiling

Three mechanisms that play important roles in boiling processes are (1) surface tension effects, (2) surface wetting characteristics of the liquid, and (3) metastable phase stability.

Anyone who has watched small bubbles rise in a carbonated beverage or a pot of boiling water has undoubtedly noticed that the bubbles are almost perfectly spherical, as if an elastic membrane were present at the interface to pull the vapor into a spherical shape. This apparent interfacial tension or *surface tension* σ is equivalent to an energy stored in the interface region per unit area. The energy excess in this region is due to the slightly larger separation of the liquid phase molecules adjacent to the gas phase.

The magnitude of the surface tension for a substance is directly linked to the strength of intermolecular forces in the material. Nonpolar liquids typically have the lowest surface tension. Water and other **polar molecules** have somewhat higher surface tension, and liquid metals, which exhibit metallic bond attraction, have very high surface tension. The surface tension of water at 20°C is 0.0728 N/m, whereas liquid mercury has a surface tension of 0.484 N/m at the same temperature. The surface tension for any pure liquid varies with temperature. It decreases almost linearly with increasing temperature, vanishing altogether at the critical point where the distinction between the phases disappears.

As a result of the surface tension at the interface, the pressure inside a spherical bubble of radius r must exceed that in the surrounding liquid by $2\sigma/r$:

$$P_v = P_l + \frac{2\sigma}{r} \qquad\qquad (4.4.1)$$

By using the relation (1) between the pressure in the two phases it can be shown that for the bubble to be in equilibrium with the surrounding liquid, the liquid must actually be superheated above the saturation temperature for the ambient liquid pressure. The amount of required superheating increases as the radius of curvature of the bubble interface decreases.

The wetting characteristics of the liquid are generally quantified in terms of a *contact angle* between the solid surface and the tangent to the interface at the point where it contacts the solid. This angle is measured through the liquid phase, as shown in Figure 4.4.1. In some systems, the wetting angle established at equilibrium may depend on the fluid motion history. For some systems the contact angle established by liquid advancing over a solid surface is larger than that established when a liquid front recedes over the surface. This behavior is referred to as *contact angle hysteresis*. Contact angle hysteresis can have an important effect on boiling and condensation processes, particularly those involving water.
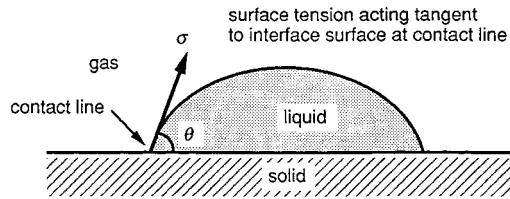

FIGURE 4.4.1 Definition of the contact angle θ.

For a bubble with a specified vapor volume, the contact angle will dictate the radius of curvature of the bubble interface. The wetting behavior in combination with the surface tension effect, thus, determines the level of superheat required for the bubble to be in equilibrium with the surrounding liquid. The liquid must be heated above this superheat level for the bubble to grow. A steady boiling process can be sustained only if the liquid is heated above this threshold superheat level.

It can be shown from basic thermodynamic analysis that a necessary and sufficient condition for phase stability is that

$$\left(\frac{\partial P}{\partial v}\right)_T < 0 \tag{4.4.2}$$

where v is the specific volume. Below the critical temperature, extrapolation of the isotherms for the liquid and vapor phases consistent with an equation of state like the van de Waals equation results in an isotherm shape similar to that shown in Figure 4.4.2.

The locus of points where $(\partial P/\partial v)_T = 0$ are termed *spinodal curves*. Regions of metastable vapor and liquid exist between the saturation curve and the spinodal curves. The effects of surface tension discussed above require that fluid surrounding a vapor bubble be in the metastable superheated liquid region. Predictions of statistical thermodynamics imply that as $(\partial P/\partial v)_T$ approaches zero, the level of fluctuations in a fluid system increases. This, in turn, increases the probability that an embryonic new phase will form as a result of density fluctuations. Initiation of a phase change in this manner is termed *homogeneous nucleation*. Generally, a pure liquid must be heated to nearly 90% of its absolute critical temperature before homogeneous nucleation of vapor bubbles occurs.

In most physical systems of engineering interest, the bulk phase is in contact with solid walls of the containing structures, or solid particulate contaminants. These solid phases may provide nucleation sites where phase change may occur if the system state is driven into the metastable range. Nucleation of vapor bubbles may preferentially occur at low liquid superheat levels in crevices in the solid surface where gas is trapped. This type of nucleation at the solid surface of a containment wall is categorized as *heterogeneous nucleation.* Because solid containment walls usually contain microscopic crevice-type
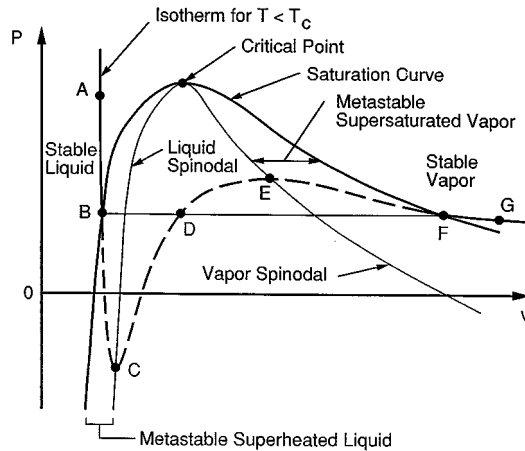
FIGURE 4.4.2 Spinodal lines and metastable regions on a *P–v* diagram.

imperfections, heterogeneous nucleation is more common than homogeneous nucleation in systems where boiling occurs.

Vapor entrapment in crevices of the heated walls of evaporator heat exchangers usually makes it easier to initiate the vaporization process. Vapor bubbles grow from these crevices until buoyancy or drag on the bubbles exceeds the surface tension force holding the droplet to the solid surface. The bubble then releases into the bulk liquid. A small remnant of vapor remains in the crevice after a bubble releases, and this remnant grows in size as further vaporization occurs until the bubble grows out of the crevice again. The result is a cyclic process of bubble growth and release known as the *ebullition cycle*. Crevices at which the ebullition cycle is sustained are said to be active nucleation sites. When the ebullition process occurs at many sites over a heated surface, the overall process is referred to as **nucleate boiling**, which is one possible mode of **pool boiling**.

Pool Boiling

Vaporization of liquid at the surface of a body immersed in an extensive pool of motionless liquid is generally referred to as pool boiling. The nature of the pool boiling process varies considerably depending on the conditions at which boiling occurs. The level of heat flux, the thermophysical properties of the liquid and vapor, the surface material and finish, and the physical size of the heated surface all may have an effect on the boiling process.

The regimes of pool boiling are most easily understood in terms of the so-called boiling curve: a plot of heat flux q'' vs. wall superheat $T_w - T_{sat}$ for the circumstances of interest. Many of the features of the classic pool boiling curve were determined in the early investigations of pool boiling conducted by Nukiyama (1934). Strictly speaking, the classic pool boiling curve defined by the work of this investigator and others applies to well-wetted surfaces for which the characteristic physical dimension L is large compared to the bubble or capillary length scale L_b defined as

$$L_b = \sqrt{\frac{\sigma}{g(\rho_l - \rho_v)}} \qquad (4.4.3)$$

The discussion in this section is limited to pool boiling of wetting liquids on surfaces with dimensions large compared with L_b. Additional information on features of the boiling curve when the liquid poorly wets the surface or when L/L_b is small can be found in Carey (1992). To make this discussion concrete, we will assume that the ambient liquid surrounding the immersed body is at the saturation temperature for the ambient pressure. If the surface temperature of the immersed body is controlled and slowly
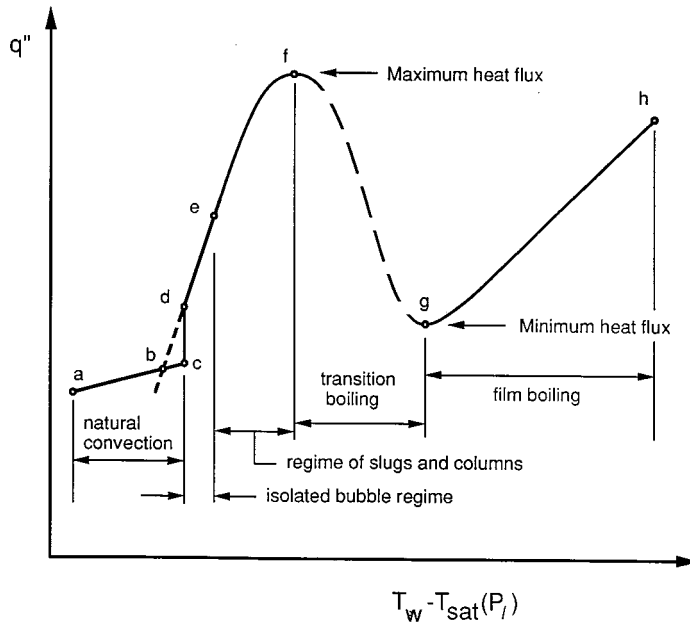
FIGURE 4.4.3 Pool boiling regimes for an independently controlled surface temperature.

increased, the boiling curve will look similar to that shown in Figure 4.4.3. The axes in this plot are logarithmic scales. The regimes of pool boiling encountered for an upward-facing horizontal flat surface as its temperature is increased are also indicated in Figure 4.4.3. The lateral extent of the surface is presumed to be much larger than L_b. At very low wall superheat levels, no nucleation sites may be active and heat may be transferred from the surface to the ambient liquid by natural convection alone and q'' increases slowly with $T_w - T_{sat}$.

Eventually, the superheat becomes large enough to initiate nucleation at some of the cavities on the surface. This *onset of nucleate boiling* (ONB) condition occurs at point *c* in Figure 4.4.3. Once nucleate boiling is initiated, any further increase in wall temperature causes the system operating point to move upward along section *d-f* of the curve in Figure 4.4.3. This portion of the curve corresponds to the nucleate boiling regime. The active sites are few and widely separated at low wall superheat levels. This range of conditions, corresponding to segment *d-e* of the curve, is sometimes referred to as the *isolated bubble regime.*

With increasing surface superheat, more sites become active, and the bubble frequency at each site generally increases. Eventually, the active sites are spaced so closely that bubbles from adjacent sites merge together during the final stages of growth and release. Vapor is being produced so rapidly that bubbles merging together form columns of vapor slugs that rise upward in the liquid pool toward its free surface. This higher range of wall superheat, corresponding to segment *e-f* of the boiling curve in Figure 4.4.3, is referred to as the *regime of slugs and columns.*

Increasing the wall superheat and heat flux within the regime of slugs and columns produces an increase in the flow rate of vapor away from the surface. Eventually, the resulting vapor drag on the liquid moving toward the surface becomes so severe that liquid is unable to reach the surface fast enough to keep the surface completely wetted with liquid. Vapor patches accumulate at some locations and evaporation of the liquid between the surface and some of these patches dries out portions of the surface.

If the surface temperature is held constant and uniform, dry portions of the surface covered with a vapor film will locally transfer a much lower heat flux than wetted portions of the surface where nucleate boiling is occurring. Because of the reduction in heat flux from intermittently dry portions of the surface, the mean overall heat flux from the surface is reduced. Thus, increasing the wall temperature within the

slugs and columns region ultimately results in a peaking and rollover of the heat flux. The peak value of heat flux is called the **critical heat flux** (CHF), designated as point *f* in Figure 4.4.3

If the wall temperature is increased beyond the critical heat flux condition, a regime is encountered in which the mean overall heat flux decreases as the wall superheat increases. This regime, which is usually referred to as the **transition boiling** regime, corresponds to segment *f-g* on the boiling curve shown in Figure 4.4.3. The transition boiling regime is typically characterized by rapid and severe fluctuations in the local surface heat flux and/or temperature values (depending on the imposed boundary condition). These fluctuations occur because the dry regions are generally unstable, existing momentarily at a given location before collapsing and allowing the surface to be rewetted.

The vapor film generated during transition boiling can be sustained for longer intervals at higher wall temperatures. Because the intermittent insulating effect of the vapor blanketing is maintained longer, the time-averaged contributions of the blanketed locations to the overall mean heat flux are reduced. The mean heat flux from the surface thus decreases as the wall superheat is increased in the transition regime. As this trend continues, eventually a point is reached at which the surface is hot enough to sustain a stable vapor film on the surface for an indefinite period of time. The entire surface then becomes blanketed with a vapor film, thus making the transition to the **film boiling** regime. This transition occurs at point *g* in Figure 4.4.3.

Within the film boiling regime, the heat flux monotonically increases as the superheat increases. This trend is a consequence of the increased conduction and/or convection transport due to the increased driving temperature difference across the vapor film. Radiative transport across the vapor layer may also become important at higher wall temperatures.

Once a surface is heated to a superheat level in the film boiling regime, if the surface temperature is slowly decreased, in general the system will progress through each of the regimes described above in reverse order. However, the path of the boiling curve may differ significantly from that observed for increasing wall superheat, depending on whether the surface heat flux or temperature is controlled.

Experimental evidence summarized by Witte and Lienhard (1982) implies that the path of the transition boiling curve is determined, to a large degree, by the wetting characteristics of the liquid on the solid surface. For a given wall superheat level in the transition boiling regime, a higher heat flux is generally obtained if the liquid wets the surface than if it poorly wets the surface. For systems that exhibit contact angle hysteresis, the transition boiling curves obtained for decreasing and increasing wall superheat may therefore be somewhat different. The transition boiling curve for decreasing wall superheat may be significantly below that for increasing superheat for such circumstances, as indicated in Figure 4.4.4.

For an electrically heated surface, the rise in temperature associated with the jump from nucleate to film boiling at the critical heat flux is very often large enough to melt component materials and burn out the component. As a result, the critical heat flux is often referred to as the *burnout heat flux* to acknowledge the potentially damaging effects of applying this heat flux level to components cooled by nucleate boiling. Once the jump to film boiling has been made, any further increase in applied heat flux increases the wall superheat, and the system follows basically the same film boiling curve as in the temperature-controlled case.

Correlations of nucleate pool boiling heat transfer data have typically been used as tools to predict nucleate boiling heat transfer in engineering systems and heat exchangers. Many investigators have proposed methods of correlating data of this type; so many, in fact, that a complete discussion of them all could easily fill a major portion of this section. In this section, three of the more commonly used correlation methods will be mentioned. However, before proceeding, two aspects of the interpretation of such correlations are worth noting. First, experimental data indicate that the subcooling of the liquid pool has a negligible effect on the nucleate boiling heat transfer rate. Consequently, the pool boiling correlations are generally regarded as being valid for both subcooled and saturated nucleate boiling. Second, it has also been observed that at moderate to high heat flux levels, a pool boiling heat transfer correlation developed for one heated surface geometry in one specific orientation often works reasonably well for other geometries and/or other orientations. Hence, although a correlation was developed for a
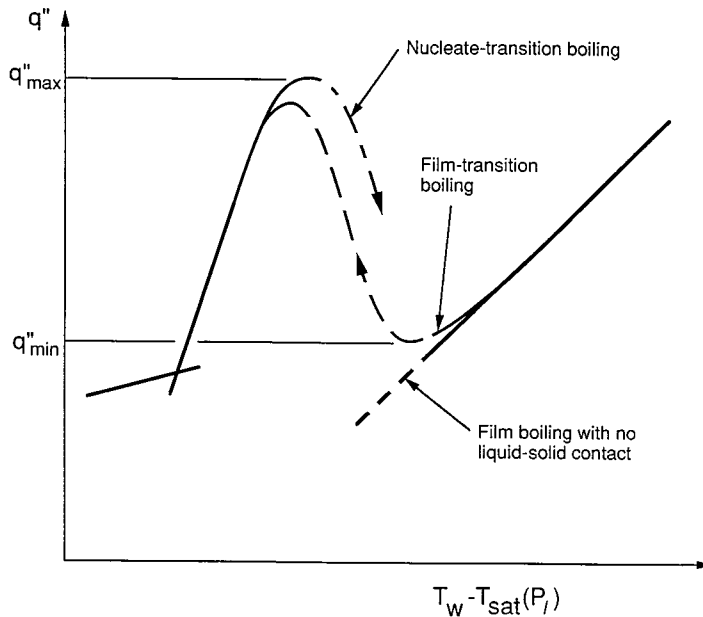
FIGURE 4.4.4 Relative locations of the nucleate transition and film transition portions of the pool boiling curve.

specific geometry and orientation, it may often be used for other geometries, at least at moderate to high heat flux levels.

Having taken note of the above points, a commonly used correlation for nucleate boiling heat transfer developed by Rohsenow (1962) is

$$
\frac{q''}{\mu_l h_{fg}} \left[\frac{\sigma}{g(\rho_l - \rho_v)} \right]^{1/2} = \left(\frac{1}{C_{sf}} \right)^{1/r} \mathrm{Pr}_l^{-s/r} \left[\frac{c_{pl}\left[T_w - T_{sat}(P_l)\right]}{h_{fg}} \right]^{1/r}
\tag{4.4.4}
$$

Values of $r = 0.33$ and $s = 1.7$ are recommended for this correlation, but for water s should be changed to 1.0. The values of C_{sf} in this correlation vary with the type of solid surface and the type of fluid in the system. This empirically accounts for material property and/or wetting angle effects. Recommended values of C_{sf} for specific liquid–solid combinations are given by Rohsenow (1962), but whenever possible, an experiment should be conducted to determine the appropriate value of C_{sf} for the particular solid–liquid combination of interest. If this is not possible, a value of $C_{sf} = 0.013$ is recommended as a first approximation.

As noted previously, the pool boiling curve generally exhibits a maximum heat flux or CHF at the transition between nucleate and transition boiling. This peak value is the maximum level of heat flux from the surface which the system can provide in a nonfilm-boiling mode at a given pressure. The mechanism responsible for the CHF has been the subject of considerable investigation and debate over the past five decades. As the heat flux increases, bubbles generated at the surface coalesce to form vapor columns or jets. Perhaps the most widely cited CHF model postulates that the CHF condition occurs when Helmholtz instability of the large vapor jets leaving the surface distorts the jets, blocking liquid flow to portions of the heated surface. Continued vaporization of liquid at locations on the surface which are starved of replacement liquid than leads to formation of a vapor blanket over part or all of the surface. According to Zuber (1959) for a flat horizontal surface, the predicted maximum heat flux q''_{max} is

$$q''_{max} = 0.131 \rho_v h_{fg} \left[\frac{\sigma_g (\rho_l - \rho_v)}{\rho_v^2} \right]^{1/4} \tag{4.4.5}$$

but Lienhard and Dhir (1973) recommend that the constant 0.131 in the above relation be replaced with 0.141. Other geometries are treated by Lienhard et al. (1973) and Lienhard and Dhir (1973b). An alternative model has been proposed by Haramura and Katto (1983).

Lienhard and Witte (1985) discuss the development and limitations of hydrodynamic CHF theories.

As shown in the Figure 4.4.3, the boundary between the transition boiling regime and the film boiling regime corresponds to a minimum in the heat flux vs. superheat curve. This condition is referred to as the **minimum heat flux** condition, referred to as the *Leidenfront point*. The minimum heat flux corresponds approximately to the lowest heat flux which will sustain stable film boiling.

For an infinite flat (upward-facing) heated surface, vapor generated at the interface during stable film boiling is released as bubbles at the nodes of a standing two-dimensional Taylor wave pattern. The following relation for the minimum heat flux q''_{min} derived by Zuber (1959) and Berenson (1961).

$$q''_{min} = 0.09 \rho_v h_{fg} \left[\frac{\sigma_g (\rho_l - \rho_v)}{(\rho_l + \rho_v)^2} \right]^{1/4} \tag{4.4.6}$$

q''_{min} correlations have been developed by Lienhard and Wong (1964) for horizontal cylinders and Gunnerson and Cronenberg (1980) for spheres.

In film boiling, transport of heat across the vapor film from the wall to the interface may occur by convection, conduction, and radiation. The radiation contribution depends on the nature of the solid surface, but when the radiation effect is small, the heat transfer for film boiling is independent of the material properties and finish of the surface. For buoyancy-driven laminar film boiling over a vertical flat isothermal surface in a pool of saturated liquid, the local heat transfer coefficient from the surface can be obtained from the following relation:

$$h = \left[\frac{k_v^3 g \rho_v (\rho_l - \rho_v) h_{fg}}{4 \mu_v (T_w - T_{sat}) x} \right]^{1/4} \tag{4.4.7}$$

At low surface temperatures, radiation effects are negligible and consideration of convective transport alone is sufficient to predict the heat transfer. At higher temperatures radiation effects must also be included. If the vapor in the film absorbs and emits radiation at infrared wavelengths, a detailed treatment of the radiation interaction with the vapor may be necessary to accurately predict the film boiling heat transfer.

Additional information mechanisms such as interfacial waves, turbulence, and variable properties is summarized in Carey (1992).

Transition pool boiling has traditionally been interpreted as a combination of nucleate and film boiling alternately occurring over the heated surface, and a model of transition boiling that accounts for contact angle effects has been proposed by Ramilison and Lienhard (1987).

Internal Convective Boiling

Flow boiling in tubes is perhaps the most complex convective process encountered in applications. In most evaporator and boiler applications, the flow is either horizontal or vertically upward. Figure 4.4.5 schematically depicts a typical low-flux vaporization process in a horizontal round tube. In this example liquid enters as subcooled liquid and leaves as superheated vapor. As indicated in Figure 4.4.5, the flow undergoes transitions in the boiling regime and the two-phase flow regime as it proceeds down the tubes. The regimes encountered depend on the entrance conditions and the thermal boundary conditions at the
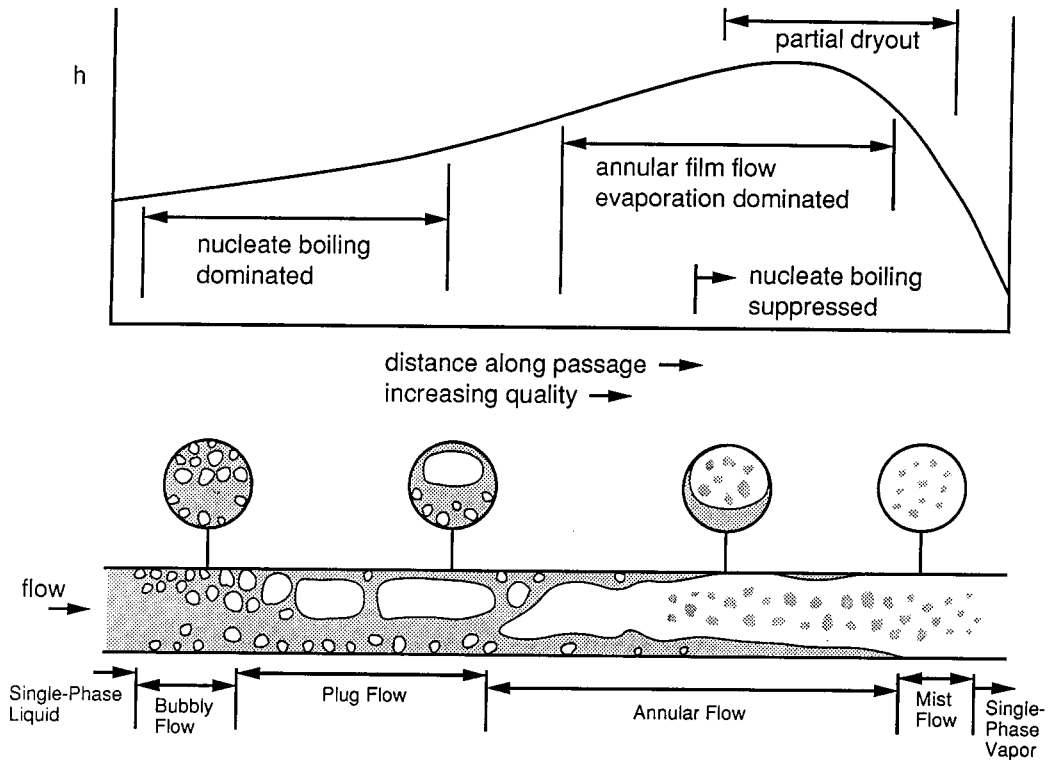
FIGURE 4.4.5 Qualitative variation of the heat transfer coefficient *h* and flow regime with quality for internal convective boiling in a horizontal tube at moderate wall superheat.

tube wall. At low quality the vaporization process is dominated by nucleate boiling, with convective effects being relatively weak. As the quality increases, the flow quickly enters the annular film flow regime in which convective evaporation of the annular liquid film is the dominant heat transfer mechanism. Often the conditions are such that liquid droplets are often entrained in the core vapor flow during annular flow evaporation. Eventually, the annular film evaporates away, leaving the wall dry. Mist-flow evaporation of entrained liquid droplets continues in the post-dryout regime until only vapor remains. Similar, sequences of flow and boiling regimes occurring in vertical upward flow, as indicated in Figure 4.4.6.

The boiling regime trends shown in Figures 4.4.5 and 4.4.6 are typical for low heat flux vaporization processes. At high wall superheat levels, transition boiling or film boiling can also occur. The transition from nucleate boiling to one of these regimes is termed a *departure from nucleate boiling* (DNB) or the CHF condition. However, the heat transfer performance of an evaporator under transition or film boiling conditions is so poor that equipment is not usually designed to operate under such conditions.

Because low-quality or subcooled flow boiling are nucleate boiling dominated, the heat transfer coefficient in these regimes is often predicted using a nucleate boiling correlation developed as a fit to pool boiling data. The usefulness of such an approach is a consequence of the fact that for most conditions of practical interest, nucleate boiling heat transfer is only weakly affected by liquid subcooling or liquid bulk convection.

For saturated convective boiling prior to dryout, relations to predict the heat transfer coefficient have typically been formulated to impose a gradual suppression of nucleate boiling and gradual increase in liquid film evaporation heat transfer as the quality increases. A number of correlations based on such an approach have been developed. An early correlation of this type developed by Chen (1966) has been widely used. One of the better methods of this type is the recently developed correlation of Kandlikar
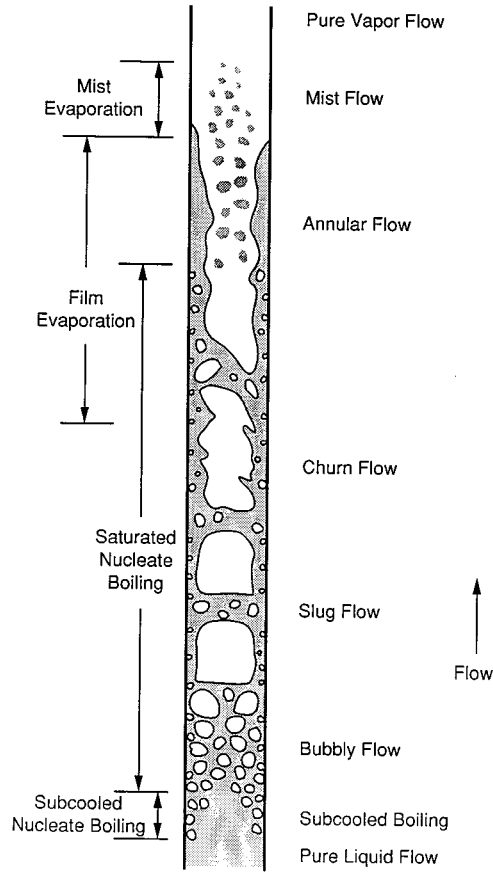
FIGURE 4.4.6 Flow regimes and boiling mechanisms for upflow convective boiling in a vertical tube at moderate wall superheat.

(1989) which has been fit to a broad spectrum of data for both horizontal and vertical tubes. For this method the heat transfer coefficient for a tube of diameter D is given by

$$h = h_l \left[C_1 Co^{C_2} \left(25 \mathrm{Fr}_{le} \right)^{C_5} + C_3 Bo^{C_4} F_K \right] \qquad (4.4.8)$$

where

$$Co = \left(\frac{1-x}{x} \right)^{0.8} \left(\frac{\rho_v}{\rho_l} \right)^{0.5} \qquad (4.4.9)$$

$$Bo = q'' / G h_{fg} \qquad (4.4.10)$$

$$Fr_{le} = G^2 / \rho_l^2 g D \qquad (4.4.11)$$

and h_l is the single-phase heat transfer coefficient for the liquid phase flowing alone in the tube computed as

$$h_l = 0.023 \left(\frac{k_l}{D} \right) \left(\frac{G(1-x)D}{\mu_l} \right)^{0.8} \mathrm{Pr}_l^{0.4} \qquad (4.4.12)$$

The constants $C_1 - C_5$ are given in Table 4.4.1. The factor F_K is a fluid-dependent parameter. For water, $F_K = 1$. For R-12 and nitrogen, recommended values of F_K are 1.50 and 4.70, respectively. Values of F_K for a variety of other fluids can be obtained from Kandlikar (1989).

TABLE 4.4.1   Constants for the Correlation of Kandlikar (1987)

	$Co < 0.65$ (Convective Region)	$Co \geq 0.65$ (Nucleate Boiling Region)
C_1	1.1360	0.6683
C_2	–0.9	–0.2
C_3	667.2	1058.0
C_4	0.7	0.7
$C_5{}^a$	0.3	0.3

[a] $C_5 = 0$ for vertical tubes and horizontal tubes with $\mathrm{Fr}_{le} > 0.04$.

Methods for predicting the conditions at which dryout or a DNB transition occurs have typically been empirical in nature. Based on fits to extensive data, Levitan and Lantsman (1975) recommended the following relations for the DNB heat flux and the quality at which dryout occurs during flow boiling of water in a tube with an 8-mm diameter.

$$q''_{\mathrm{crit}} = \left[10.3 - 7.8 \left(\frac{P}{98} \right) + 1.6 \left(\frac{P}{98} \right)^2 \right] \left(\frac{G}{1000} \right)^{1.2\left\{ [0.25(P-98)/98]-x \right\}} e^{-1.5x} \qquad (4.4.13)$$

$$x_{\mathrm{crit}} = \left[0.39 + 1.57 \left(\frac{P}{98} \right) - 2.04 \left(\frac{P}{98} \right)^2 + 0.68 \left(\frac{P}{98} \right)^3 \right] \left(\frac{G}{1000} \right)^{-0.5} \qquad (4.4.14)$$

In the above relations, q''_{crit} is in MW/m², P is the pressure in bar, and G is in kg/m²sec. To obtain values of q''_{crit} and x_{crit} for diameters other than 8 mm, Levitan and Lantsman (1975) recommended that the 8-mm values from the above relations be corrected as follows:

$$q''_{\mathrm{crit}} = \left(q''_{\mathrm{crit}} \right)_{8\mathrm{mm}} \left(\frac{8}{D} \right)^{1/2} \qquad (4.4.15)$$

$$x_{\mathrm{crit}} = \left(x_{\mathrm{crit}} \right)_{8\mathrm{mm}} \left(\frac{8}{D} \right)^{0.15} \qquad (4.4.16)$$

where D is the diameter in millimeters. A good generalized empirical correlation for predicting dryout or CHF conditions in vertical uniformly heated tubes is that recently proposed by Katto and Ohno (1984).

In many cases, post-dryout mist flow evaporation is driven primarily by convective transport from the tube wall to the gas and then to the entrained droplets. In some circumstances, impingement of droplets onto the heat surface and radiation interactions may also be important. In cases where convection is dominant, predictions of the heat transfer coefficient have been developed by modifying a single-phase correlation for the entire flow as vapor with a correction factor which accounts for the presence of the entrained droplets. Often this correction factor has been presumed to be a function of property ratios. An example of such an approach is the correlation of Dougall and Rohsenow (1963) for which the heat transfer coefficient h is given by

$$\frac{hD}{k_v} = 0.023\left[\left(\frac{GD}{\mu_v}\right)\left(x + \frac{\rho_v}{\rho_l}(1-x)\right)\right]^{0.8} \mathrm{Pr}_{v,\mathrm{sat}}^{0.4} \qquad (4.4.17)$$

For further information on mechanisms of convective boiling, see the texts of Collier (1981), Stephan (1992), and Carey (1992).

Condensation

As in the case of boiling, surface tension effects, surface wetting characteristics, and metastable phase stability also can play important roles in condensation processes. As a result of interfacial tension, the pressure inside a spherical liquid droplet of radius r must exceed that in the surrounding liquid by $2\sigma/r$. A consequence of this and basic thermodynamics is that at equilibrium the surrounding vapor must actually be slightly supersaturated. The amount of supersaturation required at equilibrium increases as the radius of curvature of the bubble interface decreases.

For a liquid droplet on a solid surface with a specified volume, the wetting contact angle dictates the radius of curvature of the droplet interface. Because of the linkage between the interface curvature and the required equilibrium supersaturation, the wetting behavior thus determines the level above which the vapor supersaturation must be raised for the droplet to grow. Steady condensation on the droplet interface can be sustained only if the vapor is driven beyond this supersaturation level by cooling or depressurization. For such conditions, the vapor is in the metastable supersaturated range indicated in Figure 4.4.2.

Condensation on external surfaces of a body immersed in a gas phase generally falls into one or two categories: **dropwise condensation** or **film condensation**. In dropwise condensation, the liquid-phase condensate collects as individual droplets which grow in size with time on the cold surface. This mode of condensation is most likely when the liquid poorly wets the solid surface. When the condensation rate is high or the liquid readily wets the surface, a film of liquid condensate covers the solid surface, and the process is referred to as film condensation.

Dropwise Condensation. Dropwise condensation may occur on a solid surface cooled below the saturation temperature of a surrounding vapor when the surface is poorly wetted except at locations where well-wetted contaminant nuclei exist. The poorly wetted surface condition can result from contamination or coating of the surface with a substance which is poorly wetted by the liquid phase of the surrounding vapor. In practice, this can be achieved for steam condensation by (1) injecting a nonwetting chemical into the vapor which subsequently deposits on the surface, (2) introducing a substance such as a fatty (i.e., oleic) acid or wax onto the solid surface, or (3) by permanently coating the surface with a low-surface-energy polymer or a noble metal. The effects of the first two methods are generally temporary, since the resulting surface films eventually are dissolved or eroded away.

During dropwise condensation, the condensate is usually observed to appear in the form of droplets which grow on the surface and coalesce with adjacent droplets. When droplets become large enough, they are generally removed from the surface by the action of gravity or drag forces resulting from the motion of the surrounding gas. As the drops roll or fall from the surface they merge with droplets in their path, effectively sweeping the surface clean of droplets. Droplets then begin to grow anew on the freshly-exposed solid surface. This sweeping and renewal of the droplet growth process is responsible for the high heat transfer coefficients associated with dropwise condensation. Theoretical aspects of dropwise condensation are described in two publications by Tanaka (1975, 1979). A discussion of correlations for the heat transfer coefficient associated with dropwise condensation is provided in the review article by Merte (1973).

External Film Condensation. If the liquid phase fully wets a cold surface in contact with a vapor near saturation conditions, the conversion of vapor to liquid will take the form of film condensation. As the name implies, the condensation takes place at the interface of a liquid film covering the solid surface. Because the latent heat of vaporization must be removed at the interface to sustain the process, the rate

of condensation is directly linked to the rate at which heat is transported across the liquid film from the interface to the surface.

The classic integral analysis of Nusselt (1916) for laminar falling-film condensation on a vertical surface considers the physical circumstances shown in Figure 4.4.7. The surface exposed to a motionless ambient of saturated vapor is taken to be isothermal with a temperature below the saturation temperature. Note that although a vertical surface is considered here, the analysis is identical for an inclined surface, except that the gravitational acceleration g is replaced by $g \sin \Omega$, with Ω being the angle between the surface and the horizontal. Because the liquid film flows down the surface because of gravity, this situation is sometimes referred to as *falling-film condensation*.
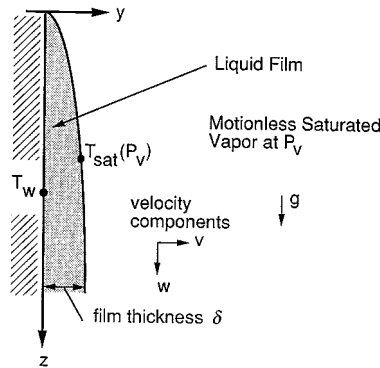

FIGURE 4.4.7 System model for the Nusselt analysis of falling-film condensation.

In its simplest form, the classic Nusselt analysis incorporates the following idealizations: (1) laminar flow, (2) constant properties, (3) that subcooling of liquid is negligible in the energy balance, (4) that inertia effects are negligible in the momentum balance, (5) that the vapor is stationary and exerts no drag, (6) that the liquid-vapor interface is smooth, and (7) that heat transfer across film is only by conduction (convection is neglected). With these idealizations, the following relation for the local heat transfer coefficient h can be obtained

$$\frac{hz}{k_l} = \left[\frac{\rho_l \left(\rho_l - \rho_v \right) g h_{fg} z^3}{4 k_l \mu_\ell \left(T_{\text{sat}} - T_w \right)} \right]^{1/4} \tag{4.4.18}$$

Modified versions of this analysis have been subsequently developed which relax many of these assumptions. Laminar film condensation on a vertical surface can also be analyzed with a full boundary layer formulation. An example of this type of approach is the analysis presented by Sparrow and Gregg (1959).

The analyses described above do not include two physical mechanisms which can significantly affect the transport: (1) the effects of waves on the liquid-vapor interface and (2) interfacial vapor shear drag on the interface. The effects of interfacial shear have been studied analytically by numerous investigators. The effects of surface waves on laminar film condensation are more difficult to incorporate into theoretical analyses. In general, interfacial waves are expected to enhance convective heat transport in the film since it intermittently thins the film, increases the interfacial area, and induces mixing. Because of these effects, laminar film condensation heat transfer data are often significantly higher than the values predicted by simple boundary layer models.

As for any boundary layer flow, when the film Reynolds number becomes large enough, it is expected that a transition to turbulent flow will occur. Eddy diffusivity models of the resulting turbulent transport have been developed by Seban (1954), Dukler (1960), and others. This methodology was later extended to evaporation of a falling liquid film (see, for example, Mills and Chung, 1973).

Subsequent studies (see, for example, Mills and Chung, 1973) have suggested that the presence of the interface tends to damp larger turbulent eddies near the interface in the liquid film. This implies that a viscous sublayer exists at the interface as well as at the wall. Recent efforts to model turbulent falling-film evaporation and condensation processes have therefore included a variation of the eddy viscosity in which it goes to zero at both the wall and the interface. The analysis tools and correlations described above work reasonably well for values of liquid Prandtl number above 1. However, deviation of the predictions using these methods from heat transfer data for liquid metals can be quite significant.

Because of its importance to the design of tube-and-shell condensers, condensation on the outside of horizontal tubes has been the subject of numerous studies. The length of the tube perimeter over which the condensate flows is usually small for commonly used tubes. Consequently, the film Reynolds number is usually low and the flow in the liquid film is laminar.

With slight modification, the Nusselt (1916) analysis of laminar falling-film condensation over a flat plate can be adapted to film condensation on an isothermal horizontal cylinder. Doing so yields the following relation for the mean heat transfer coefficient:

$$\frac{\bar{h}D}{k_l} = 0.728\left[\frac{(\rho_l - \rho_v)gh_{fg}D^3\mathrm{Pr}_l}{\rho_l v_l^2 c_{pl}(T_{\mathrm{sat}} - T_w)}\right]^{1/4} \tag{4.4.19}$$

Selin (1961) found that better agreement with film condensation data for horizontal tubes was obtained by replacing the constant factor in Equation (4.4.19) by 0.61. Correlations similar to the single-tube relation above have also been developed for the average condensation heat transfer coefficient for banks of round tubes.

Analytical treatment of laminar film condensation on a sphere is virtually the same as that for a horizontal cylinder. The only differences result from the angular variation of the body perimeter because of the spherical geometry. A general analytical prediction of the local heat transfer coefficient for laminar film condensation on arbitrary axisymmetric bodies has been developed by Dhir and Lienhard (1971).

Condensation in the Presence of a Noncondensable Gas. In nature and in a number of technological applications, condensation of one component vapor in a mixture may occur in the presence of other noncondensable components. The most common example is the condensation of water vapor in the air on a cold solid surface. If the component gases are considered to be a mixture of independent substances, condensation of one component vapor will occur if the temperature of the surface is below the saturation temperature of the pure vapor at its partial pressure in the mixture. This temperature threshold is referred to as the *dew point* of the mixture.

Because only the vapor is condensed, the concentration of the noncondensable gas at the interface is higher than its value in the far ambient. This, in turn, decreases the partial pressure of the vapor at the interface below its ambient value. The corresponding saturation temperature at the interface is therefore lower than the bulk temperature. The resulting depression of the interface temperature generally reduces the condensation heat transfer rate below that which would result for pure vapor alone under the same conditions. Space limitations here preclude a detailed discussion of the effects of noncondensable gases. The interested reader may find more-extensive discussions of this topic in the references by Collier (1981) and Carey (1992).

Internal Convective Condensation. In most power and refrigeration systems, the flow in the condenser is either horizontal or vertically downward. Figure 4.4.8 schematically depicts a typical condensation process in a horizontal round tube. Superheated vapor enters the tube and at the exit end the liquid is subcooled. At a point some distance downstream of the entrance, vapor begins to condense on the walls of the tube. The location at which this occurs is at or slightly before the bulk flow reaches the equilibrium saturation condition. In most condensers, the liquid readily wets the interior of the tube and at high vapor volume fractions the liquid forms a thin liquid film on the interior wall of the tube.
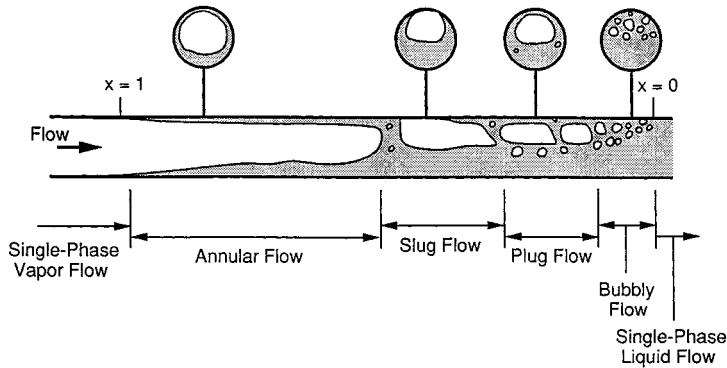
FIGURE 4.4.8 Flow regimes during horizontal cocurrent flow with condensation.

The vapor velocity is generally high at the inlet end of the condenser tube, and the liquid film is driven along the tube by strong vapor shear on the film. At low vapor flow rates, some stratification may occur and the film may be thicker on the bottom of the horizontal tube. At high vapor flow rates, turbulent stresses acting on the liquid may tend to keep the thickness of the liquid film nominally uniform over the perimeter of the tube.

In most condenser applications, shear-dominated annular flow persists to very low qualities and the overwhelming majority of the heat transfer occurs in this regime. The very last stage of the condensation process, corresponding to qualities less than a few percent, may occur in slug, plug, or bubbly two-phase flow. Generally these regimes represent such a small portion of the overall heat transfer in the condenser that some inaccuracy in estimating the heat transfer coefficient for them is tolerated. As a first estimate, the heat transfer coefficient may be predicted using a correlation for pure single-phase liquid flow in the tube at the same total flow rate, or a correlation for annular flow condensation may simply be extrapolated to zero quality.

Because most of the heat duty occurs in the annular flow regime, accurate prediction of the overall heat transfer performance of the condenser requires a predictive methodology that accurately treats the transport in this regime. For this reason, the form of most correlation methods for predicting local convective condensation heat transfer coefficients are optimized to match data in the annular flow regime. One example of such a correlation is the following relation for the local heat transfer coefficient for annular flow condensation proposed by Traviss et al. (1973):

$$\frac{hD}{k_l} = \frac{0.15\mathrm{Pr}_l\mathrm{Re}_l^{0.9}}{F_T}\left[\frac{1}{X_{tt}} + \frac{2.85}{X_{tt}^{0.476}}\right] \tag{4.4.20}$$

where

$$\mathrm{Re}_l = \frac{G(1-x)D}{\mu_l}, \qquad X_{tt} = \left(\frac{1-x}{x}\right)^{0.9}\left(\frac{\rho_v}{\rho_l}\right)^{0.5}\left(\frac{\mu_l}{\mu_v}\right)^{0.1}$$

and F_T is given by

$$F_T = 5\mathrm{Pr}_l + 5\ln\left\{1 + 5\mathrm{Pr}_l\right\} + 2.5\ln\left\{0.0031\mathrm{Re}_l^{0.812}\right\} \quad \text{for} \quad \mathrm{Re}_l > 1125$$

$$= 5\mathrm{Pr}_l + 5\ln\left\{1 + \mathrm{Pr}_l\left(0.0964\mathrm{Re}_l^{0.585} - 1\right)\right\} \quad\quad \text{for} \quad 50 < \mathrm{Re}_l < 1125$$

$$= 0.707\mathrm{Pr}_l\mathrm{Re}_l^{0.5} \quad\quad\quad\quad\quad\quad\quad\quad\quad \text{for} \quad \mathrm{Re}_l < 50$$

Carey (1992) has shown that the generic form of this correlation can be derived from a theoretical model of annular flow condensation in a round tube. Several correlations of this general type have been developed as fits to experimental data; see Carey (1992) for a summary. The predictions of these correlations may vary significantly for a given set of conditions. When possible, a correlation should be selected which has been tested against data for conditions close to those for the application of interest.

A correlation methodology that can be used to predict internal convective condensation heat transfer for slug, plug, or wavy stratified flow has also been proposed by Rossen and Meyers (1965). To predict the overall heat transfer performance of a condenser, methods to predict the local heat transfer coefficient must be combined with a scheme to numerically integrate finite-difference forms of the energy, mass, and momentum balances in the tube. For further information on such schemes see the references by Collier (1981) and Carey (1992) (Figure 4.4.9).
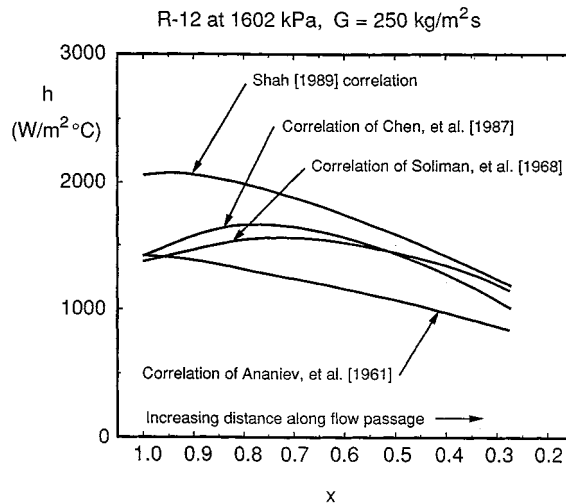
FIGURE 4.4.9 Comparison of the variation of *h* with *x* predicted by four correlation methods for internal convective condensation. References cited in this figure are listed in chapter 11 of Carey (1992).

Defining Terms

Critical heat flux (CHF): A maximum heat flux condition that characterizes the transition between nucleate boiling and transition boiling or film boiling.

Dropwise condensation: Condensation of vapor into liquid in discrete droplets, usually attained when a cold surface is poorly wetted by the liquid phase.

Film boiling: Generation of vapor at the interface of a vapor film which entirely covers the hot surface.

Film condensation: Condensation of vapor onto the interface of a liquid film that completely covers a cold surface.

Minimum heat flux: A minimum heat flux condition on the classic boiling curve that characterizes the transition between film boiling and transition boiling. Also, sometimes referred to as the Leidenfrost point, it is a lower bound for heat flux values at which stable film boiling may occur.

Nucleate boiling: Generation of vapor at a hot surface by formation of bubbles at discrete nucleation sites with full liquid wetting of the surface.

Polar molecules: Molecules which have a permanent electric dipole moment. Examples include water and ammonia.

Pool boiling: Generation of vapor at the surface of a hot body immersed in an extensive liquid pool.

Transition boiling: Generation of vapor at a hot surface with intermittent or partial liquid wetting of the surface.

References

Berenson, P.J. 1961. Film boiling heat transfer from a horizontal surface. *J. Heat Transfer*, 83, 351–356.

Carey, V.P. 1992. *Liquid-Vapor Phase Change Phenomena.* Taylor and Francis, Washington, D.C.

Chen, J.C. 1966. Correlation for boiling heat transfer to saturated fluids in convective flow. *Ind. Eng. Chem. Proc. Design and Dev.* 5(3), 322–339.

Collier, J.G. 1981. *Convective Boiling and Condensation*, 2nd ed. McGraw-Hill, New York.

Dhir, V.K. and Lienhard, J. 1971. Laminar film condensation on plane and axisymmetric bodies in nonuniform gravity. *J. Heat Transfer* 93, 97–100.

Dougall, R.S. and Rohsenow, W.M. 1963. Film boiling on the inside of vertical tubes with upward flow of the fluid at low qualities. MIT Report No. 9079-26. MIT, Cambridge, MA.

Dukler, A.E. 1960. Fluid mechanics and heat transfer in vertical falling film systems. *Chem. Eng. Prog. Symp. Ser.* 56(30), 1–10.

Gunnerson, F.S. and Cronenberg, A.W. 1980. On the minimum film boiling conditions for spherical geometries. *J. Heat Transfer* 102,335–341.

Haramura, Y. and Katto, Y. 1983. A new hydrodynamic model of the critical heat flux, applicable widely to both pool and forced convective boiling on submerged bodies in saturated liquids. *Int. J. Heat Mass Transfer* 26, 389–399.

Kandlikar, S.G. 1989. A general correlation for saturated two-phase flow boiling heat transfer inside horizontal and vertical tubes. *J. Heat Transfer* 112, 219–228.

Katto, Y. and Ohno, H. 1984. An improved version of the generalized correlation of critical heat flux for the forced convective boiling in uniformly heated vertical tubes. *Int. Heat Mass Transfer* 21, 1527–1542.

Levitan, L.L. and Lantsman, F.P. 1975. Investigating burnout with flow of a steam-water mixture in a round tube, *Therm. Eng.* (USSR). English trans., 22, 102–105.

Lienhard, J.H. and Dhir, V.K. 1973. Extended hydrodynamic theory of the peak and minimum pool boiling heat fluxes. NASA CR-2270.

Lienhard, J.H. and Witte, L.C. 1985. A historical review of the hydrodynamic theory of boiling. *Rev. Chem. Eng.* 3, 187–277.

Lienhard, J.H. and Wong, P.T.Y. 1964. The dominant unstable wavelength and minimum heat flux during film boiling on a horizontal cylinder. *J. Heat Transfer* 86, 220–226.

Merte, H. 1973. Condensation heat transfer. *Adv. Heat Transfer* 9, 181–272.

Mills, A.F. and Chung, D.K. 1973. Heat transfer across turbulent falling films. *Int. J. Heat Mass Transfer* 16, 694–696.

Nukiyama, S. 1934. The maximum and minimum values of Q transmitted from metal to boiling water under atmospheric pressure. *J. Jpn. Soc. Mech. Eng.* 37, 367–374.

Nusselt, W. 1916. Die Oberflachenkondensation des Wasser dampfes. *Z. Ver. Dtsch. Ininuere* 60, 541–575.

Ramilison, J.M. and Lienhard, J.H. 1987. Transition boiling heat transfer and the film transition regime. *J. Heat Transfer* 109, 746–752.

Rohsenow, W.M. 1962. A method of correlating heat transfer data for surface boiling of liquids. *Trans. ASME* 84, 969–975.

Rossen, H.F. and Meyers, J.A. 1965. Point values of condensing film coefficients inside a horizontal tube. *Chem. Eng. Prog. Symp. Ser.* 61(59), 190–199.

Seban, R. 1954. Remarks on film condensation with turbulent flow. *Trans. ASME* 76, 299–303.

Selin, G. 1961. Heat transfer by condensing pure vapors outside inclined tubes, in *Proc. First Int. Heat Transfer Conf.*, University of Colorado, Boulder, Part II, 279–289.

Sparrow, E.M. and Gregg, J.L. 1959. A boundary-layer treatment of laminar film condensation. *J. Heat Transfer* 81, 13–23.

Stephen, K. 1992. *Heat Transfer in Condensation and Boiling*. Springer-Verlag, New York.

Tanaka, H. 1975. A theoretical study of dropwise condensation. *J. Heat Transfer* 97, 72–78.

Tanaka, H. 1979. Further developments of dropwise condensation theory. *J. Heat Transfer* 101, 603–611.

Traviss, D.P., Rohsenow, W.M., and Baron, A.B. 1973. Forced convection condensation in tubes: a heat transfer correlation for condenser design. *ASHRAE Trans.* 79(I), 157–165.

Witte, L.C. and Lienhard, J.H. 1982. On the existence of two "transition" boiling curves. *Int. J. Heat Mass Transfer* 25, 771–779.

Zuber, N. 1959. Hydrodynamic aspects of boiling heat transfer. AEC Rep. AECU-4439.

Further Information

The texts *Heat Transfer in Condensation and Boiling* by K. Stephan (Springer-Verlag, New York, 1992) and *Liquid-Vapor Phase Change Phenomena* by V.P. Carey (Taylor and Francis, Washington, D.C., 1992) provide an introduction to the physics of boiling and condensation processes. The text by J.G. Collier, *Convective Boiling and Condensation* (2nd ed., McGraw-Hill, New York, 1981), summarizes more-advanced elements of convective boiling and condensation processes. The *ASHRAE Handbook of Fundamentals* (American Society of Heating, Refrigerating, and Air-Conditioning Engineers, Atlanta, GA, 1993) provides some information on boiling and condensation heat transfer and is a good source of thermophysical property data needed to analyze boiling and condensation processes.

Particle Gas Convection

John C. Chen

Introduction

Heat transfer in two-phase systems involving gas and solid particles are encountered in several types of operations important in chemical, power, and environmental technologies. Chief among these are gas fluidized beds which are widely used to achieve either physical processing or chemical reactions that require interfacial contact between gas and solid particles. Currently, fluidized beds operate in either the *bubbling regime* or the *fast-circulating regime*. In the first case, particles are retained in the fluidized bed while the gas passes upward past the particles, partially as rising bubbles. In the second case, gas velocities exceed terminal velocity for the individual particles and the two phases flow through the fluidized bed in cocurrent upward flow. For those applications which require thermal control, convective heat transfer between the fluidized medium and heat transfer surfaces (either immersed tubes or the vessel walls) is an essential element of the process design.

Bubbling Fluidized Beds

Bubbling fluidization occurs when the superficial gas velocity exceeds a critical value wherein the gravitational body force on the solid particles is balanced by the shear force between particles and flowing gas. The superficial gas velocity at this condition, commonly called the minimum fluidization velocity (U_{mf}), marks the boundary between gas flow through packed beds and gas flow in fluidized beds. Wen and Yu (1966) derived the following general equation to estimate U_{mf} for spherical particles:

$$\mathrm{Re}_{mf} = \left[(33.7)^2 + 0.0408\mathrm{Ar} \right]^{1/2} - 33.7 \tag{4.4.21}$$

where

$$\text{Re}_{mf} = \text{particle Reynolds number at } U_{mf} = \frac{U_{mf} d_p \rho_g}{\mu_g}$$

$$\text{Ar} = \text{Archimedes number} = \frac{d_p^3 \rho_g (\rho_s - \rho_g) g}{\mu_g^2}$$

Increasing gas velocity beyond minimum fluidization causes the excess gas to collect into discrete bubbles that grow and rise through the fluidized matrix of solid particles. In this bubbling fluidization regime, the total pressure drop over the height of the fluidized bed, *H*, is equal to the hydrostatic pressure of the solid mass,

$$\Delta P = g \rho_s (1 - \varepsilon) H \tag{4.4.22}$$

where ε = volume fraction of gas (void fraction).

Tubes carrying cooling or heating fluids are often immersed in bubbling fluidized beds to extract or add thermal energy. The effective heat transfer coefficient at the surface of such tubes has been the objective of numerous experimental and analytical investigations. Data for the circumferentially averaged heat transfer coefficient for horizontal tubes are shown in Figure 4.4.10 for various types of solid particles. Characteristics representative of such systems are
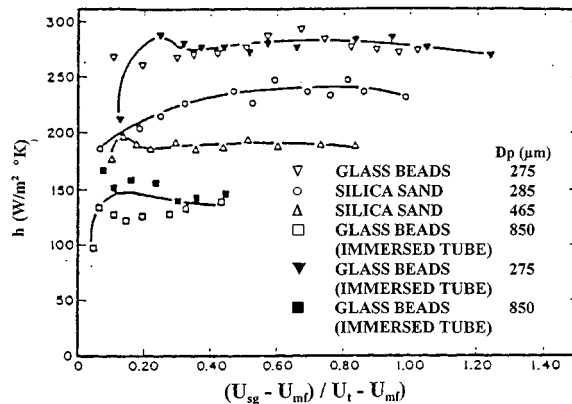
FIGURE 4.4.10 Average heat transfer coefficients for horizontal tubes immersed in bubbling fluidized beds. (From Biyikli, Tuzla and Chen, 1983.)

- The heat transfer coefficient increases sharply as the gas velocity exceeds minimum fluidization velocity,
- After the initial increase, the heat transfer coefficient remains fairly constant over a significant range of the gas velocity beyond minimum fluidization velocity,
- The absolute magnitude of the heat transfer coefficient is severalfold greater than single-phase gas convection at the same superficial velocity,
- The heat transfer coefficient increases as particle size decreases.

Kunii and Levenspiel (1991) have shown that increasing gas pressure and density significantly increases the magnitude of the heat transfer coefficient as well as promoting the occurrence of minimum fluidization at a lower value of superficial gas velocity. The effect of bundle spacing is insignificant at 1-atm pressure but becomes increasingly more important as gas pressure and density increase. The data

of Jacob and Osberg (1957) indicate that the convective heat transfer coefficient in fluidized beds increases with increasing thermal conductivity of the gas phase, for any given particle size.

Several different types of correlations have been suggested for predicting convective heat transfer coefficients at submerged surfaces in bubbling fluidized beds. The first type attributes the enhancement of heat transfer to the scouring action of solid particles on the gas boundary layer, thus decreasing the effective film thickness. These models generally correlate a heat transfer Nusselt number in terms of the fluid Prandtl number and a modified Reynolds number with either the particle diameter or the tube diameter as the characteristic length scale. Examples are

Leva's correlation for vertical surfaces and larger particles (Leva and Gummer, 1952);

$$\mathrm{Nu}_{d_p} = \frac{h_c d_p}{k_g} = 0.525 \big(\mathrm{Re}_p\big)^{0.75} \tag{4.4.23}$$

where

$$\mathrm{Re}_p = \frac{d_p \rho_g U}{\mu_g}$$

Vreedenberg's (1958) correlation for horizontal tubes refers to the particle of diameter D_t.

$$\mathrm{Nu}_{D_t} = \frac{h_c D_t}{k_g} = 420 \left(\frac{\rho_s}{\rho_g} \mathrm{Re}_t \right)^{0.3} \left(\frac{\mu_g^2}{g \rho_s^2 d_p^3} \right)^{0.3} \big(\mathrm{Pr}_g\big)^{0.3} \tag{4.4.24}$$

for

$$\left(\frac{\rho_s}{\rho_g} \mathrm{Re}_t \right) > 2250$$

where

$$\mathrm{Re}_t = \frac{D_t \rho_g U}{\mu_g}$$

Molerus and Schweinzer (1989) developed an alternative type of correlation based on the supposition that the heat transfer is dominated by gas convection through the matrix of particles in the vicinity of the heat transfer surface. Their correlation takes the form:

$$\mathrm{Nu} = \frac{h_c d_p}{k_g} = 0.0247 (\mathrm{Ar})^{0.4304} (\mathrm{Pr})^{0.33} \tag{4.4.25}$$

Figure 4.4.11 shows comparison of this model with experimental data obtained at three different pressures. The solid curve represents the relationship for fixed beds, while the dashed lines represent the behavior for fluidized beds (i.e., Equation 4.4.25) upon exceeding minimum fluidization.

A third type of model considers the heat transfer surface to be contacted alternately by gas bubbles and packets of packed particles, leading to a surface renewal process for heat transfer. Mickley and Fairbanks (1955) provided the first analysis of this renewal mechanism. Ozkaynak and Chen (1980)
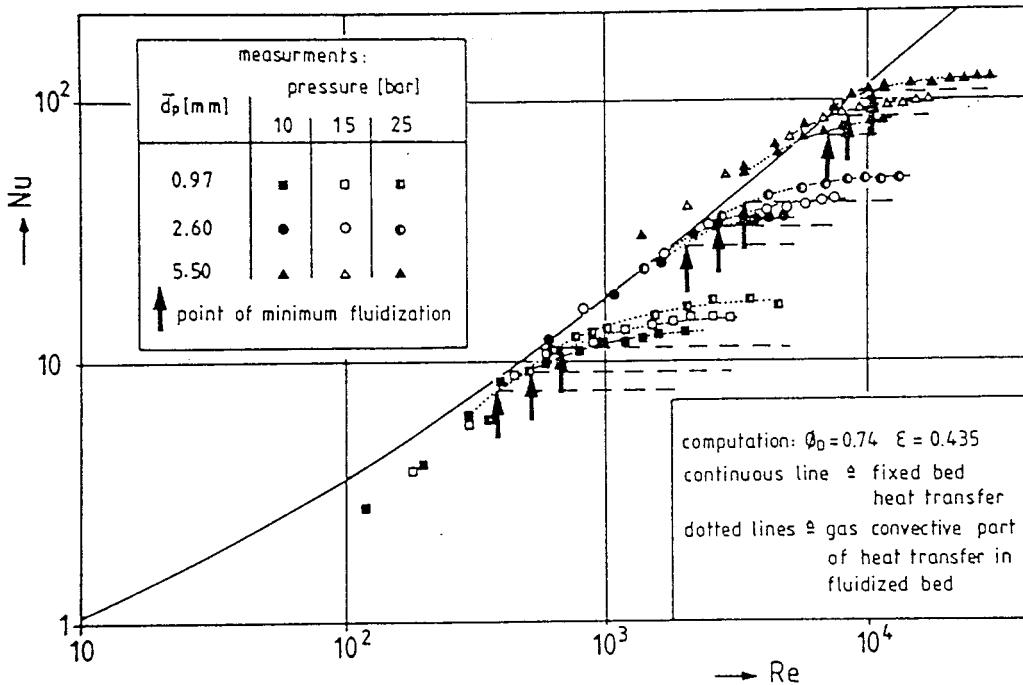
FIGURE 4.4.11 Correlation of Molerus and Schweinzer compared with experimental data (1989).

showed that if experimentally measured values of the packet contact time and residence times are used in the packet model analysis, excellent agreement is obtained.

Fast-Circulating Fluidized Beds

Fast fluidization occurs when the superficial gas velocity exceeds the terminal velocity of the solid particles, causing the particles to be suspended in cocurrent upward flow with the gas. This upward flow occurs in "rise reactors" wherein desired physical or chemical reactions occur. In most applications, the two-phase flow exits the top of the riser into a cyclone where the gas phase is separated and exhausted while the solid particles are captured and returned for reinjection at the bottom of the riser. The volumetric concentration of solid particles in these fast fluidized beds (FFBs) tend to be fairly dilute, often with average concentrations of less than 2%. Heat exchange with the particle/gas suspension is usually accomplished through the vertical wall surfaces or through vertical tubes immersed in the duct.

The heat transfer coefficient at vertical surfaces FFBs has been found to increase with increasing solid concentration, aside from other second-order parametric effects. Figure 4.4.12 shows heat transfer coefficients experimentally measured by Dou et al. (1994) for an FFB operating with sand particles of 124 μm mean diameter. Figure 4.4.12b shows that the heat transfer coefficient increased with solid mass flux, for a constant superficial gas velocity. Figure 4.4.12a shows that the heat transfer coefficient decreased parametrically with superficial gas velocity for a constant solid mass flux. Both figures indicate that heat transfer coefficients decrease with increasing elevation in the riser duct. These three parametric trends are all consistent with the hypothesis that heat transfer in FFBs increases with increasing concentration of the solid phase.

It is generally accepted that the effective heat transfer coefficient for surfaces in FFBs have contributions for gas-phase convection, particle-induced convection, and radiation:
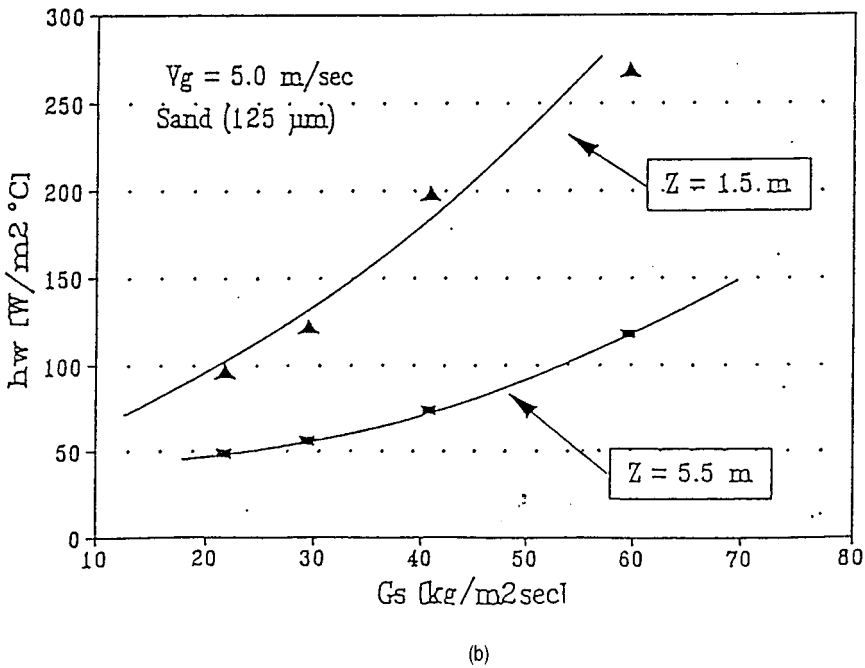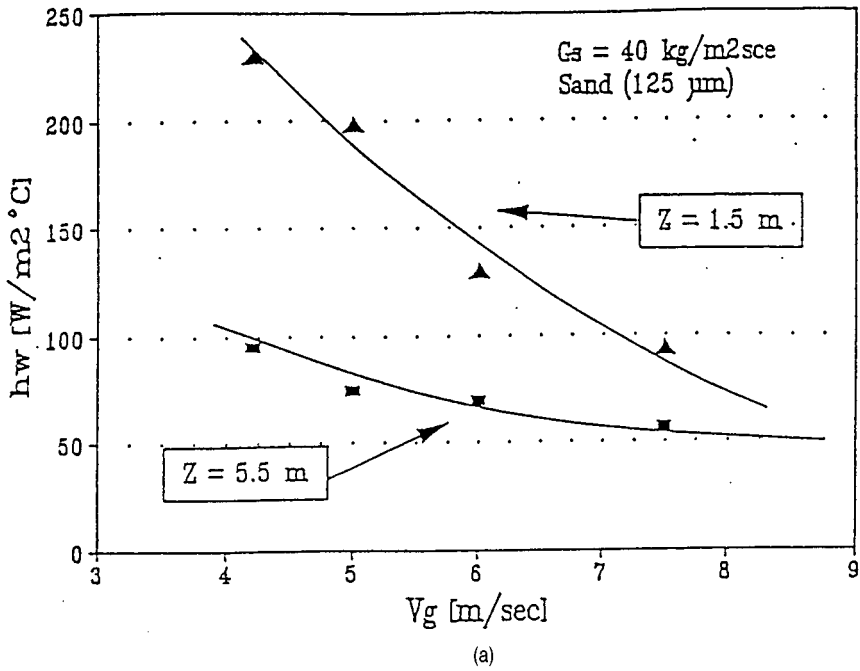
$$h = h_g + h_p + h_r \qquad (4.4.26)$$

(a)

(b)

FIGURE 4.4.12 Heat transfer coefficients in fast fluidized beds; Vg is superficial gas velocity, Gs is mass flux of particles, and Z is elevation in FFB. (From Dou, Tuzla and Chen, 1992.)

In contrast to the situation in dense-bubbling fluidized beds, the relatively dilute concentration of solid particles in FFBs often results in significant contributions from all three heat transfer mechanisms. The radiation coefficient can be obtained by a gray body model suggested by Grace (1985). The contribution of the gas phase convection (h_g) is commonly estimated based on correlations for gas flow alone at the same superficial gas velocity. Although the presence of particles may alter the turbulence characteristic of this gas flow, any errors caused by this procedure are usually small since h_g is generally smaller than the particle-phase convective coefficient h_p.

For most FFBs, the particle convective contribution to heat transfer is most important and the prediction of h_p is the major concern in thermal design. Unfortunately, mechanistically based models are still lacking and most design methods rely on empirical correlations which often combine the contributions of gas and particle phases into a single convective heat transfer coefficient (h_c). One such correlation proposed by Wen and Miller (1961) is

$$\text{Nu}_{d_p} = \frac{h_c d_p}{k_g} = \left(\frac{C_{pp}}{C_{pg}}\right)\left(\frac{\rho_{\text{susp}}}{\rho_p}\right)^{0.3}\left(\frac{V_t}{g d_p}\right)^{0.21}\text{Pr}_g \qquad (4.4.27)$$

where V_t = terminal velocity of particle.

Other correlations have been proposed by Fraley (1992) and Martin (1984). These correlations are useful as a starting point but have not yet been verified over wide parametric ranges. Large deviations can occur when compared with measurements obtained outside of the experimental parametric ranges.

References

Biyikli, K., Tuzla, K., and Chen, J.C. 1983. Heat transfer around a horizontal tube in freeboard region of fluidized beds, *AIChE J.,* 29(5), 712–716.

Dou, S., Herb, B., Tuzla, K., and Chen, J.C. 1992. Dynamic variation of solid concentration and heat transfer coefficient at wall of circulating fluidized bed, in *Fluidization VII*, Eds. Potter and Nicklin, Engineering Foundation, 793–802.

Fraley, L.D., Lin, Y.Y., Hsiao, K.H., and Solbakken, A. 1983. ASME Paper 83-HT-92, National Heat Transfer Conference, Seattle.

Grace, J.R. 1985. Heat transfer in circulating fluidized beds, *Circulating Fluidized Bed Technology I*, Peramon Press, New York, 63–81.

Jacob, A. and Osberg, G.L. 1957. Effect of gas thermal conductivity on local heat transfer in a fluidized bed, *Can. J. Chem. Eng.*, 35(6), 5–9.

Kunii, D. and Levenspiel, O. 1991. *Fluidization Engineering*, 2nd ed., Butterworth-Heinemann, Boston.

Leva, M. and Grummer, M. 1952. A correlation of solids turnovers in fluidized systems, *Chem. Eng. Prog.*, 48(6), 307–313.

Martin, H. 1984. *Chem. Eng. Process*, 18, 157–223.

Mickley, H.S. and Fairbanks, D.F. 1955. Mechanism of heat transfer to fluidized beds, *AIChE J.*, 1(3), 374–384.

Molerus, O. and Scheinzer, J. 1989. Prediction of gas convective part of the heat transfer to fluidized beds, in *Fluidization IV*, Engineering Foundation, New York, 685–693.

Ozkaynak, T.F. and Chen, J.C. 1980. Emulsion phase residence time and its use in heat transfer models in fluidized bed, *AIChE J.*, 26(4), 544–550.

Vreedenberg, H.A. 1958. Heat transfer between a fluidized bed and a horizontal tube, *Chem. Eng. Sci.*, 9(1), 52–60.

Wen, C.Y. and Yu, Y.H. 1966. A generalized method for predicting the minimum fluidization velocity, *AIChE J.*, 12(2), 610–612

Wen, C.Y. and MIller, E.N. 1961. *Ind. Eng. Chem.*, 53, 51–53.

Melting and Freezing

Noam Lior

Introduction and Overview

Melting and freezing occur naturally (Lunardini, 1981) as with environmental ice in the atmosphere (hail, icing on aircraft), on water bodies and ground regions at the Earth surface, and in the molten Earth core (Figure 4.4.13). They are also a part of many technological processes, such as preservation of foodstuffs (ASHRAE, 1990, 1993), refrigeration and air-conditioning (ASHRAE, 1990, 1993), snow and ice making for skiing and skating (ASHRAE, 1990), organ preservation and cryosurgery (Rubinsky and Eto, 1990), manufacturing (such as casting, molding of plastics, coating, welding, high-energy beam cutting and forming, crystal growth, electrodischarge machining, electrodeposition) (Flemings, 1974; Cheng and Seki, 1991; Tanasawa and Lior, 1992), and thermal energy storage using solid–liquid phase-changing materials (deWinter, 1990).
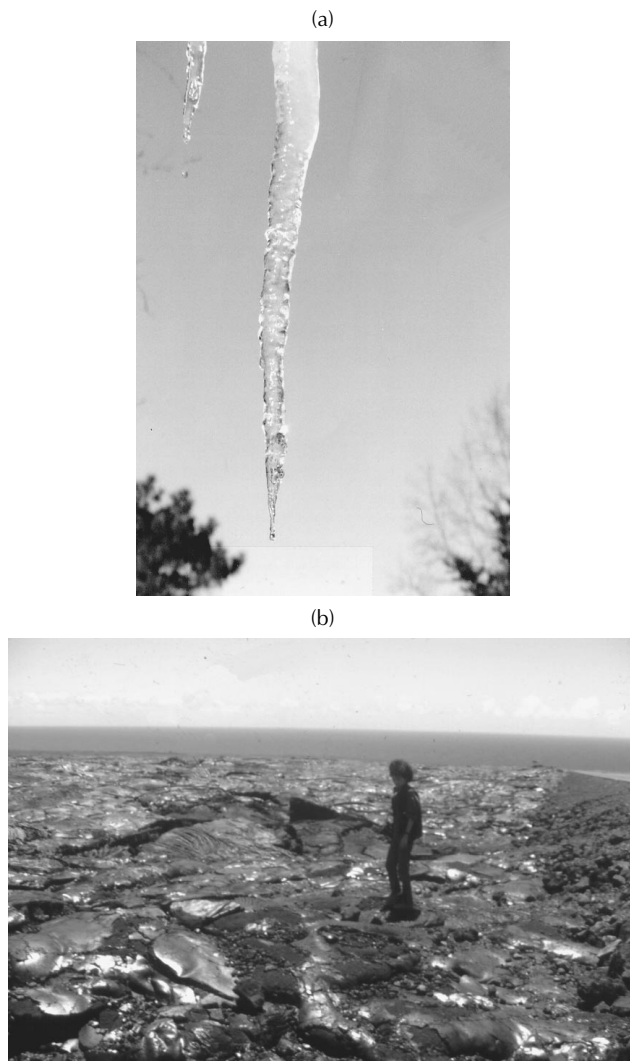
(a)

(b)

FIGURE 4.4.13 Melting and freezing in nature. (a) A melting icicle. (b) Frozen lava in Hawaii.

In simple thermodynamic systems (i.e., without external fields, surface tension, etc.) of a pure material, melting or freezing occurs at certain combinations of temperature and pressure. Since pressure typically has a relatively smaller influence, only the fusion (freezing or melting) temperature is often used to identify this phase transition. Fusion becomes strongly dependent on the concentration when the material contains more than a single species. Furthermore, melting and freezing are also sensitive to external effects, such as electric and magnetic fields, in more-complex thermodynamic systems.

The equilibrium thermodynamic system parameters during phase transition can be calculated from the knowledge that the partial molar Gibbs free energies or chemical potentials of each component in the two phases must be equal. One important result of using this principle for simple single-component systems is the Clapeyron equation relating the temperature (T) and pressure (P) during the phase transition, such that

$$\frac{dP}{dT} = \frac{h_{s\ell}}{T\Delta v} \qquad (4.4.28)$$

where $h_{s\ell}$ is the enthalpy change from phase A to phase B ($= h_B - h_A$, the latent heat of fusion with appropriate sign) and Δv is the specific volume difference between phases A and B ($= v_B - v_A$). Considering for example that phase A is a solid and B a liquid ($h_{s\ell}$ is then positive), examination of Equation (4.4.28) shows that increasing the pressure will result in an increase in the melting temperature if $\Delta v > 0$ (i.e., when the specific volume of the liquid is higher than that of the solid, which is a property of tin, for example), but will result in a decrease of the melting temperature when $\Delta v < 0$ (for water, for example).

In some materials, called glassy, the phase change between the liquid and solid occurs with a gradual transition of the physical properties, from those of one phase to those of the other. When the liquid phase flows during the process, the flow is strongly affected because the viscosity increases greatly as the liquid changes to solid. Other materials, such as pure metals and ice, and eutectic alloys, have a definite line of demarcation between the liquid and the solid, the transition being abrupt. This situation is easier to analyze and is therefore more thoroughly addressed in the literature.

Gradual transition is most distinctly observed in mixtures. Consider the equilibrium phase diagram for a binary mixture (or alloy) composed of species a and b, shown in Figure 4.4.14. χ is the concentration of species b in the mixture, ℓ denotes the liquid, s the solid, s_a a solid with a lattice structure of species a in its solid phase but containing some molecules of species b in that lattice, and s_b a solid with a lattice structure of species b in its solid phase but containing some molecules of species a in that lattice. "Liquidus" denotes the boundary above which the mixture is just liquid, and "solidus" is the boundary separating the final solid mixture of species a and b from the solid–liquid mixture zones and from the other zones of solid s_a and solid s_b.

For illustration, assume that a liquid mixture is at point 1, characterized by concentration χ_1 and temperature T_1 (Figure 4.4.14), and is cooled (descending along the dashed line) while maintaining the concentration constant. When the temperature drops below the liquidus line, solidification starts, creating a mixture of liquid and of solid s_a. Such a two-phase mixture is called the **mushy zone**. At point 2 in that zone, the solid phase (s_a) portion contains a concentration χ_{2,s_a} of component b, and the liquid phase portion contains a concentration $\chi_{2,\ell}$ of component b. The ratio of the mass of the solid s_a to that of the liquid is determined by the lever rule, and is $(\chi_{2,\ell} - \chi_2)/(\chi_2 - \chi_{2,s_a})$ at point 2. Further cooling to below the solidus line, say to point 3, results in a solid mixture (or alloy) of s_a and s_b, containing concentrations χ_{3,s_A} and χ_{3,s_B} of species b, respectively. The ratio of the mass of the solid s_a to that of s_b is again determined by the lever rule, and is $(\chi_{3,s_b} - \chi_3)/(\chi_3 - \chi_{3,s_a})$ at point 3.

A unique situation occurs if the initial concentration of the liquid is χ_e: upon constant-concentration cooling, the liquid forms the solid mixture $s_a + s_b$ having the same concentration and without the formation of a two-phase zone. χ_e is called the **eutectic concentration**, and the resulting solid mixture (or alloy) is called a *eutectic*.
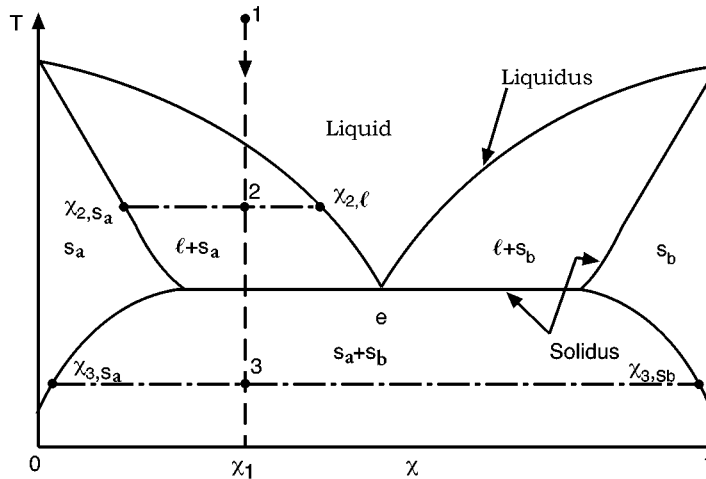
FIGURE 4.4.14 A liquid–solid phase diagram of a binary mixture.

   The presence of a two-phase mixture zone with temperature-dependent concentration and phase proportion obviously complicates heat transfer analysis, and requires the simultaneous solution of both the heat and mass transfer equations. Furthermore, the liquid usually does not solidify on a simple planar surface. Crystals of the solid phase are formed at some preferred locations in the liquid, or on colder solid surfaces immersed in the liquid, and as freezing progesses the crystals grow in the form of intricately shaped fingers, called dendrites. This complicates the geometry significantly and makes mathematical modeling of the process very difficult. An introduction to such problems and further references are available in Hayashi and Kunimine (1992) and Poulikakos (1994).

   Flow of the liquid phase often has an important role in the inception of, and during, melting and freezing (see Incropera and Viskanta, 1992). The flow may be forced, such as in the freezing of a liquid flowing through or across a cooled pipe, and/or may be due to natural convection that arises whenever there are density gradients in the liquid, here generated by temperature and possibly concentration gradients. It is noteworthy that the change in phase usually affects the original flow, such as when the liquid flowing in a cooled pipe gradually freezes and the frozen solid thus reduces the flow passage, or when the evolving dendritic structure gradually changes the geometry of the solid surfaces that are in contact with the liquid. Under such circumstances, strong coupling may exist between the heat transfer and fluid mechanics, and also with mass transfer when more than a single species is present. The process must then be modeled by an appropriate set of continuity, momentum, energy, mass conservation, and state equations, which need to be solved simultaneously.

   More-detailed information about melting and freezing can be found in the monograph by Alexiades and Solomon (1993) and in the comprehensive reviews by Fukusako and Seki (1987) and Yao and Prusa (1989).

Melting and Freezing of Pure Materials

Thorough mathematical treatment of melting and freezing is beyond the scope of this section, but examination of the simplified one-dimensional case for a pure material and without flow effects provides important insights into the phenomena, identifies the key parameters, and allows analytical solutions and thus qualitative predictive capability for at least this class of problems.

   In the freezing model, described in Figure 4.4.15, a liquid of infinite extent is to the right ($x > 0$) of the infinite surface at $x = 0$, initially at a temperature T_i higher than the fusion temperature T_f. At time $t = 0$ the liquid surface temperature at $x = 0$ is suddenly lowered to a temperature $T_0 < T_f$, and maintained at that temperature for $t > 0$. Consequently, the liquid starts to freeze at $x = 0$, and the freezing interface (separating in Figure 4.4.15 the solid to its left from the liquid on its right) located
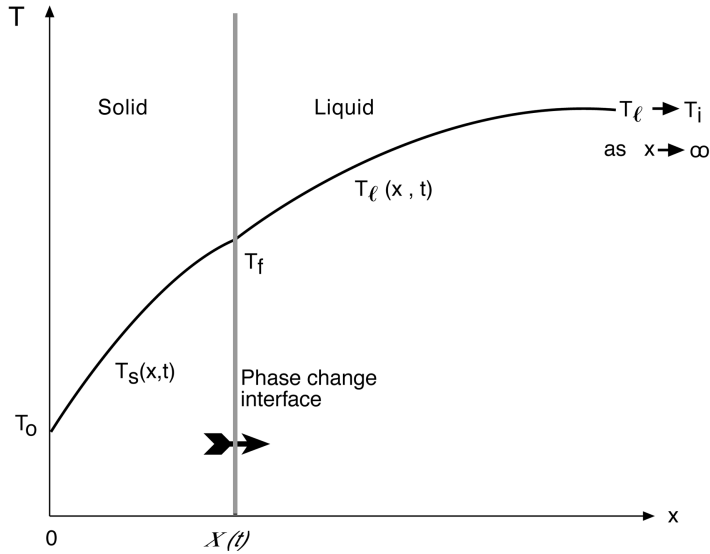
FIGURE 4.4.15 Freezing of semi-inifinite liquid with heat conduction in both phases.

at the position $x = X(t)$ moves gradually to the right (in the positive x direction). We note that in this problem heat is conducted in both phases.

Assuming for simplification that heat transfer is by conduction only — although at least natural convection (Incropera and Viskanta, 1992) and sometimes forced convection and radiation also take place — the governing equations are

In the liquid: The transient heat conduction equation is

$$\frac{\partial T_\ell(x,t)}{\partial t} = \alpha_\ell \frac{\partial^2 T_\ell(x,t)}{\partial x^2} \quad \text{in} \quad X(t) < x < \infty \quad \text{for} \quad t > 0 \tag{4.4.29}$$

$$T_\ell(x,t) = T_i \quad \text{in} \quad x > 0, \quad \text{at} \quad t = 0 \tag{4.4.30}$$

where α_ℓ is the thermal diffusivity of the liquid, with the initial condition and the boundary condition

$$T_\ell(x \to \infty, t) \to T_i \quad \text{for} \quad t > 0 \tag{4.4.31}$$

In the solid: The transient heat conduction equation is

$$\frac{\partial T_s(x,t)}{\partial t} = \alpha_s \frac{\partial^2 T_s(x,t)}{\partial x^2} \quad \text{in} \quad 0 < x < X(t) \quad \text{for} \quad t > 0 \tag{4.4.32}$$

where α_s is the thermal diffusivity of the solid, with the boundary condition

$$T_s(0,t) = T_0 \quad \text{for} \quad t > 0 \tag{4.4.33}$$

The remaining boundary conditions are those of temperature continuity and heat balance at the solid–liquid phase-change interface $X(t)$,

$$T_\ell[X(t)] = T_s[X(t)] = T_f \quad \text{for} \quad t > 0 \tag{4.4.34}$$

$$k_s\left(\frac{\partial T_s}{\partial x}\right)_{[X(t)]} - k_\ell\left(\frac{\partial T_\ell}{\partial x}\right)_{[X(t)]} = \rho h_{s\ell}\frac{dX(t)}{dt} \quad \text{for} \quad t > 0 \tag{4.4.35}$$

where k_s and k_ℓ are the thermal conductivities of the solid and liquid, respectively, ρ is the density (here it is assumed for simplicity to be the same for the liquid and solid), and $h_{s\ell}$ is the latent heat of fusion. The two terms on the left-hand side of Equation (4.4.35) thus represent the conductive heat flux away from the phase-change interface, into the solid at left and the liquid at right, respectively. Energy conservation at the interface requires that the sum of these fluxes leaving the interface be equal to the amount of heat generated due to the latent heat released there, represented by the term on the right-hand side of the equation.

The analytical solution of Equations (4.4.29) to (4.4.35) yields the temperature distributions in the liquid and solid phases,

$$T_\ell(x,t) = T_i - \left(T_i - T_f\right)\frac{\text{erfc}\left(\dfrac{x}{2\sqrt{\alpha_\ell t}}\right)}{\text{erfc}\left(\lambda\sqrt{\alpha_s/\alpha_\ell}\right)} \tag{4.4.36}$$

$$T_s(x,t) = T_0 + \left(T_f - T_0\right)\frac{\text{erfc}\left(\dfrac{x}{2\sqrt{\alpha_s t}}\right)}{\text{erfc}\,\lambda} \tag{4.4.37}$$

where erf and erfc are the *error function* and the *complementary error function*, respectively, and λ is a constant, obtained from the solution of the equation

$$\frac{e^{\lambda^2}}{\text{erf}\,\lambda} - \frac{k_\ell}{k_s}\sqrt{\frac{\alpha_s}{\alpha_\ell}}\frac{T_i - T_f}{T_f - T_0}\frac{e^{(\alpha_s/\alpha_\ell)\lambda^2}}{\text{erfc}\left(\lambda\sqrt{\alpha_s/\alpha_\ell}\right)} = \frac{\lambda\sqrt{\pi}}{\text{Ste}_s} \tag{4.4.38}$$

where Ste is the Stefan number (dimensionless), here defined for the solid as

$$\text{Ste}_s \equiv \frac{c_s\left(T_f - T_0\right)}{h_{s\ell}} \tag{4.4.39}$$

and c_s is the specific heat of the solid. Solutions of Equation (4.4.38) are available for some specific cases in several of the references, and can be obtained relatively easily by a variety of commonly used software packages.

The solution of Equations (4.4.29) to (4.4.35) also gives an expression for the transient position of the freezing interface,

$$X(t) = 2\lambda\left(\alpha_s t\right)^{1/2} \tag{4.4.40}$$

where λ is the solution of Equation 4.4.38, and thus the expression for the rate of freezing, i.e., the velocity of the motion of the solid liquid interface, is

$$\frac{dX(t)}{dt} = \lambda \alpha_s^{1/2} t^{1/2} \tag{4.4.41}$$
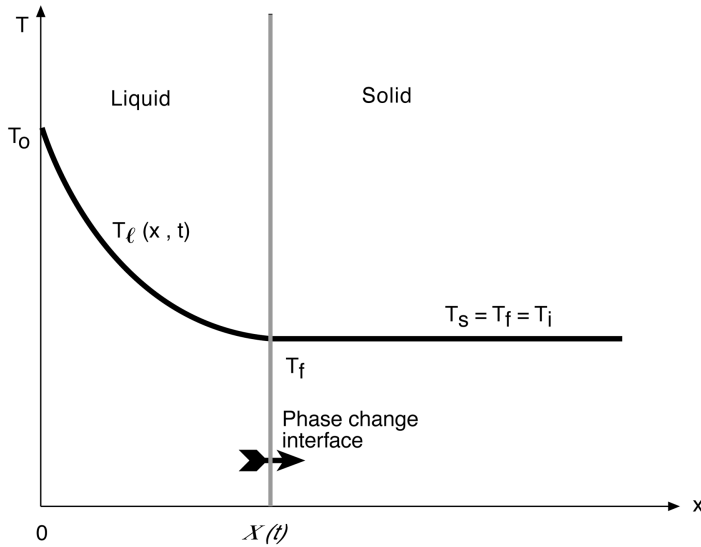
FIGURE 4.4.16 Melting of semi-infinite solid with conduction in the liquid phase only.

For a simple one-dimensional melting example of an analytical solution for melting, consider the semi-infinite solid described in Figure 4.4.16, initially at the fusion temperature T_f. For time $t > 0$ the temperature of the surface (at $x = 0$) is raised to $T_0 > T_f$, and the solid consequently starts to melt there. In this case the temperature in the solid remains constant, $T_s = T_f$, so the temperature distribution needs to be calculated only in the liquid phase. It is assumed that the liquid formed by melting remains motionless and in place. Very similarly to the above-described freezing case, the equations describing this problem are the heat conduction equation

$$\frac{\partial T_\ell(x,t)}{\partial t} = \alpha_\ell \frac{\partial^2 T_\ell(x,t)}{\partial x^2} \quad \text{in} \quad 0 < x < X(t) \quad \text{for} \quad t > 0 \tag{4.4.42}$$

with the initial condition

$$T_\ell(x,t) = T_f \quad \text{in} \quad x > 0, \quad \text{at} \quad t = 0 \tag{4.4.43}$$

the boundary condition

$$T_\ell(0,t) = T_0 \quad \text{for} \quad t > 0 \tag{4.4.44}$$

and the liquid–solid interfacial temperature and heat flux continuity conditions

$$T_\ell[X(t)] = T_f \quad \text{for} \quad t > 0 \tag{4.4.45}$$

$$-k_\ell \left(\frac{\partial T_\ell}{\partial x}\right)_{[X(t)]} = \rho h_{\ell s} \frac{dX(t)}{dt} \quad \text{for} \quad t > 0 \tag{4.4.46}$$

The analytical solution of this problem yields the temperature distribution in the liquid,

$$T_\ell(x,t) = T_0 - \left(T_0 - T_f\right)\frac{\mathrm{erf}\left(\dfrac{x}{2\sqrt{\alpha_\ell t}}\right)}{\mathrm{erf}\,\lambda'} \quad \text{for} \quad t > 0 \tag{4.4.47}$$

where λ' is the solution of the equation

$$\lambda' e^{\lambda'^2}\,\mathrm{erf}(\lambda') = \frac{\mathrm{Ste}_\ell}{\sqrt{\pi}} \tag{4.4.48}$$

with Ste_ℓ here defined for the liquid as

$$\mathrm{Ste}_\ell \equiv \frac{c_\ell\left(T_0 - T_f\right)}{h_{s\ell}} \tag{4.4.49}$$

λ' as a function of Ste, for $0 \le \mathrm{Ste} \le 5$, is given in Figure 4.4.17. The interface position is

$$X(t) = 2\lambda'\left(\alpha_\ell t\right)^{1/2} \tag{4.4.50}$$
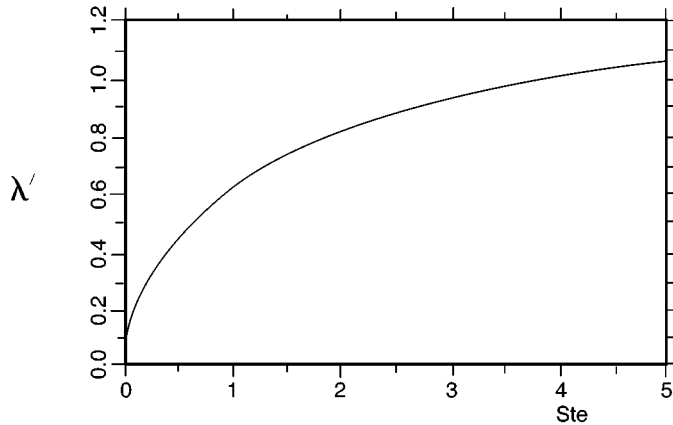
FIGURE 4.4.17 The root λ' of Equation 4.4.48.

The solution of the *freezing* problem under similar conditions, i.e., of a semi-infinite liquid initially at temperature T_f where $T(0,t)$ is abruptly reduced to $T_0 < T_f$ for $t > 0$, is identical to the above if every subscript ℓ is replaced by s and the latent heat $h_{s\ell}$ is replaced by $-h_{s\ell}$.

Example: The temperature of the vertical surface of a large volume of solid paraffin wax used for heat storage, initially at the fusion temperature, $T_i = T_f = 28°C$, is suddenly raised to $58°C$. Any motion in the melt may be neglected. How long would it take for the paraffin to solidify to a depth of 0.1 m? Given properties: $\alpha_\ell = (1.09)\,10^{-7}\ \mathrm{m^2/sec}$, $\rho_s = \rho_\ell = 814\ \mathrm{kg/m^3}$, $h_{s\ell} = 241\ \mathrm{kJ/kg}$, $c_\ell = 2.14\ \mathrm{kJ/kg°C}$. To find the required time we use Equation (4.4.50), in which the value of λ' needs to be determined. λ' is calculated from Equation (4.4.48), which requires the knowledge of Ste_ℓ. From Equation (4.4.49)

$$\text{Ste}_\ell = \frac{(2.14 \ \text{kJ/kg°C})(58°\text{C} - 28°\text{C})}{241.2 \ \text{kJ/kg}} = 0.266$$

The solution of Equation (4.4.48) as a function of Ste_ℓ is given in Figure 4.4.17, yielding $\lambda \approx 0.4$. By using Equation (4.4.50), the time of interest is calculated by

$$t = \frac{[X(t)]^2}{4\lambda^2 \alpha_\ell} = \frac{(0.1 \ \text{m})^2}{4(0.4)^2 \left[(1.09)10^7 \ \text{m}^2/\text{sec}\right]} = (1.43)10^5 \ \text{sec} = 39.8 \ \text{hr}$$

The axisymmetric energy equation in *cylindrical coordinates*, applicable to both the solid phase and immobile liquid phase (with appropriate assignment of the properties) is

$$\frac{\partial T(r,t)}{\partial t} = \frac{1}{\rho c} \frac{\partial}{\partial r} \left(\frac{k}{r} \frac{\partial T(r,t)}{\partial r} \right) \quad \text{for} \quad t > 0 \tag{4.4.51}$$

and the temperature and heat balance conditions at the solid–liquid phase-change interface $r = R(t)$ are

$$T_\ell[R(t)] = T_s[R(t)] \quad \text{for} \quad t > 0 \tag{4.4.52}$$

$$k_s \left(\frac{\partial T_s}{\partial r} \right)_{R(t)} - k_\ell \left(\frac{\partial T_\ell}{\partial r} \right)_{R(t)} = h_{s\ell} \frac{dR(t)}{dt} \tag{4.4.53}$$

Because of the nature of the differential equations describing nonplanar and multidimensional geometries, analytical solutions are available for only a few cases, such as line heat sources in cylindrical coordinate systems or point heat sources in spherical ones, which have very limited practical application. Other phase-change problems in nonplanar geometries, and in cases when the melt flows during phase change, are solved by approximate and numerical methods (Yao and Prusa, 1989; Alexiades and Solomon, 1993).

Some Approximate Solutions

Two prominent approximate methods used for the solution of melting and freezing problems are the integral method and the *quasi-static* approximation. The integral method is described in Goodman (1964), and only the quasi-static approximation is described here.

To obtain rough estimates of melting and freezing processes quickly, in cases where heat transfer takes place in only one phase, it is assumed in this approximation that effects of sensible heat are negligible relative to those of latent heat ($\text{Ste} \to 0$), thus eliminating the sensible-heat left-hand side of the energy equations (such as (4.4.29), (4.4.32), and (4.4.51)). This is a significant simplification, since the energy equation then becomes independent of time, and solutions to the steady-state heat conduction problem are much easier to obtain. At the same time, the transient phase-change interface condition (such as Equations (4.4.35) and (4.4.53)) 5 is retained, allowing the estimation of the transient interface position and velocity. This is hence a quasi-static approximation, and its use is shown below.

We emphasize that these are just approximations, without full information on the effect of specific problem conditions on the magnitude of the error incurred when using them. In fact, in some cases, especially with a convective boundary condition, they may produce incorrect results. It is thus necessary to examine the physical viability of the results, such as overall energy balances, when using these approximations.

All of the examples are for melting, but freezing problems have the same solutions when the properties are taken to be those of the solid and $h_{s\ell}$ is replaced everywhere by $-h_{s\ell}$. It is assumed here that the problems are one-dimensional, and that the material is initially at the fusion temperature T_f.

Examples of the Quasi-Static Approximation for Cartesian Coordinate Geometries. Given a semi-infinite solid (Figure 4.4.16), on which a *time-dependent temperature* $T_0(t) > T_f$ *is imposed at* x = *0*, the above-described quasi-static approximation of Equations (4.4.42) to (4.4.46) easily yields the solution

$$X(t) = \left[2\frac{k_\ell}{\rho h_{s\ell}} \int_0^t \left[T_0(t) - T_f \right] dt \right]^{1/2} \quad \text{for} \quad t \geq 0 \tag{4.4.54}$$

$$T_\ell(x,t) = T_0(t) - \left[T_0(t) - T_f \right] \frac{x}{X(t)} \quad \text{in} \quad 0 \leq x \leq X(t) \quad \text{for} \quad t \geq 0 \tag{4.4.55}$$

The heat flux needed for melting, $q(x,t)$, can easily be determined from the temperature distribution in the liquid (Equation 4.4.55), which is linear because of the steady-state form of the heat conduction equation in this quasi-static approximation, so that

$$q(x,t) = -k_\ell \frac{dT_\ell(x,t)}{dx} = k_\ell \frac{T_0(t) - T_f}{X(t)} \tag{4.4.56}$$

For comparison of this approximate solution to the exact one (Equations (4.4.47) and (4.4.50)), consider the case where $T_0(t) = T_0$ = constant. Rearranging to use the Stefan number, Equations (4.4.54) and (4.4.55) become

$$X(t) = 2\left(\text{Ste}_\ell/2\right)^{1/2} \left(\alpha_\ell t\right)^{1/2} \quad \text{for} \quad t > 0 \tag{4.4.57}$$

$$T(x,t) = T_0 - \left[T_0 - T_f \right] \frac{x / \left[2\left(\alpha_\ell t\right)^{1/2} \right]}{\left(\text{Ste}_\ell/2\right)^{1/2}} \quad \text{in} \quad 0 \leq x \leq X(t) \quad \text{for} \quad t \geq 0 \tag{4.4.58}$$

It is easy to show that λ' in the exact solution (Equation 4.4.48) approaches the value $(\text{Ste}_\ell/2)^{1/2}$ when $\text{Ste}_\ell \to 0$, and that otherwise $\lambda' < (\text{Ste}_\ell/2)^{1/2}$. The approximate solution is therefore indeed equal to the exact one when $\text{Ste}_\ell \to 0$, and it otherwise overestimates the values of both $X(t)$ and $T(x,t)$. While the errors depend on the specific problem, they are confined to about 10% in the above-described case (Alexiades and Solomon, 1993).

For the same melting problem but with the *boundary condition of an imposed time-dependent heat flux* $q_0(t)$,

$$-k_\ell \left(\frac{dT_\ell}{dx} \right)_{0,t} = q_0(t) \quad \text{for} \quad t > 0 \tag{4.4.59}$$

the quasi-static approximate solution is

$$X(t) \equiv \frac{1}{\rho h_{s\ell}} \int_0^t q_0(t) \, dt \quad \text{for} \quad t > 0 \tag{4.4.60}$$

$$T_\ell(x,t) = T_f + \frac{q_0}{k_\ell}\left[\frac{q_0}{\rho h_{s\ell}}t - x\right] \quad \text{in} \quad 0 \le x \le X(t) \quad \text{for} \quad t > 0 \tag{4.4.61}$$

For the same case if the *boundary condition is a convective heat flux* from an ambient fluid at the transient temperature $T_a(t)$, characterized by a heat transfer coefficient $\bar{h}$,

$$-k_\ell\left(\frac{dT_\ell}{dx}\right)_{0,t} = \bar{h}\left[T_a(t) - T_\ell(0,t)\right] \quad \text{for} \quad t \ge 0 \tag{4.4.62}$$

the quasi-static approximate solution is

$$X(t) = -\frac{k_\ell}{\bar{h}} + \left\{\left(\frac{k_\ell}{\bar{h}}\right)^2 + 2\frac{k_\ell}{\rho h_{s\ell}}\int_0^t \left[T_a(t) - T_f\right]dt\right\}^{1/2} \quad \text{for} \quad t \ge 0 \tag{4.4.63}$$

$$T_\ell(x,t) = T_f(t)\left[T_a(t) - T_f\right]\frac{\bar{h}\left[X(t) - x\right]}{\bar{h}X(t) + k_\ell} \quad \text{in} \quad 0 \le x \le X(t) \quad \text{for} \quad t > 0 \tag{4.4.64}$$

Examples of the Quasi-Static Approximation for Cylindrical Coordinate Geometries. It is assumed in these examples that the cylinders are very long and that the problems are axisymmetric. Just as in the Cartesian coordinate case, the energy equation (4.4.51) is reduced by the approximation to its steady-state form. Here

$$T_\ell(r_i,t) = T_0(t) > T_f \quad \text{for} \quad t > 0 \tag{4.4.65}$$

Consider the *outward-directed melting* of a hollow cylinder due to a temperature imposed at the internal radius r_i. The solution is

$$T_\ell(r,t) = T_f + \left[T_0(t) - T_f\right]\frac{\ln\left[r/R(t)\right]}{\ln\left[r_i/R(t)\right]} \quad \text{in} \quad r_i \le r \le R(t) \quad \text{for} \quad t > 0 \tag{4.4.66}$$

and the transient position of the phase front, $R(t)$, can be calculated from the transcendental equation

$$2R(t)^2 \ln\frac{R(t)}{r_i} = R(t)^2 - r_i^2 + \frac{4k_\ell}{\rho h_{s\ell}}\int_0^t \left[T_0(t) - T_f\right]dt \tag{4.4.67}$$

If the melting for the same case occurs due to the imposition of a *heat flux q_0 at r_p*

$$-k_\ell\left(\frac{dT_\ell}{dx}\right)_{r_i,t} = q_0(t) > 0 \quad \text{for} \quad t > 0 \tag{4.4.68}$$

the solution is

$$T_\ell(r,t) = T_f - \frac{q_0(t)r_i}{k_\ell}\ln\frac{r}{R(t)} \quad \text{in} \quad r_i \le r \le R(t) \quad \text{for} \quad t > 0 \tag{4.4.69}$$

$$R(t) = \left(r_i^2 + 2\frac{r_i}{\rho h_{s\ell}} \int_0^t q_0(t)\, dt \right)^{1/2} \quad \text{for} \quad t > 0 \tag{4.4.70}$$

If the melting for the same case occurs due to the imposition of a *convective heat flux from a fluid at the transient temperature* $T_a(t)$, *with a heat transfer coefficient* $\bar{h}$, *at* r_i

$$-k_\ell \left(\frac{dT_\ell}{dr} \right)_{r_i,t} = \bar{h}\left[T_a(t) - T_f(r_i,t) \right] > 0 \quad \text{for} \quad t > 0 \tag{4.4.71}$$

The solution is

$$T_\ell(r,t) = T_f + \left[T_a(t) - T_f \right] \frac{\ln\left[r/R(t) \right]}{\ln\left[r_i/R(t) \right] - k_\ell/\bar{h} r_i} \quad \text{in} \quad r_i \le r \le R(t) \quad \text{at} \quad t > 0 \tag{4.4.72}$$

with $R(t)$ calculated from the transcendental equation

$$2R(t)^2 \ln \frac{R(t)}{r_i} = \left(1 - \frac{2k_\ell}{\bar{h} r_i} \right)\left[R(t)^2 - r_i^2 \right] + \frac{4k_\ell}{\rho h_{s\ell}} \int_0^t \left[T_a(t) - T_f \right] dt \tag{4.4.73}$$

The solutions for *inward melting* of a cylinder, where heating is applied at the outer radius r_o, are the same as the above-described ones for the outward-melting cylinder, if the replacements $r_i \to r_o$, $q_0 \to -q_0$, and $\bar{h} \to -\bar{h}$ are made. If such a cylinder is not hollow, then $r_i = 0$ is used.

Estimation of Freezing and Melting Time

There are a number of approximate formulas for estimating the freezing and melting times of different materials having a variety of shapes. The American Society of Heating, Refrigerating, and Air-Conditioning Engineers (ASHRAE) provides a number of such approximations for estimating the freezing and thawing times of foods (ASHRAE, 1993). For example, if it can be assumed that the freezing or thawing occurs at a single temperature, the time to freeze or thaw, t_f, for a body that has shape parameters P and R (described below) and thermal conductivity k, initially at the fusion temperature T_f, and which is exchanging heat via heat transfer coefficient $\bar{h}$ with an ambient at the constant T_a, can be approximated by Plank's equation

$$t_f = \frac{h_{s\ell}\rho}{\left| T_f - T_a \right|}\left(\frac{Pd}{\bar{h}} + \frac{Rd^2}{k} \right) \tag{4.4.74}$$

where d is the diameter of the body if it is a cylinder or a sphere, or the thickness when it is an infinite slab, and where the shape coefficients P and R for a number of body forms are given in Table 4.4.2. Shape coefficients for other body forms are also available. To use Equation 4.4.74 for freezing, k and ρ should be the values for the food in its frozen state. In thawing, they should be for the unfrozen food. Other simple approximations for melting and thawing times can be found in Cleland et al. (1987).

Example of Using Plank's Equation (4.4.74) for Estimating Freezing Time. Estimate the time needed to freeze a fish, the shape of which can be approximated by a cylinder 0.5 m long having a diameter of 0.1 m. The fish is initially at its freezing temperature, and during the freezing process it is surrounded by air at $T_a = -25°C$, with the cooling performed with a convective heat transfer coefficient $\bar{h} = 68$ W/m² K. For the fish, $T_f = -1°C$, $h_{s\ell} = 200$ kJ/kg, $\rho_s = 992$ kg/m³, and $k_s = 1.35$ W/m K.

<div align="center">

TABLE 4.4.2   Shape Factors for Equation (4.4.74)

Forms	*P*	*R*
Slab	1/2	1/8
Cylinder	1/4	1/16
Sphere	1/6	1/24

</div>

From ASHRAE, in *Fundamentals*, ASHRAE, Atlanta,
  1993, chap. 29. With permission.

By using Table 4.4.2, the geometric coefficients for the cylindrical shape of the fish are $P = {}^1\!/_2$ and $R = {}^1\!/_{16}$, while *d* is the cylinder diameter, = 0.1 m. Substituting these values into Equation (4.4.74) gives

$$t_f = \frac{200,000 \cdot 992}{-1-(-25)}\left(\frac{1/4(0.1)}{68} + \frac{1/16(0.1)^2}{1.35}\right) = 6866 \text{ sec} = 1.9 \text{ hr}$$

In fact, freezing or melting of food typically takes place over a range of temperatures, and approximate Plank-type formulas have been developed for various specific foodstuffs and shapes to represent reality more closely than Equation (4.4.74) (ASHRAE, 1993).

Alexiades and Solomon (1993) provide several easily computable approximate equations for estimating the time needed to melt a simple solid body initially at the fusion temperature T_f. It is assumed that conduction occurs in one phase (the liquid) only, that the problems are axi- and spherically symmetric for cylindrical and spherical bodies, respectively, and that the melting process for differently shaped bodies can be characterized by a single geometric parameter, *r*, in the body domain $0 \le r \le L$, using a shape factor, ω, defined by

$$\omega = \frac{LA}{V} - 1 \tag{4.4.75}$$

where *A* is the surface area across which the heat is transferred into the body and *V* is the body volume, to account for the specific body shape:

$$\omega = \begin{cases} 0 & \text{for a slab insulated at one end} \\ 1 & \text{for a cylinder} \\ 2 & \text{for a sphere} \end{cases} \tag{4.4.76}$$

$0 \le \omega \le 2$ always, and ω may be assigned appropriate values for shapes intermediate between the slab, cylinder, and sphere. For example, a football-shaped body, somewhere between a cylinder and sphere, may be assigned $\omega = 1.5$, and a short cylinder with a large diameter-to-height ratio may have $\omega = 0.5$.

For the case where the temperature $T_0 > T_f$ is imposed on the boundary at $t = 0$, the melt time, t_m can be estimated by

$$t_m = \frac{L^2}{2\alpha_\ell(1+\omega)\text{Ste}_\ell}\left[1 + \left(0.25 + 0.17\omega^{0.7}\right)\text{Ste}_\ell\right] \tag{4.4.77}$$

valid for $0 \le \text{Ste}_\ell \le 4$.

If the *heat input is convective*, with a heat transfer coefficient $\bar{h}$ from a fluid at temperature T_a, the approximate melt time is

$$t_m = \frac{L^2}{2\alpha_\ell(1+\omega)\text{Ste}_\ell}\left[1 + \frac{2k_\ell}{\bar{h}L} + \left(0.25 + 0.17\omega^{0.7}\right)\text{Ste}_\ell\right] \qquad (4.4.78)$$

valid for $0 \leq \text{Ste}_\ell \leq 4$ and $\bar{h}L/k_\ell \geq 0.1$, and the temperature, $T(0,t)$, of the surface across which the heat is supplied can be estimated from the implicit time-temperature relationship:

$$t = \frac{\rho c_\ell k_\ell}{2\bar{h}^2\text{Ste}_\ell}\left[1.18\text{Ste}_\ell\left(\frac{T(0,t) - T_f}{T_a - T(0,t)}\right)^{1.83} + \left(\frac{T_a - T_f}{T_a - T(0,t)}\right)^2 - 1\right] \qquad (4.4.79)$$

Both equations (4.4.78) and (4.4.79) are claimed to be accurate within 10%.

The suitability of using several simplified analytical solutions for the estimation of freezing and melting times for more-realistic problems was assessed by Dilley and Lior (1986).

Defining Terms

Eutectic concentration: A concentration of a component of a multicomponent liquid at which the liquid would upon freezing form a solid containing the same concentration, and at which the freezing process is completed at a single temperature.

Mushy zone: The zone composed of both liquid and solid, bounded by the liquidus and solidus curves, in a freezing or melting process.

References

Alexiades, V. and Solomon, A.D. 1993. *Mathematical Modeling of Melting and Freezing Processes,* Hemisphere Publishing, Washington, D.C.

ASHRAE (American Society of Heating, Refrigerating, and Air-Conditioning Engineers). 1993. Cooling and freezing times of foods, in *Fundamentals*, ASHRAE, Atlanta, GA, chap. 29.

ASHRAE (American Society of Heating, Refrigerating, and Air-Conditioning Engineers). 1990. *Refrigeration*, ASHRAE, Atlanta, GA.

Cheng, K.C. and Seki, N., Eds. 1991. *Freezing and Melting Heat Transfer in Engineering,* Hemisphere Publishing, Washington, D.C.

Cleland, D.J., Cleland, A.C., and Earle, R.L. 1987. Prediction of freezing and thawing times for multidimensional shapes by simple formulae: Part 1, regular shapes; Part 2, irregular shapes. *Int. J. Refrig.,* 10, 156–166; 234–240.

DeWinter, F. 1990. Energy storage of solar systems; in *Solar Collectors, Energy Storage, and Materials*, MIT Press, Cambridge, MA, Section II.

Dilley, J.F. and Lior, N. 1986. The evaluation of simple analytical solutions for the prediction of freeze-up time, freezing, and melting. *Proc. 8th International Heat Transfer Conf.*, 4, 1727–1732, San Francisco.

Flemings, M.C. 1974. *Solidification Processes*, McGraw-Hill, New York.

Fukusako, S. and Seki, N. 1987. Fundamental aspects of analytical and numerical methods on freezing and melting heat-transfer problems, in *Annual Review of Numerical Fluid Mechanics and Heat Transfer*, Vol. 1, T.C. Chawla, Ed., Hemisphere, Publishing, Washington, D.C., chap. 7, 351–402.

Goodman, T.R. 1964. Application of integral methods to transient nonlinear heat transfer, in *Advances in Heat Transfer*, Vol. 1, T.F. Irvine and J.P. Hartnett, Eds., Academic Press, San Diego, 51–122.

Hayashi, Y. and Kunimine, K. 1992. Solidification of mixtures with supercooling, in *Heat and Mass Transfer in Materials Processing*, I. Tanasawa and N. Lior, Eds., Hemisphere Publishing, New York, 265–277.

Incropera, F.P. and Viskanta, R. 1992. Effects of convection on the solidification of binary mixtures, in *Heat and Mass Transfer in Materials Processing*, I. Tanasawa and N Lior, Eds., Hemisphere Publishing, New York, 295–312.

Lunardini, V.J. 1981. *Heat Transfer in Cold Climate*, Van Nostrand-Reinhold, Princeton, NJ.

Poulikakos, D. 1994. *Conduction Heat Transfer,* Prentice-Hall, Englewood Cliffs, NJ.

Rubinsky, B. and Eto, T.K. 1990. Heat transfer during freezing of biological materials, in *Annual Review of Heat Transfer*, Vol. 3, C.L. Tien, Eds., Hemisphere Publishing, Washington, D.C., chap. 1, 1–38.

Tanasawa, I. and Lior, N., Ed. 1992. *Heat and Mass Transfer in Materials Processing*, Hemisphere Publishing, New York.

Yao, L.S. and Prusa, J. 1989. Melting and freezing, in *Advances in Heat Transfer*, Vol. 19, J.P. Hartnett and T.F. Irvine, Eds., Academic Press, San Diego, 1–95.

Further Information

Many textbooks on heat transfer (some listed in the References section above) contain material about melting and freezing, and many technical journals contain articles about this subject. Some of the major journals, classified by orientation, are

General: *ASME Journal of Heat Transfer, International Journal of Heat & Mass Transfer, Numerical Heat Transfer, Canadian Journal of Chemical Engineering, AIChE Journal*

Refrigeration: *Transactions of the ASHRAE, International Journal of Refrigeration, Referigeration, Journal of Food Science, Bulletin of the International Institute of Refrigeration*

Manufacturing: *ASME Journal of Engineering for Industry, Journal of Crystal Growth, Materials Science and Engineering A*

Geophysical, climate, cold regions engineering: *Limnology and Oceanography, Journal of Geophysical Research, ASCE Journal of Cold Regions Engineering, Cold Regions Science and Technology*

Medical: *Cryobiology, ASME Journal of Biomechanical Engineering, Journal of General Physiology*

4.5   Heat Exchangers

Ramesh K. Shah and Kenneth J. Bell

The two major categories of heat exchangers are shell-and-tube exchangers and compact exchangers. Basic constructions of gas-to-gas compact heat exchangers are plate-fin, tube-fin and all prime surface recuperators (including polymer film and laminar flow exchangers), and compact regenerators. Basic constructions of liquid-to-liquid and liquid-to-phase-change compact heat exchangers are gasketed and welded plate-and-frame, welded stacked plate (without frames), spiral plate, printed circuit, and dimple plate heat exchangers.

Shell-and-tube exchangers are custom designed for virtually any capacity and operating condition, from high vacuums to ultrahigh pressures, from cryogenics to high temperatures, and for any temperature and pressure differences between the fluids, limited only by the materials of construction. They can be designed for special operating conditions: vibration, heavy fouling, highly viscous fluids, erosion, corrosion, toxicity, radioactivity, multicomponent mixtures, etc. They are made from a variety of metal and nonmetal materials, and in surface areas from less than 0.1 to 100,000 m^2 (1 to over 1,000,000 ft^2). They have generally an order of magnitude less surface area per unit volume than the compact exchangers, and require considerable space, weight, support structure, and footprint.

Compact heat exchangers have a large heat transfer surface area per unit volume of the exchanger, resulting in reduced space, weight, support structure and footprint, energy requirement and cost, as well as improved process design, plant layout and processing conditions, together with low fluid inventory compared with shell-and-tube exchangers. From the operating condition and maintenance point of view, compact heat exchangers of different constructions are used for specific applications, such as for high-temperature applications (up to about 850°C or 1550°F), high pressure applications (over 200 bars), and moderate fouling applications. However, applications do not involve both high temperature and pressure simultaneously. Plate-fin exchangers are generally brazed, and the largest size currently manufactured is $1.2 \times 1.2 \times 6$ m ($4 \times 4 \times 20$ ft). Fouling is one of the major potential problems in many compact exchangers except for the plate heat exchangers. With a large frontal area exchanger, flow maldistribution could be another problem. Because of short transient times, a careful design of controls is required for startup of some compact heat exchangers compared with shell-and-tube exchangers. No industry standards or recognized practice for compact heat exchangers is yet available.

This section is divided into two parts: Compact Heat Exchangers and Shell-and-Tube Exchangers, written by R. K. Shah and K. J. Bell, respectively. In the compact heat exchangers section, the following topics are covered: definition and description of exchangers, heat transfer and pressure drop analyses, heat transfer and flow friction correlations, exchanger design (rating and sizing) methodology, flow maldistribution, and fouling. In the shell-and-tube heat exchangers section, the following topics are covered: construction features, principles of design, and an approximate design method with an example.

Compact Heat Exchangers

Ramesh K. Shah

Introduction

A heat exchanger is a device to provide for transfer of internal thermal energy (enthalpy) between two or more fluids, between a solid surface and a fluid, or between solid particulates and a fluid, in thermal contact without external heat and work interactions. The fluids may be single compounds or mixtures. Typical applications involve heating or cooling of a fluid stream of concern, evaporation or condensation of single or multicomponent fluid stream, and heat recovery or heat rejection from a system. In other applications, the objective may be to sterilize, pasteurize, fractionate, distill, concentrate, crystallize, or control process fluid. In some heat exchangers, the fluids transferring heat are in direct contact. In other heat exchangers, heat transfer between fluids takes place through a separating wall or into and out of a

wall in a transient manner. In most heat exchangers, the fluids are separated by a heat transfer surface and do not mix. Such exchangers are referred to as *direct transfer type*, or simply *recuperators*. Exchangers in which there is an intermittent flow of heat from the hot to cold fluid (via heat storage and heat rejection through the exchanger surface or matrix) are referred to as *indirect transfer type* or simply *regenerators.*

The heat transfer surface is a surface of the exchanger core which is in direct contact with fluids and through which heat is transferred by conduction in a recuperator. The portion of the surface which also separates the fluids is referred to as a *primary* or *direct surface.* To increase heat transfer area, appendages known as fins may be intimately connected to the primary surface to provide an *extended*, *secondary*, or *indirect surface.* Thus, the addition of fins reduces the thermal resistance on that side and thereby increases the net heat transfer from the surface for the same temperature difference.

Heat exchangers may be classified according to transfer process, construction, flow arrangement, surface compactness, number of fluids, and heat transfer mechanisms as shown in Figure 4.5.1.
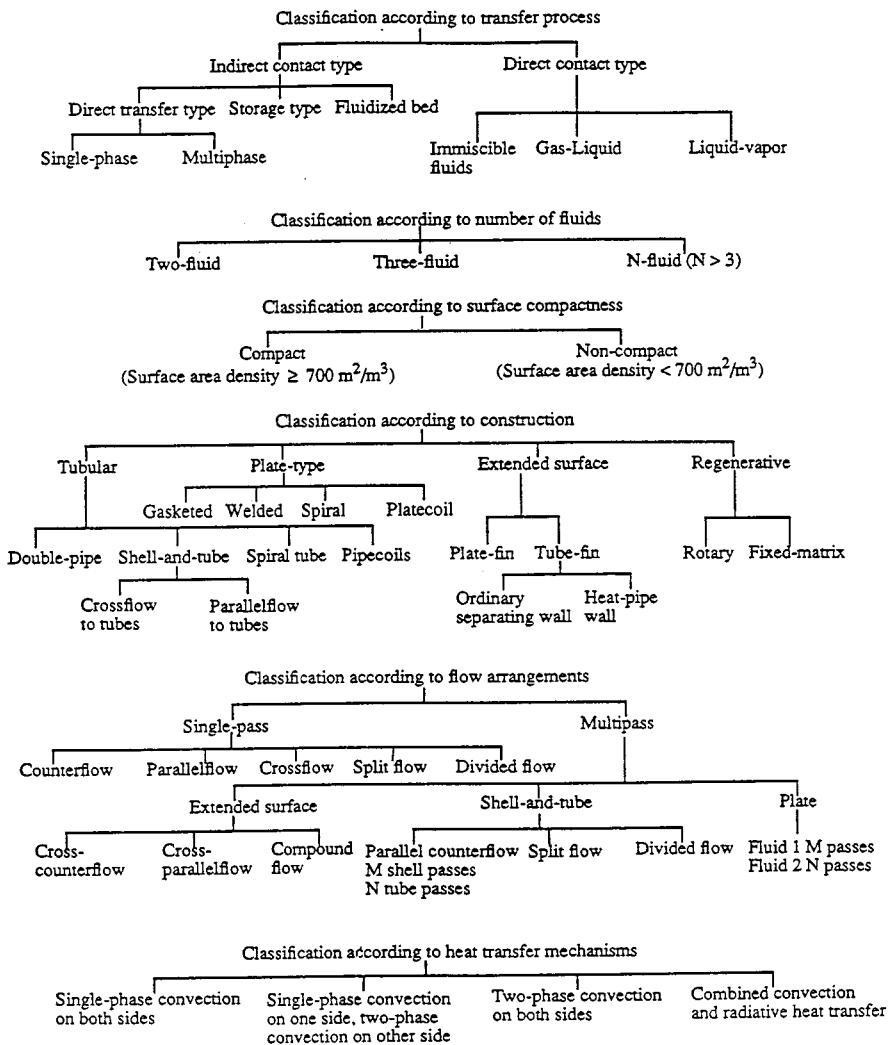

FIGURE 4.5.1 Classification of heat exchangers.

A gas-to-fluid heat exchanger is referred to as a compact heat exchanger if it incorporates a heat transfer surface having a surface area density above about 700 m^2/m^3 (213 ft^2/ft^3) on at least one of the fluid sides which usually has gas flow. It is referred to as a laminar flow heat exchanger if the surface area density is above about 3000 m^2/m^3 (914 ft^2/ft^3), and as a micro heat exchanger if the surface area density is above about 10,000 m^2/m^3 (3050 ft^2/ft^3). A liquid/two-phase heat exchanger is referred to as a compact heat exchanger is the surface area density on any one fluid side is above about 400 m^2/m^3 (122 ft^2/ft^3). A typical process industry shell-and-tube exchanger has a surface area density of less than 100 m^2/m^3 on one fluid side with plain tubes, and two to three times that with the high-fin-density low-finned tubing. Plate-fin, tube-fin, and rotary regenerators are examples of compact heat exchangers for gas flows on one or both fluid sides, and gasketed and welded plate heat exchangers are examples of compact heat exchangers for liquid flows.

Types and Description

Gas-to-Fluid Exchangers.

The important design and operating considerations for compact extended surface exchangers are (1) usually at least one of the fluids is a gas or specific liquid that has low *h*; (2) fluids must be clean and relatively noncorrosive because of small hydraulic diameter (D_h) flow passages and no easy techniques for mechanically cleaning them; (3) the fluid pumping power (i.e., pressure drop) design constraint is often equally as important as the heat transfer rate; (4) operating pressures and temperatures are somewhat limited compared with shell-and-tube exchangers as a result of the joining of the fins to plates or tubes such as brazing, mechanical expansion, etc.; (5) with the use of highly compact surfaces, the resultant shape of a gas-to-fluid exchanger is one having a large frontal area and a short flow length (the header design of a compact heat exchanger is thus important for a uniform flow distribution among the very large number of small flow passages); (6) the market potential must be large enough to warrant the sizable manufacturing research and tooling costs for new forms to be developed.

Some advantages of plate-fin exchangers over conventional shell-and-tube exchangers are as follows. Compact heat exchangers, generally fabricated from thin metallic plates, yield large heat transfer surface area per unit volume (β), typically up to ten times greater than the 50 to 100 m^2/m^3 provided by a shell-and-tube exchanger for general process application and from 1000 to 6000 m^2/m^3 for highly compact gas side surfaces. Compact liquid or two-phase side surfaces have a β ratio ranging from 500 to 600 m^2/m^3. A compact exchanger provides a tighter temperature control; thus it is useful for heat-sensitive materials, improves the product (e.g., refining fats from edible oil) and its quality (such as a catalyst bed). Also, a compact exchanger could provide rapid heating or cooling of a process stream, thus improving the product quality. The plate-fin exchangers can accommodate multiple (up to 12 or more) fluid streams in one exchanger unit with proper manifolding, thus allowing process integration and cost-effective compact solutions.

Fouling is one of the potential major problems in compact heat exchangers (except for plate-and-frame heat exchangers), particularly those having a variety of fin geometries or very fine circular or noncircular flow passages that cannot be cleaned mechanically. Chemical cleaning may be possible; thermal baking and subsequent rinsing is possible for small-size units. Hence, extended surface compact heat exchangers may not be used in heavy fouling applications.

Liquid-to-Liquid Exchangers.

Liquid-to-liquid and phase-change exchangers are plate-and-frame and welded plate heat exchangers (PHE), spiral plate, and printed circuit exchangers; some of them are described next in some detail along with other compact heat exchangers and their applications.

Plate-Fin Heat Exchangers.

This type of exchanger has "corrugated" fins or spacers sandwiched between parallel plates (referred to as plates or parting sheets) as shown in Figure 4.5.2. Sometimes fins are incorporated in a flat tube with rounded corners (referred to as a formed tube), thus eliminating a need for the side bars. If liquid or
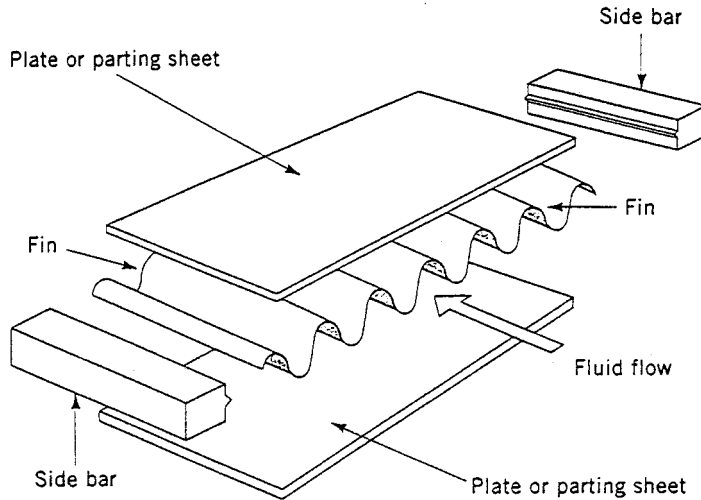
FIGURE 4.5.2 Typical components of a plate-fin exchanger.

phase-change fluid flows on the other side, the parting sheet is usually replaced by a flat tube with or without inserts/webs. Other plate-fin constructions include drawn-cup (see Figure 4.5.3) or tube-and-
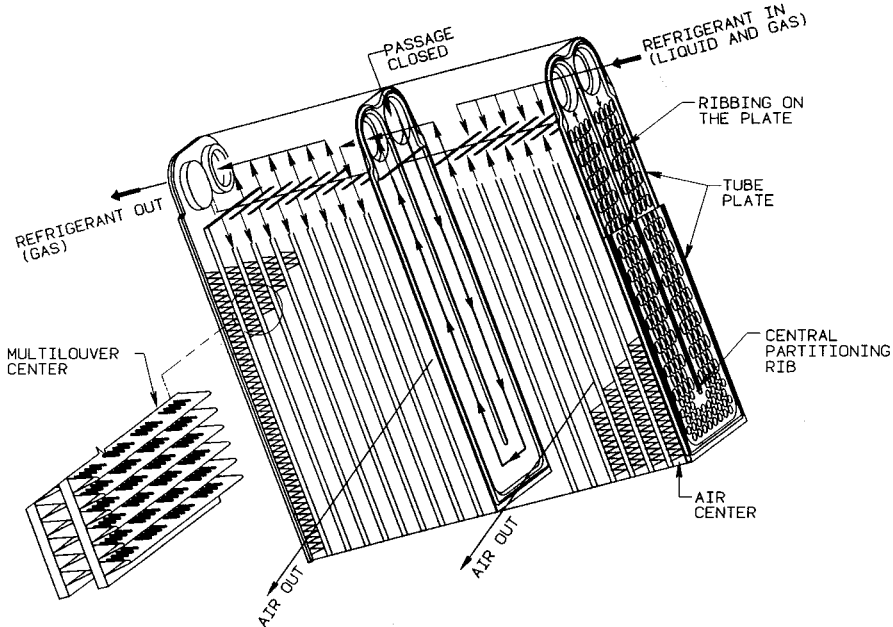
FIGURE 4.5.3 U-channel ribbed plates and multilouver fin automotive evaporator. (Courtesy of Delphi Harrison Thermal Systems, Lockport, NY.)

center configurations. Fins are die- or roll-formed and are attached to the plates by brazing, soldering, adhesive bonding, welding, mechanical fit, or extrusion. Fins may be used on both sides in gas-to-gas heat exchangers. In gas-to-liquid applications, fins are usually used only on the gas side; if employed on the liquid side, they are used primarily for structural strength and flow-mixing purposes. Fins are also sometimes used for pressure containment and rigidity.
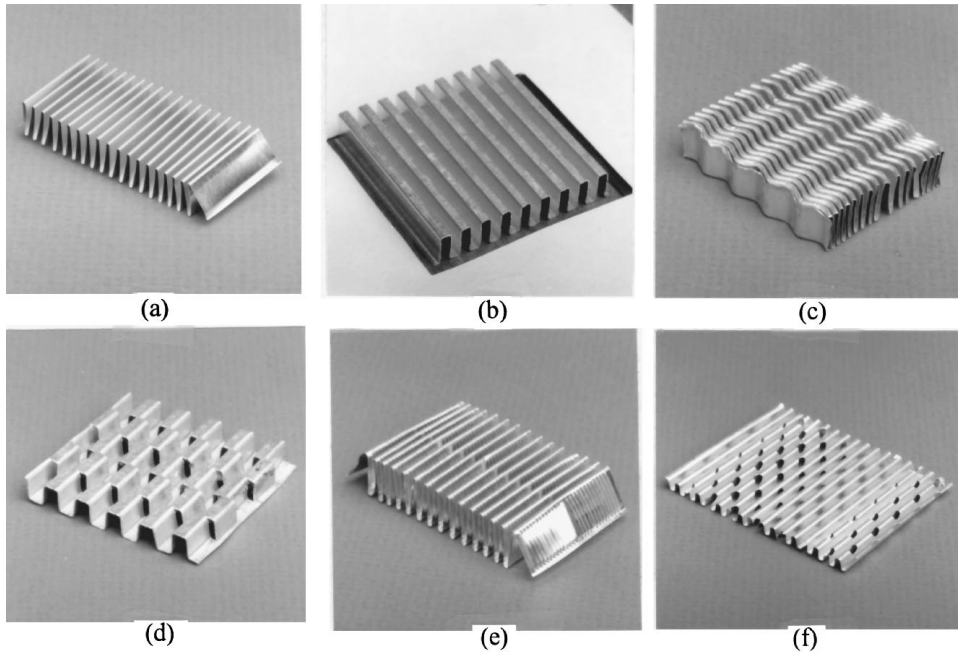
FIGURE 4.5.4 Fin geometries for plate-fin heat exchangers: (a) plain triangular fin, (b) plain rectangular fin, (c) wavy fin, (d) offset strip fin, (e) multilouver fin, and (f) perforated fin.

Plate fins are categorized as (1) plain (i.e., uncut) and straight fins, such as plain triangular and rectangular fins; (2) plain but wavy fins (wavy in the main fluid flow direction); and (3) interrupted fins such as offset strip, louver, and perforated. Examples of commonly used fins are shown in Figure 4.5.4.

Plate-fin exchangers have been built with a surface area density of up to about 5900 m^2/m^3 (1800 ft^2/ft^3). There is a total freedom of selecting fin surface area on each fluid side, as required by the design, by varying fin height and fin density. Although typical fin densities are 120 to 700 fins/m (3 to 18 fins/in.), applications exist for as many as 2100 fins/m (53 fins/in.). Common fin thicknesses range from 0.05 to 0.25 mm (0.002 to 0.010 in.). Fin heights range from 2 to 25 mm (0.08 to 1.0 in.). A plate-fin exchanger with 600 fins/m (15.2 fins/in.) provides about 1300 m^2 (400 ft^2/ft^3) of heat transfer surface area per cubic meter volume occupied by the fins. Plate-fin exchangers are manufactured in virtually all shapes and sizes, and made from a variety of materials.

Tube-Fin Heat Exchangers.
In this type of exchanger, round and rectangular tubes are the most common, although elliptical tubes are also used. Fins are generally used on the outside, but they may be used on the inside of the tubes in some applications. They are attached to the tubes by a tight mechanical fit, tension winding, adhesive bonding, soldering, brazing, welding, or extrusion. Fins on the outside of the tubes may be categorized as follows: (1) normal fins on individual tubes, referred to as individually finned tubes or simply as *finned tubes*, as shown in Figures 4.5.6 and 4.5.5a; (2) flat or continuous (plain, wavy, or interrupted) external fins on an array of tubes, as shown in Figures 4.5.7 and 4.5.5b; (3) longitudinal fins on individual tubes. The exchanger having flat (continuous) fins on tubes has also been referred to as a *plate-fin and tube* exchanger in the literature. In order to avoid confusion with plate-fin surfaces, we will refer to it as a tube-fin exchanger having flat (plain, wavy, or interrupted) fins. Individually finned tubes are probably more rugged and practical in large tube-fin exchangers. Shell-and-tube exchangers sometimes employ low-finned tubes to increase the surface area on the shell side when the shell-side heat transfer coefficient is low compared with the tube side coefficient. The exchanger with flat fins is usually less expensive on a unit heat transfer surface area basis because of its simple and mass-production-type construction
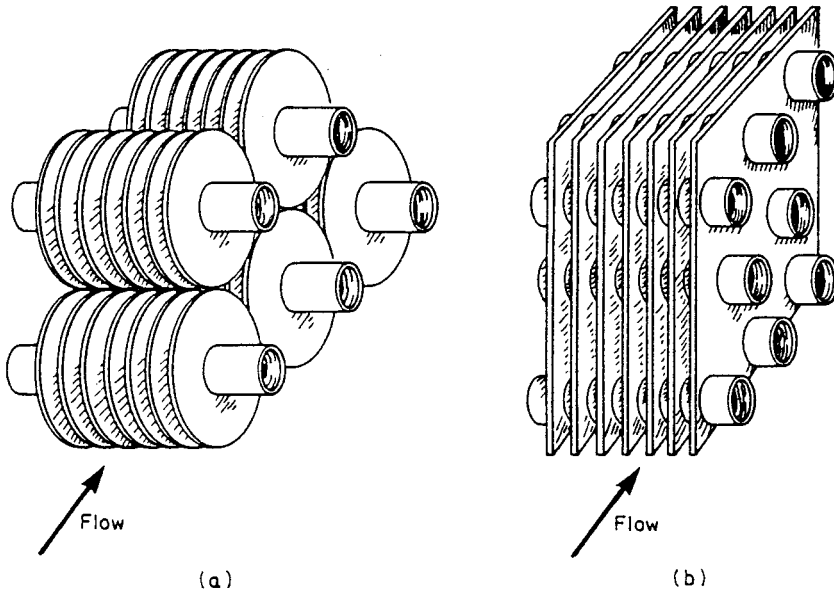
FIGURE 4.5.5 (a) Individually finned tubes, (b) flat or continuous fins on an array of tubes.
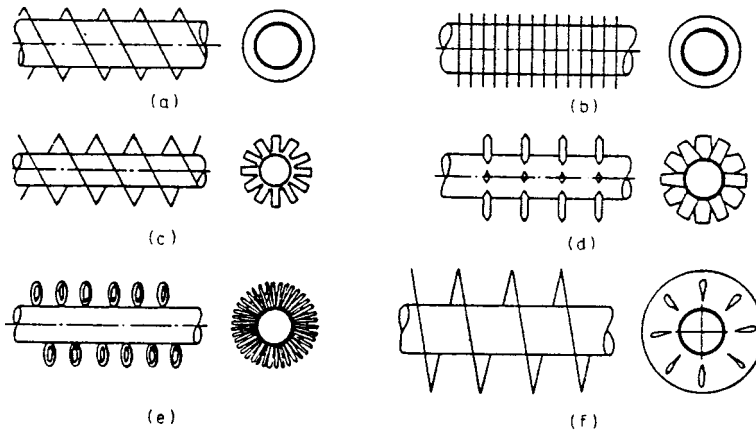
FIGURE 4.5.6 Individually finned tubes: (a) helical, (b) annular disk, (c) segmented, (d) studded, (e) wire loop, and (f) slotted helical.

features. Longitudinal fins are generally used in condensing applications and for viscous fluids in double-pipe heat exchangers.

Tube-fin exchangers can withstand high pressures on the tube side. The highest temperature is again limited by the type of bonding, the materials employed, and the material thickness. Tube-fin exchangers with an area density of about 3300 m^2/m^3 (1000 ft^2/ft^2) are commercially available. On the fin side, the desired surface area can be employed by using the proper fin density and fin geometry. The typical fin densities for flat fins vary from 250 to 800 fins/m (6 to 20 fins/in.), fin thicknesses vary from 0.08 to 0.25 mm (0.003 to 0.010 in.), and fin flow lengths from 25 to 250 mm (1 to 10 in.). A tube-fin exchanger having flat fins with 400 fins/m (10 fins/in.) has a surface area density of about 720 m^2/m^3(220 ft^2/ft^3). These exchangers are extensively used as condensers and evaporators in air-conditioning and refrigeration applications, as condensers in electric power plants, as oil coolers in propulsive power plants, and as air-cooled exchangers (also referred to as a fin-fan exchanger) in process and power industries.
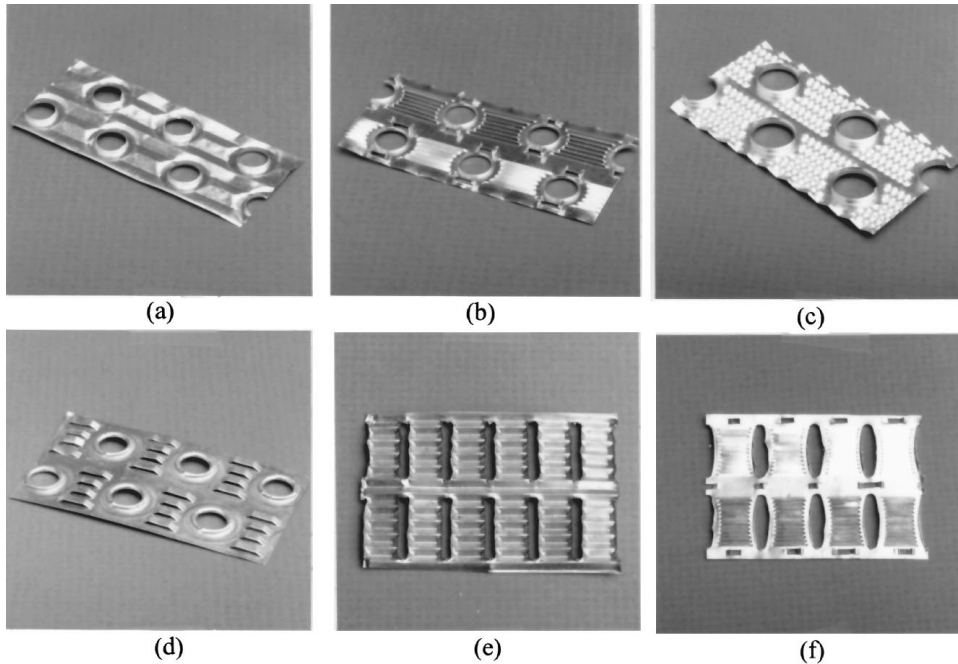
FIGURE 4.5.7 Flat or continuous fins on an array of tubes: On round tubes: (a) wavy fin, (b) multilouver fin, (c) fin with structured surface roughness (dimples), (d) parallel louver fin; (e) louver fin on flat tubes; (f) multilouver fin on elliptical tubes.

Regenerators.

The regenerator is a storage-type exchanger. The heat transfer surface or elements are usually referred to as a matrix in the regenerator. In order to have continuous operation, either the matrix must be moved periodically into and out of the fixed streams of gases, as in a *rotary* regenerator (Figure 4.5.8a), or the gas flows must be diverted through valves to and from the fixed matrices as in a *fixed-matrix* regenerator (Figure 4.5.8b). The latter is also sometimes referred to as a *periodic-flow regenerator* or a *reversible heat accumulator*. A third type of regenerator has a fixed matrix (in the disk form) and the fixed stream of gases, but the gases are ducted through rotating hoods (headers) to the matrix as shown in Figure 4.5.8c. This Rothemuhle regenerator is used as an air preheater in some power-generating plants. The thermodynamically superior counterflow arrangement is usually employed in regenerators.

The **rotary regenerator** is usually a disk type in which the matrix (heat transfer surface) is in a disk form and fluids flow axially. It is rotated by a hub shaft or a peripheral ring gear drive. For a rotary regenerator, the design of seals to prevent leakage of hot to cold fluids and vice versa becomes a difficult task, especially if the two fluids are at significantly differing pressures. Rotating drives also pose a challenging mechanical design problem.

Major advantages of rotary regenerators are the following. For a highly compact regenerator, the cost of the regenerator surface per unit of heat transfer area is usually substantially lower than that for the equivalent recuperator. A major disadvantage of a regenerator is an unavoidable carryover of a small fraction of the fluid trapped in the passage to the other fluid stream just after the periodic flow switching. Since fluid contamination (small mixing) is prohibited with liquids, the regenerators are used exclusively for gas-to-gas heat or energy recovery applications. Cross contamination can be minimized significantly by providing a purge section in the disk and using double-labyrinth seals.

Rotary regenerators have been designed for a surface area density of up to about 6600 m²/m³ (2000 ft²/ft³), and exchanger effectivenesses exceeding 85% for a number of applications. They can employ thinner stock material, resulting in the lowest amount of material for a given effectiveness and pressure
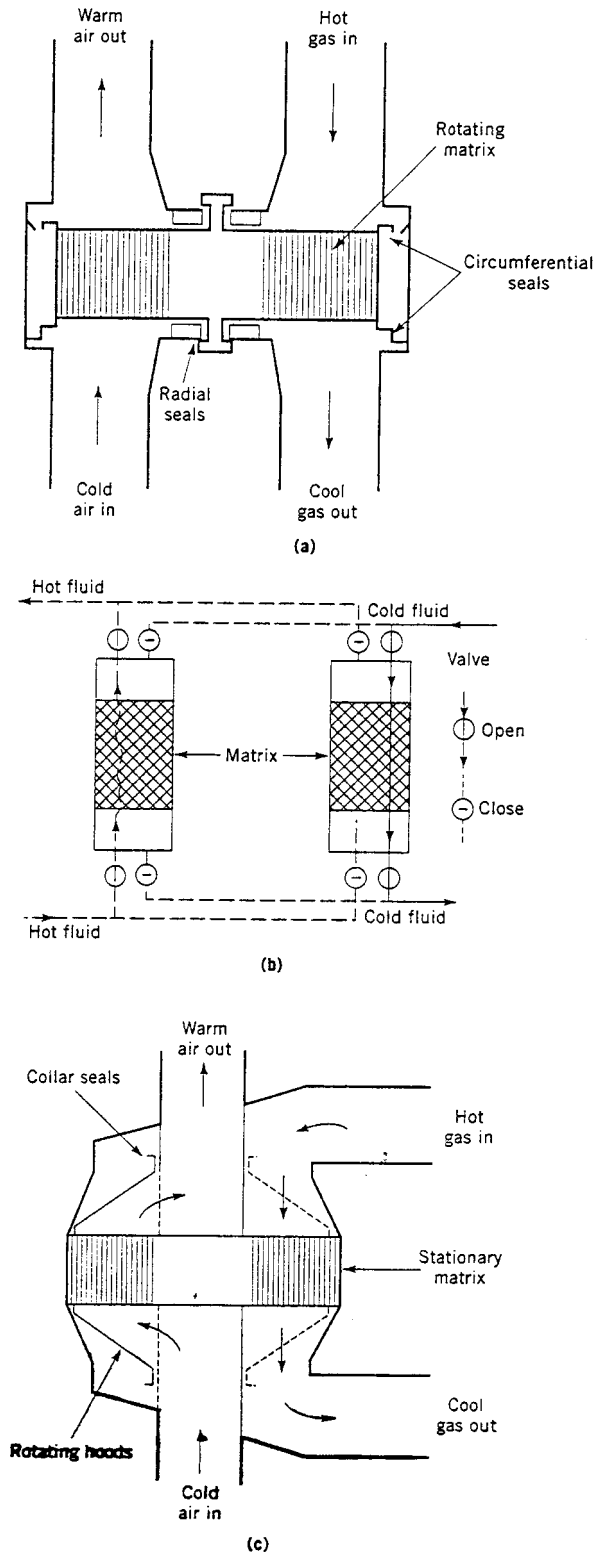
FIGURE 4.5.8 Regenerators: (a) rotary, (b) fixed-matrix, and (c) Rothemuhle.

drop of any heat exchanger known today. The metal rotary regenerators have been designed for continuous inlet temperatures up to about 790°C (1450°F) and ceramic matrices for higher-temperature applications; these regenerators are designed up to 400 kPa or 60 psi pressure differences between hot and cold gases. Plastic, paper, and wool are used for regenerators operating below 65°C (150°F) inlet temperature of the hot gas and 1 atm pressure. Typical regenerator rotor diameters and rotational speeds are as follows: up to 10 m (33 ft) and 0.5 to 3 rpm for power plant regenerators, 0.25 to 3 m (0.8 to 9.8 ft) and up to 10 rpm for air-ventilating regenerators, and up to 0.6 m (24 in.) and up to 18 rpm for vehicular regenerators. Refer to Shah (1994) for the description of **fixed-matrix regenerator**, also referred to as a *periodic-flow*, *fixed bed*, *valved*, or *stationary* regenerator.

Plate-Type Heat Exchangers.

These exchangers are usually built of thin plates (all prime surface). The plates are either smooth or have some form of corrugations, and they are either flat or wound in an exchanger. Generally, these exchangers cannot accommodate very high pressures, temperatures, and pressure and temperature differentials. These exchangers may be further classified as plate, spiral plate, lamella, and plate-coil exchangers as classified in Figure 4.5.1. The plate heat exchanger, being the most important of these, is described next.

The **plate-and-frame** or **gasketed PHE** consists of a number of thin rectangular corrugated or embossed metal plates sealed around the edges by gaskets and held together in a frame as shown in Figure 4.5.9. The plate pack with fixed and movable end covers is clamped together by long bolts, thus compressing the gaskets and forming a seal. Sealing between the two fluids is accomplished by elastomeric molded gaskets (typically 5 mm or 0.2 in. thick) that are fitted in peripheral grooves mentioned earlier. The most conventional flow arrangement is one pass to one pass counterflow with all inlet and outlet connections on the fixed end cover. By blocking flow through some ports with proper gasketing, either one or both fluids could have more than one pass. Also more than one exchanger can be accommodated in a single frame with the use of intermediate connector plates such as up to five "exchangers" or sections to heat, cool, and regenerate heat between raw milk and pasteurized milk in a milk pasteurization application.

FIGURE 4.5.9 A plate-and-frame or gasketed PHE.

TABLE 4.5.1   Some Geometric and Operating Condition Characteristics of Plate-and-Frame Heat Exchangers

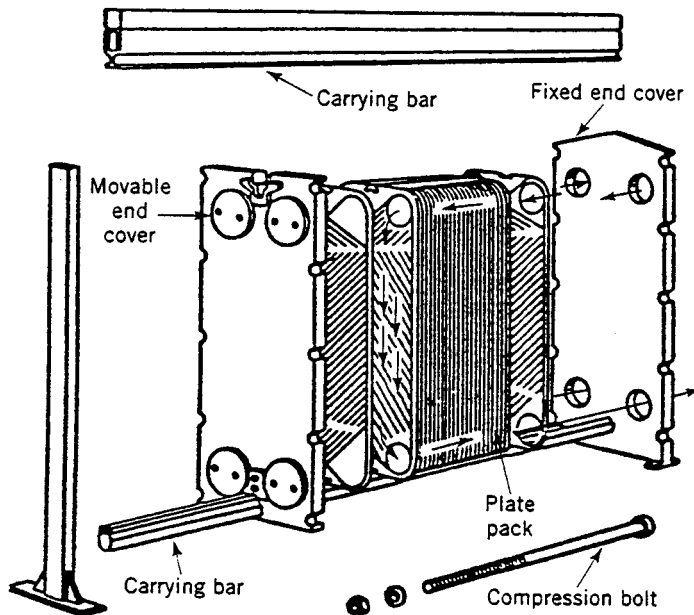| Unit		Operation	
Maximum surface area	2500 m^2	Pressure	0.1 to 2.5 MPa
Number of plates	3–700	Temperature	–40 to 260°C
Port size	Up to 400 mm	Maximum port velocity	6 m/sec
Plates		Channel flow rates	0.05 to 12.5 m^3/hr
Thickness	0.5–1.2 mm	Max unit flow rate	2500 m^3/hr
Size	0.03–3.6 m^2	**Performance**	
Spacing	1.5–5 mm	Temperature approach	As low as 1°C
Width	70–1200 mm	Heat exchanger efficiency	Up to 93%
Length	0.6–5 m	Heat transfer coefficients for water-water duties	3000 to 7000 W/m^2 K

Source: From Shah, R.K., in *Encyclopedia of Energy Technology and the Environment*, A. Bision and S.G. Boots, Eds., John Wiley & Sons, New York, 1994, 1651–1670. With permission.

Typical PHE dimensions and performance parameters are given in Table 4.5.1 (Shah, 1994). Any metal which can be cold-worked is suitable for PHE applications. The most common plate materials are stainless steel (AISI 304 or 316) and titanium. Plates made from Incoloy 825, Inconel 625, Hastelloy C-276 are also available. Nickel, cupronickel, and monel are rarely used. Carbon steel is not used because of low corrosion resistance for thin plates. The heat transfer surface area per unit volume for plate exchangers ranges from 120 to 660 m^2/m^3 (37 to 200 ft^2/ft^3).

In PHEs, the high turbulence due to plates reduces fouling from about 10 to 25% of that of a shell-and-tube exchanger. High thermal performance can be achieved in plate exchangers because the high degree of counterflow in PHEs makes temperature approaches of up to 1°C (2°F) possible. The high thermal effectiveness (up to about 93%) makes low-grade heat recovery economical. PHEs are most suitable for liquid-liquid heat transfer duties.

Welded PHEs. One of the limitations of gasketed PHE is the presence of the gaskets which restricts the use to compatible fluids and which limits operating temperatures and pressures. In order to overcome this limitation, a number of welded PHE designs have surfaced with a welded pair of plates for one or both fluid sides. However, the disadvantage of such design is the loss of disassembling flexibility on the fluid side where the welding is done. Essentially, welding is done around the complete circumference where the gasket is normally placed. A *stacked plate heat exchanger* is another welded PHE design from Pacinox in which rectangular plates are stacked and welded at the edges. The physical size limitations of PHEs (1.2 m wide × 4 m long max, 4 × 13 ft) are considerably extended to 1.5 m wide × 20 m long (5 × 66 ft) in this exchanger. A maximum surface area of (10,000 m^2 or over 100,000 ft^2) can be accommodated in one unit. The potential maximum operating temperature is 815°C (1500°F) with an operating pressure of up to 20 MPa (3000 psig) when the stacked plate assembly is placed in a cylindrical pressure vessel. For operating pressures below 2 MPa (300 psig) and operating temperatures below 200°C (400°F), the plate bundle is not contained in a pressure vessel, but is bolted between two heavy plates. Some of the applications of this exchanger are catalytic reforming, hydrosulfurization, crude distillation, synthesis converter feed effluent exchanger for methanol, propane condenser, etc.

A number of other PHE constructions have been developed to address some of the limitations of the conventional PHEs. A double-wall PHE is used to avoid mixing of the two fluids. A wide-gap PHE is used for fluids having high fiber content or coarse particles. A graphite PHE is used for highly corrosive fluids. A flow-flex exchanger has plain fins on one side between plates and the other side has conventional plate channels, and is used to handle asymmetric duties (flow rate ratio of 2 to 1 and higher).

A vacuum **brazed PHE** is a compact PHE for high-temperature and high-pressure duties, and it does not have gaskets, tightening bolts, frame, or carrying and guide bars. It simply consists of stainless steel plates and two end plates. The brazed unit can be mounted directly on piping without brackets and foundations.

Printed Circuit Heat Exchangers. This exchanger, as shown in Figure 4.5.10, has only primary heat transfer surfaces as PHEs. Fine grooves are made in the plate by using the same techniques as those employed for making printed electrical circuits. High surface area densities (650 to 1350 m^2/m^3 or 200 to 400 ft^2/ft^3 for operating pressures of 500 to 100 bar respectively) are achievable. A variety of materials including stainless steel, nickel, and titanium alloys can be used. It has been successfully used with relatively clean gases, liquids and phase-change fluids in chemical processing, fuel processing, waste heat recovery, and refrigeration industries. Again, this exchanger is a new construction with limited special applications currently.
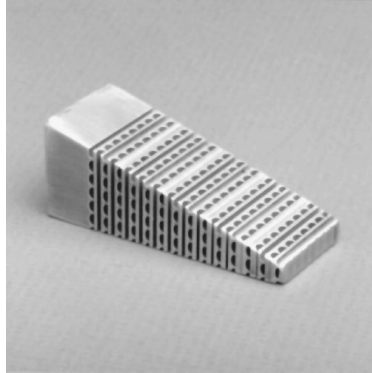
FIGURE 4.5.10 A section of a printed circuit heat exchanger. (Courtesy of Heatric Ltd., Dorset, U.K.)

Exchanger Heat Transfer and Pressure Drop Analysis

In this subsection, starting with the thermal circuit associated with a two-fluid exchanger, ε-NTU, P-NTU, and mean temperature difference (MTD) methods used for an exchanger analysis are presented, followed by the fin efficiency concept and various expressions. Finally, pressure drop expressions are outlined for various single-phase exchangers.

Two energy conservation differential equations for a two-fluid exchanger with any flow arrangement are (see Figure 4.5.11 for counterflow)

$$dq = q'' \, dA = -C_h \, dT_h = \pm C_c \, dT_c \qquad (4.5.1)$$

where the ± sign depends upon whether dT_c is increasing or decreasing with increasing dA or dx. The local overall rate equation is

$$dq = q'' \, dA = U\left(T_h - T_c\right)_{\text{local}} dA = U \, \Delta T \, dA \qquad (4.5.2)$$

Integration of Equations (4.5.1) and (4.5.2) across the exchanger surface area results in

$$q = C_h\left(T_{h,i} - T_{h,o}\right) = C_c\left(T_{c,o} - T_{c,i}\right) \qquad (4.5.3)$$

and

$$q = UA \, \Delta T_m = \Delta T_m / R_o \qquad (4.5.4)$$

where ΔT_m is the true mean temperature difference (or MTD) that depends upon the exchanger flow arrangement and degree of fluid mixing within each fluid stream. The inverse of the overall thermal conductance UA is referred to as the overall thermal resistance R_o as follows (see Figure 4.5.12).
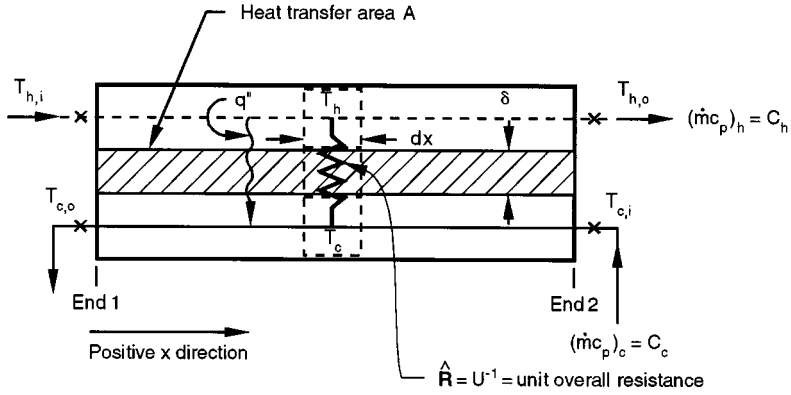
FIGURE 4.5.11 Nomenclature for heat exchanger variables.
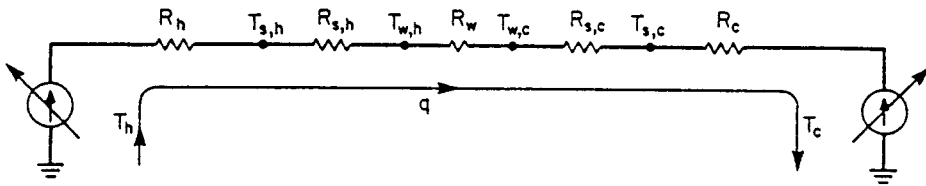
FIGURE 4.5.12 Thermal circuit for heat transfer in an exchanger.

$$R_o = R_h + R_{s,h} + R_w + R_{s,c} + R_c \qquad (4.5.5)$$

where the subscripts h, c, s, and w denote hot, cold, fouling (or scale), and wall, respectively. In terms of the overall and individual heat transfer coefficients, Equation (4.5.5) is represented as

$$\frac{1}{UA} = \frac{1}{(\eta_o hA)_h} + \frac{1}{(\eta_o h_s A)_h} + R_w + \frac{1}{(\eta_o h_s A)_c} + \frac{1}{(\eta_o hA)_c} \qquad (4.5.6)$$

where η_o = the overall surface efficiency of an extended (fin) surface and is related to the fin efficiency η_f, fin surface area A_f, and the total surface area A as follows:

$$\eta_o = 1 - \frac{A_f}{A}\left(1 - \eta_f\right) \qquad (4.5.7)$$

The wall thermal resistance R_w of Equation (4.5.5) is given by

$$
R_w = \begin{cases}
\delta/A_w k_w & \text{for a flat wall} \\[2ex]
\dfrac{\ln(d_o/d_j)}{2\pi k_w L N_t} & \text{for a circular tube with a single-layer wall} \\[3ex]
\dfrac{1}{2\pi L N_t}\left[\displaystyle\sum_j \dfrac{\ln(d_{j+1}/d_j)}{k_{w,j}}\right] & \text{for a circular tube with a multiple-layer wall}
\end{cases}
\tag{4.5.8}
$$

If one of the resistances on the right-hand side of Equation (4.5.5) or (4.5.6) is significantly higher than the other resistances, it is referred to as the *controlling thermal resistance*. A reduction in the controlling thermal resistance will have much more impact in reducing the exchanger surface area (*A*) requirement compared with the reduction in *A* as a result of the reduction in other thermal resistances.

UA of Equation (4.5.6) may be defined in terms of hot or cold fluid side surface area or wall conduction area as

$$
UA = U_h A_h = U_c A_c = U_w A_w
\tag{4.5.9}
$$

When R_w is negligible, $T_{w,h} = T_{w,c} = T_w$ of Figure 4.5.12 is computed from

$$
T_w = \frac{T_h + \left[(R_h + R_{s,h})/(R_c + R_{s,c})\right] T_c}{1 + \left[(R_h + R_{s,h})/(R_c + R_{s,c})\right]}
\tag{4.5.10}
$$

When $R_{s,h} = R_{s,c} = 0$, Equation (4.5.10) reduces to

$$
T_w = \frac{T_h/R_h + T_c/R_c}{1/R_h + 1/R_c} = \frac{(\eta_o h A)_h T_h + (\eta_o h A)_c T_c}{(\eta_o h A)_h + (\eta_o h A)_c}
\tag{4.5.11}
$$

ε-NTU, P-NTU, and MTD Methods. If we consider the fluid outlet temperatures or heat transfer rate as dependent variables, they are related to independent variable/parameters of Figure 4.5.11 as follows.

$$
T_{h,o},\ T_{c,o},\ \text{or}\ \ q = \phi\{T_{h,i},\ T_{c,i},\ C_c,\ C_h,\ U,\ A,\ \text{flow arrangement}\}
\tag{4.5.12}
$$

Six independent and three dependent variables of Equation (4.5.12) for a given flow arrangement can be transferred into two independent and one dependent dimensionless groups; three different methods are presented in Table 4.5.2 based on the choice of three dimensionless groups. The relationship among three dimensionless groups is derived by integrating Equations (4.5.1) and (4.5.2) across the surface area for a specified exchanger flow arrangement. Such expressions are presented later in Table 4.5.4 for the industrially most important flow arrangements. Now we briefly describe the three methods.

In *the ε-NTU method*, the heat transfer rate from the hot fluid to the cold fluid in the exchanger is expressed as

$$
q = \varepsilon C_{\min}\left(T_{h,i} - T_{c,i}\right)
\tag{4.5.13}
$$

TABLE 4.5.2   General Functional Relationships and Dimensionless Groups for ε-NTU, P-NTU, and MTD Methods

ε-NTU Method	P-NTU Method[a]	MTD Method[a]
$q = \varepsilon C_{min}(T_{h,i} - T_{c,i})$	$q = P_1 C_1 \lvert T_{1,i} - T_{2,i}\rvert$	$q = UAF\Delta T_{lm}$
$\varepsilon = \phi(\text{NTU}, C^*, \text{flow arrangement})$	$P_1 = \phi(\text{NTU}_1, R_1, \text{flow arrangement})$	$F = \phi(P, R, \text{flow arrangement})$[b]
$\varepsilon = \dfrac{C_h\left(T_{h,i} - T_{h,o}\right)}{C_{min}\left(T_{h,i} - T_{c,i}\right)} = \dfrac{C_c\left(T_{c,o} - T_{c,i}\right)}{C_{min}\left(T_{h,i} - T_{c,i}\right)}$	$P_1 = \dfrac{T_{1,o} - T_{1,i}}{T_{2,i} - T_{1,i}}$	$F = \dfrac{\Delta T_m}{\Delta T_{lm}}$
$\text{NTU} = \dfrac{UA}{C_{min}} = \dfrac{1}{C_{min}}\displaystyle\int_A U\,dA$	$\text{NTU}_1 = \dfrac{UA}{C_1} = \dfrac{\lvert T_{1,o} - T_{1,i}\rvert}{\Delta T_m}$	$\text{LMTD} = \Delta T_{lm} = \dfrac{\Delta T_1 - \Delta T_2}{\ln\left(\Delta T_1 / \Delta T_2\right)}$
$C^* = \dfrac{C_{min}}{C_{max}} = \dfrac{\left(\dot m c_p\right)_{min}}{\left(\dot m c_p\right)_{max}}$	$R_1 = \dfrac{C_1}{C_2} = \dfrac{T_{2,i} - T_{2,o}}{T_{1,o} - T_{1,i}}$	$\Delta T_1 = T_{h,i} - T_{c,o} \quad \Delta T_2 = T_{h,o} - T_{c,i}$

[a]   Although P, R, and NTU_1 are defined on fluid side 1, it must be emphasized that all the results of the P-NTU and MTD methods are valid if the definitions of P, NTU, and R are consistently based on C_c, C_s, C_h, or C.

[b]   P and R are defined in the P-NTU method.

Here the exchanger effectiveness ε is an efficiency factor. It is a ratio of the actual heat transfer rate from the hot fluid to the cold fluid in a given heat exchanger of any flow arrangement to the maximum possible heat transfer rate q_{max} thermodynamically permitted. The q_{max} is obtained in a *counterflow* heat exchanger (recuperator) of *infinite surface area* operating with the fluid flow rates (heat capacity rates) and fluid inlet temperatures equal to those of an actual exchanger (constant fluid properties are idealized). As noted in Table 4.5.1, the exchanger effectiveness ε is a function of NTU and C^* in this method. The number of transfer units NTU is a ratio of the overall conductance UA to the smaller heat capacity rate C_{min}. NTU designates the dimensionless "heat transfer size" or "thermal size" of the exchanger. Other interpretations of NTU are given by Shah (1983). The heat capacity rate ratio C^* is simply a ratio of the smaller to the larger heat capacity rate for the two fluid streams. Note that $0 \le \varepsilon \le 1$, $0 \le \text{NTU} \le \infty$ and $0 \le C^* \le 1$.

The P-NTU method represents a variant of the ε-NTU method. The ε-NTU relationship is different depending upon whether the shell fluid is the C_{min} or C_{max} fluid in the (stream unsymmetric) flow arrangements commonly used for shell-and-tube exchangers. In order to avoid possible errors and to avoid keeping track of the C_{min} fluid side, an alternative is to present the temperature effectiveness P as a function of NTU and R, where P, NTU, and R are defined consistently either for Fluid 1 side or Fluid 2 side; in Table 4.5.2, they are defined for Fluid 1 side (regardless of whether that side is the hot or cold fluid side), and Fluid 1 side is clearly identified for each flow arrangement in Table 4.5.4; it is the shell side in a shell-and-tube exchanger. Note that

$$q = P_1 C_1 \left| T_{1,i} - T_{2,i} \right| = P_2 C_2 \left| T_{2,i} - T_{1,i} \right| \tag{4.5.14}$$

$$P_1 = P_2 R_2 \qquad P_2 = P_1 R_1 \tag{4.5.15}$$

$$\text{NTU}_1 = \text{NTU}_2 R_2 \qquad \text{NTU}_2 = \text{NTU}_1 R_1 \tag{4.5.16}$$

and

$$R_1 = 1/R_2 \tag{4.5.17}$$

In *the MTD method*, the heat transfer rate from the hot fluid to the cold fluid in the exchanger is given by

$$q = UA\,\Delta T_m = UAF\,\Delta T_{\text{lm}} \tag{4.5.18}$$

where ΔT_m the log-mean temperature difference (LMTD), and F the LMTD correction factor, a ratio of true (actual) MTD to the LMTD, where

$$\text{LMTD} = \Delta T_{\text{lm}} = \frac{\Delta T_1 - \Delta T_2}{\ln\left(\Delta T_1/\Delta T_2\right)} \tag{4.5.19}$$

Here ΔT_1 and ΔT_2 are defined as

$$\Delta T_1 = T_{h,i} - T_{c,o} \qquad \Delta T_2 = T_{h,o} - T_{c,i} \qquad \text{for all flow arrangements} \tag{4.5.20}$$
$$\text{except for parallel flow}$$

$$\Delta T_1 = T_{h,i} - T_{c,i} \qquad \Delta T_2 = T_{h,o} - T_{c,o} \qquad \text{for parallel flow} \tag{4.5.21}$$

The LMTD represents a true MTD for a counterflow arrangement under the idealizations listed below. Thus, the LMTD correction factor F represents a degree of departure for the MTD from the counterflow LMTD; it does not represent the effectiveness of a heat exchanger. It depends on two dimensionless group P_1 and R_1 or P_2 and R_2 for a given flow arrangement.

TABLE 4.5.3   Relationships between Dimensionless Groups of the P-NTU and LMTD Methods and Those of the ε-NTU Method

$$P_1 = \frac{C_{\min}}{C_1}\,\varepsilon = \begin{cases} \varepsilon & \text{for} \quad C_1 = C_{\min} \\ \varepsilon C^* & \text{for} \quad C_1 = C_{\max} \end{cases}$$

$$R_1 = \frac{C_1}{C_2} = \begin{cases} C^* & \text{for} \quad C_1 = C_{\min} \\ 1/C^* & \text{for} \quad C_1 = C_{\max} \end{cases}$$

$$\text{NTU}_1 = \text{NTU}\,\frac{C_{\min}}{C_1} = \begin{cases} \text{NTU} & \text{for} \quad C_1 = C_{\min} \\ \text{NTU}\,C^* & \text{for} \quad C_1 = C_{\max} \end{cases}$$

$$F = \frac{\text{NTU}_{\text{cf}}}{\text{NTU}} = \frac{1}{\text{NTU}\left(1 - C^*\right)} \ln\left[\frac{1 - C^*\varepsilon}{1 - \varepsilon}\right] \xrightarrow[C^* = 1]{} \frac{\varepsilon}{\text{NTU}(1 - \varepsilon)}$$

$$F = \frac{1}{\text{NTU}_1\left(1 - R_1\right)} \ln\left[\frac{1 - RP_1}{1 - P_1}\right] \xrightarrow[R_1 = 1]{} \frac{P_1}{\text{NTU}_1\left(1 - P_1\right)}$$

The relationship among the dimensionless groups of the ε-NTU, P-NTU, and MTD methods are presented in Table 4.5.3. The closed-form formulas for industrially important exchangers are presented in terms of P_1, NTU_1, and R_1 in Table 4.5.4. These formulas are valid under idealizations which include: (1) steady-state conditions; (2) negligible heat losses to the surrounding; (3) no phase changes in the fluid streams flowing through the exchanger, or phase changes (condensation or boiling) occurring at constant temperature and constant effective specific heat; (4) uniform velocity and temperature at the entrance of the heat exchanger on each fluid side; (5) the overall extended surface efficiency η_o is uniform and constant; (6) constant individual and overall heat transfer coefficients; (7) uniformly distributed heat transfer area on each fluid side; (7) the number of baffles as large in shell-and-tube exchangers; (8) no flow maldistribution; and (9) negligible longitudinal heat conduction in the fluid and exchanger wall.

The overall heat transfer coefficient can vary as a result of variations in local heat transfer coefficients due to two effects: (1) change in heat transfer coefficients in the exchanger as a result of changes in the fluid properties or radiation due to rise or drop of fluid temperatures and (2) change in heat transfer coefficients in the exchanger due to developing thermal boundary layers; it is referred to as the *length effect*. The first effect due to fluid property variations (or radiation) consists of two components: (1) distortion of velocity and temperature profiles at a given flow cross section due to fluid property variations — this effect is usually taken into account by the so-called property ratio method, with the correction scheme of Equations (4.5.55) and (4.5.56) — and (2) variations in the fluid temperature along the axial and transverse directions in the exchanger depending upon the exchanger flow arrangement — this effect is referred to as the *temperature effect*. The resultant axial changes in the overall mean heat transfer coefficient can be significant; the variations in U_{local} could be nonlinear, dependent upon the type of the fluid. The effect of varying U_{local} can be taken into account by evaluating U_{local} at a few points in the exchanger and subsequently integrating U_{local} values by the Simpson or Gauss method (Shah, 1993). The temperature effect can increase or decrease mean U slightly or significantly, depending upon the fluids and applications. The length effect is important for developing laminar flows for which high heat transfer coefficients are obtained in the thermal entrance region. However, in general it will have less impact on the overall heat transfer coefficient because the other thermal resistances in series in an exchanger may be controlling. The length effect reduces the overall heat transfer coefficient compared with the mean value calculated conventionally (assuming uniform mean heat transfer coefficient on each fluid side). It is shown that this reduction is up to about 11% for the worst case (Shah, 1993).

Shah and Pignotti (1997) have shown that the following are the specific number of baffles beyond which the influence of the finite number of baffles on the exchanger effectiveness is not significantly larger than 2%: $N_b \geq 10$ for 1-1 TEMA E counterflow exchanger; $N_b \geq 6$ for 1-2 TEMA E exchanger for $NTU_s \leq 2$, $R_s \leq 5$; $N_b \geq 9$ for 1-2 TEMA J exchanger for $NTU_s \leq 2$, $R_s \leq 5$; $N_b \geq 5$ for 1-2 TEMA G exchanger for $NTU_s \leq 3$, all R_s; $N_b \geq 11$ for 1-2 TEMA H exchanger for $NTU_s \leq 3$, all R_s. Various shell-and-tube heat exchangers (such as TEMA E, G, H, J, etc.) are classified by the Tubular Exchanger Manufacturers' Association (TEMA, 1988).

If any of the basic idealizations are not valid for a particular exchanger application, the best solution is to work directly with either Equations 4.5.1 and 4.5.2 or their modified form by including a particular effect, and to integrate them over a small exchanger segment numerically in which all of the idealizations are valid.

Fin Efficiency and Extended Surface Efficiency.

Extended surfaces have fins attached to the primary surface on one or both sides of a two-fluid or a multifluid heat exchanger. Fins can be of a variety of geometries — plain, wavy, or interrupted — and can be attached to the inside, outside, or both sides of circular, flat, or oval tubes, or parting sheets. Fins are primarily used to increase the surface area (when the heat transfer coefficient on that fluid side is relatively low) and consequently to increase the total rate of heat transfer. In addition, enhanced fin geometries also increase the heat transfer coefficient compared to that for a plain fin. Fins may also be used on the high heat transfer coefficient fluid side in a heat exchanger primarily for structural strength purposes (for example, for high-pressure water flow through a flat tube) or to provide a thorough mixing of a highly viscous liquid (such as for laminar oil flow in a flat or a round tube). Fins are attached to the primary surface by brazing, soldering, welding, adhesive bonding, or mechanical expansion, or they are extruded or integrally connected to the tubes. Major categories of extended surface heat exchangers are plate-fin (Figures 4.5.2 to 4.5.4) and tube-fin (Figures 4.5.5 to 4.5.7) exchangers. Note that shell-and-tube exchangers sometimes employ individually finned tubes — low finned tubes (similar to Figure 4.5.5a but with low-height fins) (Shah, 1985).

The concept of fin efficiency accounts for the reduction in temperature potential between the fin and the ambient fluid due to conduction along the fin and convection from or to the fin surface depending upon the fin cooling or heating situation. The fin efficiency is defined as the ratio of the actual heat transfer rate through the fin base divided by the maximum possible heat transfer rate through the fin

TABLE 4.5.4 P_1 - NTU_1 Formulas and Limiting Values P_1 and $R_1 = 1$ and $NTU_1 \to \infty$ for Various Exchanger Flow Arrangements[a]

Flow Arrangement	Eq. no.	General formula	Value for $R_1 = 1$	Value for $NTU_1 \to \infty$
	I.1.1	$P_1 = \dfrac{1 - \exp[-NTU_1(1 - R_1)]}{1 - R_1 \exp[-NTU_1(1 - R_1)]}$	$P_1 = \dfrac{NTU_1}{1 + NTU_1}$	$P_1 \to 1$ for $R_1 \le 1$ $P_1 \to 1/R_1$ for $R_1 \ge 1$
	I.1.2	$NTU_1 = \dfrac{1}{(1 - R_1)} \ln\left[\dfrac{1 - R_1 P_1}{1 - P_1}\right]$	$NTU_1 = \dfrac{P_1}{1 - P_1}$	$NTU_1 \to \infty$
Counterflow exchanger, stream symmetric.	I.1.3	$F = 1$	$F = 1$	$F = 1$
	I.2.1	$P_1 = \dfrac{1 - \exp[-NTU_1(1 + R_1)]}{1 + R_1}$	$P_1 = \dfrac{1}{2}[1 - \exp(-2NTU_1)]$	$P_1 \to \dfrac{1}{1 + R_1}$
	I.2.2	$NTU_1 = \dfrac{1}{1 + R_1} \ln\left[\dfrac{1}{1 - P_1(1 + R_1)}\right]$	$NTU_1 = \dfrac{1}{2} \ln\left[\dfrac{1}{1 - 2P_1}\right]$	$NTU_1 \to \infty$
Parallel flow exchanger, stream symmetric.	I.2.3	$F = \dfrac{(R_1 + 1) \ln\left[\dfrac{1 - R_1 P_1}{1 - P_1}\right]}{(R_1 - 1) \ln[1 - P_1(1 + R_1)]}$	$F = \dfrac{2P_1}{(P_1 - 1) \ln(1 - 2P_1)}$	$F \to 0$
	II.1	$P_1 = 1 - \exp(NTU_1)$ $\quad - \exp[-(1 + R_1)NTU_1]$ $\quad \cdot \sum\limits_{n=1}^{\infty} R_1^n P_n(NTU_1)$ $P_n(y) = \dfrac{1}{(n+1)!} \sum\limits_{j=1}^{n} \dfrac{(n+1-j)}{j!} y^{n+j}$	same as Eq. (II.1) with $R_1 = 1$	$P_1 \to 1$ for $R_1 \le 1$ $P_1 \to \dfrac{1}{R_1}$ for $R_1 \ge 1$
Single-pass crossflow exchanger, both fluids unmixed, stream symmetric				

TABLE 4.5.4 (continued) P_1 - NTU_1 Formulas and Limiting Values P_1 and $R_1 = 1$ and $NTU_1 \to \infty$ for Various Exchanger Flow Arrangements[a]
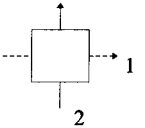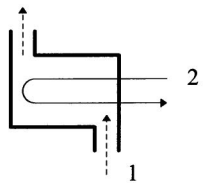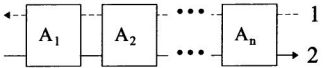
Flow Arrangement	Eq. no.	General formula	Value for $R_1 = 1$	Value for $NTU_1 \to \infty$
Single-pass crossflow exchanger, fluid 1 unmixed, fluid 2 mixed.	II.2.1	$P_1 = [1 - \exp(-KR_1)]/R_1$ $K = 1 - \exp(-NTU_1)$	$P_1 = 1 - \exp(-K)$	$P_1 \to \dfrac{1 - \exp(-R_1)}{R_1}$
	II.2.2	$NTU = \ln\left[\dfrac{1}{1 + \dfrac{1}{R_1}\ln(1 - R_1 P_1)}\right]$	$NTU_1 = \ln\left[\dfrac{1}{1 + \ln(1 - P_1)}\right]$	$NTU_1 \to \infty$
	II.2.3	$F = \dfrac{\ln[(1 - R_1 P_1)/(1 - P_1)]}{(R_1 - 1)\ln\left[1 + \dfrac{1}{R_1}\ln(1 - R_1 P_1)\right]}$	$F = \dfrac{P_1}{(P_1 - 1)\ln[1 + \ln(1 - P_1)]}$	$F \to 0$
Single-pass crossflow exchanger, fluid 1 mixed, fluid 2 unmixed.	II.3.1	$P = 1 - \exp(-K/R_1)$ $K = 1 - \exp(-R_1 NTU_1)$	$P = 1 - \exp(-K)$ $K = 1 - \exp(-NTU_1)$	$P_1 \to 1 - \exp(-1/R_1)$
	II.3.2	$NTU_1 = \dfrac{1}{R_1}\ln\left[\dfrac{1}{1 + R_1}\ln(1 - P_1)\right]$	$NTU_1 = \ln\left[\dfrac{1}{1 + \ln(1 - P_1)}\right]$	$NTU_1 \to \infty$
	II.3.3	$F = \dfrac{\ln(1 - R_1 P_1)/(1 - P_1)]}{(1 - 1/R_1)\ln[1 + R_1\ln(1 - P_1)]}$	$F = \dfrac{P_1}{(P_1 - 1)\ln[1 + \ln(1 - P_1)]}$	$P_1 \to \dfrac{1}{1 + R_1}$
Single-pass crossflow exchanger, both fluids mixed, stream symmetric.	II.4	$P_1 = \left[\dfrac{1}{K_1} + \dfrac{R_1}{K_2} - \dfrac{1}{NTU_1}\right]^{-1}$ $K_1 = 1 - \exp(-NTU_1)$ $K_2 = 1 - \exp(-R_1 NTU_1)$	$P_1 = \left[\dfrac{2}{K_1} - \dfrac{1}{NTU_1}\right]^{-1}$	$P_1 \to \dfrac{1}{1 + R_1}$

TABLE 4.5.4 (continued) P_1 - NTU_1 Formulas and Limiting Values P_1 and $R_1 = 1$ and $NTU_1 \to \infty$ for Various Exchanger Flow Arrangements[a]
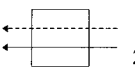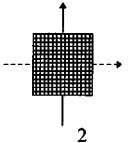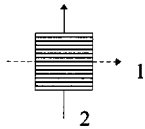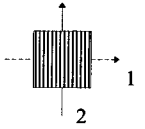
Flow Arrangement	Eq. no.	General formula	Value for $R_1 = 1$	Value for $NTU_1 \to \infty$
	III.1.1	$P_1 = \dfrac{2}{1 + R_1 + E \coth(E\, NTU_1 / 2)}$	$P_1 = \dfrac{1}{1 + \coth(NTU_1 / \sqrt{2}) / \sqrt{2}}$	$P_1 \to \dfrac{2}{1 + R_1 + E}$
		$E = \left[1 + R_1^2\right]^{1/2}$		
	III.1.2	$NTU_1 = \dfrac{1}{E} \ln\left[\dfrac{2 - P_1(1 + R_1 - E)}{2 - P_1(1 + R_1 + E)}\right]$	$NTU_1 = \ln\left[\dfrac{2 - P_1}{2 - 3P_1}\right]$	$NTU_1 \to \infty$
1-2 TEMA E shell-and-tube exchanger, shell fluid mixed, stream symmetric	III.1.3	$F = \dfrac{E \ln[(1 - R_1 P_1)/(1 - P_1)]}{(1 - R_1)\ln\left[\dfrac{2 - P_1(1 + R_1 - E)}{2 - P_1(1 + R_1 + E)}\right]}$	$F = \dfrac{P_1/(1 - P_1)}{\ln[(2 - P_1)/(2 - 3P_1)]}$	$F \to 0$
	IV.1.1	$P_1 = \dfrac{\prod\limits_{i=1}^{n}(1 - R_1 P_{1,A_i}) - \prod\limits_{i=1}^{n}(1 - P_{1,A_i})}{\prod\limits_{i=1}^{n}(1 - R_1 P_{1,A_i}) - R_1 \prod\limits_{i=1}^{n}(1 - P_{1,A_i})}$	$P_1 = \dfrac{\sum\limits_{i=1}^{n}\dfrac{P_{1,A_i}}{1 - P_{1,A_i}}}{1 + \sum\limits_{i=1}^{n}\dfrac{P_{1,A_i}}{1 - P_{1,A_i}}}$	same as Eq. (I.1.1) counterflow
	IV.1.2	$R_1 = R_{1,A_i}, \quad i = 1, \dots, n$	$1 = R_{1,A_i}, \quad i = 1, \dots, n$	same as Eq. (IV.1.2)
	IV.1.3	$NTU_1 = \sum\limits_{i=1}^{n} NTU_{1,A_i}$	same as for Eq. (IV.1.3)	same as Eq. (IV.1.3)
Series coupling of n exchangers, overall counterflow arrangement. Stream symmetric if all A_1 are stream symmetric.	IV.1.4	$F = \dfrac{1}{NTU_1}\sum\limits_{i=1}^{n} NTU_{1,A_i} F_{A_i}$	same as Eq. (IV.1.4)	same as Eq. (IV.1.4)

[a] In this table, all variables, except P_1, R_1, NTU_1 and F, are local or dummy variables not necessarily related to similar ones defined in the nomenclature and the text. Source: Shah, R.K. and Mueller, A.C., 1988. With permission.
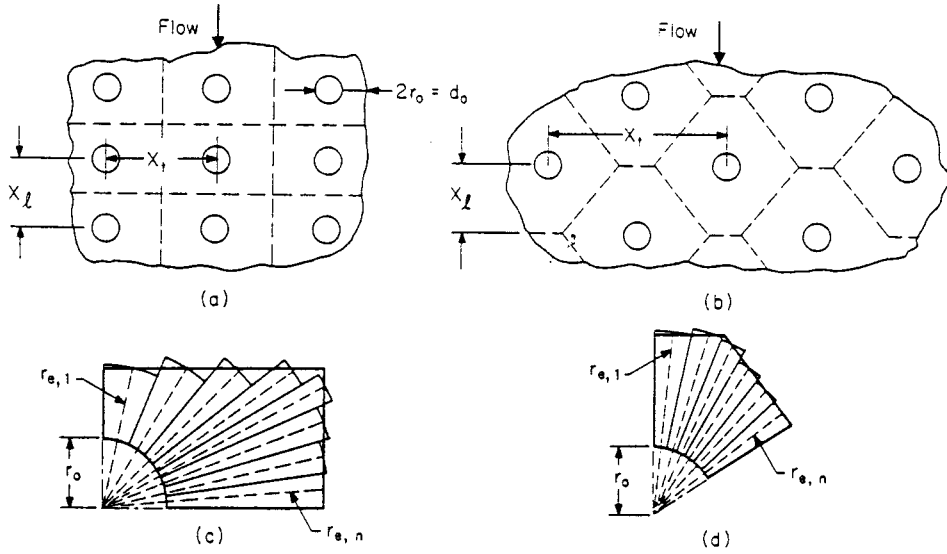
FIGURE 4.5.13 A flat fin over (a) an in-line and (b) staggered tube arrangement; the smallest representative segment of the fin for (c) an in-line and (d) a staggered tube arrangement.

base which would be obtained if the entire fin were at the base temperature (i.e., its material thermal conductivity were infinite). Since most of the real fins are "thin", they are treated as one-dimensional (1-D) with standard idealizations used for the analysis (Huang and Shah, 1992). This 1-D fin efficiency is a function of the fin geometry, fin material thermal conductivity, heat transfer coefficient at the fin surface, and the fin tip boundary condition; it is not a function of the fin base or fin tip temperature, ambient temperature, and heat flux at the fin base or fin tip in general. Fin efficiency formulas for some common fins are presented in Table 4.5.5 (Shah, 1985). Huang and Shah (1992) also discuss the influence on η_f if any of the basic idealizations used in the fin analysis are violated.
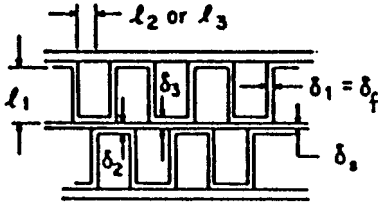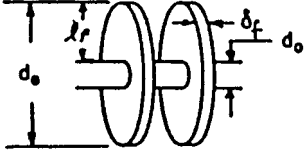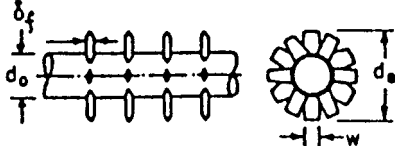
The fin efficiency for flat fins (Figure 4.5.5b) is obtained by a sector method (Shah, 1985). In this method, the rectangular or hexagonal fin around the tube (Figures 4.5.7a and b) or its smallest symmetrical section is divided into *n* sectors (Figure 4.5.13). Each sector is then considered as a circular fin with the radius $r_{e,i}$ equal to the length of the centerline of the sector. The fin efficiency of each sector is subsequently computed using the circular fin formula of Table 4.5.5. The fin efficiency η_f for the whole fin is then the surface area weighted average of $\eta_{f,i}$ of each sector.

$$\eta_f = \frac{\displaystyle\sum_{i=1}^{n} \eta_{f,i} A_{f,i}}{\displaystyle\sum_{i=1}^{n} A_{f,i}} \tag{4.5.22}$$

Since the heat flow seeks the path of least thermal resistance, actual η_f will be equal to or higher than that calculated by Equation (4.5.22); hence, Equation (4.5.22) yields a somewhat conservative value of η_f.

The η_f values of Table 4.5.5 or Equation (4.5.22) are not valid in general when the fin is thick, when it is subject to variable heat transfer coefficients or variable ambient fluid temperature, or when it has a temperature depression at the fin base. See Huang and Shah (1992) for details. For a thin rectangular fin of constant cross section, the fin efficiency as presented in Table 4.5.5 is given by

TABLE 4.5.5   Fin Efficiency Expressions for Plate-Fin and Tube-Fin Geometries of Uniform Fin Thickness

Geometry	Fin Efficiency Formula
	$m_i = \left[\dfrac{2h}{k_f \delta_i} \left(1 + \dfrac{\delta_i}{l_f} \right) \right]^{1/2} \quad E_1 = \dfrac{\tanh(m_i l_1)}{m_i l_1} \quad i = 1, 2$

Plain, wavy, or offset strip fin
of rectangular cross section

$$\eta_f = E_1$$
$$l_1 = \frac{b}{2} - \delta_1 \quad \delta_1 = \delta_f$$

Triangular fin heated
from one side

$$\eta_f = \frac{hA_1(T_0 - T_a)\dfrac{\sinh(m_1 l_1)}{m_1 l_1} + q_e}{\cosh(m_1 l_1)\left[hA_1(T_0 - T_a) + q_e \dfrac{T_0 - T_a}{T_1 - T_a} \right]}$$

Plain, wavy, or louver fin
of triangular cross section

$$\eta_f = E_1$$
$$l_1 = \frac{l}{2} \quad \delta_1 = \delta_f$$

Double sandwich fin

$$\eta_f = \frac{E_1 l_1 + E_2 l_2}{l_1 + l_2} \frac{1}{1 + m_1^2 E_1 E_2 l_1 l_2}$$
$$\delta_1 = \delta_f \quad \delta_2 = \delta_3 = \delta_f + \delta_s$$
$$l_1 = b - \delta_f + \frac{\delta_s}{2} \quad l_2 = l_3 = \frac{p_f}{2}$$

Circular fin

$$\eta_j = \begin{cases} a(ml_e)^{-b} & \text{for } \Phi > 0.6 + 2.257(r^*)^{-0.445} \\ \dfrac{\tanh \Phi}{\Phi} & \text{for } \Phi \le 0.6 + 2.257(r^*)^{-0.445} \end{cases}$$
$$a = (r^*)^{-0.246} \quad \Phi = ml_e(r^*)^{\exp(0.13ml_e - 1.3863)}$$
$$b = \begin{cases} 0.9107 + 0.0893r^* & \text{for } r^* \le 2 \\ 0.9706 + 0.17125 \ln r^* & \text{for } r^* > 2 \end{cases}$$
$$m = \left(\frac{2h}{k_f \delta_f} \right)^{1/2} \quad l_e = l_j + \frac{\delta_f}{2} \quad r^* = \frac{d_e}{d_o}$$

Studded fin

$$\eta_j = \frac{\tanh(ml_e)}{ml_e}$$
$$m = \left[\frac{2h}{k_f \delta_f} \left(1 + \frac{\delta_f}{w} \right) \right]^{1/2} \quad l_e = l_j + \frac{\delta_f}{2} \quad l_f = \frac{(d_e - d_o)}{2}$$

$$\eta_f = \frac{\tanh(m\ell)}{m\ell} \tag{4.5.23}$$

where $m = [2h(1 + \delta_f \ell_f)/k_f \delta_f]^{1/2}$. For a thick rectangular fin of constant cross section, the fin efficiency (a counterpart of Equation (4.5.23) is given by (Huang and Shah, 1992)

$$\eta_f = \frac{\left(\text{Bi}^+\right)^{1/2}}{K\text{Bi}} \tanh\left[K\left(\text{Bi}^+\right)^{1/2}\right] \tag{4.5.24}$$

where $\text{Bi}^+ = \text{Bi}/(1 + \text{Bi}/4)$, $\text{Bi} = (h\delta_f/2k_f)^{1/2}$, $K = 2\ell/\delta_f$. Equation (4.5.23) is accurate (within 0.3%) for a "thick" rectangular fin having $\eta_f > 80\%$; otherwise, use Equation (4.5.24) for a thick fin.

In an extended-surface heat exchanger, heat transfer takes place from both the fins ($\eta_f < 100\%$) and the primary surface ($\eta_f = 100\%$). In that case, the total heat transfer rate is evaluated through a concept of extended surface efficiency η_o defined as

$$\eta_o = \frac{A_p}{A} + \eta_f \frac{A_f}{A} = 1 - \frac{A_f}{A}\left(1 - \eta_f\right) \tag{4.5.25}$$

where A_f is the fin surface area, A_p is the primary surface area, and $A = A_f + A_p$. In Equation 4.5.25, heat transfer coefficients over the finned and unfinned surfaces are idealized to be equal. Note that $\eta_o \geq \eta_f$ and η_o is always required for the determination of thermal resistances of Equation (4.5.5) in heat exchanger analysis.

Pressure Drop Analysis.

Usually a fan, blower, or pump is used to flow fluid through individual sides of a heat exchanger. Due to potential initial and operating high cost, low fluid pumping power requirement is highly desired for gases and viscous liquids. The fluid pumping power $\wp$ is approximately related to the core pressure drop in the exchanger as (Shah, 1985).

$$\wp = \frac{\dot{m}\Delta p}{\rho} \approx \begin{cases} \dfrac{1}{2g_c}\dfrac{\mu}{\rho^2}\dfrac{4L}{D_h}f\,\text{Re} & \text{for laminar flow} \tag{4.5.26} \\[3ex] \dfrac{0.046}{2g_c}\dfrac{\mu^{0.2}}{\rho^2}\dfrac{4L}{D_h}\dfrac{\dot{m}^{2.8}}{A_0^{1.8}D_h^{0.2}} & \text{for turbulent flow} \tag{4.5.27} \end{cases}$$

It is clear from Equations (4.2.26) and (4.2.27) that the fluid pumping power is strongly dependent upon the fluid density ($\wp \propto 1/\rho^2$) particularly for low-density fluids in laminar and turbulent flows, and upon the viscosity in laminar flow. In addition, the pressure drop itself can be an important consideration when blowers and pumps are used for the fluid flow since they are head limited. Also for condensing and evaporating fluids, the pressure drop affects the heat transfer rate. Hence, the pressure drop determination in the exchanger is important.

The pressure drop associated with a heat exchanger consists of (1) core pressure drop, and (2) the pressure drop associated with the fluid distribution devices such as inlet and outlet manifolds, headers, tanks, nozzles, ducting, and so on, which may include bends, valves, and fittings. This second Δp component is determined from Idelchik (1994) and Miller (1990). The core pressure drop may consist of one or more of the following components depending upon the exchanger construction: (1) friction losses associated with fluid flow over heat transfer surface (this usually consists of skin friction, form (profile) drag, and internal contractions and expansions, if any); (2) the momentum effect (pressure drop or rise due to fluid density changes) in the core; (3) pressure drop associated with sudden contraction and expansion at the core inlet and outlet, and (4) the gravity effect due to the change in elevation

between the inlet and outlet of the exchanger. The gravity effect is generally negligible for gases. For vertical flow through the exchanger, the pressure drop or rise ("static head") due to the elevation change is given by

$$\Delta p = \pm \frac{\rho_m g L}{g_c} \qquad (4.5.28)$$

Here the "+" sign denotes vertical upflow (i.e., pressure drop), the "–" sign denotes vertical downflow (i.e., pressure rise). The first three components of the core pressure drop are now presented for plate-fin, tube-fin, plate, and regenerative heat exchangers.

Plate-fin heat exchangers. For the plate-fin exchanger (Figure 4.5.2), all three components are considered in the core pressure drop evaluation as follows:

$$\frac{\Delta p}{p_i} = \frac{G^2}{2g_c} \frac{1}{p_i \rho_i} \left[\left(1 - \sigma^2 + K_c\right) + f \frac{L}{r_h} \rho_i \left(\frac{1}{\rho}\right)_m + 2\left(\frac{\rho_i}{\rho_o} - 1\right) - \left(1 - \sigma^2 - K_e\right)\frac{\rho_i}{\rho_o} \right] \qquad (4.5.29)$$

where f is the Fanning friction factor, K_c and K_e are flow contraction (entrance) and expansion (exit) pressure loss coefficients (see Figure 4.5.14), and σ is a ratio of minimum free flow area to frontal area. K_c and K_e for four different entrance flow passage geometries are presented by Kays and London (1984). The entrance and exit losses are important at low values of σ and L (short cores), high values of Re, and for gases; they are negligible for liquids. The values of K_c and K_e apply to long tubes for which flow is fully developed at the exit. For partially developed flows, K_c and K_e is higher than that for fully developed flows. For interrupted surfaces, flow is never a fully developed boundary layer type. For highly interrupted fin geometries, the entrance and exit losses are generally small compared to the core pressure drop and the flow is well mixed; hence, K_c and K_e for Re $\rightarrow \infty$ should represent a good approximation. The mean specific volume v_m or $(1/\rho)_m$ in Equation (4.5.29) is given as follows. For liquids with any flow arrangement, or for a perfect gas with $C^* = 1$ and any flow arrangement (except for parallel flow),

$$\left(\frac{1}{\rho}\right)_m = v_m = \frac{v_i + v_o}{2} = \frac{1}{2}\left(\frac{1}{\rho_i} + \frac{1}{\rho_o}\right) \qquad (4.5.30)$$

where v is the specific volume in m³/kg. For a perfect gas with $C^* = 0$ and any flow arrangement,

$$\left(\frac{1}{\rho}\right)_m = \frac{\tilde{R}}{p_{ave}} T_{lm} \qquad (4.5.31)$$

Here $\tilde{R}$ is the gas constant in J/(kg K), $p_{ave} = (p_i + p_o)/2$, and $T_{lm} = T_{const} + \Delta T_{lm}$ where T_{const} is the mean average temperature of the fluid on the other side of the exchanger; the LMTD ΔT_{lm} is defined in Table 4.5.2. The core frictional pressure drop in Equation 4.5.29 may be approximated as

$$\Delta p \approx \frac{4 f L G^2}{2 g_c D_h}\left(\frac{1}{\rho}\right)_m \qquad (4.5.32)$$

Tube-fin heat exchangers. The pressure drop inside a circular tube is computed using Equation (4.5.29) with proper values of f factors, and K_c and K_e from Figure (4.5.18) for circular tubes.

For flat fins on an array of tubes (see Figure 4.5.5b), the components of the core pressure drop (such as those in Equation 4.5.29) are the same with the following exception: the core friction and momentum effect take place within the core with $G = \dot{m}/A_0$, where A_o is the minimum free-flow area within the
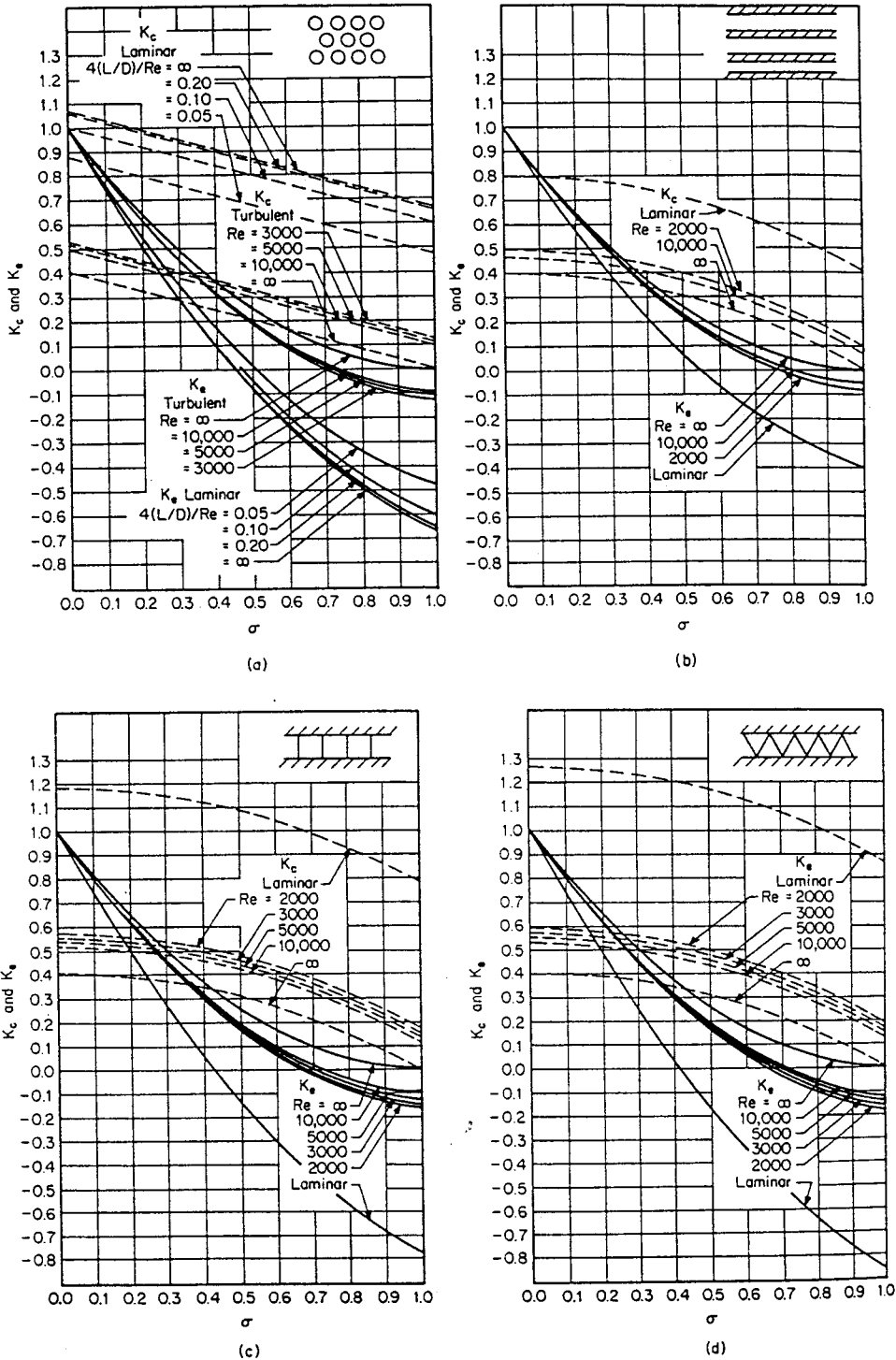
FIGURE 4.5.14 Entrance and exit pressure loss coefficients: (a) circular tubes, (b) parallel plates, (C) square passages, and (d) triangular passages. (From Kays, W.M. and London, A.L., *Compact Heat Exchangers*, 3rd ed., McGraw-Hill, New York, 1984. With permission.) For each of these flow passages, shown in the inset, the fluid flows perpendicular to the plane of the paper into the flow passages.

core, and the entrance and exit losses occur at the leading and trailing edges of the core with the associated flow area A_0' such that

$$\dot{m} = GA_o = G'A_o' \quad \text{or} \quad G'\sigma' = G\sigma \tag{4.5.33}$$

where σ' is the ratio of free-flow area to frontal area at the fin leading edges. The pressure drop for flow normal to a tube bank with flat fins is then given by

$$\frac{\Delta p}{p_i} = \frac{G^2}{2g_c} \frac{1}{p_i\rho_i}\left[f\frac{L}{r_h}\rho_i\left(\frac{1}{\rho}\right)_m + 2\left(\frac{\rho_i}{\rho_o} - 1\right)\right] + \frac{G'^2}{2g_c}\frac{1}{p_i\rho_i}\left[\left(1 - \sigma'^2 - K_c\right) - \left(1 - \sigma'^2 - K_e\right)\frac{\rho_i}{\rho_o}\right] \tag{4.5.34}$$

For individually finned tubes as shown in Figure 4.5.5a, flow expansion and contraction take place along each tube row, and the magnitude is of the same order as that at the entrance and exit. Hence, the entrance and exit losses are generally lumped into the core friction factor. Equation (4.5.29) then reduces for individually finned tubes to

$$\frac{\Delta p}{p_i} = \frac{G^2}{2g_c}\frac{1}{p_i\rho_i}\left[f\frac{L}{r_h}\rho_i\left(\frac{1}{\rho}\right)_m + 2\left(\frac{\rho_i}{\rho_o} - 1\right)\right] \tag{4.5.35}$$

Regenerators. For regenerator matrices having cylindrical passages, the pressure drop is computed using Equation (4.5.29) with appropriate values of f, K_c, and K_e. For regenerator matrices made up of any porous material (such as checkerwork, wire, mesh, spheres, copper wools, etc.), the pressure drop is calculated using Equation (4.5.35) in which the entrance and exit losses are included in the friction factor f.

Plate heat exchangers. Pressure drop in a PHE consists of three components: (1) pressure drop associated with the inlet and outlet manifolds and ports, (2) pressure drop within the core (plate passages), and (3) pressure drop due to the elevation change. The pressure drop in the manifolds and ports should be kept as low as possible (generally < 10%, but it is found as high as 25 to 30% of higher in some designs). Empirically, it is calculated as approximately 1.5 times the inlet velocity head per pass. Since the entrance and exit losses in the core (plate passages) cannot be determined experimentally, they are included in the friction factor for the given plate geometry. The pressure drop (rise) caused by the elevation change for liquids is given by Equation (4.5.28). Hence, the pressure drop on one fluid side in a PHE is given by

$$\Delta p = \frac{1.5G^2N_p}{2g_c\rho_i} + \frac{4fLG^2}{2g_cD_e}\left(\frac{1}{\rho}\right)_m + \left(\frac{1}{\rho_o} - \frac{1}{\rho_i}\right)\frac{G^2}{g_c} \pm \frac{\rho_m gL}{g_c} \tag{4.5.36}$$
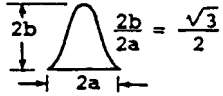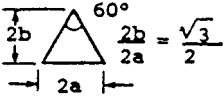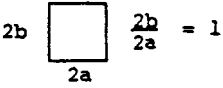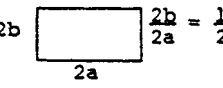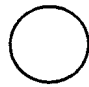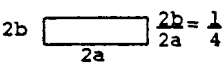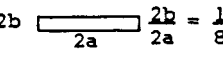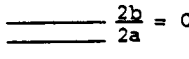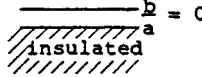
where N_p is the number of passes on the given fluid side and D_e is the equivalent diameter of flow passages (usually twice the plate spacing). Note that the third term on the right-hand side of the equality sign of Equation (4.5.36) is for the momentum effect which is generally negligible in liquids.

Heat Transfer and Flow Friction Correlations

Accurate and reliable surface heat transfer and flow friction characteristics are a key input to the exchanger heat transfer and pressure drop analyses or to the rating and sizing problems (Shah, 1985). Some important analytical solutions and empirical correlations are presented next for selected exchanger geometries.

The heat transfer rate in laminar duct flow is very sensitive to the thermal boundary condition. Hence, it is essential to identify carefully the thermal boundary condition in laminar flow. The heat transfer rate in turbulent duct flow is insensitive to the thermal boundary condition for most common fluids (Pr >

TABLE 4.5.6 Solutions for Heat Transfer and Friction for Fully Developed Flow-Through Specified Ducts

Geometry ($L/D_h > 100$)	Nu_{H1}	Nu_{H2}	Nu_τ	$f Re$	j_{H1}/f [a]	Nu_{H1}/Nu_τ
$\frac{2b}{2a} = \frac{\sqrt{3}}{2}$	3.014	1.474	2.39[b]	12.630	0.269	1.26
$60°$ $\frac{2b}{2a} = \frac{\sqrt{3}}{2}$	3.111	1.892	2.47	13.333	0.263	1.26
$\frac{2b}{2a} = 1$	3.608	3.091	2.976	14.227	0.286	1.21
(hexagon)	4.002	3.862	3.34[b]	15.054	0.299	1.20
$\frac{2b}{2a} = \frac{1}{2}$	4.123	3.017	3.391	15.548	0.299	1.22
(circle)	4.364	4.364	3.657	16.000	0.307	1.19
$\frac{2b}{2a} = \frac{1}{4}$	5.331	2.94	4.439	18.233	0.329	1.20
$\frac{2b}{2a} = \frac{1}{8}$	6.490	2.94	5.597	20.585	0.355	1.16
$\frac{2b}{2a} = 0$	8.235	8.235	7.541	24.000	0.386	1.09
$\frac{b}{a} = 0$ insulated	5.385	—	4.861	24.000	0.253	1.11

[a] This heading is the same as Nu_{H1} $Pr^{-1/3}/f$ Re with Pr = 0.7.

[b] Interpolated values.

0.7); the exception is liquid metals (Pr < 0.03). Hence, there is generally no need to identify the thermal boundary condition in turbulent flow for all fluids except liquid metals.

Fully developed laminar flow analytical solutions for some duct shapes of interest in compact heat exchangers are presented in Table 4.5.6 for three important thermal boundary conditions denoted by the subscripts *H*1, *H*2, and *T* (Shah and London, 1978; Shah and Bhatti, 1987). Here, *H*1 denotes constant axial wall heat flux with constant peripheral wall temperature, *H*2 denotes constant axial and peripheral wall heat flux, and *T* denotes constant wall temperature. The entrance effects, flow maldistribution, free convection, property variation, fouling, and surface roughness all affect fully developed analytical solutions. In order to account for these effects in real plate-fin plain fin geometries having fully developed flows, it is best to reduce the magnitude of the analytical Nu by at least 10% and to increase the value of the analytical *f*Re by 10% for design purposes.

The initiation of transition flow, the lower limit of the critical Reynolds number (Re_{crit}), depends upon the type of entrance (e.g., smooth vs. abrupt configuration at the exchanger flow passage entrance). For a sharp square inlet configuration, Re_{crit} is about 10 to 15% lower than that for a rounded inlet configuration. For most exchangers, the entrance configuration would be sharp. Some information on Re_{crit} is provided by Ghajar and Tam (1994).

Transition flow and fully developed turbulent flow Fanning friction factors (within ±2% accuracy) are given by Bhatti and Shah (1987) as

$$f = A + B\text{Re}^{-1/m} \qquad (4.5.37)$$

where

$$A = 0.0054, \qquad B = 2.3 \times 10^{-8}, \qquad m = -2/3, \qquad \text{for} \quad 2100 \leq \text{Re} \leq 4000$$

$$A = 0.00128, \qquad B = 0.1143, \qquad m = 3.2154, \qquad \text{for} \quad 4000 \leq \text{Re} \leq 10^7$$

The transition flow and fully developed turbulent flow Nusselt number correlation for a circular tube is given by Gnielinski as reported in Bhatti and Shah (1987) as

$$\text{Nu} = \frac{(f/2)(\text{Re} - 1000)\text{Pr}}{1 + 12.7(f/2)^{1/2}\left(\text{Pr}^{2/3} - 1\right)} \qquad (4.5.38)$$

which is accurate within about ±10% with experimental data for $2300 \leq \text{Re} \leq 5 \times 10^6$ and $0.5 \leq \text{Pr} \leq 2000$.

A careful observation of accurate experimental friction factors for all noncircular smooth ducts reveals that ducts with laminar fRe < 16 have turbulent f factors lower than those for the circular tube; whereas ducts with laminar fRe > 16 have turbulent f factors higher than those for the circular tube (Shah and Bhatti, 1988). Similar trends are observed for the Nusselt numbers. Within ±15% accuracy, Equations (4.5.37) and (4.5.38) for f and Nu can be used for noncircular passages with the hydraulic diameter as the characteristic length in f, Nu, and Re; otherwise, refer to Bhatti and Shah (1987) for more accurate results for turbulent flow.

For hydrodynamically and thermally developing flows, the analytical solutions are boundary condition dependent (for laminar flow heat transfer only) and geometry dependent. The hydrodynamic entrance lengths for developing laminar and turbulent flows are given by Shah and Bhatti (1987) and Bhatti and Shah (1987) as

$$\frac{L_{hy}}{D_h} = \begin{cases} 0.0565\text{Re} & \text{for laminar flow } (\text{Re} \leq 2100) \qquad (4.5.39) \\ 1.359\text{Re}^{1/4} & \text{for turbulent flow } \left(\text{Re} \geq 10^4\right) \qquad (4.5.40) \end{cases}$$

Analytical results are useful for well-defined constant-cross-sectional surfaces with essentially unidirectional flows. The flows encountered in heat exchangers are generally very complex having flow separation, reattachment, recirculation, and vortices. Such flows significantly affect Nu and f for the specific exchanger surfaces. Since no analytical or accurate numerical solutions are available, the information is derived experimentally. Kays and London (1984) and Webb (1994) present most of the experimental results reported in the open literature. In the following, empirical correlations for only some important surfaces are summarized due to space limitations. Refer to section 4.2, subsection External Flow Forced Convection for bare tube banks.

Plate-Fin Extended Surfaces.

Offset strip fins. This is one of the most widely used enhanced fin geometries (Figure 4.5.15) in aircraft, cryogenics, and many other industries that do not require mass production. This surface has one of the highest heat transfer performances relative to the friction factor. The most comprehensive correlations for j and f factors for the offset strip fin geometry is provided by Manglik and Bergles (1995) as follows.
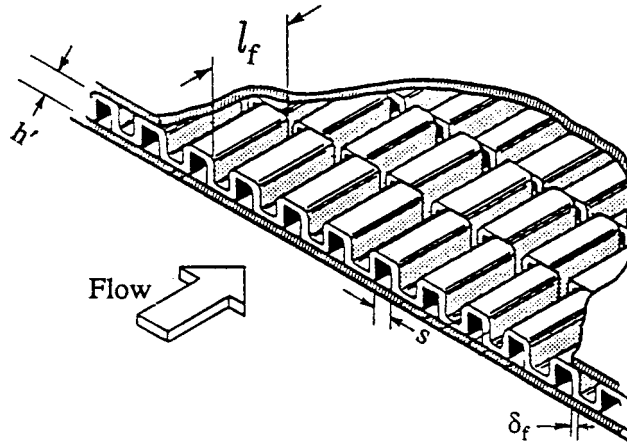
FIGURE 4.5.15 An offset strip fin geometry.

$$j = 0.6522 \mathrm{Re}^{-0.5403} \left(\frac{s}{h'}\right)^{-0.1541} \left(\frac{\delta_f}{l_f}\right)^{0.1499} \left(\frac{\delta_f}{s}\right)^{-0.0678}$$

$$\times \left[1 + 5.269 \times 10^{-5} \mathrm{Re}^{1.340} \left(\frac{s}{h'}\right)^{0.504} \left(\frac{\delta_f}{l_f}\right)^{0.456} \left(\frac{\delta_f}{s}\right)^{-1.055}\right]^{0.1} \tag{4.5.41}$$

$$f = 9.6243 \mathrm{Re}^{-0.7422} \left(\frac{s}{h'}\right)^{-0.1856} \left(\frac{\delta_f}{l_f}\right)^{0.3053} \left(\frac{\delta_f}{s}\right)^{-0.2659}$$

$$\times \left[1 + 7.669 \times 10^{-8} \mathrm{Re}^{4.429} \left(\frac{s}{h'}\right)^{0.920} \left(\frac{\delta_f}{l_f}\right)^{3.767} \left(\frac{\delta_f}{s}\right)^{0.236}\right]^{0.1} \tag{4.5.42}$$

where

$$D_h = 4A_o \Big/ \left(A/l_f\right) = 4sh'l_f \Big/ \left[2\left(sl_f + h'l_f + \delta_f h'\right) + \delta_f s\right] \tag{4.5.43}$$

Geometric symbols in Equation (4.5.43) are shown in Figure 4.5.15.

These correlations predict the experimental data of 18 test cores within ±20% for $120 \leq \mathrm{Re} \leq 10^4$. Although all the experimental data for these correlations are obtained for air, the *j* factor takes into consideration minor variations in the Prandtl number, and the above correlations should be valid for $0.5 < \mathrm{Pr} < 15$.

Louver fins. Louver or multilouver fins are extensively used in the auto industry because of their mass production manufacturability and hence lower cost. The louver fin has generally higher *j* and *f* factors than those for the offset strip fin geometry, and also the increase in the friction factors is in general higher than the increase in the *j* factors. However, the exchanger can be designed for higher heat transfer and the same pressure drop compared to that with the offset strip fins by a proper selection of exchanger frontal area, core depth, and fin density. Published literature and correlations on the louver fins are summarized by Webb (1994) and Cowell et al. (1995), and the understanding of flow and heat transfer phenomena is summarized by Cowell et al. (1995). Because of the lack of systematic studies reported

in the open literature on modern louver fin geometries, no correlation can be recommended for the design purpose.

Tube-Fin Extended Surfaces.

Two major types of tube-fin extended surfaces as shown in Figure 4.5.5 are (1) individually finned tubes and (2) flat fins (also sometimes referred to as plate fins) with or without enhancements/interruptions on an array of tubes. An extensive coverage of the published literature and correlations for these extended surfaces are provided by Webb (1994), Kays and London (1984), and Rozenman (1976). Empirical correlations for some important geometries are summarized below.

Individually finned tubes. This fin geometry, helically wrapped (or extruded) circular fins on a circular tube as shown in Figure 4.5.5a, is commonly used in process and waste heat recovery industries. The following correlation for *j* factors is recommended by Briggs and Young (see Webb, 1994) for individually finned tubes on staggered tube banks.

$$j = 0.134 \text{Re}_d^{-0.319} \left(s/l_f \right)^{0.2} \left(s/\delta_f \right)^{0.11} \tag{4.5.44}$$

where l_f is the radial height of the fin, δ_f the fin thickness, $s = p_f - \delta_f$ is the distance between adjacent fins and p_f is the fin pitch. Equation (4.5.44) is valid for the following ranges: $1100 \le \text{Re}_d \le 18,000$, $0.13 \le s/l_f \le 0.63$, $1.01 \le s/\delta_f \le 6.62$, $0.09 \le l_f/d_o \le 0.69$, $0.011 \le \delta_f/d_o \le 0.15$, $1.54 \le X_t/d_o \le 8.23$, fin root diameter d_o between 11.1 and 40.9 mm, and fin density $N_f (= 1/p_f)$ between 246 and 768 fin/m. The standard deviation of Equation (4.5.44) with experimental results was 5.1%.

For friction factors, Robinson and Briggs (see Webb, 1994) recommended the following correlation:

$$f_{tb} = 9.465 \text{Re}_d^{-0.316} \left(X_t/d_o \right)^{-0.927} \left(X_t/X_d \right)^{0.515} \tag{4.5.45}$$

Here $X_d = (X_t^2 + X_l^2)^{1/2}$ is the diagonal pitch, and X_t and X_l are the transverse and longitudinal tube pitches, respectively. The correlation is valid for the following ranges: $2000 \le \text{Re}_d \le 50,000$, $0.15 \le s/l_f \le 0.19$, $3.75 \le s/\delta_f \le 6.03$, $0.35 \le l_f/d_o \le 0.56$, $0.011 \le \delta_f/d_o \le 0.025$, $1.86 \le X_t/d_o \le 4.60$, $18.6 \le d_o \le 40.9$ mm, and $311 \le N_f \le 431$ fin/m. The standard deviation of Equation (4.5.45) with correlated data was 7.8%

For crossflow over low-height finned tubes, a simple but accurate correlation for heat transfer is given by Ganguli and Yilmaz (1987) as

$$j = 0.255 \text{Re}_d^{-0.3} \left(d_e/s \right)^{-0.3} \tag{4.5.46}$$

A more accurate correlation for heat transfer is given by Rabas and Taborek (1987). Chai (1988) provides the best correlation for friction factors:

$$f_{tb} = 1.748 \text{Re}_d^{-0.233} \left(\frac{l_f}{s} \right)^{0.552} \left(\frac{d_o}{X_t} \right)^{0.599} \left(\frac{d_o}{X_1} \right)^{0.1738} \tag{4.5.47}$$

This correlation is valid for $895 < \text{Re}_d < 713,000$, $20 < \theta < 40°$, $X_t/d_o < 4$, $N \ge 4$, and θ is the tube layout angle. It predicts 89 literature data points within a mean absolute error of 6%; the range of actual error is from –16.7 to 19.9%.

Flat plain fins on a staggered tubebank. This geometry, as shown in Figure 4.5.5b, is used in air-conditioning/refrigeration industry as well as where the pressure drop on the fin side prohibits the use of enhanced/interrupted flat fins. An inline tubebank is generally not used unless very low fin side pressure drop is the essential requirement. Heat transfer correlation for Figure 4.5.5b flat plain fins on

staggered tubebanks is provided by Gray and Webb (see Webb, 1994) as follows for four or more tube rows.

$$j_4 = 0.14 \mathrm{Re}_d^{-0.328} \left(X_t / X_l \right)^{-0.502} \left(s/d_o \right)^{0.031} \tag{4.5.48}$$

For the number of tube rows N from 1 to 3, the j factor is lower and is given by

$$\frac{j_N}{j_4} = 0.991 \left[2.24 \mathrm{Re}_d^{-0.092} \left(N/4 \right)^{-0.031} \right]^{0.607(4-N)} \tag{4.5.49}$$

Gray and Webb (see Webb, 1994) hypothesized the friction factor consisting of two components: one associated with the fins and the other associated with the tubes as follows.

$$f = f_f \frac{A_f}{A} + f_t \left(1 - \frac{A_f}{A} \right) \left(1 - \frac{\delta_f}{p_f} \right) \tag{4.5.50}$$

where

$$f_f = 0.508 \mathrm{Re}_d^{-0.521} \left(X_t / d_o \right)^{1.318} \tag{4.5.51}$$

and f_t (defined the same way as f) is the Fanning friction factor associated with the tube and can be determined from Eu of Figure 19 of Zukauskas (1987) as $f_t = \mathrm{Eu} N (X_t - d_o)/\pi d_o$. Equation (4.5.50) correlated 90% of the data for 19 heat exchangers within ±20%. The range of dimensionless variables of Equations (4.5.50) and (4.5.51) are $500 \le \mathrm{Re} \le 24{,}700$, $1.97 \le X_t/d_o \le 2.55$, $1.7 \le X_l/d_o \le 2.58$, and $0.08 \le s/d_o \le 0.64$.

Exchanger Design Methodology

The problem of heat exchanger design is complex and multidisciplinary (Shah, 1991). The major design considerations for a new heat exchanger include process/design specifications, thermal and hydraulic design, mechanical design, manufacturing and cost considerations, and trade-offs and system-based optimization, as shown in Figure 4.5.16 with possible strong interactions among these considerations as indicated by double-sided arrows. The thermal and hydraulic design methods are mainly analytical, and the structural design is analytical to some extent. Most of the other major design considerations involve qualitative and experience-based judgments, trade-offs, and compromises. Therefore, there is no unique solution to designing a heat exchanger for given process specifications. Further details on this design methodology is given by Shah (1991).

Two important heat exchanger design problems are the rating and sizing problems. Determination of heat transfer and pressure drop performance of either an existing exchanger or an already sized exchanger is referred to as the rating problem. The objective here is to verify vendor's specifications or to determine the performance at off-design conditions. The rating problem is also sometimes referred to as the performance problem. In contrast, the design of a new or existing type of exchanger is referred to as the sizing problem. In a broad sense, it means the determination of the exchanger construction type, flow arrangement, heat transfer surface geometries and materials, and the physical size of an exchanger to meet the specified heat transfer and pressure drops. However, from the viewpoint of quantitative thermal-hydraulic analysis, we will consider that the selection of the exchanger construction type, flow arrangement, and materials has already been made. Thus, in the sizing problem, we will determine the physical size (length, width, height) and surface areas on each side of the exchanger. The sizing problem is also sometimes referred to as the design problem.
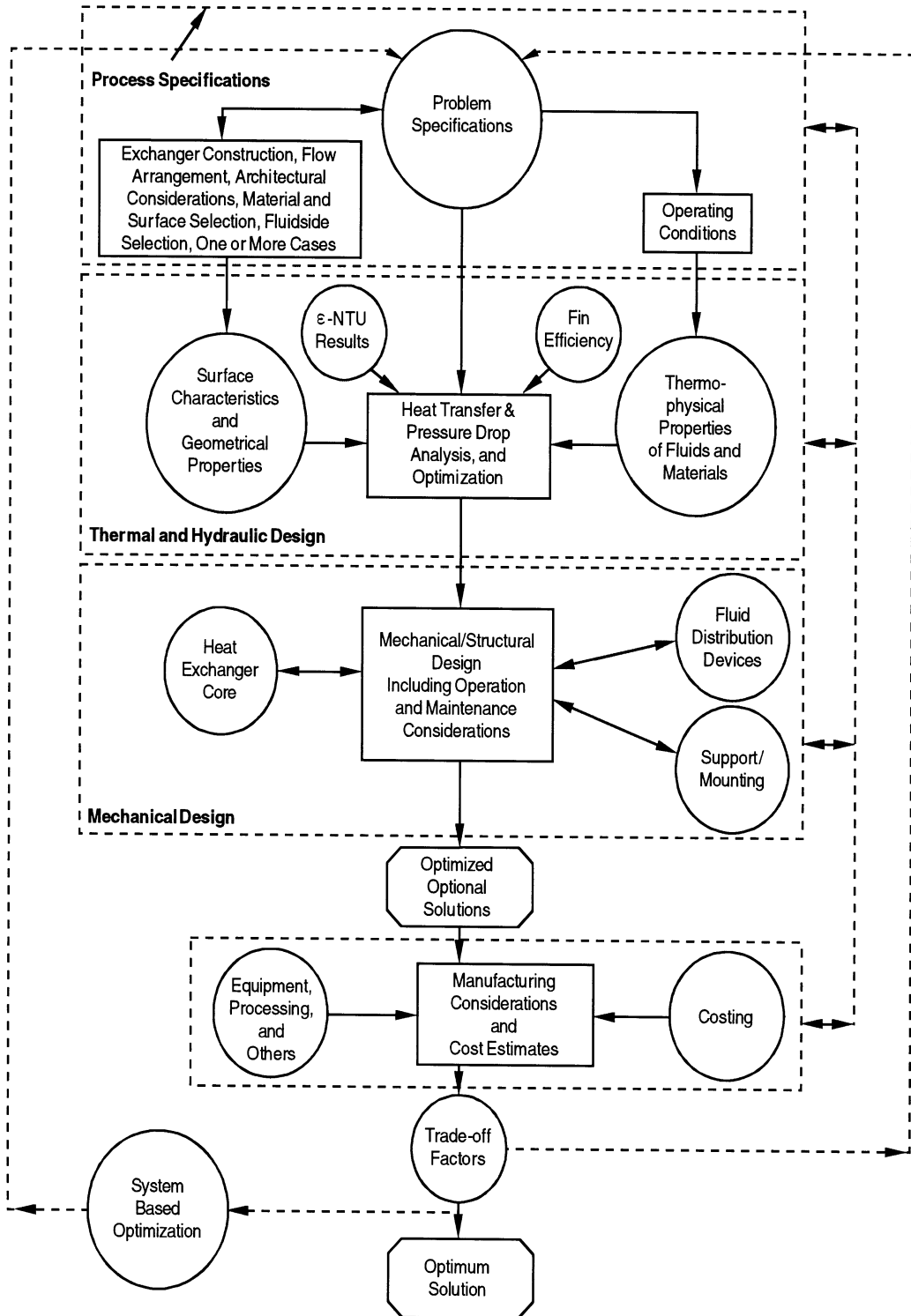
FIGURE 4.5.16 Heat exchanger design methodology.

The step-by-step solution procedures for the rating and sizing problems for counterflow and cross-flow single-pass plate-fin heat exchangers have been presented with a detailed illustrative example by Shah (1981). Shah (1988a) presented further refinements in these procedures as well as step-by-step procedures for two-pass cross-counterflow plate-fin exchangers, and single-pass crossflow and two-pass cross-counterflow tube-fin exchangers. Also, step-by-step solution procedures for the rating and sizing problems for rotary regenerators (Shah, 1988b), heat pipe heat exchangers (Shah and Giovannelli, 1988) and PHEs (Shah and Wanniarachchi, 1991) are available. As an illustration, the step-by-step solution procedures will be covered here for a single-pass crossflow exchanger.

Rating Problem for a Crossflow Plate-Fin Exchanger.

Following is a step-by-step procedure for rating a crossflow plate-fin exchanger. Inputs to the rating problem for a two-fluid exchanger are the exchanger construction, flow arrangement and overall dimensions, complete details on the materials and surface geometries on both sides including their nondimensional heat transfer and pressure drop characteristics (*j* and *f* vs. Re), fluid flow rates, inlet temperatures, and fouling factors. The fluid outlet temperatures, total heat transfer rate, and pressure drops on each side of the exchanger are then determined as the rating problem solution.

1. Determine the surface geometric properties on each fluid side. This includes the minimum free-flow area A_o, heat transfer surface area A (both primary and secondary), flow lengths L, hydraulic diameter D_h, heat transfer surface area density β, the ratio of minimum free-flow area to frontal area σ, fin length l_f, and fin thickness δ for fin efficiency determination, and any specialized dimensions used for heat transfer and pressure drop correlations.

2. Compute the fluid bulk mean temperature and fluid thermophysical properties on each fluid side. Since the outlet temperatures are not known for the rating problem, they are estimated initially. Unless it is known from past experience, assume an exchanger effectiveness as 60 to 75% for most single-pass crossflow exchangers, or 80 to 85% for single-pass counterflow exchangers. For the assumed effectiveness, calculate the fluid outlet temperatures.

$$T_{h,o} = T_{h,i} - \varepsilon\left(C_{\min}/C_h\right)\left(T_{h,i} - T_{c,i}\right) \tag{4.5.52}$$

$$T_{c,o} = T_{c,i} - \varepsilon\left(C_{\min}/C_c\right)\left(T_{h,i} - T_{c,i}\right) \tag{4.5.53}$$

Initially, assume $C_c/C_h = \dot{m}_c/\dot{m}_h$ for a gas-to-gas exchanger, or $C_c/C_h = \dot{m}_c c_{p,c}/\dot{m}_h c_{p,h}$ for a gas-to-liquid exchanger with very approximate values of c_p for the fluids in question.

For exchangers with $C^* > 0.5$ (usually gas-to-gas exchangers), the bulk mean temperatures on each fluid side will be the arithmetic mean of the inlet and outlet temperatures on each fluid side (Shah, 1981). For exchangers with $C^* > 0.5$ (usually gas-to-gas exchangers), the bulk mean temperature on the $C_{\max}$ side will be the arithmetic mean of inlet and outlet temperatures; the bulk mean temperature on the $C_{\min}$ side will be the log-mean average temperature obtained as follows:

$$T_{m,C_{\min}} = T_{m,C_{\max}} \pm \Delta T_{\text{lm}} \tag{4.5.54}$$

where ΔT_{lm} is the LMTD based on the terminal temperatures (see Equation 4.5.19). Use the plus sign if the $C_{\min}$ side is hot; otherwise, use the negative sign.

Once the bulk mean temperature is obtained on each fluid side, obtain the fluid properties from thermophysical property books or from handbooks. The properties needed for the rating problem are μ, c_p, k, Pr, and ρ. With this c_p, one more iteration may be carried out to determine $T_{h,o}$ or $T_{c,o}$ from Equation 4.5.52 or 4.5.53 on the $C_{\max}$ side, and subsequently T_m on the $C_{\max}$ side, and refine fluid properties accordingly.

3. Calculate the Reynolds number $Re = GD_h/\mu$ and/or any other pertinent dimensionless groups (from the basic definitions) needed to determine the nondimensional heat transfer and flow friction characteristics (e.g., j or Nu and f) of heat transfer surfaces on each side of the exchanger. Subsequently, compute j or Nu and f factors. Correct Nu (or j) for variable fluid property effects (Shah, 1981) in the second and subsequent iterations from the following equations.

$$\text{For gases:} \qquad \frac{\text{Nu}}{\text{Nu}_{cp}} = \left[\frac{T_w}{T_m}\right]^{n'} \qquad \frac{f}{f_{cp}} = \left[\frac{T_w}{T_m}\right]^{m'} \qquad (4.5.55)$$

$$\text{For liquids:} \qquad \frac{\text{Nu}}{\text{Nu}_{cp}} = \left[\frac{\mu_w}{\mu_m}\right]^{n'} \qquad \frac{f}{f_{cp}} = \left[\frac{\mu_w}{\mu_m}\right]^{m'} \qquad (4.5.56)$$

where the subscript cp denotes constant properties, and m' and n' are empirical constants provided in Table 4.5.7. Note that T_w and T_m in Equations (4.5.55) and (4.5.56) and in Tables 4.5.7a and b and are absolute temperatures.

TABLE 4.5.7a Property Ratio Method Exponents of Equations (4.5.55) and (4.5.56) for Laminar Flow

Fluid	Heating	Cooling
Gases	$n' = 0.00$, $m' = 1.00$ for $1 < T_w/T_m < 3$	$n' = 0.0$, $m' = 0.81$ for $0.5 < T_w/T_m < 1$
Liquids	$n' = -0.14$, $m' = 0.58$ for $\mu_w/\mu_m < 1$	$n' = -0.14$, $m' = 0.54$ for $\mu_w/\mu_m > 1$

Source: Shah, R.K., in *Heat Exchangers: Thermal-Hydraulic Fundamentals and Design*, S. Kakaç et al., Eds., Hemisphere Publishing, Washington, D.C., 1981. With permission.

TABLE 4.5.7b Property Ratio Method Correlations of Exponents of Equations (4.5.55) and (4.5.56) for Turbulent Flow

Fluid	Heating	Cooling
Gases	$\text{Nu} = 5 + 0.012\,Re^{0.83}\,(\text{Pr} + 0.29)\,(T_w/T_m)^n$ $n = -[\log_{10}(T_w/T_m)]^{1/4} + 0.3$ for $1 < T_w/T_m < 5$, $0.6 < \text{Pr} < 0.9$, $10^4 < Re < 10^6$, and $L/D_h > 40$ $m' = -0.1$ for $1 < T_w/T_m < 2.4$	$n' = 0$ $m' = -0.1$ (tentative)
Liquids	$n' = -0.11$[a] for $0.08 < \mu_w/\mu_m < 1$ $f/f_{cp} = (7 - \mu_m/\mu_w)/6$[b] or $m' = 0.25$ for $0.35 < \mu_w/\mu_m < 1$	$n' = -0.25$[a] for $1 < \mu_w/\mu_m < 40$ $m' = 0.24$[b] for $1 < \mu_w/\mu_m < 2$

[a]　Valid for $2 \le \text{Pr} \le 140$, $10^4 \le Re \le 1.25 \times 10^5$.
[b]　Valid for $1.3 \le \text{Pr} \le 10$, $10^4 \le Re \le 2.3 \times 10^5$.
Source: Shah, R.K., in *Heat Exchangers: Thermal-Hydraulic Fundamentals and Design*, S. Kakaç et al., Eds., Hemisphere Publishing, Washington, D.C., 1981. With permission.

4. From Nu or j, compute the heat transfer coefficients for both fluid streams.

$$h = \text{Nu}\,k/D_h = jGc_p\text{Pr}^{-2/3} \qquad (4.5.57)$$

Subsequently, determine the fin efficiency η_f and the extended surface efficiency η_o

$$\eta_f = \frac{\tanh m\ell}{m\ell} \quad \text{where} \quad m^2 = \frac{h\tilde{P}}{k_f A_k} \tag{4.5.58}$$

where $\tilde{P}$ is the wetted perimeter of the fin surface.

$$\eta_o = 1 - \frac{A_f}{A}\left(1 - \eta_f\right) \tag{4.5.59}$$

Also calculate the wall thermal resistance $R_w = \delta/A_w k_w$. Finally, compute the overall thermal conductance *UA* from Equation (4.5.6) knowing the individual convective film resistances, wall thermal resistances, and fouling resistances, if any.

5. From the known heat capacity rates on each fluid side, compute $C^* = C_{min}/C_{max}$. From the known *UA*, determine NTU = UA/C_{min}. Also calculate the longitudinal conduction parameter λ. With the known *NTU*, C^*, λ, and the flow arrangement, determine the exchanger effectiveness ε from either closed-form equations of Table 4.5.4 or tabular/graphical results from Kays and London (1984).

6. With this ε, finally compute the outlet temperatures from Equations (4.5.52) and (4.5.53). If these outlet temperatures are significantly different from those assumed in Step 2, use these outlet temperatures in Step 2 and continue iterating Steps 2 to 6, until the assumed and computed outlet temperatures converge within the desired degree of accuracy. For a gas-to-gas exchanger, most probably one or two iterations will be sufficient.

7. Finally, compute the heat duty from

$$q = \varepsilon C_{min}\left(T_{h,i} - T_{c,i}\right) \tag{4.5.60}$$

8. For the pressure drop calculations, first we need to determine the fluid densities at the exchanger inlet and outlet (ρ_i and ρ_o) for each fluid. The mean specific volume on each fluid side is then computed from Equation (4.5.30).

Next, the entrance and exit loss coefficients, K_c and K_e, are obtained from Figure 4.5.14 for known σ, Re, and the flow passage entrance geometry.

The friction factor on each fluid side is corrected for variable fluid properties using Equation (4.5.55) or (4.5.56). Here, the wall temperature T_w is computed from

$$T_{w,h} = T_{m,h} - \left(R_h + R_{s,h}\right)q \tag{4.5.61}$$

$$T_{w,c} = T_{m,c} + \left(R_c + R_{s,c}\right)q \tag{4.5.62}$$

where the various resistance terms are defined by Equation (4.5.6).

The core pressure drops on each fluid side are then calculated from Equation (4.5.29). This then completes the procedure for solving the rating problem.

Sizing Problem for a Crossflow Plate-Fin Exchanger.

As defined earlier, we will concentrate here to determine the physical size (length, width, and height) of a single-pass crossflow exchanger for specified heat duty and pressure drops. More specifically, inputs to the sizing problem are surface geometries (including their nondimensional heat transfer and pressure drop characteristics), fluid flow rates, inlet and outlet fluid temperatures, fouling factors, and pressure drops on each side.

For the solution to this problem, there are four unknowns — two flow rates or Reynolds numbers (to determine correct heat transfer coefficients and friction factors) and two surface areas — for the two-

fluid crossflow exchanger. The following four equations (Equations (4.5.63), (4.5.65), and (4.5.67) are used to solve iteratively the surface areas on each fluid side: *UA* in Equation (4.5.63) is determined from NTU computed from the known heat duty or ε and C^*; *G* in Equation (4.5.65) represents two equations, for Fluids 1 and 2 (Shah, 1988a); and the volume of the exchanger in Equation (4.5.67) is the same based on the surface area density of Fluid 1 or Fluid 2.

$$\frac{1}{UA} \approx \frac{1}{\left(\eta_o hA\right)_h} + \frac{1}{\left(\eta_o hA\right)_c} \tag{4.5.63}$$

Here we have neglected the wall and fouling thermal resistances. This equation in nondimensional form is given by

$$\frac{1}{\text{NTU}} = \frac{1}{\text{ntu}_h\left(C_h/C_{\min}\right)} + \frac{1}{\text{ntu}_c\left(C_c/C_{\min}\right)} \tag{4.5.64}$$

$$G_i = \left[\frac{2g_c\Delta p}{\text{Deno}}\right]_i^{1/2} \qquad i = 1,2 \tag{4.5.65}$$

where

$$\text{Deno}_i = \left[\frac{f}{j}\frac{\text{ntu}}{\eta_o}\text{Pr}^{2/3}\left(\frac{1}{\rho}\right)_m + 2\left(\frac{1}{\rho_o} - \frac{1}{\rho_i}\right) + \left(1 - \sigma^2 + K_c\right)\frac{1}{\rho_i} - \left(1 - \sigma^2 - K_e\right)\frac{1}{\rho_o}\right]_i \tag{4.5.66}$$

$$V = \frac{A_1}{\alpha_1} = \frac{A_2}{\alpha_2} \tag{4.5.67}$$

In the iterative solutions, the first time one needs ntu_h and ntu_c to start the iterations. These can be either determined from the past experience or by estimations. If both fluids are gases or both fluids are liquid, one could consider that the design is "balanced," i.e., that the thermal resistances are distributed approximately equally on the hot and cold sides. In that case, $C_h = C_c$, and

$$\text{ntu}_h \approx \text{ntu}_c \approx 2\text{NTU} \tag{4.5.68}$$

Alternatively, if we have liquid on one side and gas on the other side, consider 10% thermal resistance on the liquid side, i.e.,

$$0.10\left(\frac{1}{UA}\right) = \frac{1}{\left(\eta_o hA\right)_{\text{liq}}} \tag{4.5.69}$$

Then, from Equations (4.5.63) and (4.5.64) with $C_{\text{gas}} = C_{\min}$, we can determine the ntu values on each side as follows:

$$\text{ntu}_{\text{gas}} = 1.11\text{NTU}, \qquad \text{ntu}_{\text{liq}} = 10C^*\text{NTU} \tag{4.5.70}$$

Also note that initial guesses of η_o and *j/f* are needed for the first iteration to solve Equation (4.5.66). For a good design, consider $\eta_o = 0.80$ and determine an approximate value of *j/f* from the plot of *j/f* vs.

Re curve for the known *j* and *f* vs. Re characteristics of each fluid side surface. The specific step-by-step design procedure is as follows:

1. In order to compute the fluid bulk mean temperature and the fluid thermophysical properties on each fluid side, determine the fluid outlet temperatures from the specified heat duty

$$q = \left(\dot{m} c_p \right)_h \left(T_{h,i} - T_{h,o} \right) = \left(\dot{m} c_p \right)_c \left(T_{c,o} - T_{c,i} \right) \tag{4.5.71}$$

or from the specified exchanger effectiveness using Equation (4.5.52) and (4.5.53). For the first time, estimate the values of c_p.

For exchangers with $C^* \geq 0.5$, the bulk mean temperature on each fluid side will be the arithmetic mean of inlet and outlet temperatures on each side. For exchangers with $C^* < 0.5$, the bulk mean temperature on the C_{max} side will be the arithmetic mean of the inlet and outlet temperatures on that side and the bulk mean temperature on the C_{min} side will be the log-mean average as given by Equation (4.5.54). With these bulk mean temperatures, determine c_p and iterate one more time for the outlet temperatures if warranted. Subsequently, determine μ, c_p, k, Pr, and ρ on each fluid side.

2. Calculate C^* and ε (if q is given), and determine NTU from the ε-NTU expression, tables, or graphical results for the selected flow arrangement (in this case, it is unmixed–unmixed cross-flow, Table 4.5.4). The influence of longitudinal heat conduction, if any, is ignored in the first iteration since we don't know the exchanger size yet.

3. Determine ntu on each side by the approximations discussed with Equations (4.5.68) and (4.5.70) unless it can be estimated from past experience.

4. For the selected surfaces on each fluid side, plot *j/f* vs. Re curve from the given surface characteristics and obtain an approximate value of *j/f*. If fins are employed, assume $\eta_o = 0.80$ unless a better value can be estimated.

5. Evaluate G from Equation (4.5.65) on each fluid side using the information from Steps 1 to 4 and the input value of Δp.

6. Calculate Reynolds number Re, and determine *j* and *f* on each fluid side from the given design data for each surface.

7. Compute h, η_f, and η_o using Equations (4.5.57) to (4.5.59). For the first iteration, determine U_1 on Fluid 1 side from the following equation derived from Equations (4.5.6) and (4.5.67).

$$\frac{1}{U_1} = \frac{1}{\left(\eta_o h \right)_1} + \frac{1}{\left(\eta_o h_s \right)_1} + \frac{\alpha_1/\alpha_2}{\left(\eta_o h_s \right)_2} + \frac{\alpha_1/\alpha_2}{\left(\eta_o h \right)_2} \tag{4.5.72}$$

where $\alpha_1/\alpha_2 = A_1/A_2$, $\alpha = A/V$, V is the exchanger total volume, and subscripts 1 and 2 denote Fluid 1 and 2 sides. For a plate-fin exchanger, α terms are given by Shah (1981) and Kays and London (1984):

$$\alpha_1 = \frac{b_1 \beta_1}{b_1 + b_2 + 2a} \qquad \alpha_2 = \frac{b_2 \beta_2}{b_1 + b_2 + 2a} \tag{4.5.73}$$

Note that the wall thermal resistance in Equation (4.5.72) is ignored in the first iteration. In second and subsequent iterations, compute U_1 from

$$\frac{1}{U_1} = \frac{1}{\left(\eta_o h \right)_1} + \frac{1}{\left(\eta_o h_s \right)_1} + \frac{\delta A_1}{k_w A_w} + \frac{A_1/A_2}{\left(\eta_o h_s \right)_2} + \frac{A_1/A_2}{\left(\eta_o h \right)_2} \tag{4.5.74}$$

where the necessary geometry information A_1/A_2 and A_1/A_w is determined from the geometry calculated in the previous iteration.

8. Now calculate the core dimensions. In the first iteration, use NTU computed in Step 2. For subsequent iterations, calculate longitudinal conduction parameter λ (and other dimensionless groups for a crossflow exchanger). With known ε, C^*, and λ, determine the correct value of NTU using either a closed-form equation or tabular/graphical results (Kays and London, 1984). Determine A_1 from NTU using U_1 from the previous step and known $C_{\min}$.

$$A_1 = \mathrm{NTU}\, C_{\min}/U_1 \tag{4.5.75}$$

and hence

$$A_2 = (A_2/A_1)A_1 = (\alpha_2/\alpha_1)A_1 \tag{4.5.76}$$

A_o from known $\dot{m}$ and G is given by

$$A_{o,1} = (\dot{m}/G)_1 \qquad A_{o,2} = (\dot{m}/G)_2 \tag{4.5.77}$$

so that

$$A_{fr,1} = A_{o,1}/\sigma_1 \qquad A_{fr,2} = A_{o,2}/\sigma_2 \tag{4.5.78}$$

where σ_1 and σ_2 are generally specified for the surface or can be computed for plate-fin surfaces from Shah (1981) and Kays and London (1984):

$$\sigma_1 = \frac{b_1\beta_1 D_{h,1}/4}{b_1 + b_2 + 2\delta} \qquad \sigma_2 = \frac{b_2\beta_2 D_{h,2}/4}{b_1 + b_2 + 2\delta} \tag{4.5.79}$$

Now compute the fluid flow lengths on each side (see Figure 4.5.17) from the definition of the hydraulic diameter of the surface employed on each side.

$$L_1 = \left(\frac{D_h A}{4A_o}\right)_1 \qquad L_2 = \left(\frac{D_h A}{4A_o}\right)_2 \tag{4.5.80}$$

Since $A_{fr,1} = L_2 L_3$ and $A_{fr,2} = L_1 L_3$, we can obtain

$$L_3 = \frac{A_{fr,1}}{L_2} \qquad \text{or} \qquad L_3 = \frac{A_{fr,2}}{L_1} \tag{4.5.81}$$

Theoretically, L_3 calculated from both expressions of Equation (4.5.81) should be identical. In reality, they may differ slightly because of the round-off error. In that case, consider an average value for L_3.

9. Finally, compute the pressure drop on each fluid side, after correcting f factors for variable property effects, in a manner similar to Step 8 of the rating problem for a Crossflow Plate Fin Exchanger.

10. If the calculated values of Δp are within and close to input specifications, the solution to the sizing problem is completed. Finer refinements in the core dimensions, such as integer numbers of flow passages, etc., may be carried out at this time. Otherwise, compute the new value of G on each fluid side using Equation (4.5.29) in which Δp is the input-specified value, and f, K_c, K_e, and geometric dimensions are from the previous iteration.
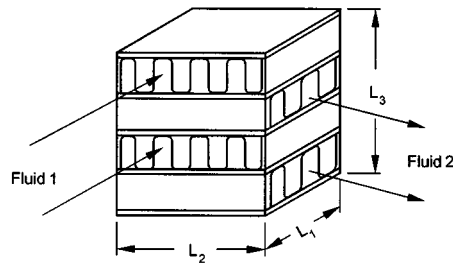
FIGURE 4.5.17 A single-pass crossflow exchanger.

11. Repeat (iterate) Steps 6 to 10 until both transfer and pressure drops are met as specified. It should be emphasized that since we have imposed no constraints on the exchanger dimensions, the above procedure will yield L_1, L_2, and L_3 for the selected surfaces such that the design will meet exactly the heat duty and pressure drops on both fluid sides.

Flow Maldistribution

In the previously presented heat transfer (ε-NTU, MTD, etc. methods) and pressure drop analyses, it is presumed that the fluid is uniformly distributed through the core. In practice, flow maldistribution does occur to some extent and often severely, and may result in a significant reduction in exchanger heat transfer performance and an increase in the pressure drop. Hence, it may be necessary for the designer to take into account the effect of flow maldistribution causing undesirable performance deterioration up front while designing a heat exchanger.

Some maldistributions are geometry-induced (i.e., the result of exchanger fabrication conditions, such as header design or manufacturing tolerances, or the duct geometry/structure upstream of the exchanger), and other maldistributions are the result of exchanger operating conditions. Gross, passage-to-passage and manifold-induced flow maldistributions are examples of the former category, while viscosity, natural convection, and density-difference-induced flow maldistributions are of the latter category. Flow maldistributions associated with two-phase and multiphase flow are too complex, with only limited information available in the literature. The analysis methods and results for some of the above flow maldistributions for single-phase flows are given by Shah (1985), Mueller and Chiou (1987), and Putnam and Rohsenow (1985).

Fouling in Heat Exchangers

Fouling, Its Effect, and Mechanisms.

Fouling refers to undesired accumulation of solid material (by-products of the heat transfer processes) on heat exchanger surfaces which results in additional thermal resistance to heat transfer, thus reducing exchanger performance. The fouling layer also blocks the flow passage/area and increases surface roughness, thus either reducing the flow rate in the exchanger or increasing the pressure drop or both. The foulant deposits may be loose such as magnetite particles or hard and tenacious such as calcium carbonate scale; other deposits may be sediment, polymers, coking or corrosion products, inorganic salts, biological growth, etc. Depending upon the fluids, operating conditions, and heat exchanger construction, the maximum fouling layer thickness on the heat transfer surface may result in a few hours to a number of years.

Fouling could be very costly depending upon the nature of fouling and the applications. It increases capital costs: (1) oversurfacing heat exchanger, (2) provisions for cleaning, and (3) use of special materials and constructions/surface features. It increases maintenance costs: (1) cleaning techniques, (2) chemical additives, and (3) troubleshooting. It may cause a loss of production: (1) reduced capacity and (2) shutdown. It increases energy losses: (1) reduced heat transfer, (2) increased pressure drop, and (3) dumping dirty streams. Fouling promotes corrosion, severe plugging, and eventual failure of uncleaned

heat exchangers. In a fossil-fired exhaust environment, gas-side fouling produces a potential fire hazard in heat exchangers.

The following are the major fouling mechanisms:

- *Crystallization or precipitation fouling* results from the deposition/formation of crystals of dissolved substances from the liquid onto heat transfer surface due to solubility changes with temperature beyond the saturation point. If the deposited layer is hard and tenacious, it is often referred to as scaling. If it is porous and mushy, it is called sludge.
- *Particulate fouling* results from the accumulation of finely divided substances suspended in the fluid stream onto heat transfer surface. If the settling occurs as a result of gravity, it is referred to as sedimentation fouling.
- *Chemical reaction fouling* is defined as the deposition of material produced by chemical reaction (between reactants contained in the fluid stream) in which the heat transfer surface material does not participate.
- *Corrosion fouling* results from corrosion of the heat transfer surface that produces products fouling the surface and/or roughens the surface, promoting attachment of other foulants.
- *Biological fouling* results from the deposition, attachment, and growth of biological organisms from liquid onto a heat transfer surface. Fouling due to microorganisms refers to microbial fouling and fouling due to macroorganisms refers to macrobial fouling.
- *Freezing fouling* results from the freezing of a single-component liquid or higher-melting-point constituents of a multicomponent liquid onto a subcooled heat transfer surface.

Biological fouling occurs only with liquids since there are no nutrients in gases. Also crystallization fouling is not too common with gases since most gases contain few dissolved salts (mainly in mists) and even fewer inverse-solubility salts. All other types of fouling occur in both liquid and gas. More than one mechanism is usually present in many fouling situations, often with synergetic results. Liquid-side fouling generally occurs on the exchanger side where the liquid is being heated, and gas-side fouling occurs where the gas is being cooled; however, reverse examples can be found.

Importance of Fouling.
Fouling in liquids and two-phase flows has a significant detrimental effect on heat transfer with some increase in pressure drop. In contrast, fouling in gases reduces heat transfer somewhat (5 to 10% in general) in compact heat exchangers, but increases pressure drop significantly up to several hundred percent. For example, consider $U = 1400$ W/m²K as in a process plant liquid-to-liquid heat exchanger. Hence, $R = 1/U = 0.00072$ m²K/W. If the fouling factors ($r_{s,h} + r_{s,c}$) together amount to 0.00036 (considering a typical TEMA value of the fouling factor as 0.00018), 50% of the heat transfer area requirement A for given q is chargeable to fouling. However, for gas flows on both sides of an exchanger, $U \approx 280$ W/m²K, and the same fouling factor of 0.00036 would represent only about 10% of the total surface area. Thus, one can see a significant impact on the heat transfer surface area requirement due to fouling in heat exchangers having high U values (such as having liquids or phase-change flows).

Considering the core frictional pressure drop (Equation (4.5.32) as the main pressure drop component, the ratio of pressure drops of fouled and cleaned exchangers is given by

$$\frac{\Delta p_F}{\Delta p_C} = \frac{f_F}{f_C}\left(\frac{D_{h,C}}{D_{h,F}}\right)\left(\frac{u_{m,F}}{u_{m,C}}\right)^2 = \frac{f_F}{f_C}\left(\frac{D_{h,C}}{D_{h,F}}\right)^5 \tag{4.5.82}$$

where the term after the second equality sign is for a circular tube and the mass flow rates under fouled and clean conditions remain the same. Generally, $f_F > f_C$ due to the fouled surface being rough. Thus, although the effect of fouling on the pressure drop is usually neglected, it can be significant, particularly for compact heat exchangers with gas flows. If we consider $f_F = f_C$, and the reduction in the tube inside

diameter due to fouling by only 10 and 20%, the resultant pressure drop increase will be 69 and 205%, respectively, according to Equation (4.5.82) regardless of whether the fluid is liquid or gas!

Accounting of Fouling in Heat Exchangers.

Fouling is an extremely complex phenomenon characterized by a combined heat, mass, and momentum transfer under transient condition. Fouling is affected by a large number of variables related to heat exchanger surfaces, operating conditions, and fluids. Fouling is time dependent, zero at $\tau = 0$; after the induction or delay period τ_d, the fouling resistance is either pseudolinear, falling rate, or asymptotic.

Fouling is characterized by all or some of the following sequential events: initiation, transport, attachment, removal, and aging (Epstein, 1983). Research efforts are concentrated on quantifying these events by semitheoretical models (Epstein, 1978) with very limited success on specific fouling situations. Hence, the current heat exchanger design approach is to use a constant (supposedly an asymptotic) value of the fouling factor $r_s = 1/h_s$. Equation (4.5.6) presented earlier includes the fouling resistances on the hot and cold sides for a nontubular extended-surface exchanger. Here $1/h_s = r_s$ is generally referred to as the *fouling factor*. Fouling factors for some common fluids are presented in Tables 4.5.8 and 4.5.9.

The specification of fouling effects in a process heat exchanger is usually represented in the following form, wherein the combined fouling factor $r_{s,t}$ is the sum of the fouling factors on the hot and cold sides:

Combined fouling factor
$$r_{s,t} = \frac{1}{U_C} - \frac{1}{U_F} \tag{4.5.83}$$

Cleanliness factor
$$\mathrm{CF} = U_F / U_C \tag{4.5.84}$$

Percentage oversurface
$$\%\mathrm{OS} = \left(\frac{A_F}{A_C} - 1 \right) 100 \tag{4.5.85}$$

Here the subscripts F and C denote fouled and clean exchanger values. From Equation (4.5.6) with $A_h = A_c = A$, $\eta_o = 1$, $\Delta T_{m,F} = \Delta T_{m,C}$, it can be shown that

$$\frac{A_F}{A_C} = \frac{U_C}{U_F} = 1 + U_C r_{s,t} \tag{4.5.86}$$

where $r_{s,t} = r_{s,h} + r_{s,c}$. In heat exchanger design, constant (supposedly an asymptotoic) values of $r_{s,h}$ and $r_{s,c}$ are used. Accordingly, extra heat transfer surface area is provided to take into account the deleterious effect of fouling. Thus, the heat exchanger will be "oversized" for the initial clean condition, "correctly sized" for asymptotic fouling (if it occurs in practice), and "undersized" just before the cleaning operation for nonasymptotic fouling.

Influence of Operating and Design Variables.

Based on operational experience and research over the last several decades, many variables have been identified that have a significant influence on fouling. The most important variables are summarized next.

Flow velocity. Flow velocity is one of the most important variables affecting fouling. Higher velocities increase fluid shear stress at the fouling deposit–fluid interface and increase the heat transfer coefficient; but, at the same time, increased pressure drop and fluid pumping power may erode the surface and may accelerate the corrosion of the surface by removing the protective oxide layer. The fouling buildup in general is inversely proportional to $u_m^{1.5}$. For water, the velocity should be kept above 2 m/sec to suppress fouling, and the absolute minimum should be above 1 m/sec to minimize fouling.

Surface temperature. Higher surface temperatures promote chemical reaction, corrosion, crystal formation (with inverse solubility salts), and polymerization, but reduce biofouling for temperatures above the optimum growth, avoid potential freezing fouling, and avoid precipitation of normal-solubility salts.

TABLE 4.5.8   Fouling Factors for Various Fluid Streams Used in Heat Exchangers

Water Type	Fouling Factors $(m^2 \cdot K)/W$
Seawater (43°C maximum outlet)	0.000275 to 0.00035
Brackish water (43°C maximum outlet)	0.00035 to 0.00053
Treated cooling tower water (49°C maximum outlet)	0.000175 to 0.00035
Artificial spray pond (49°C maximum outlet)	0.000175 to 0.00035
Closed-loop treated water	0.000175
River water	0.00035 to 0.00053
Engine jacket water	0.000175
Distilled water or closed-cycle condensate	0.00009 to 0.000175
Treated boiler feedwater	0.00009
Boiler blowdown water	0.00035 to 0.00053

Liquids	
No. 2 fuel oil	0.00035
No. 6 fuel oil	0.0009
Transformer oil	0.000175
Engine lube oil	0.000175
Refrigerants	0.000175
Hydraulic fluid	0.000175
Industrial organic HT fluids	0.000175 to 0.00035
Ammonia	0.000175
Ammonia (oil bearing)	0.00053
Methanol solutions	0.00035
Ethanol solutions	0.00035
Ethylene glycol solutions	0.00035
MEA and DEA solutions	0.00035
DEG and TEG solutions	0.00035
Stable side draw and bottom products	0.000175 to 0.00035
Caustic solutions	0.00035

Gas or Vapor	
Steam (non-oil-bearint)	0.0009
Exhaust steam (oil-bearing)	0.00026 to 0.00035
Refrigerant (oil-bearing)	0.00035
Compressed air	0.000175
Ammonia	0.000175
Carbon dioxide	0.00035
Coal flue gas	0.00175
Natural gas flue gas	0.00090
Acid gas	0.00035 to 0.00053
Solvent vapor	0.000175
Stable overhead products	0.000175

Natural Gas and Petroleum Streams	
Natural gas	0.000175 to 0.00035
Overhead products	0.000175 to 0.00035
Lean oil	0.00035
Rich oil	0.000175 to 0.00035
Natural gasoline and liquefied petroleum gases	0.000175 to 0.00035

Oil Refinery Streams	
Crude and vacuum unit gases and vapors	
Atmospheric tower overhead vapors	0.00017
Light naphthas	0.00017
Vacuum overhead vapors	0.00035

TABLE 4.5.8   (continued)   Fouling Factors for Various Fluid Streams Used in Heat Exchangers

Oil Refinery Streams

Crude and vacuum liquids

Gasoline	0.00035
Naphtha and light distillates	0.00035 to 0.00053
Kerosene	0.00035 to 0.00053
Light gas oil	0.00035 to 0.00053
Heavy gas oil	0.00053 to 0.0009
Heavy fuel oil	0.00053 to 0.00123
Vacuum tower bottoms	0.00176
Atmospheric tower bottoms	0.00123

Cracking and coking unit streams

Overhead vapors	0.00035
Light cycle oil	0.00035 to 0.00053
Heavy cycle oil	0.00053 to 0.0007
Light coker gas oil	0.00053 to 0.0007
Heavy coker gas oil	0.00070 to 0.0009
Bottoms slurry oil (1.5 m/sec minimum)	0.00053
Light liquid products	0.00035

Catalytic reforming, hydrocracking, and
  hydrodesulfurization streams

Reformer charge	0.00026
Reformer effluent	0.00026
Hydrocharger charge and effluent[a]	0.00035
Recycle gas	0.000175
Liquid product over 50°C (API)[b]	0.000175
Liquid product 30 to 50°C (API)[b]	0.00035

Light ends processing streams

Overhead vapors and gases	0.000175
Liquid products	0.000175
Absorption oils	0.00035 to 0.00053
Alkylation trace acid streams	0.00035
Reboiler streams	0.00035 to 0.00053

[a]   Depending on charge characteristics and storage history, charge fouling resistance may be many times this value.

[b]   American Petroleum Institute.

Source: Chenoweth, J., Final Report, HTRI/TEMA Joint Committee to Review the Fouling Section of TEMA Standards, HTRI, Alhambra, CA, 1988. With permission.

It is highly recommended that the surface temperature be maintained below the reaction temperature; it should be kept below 60°C for cooling tower water.

Tube material. The selection of the tube material is important from the corrosion point of view which in turn could increase crystallization and biological fouling. Copper alloys can reduce certain biofouling, but their use is limited by environmental concerns with river, ocean, and lake waters.

There are many other variables that affect fouling. It is beyond the scope here, but the reader may refer to TEMA (1988).

Fouling Control and Cleaning Techniques.

Control of fouling should be attempted first before any cleaning method is attempted. For gas-side fouling, one should verify that fouling exists, identify the sequential event that dominates the foulant accumulation, and characterize the deposit. For liquid-side fouling, fouling inhibitors/additives should be employed while the exchanger is in operation; for example, use antidispersant polymers to prevent sedimentation fouling, "stabilizing" compounds to prevent polymerization and chemical reaction fouling, corrosion inhibitors to prevent corrosion fouling, biocide/germicide to prevent biofouling, softeners, acids, and polyphosphates to prevent crystallization fouling.

TABLE 4.5.9   Fouling Factors and Design Parameters for Finned Tubes in Fossil Fuel Exhaust Gases

Type of Flue Gas	Fouling Factor, $m^2 K/W$	Minimum Spacing between Fins, m	Maximum Gas Velocity to Avoid Erosion, m/sec
Clean Gas (Cleaning Devices Not Required)			
Natural Gas	0.0000881–0.000528	0.00127–0.003	30.5–36.6
Propane	0.000176–0.000528	0.00178	—
Butane	0.000176–0.000528	0.00178	—
Gas turbine	0.000176	—	—
Average Gas (Provisions for Future Installation of Cleaning Devices)			
No. 2 oil	0.000352–0.000704	0.00305–0.00384	25.9–30.5
Gas turbine	0.000264	—	—
Diesel engine	0.000528	—	—
Dirty Gas (Cleaning Devices Required)			
No. 6 oil	0.000528–0.00123	0.00457–0.00579	18.3–24.4
Crude oil	0.000704–0.00264	0.00508	—
Residual oil	0.000881–0.00352	0.00508	—
Coal	0.000881–0.00881	0.00587–0.00864	15.2–21.3

Source: Weierman, R.C., 1982. Design of Heat Transfer Equipment for Gas-Side Fouling Service, Workshop on an Assessment of Gas-Side Fouling in Fossil Fuel Exhaust Environments, W.J. Marner and R.L. Webb, Eds., JPL Publ. 82-67, Jet Propulsion Laboratory, California Institute of Technology, Pasadena. With permission.

If the foulant control is not effective, the exchanger must be cleaned either on-line or off-line. On-line cleaning includes flow-driven brushes/sponge balls inside tubes, power-driven rotating brushes inside tubes, acoustic horns/mechanical vibrations for tube banks with gases, soot blowers, and shutting off of the cold gas supply, flowing hot gas, or reversing of the fluids. Off-line cleaning methods, without dismantling the exchanger include chemical cleaning (circulate acid/detergent solutions), circulating of particulate slurry (such as sand and water), and thermal melting of frost layers. Off-line cleaning with a heat exchanger opened includes high-pressure steam or water cleaning, and thermal baking of an exchanger and then rinsing for small heat exchanger modules removed from the container of the modular exchangers.

Nomenclature

A total heat transfer area (primary + fin) on one fluid side of a heat exchanger, A_p: primary surface area, A_f: fin surface area, m^2

A_{fr} frontal area on one side of an exchanger, m^2

A_k total wall cross-sectional area for heat conduction in fin or for longitudinal conduction in the exchanger, m^2

A_o minimum free-flow area on one fluid side of a heat exchanger, m^2

b plate spacing, $h' + \delta_f$, m

C flow stream heat capacity rate with a subscript c or h, $\dot{m}c_p$, W/°C

C^* heat capacity rate ratio, C_{min}/C_{max}, dimensionless

c_p specific heat of fluid at constant pressure, J/kg K

D_h hydraulic diameter of flow passages, $4A_o L/A$, m

d_e fin tip diameter of an individually finned tube, m

d_i, d_o tube inside and outside diameters, respectively, m

Eu N-row average Euler number, $\Delta p/(\rho\, u_m^2\, N/2g_c)$, $\rho\Delta p g_c/(NG^2/2)$, dimensionless

F	log-mean temperature difference correction factor, dimensionless
f	Fanning friction factor, $\rho \Delta p g_c D_h/(2LG^2)$, dimensionless
f_{tb}	Fanning friction factor per tube row for crossflow over a tube bank outside, $\rho \Delta p g_c/(2NG^2)$
G	mass velocity based on the minimum free flow area, $\dot{m}/A_o$, kg/m²sec
g	gravitational acceleration, m²/sec
g_c	proportionality constant in Newton's second law of motion, $g_c = 1$ and dimensionless in SI units
H	fin length for heat conduction from primary surface to either fin tip or midpoint between plates for symmetric heating, m
h	heat transfer coefficient, W/m²K
h'	height of the offset strip fin (see Figure 4.5.15), m
j	Colburn factor, $\mathrm{NuPr}^{-1/3}/\mathrm{Re}$, $\mathrm{StPr}^{2/3}$, dimensionless
k	fluid thermal conductivity, W/m K
k_f	thermal conductivity of the fin material, W/m K
k_w	thermal conductivity of the matrix (wall) material, W/m K
L	fluid flow (core or tube) length on one side of an exchanger, m
l	fin length for heat conduction from primary surface to the midpoint between plates for symmetric heating, see Table 4.5.5 for other definitions of l, m
l_f	offset trip fin length or fin height for individually finned tubes, l_f represents the fin length in the fluid flow direction for an uninterrupted fin with $l_f = L$ in most cases, m
m	fin parameter, 1/m
N	number of tube rows
N_f	number of fins per meter, 1/m
N_t	total number of tubes in an exchanger
NTU	number of heat transfer units, $UA/C_{\min}$, it represents the total number of transfer units in a multipass unit, $\mathrm{NTU}_s = UA/C_{\mathrm{shell}}$, dimensionless
Nu	Nusselt number, hD_h/k, dimensionless
ntu_c	number of heat transfer units based on the cold side, $(\eta_o hA)_c/C_c$, dimensionless
ntu_h	number of heat transfer units based on the hot side, $(\eta_o hA)_h/C_h$, dimensionless
$\dot{m}$	mass flow rate, kg/sec
P	temperature effectiveness of one fluid, dimensionless
$\wp$	fluid pumping power, W
Pr	fluid Prandtl number, $\mu c_p/k$, dimensionless
p	fluid static pressure, Pa
Δp	fluid static pressure drop on one side of heat exchanger core, Pa
p_f	fin pitch, m
q	heat duty, W
q_e	heat transfer rate (leakage) at the fin tip, W
q''	heat flux, W/m²
R	heat capacity rate ratio used in the P-NTU method, $R_1 = C_1/C$, $R_2 = C_2/C_1$, dimensionless
R	thermal resistance based on the surface area A, compare Equations 4.5.5 and 4.5.6 for definitions of specific thermal resistances, K/W
Re	Reynolds number, GD_h/μ, dimensionless
Re_d	Reynolds number, $\rho u_m d_o/\mu$, dimensionless
r_h	hydraulic radius, $D_h/4$, $A_o L/A$, m
r_s	fouling factor, $1/h_s$, m²K/W
St	Stanton number, h/Gc_p, dimensionless
s	distance between adjacent fins, $p_f - \delta_f$ m
T	fluid static temperature to a specified arbitrary datum, °C
T_a	ambient temperature, °C
T_o	fin base temperature, °C
T_l	fin tip temperature, °C
U	overall heat transfer coefficient, W/m² K
u_m	mean axial velocity in the minimum free flow area, m/sec

V	heat exchanger total volume, m^3
X_d	diagonal tube pitch, m
X_l	longitudinal tube pitch, m
X_t	transverse tube pitch, m
α	ratio of total heat transfer area on one side of an exchanger to the total volume of an exchanger, A/V, m^2/m^3
β	heat transfer surface area density, a ratio of total transfer area on one side of a plate-fin heat exchanger to the volume between the plates on that side, m^2/m^3
ε	heat exchanger effectiveness, it represents an overall exchanger effectiveness for a multiplass unit, dimensionless
δ	wall thickness, m
δ_f	fin thickness, m
η_f	fin efficiency, dimensionless
η_o	extended surface efficiency, dimensionless
λ	longitudinal wall heat conduction parameter based on the total conduction area, $\lambda = k_w A_{k,t}/C_{min}L$, $\lambda_c = k_w A_{k,c}/C_c L$, $\lambda_h = k_w A_{k,h}/C_h L$, dimensionless
μ	fluid dynamic viscosity, Pa·s
ρ	fluid density, kg/m^3
σ	ratio of free flow area to frontal area, A_o/A_{fr}, dimensionless

Subscripts

C	clean surface value
c	cold fluid side
F	fouled surface value
f	fin
h	hot fluid side
i	inlet to the exchanger
o	outlet to the exchanger
s	scale or fouling
w	wall or properties at the wall temperature
1	one section (inlet or outlet) of the exchanger
2	other section (outlet or inlet) of the exchanger

References

Bhatti, M.S. and Shah, R.K. 1987. Turbulent and transition flow convective heat transfer in ducts, in *Handbook of Single-Phase Convective Heat Transfer,* S. Kakaç, R. K. Shah, and W. Aung, Eds., John Wiley & Sons, New York, chap. 4, 166 pp.

Chai, H.C. 1988. A simple pressure drop correlation equation for low finned tube crossflow heat exchangers, *Int. Commun. Heat Mass Transfer*, 15, 95–101.

Chenoweth, J. 1988. Final Report, HTRI/TEMA Joint Committee to Review the Fouling Section of TEMA Standards, HTRI, Alhambra, CA.

Cowell, T.A., Heikal, M.R., and Achaichia, A. 1995. Flow and heat transfer in compact louvered fin surfaces, *Exp. Thermal Fluid Sci.*,10, 192–199.

Epstein, N. 1978. Fouling in heat exchangers, in *Heat Transfer 1978*, Vol. 6, Hemisphere Publishing, New York, 235–254.

Epstein, N. 1983. Thinking about heat transfer fouling: a 5×5 matrix, *Heat Transfer Eng.*, 4(1), 43–56.

Foumeny, E.A. and Heggs, P.J. 1991. *Heat Exchange Engineering*, Vol. 2, *Compact Heat Exchangers: Techniques for Size Reduction*, Ellis Horwood Ltd., London.

Ganguli, A. and Yilmaz, S.B. 1987. New heat transfer and pressure drop correlations for crossflow over low-finned tube banks, *AIChE Symp. Ser. 257*, 83, 9–14.

Ghajar, A.J. and Tam, L.M. 1994. Heat transfer measurements and correlations in the transition region for a circular tube with three different inlet configurations, *Exp. Thermal Fluid Sci.*, 8, 79–90.

Huang, L.J. and Shah, R.K. 1992. Assessment of calculation methods for efficiency of straight fins of rectangular profiles, *Int. J. Heat Fluid Flow*, 13, 282–293.

Idelchik, I.E. 1994. *Handbook of Hydraulics Resistance*, 3rd ed., CRC Press, Boca Raton, FL.

Kakaç, S., Ed. 1991. *Boilers, Evaporators, and Condensers*, John Wiley & Sons, New York.

Kakaç, S., Bergles, A.E., and Mayinger, F. 1981. *Heat Exchangers: Thermal-Hydraulic Fundamentals and Design*, Hemisphere Publishing, Washington, D.C.

Kakaç, S., Shah, R.K., and Bergles, A.E. 1983. *Low Reynolds Number Flow Heat Exchangers*, Hemisphere Publishing, Washington, D.C.

Kakaç, S., Bergles, A.E., and Fernandes, E.O. 1988. *Two-Phase Flow Heat Exchangers: Thermal Hydraulic Fundamentals and Design*, Kluwer Academic Publishers, Dordrecht, Netherlands.

Kays, W.M. and London, A.L. 1984. *Compact Heat Exchangers*, 3rd ed., McGraw-Hill, New York.

Manglik, R.M. and Bergles, A.E. 1995. Heat transfer and pressure drop correlations for the rectangular offset-strip-fin compact heat exchanger, *Exp. Thermal Fluid Sci.*, 10, 171–180.

Miller, D.S. 1990. *Internal Flow Systems, 2nd ed., BHRA (Information Services),* Cranfield, Bedford, U.K.

Mueller, A.C. and Chiou, J.P. 1987. *Review of Various Types of Flow Maldistribution in Heat Exchangers*, Book No. H00394, HTD-Vol. 75, ASME, New York, 3–16.

Putnam, G.R. and Rohsenow, W.M. 1985. Viscosity induced nonuniform flow in laminar flow heat exchangers, *Int. J. Heat Mass Transfer*, 28, 1031–1038.

Rabas, T.J. and Taborek, J. 1987. Survey of turbulent forced-convection heat transfer and pressure drop characteristics of low-finned tube banks in cross flow, *Heat Transfer Eng.*, 8(2), 49–62.

Roetzel, W., Heggs, P.J., and Butterworth, D., Eds. 1991. *Design and Operation of Heat Exchangers*, Springer-Verlag, Berlin.

Rozenman, T. 1976. Heat transfer and pressure drop characteristics of dry cooling tower extended surfaces, Part I: Heat transfer and pressure drop data, Report BNWL-PFR 7-100; Part II: Data analysis and correlation, Report BNWL-PFR 7-102, Battelle Pacific Northwest Laboratories, Richland, WA.

Shah, R.K. 1981. Compact heat exchangers, in *Heat Exchangers: Thermal-Hydraulic Fundamentals and Design*, S. Kakaç, A.E. Bergles, and F. Mayinger, Eds., Hemisphere Publishing, Washington, D.C., 111–151.

Shah, R.K. 1983. Heat Exchanger Basic Design Methods, in *Low Reynolds Number Flow Heat Exchanger*, S. Kakaç, R.K. Shah and A.E. Bergles, Eds., pp. 21–72, Hemisphere, Washington, D.C.

Shah, R.K. 1985. Compact heat exchangers, in *Handbook of Heat Transfer Applications*, 2nd ed., W.M. Rohsenow, J.P. Hartnett, and E.N. Ganic, Eds., McGraw-Hill, New York, Chap. 4, Part 3.

Shah, R.K. 1988a. Plate-fin and tube-fin heat exchanger design procedures, in *Heat Transfer Equipment Design*, R.K. Shah, E.C. Subbarao, and R.A. Mashelkar, Eds., Hemisphere Publishing, Washington, D.C., 255–266.

Shah, R.K. 1988b. Counterflow rotary regenerator thermal design procedures, in *Heat Transfer Equipment Design*, R.K. Shah, E.C. Subbarao, and R.A. Mashelkar, Eds., Hemisphere Publishing, Washington, D.C., 267–296.

Shah, R.K. 1991. Multidisciplinary approach to heat exchanger design, in *Industrial Heat Exchangers*, J.-M. Buchlin, Ed., Lecture Series No. 1991-04, von Kármán Institute for Fluid Dynamics, Rhode Saint Genèse, Belgium.

Shah, R.K. 1993. Nonuniform heat transfer coefficients for heat exchanger thermal design, in *Aerospace Heat Exchanger Technology 1993*, R.K. Shah and A. Hashemi, Eds., Elsevier Science, Amsterdam, Netherlands, 417–445.

Shah, R.K. 1994. Heat exchangers, in *Encyclopedia of Energy Technology and The Environment*, A. Bision and S.G. Boots, Eds., John Wiley & Sons, New York, 1651–1670.

Shah, R.K., Bell, K.J., Mochizuki, S., and Wadekar, V. V., Eds., 1997. *Compact Heat Exchangers for the Process Industries*, Begell House, New York.

Shah, R.K. and Bhatti, M.S. 1987. Laminar convective heat transfer in ducts, in *Handbook of Single-Phase Convective Heat Transfer*, S. Kacaç, R.K. Shah, and W. Aung, Eds., John Wiley, New York, Chap. 3, 137 pp.

Shah, R.K. and Bhatti, M.S. 1988. Assessment of correlations for single-phase heat exchangers, in *Two-Phase Flow Heat Exchangers: Thermal-Hydraulic Fundamentals and Design*, S. Kakaç, A.E. Bergles, and E.O. Fernandes, Eds., Kluwer Academic Publishers, Dordrecht, The Netherlands, 81–122.

Shah, R.K. and Giovannelli, A.D. 1988. Heat pipe heat exchanger design theory, in *Heat Transfer Equipment Design*, R.K. Shah, E.C. Subbarao, and R.A. Mashelkar, Eds., Hemisphere Publishing, Washington, D.C., 609–653.

Shah, R.K. and Hashemi, A., Eds. 1993. *Aerospace Heat Exchanger Technology*, Elsevier Science, Amsterdam.

Shah, R.K., Kraus, A.D., and Metzger, D.E., Eds., 1990. *Compact Heat Exchangers — A Festschrift for Professor A.L. London*, Hemisphere, Washington, D.C.

Shah, R.K. and London, A.L. 1978. Laminar flow forced convection in ducts, Suppl. 1 to *Advances in Heat Transfer*, Academic Press, New York.

Shah, R.K. and Mueller, A.C. 1988. Heat Exchange, in *Ullmann's Encyclopedia of Industrial Chemistry*, Unit Operations II, vol. B3, chap. 2, 108 pages, VCH, Weinheim, Germany.

Shah, R.K. and Pignotti, A. 1997. The influence of a finite number of baffles on the shell-and-tube heat exchanger performance, *Heat Transfer Eng.*, 18.

Shah, R.K., Subbarao, E.C., and Mashelkar, R.A., Eds. 1988. *Heat Transfer Equipment Design*, Hemisphere Publishing, Washington, D.C.

Shah, R.K. and Wanniarachchi, A.S. 1991. Plate heat exchanger design theory, in *Industrial Heat Exchangers*, J.-M. Buchlin, Ed., Lecture Series No. 1991-04, von Kármán Institute for Fluid Dynamics, Rhode Saint Genèse, Belgium.

Taylor, M.A. 1987. *Plate-Fin Heat Exchangers: Guide to Their Specificaitons and Use*, 1st ed., HTFS, Harwell Laboratory, Oxon, U.K., rev. 1990.

TEMA, 1988. *Standards of the Tubular Exchanger Manufacturers Association*, 7th ed., Tubular Exchanger Manufacturers Association, New York.

Webb, R.L. 1994. *Principles of Enhanced Heat Transfer*, John Wiley & Sons, New York.

Weierman, R.C. 1982. Design of Heat Transfer Equipment for Gas-Side Fouling Service, Workshop on an Assessment of Gas-Side Fouling in Fossil Fuel Exhaust Environments, W.J. Marner and R.L. Webb, Eds., JPL Publ. 82-67, Jet Propulsion Laboratory, California Institute of Technology, Pasadena.

Zukauskas, A. 1987. Convective heat transfer in cross flow, in *Handbook of Single-Phase Convective Heat Transfer*, S. Kacaç, R.K. Shah, and W. Aung, John Wiley, New York, Chap. 6.

Further Information

Heat exchangers play a crucial and dominant role in many developments related to energy conservation, recovery, utilization, economic development of new energy sources, and environmental issues such as air and water pollution control, thermal pollution, waste disposal, etc. Many new and innovative heat exchangers have been developed for these and many other applications worldwide. A broad overview is provided for various heat exchangers and basic design theory for single-phase heat exchangers. For further details and study, the reader may refer to the following references: Kakaç et al. (1981; 1983; 1988), Taylor (1987), Shah et al. (1990), Foumeny and Heggs (1991), Kakaç (1991), Roetzel et al. (1991), Shah and Hashemi (1993), and Shah et al. (1997).

Shell-and-Tube Heat Exchangers

Kenneth J. Bell

Introduction

A shell-and-tube heat exchanger is essentially a bundle of tubes enclosed in a shell and so arranged that one fluid flows through the tubes and another fluid flows across the outside of the tubes, heat being transferred from one fluid to the other through the tube wall. A number of other mechanical components are required to guide the fluids into, through, and out of the exchanger, to prevent the fluids from mixing, and to ensure the mechanical integrity of the heat exchanger. A typical shell-and-tube heat exchanger is shown in Figure 4.5.18 (TEMA, 1988), but the basic design allows many modifications and special features, some of which are described below.

1. Stationary Head-Channel
2. Stationary Head Flange-Channel or Bonnet
3. Channel Cover
4. Stationary Head Nozzle
5. Stationary Tubesheet
6. Tubes
7. Shell
8. Shell Cover
9. Shell Flange-Stationary Head End
10. Shell Flange-Rear Head End
11. Shell Nozzle
12. Shell Cover Flange

13. Floating Tubesheet
14. Floating Head Cover
15. Floating Head Cover Flange
16. Floating Head Backing Device
17. Tierods and Spacers
18. Transverse Baffles or Support Plates
19. Impingement Plates
20. Pass Partition
21. Vent Connection
22. Drain Connection
23. Instrument Connection
24. Support Saddle
25. Lifting Lug

Nomenclature of Heat Exchanger Components

For the purpose of establishing standard terminology, Figure 4.5.18 illustrates various types of heat exchangers. Typical parts and connections, for illustrative purposes only, are numbered for identification:
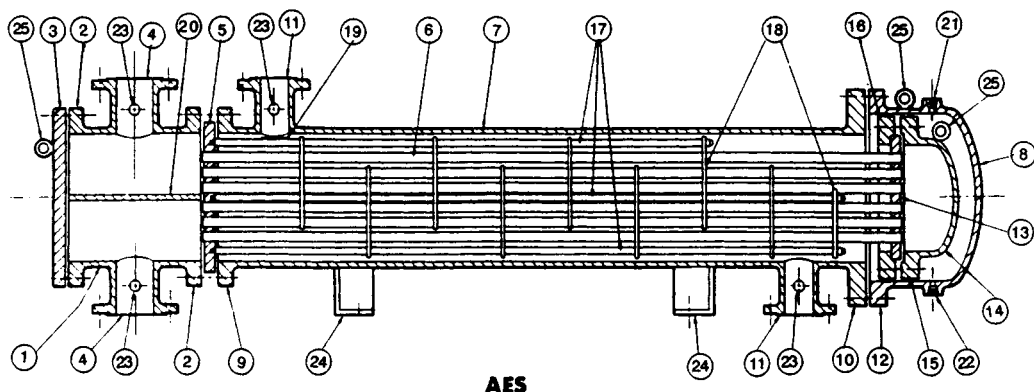
FIGURE 4.5.18 Longitudinal section of a typical shell-and-tube heat exchanger (TEMA AES) with nomenclature. (Modified from TEMA, *Standards* 7th ed., Tubular Exchanger Manufacturers Association, Tarrytown, NY, 1988.)

Shell-and-tube heat exchangers have been constructed with heat transfer areas from less than 0.1 m^2 (1 ft^2) to over 100,000 m^2 (1,000,000 ft^2), for pressures from deep vacuum to over 1000 bar (15,000 psi), for temperatures from near 0 to over 1400 K (2000°F), and for all fluid services including single-phase heating and cooling and multiphase vaporization and condensation. The key to such flexibility is the wide range of materials of construction, forming and joining methods, and design features that can be built into these exchangers (see Schlünder, Vol. 4, 1983; Saunders, 1988; and Yokell, 1990). Most

shell-and-tube heat exchangers are manufactured in conformity with TEMA _Standards_ (1988) and the _ASME Boiler and Pressure Vessel Code_ (latest edition), but other codes and standards may apply.

Construction Features

In the design process, it is important to consider the mechanical integrity under varying operational conditions and the maintainability (especially cleaning) of the exchanger as equally important with the thermal-hydraulic design.

Tubes. Tubes used in shell-and-tube exchangers range from 6.35 mm ($^1/_4$ in.) to 50.8 mm (2 in.) and above in outside diameter, with the wall thickness usually being specified by the Birmingham wire gauge (BWG). Tubes are generally available in any desired length up to 30 m (100 ft) or more for plain tubes. While plain tubes are widely used, a variety of internally and/or externally enhanced tubes is available to provide special heat transfer characteristics when economically justified (see subsection on enhancement in Section 4.8). Low fin tubes having circumferential fins typically 0.8 to 1.6 mm (0.032 to 0.062 in.) high, spaced 630 to 1260 fins/m (16 to 32 fins/in.) are often employed, especially when the shell-side heat transfer coefficient is substantially smaller than the tube-side coefficient. The outside heat transfer area of a low fin tube is three to six times the inside area, resulting in a smaller heat exchanger shell for the same service, which may offset the higher cost of the tube per unit length.

The tubes are inserted into slightly oversized holes drilled (or, occasionally, punched) through the tubesheets (items 5 and 13, Figure 4.5.18). The tubes are secured by several means, depending upon the mechanical severity of the application and the need to avoid leakage between the streams. In some low-severity applications, the tubes are roller-expanded into smooth holes in the tubesheet. For a stronger joint, two shallow circumferential grooves are cut into the wall of the hole in the tubesheet and the tube roller-expanded into the grooves; to eliminate the possibility of leakage, a seal weld can be run between the outer end of the tube and the tubesheet. Alternatively, the tubes may be strength-welded into the tubesheet.

Tube Supports. It is essential to provide periodic support along the length of the tubes to prevent sagging and destructive vibration caused by the fluid flowing across the tube bank. A secondary role played by the tube supports is to guide the flow back and forth across the tube bank, increasing the velocity and improving the heat transfer on the shell side (but also increasing the pressure drop). The tube support is usually in the form of single segmental baffles (item 18 in Figure 4.5.18) — circular plates with holes drilled to accommodate the tubes and with a segment sheared off to form a "window" or "turnaround" to allow the shell-side fluid to pass from one cross-flow section to the next. The baffles must overlap at least one full row of tubes to give the bundle the necessary rigidity against vibration. When minimizing shell-side pressure drop is not a priority, a baffle cut of 15 to 25% of the shell inside diameter is customary. Baffle spacing is determined first by the necessity to avoid vibration and secondarily to approximately match the free cross-flow area between adjacent baffles to the flow area in the window; i.e., small baffle cuts correspond to closer baffle spacing.

In situations such as low-pressure gas flows on the shell side where pressure drop is severely limited, double segmental and strip baffle arrays can be used. More recently, a helical baffle arrangement has been introduced (Kral et al., 1996) which causes the shell-side fluid to spiral through the exchanger giving improved heat transfer vs. pressure drop characteristics. Where vibration prevention and/or minimum pressure drop are the main concerns, grids of rods or strips can be used (Gentry et al., 1982).

Shells. The shell is the cylinder which confines the shell-side fluid (item 7 in Figure 4.5.18), fitted with nozzles for fluid inlet and exit. Diameters range from less than 50 mm (2 in.) to 3.05 m (10 ft) commonly, and at least twice that value for special applications. In diameters up to 610 mm (24 in.), shells are usually made from standard pipe or tubular goods by cutting to the desired length; in larger sizes, metal plates are rolled to the desired diameter and welded.

A variety of nozzle arrangements are used for special purposes, and TEMA has a standard code to identify the major types, as well as the various front and rear head configurations on the tube side. Figure 4.5.19 shows these configurations with the corresponding code letters.

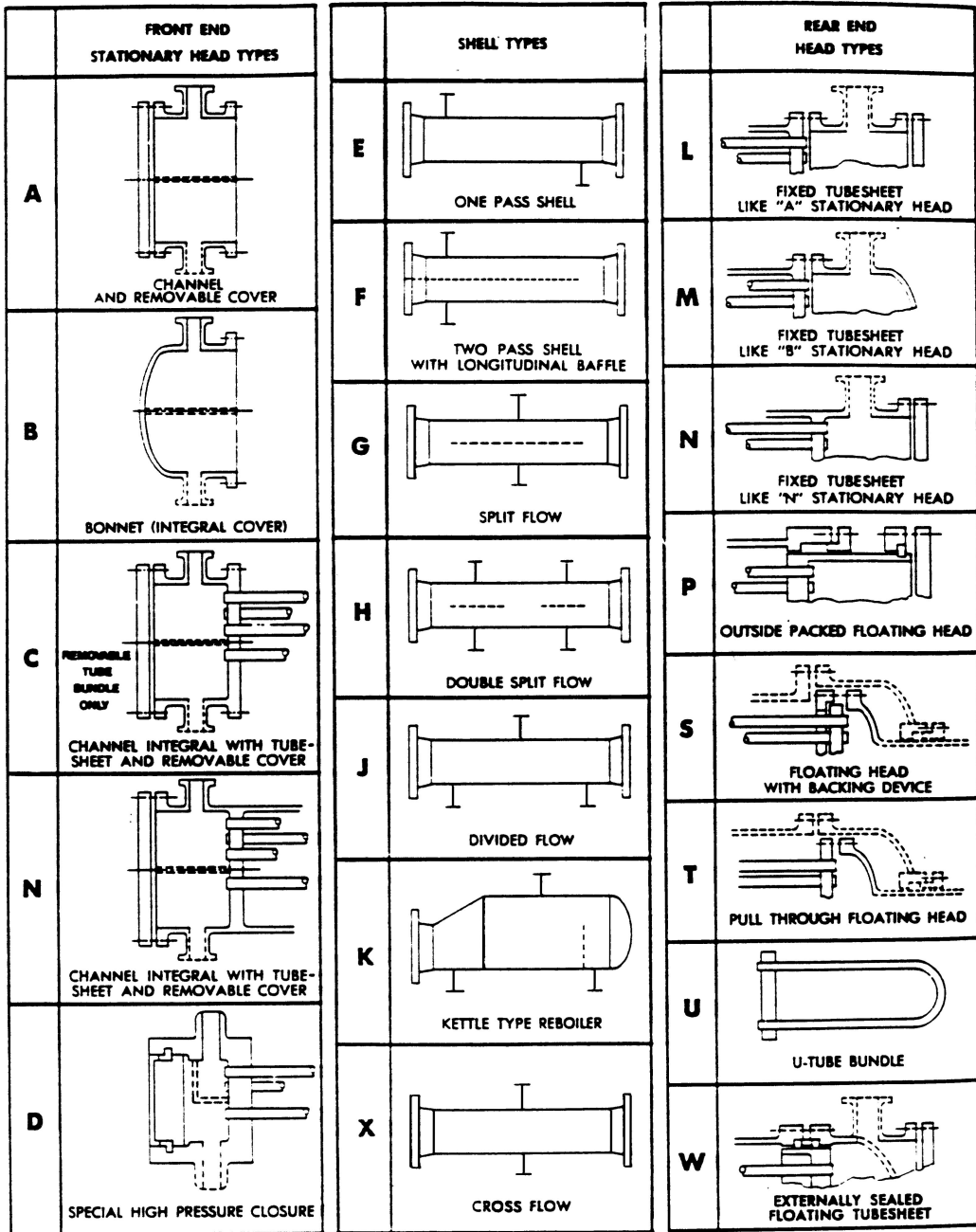| FRONT END STATIONARY HEAD TYPES	SHELL TYPES	REAR END HEAD TYPES
A — CHANNEL AND REMOVABLE COVER	E — ONE PASS SHELL	L — FIXED TUBESHEET LIKE "A" STATIONARY HEAD
B — BONNET (INTEGRAL COVER)	F — TWO PASS SHELL WITH LONGITUDINAL BAFFLE	M — FIXED TUBESHEET LIKE "B" STATIONARY HEAD
C — CHANNEL INTEGRAL WITH TUBE-SHEET AND REMOVABLE COVER (REMOVABLE TUBE BUNDLE ONLY)	G — SPLIT FLOW	N — FIXED TUBESHEET LIKE "N" STATIONARY HEAD
N — CHANNEL INTEGRAL WITH TUBE-SHEET AND REMOVABLE COVER	H — DOUBLE SPLIT FLOW	P — OUTSIDE PACKED FLOATING HEAD
	J — DIVIDED FLOW	S — FLOATING HEAD WITH BACKING DEVICE
D — SPECIAL HIGH PRESSURE CLOSURE	K — KETTLE TYPE REBOILER	T — PULL THROUGH FLOATING HEAD
	X — CROSS FLOW	U — U-TUBE BUNDLE
		W — EXTERNALLY SEALED FLOATING TUBESHEET

FIGURE 4.5.19 TEMA nomenclature for shell and tube configurations. (From TEMA, *Standards,* 7th ed., Tubular Exchanger Manufacturers Association, Tarrytown, NY, 1988. With permission.)

The E shell (center column, top) has the nozzles on opposite ends of the shell and is the most common configuration. It is used for any of the thermal services (single-phase heating or cooling, vaporization, and condensation). The nozzles may be on opposite sides of the shell as shown, or on the same side; the choice is largely determined by plumbing convenience. The E shell allows countercurrent flow (see below) of the two streams if there is one tube-side pass (i.e., the tube-side fluid flows through all of the tubes in parallel).

The F shell has both nozzles at one end of the shell and uses a longitudinal baffle on the shell side (shown dashed in the drawing) to force the shell-side fluid to flow to the far end of the heat exchanger and then back to the exit nozzle on the other side of the longitudinal baffle. Ideally, this allows countercurrent flow of the two streams if there are two tube-side passes (i.e., the tube-side fluid flows through half of the tubes in one direction, is turned around in the rear head, and returns through the other half of the tubes — see discussion of head types below). However, the longitudinal baffle must be carefully sealed to the shell to prevent leakage of the shell-side fluid across it; this is done by welding the longitudinal baffle to the shell and front tubesheet (which limits some design options) or by using mechanical seals. The F shell is mainly used for sensible heat transfer services.

The G shell has both nozzles at the center of the shell, with a centrally located longitudinal baffle to force the fluid to the ends of the shell before returning. While the G shell is used for all services, its main application is as a shellside vaporizer with either forced or natural (thermosiphon) convection of the boiling fluid; in the latter service, limited leakage across the baffle generally does not greatly degrade the thermal performance and the longitudinal baffle does not need to be perfectly sealed against the shell.

The H shell is effectively a double G shell and is employed in the same services. It is considered when the calculated shell-side pressure drop for a G arrangement is too high and threatens to limit the circulation rate.

The J shell, with one nozzle on top of the shell and two on the bottom, or vice versa, is commonly used in vacuum-condensing applications because of its low pressure drop. Two J shells (one inverted) may be mated in series for long-condensing-range mixtures. The nozzles are usually different diameters, with the large diameter accommodating the inlet vapor. The baffles are vertically cut.

The K shell (or kettle reboiler or flooded chiller) is exclusively intended for vaporization of liquid on the shell side, with a condensing vapor (usually steam) or a hot liquid on the tube side as the heating medium. The tubesheet diameter is large enough to accommodate the tube bundle, but the shell transitions to a larger diameter to allow the vapor to disengage from the liquid pool and exit from the top nozzle. A weir or other level control is used to maintain the liquid level, usually just above the top tubes in the bundle.

The X shell is intended to provide a well-distributed cross flow of the shell-side fluid, the fluid usually entering at the top and exiting at the bottom but occasionally used for upflow or horizontal cross flow. To obtain good distribution, multiple nozzles from a properly designed manifold may be required. Alternatively, the upper tubes in the bundle may be omitted to allow internal redistribution, or a large plenum chamber may be welded to the top of the shell ("vapor dome" or "bathtub nozzle"), or a diverging transition section may be placed between the inlet piping and the top of the shell. The tube supports may be complete circles since there is little or no longitudinal shell-side flow. The X shell gives the lowest shell-side pressure drop of any configuration and is often used for low-pressure vapor condensers.

Front Head. TEMA recognizes several front head designs as shown in the first column of Figure 4.5.19. Any of these designs will get the tube-side fluid into the tubes, but each has special features which recommend it to meet special needs. In Figure 4.5.19 the dashed lines indicate optional features depending upon need.

The A head, a channel with removable cover, bolts directly to the shell flange as shown in Figure 4.5.18, the tubesheet in that case being held between them and sealed with gaskets. Alternatively, the tubesheet may be integral with the shell (see the L rear head in Figure 4.5.19). A removable channel cover permits inspection, cleaning, removal, and replacement of tubes without disturbing the piping. The dashed lines at the center and the lower nozzle indicate that a pass partition plate may be welded

in the channel (and gasketed against the tubesheet and channel cover) to provide for two tube-side passes (as shown in Figure 4.5.18 and required by the F shell design). Additional pass partitions may be provided to allow four, six, or any even number of tube-side passes. This permits the designer to utilize the available tube-side pressure drop to increase velocity, improve the heat transfer coefficient, and possibly reduce fouling. A second nozzle is required on the channel for multipass designs.

The B, or bonnet, front head reduces the number of gasketed joints and thus the opportunity for leakage, but it does not permit inspection of the tubes without breaking the piping connection. It is generally less expensive than the A head.

C and N heads retain the removable cover feature of the A head but, respectively, replace the channel-to-tubesheet and the tubesheet-to-shell gasketed connections with welds to minimize leakage possibilities. The N head is particularly used in nuclear services.

The D head is mainly used in feed-water heater applications where tube-side pressures are in the 100 to 400 bar range. The internal partition (optional) need only withstand the 1 to 2 bar pressure drop through the tubes so it can be of lightweight construction. The high-pressure closure against the atmosphere uses a shear key ring to lock the main closure in place.

Rear Head. A variety of rear head designs are used in shell-and-tube exchangers, primarily because of the need to accommodate thermally induced stresses. During operation, the tubes and the shell have different temperatures and therefore will expand (or try to) different amounts, even if there were no residual stresses in the exchanger before start-up and even if the entire exchanger is made out of the same material. The thermal stress problem is exacerbated if there are residual stresses, or if the exchanger is made of different materials, or during transient operation (including start-up and shutdown). If the temperature differences are small, the structure may be able to accommodate the thermal stresses safely; usually, however, it is necessary to make specific provision to allow the shell and the tubes to expand or contract independently. Failure to do so can result in buckling, bending, or even rupture of the shell or the tubes, or destruction of the tube-to-tubesheet joint.

A simple solution is to incorporate an expansion joint or a bellows into the shell (or in certain special applications, into the tube-side piping internal to the shell cover). However, this solution cannot cover the entire range of pressures and temperature differences encountered in practice. Further, it is usually possible to incorporate other desirable features, such as removable bundles, with thermal stress relief in the variety of rear head designs available. These are shown in the last column of Figure 4.5.19.

The L and M rear heads correspond to the A and B front heads previously described. As shown, they require a fixed tubesheet design; that is, the tubesheets are rigidly fastened to the shell, and thermal stress relief, if necessary, must be provided by a shell-side expansion joint or bellows. The tube bundle cannot be removed for inspection or mechanical cleaning on the shell side. However, the outer tube limit (OTL) — the diameter of the tube field circumscribing the outermost tubes in the bundle — can be as little as 0.4 in. (10 mm) less than the inside diameter of a pipe shell and 0.5 in. (12.7 mm) for a rolled shell. Therefore, the tube field can be very full, giving more tubes and minimizing bypass flow. Similar comments apply to the N rear head, except that more clearance must be left between the outermost tubes and the shell.

The type P head uses packing between the skirt on the rear tubesheet and the shell extension to seal the shell-side fluid against leakage. The compression on the packing has to be adjusted to prevent excessive leakage on the one hand and to allow limited movement of the tube-side head on the other, so the shell-side fluid must be benign and cheap (not surprisingly, it is often cooling water). On the other hand, leakage between the two fluids can occur only through tube hole leaks. Because of the tubesheet skirt, clearance between the outermost tubes and the shell must increase compared with types L or M; accordingly, fewer tubes are possible in a given shell, and sealing strips to partially block the bundle-to-shell bypass stream are recommended. When the floating head cover and packing gland are removed, the tube bundle can be pulled out of the shell for inspection and cleaning.

The TEMA S split-ring floating head design uses a split backing ring to hold the floating head cover and its gasket to the tubesheet. The split backing ring is bolted to the cover with a bolt circle outside

the diameter of the tubesheet. Therefore, when the split ring is removed, the entire tube bundle may be pulled out of the shell. Tube count is similar to type P design and sealing strips are recommended. Usually, the split-ring floating head is used with an even number of tube passes so that a plain bonnet-type shell cover can be used. However, as shown by the dashed lines in Figure 4.5.19, single tube-side pass design (and countercurrent flow) can be achieved by use of a packing gland on the exit piping through the bonnet; alternatively, a deep bonnet can be used together with an expansion joint or bellows on the tube-side exit piping.

The pull-through floating head, type T, uses a floating head cover that flanges directly to the tubesheet, reducing the possibility of internal leakage compared with type S, but also eliminating more tubes around the periphery. Sealing strips are a virtual necessity. Single tube-side pass design is similar to type S, but is rarely used.

TEMA type U uses a bundle of U tubes and hence requires no rear head at all. The U-tube bundle effectively eliminates the thermal stress problem between shell and tubes, because each tube is free to expand or contract independently. The U bundle is also the cheapest construction because the cost of a second tubesheet is avoided. However, there are a number of drawbacks: designs must have an even number of tube-side passes, mechanical cleaning of the smaller bend radius tubes in the U bend is impossible, individual tubes cannot be replaced except in the outer row, some tube count is lost because of minimum bend limits, and the U bend must be carefully supported against vibration or kept out of the cross-flow stream by placing the shell nozzle upstream of the bend. The tube side in the U bend is susceptible to erosion, especially with two-phase or particulate-containing fluids.

Type W uses two sets of packing, often with a lantern ring in between. This construction is generally limited to benign fluids and low to very moderate pressures and temperatures.

Other Features. Numerous other components are necessary or optional to construction of shell-and-tube exchangers. Probably the most complete discussion is given by Yokell (1990).

Principles of Design

Design Logic. The design of a shell-and-tube exchanger involves the following steps:

1. Selection of a set of design features which are required for mechanical integrity and ease of maintenance, and which will likely lead to satisfying the thermal requirements within the allowable pressure drops, and at lowest cost.
2. Selection of a set of dimensions for the actual exchanger.
3. For the dimensions selected in (2), calculation of the thermal performance of the heat exchanger and both tube-side and shell-side pressure drops, using available rating procedures.
4. Comparison of the thermal performance calculated in (3) with that required and examination of the pressure drops calculated in (3) to ensure that the allowed pressure drops are reasonably used but not exceeded.
5. Adjustment of the dimensions selected in (2) and repetition of steps (3) and (4) until the criteria are satisfied.
6. Completion of the mechanical design to satisfy code requirements.
7. Cost estimation.

Basic Design Equations. The basic design equation for a shell-and-tube exchanger in steady-state service is

$$A^* = \int_0^{q_T} \frac{dq}{U^*\left(T_h - T_c\right)} \tag{4.5.87}$$

where A^* is the heat transfer area required in the heat exchanger, m^2 (ft^2); q_T is the heat transfer rate of the heat exchanger, W (Btu/hr); U^* is the local overall heat transfer coefficient referenced to area A^*, W/m^2 K (Btu/hr ft^2 °F); and T_h and T_c are the local hot and cold stream temperatures, K (°F). The $*$

superscript on A^* and U^* only means that a consistent reference area must be used in defining these terms. For example, for an exchanger with plain tubes, it is customary to use the total outside heat transfer area of all of the tubes in the exchanger, A_o, as the reference area, and then U_o is the overall heat transfer coefficient referenced to A_o. If the exchanger has low-finned tubes, A^* may refer either to the total outside area including fins or to the inside tube heat transfer area; the choice is optional, but must be spelled out. Since T_h and T_c generally vary with the amount of heat transferred (following the first law of thermodynamics, and excepting isobaric phase transition of a pure component) and U^* may vary with local heat transfer conditions, in principle Equation 4.5.87 must be numerically integrated with T_h, T_c, and U^* calculated along the path of integration, and this process is performed by the most-advanced computer-based design methods.

For many applications, certain reasonable assumptions can be made allowing the analytical integration of Equation 4.5.87 to give (Schlünder, Vol. 1, 1983; Hewitt et al., 1994)

$$A^* = \frac{q_T U^*}{(\text{MTD})} \tag{4.5.88}$$

where MTD is the mean temperature difference for the particular flow conditions and configuration. The key assumptions are that there is no significant bypassing of fluid around the heat transfer surface, that the overall heat transfer coefficient is constant, and that the specific heats of the two streams are constant over their temperature ranges in the exchanger; isothermal phase transitions, such as vaporizing or condensing a pure component at constant pressure, are also allowed.

If the two streams are in countercurrent flow, i.e., if they flow always in the opposite direction to one another,

$$\text{MTD} = (\text{LMTD})_{\text{countercurrent}} = \frac{\left(T_{h,i} - T_{c,o}\right) - \left(T_{h,o} - T_{c,i}\right)}{\ln\left(\dfrac{T_{h,i} - T_{c,o}}{T_{h,o} - T_{c,i}}\right)} \tag{4.5.89}$$

where $(\text{LMTD})_{\text{countercurrent}}$ is the "logarithmic mean temperature difference for countercurrent flow" and the subscripts i and o indicate "inlet" and "outlet," respectively. E shells with a single tube-side pass and F shells with two tube-side passes are almost always designed for countercurrent flow. (While the flow between adjacent baffles is basically cross flow, it can be shown that the total shell-side flow pattern is equivalent to countercurrent flow if there are more than three or four baffles).

Very occasionally, usually when close control of tube wall temperatures is required, cocurrent flow is specified, with the two streams flowing in the same direction through the exchanger. For this case,

$$\text{MTD} = (\text{LMTD})_{\text{cocurrent}} = \frac{\left(T_{h,i} - T_{c,i}\right) - \left(T_{h,o} - T_{c,o}\right)}{\ln\left(\dfrac{T_{h,i} - T_{c,i}}{T_{h,o} - T_{c,o}}\right)} \tag{4.5.90}$$

where the symbols have the same meaning as before. $(\text{LMTD})_{\text{countercurrent}}$ is always equal to or greater than $(\text{LMTD})_{\text{cocurrent}}$, so wherever possible, countercurrent design and operation is preferred.

However, most shell-and-tube exchangers have nozzle and tube pass configurations which lead to mixed countercurrent and cocurrent flow regions (as well as cross flow in the X shell). For these cases,

$$\text{MTD} = F(\text{LMTD})_{\text{countercurrent}} \tag{4.5.91}$$

where (LMTD)$_{countercurrent}$ is calculated from Equation (4.5.89) and *F* is the "configuration correction factor" for the flow configuration involved. *F* has been found as a function of dimensionless temperature ratios for most flow configurations of interest and is given in analytical and/or graphical form in the earlier part of this section by Shah and in many heat transfer references (e.g., Schlünder, Vol. 1, 1983). *F* is equal to unity for pure countercurrent flow and is less than unity for all other cases; practical considerations limit the range of interest to values above 0.7 at the lowest and more comfortably to values above 0.8. Values of zero or below indicate conditions that violate the second law of thermodynamics.

The Overall Heat Transfer Coefficient. The overall heat transfer coefficient *U**, referenced to the heat transfer area *A**, is related to the individual (film) heat transfer coefficients and the fouling resistances by

$$U^* = \frac{1}{\dfrac{A^*}{h_i A_i} + R_{fi}\dfrac{A^*}{A_i} + \dfrac{A^* \ln(d_o/d_i)}{2\pi N_t L k_w} + R_{fo}\dfrac{A^*}{A_o} + \dfrac{A^*}{h_o A_o}} \qquad (4.5.92)$$

where h_i and h_o are, respectively, the tube-side and shell-side film heat transfer coefficients, W/m^{2}K (Btu/hr ft^2 °F), each referenced to its corresponding heat transfer area; R_{fi} and R_{fo} the corresponding fouling resistances (see below), m^{2}K/W (hr ft^2 °F/Btu); N_t the total number of tubes in the heat exchanger; *L* the effective tube length between the inside surfaces of the tubesheets, m (ft); d_o and d_i the outside and inside tube diameters, m (ft); and k_w the thermal conductivity of the tube wall material, W/m K (Btu/hr ft°F). For the special but important case of plain tubes

$$A^* = A_o = N_t(\pi d_o L) \qquad (4.5.93)$$

and Equation (4.5.92) reduces to

$$U_o = \frac{1}{\dfrac{d_o}{h_i d_i} + R_{fi}\dfrac{d_o}{d_i} + \dfrac{d_o \ln(d_o/d_i)}{2k_w} + R_{fo} + \dfrac{1}{h_o}} \qquad (4.5.94)$$

If finned tubes are used, the root diameter d_r of the fins replaces d_o in Equation (4.5.92) and A_o includes the surface area of the fins as well as the bare tube surface between the fins; it is also necessary to include a fin efficiency (typically about 0.8 to 0.95) multiplier in the numerators of the last two terms on the right side of Equation (4.5.92) to account for resistance to conduction in the fins. The treatment of fin efficiency is fully developed in Kern and Kraus (1972). Efficiencies of some of the important geometries are given in the earlier half of this section.

Film Heat Transfer Coefficients. Calculation of single-phase tube-side heat transfer coefficients for plain tubes is discussed in Section 4.1; special correlations are required for internally enhanced tubes, see discussion of enhancement in Section 4.8. Intube condensation and vaporization are covered in the subsection on boiling and condensation in Section 4.4.

Shell-side heat transfer calculations are more complex owing to the large number and range of design variables and process conditions that can occur. The most accurate methods are proprietary and computer based. The best known of these methods are those of Heat Transfer Research, Inc. (HTRI), College Station, TX; Heat Transfer and Fluid Flow Services (HTFS), Harwell, U.K.; and B-JAC, Midlothian, VA. For single-phase flow, the Delaware method appears to be the best in the open literature, and it is feasible for both had and computer use; various presentations of the method appear in many references, including Schlünder, Vol. 3 (1983) and Hewitt et al. (1994). These references also give methods for

shell-side vaporizing and condensing design. An approximate design procedure is given in the next subsection.

Fouling. Fouling is the formation of any undesired deposit on the heat transfer surface, and it presents an additional resistance to the flow of heat. Several different types of fouling are recognized:

Sedimentation: deposition of suspended material on the surface.

Crystallization: precipitation of solute from supersaturated solutions.

Corrosion: formation of corrosion products on the surface.

Thermal degradation/polymerization: formation of insoluble products by oxidation, charring, and/or polymerization of a process stream.

Biofouling: growth of large organisms (e.g., barnacles) that interfere with flow to or past a heat transfer surface ("macrobiofouling") or small organisms (e.g., algae) that form a fouling layer on the surface ("microbiofouling").

The effect of fouling on design is twofold: Extra surface must be added to the heat exchanger to overcome the additional thermal resistance, and provision must be made to allow cleaning either by chemical or mechanical means. The fouling resistances included in Equation (4.5.92) result in requiring extra surface by reducing U^* (though they do not properly account for the time-dependent nature of fouling) and should be chosen with care. Table 4.5.8, based on the TEMA *Standards* provides some guidance, but prior experience with a given service is the best source of values. Ranges of typical values for major classes of service are included in Table 4.5.10.

Other things being equal, a fouling stream that requires mechanical cleaning should be put in the tubes because it is easier to clean the tube side. If this is not possible or desirable, then a removable bundle with a rotated square tube layout should be chosen to facilitate cleaning.

Pressure Drop. Tube-side pressure drop in plain tubes is discussed in Section 3.4. These calculations are straightforward and quite accurate as long as the tubes are smooth and clean; however, even a small amount of roughening due to corrosion or fouling (sometimes with a significant reduction of flow area) can double or triple tube-side pressure drop. Special correlations are required for internally enhanced tubes.

Calculation of shell-side pressure drop is implicit in the design methods mentioned above for heat transfer. Roughness has less effect on shell-side pressure drop than on tube side, but fouling still may have a very substantial effect if the deposits fill up the clearances between the baffles and the shell and between the tubes and the baffles, or if the deposits are thick enough to narrow the clearances between adjacent tubes. Existing design methods can predict these effects if the thickness of the fouling layer can be estimated.

Limitations of Design. It should be recognized that even under the best of conditions — new, clean exchangers with conventional construction features — heat exchanger design is not highly accurate. The best methods, when compared with carefully taken test data, show deviations of ±20% on overall heat transfer and ±40% on shell-side pressure drop (Palen and Taborek, 1969). These ranges are considerably worsened in fouling services. In these cases, the thermal *system* should be designed for operational flexibility, including carefully chosen redundancy of key components, and easy maintenance.

Approximate Design Method

Because of the complexity of rigorous design methods, it is useful to have an estimation procedure that can quickly give approximate dimensions of a heat exchanger for a specified service. Such a method is given here for purposes of preliminary cost estimation, plant layout, or checking the results of computer output. This method is based upon Equation (4.5.88) with $A^* = A_o$ and $U^* = U_o$ and depends upon rapidly estimating values for q_T, MTD, and U_o. The procedure is as follows:

TABLE 4.5.10   Typical Film Heat Transfer Coefficients for Shell-and-Tube Heat Exchangers

Fluid Conditions		h, W/m²K[a,b]	Fouling resistance, m² K/W[a]
Sensible heat transfer			
Water[c]	Liquid	5000–7500	$1–2.5 \times 10^{-4}$
Ammonia	Liquid	6000–8000	$0–1 \times 10^{-4}$
Light organics[d]	Liquid	1500–2000	$0–2 \times 10^{-4}$
Medium organics[e]	Liquid	750–1500	$1–4 \times 10^{-4}$
Heavy organics[f]	Liquid		
	Heating	250–750	$2–10 \times 10^{-4}$
	Cooling	150–400	$2–10 \times 10^{-4}$
Very heavy organics[g]	Liquid		
	Heating	100–300	$4–30 \times 10^{-3}$
	Cooling	60–150	$4–30 \times 10^{-3}$
Gas[h]	Pressure 100–200 kN/m² abs	80–125	$0–1 \times 10^{-4}$
Gas[h]	Pressure 1 MN/m² abs	250–400	$0–1 \times 10^{-4}$
Gas[h]	Pressure 10 MN/m² abs	500–800	$0–1 \times 10^{-4}$
Condensing heat transfer			
Steam, ammonia	Pressure 10 kN/m² abs, no noncondensables[i,j]	8000–12000	$0–1 \times 10^{-4}$
Steam, ammonia	Pressure 10 kN/m² abs, 1% noncondensables[k]	4000–6000	$0–1 \times 10^{-4}$
Steam, ammonia	Pressure 10 kN/m² abs, 4% noncondensables[k]	2000–3000	$0–1 \times 10^{-4}$
Steam, ammonia	Pressure 100 kN/m² abs, no noncondensables[i,j,k,l]	10000–15000	$0–1 \times 10^{-4}$
Steam, ammonia	Pressure 1 MN/m² abs, no noncondensables[i,j,k,l]	15000–25,000	$0–1 \times 10^{-4}$
Light organics[d]	Pure component, pressure 10 kN/m² abs, no noncondensables[i]	1500–2000	$0–1 \times 10^{-4}$
Light organics[d]	Pressure 10 kN/m² abs, 4% noncondensables[k]	750–1000	$0–1 \times 10^{-4}$
Light organics[d]	Pure component, pressure 100 kN/m² abs, no noncondensables	2000–4000	$0–1 \times 10^{-4}$
Light organics[d]	Pure component, pressure 1 MN/m² abs	3000–4000	$0–1 \times 10^{-4}$
Medium organics[e]	Pure component or narrow condensing range, pressure 100 kN/m² abs[m,n]	1500–4000	$1–3 \times 10^{-4}$
Heavy organics	Narrow condensing range pressure 100 kN/m² abs[m,n]	600–2000	$2–5 \times 10^{-4}$
Light multicomponent mixtures, all condensable[d]	Medium condensing range, pressure 100 kN/m² abs[k,m,o]	1000–2500	$0–2 \times 10^{-4}$
Medium multicomponent mixtures, all condensable[e]	Medium condensing range, pressure 100 kN/m² abs[k,m,o]	600–1500	$1–4 \times 10^{-4}$
Heavy multicomponent mixtures, all condensable[f]	Medium condensing range, pressure 100 kN/m² abs[k,m,o]	300–600	$2–8 \times 10^{-4}$
Vaporizing heat transfer[p,q]			
Water[r]	Pressure < 0.5 MN/m² abs, $\Delta T_{SH,max} = 25$ K	3000–10000	$1–2 \times 10^{-4}$
Water[r]	Pressure < 0.5 MN/m² abs, pressure < 10 MN/m² abs, $\Delta T_{SH,max} = 20$ K	4000–15000	$1–2 \times 10^{-4}$

TABLE 4.5.10   (continued)   Typical Film Heat Transfer Coefficients for Shell-and-Tube Heat Exchangers

Fluid Conditions		h, W/m²K[a,b]	Fouling resistance, m² K/W[a]
Ammonia	Pressure < 3 MN/m² abs, $\Delta T_{\text{SH,max}} = 20$ K	3000–5000	0–2×10^{-4}
Light organics[d]	Pure component, pressure < 2 MN/m² abs, $\Delta T_{\text{SH,max}} = 20$ K	1000–4000	1–2×10^{-4}
Light organics[d]	Narrow boiling range,[s] pressure < 2 MN/m² abs, $\Delta T_{\text{SH,max}} = 15$ K	750–3000	0–2×10^{-4}
Medium organics[e]	Pure component, pressure < 2 MN/m² abs, $\Delta T_{\text{SH,max}} = 20$ K	1000–3500	1–3×10^{-4}
Medium organics[e]	Narrow boiling range,[s] pressure < 2 MN/m² abs, $\Delta T_{\text{SH,max}} = 15$ K	600–2500	1–3×10^{-4}
Heavy organics[f]	Pure component, pressure < 2 MN/m² abs, $\Delta T_{\text{SH,max}} = 20$ K	750–2500	2–5×10^{-4}
Heavy organics[g]	Narrow boiling range,[s] pressure < 2 MN/m² abs, $\Delta T_{\text{SH,max}} = 15$ K	400–1500	2–8×10^{-4}
Very heavy organics[h]	Narrow boiling range,[s] pressure < 2 MN/m² abs, $\Delta T_{\text{SH,max}} = 15$ K	300–1000	2–10×10^{-4}

Source: Schlünder, E.U., Ed., *Heat Exchanger Design Handbook*, Begell House, New York, 1983. With permision.

[a] Heat transfer coefficients and fouling resistances are based on area in contact with fluid. Ranges shown are typical, not all encompassing. Temperatures are assumed to be in normal processing range; allowances should be made for very high or low temperatures.

[b] Allowable pressure drops on each side are assumed to be about 50–100 kN/m² except for (1) low-pressure gas and two-phase flows, where the pressure drop is assumed to be about 5% of the absolute pressure; and (2) very viscous organics, where the allowable pressure drop is assumed to be about 150–250 kN/m².

[c] Aqueous solutions give approximately the same coefficients as water.

[d] Light organics include fluids with liquid viscosities less than about 0.5×10^{-3} Nsec/m², such as hydrocarbons through C_8, gasoline, light alcohols and ketones, etc.

[e] Medium organics include fluids with liquid viscosities between about 0.5×10^{-3} and 2.5×10^{-3} Nsec/m², such as kerosene, straw oil, hot gas oil, and light crudes.

[f] Heavy organics include fluids with liquid viscosities greater than 2.5×10^{-3} Nsec/m², but not more than 50×10^{-3} Nsec/m², such as cold gas oil, lube oils, fuel oils, and heavy and reduced crudes.

[g] Very heavy organics include tars, asphalts, polymer melts, greases, etc., having liquid viscosities greater than about 50×10^{-3} Nsec/m². Estimation of coefficients for these materials is very uncertain and depends strongly on the temperature difference, because natural convection is often a significant contribution to heat transfer in heating, whereas congelation on the surface and particularly between fins can occur in cooling. Since many of these materials are thermally unstable, high surface temperatures can lead to extremely severe fouling.

[h] Values given for gases apply to such substances as air, nitrogen, carbon dioxide, light hydrocarbon mixtures (no condensation), etc. Because of the very high thermal conductivities and specific heats of hydrogen and helium, gas mixtures containing appreciable fractions of these components will generally have substantially higher heat transfer coefficients.

[i] Superheat of a pure vapor is removed at the same coefficient as for condensation of the saturated vapor if the exit coolant temperature is less than the saturation temperature (at the pressure existing in the vapor phase) and if the (constant) saturation temperature is used in calculating the MTD. But see note k for vapor mixtures with or without noncondensable gas.

[j] Steam is not usually condensed on conventional low-finned tubes; its high surface tension causes bridging and retention of the condensate and a severe reduction of the coefficient below that of the plain tube.

TABLE 4.5.10 (continued) Typical Film Heat Transfer Coefficients for Shell-and-Tube Heat Exchangers

Fluid Conditions	h, W/m²Kᵃ,ᵇ	Fouling resistance, m² K/Wᵃ

ᵏ   The coefficients cited for condensation in the presence of noncondensable gases or for multicomponent mixtures are only for very rough estimation purposes because of the presence of mass transfer resistances in the vapor (and to some extent, in the liquid) phase. Also, for these cases, the vapor-phase temperature is not constant, and the coefficient given is to be used with the MTD estimated using vapor-phase inlet and exit temperatures, together with the coolant temperatures.

ˡ   As a rough approximation, the same relative reduction in low-pressure condensing coefficients due to noncondensable gases can also be applied to higher pressures.

ᵐ   Absolute pressure and noncondensables have about the same effect on condensing coefficients for medium and heavy organics as for light organics. For large fractions of noncondensable gas, interpolate between pure component condensation and gas cooling coefficients.

ⁿ   Narrow condensing range implies that the temperature difference between dew point and bubble point is less than the smallest temperature difference between vapor and coolant at any place in the condenser.

ᵒ   Medium condensing range implies that the temperature difference between dew point and bubble point is greater than the smallest temperature difference between vapor and coolant, but less than the temperature difference between inlet vapor and outlet coolant.

ᵖ   Boiling and vaporizing heat transfer coefficients depend very strongly on the nature of the surface and the structure of the two-phase flow past the surface in addition to all of the other variables that are significant for convective heat transfer in other modes. The flow velocity and structure are very much governed by the geometry of the equipment and its connecting piping. Also, there is a maximum heat flux from the surface that can be achieved with reasonable temperature differences between surface and saturation temperatures of the boiling fluid; any attempt to exceed this maximum heat flux by increasing the surface temperature leads to partial or total coverage of the surface by a film of vapor and a sharp decrease in the heat flux.

Therefore, the vaporizing heat transfer coefficients given in this table are only for very rough estimating purposes and assume the use of plain or low-finned tubes without special nucleation enhancement.

$\Delta T_{\mathrm{SH,max}}$ is the maximum allowable temperature difference between surface and saturation temperature of the boiling liquid. No attempt is made in this table to distinguish among the various types of vapor-generation equipment, since the major heat transfer distinction to be made is the propensity of the process stream to foul. Severely fouling streams will usually call for a vertical thermosiphon or a forced-convection (tube-side) reboiler for ease of cleaning.

ᑫ   Subcooling heat load is transferred at the same coefficient as latent heat load in kettle reboilers, using the saturation temperature in the MTD. For horizontal and vertical thermosiphons and forced-circulation reboilers, a separate calculation is required for the sensible heat transfer area, using appropriate sensible heat transfer coefficients and the liquid temperature profile for the MTD.

ʳ   Aqueous solutions vaporize with nearly the same coefficient as pure water if attention is given to boiling-point elevation, if the solution does not become saturated, and if care is taken to avoid dry wall conditions.

ˢ   For boiling of mixtures, the saturation temperature (bubble point) of the final liquid phase (after the desired vaporization has taken place) is to be used to calculate the MTD. A narrow-boiling-range mixture is defined as one for which the difference between the bubble point of the incoming liquid and the bubble point of the exit liquid is less than the temperature difference between the exit hot stream and the bubble point of the exit boiling liquid. Wide-boiling-range mixtures require a case-by-case analysis and cannot be reliably estimated by these simple procedures.

Estimation of q_T   For sensible heat transfer,

$$q_T = \dot{m}_h c_{p,h}\left(T_{h,i} - T_{h,o}\right) = \dot{m}_c c_{p,c}\left(T_{c,o} - T_{c,i}\right) \tag{4.5.95}$$

where $\dot{m}$ is the mass flow rate, c_p the specific heat, and T the stream temperature, with subscripts h and c denoting the hot and cold streams, respectively, and i and o inlet and outlet, respectively.

   For isothermal phase change,

$$q_T = \dot{m}h_{fg} \tag{4.5.96}$$

where $\dot{m}$ is the mass rate of condensation or vaporization and h_{fg} is the latent heat of phase transformation.

For more complex cases, such as partial or multicomponent condensation, more elaborate analyses are required, although this method can still be used with care to give rough estimates.

Estimation of MTD. The first step is to calculate or estimate $\text{LMTD}_{\text{countercurrent}}$ from Equation (4.5.89) and then estimate F as follows:

1. If the two streams are in countercurrent flow, $F = 1$.
2. If the two streams are in a combination of countercurrent and cocurrent flows (i.e., multiple tube passes) and the outlet temperatures of the two streams are equal, $F = 0.8$.
3. If the exchanger has multiple passes and $T_{h,o} > T_{c,o}$, then $0.8 < F < 1.0$, with the actual value depending upon the temperature ranges of the two streams and $(T_{h,o} - T_{c,o})$. It is usually sufficiently accurate to take $F = 0.9$ in this case, but a more accurate value can be obtained from the earlier half of this section by Shah.
4. Design of a multiple tube pass exchanger with $T_{h,o} < T_{c,o}$ (i.e., a temperature cross) leads to $F < 0.8$, which is inefficient, of uncertain inaccuracy, and perhaps even thermodynamically impossible. The problem can be handled with multiple shells in series. Consult Shah's discussion.
5. Then, $\text{MTD} = F(\text{LMTD})_{\text{countercurrent}}$, (Equation 4.5.91).

Estimation of U_o. The best way to estimate U_o is to use Equation (4.5.94), together with values of h_o, h_i, $R_{f,o}$, and $R_{f,i}$, chosen from Table 4.5.10. This table includes ranges of values that are typical of the fluids and services indicated assuming normally allowable pressure drops, exchanger construction, and fouling. However, care should be taken in selecting values to consider possible unusual conditions, e.g., especially high or low velocities (implying correspondingly high or low allowable pressure drops), and especially fouling. In selecting values from the table, the user should carefully read the footnotes for each entry.

Calculation of A_o. The total outside tube heat transfer area required in the heat exchanger is now found from Equation (4.5.88).

Estimation of Exchanger Dimensions. Figure 4.5.20 shows the relationship among A_o, effective tube length L, and inside shell diameter for a fully tubed, fixed tubesheet heat exchanger with one tube-side pass, with $3/4$ in. (19.05 mm) plain tubes on a $15/16$ in. (23.8 mm) pitch equilateral triangular tube layout. These curves are constructed using tube count tables (e.g., Saunders, 1988). The dashed lines marked 3:1, 6:1, 8:1, 10:1, and 15:1 indicate ratios of tube length to shell inside diameter for guidance in selection. Exchangers of less than 3:1 ratio are expensive because of the large-diameter shell and tubesheet, with more holes to be drilled and tubes rolled and/or welded, and shell-side flow distribution is likely to be poor and lead to excessive fouling. Exchangers greater than 15:1 ratio are probably beyond the point of saving money by reducing shell diameter and number of tubes and may require excessive clear way for pulling the bundle; the bundles may be springy and difficult to handle during maintenance. Most heat exchangers fall into the 6:1 to 10:1 range.

Figure 4.5.20 is a very specific case which is used as a reference. In order to extend its usefulness to other tube diameters, layouts, bundle constructions, etc., Equation (4.5.97) is used:

$$A_o' = A_o F_1 F_2 F_3 \tag{4.5.97}$$

where A_o' is the value to be used with Figure 4.5.20, A_o is the required area calculated from Equation (4.5.88), and

F_1 is the correction factor for the tube layout. $F_1 = 1.00$ for $3/4$ in. (19.05 mm) outside diameter tubes on a $15/16$ in. (23.8 mm) triangular pitch. Values of F_1 for other tube diameters and pitches are given in Table 4.5.11.

F_2 is the correction factor for the number of tube-side passes. $F_2 = 1.00$ for one tube-side pass, and Table 4.5.12 gives values of F_2 for more passes.
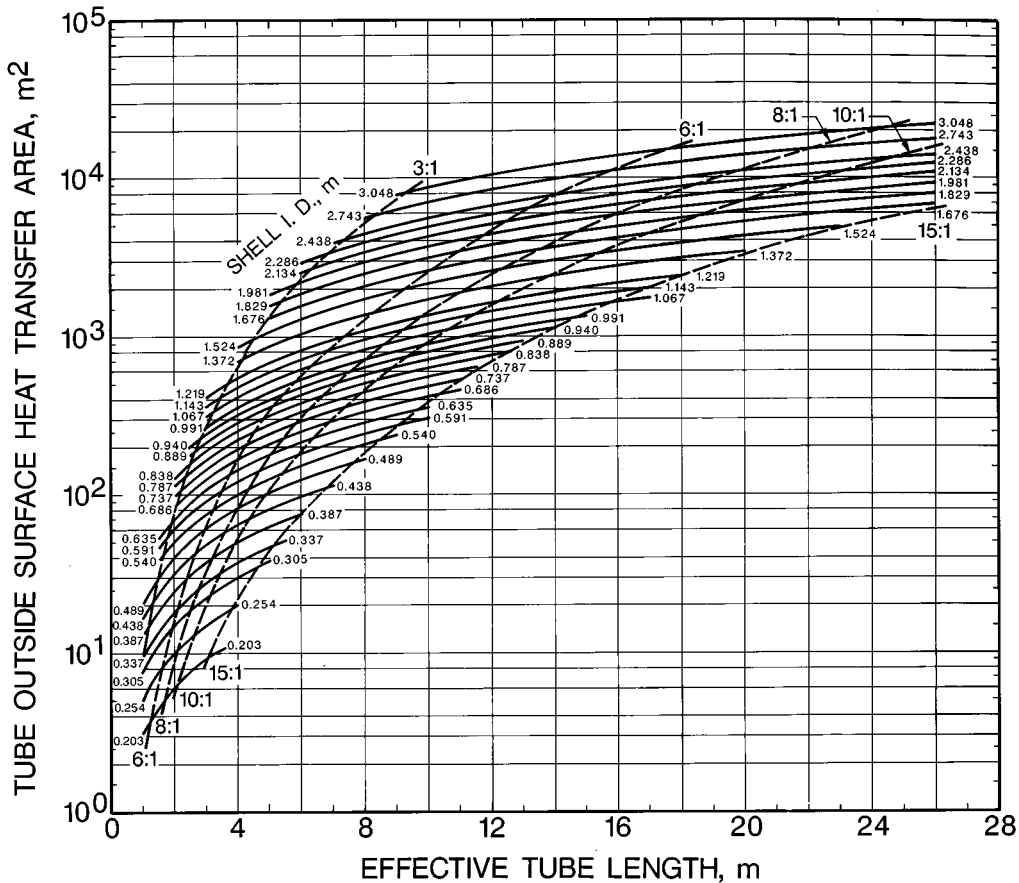
FIGURE 4.5.20 Heat transfer area as a function of shell inside diameter and effective tube length for 19.05 mm ($^3/_4$ in.) tubes on a 23.8 mm ($^{15}/_{16}$ in.) equilateral triangular tube layout, fixed tubesheet, one tube-side pass, fully tubed shell. (From Schlünder, E. U., Ed. *Heat Exchanger Design Handbook*, Begell House, New York, 1983. With permission.)

F_3 is the correction factor for shell construction/tube bundle configuration. $F_3 = 1.00$ for fixed tubesheet, fully tubed shells, and Table 4.5.13 gives values of F_3 for the standard TEMA types.

Once a value of A'_o has been calculated from Equation (4.5.97), enter the ordinate of Figure 4.5.20 at that value and move horizontally, picking off the combinations of shell inside diameter and tube length that meet that requirement. The final choice can then be made from among those possibilities.

Example of the Approximate Design Method

Problem Statement. Estimate the dimensions of a shell-and-tube heat exchanger to cool 100,000 lb$_m$/hr (12.6 kg/sec) of liquid toluene from 250 to 110°F (121.1 to 43.3°C) using cooling tower water available at 80°F (26.7°C). Use split-ring floating head construction (TEMA S) with $^3/_4$ in. (19.05 mm) outside diameter × 14 BWG (0.083 in. = 2.11 mm wall) low-carbon steel tubes on $^{15}/_{16}$ in. (23.8 mm) equilateral triangular pitch. This construction implies one shell-side pass and an even number of tube-side passes — assume two for the present. Choose cooling water exit temperature of 100°F (37.8°C). Specific heat of toluene is 0.52 Btu/lb$_m$°F (2177 J/kgK) and viscosity at 180°F (82.2°C) is 0.82 lb/$_m$/ft hr ($0.34 × 10^{-3}$ Nsec/m^2 or 0.34 cP).

TABLE 4.5.11 Values of F$_1$ for Various Tube Diameters and Layouts

Tube Outside Diameter, in. (mm)	Tube Pitch, in. (mm)	Layout	F$_1$
5/8 (15.88)	13/16 (20.6)	▷	0.90
5/8 (15.88)	13/16 (20.6)	◇ □	1.04
3/4 (19.05)	15/16 (23.8)	◁	1.00
3/4 (19.05)	15/16 (23.8)	◇ □	1.16
3/4 (19.05)	1 (25.4)	◁	1.14
3/4 (19.05)	1 (25.4)	◇ □	1.31
1 (25.4)	1 1/4 (31.8)	◁	1.34
1 (25.4)	1 1/4 (31.8)	◇ □	1.54

$$F_1 = \frac{\text{(Heat transfer area / cross-sectional area of unit cell)}\,\text{Reference}}{\text{(Heat transfer area / cross-sectional area of unit cell)}\,\text{New Case}}$$

This table may also be used for low-finned tubing in the following way. The value estimated for h_o from Table 4.5.10 should be multiplied by the fin efficiency (usually between 0.75 and 1 for a good application; 0.85 is a good estimate) and used in Equation 4.5.92 with $A^* = A_o$, the total outside heat transfer area including fins. Then this value of A_o is divided by the ratio of the finned tube heat transfer area to the plain tube area (per unit length). The result of this calculation is used as A_o in Equation 4.5.96 to find A_o' to enter Figure 4.5.20.

Source: Schlünder, E.U., Ed., *Heat Exchanger Design Handbook*, Begell House, New York, 1983. With permission.

TABLE 4.5.12 Values of F$_2$ for Various Numbers of Tube Side Passes[a]

Inside Shell Diameter, in. (mm)	F_2 Number of Tube-Side Passes			
	2	4	6	8
Up to 12 (305)	1.20	1.40	1.80	—
13$^1/_4$ to 17$^1/_4$ (337 to 438)	1.06	1.18	1.25	1.50
19$^1/_4$ to 23$^1/_4$ (489 to 591)	1.04	1.14	1.19	1.35
25 to 33 (635 to 838)	1.03	1.12	1.16	1.20
35 to 45 (889 to 1143)	1.02	1.08	1.12	1.16
48 to 60 (1219 to 1524)	1.02	1.05	1.08	1.12
Above 60 (above 1524)	1.01	1.03	1.04	1.06

[a] Since U-tube bundles must always have at least two passes, use of this table is essential for U-tube bundle estimation. Most floating head bundles also require an even number of passes.

Source: Schlünder, E.U., Ed., *Heat Exchanger Design Handbook*, Begell House, New York, 1985. With permission.

Solution.

$$q_T = \left(100{,}000 \ \text{lb}_m/\text{hr}\right)\left(0.52 \ \text{Btu/lb}_m\,°\text{F}\right)\left(250 - 110\right)°\text{F}$$

$$= 7.28 \times 10^6 \ \text{Btu/hr} = 2.14 \times 10^6 \ \text{W}$$

TABLE 4.5.13 F_3 for Various Tube Bundle Constructions

Type of Tube Bundle Construction	F_3 Inside Shell Diameter, in. (mm)				
	Up to 12 (305)	13–22 (330–559)	23–36 (584–914)	37–48 (940–1219)	Above 48 (1219)
Split backing ring (TEMA S)	1.30	1.15	1.09	1.06	1.04
Outside packed floating heat (TEMA P)	1.30	1.15	1.09	1.06	1.04
U-Tube* (TEMA U)	1.12	1.08	1.03	1.01	1.01
Pull-through floating head (TEMA T)	—	1.40	1.25	1.18	1.15

[a] Since U-tube bundles must always have at least two tube-side passes, it is essential to use Table 4.5.12 also for this configuration.

Source: Schlünder, E.U., Ed., *Heat Exchanger Design Handbook*, Begell House, New York, 1983. With permission.

$$\text{LMTD}_{\text{countercurrent}} = \frac{(250-100)-(110-80)}{\ln\dfrac{250-100}{110-80}} = 74.6°F = 41.4°C$$

Since there are at least two tube-side passes, flow is not countercurrent, and $T_{h_o} > T_{c_o}$, estimate $F \approx 0.9$. Therefore, MTD = 0.9 (74.6°F) = 67.1°F = 37.3°C.

Estimation of U_o. Light organic liquid cooled by liquid water. (Note that 1 Btu/hr ft² °F = 5.678 W/m²K).

Water (in tubes) h_i	1000 Btu/hr ft² °F	5700 W/m²K
Toluene (in shell) h_o	300 Btu/hr ft² °F	1700 W/m²K
Tube-side fouling R_{f_i}	0.001 hr ft² °F/Btu	1.8×10^{-4} m²K/W
Shell-side fouling R_{f_o}	0.0005 hr ft² °F/Btu	8.8×10^{-5} m²K/W

Tube wall resistance (for estimation purposes, this term can be approximated by x_w/k_w, where x_w is the wall thickness):

$$\frac{x_w}{k_w} = \frac{0.083 \text{ in.}}{(12 \text{ in./ft})(26 \text{ Btu/hr ft °F})} = 2.7 \times 10^{-4} \frac{\text{hr ft}^2 \text{ °F}}{\text{Btu}} = 4.6 \times 10^{-5} \frac{\text{m}^2\text{K}}{\text{W}}$$

Then,

$$U_o = \frac{1}{\dfrac{0.750}{1000(0.584)} + \dfrac{0.001(0.750)}{0.584} + 2.7 \times 10^{-4} + 0.0005 + \dfrac{1}{300}}$$

$$= 150 \text{ Btu/hr ft °F} = 848 \text{ W/m}^2\text{K}$$

$$A_o = \frac{7.28 \times 10^6 \text{ Btu/hr}}{(150 \text{ Btu/hr ft}^2 \text{ °F})(67.1°F)} = 723 \text{ ft}^2 = 67.7 \text{ m}^2$$

Correct for changes in construction features (preliminary examination of Figure 4.5.20 indicates shell inside diameter will be in the range of 500 mm, or 20 in.):

F_1: F_1 = 1.00 since the same tube size and layout is used;
F_2: F_2 = 1.04, assuming two passes;
F_3: F_3 = 1.15, TEMA S construction;

A'_o $= (723 \text{ ft}^2) \ (1.00)(1.04)(1.15) = 865 \text{ ft}^2 = 81 \text{ m}^2.$

From Figure 4.5.20, entering at A'_o, pick off the following combinations of shell inside diameter and tube length:

Shell Inside Diameter		Effective Tube Length		L/D_s
in.	mm	ft	m	
27	686	6.6	2.0	2.9
25	635	7.5	2.3	3.6
$23^1/_4$	591	9.2	2.8	4.7
$21^1/_4$	540	10.8	3.3	6.1
$19^1/_4$	489	13.1	4.0	8.2
$17^1/_4$	438	16.7	5.1	11.6

Any of these combinations would supply the desired area; the $21^1/_4$ in. (540 mm) and $19^1/_4$ in. (489 mm) would appear to be likely choices.

References

American Society of Mechanical Engineers. 1995. *ASME Boiler and Pressure Vessel Code*, Section VIII. New editions published every 3 years. ASME, New York.

Gentry, C.C., Young, R.K., and Small, W.M. 1982. RODbaffle heat exchanger thermal-hydraulic predictive methods, in *Proceedings of the Seventh International Heat Transfer Conference*, Munich, Germany, 6, 197–202.

Hewitt, G.F., Shires, G.L., and Bott, T.R. 1994. *Process Heat Transfer*, CRC/Begell House, Boca Raton, FL.

Kern, D.Q. and Kraus, A.D. 1972. *Extended Surface Heat Transfer*, McGraw-Hill, New York.

Kral, D., Stehlik, P., Van der Ploeg, H.J., and Master, B.I., 1996. Helical baffles in shell and tube heat exchangers. Part I: Experimental verification, *Heat Transfer Eng.*, 17(1), 93–101.

Palen, J.W. and Taborek, J. 1969. Solution of shell side flow pressure drop and heat transfer by stream analysis method, *Chem. Eng. Prog. Symp. Ser. No. 92, Heat Transfer-Philadelphia,* 65, 53–63.

Saunders, E.A.D. 1988. *Heat Exchangers: Selection, Design, and Construction,* Longman Scientific & Technical/John Wiley & Sons, New York.

Schlünder, E.U., Ed. 1983. *Heat Exchanger Design Handbook*, Begell House, New York.

Singh, K.P. and Soler, A.I. 1984. *Mechanical Design of Heat Exchangers and Pressure Vessel Components*, Arcturus, Cherry Hill, NJ.

TEMA. 1988. *Standards*, 7th ed., Tubular Exchanger Manufacturers Association, Tarrytown, NY.

Yokell, S. 1990. *A Working Guide to Shell and Tube Heat Exchangers*, McGraw-Hill, New York.

4.6   Temperature and Heat Transfer Measurements

Robert J. Moffat

There are two different kinds of material to consider with respect to experimental methods: the unit operations of measurement (transducers and their environmental errors) and the strategy of experimentation. This section deals only with the unit operations: transducers, their calibrations, and corrections for environmental errors.

Temperature Measurement

An International Practical Temperature Scale (IPTS) has been defined in terms of a set of fixed points (melting points of pure substances) along with a method for interpolating between the fixed points. The IPTS agrees with the thermodynamic temperature scale within a few degrees Kelvin over most of its range. The IPTS is the basis for all commerce and science, and all calibrations are made with respect to the IPTS temperature. The scale is revised periodically.

Accurate calibrations are not enough to ensure accurate data, however. If a sensor has been installed to measure a gas temperature or a surface temperature, any difference between the sensor temperature and the measurement objective due to heat transfer with the environment of the sensor is an "error." In most temperature-measuring applications, the environmental errors are far larger than the calibration tolerance on the sensor and must be dealt with just as carefully as the calibration.

Thermocouples

Any pair of thermoelectrically dissimilar materials can be used as a thermocouple. The pair need only be joined together at one end and connected to a voltage-measuring instrument at the other to form a usable system. A thermocouple develops its signal in response to the temperature difference from one end of the pair to the other. The temperature at one end, known as the *reference junction* end, must be known accurately before the temperature at the other end can be deduced from the voltage.

Thermocouples are the most commonly used electrical output sensors for temperature measurement. With different materials for different ranges, thermocouples have been used from cryogenic temperatures (a few Kelvin) to over 3000 K. In the moderate temperature range, ambient to 1200°C, manufacturer's quoted calibration accuracy can be as good as ±3/8% of reading (referred to 0°C) for precision-grade base metal thermocouples. Broader tolerances apply at very high temperature and very low temperatures. Thermocouple signals are DC voltages in the range from a few microvolts to a few tens of microvolts per degree C. Because of their low signal levels, thermocouple circuits must be protected from ground loops, galvanic effects, and from pickup due to electrostatic or electromagnetic interactions with their surroundings. Thermocouples are low-impedance devices. Multiple channels of thermocouples can be fed to a single voltage reader using low-noise-level scanners or preamplifiers and electronic multiplexers.

The alloys most frequently used for temperature measurement are listed in Table 4.6.1. These alloys have been developed, over the years, for the linearity, stability, and reproducibility of their EMF vs. temperature characteristics and for their high-temperature capability.

Calibration data for thermocouples are periodically reviewed by the National Institutes of Science and Technology based on the then-current IPTS. Values in Table 4.6.1 illustrate the approximate levels which can be expected, and are from the National Bureau of Standards Monograph 125. Maximum temperatures listed in this table are estimates consistent with a reasonable service lifetime. Allowable atmosphere refers to the composition in contact with the thermoelements themselves. Accuracy estimates are provided for two levels of precision: standard grade and precision grade where these data are available.

Noble metal and refractory metal thermocouples are often used with substitute lead wires, as a cost-saving measure. These lead wires, described in Table 4.6.2 are cheaper and easier to handle than the high temperature thermocouples. They have the same temperature–EMF characteristics as their primary thermoelements, but only over the range of temperatures the lead wires will usually encounter (up to a few hundred degrees C). Except for the substitute alloys, thermocouple extension wires have the same

TABLE 4.6.1   Application Characteristics of Some Common Thermocouple Alloys

Max T °F	Max T °C	Allowable Atmos. (Hot)	Material Names	ANSI Type[a]	Color Code	Output mV/100°F	Accuracy, %	
							Standard[a]	Precision[a]
5072	2800	Inert, H$_2$, vacuum	Tungsten/tungsten 26% rhenium	—	—	0.86	—	—
5000	2760	Inert, H$_2$, vacuum	Tungsten 5% rhenium/tungsten 26% rhenium	—	—	0.76	—	—
4000	2210	Inert, H$_2$	Tungsten 3% rhenium/tungsten 35% rhenium	—	—	0.74	—	—
3720	1800	Oxidizing[b]	Platinum 30% rhodium/platinum 6% rhodium	B	—	0.43	1/2	1/4
2900	1600	Oxidizing[b]	Platinum 13% rhodium/platinum	R	—	0.64	1/4	1/4
2800	1540	Oxidizing[b]	Platinum 10% rhodium/platinum	S	—	0.57	1/4	1/4
2372	1300	Oxidizing[b,c]	Platinel II (5355)/Platinel II (7674)	—	—	2.20	5/8	—
2300	1260	Oxidizing	Chromel/Alumel,[d] Tophel/Nial,[e] Advance T1/T2,[f] Thermo-Kanathal P/N[g]	K	Yellow red	2.20	4°F, or 3/4%	2°F, or 3/8%
1800	980	Reducing[a]	Chromel/constantan	E	Purple red	4.20	1/2	3/8
1600	875	Reducing	Iron/constantan	J	White red	3.00	4°F, or 3/4%	2°F, or 3/8%
750	400	Reducing	Copper/constantan	T	Blue red	2.50	3/4	3/8

[a] Per ANSI C96.1 Standard.

[b] Avoid contact with carbon, hydrogen, metallic vapors, silica, reducing atmosphere.

[c] @ Engelhard Corp.

[d] @ Hoskins Mfg. Co.

[e] Wilber B. Driver Co.

[f] Driver-Harris Co.

[g] The Kanthal Corp.

TABLE 4.6.2   Substitute Material Extension Wires for Thermocouples

Thermocouple Material	Thermocouple Type[a]	Extension Wire, Type[a]	Color for (+) Wire	Color for (–) Wire	Overall Color
Tungsten/tungsten 26% rhenium	—	Alloys 200/226[b]	—	—	—
Tungsten 5% rhenium/tungsten 26% rhenium	—	Alloys (405/426)[b]	White	Red	Red[b]
Tungsten 3% rhenium/tungsten 25% rhenium	—	Alloys (203/225)[b]	White/yellow	White/red	Yellow/red[b]
Platinum/platinum rhodium	S, R	SX, SR	Black	Red	Green
Platinel II-5355/Platinel II-7674	—	P2X[d]	Yellow	Red	Black[d]
Chromel/Alumel, Tophel/Nial, Advance, Thermokanthal[c]	K	KX	Yellow	Red	Yellow
Chromel/constantan	E	EX	Purple	Red	Purple
Iron/constantan	J	JX	White	Red	Black
Copper/constantan	T	TX	Blue	Red	Blue

[a] ANSI, except where noted otherwise.
[b] Designations affixed by Hoskins Mfg. Co.
[c] Registered trade mark names.
[d] Engelhard Mfg. Co.

composition as thermocouple wires, differing only in the type of insulation and the accuracy of calibration, which is not held as closely for extension wire as for thermocouple-grade wire.

Any instrument capable of reading low DC voltages (on the order of millivolts) with 5 to 10 µV resolution will suffice for temperature measurements. *Galvanometric measuring instruments* can be used, but, since they draw current, the voltage available at the terminals of the instrument depends not only on the voltage output of the thermocouple loop but also on the resistance of the instrument and the loop together. Such instruments are normally marked to indicate the external resistance for which they have been calibrated. *Potentiometric instruments*, either manually balanced or automatically balanced, draw no current when in balance, hence can be used with thermocouple loops of any arbitrary resistance without error. High-input impedance *voltmeters* draw very low currents and, except for very high resistance circuits, are not affected by the loop resistance.

Thermocouple Theory. Equation (4.6.1) is the general form describing the EMF generated in a two-wire thermocouple (Moffat, 1962). The same form can be derived from either the free-electron theory of metals or from thermodynamic arguments alone: the output of a thermocouple can be described as the sum of a set of terms, one arising in each wire in the circuit.

The junctions do not generate the EMF: they are merely electrical connections between the wires. For a two-wire circuit,

$$\text{EMF} = \int_0^L \varepsilon_1 \frac{dT}{dx} dx + \int_L^0 \varepsilon_2 \frac{dT}{dx} dx \tag{4.6.1}$$

where
ε_1 and $\varepsilon_2 =$ the total thermoelectric power of materials 1 and 2, respectively, mV/C. The value of ε is equal to the sum of the Thomson coefficient and the temperature derivative of the Peltier coefficient for the material.
$T =$ temperature, C
$x =$ distance along the wire, m
$L =$ length of the wire, m

This form for expressing the output of a two-wire circuit applies regardless of whether the wires are uniform in composition or not. If a circuit contained four wires (two thermocouple wires and two extension wires), then Equation (4.6.1) would be written with four terms, one for each length of wire.

When the wire is uniform in composition and both wires begin at (T_o) and both end at (T_L) the two terms can be collected into one integral:

$$\text{EMF} = \int_{T_0}^{T_L} \left(\varepsilon_1 - \varepsilon_2 \right) dT \tag{4.6.2}$$

The EMF–temperature (E–T) tables produced by NIST and others are "solutions" to Equation (4.6.2) and can be used only when the following three conditions are met:

1. The thermoelectric power, ε, is not a function of position; i.e., the wires are homogeneous;
2. There are only two wires in the circuit;
3. Each wire begins at T_o and ends at T_L

When the circuit consists entirely of pairs of materials, Equation 4.6.2 can be used directly as the basis for understanding the source of the EMF. As an example, consider the three-pair system shown in Figure 4.6.1. For that circuit, Equation (4.6.2) would have three terms: one for each pair. The total EMF generated by the circuit would be the sum of the EMFs generated in the thermocouple pair and in the extension wire pair. The pair of copper wires would not contribute to the net EMF, assuming the two copper wires were perfectly matched. The EMF contributed by each pair would be proportional to the temperature difference from end to end of that pair, as shown in Equation (4.6.3) and (4.6.4).

$$\text{EMF} = \int_{T_1}^{T_2} \left(\varepsilon_{cu} - \varepsilon_{cu} \right) dT + \int_{T_2}^{T_3} \left(\varepsilon_+ - \varepsilon_- \right)_{\text{LEADS}} dT + \int_{T_3}^{T_4} \left(\varepsilon_+ - \varepsilon_- \right)_{\text{TC}} dT \tag{4.6.3}$$

$$\text{EMF} = 0 + (T3 - T2)\left(\varepsilon_+ - \varepsilon_- \right)_{\text{LEADS}} + (T4 - T3)\left(\varepsilon_+ - \varepsilon_- \right)_{\text{TC}} \tag{4.6.4}$$
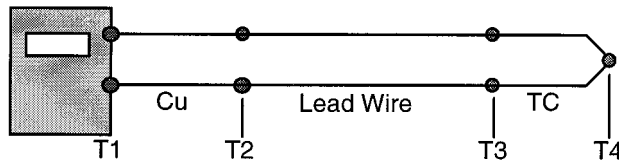

FIGURE 4.6.1 A three-pair circuit.

Most thermocouple circuits consist only of pairs of wires and can be understood in terms of these two equations, but some require a more detailed treatment. A graphical method of analysis is available, based on Equation (4.6.1).

The temperature–EMF calibrations of the more common materials are shown in Figure 4.6.2 derived from NBS Monograph 125 and other sources. This figure provides the input data for a simple graphical technique for describing the EMF generation in a circuit. Each curve in Figure 4.6.2 represents the output which would be derived from a thermocouple made of material X used with platinum when the cold end is held at 0°C and the hot end is held at *T*.

Those elements commonly used as "first names" for thermocouple pairs, i.e., Chromel (Chromel-Alumel), iron (-constantan), copper (-constantan), have positive slopes in Figure 4.6.2.

The simplest thermocouple circuit for temperature measurement consists of two wires joined together at one end (forming the "measuring junction") with their other ends connected directly to a measuring instrument, as shown in the upper portion of Figure 4.6.3. The EMF generation in this circuit is graphically represented in the lower portion, an E–T diagram, using the data in Figure 4.6.2. The E–T
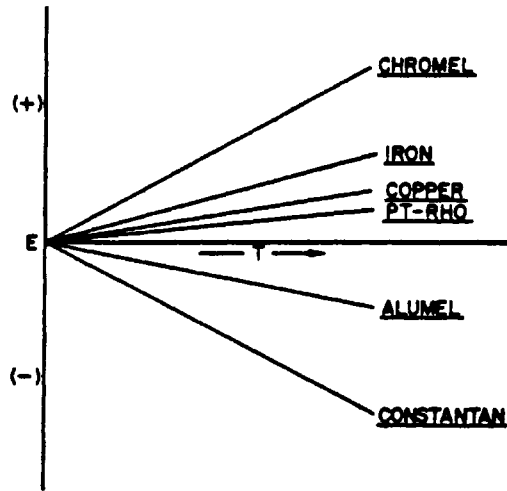
FIGURE 4.6.2 E–T calibrations for several common thermocouple materials.
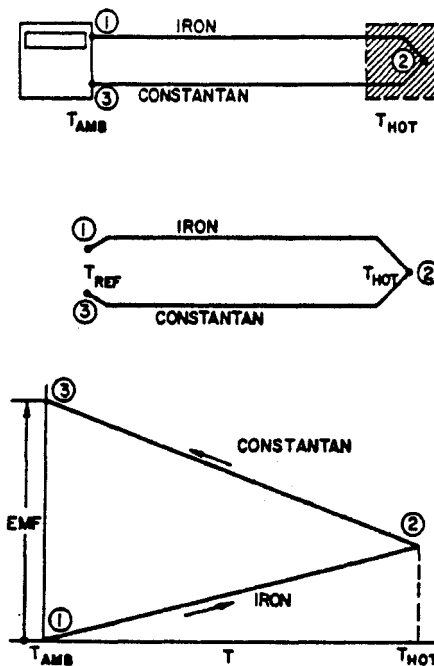
FIGURE 4.6.3 E–T diagram of a thermocouple using an ambient reference.

diagram is used for examining the EMF generated in the circuit, to be certain that it arises only from the desired thermocouple materials, and that all segments of the circuit are properly connected. The E–T diagram is not used for evaluating the output — that is done using the tables after the circuit has been shown to be correctly wired.

To construct an E–T diagram, first sketch the physical system considered and assign a number to each "point of interest" on that sketch and a temperature. On E–T coordinates, locate point 1 at 0/mV and at its assigned temperature. Then start a line from point 1, moving toward the temperature of point 2, and copying the shape of the calibration curve of the iron wire (see Figure 4.6.2). From 2 to 3, use the constantan calibration curve. The difference in elevation of points 1 and 3 describes the net EMF

generated in the circuit between points 1 and 3, and describes the polarity. When point 3 lies physically above point 1 in the E–T diagram, it is, by convention, electrically negative with respect to point 1.

The simple triangular shape shown in Figure 4.6.3 identifies a proper circuit. Any thermocouple circuit whose E–T diagram is equivalent to that is appropriate for temperature measurement and its EMF may be interpreted using the conventional tables. Any circuit whose E–T diagram is not equivalent to the pattern circuit should be rewired.

Thermocouples generate their signal in response to the temperature difference between the two ends of the loop. For accurate measurements, the temperature of the "reference junction" must be known. Laboratory users often use an ice bath made from a good-quality Dewar flask or vacuum-insulated bottle of at least 1 pt capacity, as shown in Figure 4.6.4. The flask should be filled with finely crushed ice and then flooded with water to fill the interstices between the ice particles. The reference thermocouple is inserted into a thin-walled glass tube containing a small amount of silicone oil and submerged six or eight diameters into the ice pack. The oil assures good thermal contact between the thermocouple junction and the ice/water mixture. The tube should be sealed at the top to prevent atmospheric moisture from condensing inside it, which would cause corrosion when using iron-constantan thermocouples. Figure 4.6.5 shows in iron-constantan thermocouple circuit with an ice bath. The individual thermocouple wires are connected to copper wires in the ice bath, and the two copper wires taken to the voltmeter. The lower portion of this figure shows the E–T diagram for this circuit, and proves that the output of this circuit is entirely due to the temperature difference from end to end of the iron-constantan loop: the two copper wires do not contribute to the output.
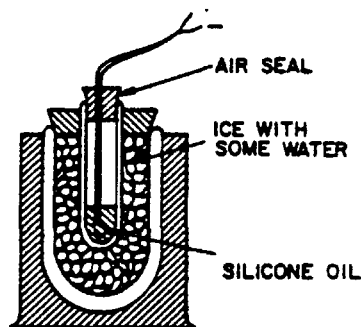

FIGURE 4.6.4 Characteristics of a good ice bath.

Calibration. Thermocouple calibrations are provided by the wire manufacturers to tolerances agreed upon industry-wide, as summarized in Table 4.6.1. These tolerances include two components: the uncertainty in the average slope of the calibration curve of the wire, and the effects of local inhomogeneities in the wire. It is difficult to improve the accuracy of a thermocouple by calibrating it. For a truly significant calibration, the thermocouple would have to be exposed to the same temperature during calibration, at every point along it, that it would encounter in service. In an oven calibration, most of the signal is generated in the material at the mouth of the oven, as could be recognized by considering the temperature gradient distribution along the wire. The material inside the oven contributes little or nothing to the signal.

Thermistors

Thermistors are electrical resistance temperature transducers whose resistance varies inversely, and exponentially, with temperature. The resistance of a 5000 Ω thermistor may go down by 200 Ω for each degree C increase in temperature in the vicinity of the initial temperature. Interrogated by a 1.0 mA current source, this yields a signal of 200 mV/°C. As a consequence of this large signal, thermistors are frequently used in systems where high sensitivity is required. It is not uncommon to find thermistor data logged to the nearest 0.001°C. This does not mean that the data are accurate to 0.001°C, simply
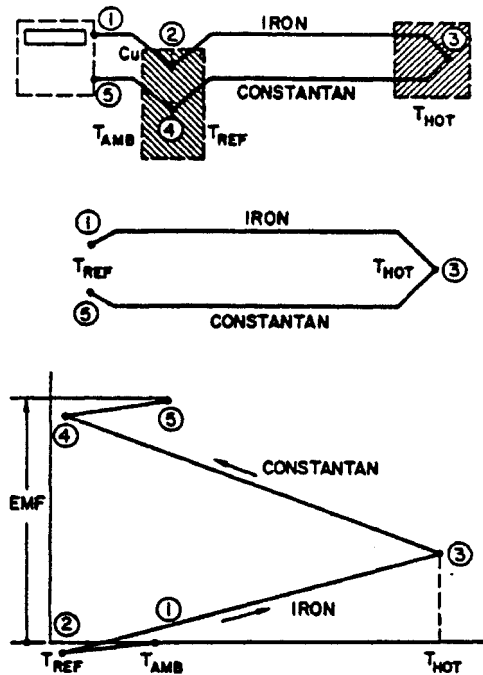
FIGURE 4.6.5 A thermocouple circuit using an ice bath reference, and its E–T diagram.

that the data are readable to that precision. A thermistor probe is sensitive to the same environmental errors which afflict any immersion sensor: its accuracy depends on its environment.

Thermistor probes can be used between –183°C (the oxygen point) and +327°C (the lead point) but most applications are between –80 and +150°C. The sensitivity of a thermistor (i.e., the percent change in resistance per degree C change in thermistor temperature) varies markedly with temperature, being highest at cryogenic temperatures.

Thermistor probes range in size from 0.25-mm spherical beads (glass covered) to 6-mm-diameter steel-jacketed cylinders. Lead wires are proportionately sized. Disks and pad-mounted sensors are available in a wide range of shapes, usually representing a custom design "gone commercial." Aside from the unmounted spherical probes and the cylindrical probes, there is nothing standard about the probe shapes.

Calibration. Thermistor probes vary in resistance from a few hundred ohms to megohms. Probe resistance is frequently quoted at 25°C, with no power dissipation in the thermistor. The commercial range is from about 2000 to 30,000 Ω. Representative values of the sensitivity coefficient (% change in resistance per degree C) is given in Table 4.6.3 and resistance values themselves, in Table 4.6.4.

TABLE 4.6.3   Thermistor Temperature Coefficient Variations with Temperature

Temp. °C	Condition	$\Delta R/R$, %
–183	Liquid oxygen	–61.8
–80	Dry ice	–13.4
–40	Frozen mercury	–9.2
0	Ice point	–6.7
25	Room temperature	–5.2
100	Boiling water	–3.6
327	Melting lead	–1.4

TABLE 4.6.4   Thermistor Resistance Variation with Temperature

Temp., °C	Res., Ω	Temp., °C	Res., Ω
–80	1.66 M	0	7355
–40	75.79 K	25	2252
–30	39.86 K	100	152.8
–20	21.87 K	120	87.7
–10	12.46 K	150	41.9

Proprietary probes are available which "linearize" thermistors by placing them in combination with other resistors to form a circuit whose overall resistance varies linearly with temperature over some range. These compound probes can be summed, differenced, and averaged as can any linear sensor. Modern manufacturing practices allow matched sets to be made, interchangeable within +/–0.1°C.

Thermal Characteristics. Thermistor probes are generally interrogated using a low current, either AC or DC. A level of about 10 µA would be typical. With a probe resistance of 10 K Ω, 0.01 W must be dissipated into its surrounding material. This current results in the probe running slightly above the temperature of the medium into which it is installed: the "self-heating" effect. Since thermistors are often used where very small changes in temperature are important, even small amounts of self-heating may be important.

The self-heating response is discussed in terms of the "dissipation constant" of the probe, in milliwatts per degree C. The dissipation constant depends on the thermal resistance between the thermistor and its surroundings. For fluid-sensing probes, the self-heating varies with velocity and thermal conductivity, while for solid immersion probes, it varies with the method of attachment and type of substrate.

Dissipation constants for representative probes are given in Table 4.6.5. The self-heating effect must be considered in calibration as well as in use.

The transient response of a thermistor is more complex than that of a thermocouple and, size for size, they are not as well suited to transient measurements.

TABLE 4.6.5   Representative Thermal Dissipation Constants for Two Thermistor Probe Designs

Environment	1.0-cm Disk	5.0-cm Cylinder
Still air	8 mW/C	1 mW/C
Still oil	55	—
Still water	—	3.5
Oil at 1 m/sec	250	—

Thermistor probes are sold with calibration tables of resistance vs. temperature at some specified accuracy, on the order of +/–0.1 or 0.2 K, depending on the grade of probe purchased. These tables are typically in increments of 1 K. For computer interpretation, they should be fit to the Steinhart-Hart form[2] and the coefficients determined for least error.

$$\frac{1}{T} = A_0 + A_1 \ln(R) + A_3 \ln\left(R^3\right) \tag{4.6.5}$$

Resistance Temperature Detectors

The terms *resistance temperature detector* (RTD) and *resistance thermometer* are used interchangeably to describe temperature sensors containing either a fine wire or a thin film metallic element whose resistance increases with temperature. In use, a small current (AC or DC) is passed through the element, and its resistance measured. The temperature of the element is then deduced from the measured resistance using a calibration equation or table lookup.

RTDs are used both for standards and calibration laboratories and for field service. Field-service probes are generally encased in stainless steel protective tubes with either wire or film elements bonded to sturdy support structures. They are made to take considerable physical abuse. Laboratory standard-grade probes are often enclosed in quartz tubes, with the resistance wire mounted in a strain-free manner on a delicate mandrel.

High-quality resistance thermometers have been used as defining instruments over part of the range of the IPTS. Because of this association with high-precision thermometry, resistance thermometers in general have acquired a reputation for high precision and stability. Commercial probes, however, are far different in design from the standards-grade probes, and their stability and precision depend on their design and manufacture.

RTDs are often recommended for single-point measurements in steady-state service at temperatures below 1000°C where longtime stability and traceable accuracy are required and where reasonably good heat transfer conditions exist between the probe and its environment.

They are not recommended for use in still air, or in low-conductivity environments. RTDs self-heat, which causes an error when the probes are used in a situation with poor heat transfer. They are not recommended for transient service or dynamic temperature measurements unless specifically designed for such service. The probes tend to have complex transient characteristics and are not amenable to simple time-constant compensation.

Physical Characteristics. The physical characteristics of any given resistance thermometer represent a compromise between two opposing sets of requirements. For accuracy, repeatability, and speed of response, a delicate, low-mass sensing element is desired, supported in a strain-free manner in good thermal contact with its surroundings. For durability, a rugged sensor is indicated, mounted firmly to a sturdy structure inside a robust, sealed protection tube.

Both the short-term calibration (resistance vs. specimen temperature) and the long-term stability (drift) are directly affected by the mechanical configuration of the probe. The electrical resistance of the sensing element is a function of its temperature and state of mechanical strain (Figure 4.6.6).
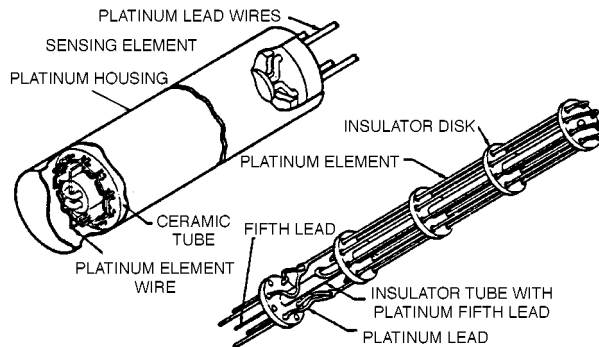
FIGURE 4.6.6 Slack-wire platinum resistance thermometer.

The sensing elements used in field-service RTD probes range from thin metallic films deposited on rectangular ceramic wafers ($0.5 \times 1.0 \times 2.0$ mm) with pigtail leads (0.25 mm diameter and 2.5 cm long) to glass-encapsulated, wire-wound mandrels (4 mm in diameter and 2.0 cm long), again with pigtail leads. Bonding the sensor to its support provides good mechanical protection to the element, but subjects the element to strain due to thermal expansion. As long as this process is repeatable, the calibration is stable.

Electrical Characteristics. RTDs are available commercially with resistances from 20 to 20,000 Ω with 100 Ω being common. Bifilar windings are frequently used in wire-wound elements, to reduce the

electrical noise pickup. This is more important in the quartz-jacketed probes than in those with stainless steel protection tubes. Twisted pair lead wires are recommended.

Thermal Characteristics. Figure 4.6.7 shows a simplified cross section of a typical resistance thermometer and a thermal circuit which can be used to discuss its behavior. In forming such a thermal circuit model, each element of the probe is described by its resistive and capacitive attributes following conventional heat transfer practice. The principal components are

- The external thermal resistance per unit length;
- The thermal capacitance of the protective tube per unit length, C_T;
- The radial internal thermal resistance between the sensor and the protective tube, R_{int};
- The capacitance of the sensor element and its support, C_{sensor};
- The axial internal thermal resistance of the stem, per unit length, R_T.
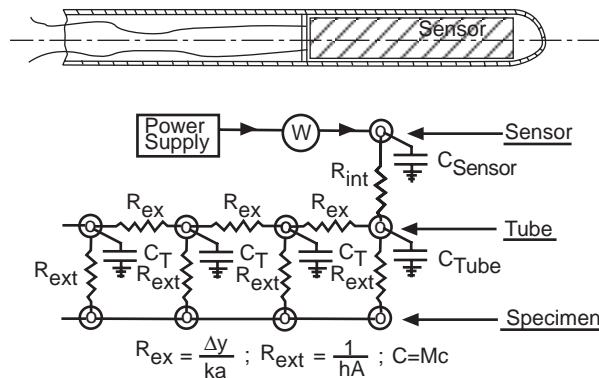

FIGURE 4.6.7 Thermal circuit representation of a typical resistance thermometer.

This circuit can be used to predict the temperature distribution within the probe both at steady state and during transients and can be refined, if needed, by subdividing the resistance and capacitance entities.

Steady-State Self-Heating. Interrogating an RTD by passing a current through it dissipates power in the element, shown in Figure 4.6.7 as W, which goes off as heat transfer through the internal and external resistances. This self-heating causes the sensing element to stabilize at a temperature higher than its surroundings and constitutes an "error" if the intent is to measure the surrounding temperature. The amount of the self-heating error depends on three factors:

- The amount of power dissipated in the element,
- The internal thermal resistance of the probe, as a consequence of its design, and
- The external thermal resistance between the surface of the probe and the surrounding material.

The self-heating temperature rise is given by Equation (4.6.6):

$$T_{sens} - T_{surr} = W\left(R_{int} + R_{ext}\right) \tag{4.6.6}$$

The internal thermal resistance of a probe, R_{int}, measured in degree C per watt, describes the temperature rise of the sensing element above the surface temperature of the probe, per unit of power dissipated. The internal thermal resistance can be deduced from measurements of the sensor temperature at several different current levels when the probe is maintained in a well-stirred ice bath, where the external thermal resistance is very low. The slope of the apparent temperature vs. power dissipated line, °C/W, is the internal thermal resistance. When an RTD is used in a gas or liquid, the external resistance between the

probe and its surroundings must be estimated from standard heat transfer data. The external resistance is 1/(hA), °C/W.

A typical cylindrical probe exposed to still air will display self-heating errors on the order of 0.1 to 1.0°C per mW (commercial probes of 1.5 to 5 mm in diameter). At 1 m/sec air velocity, the self-heating error is reduced to between 0.03 and 0.3°C. In water at 1 m/sec velocity, the self-heating effect would be reduced by a factor of four or five compared to the values in moving air, depending on the relative importance of the internal and the external thermal resistances.

Calibration and Drift. The relationship between resistance and temperature must be determined for each probe or acquired from the manufacturer. Generally speaking, the reported values will require interpolation.

The resistance–temperature characteristic of a probe may drift (i.e., change with time) while the probe is in service. Manufacturers of laboratory-grade probes will specify the expected drift rate, usually in terms of the expected error in temperature over an interval of time. Two sample specifications are "0.01 C per 100 hours" for a low-resistance, high-temperature probe (0.22 Ω at 0°C, 1100°C maximum service temperature) and "0.01 C per year" for a moderate-resistance, moderate-temperature probe (25.5 Ω at 0°C, 250°C maximum service temperature). Drift of the resistance-temperature relationship takes place more rapidly at high temperatures.

Radiation Devices

Surface temperatures and gas temperatures can be deduced from radiation measurements. Surface-temperature measurements are based on the emitted infrared energy, while gas-temperature measurements use specific emission lines from the gas itself or from a tracer inserted into the gas.

Commercial surface-temperature measurement systems (single-point) are available, at low cost, which can measure temperature to +/–1% of reading, above 38°C, if the emissivity of the surface is known. The device referenced requires a spot size of 1.25 cm diameter, viewed from 75 cm. Spectroscopic gas-temperature measurements can be accurate to +/–3 or 4% of reading, but require a significant investment in effort as well as equipment (on the order of 1 to 2 years and $100,000 to $200,000). Several techniques based on Raman scattering have been used in combustion systems. Planar-lasar-induced fluorescence has shown considerable promise as one of the newer methods.

Infrared emission from a surface is described by two laws: the Stefan Boltzmann law describing the total emitted radiation as a function of temperature, and Planck's law describing its distribution as a function of temperature. These laws form the basis for all radiation-based surface-temperature detectors.

Early radiometers focused the total infrared energy on a thermopile bolometer and used the temperature rise across its calibrated heat loss path to measure the incident energy flux. Solid-state photon detectors have replaced thermopile bolometers as the detector of choice. Such a detector will respond to any photon having energy above a certain level (specific to the detector). Since the energy of a photon is inversely proportional to its wavelength, detectors respond to all wavelengths below some value. Modern detectors use band-pass filters to limit the wavelength band of photons admitted to the detector and rely on Planck's law to infer the temperature from the energy flux:

$$E_{b,\lambda} = \frac{C_1 \lambda^{-5}}{e^{C_2/\lambda T} - 1} \tag{4.6.7}$$

where $E_{b,\lambda}$ = radiated power at the wavelength λ, W/m^2
     T = temperature, K
     C_1 = 3.743×10^8, Wμm^4/m^2
     C_2 = 1.4387×10^4, μmK

Commercial radiation temperature detectors use different wave bands for different temperature ranges, with different detectors for each band. The emissivity of the surface must be known, as a function of temperature, in the wavelength band used by the detector.

Radiation detectors are vulnerable to interference from four sources: low signal-to-noise ratio at low temperatures (below a few hundred degrees C); radiation from the surroundings reflecting into the detector (also usually more important at low temperatures); low spatial resolution (also more evident at low temperatures); uncertainty in the emissivity of the surface (at all temperatures); and absorption of radiation into water vapor and CO_2 in the line of sight (at any temperature).

A fiber-optic blackbody temperature detector system is offered by the Luxtron Corporation for standards room and field service above 300°C. The unit consists of a blackbody capsule fiber-optically coupled to a filtered, band-limited photon detector. Accuracy of 0.01 to 0.1°C is claimed, depending on temperature level.

A fluoroptic temperature-measuring system is also offered by the same company, for use only at lower temperatures (–200 to +450°C). This system uses an ultraviolet-stimulated phosphor on the end of an optical fiber as its sensor. The fluorescent signal from the phosphor decays with time, and its "time constant" is a function of temperature. Accuracy of +/–0.5°C is claimed for measurements within +/–50°C of a calibration point, or +/–1°C within 100°C.

Temperature-Sensitive Paints, Crayons, and Badges

Temperature-sensitive paints, crayons, and badges are available from several suppliers (Omega Engineering, Inc., Stamford, CT, and others in Germany and Japan). Each undergoes an irreversible change (e.g., a change in color or a change from solid to liquid) at one specified temperature. With a range of paints, temperatures from ambient to about 1500°C can be covered. The accuracy generally quoted is about +/–1% of level, although melting standards are available to +/–0.5°C.

The phase-change materials melt at well-defined temperatures, yielding easily discernible evidence that their event temperature has been exceeded. When more than one phase-change paint is applied to the same specimen, there can be interference if the melt from the low-melting paint touches the high-melting material. Color change materials do not interfere, but are more difficult to interpret. The calibration of high-temperature paints (both phase change and color change) may shift when they are used on heavily oxidized materials, due to alloying of the oxide with the paint. Recommended practice is to calibrate the paints on specimens of the application material. The event temperature which will cause transformation depends on the time at temperature: short exposure to a high temperature often has the same effect as long exposure to a lower temperature.

The paints and crayons are nonmetallic and, therefore, tend to have higher emissivities for thermal radiation than metals. They should be used only over small areas of metallic surfaces, compared with the metal thickness, or else their different emissivities may lead to a shift in the operating temperature of the parts.

The principal disadvantages of the paints and crayons are that they require visual interpretation, which can be highly subjective, and they are one-shot, irreversible indicators which respond to the highest temperature encountered during the test cycle. They cannot record whether the peak was reached during normal operation or during soak-back.

Liquid crystals can be divided into three groups, depending on their molecular arrangements: (1) smectic, (2) nematic, and (3) cholesteric. Most of the temperature-sensitive liquid crystals now in use are cholesteric: made from esters of cholesterol. Their molecules are arranged in planar layers of molecules with their long axes parallel and in the plane of the layer. The molecules in each layer are rotated with respect to those in its neighboring layers by about 15 min of arc in a continuous, helical pattern along an axis normal to the layers.

The colors reflected from cholesteric liquid crystals are thought to be due to Bragg diffraction from the aligned layers. The "wrap angle" between adjacent layers increases with temperature; hence, the color of the liquid crystal shifts toward short wavelengths (toward blue) as the temperature is raised. The color can also be affected by electric fields, magnetic fields, pressure, shear stress, and some chemical vapors.

Warm cholesterics are colorless liquids and they pass through a series of bright colors as they are heated through their "color-play" temperature band. The first color to appear is a deep red, followed by

yellow, green, blue, and violet. Further heating yields a colorless liquid again. This cycle is reversible and repeatable, and the color–temperature relationship can be calibrated.

Liquid crystals selectively reflect only a small fraction of the incident light; hence, to enhance the brightness of the color image, they must be backed up with black paint or a nonreflecting surface.

A typical calibration is shown in Figure 4.6.8 for liquid crystals painted over black paint on an aluminum calibration strip. The upper part of Figure 4.6.8 describes the color variation, while the lower part shows the imposed linear temperature distribution. The hot end is blue, the cold end is red. Color-play intervals range from 0.5 to 10.0°C. Liquid crystals whose color-play interval is on the order of 0.5 to 2.0°C are often referred to as *narrow-band* materials, while those whose interval extends to 5.0 to 10°C are called *wide band*. Narrow-band images are easy to interpret by eye. Wide-band images show only subtle variations of color for small changes in temperature, and accurate work requires digital image handling or multiple images taken with different filters.
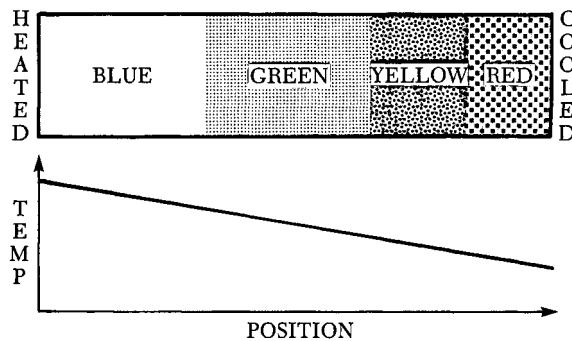

FIGURE 4.6.8 Schematic representation of a calibration strip.

Several different narrow-band liquid crystals can be mixed together to make a single, multi-event paint covering a wide range of temperatures, provided their color-play intervals do not overlap. Such a mixture yields a set of color-play bands, one for each component.

Calibration. Liquid crystals are sold by event temperature and color-play bandwidth, with a nominal accuracy of +/–1°C on the event temperature. In many applications, especially if the image is to be visually interpreted, no further calibration is needed.

The accuracy attainable with a liquid crystal is related to the width of the color-play interval. With narrow-band material (a color-play interval of about 1.0°C), visual interpretation can be done with an uncertainty of 0.25 to 0.5°C. With digital image interpretation, spectrally controlled lighting and appropriate corrections for reflected light interference, the uncertainty can be held below 0.25°C.

Early users reported that the perceived color of a liquid crystal depended on both the lighting angle and the viewing angle. This dependence can be eliminated by using a light source along the line of sight (coaxial viewing and illumination).

Multiple-Event Paints. Several narrow-band paints can be mixed together to make a single paint with all the characteristics of each component, if their color-play intervals do not overlap. Each component retains its original calibration and acts independently of the other components.

Figure 4.6.9 shows the image from a five-event paint used to map the adiabatic wall temperature isotherms around a heated block in mixed convection. The outermost isotherm is 30°C, and the events are spaced apart at 5°C intervals. Determination of the temperatures from a multiple-event image requires that the temperature be known at one point in the image.

Liquid Crystals in Water. Liquid crystals can be used to mark the temperature distribution in water and some other liquids by adding a small quantity of encapsulated liquid crystal material to the liquid and photographing the color distribution using planar lighting. Velocity and temperature distributions can be
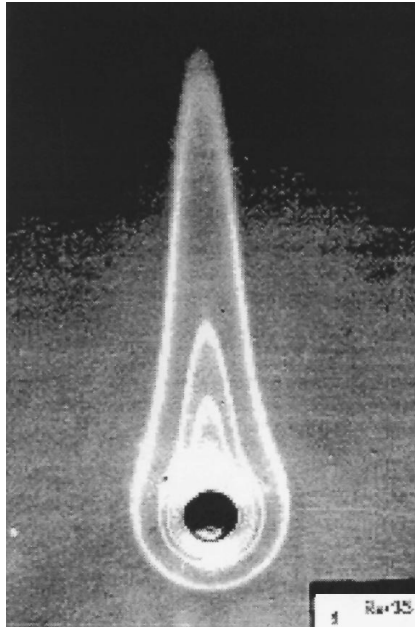
FIGURE 4.6.9 Multi-event liquid crystal used to visualize the isotherm pattern above a heated spot in mixed convection.
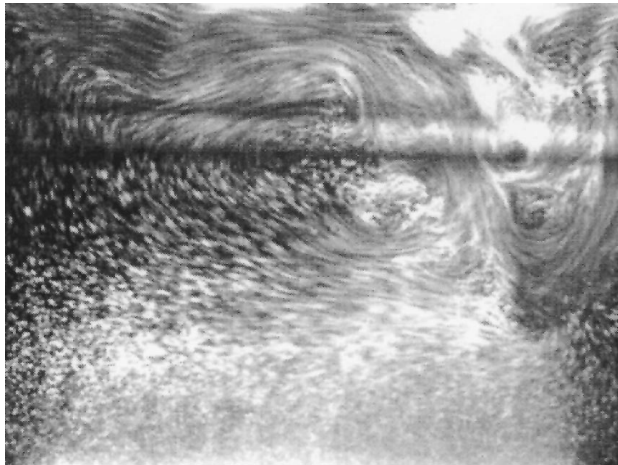
FIGURE 4.6.10 Liquid crystal visualization of the velocity and temperature distribution in a water-filled tank.

determined by photographing the liquid crystal particles using a known exposure time. The temperature is deduced from the particle color, and the velocity by the length of the streak its image forms. Figure 4.6.10 shows the velocity and temperature distributions in a shear-driven, water-filled cavity 30 sec after the impulsive start of belt motion. In this view, the belt is at the top of the image, and moved from left to right. The water was stably stratified initially, with the top being 4°C hotter than the bottom. This technique was demonstrated by Rhee et al. (1984) and has been used by several workers.

Image Processing. Several schemes have been proposed to remove the subjectivity from interpretation of liquid crystal images. Akino et al. (1989), and others, have processed RGB video images of narrow-band images using multiple filters to extract images of specified isochromes, related to temperatures through a calibration. Hollingsworth et al. (1989) processed RGB images of wide-band images using

chromaticity coordinates (hue, saturation, and intensity) and extracted temperature at each pixel, rather than along isochromes.

Heat Flux

Heat flux to or from a surface can be measured directly, using heat flux meters, or inferred from an overall energy balance, or inferred from temperature–time measurements at the surface or within the body. There are no primary standards for heat flux measurement.

Three general classes of heat flux meters are in common use: slug calorimeters, planar heat flux gauges (sometimes called Schmidt–Boelter gauges), and circular foil gauges (sometimes called Gardon gauges). Sensitivities range from microvolts per kW/m^2 to millivolts per W/m^2. Planar gauges can be used for radiant or convective heat loads. Circular foil gauges should be used only for radiant loads.

Slug Calorimeter

The slug calorimeter is an energy balance transducer consisting of a known mass of material instrumented so that its temperature can be measured. A simple version is shown in Figure 4.6.11. If losses are negligibly small and the mass and the specific heat are constant, the instantaneous heat flux is deduced from

$$\dot{q}_{in}'' A = Mc \frac{\partial T}{\partial t} \tag{4.6.8}$$

where T = Average temperature of the slug, C
M = Mass of the slug, kg
c = Specific heat, J/kg·C
A = Face area, m^2
τ = Time
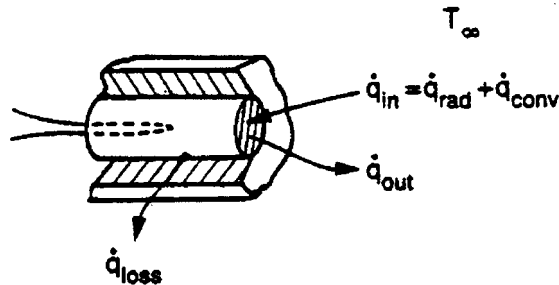
FIGURE 4.6.11 A simple slug calorimeter.

The variation of slug temperature with time is used to infer net heat transfer rate to the gauge. Slug calorimeters are used mainly when the heat flux, or the heat transfer coefficient, is expected to be relatively constant. They are of less value when the input flux changes arbitrarily because of the inaccuracies inherent in differentiating the signals.

Planar Heat Flux Gauge

Planar heat flux gauges use Fourier's law to deduce the heat flux from a steady-state measurement of the temperature difference across a thin sheet of thermally insulating material. The planar gauge geometry is shown in Figure 4.6.12. The working equation for a planar gauge is

FIGURE 4.6.12 A typical planar heat flux gauge.

$$\text{EMF} = N\varepsilon\,\Delta T = \frac{N\varepsilon t}{k}\dot{q}''$$ (4.6.9)

where $N =$ number of junction pairs,
$e =$ thermoelectric power of the thermoelement, mV/C
$t =$ thickness of the insulator, m
$k =$ conductivity of the insulator, W/m·C
$q'' =$ heat flux through the gauge, W/m²

The figure shows one thermocouple junction on the top and one on the bottom surface of the insulator. Most gauges use multiple junctions. The thermoelements may be wire (down to 0.025 mm diameter) or thin films deposited on the insulator (10 to 20 Å). The assembly is usually sandwiched between two sheets of protective material to form an integral unit. Up to 150°C application temperature, these units are often made of Kapton, and provided with a contact adhesive. They may be as thin as 0.15 mm overall.

Gauges should not be removed and reinstalled without recalibration, as the act of removing them from the surface may delaminate the gauge, changing its thermal resistance, and therefore its calibration.

Circular Foil Gauges

A circular foil gauge consists of a thin circular disk of metal supported by its edge from a structure of constant and uniform temperature. The circular foil gauge is often called a Gardon gauge. A constantan foil is often used, with a copper support structure. Two copper wires complete the circuit: one attached to the center of the foil disk and one to the support structure. The copper–constantan thermocouple thus formed produces an EMF determined by the temperature difference from the center of the foil disk to its rim. That temperature difference is directly proportional to the average heat flux on the disk. A cross-sectional view of a circular foil gauge is shown in Figure 4.6.13.

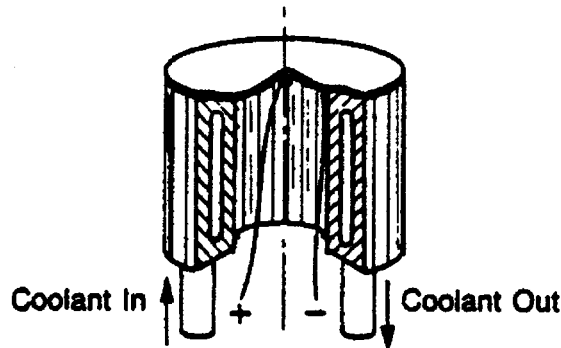**FIGURE 4.6.13** A water-cooled circular foil gauge (Gardon gauge).

The working equation for a circular foil gauge is

$$\text{EMF} = \varepsilon\frac{R^2}{4kt}\dot{q}''$$ (4.6.10)

where $\varepsilon =$ thermoelectric power, mV/C

$R =$ radius of the disk, m
$k =$ thermal conductivity of the disk, W/m·C
$t =$ thickness of the disk, m
$q'' =$ heat flux absorbed by the disk, W/m² (must be uniform)

The output signal is thus directly proportional to the heat flux on the disk. Cooling passages are frequently built into the support structure to maintain the edge of the disk (the heat sink for the foil disk) at constant temperature.

Calibration

Calibration of the Gardon-type heat flux meters is most easily done by comparison, using a radiation calibrator.

Planar gauges can be calibrated either by conduction or radiation, but the results will depend on the calibration method for some guages.

Sensor Environmental Errors

Temperature sensors generate signals in response to their own temperatures, but are usually installed to measure the temperature of some fluid or solid. There is heat transfer between the sensor and all of its surroundings, with the result that the sensor usually equilibrates at some temperature different from the fluid or solid it is installed in. This difference is considered an error in the measurement.

Similarly, heat flux gauges are generally installed so one can infer the heat flux which would have been there had the gauge not altered the system behavior. But heat flux gauges do disturb the system, and the heat flux at the gauge location, when the gauge is there, may be significantly different from that which would have been there without the gauge. This system disturbance effect must also be considered an error.

Steady-State Errors in Gas-Temperature Measurement

All immersion-type temperature sensors (thermocouples, resistance detectors, and thermistors) are subject to the same environmental errors, which are frequently larger than the calibration errors of the sensors. Large probes are usually affected more than small ones; hence, RTDs and thermistors (selected by investigators who wish to claim high accuracy for their data) are more vulnerable to environmental errors (due to their larger size and their self-heating errors). This aspect of accuracy is sometimes overlooked.

Sensor installations for gas-temperature measurements should be checked for all three of the usual steady-state environmental errors: velocity error, radiation error, and conduction error. The same equations apply to all sensors, with appropriate dimensions and constants.

$$\text{velocity error:} \qquad E_v = (1 - \alpha)\frac{V^2}{2g_c J c_p} \qquad\qquad (4.6.11)$$

$$\text{radiation error:} \qquad E_r = \frac{\sigma\varepsilon}{h}\left(T_{\text{sens}}^4 - T_{\text{surr}}^4\right) \qquad\qquad (4.6.12)$$

$$\text{conduction error:} \qquad E_c = \frac{T_{\text{gas}} - T_{\text{mount}}}{\cosh\left[L\sqrt{\dfrac{hA_c}{kA_k}}\right]} \qquad\qquad (4.6.13)$$

where $E_v =$ velocity error, °
$\alpha =$ recovery factor, —

$$V =$$ velocity, ft/sec

$$g_c =$$ universal gravitational constant

$$J =$$ Joules constant, ff/bf/Btu

$$c_p =$$ specific heat, Btu/lbm, °F

and $$E_r =$$ radiation error, °R

$$\sigma =$$ Stefan-Boltzmann constant

$$\varepsilon =$$ emissivity

$$h =$$ heat transfer coefficient, Btu/secft², °F

$$T_{sens} =$$ indicated temperature, °R

$$T_{surr} =$$ surrounding temperature, °R

$$E_c =$$ conduction error, °R

$$T_{gas} =$$ gas temperature, °R

$$T_{mount} =$$ mount temperature, °R

$$L =$$ length of exposed junction, ft

$$h =$$ heat transfer coefficient, Btu/secft², °F

$$A_c =$$ heat transfer area, ft²

$$k =$$ thermal conductivity, Btu/secft

$$A_k =$$ conduction area, ft²

Velocity error depends upon the recovery factor, which varies with the Prandtl number of the fluid. The Prandtl numbers of most liquids are greater than 1; hence, the recovery factor α is greater than 1 and probes tend to read higher than the stagnation temperature in high-speed liquid flows. With thermistors and RTDs in liquids, the self-heating effect and the velocity error both tend to cause high readings. In gases, where the Prandtl number is less than 1, the two effects are of opposite sign and may partly cancel each other.

Radiation and conduction errors vary inversely with the heat transfer coefficient. Both tend to be larger for larger-diameter probes since, all other factors remaining the same, the heat transfer coefficient will be lower for a large-diameter probe. This results in larger radiation and conduction errors. In liquids, radiation error is not a problem, but velocity error and conduction error may both be significant. Conduction error becomes a problem in liquid-temperature measurements when thermowells are used. The depth of immersion of the well is frequently too short to eliminate conduction error.

Steady-State Errors in Solid and Surface-Temperature Measurements

When probes are used to measure solid temperature by inserting them into a hole in the specimen, they are subject to conduction errors proportional to their size and conductivity. A general rule of thumb is to keep the insertion depth at least 20 times the diameter (or wall thickness) of the probe. This assumes a close-fitting hole, backfilled with a material with higher thermal conductivity than air. For more-exact advice regarding a specific installation, a careful thermal circuit analysis of the installation should be developed, and its results used to guide the selection of diametrical clearance, backfill materials, and penetration depth.

A thermocouple attached to a hot surface surrounded by cooler fluid will exchange heat with the fluid by convection and with the surrounding solids by radiation. Heat lost from the thermocouple must be made up from the surface by conduction, which will result in a cold spot at the point of attachment.

Figure 4.6.14 shows the system disturbance error caused by a surface-attached thermocouple, as a fraction of the maximum possible error for the installation. If the surface is irradiated (e.g., by heating lamps), the irradiation will raise the surface temperature, but will also affect the system disturbance error. The effect on the system disturbance error caused by turning on the irradiation is similar to that of raising the temperature of the surrounding fluid to a new value, $T_\infty°$,

where $T_{ind} =$ indicated temperature from an otherwise error-free thermocouple, °C

$$T_s =$$ undisturbed substrate temperature, °C
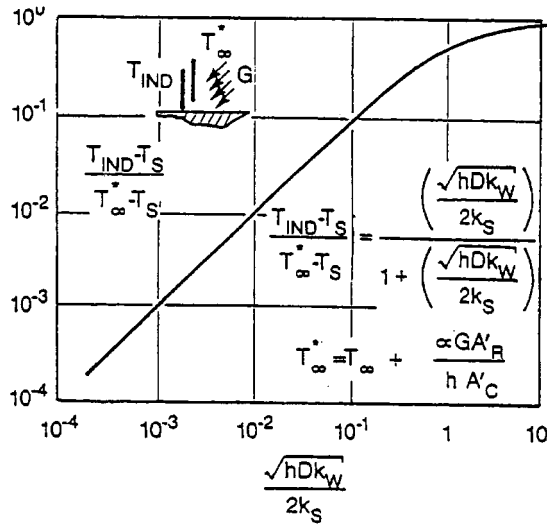
FIGURE 4.6.14 System disturbance errors caused by an attached thermocouple (worst case).

T_∞° = effective fluid temperature, °C

h = heat transfer coefficient, TC to fluid, W/m, °C

D = outside diameter of TC, m

k_w = effective thermal conductivity of TC, W/m, °C

k_s = thermal conductivity of substrate, W/m, °C

The effective gas temperature is defined in terms of the incident irradiation and the heat transfer coefficient as

$$T_\infty^* = T_\infty + \frac{\alpha G A_R}{h A_C} T_\infty^* \qquad (4.6.14)$$

where T_∞ = actual gas temperature, °C

α = absorptivity of the TC for thermal radiation

G = incident thermal radiation flux, W/m²

A_R/A_c = ratio of irradiated surface to convective surface

h = heat transfer coefficient between the TC and the gas, W/m°C

Steady-State Errors in Heat Flux Gauges for Convective Heat Transfer

If the gauge is not flush with the surface, it may disturb the flow, and if it is not at the same temperature as the surface, it will disturb the heat transfer. Thus, the gauge may properly report the heat flux which is present when the gauge is present, but that may be significantly different from the heat flux which would have been there if the gauge had not been there.

For planar gauges, both effects are usually small. The thermal resistance of such a gauge is generally small, and they are thin enough to avoid disturbing most flows. Circular foil gauges pose a more serious problem, since they are often cooled significantly below the temperature of the surrounding surface. Dropping the wall temperature at the gauge location can significantly increase the local heat load in two ways: one due to the fact that, for a given value of *h*, a cold spot receives a higher heat load from the gas stream. The second effect arises because the value of the heat transfer coefficient itself depends on the local wall temperature distribution: a local cold spot under a hot gas flow will experience a higher heat transfer coefficient than would have existed had the surface been of uniform temperature.

Evaluating the Heat Transfer Coefficient

The heat transfer coefficient is a defined quantity, given by

$$h = \frac{\dot{q}''_{conv}}{\left(T_o - T_{ref}\right)} \tag{4.6.15}$$

where h = heat transfer coefficient, W/m², °C
$\dot{q}''_{conv}$ = convective heat flux, W/m²
T_o = temperature of the considered surface, °C
T_{ref} = temperature used as reference for this definition, °C

Different reference temperatures are conventionally used for different situations:

- T_∞: The free-stream temperature. Used for isolated objects of uniform temperature in a uniform free stream, where an average value of h is desired which describes the overall heat transfer between the object and the flow. Also used in boundary layer heat transfer analyses where local values of h are needed to deal with locally varying conditions.
- T_m: The mixed mean fluid temperature. Used for internal flows where the intent of the calculation is to describe the changes in mixed mean fluid temperature (e.g., heat exchangers).
- $T_{adiabatic}$: The adiabatic surface temperature. Used for isolated objects or small regions of uniform temperature in either internal or external flows, where the overall thermal boundary conditions are neither uniform heat flux nor uniform temperature.

For a given data set, the value of the heat transfer coefficient will depend on the reference temperature chosen, and h should be subscripted to inform later users which reference was used: e.g., h_∞, h_m, or $h_{adiabatic}$.

Direct Methods

The two most commonly used methods for measuring the heat transfer coefficient are both derived from the same energy balance equation:

$$hA\left(T_o - T_{ref}\right) = \dot{e}_{in} + \dot{q}_{cond,in} + \dot{q}_{rad,in} - Mc\frac{dT}{d\tau} \tag{4.6.16}$$

where h = the heat transfer coefficient, W/m, °C
A = the area available for convective transport, m²
T_{ref} = the reference temperature used in defining h, °C
T_o = the average surface temperature over the area A, °C
$\dot{e}_{in}$ = externally provided input, W
$\dot{q}_{cond,in}$ = net energy conducted in, W
$\dot{q}_{rad,in}$ = net energy radiated in, W
$Mc\ dT/d\tau$ = rate of increase of thermal energy stored within the system, W

Steady State. In the steady-state method, the transient term is zero (or nearly so), and h is determined by measuring the input power and the operating temperature, and correcting for losses. Equation (4.6.16) can be applied to differentially small elements or to whole specimens. The considered region must be reasonably uniform in temperature, so the energy storage term and the convective heat transfer term use the same value.

For tests of isolated objects, or embedded calorimeter sections, steady-state tests usually use high-conductivity specimens (e.g., copper or aluminum) with embedded electric heaters. The resulting value of h is the average over the area of the specimen. The Biot number, hL/k, for the specimen should be low (on the order of 0.01 or less) if only one temperature sensor is used in the specimen, so the surface temperature can be determined from the embedded sensor.

If a single heated element is used within an array of unheated elements, the resulting heat transfer coefficient is implicitly defined as $h_{\mathrm{adiabatic}}$ and should be identified as such. Heat transfer coefficients measured with single-active-element tests cannot be used with the mixed mean fluid temperature.

When the variation of h over a surface is required, one common steady-state technique is to stretch a thin foil (stainless steel, or carbon impregnated paper, or gold deposited on polycarbonate) over an insulating substrate, and electrically heat the foil surface. Liquid crystals or infrared techniques can be used to map the surface temperature, from which the heat transfer coefficient distribution can be determined. The "heated foil with liquid crystal" approach was used by Cooper et al. in 1975 to measure heat transfer coefficients, and has since been used by many others. Hippensteele et al. (1985) have made extensive use of the foil technique in studies of gas turbine heat transfer. An example of their work on the end wall of a turbine cascade is shown in Figure 4.6.15.
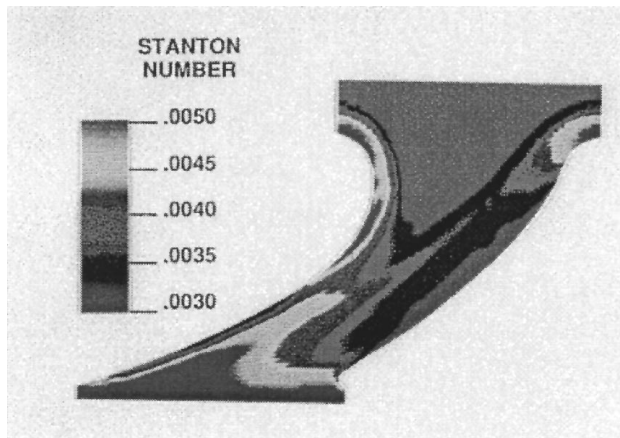
FIGURE 4.6.15 Heat transfer coefficient distribution on the end wall of a turbine cascade. (From Hippensteele, S.A. et al., NASA Technical Memorandum 86900, March, 1985. With permission.)

Hollingsworth et al. (1989) used a stainless steel foil heater for a study in air for an electronics cooling application, illustrated in Figure 4.6.16.
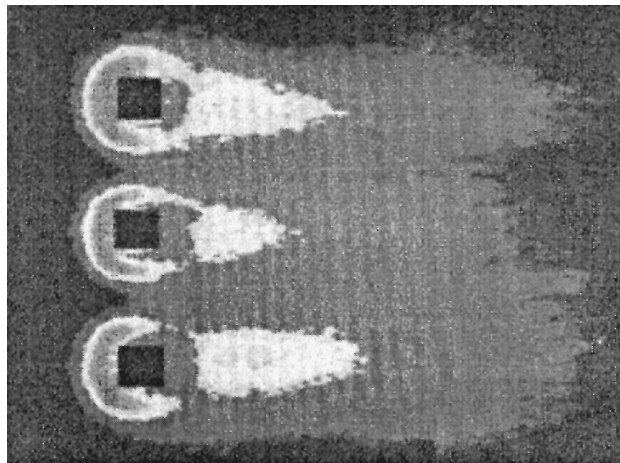
FIGURE 4.6.16 Visualization of the heat transfer coefficient distribution on a heated plate around three unheated cubes.

Another steady-state technique which reveals the distribution of *h* on the surface was introduced by den Ouden and Hoogendoorn (1974) and is currently in use by Meinders (1996). It uses a uniform and constant-temperature substrate (originally, a tank of warm water, now a copper block) covered with a layer of known thermal resistance (originally, a plate of glass, now a thin layer of epoxy). The surface was painted with liquid crystals (now visualized using infrared imaging) and the surface-temperature distribution determined. The inner (uniform) and outer (measured) temperature distributions are then used as boundary conditions to a three-dimensional conduction solver which calculates the total heat flux at each point on the surface. The total heat flux is corrected for radiation to yield the net convective transport at each point, from which *h* can be determined.

This method appears to have an advantage in accuracy over the heated foil technique because of the more accurate handling of substrate conduction.

Transient Lumped Parameter Systems. In the lumped parameter transient method, the specimen is assumed to be uniform in temperature at every instant through the transient. The power, $\dot{e}_{in}$, in Equation (4.6.16) is usually zero, although that is not necessary (one could simply change the power level at time zero to initiate the transient). At time zero, a transient is initiated, and the response curve recorded.

The data can be interpreted, and the validity of the first-order assumption tested at the same time by plotting $(T - T_{final})/(T_{initial} - T_{final})$ on the log scale of semilog coordinates, with time on the algebraic scale. If the line is straight, then the system is first order and the characteristic time can be determined from any two points on the line by

$$\tau = \frac{(t_2 - t_1)}{\ln\left\{\dfrac{T_{fin} - T_1}{T_{fin} - T_2}\right\}} \tag{4.6.17}$$

where τ =   characteristic time, *Mc/hA*, sec
      t_1 =   time at the first instant
      t_2 =   time at the second instant
      T_1 =   specimen temperature at the first instant, °C
      T_2 =   specimen temperature at the second instant, °C
      T_{fin} =   specimen temperature after a long time (fluid temperature), °C

The heat transfer coefficient is extracted from the time-constant definition.

Indirect Methods

An increasingly popular method is the extraction of *h* from surface-temperature variations after a step in flow temperature using an inverse calculation method (see the section on inferential methods of heat flux measurement). The simplest inverse method assumes one-dimensional conduction into an infinitely thick plate of constant material properties. Even highly irregular geometries can be studied with this technique, if the streamwise extent of the specimen is small and the testing time is short. A short time interval is necessary so the penetration of the thermal wave is limited to a thin layer near the surface. The short streamwise extent is necessary so the temperature response of the surface upstream does not alter the thermal step applied to the downstream surface. This technique has been used to determine the heat transfer coefficient distribution on the inside walls of passages of irregular shape, by making the passage in a transparent material.

Naphthalene Sublimination. The equations for mass diffusion are similar to those for heat transfer, except for replacing the Prandtl number in the heat transfer equation by the Schmidt number in the diffusion equation. Thus, one could expect that the distribution of the mass transfer coefficients on a surface would mimic the distribution of the heat transfer coefficients.

The most commonly used analog technique is naphthalene sublimination. As early as 1940, the mass transfer/heat transfer similarity was used to estimate the heat transfer coefficient distribution. Naphthalene

is a solid material which sublimes at a reasonable rate in air at ambient temperature. Specimens can be cast in naphthalene with good precision, and the recession of the surface mapped as a function of position and time using automated or semiautomated measuring equipment. The surface recession over a known interval of time is a measure of the mass transfer rate, from which the mass transfer coefficient can be deduced.

Naphthalene experiments are generally done at uniform temperature; hence, a uniform vapor pressure exists at the surface. This corresponds to the heat transfer situation of heat transfer from a uniform temperature surface. No counterpart of the uniform heat flux situation has been produced using naphthalene, nor have there been experiments corresponding to variable wall temperature.

Naphthalene sublimation experiments do not suffer from any counterpart of the conduction heat transfer in the substrate. Conduction makes it difficult to work near discontinuities in wall temperature in a heat transfer experiment. Details of the fine structure of mass transfer near obstructions and discontinuities can be resolved in naphthalene experiments, but those details might not exist in a heat transfer process. The Prandtl number of air is much lower than the Schmidt number of naphthalene diffusing in air; hence, thermal conduction would tend to blur out sharp gradients in the temperature field more than diffusion would blur out gradients in naphthalene concentration.

The Schmidt number of naphthalene in air is about 2.5, far different than the Prandtl number of air (0.71); hence, the mass transfer coefficient deduced from a naphthalene experiment is not numerically equal to the heat transfer coefficient which would have existed at those conditions. The usual recommendation is to adjust for the Prandtl number of Schmidt number using a relation of the form:

$$\text{St}\,\text{Pr}^{2/3} = f\{\text{Re}\} = \text{Sh}_j\text{Sc}_j^{2/3} \tag{4.6.18}$$

based on laminar results. That recommendation has not been seriously tested by experiments in turbulent and separated flows. By using nominal values of the Schmidt number and Prandtl number, the heat transfer Stanton number would be 2.3 times higher than the measured Sherwood number and an uncertainty of 10% in that ratio would alter the inferred heat transfer coefficient by 23%.

System Performance Matching. Sometimes the "effective average heat transfer coefficient" for a system is inferred from the overall behavior of the system, e.g., estimating *h* from the effectiveness of a heat exchanger. Values deduced by this means cannot be expected to agree well with direct measurements unless a very sophisticated system description model is used.

References

Moffat, R.J., The gradient approach to thermocouple circuitry, *Temperature, Its Measurement and Control in Science and Industry*, Rienhold, New York, 1962.

Steinhart, J.S. and Hart, S.R., Calibration curves for thermistors, *Deep Sea Res.*, 15, 497, 1968.

Rhee, H.S., Koseff, J.R., and Street, R.L., Flow visualization of a recirculating flow by rheoscopic liquid and liquid crystal techniques, *Exp. Fluids*, 2, 57–64, 1984.

Hollingsworth, K., Boehman, A.L., Smith, E.G., and Moffat, R.J., Measurement of temperature and heat transfer coefficient distributions in a complex flow using liquid crystal thermography and true-color image processing, in *Coll. Pap. Heat Transfer, ASME HTD*, 123, 35–42, Winter Annual Meeting, 1989.

Cooper, T.E., Field, R.J., and Meyer, J.F., Liquid crystal thermography and its application to the study of convective heat transfer, *J. Heat Transfer*, 97, 442–450, 1975.

Hippensteele, S.A., Russell, L.M., and Torres, F.J., Local Heat Transfer Measurements on a Large Scale Model Turbine Blade Airfoil Using a Composite of a Heater Element and Liquid Crystals, NASA Technical Memorandum 86900, March 1985.

den Ouden, C. and Hoogendoorn, C.J., Local convective heat transfer coefficients for jets impinging on a plate: experiments using a liquid crystal technique, in *Proc. of the 5th Int. Heat Transfer Conf.,* Vol. 5, AIChE, New York, 1974, 293–297.

Personal Communication from Erwin Meinders, March 1996. Work in progress at the Technical University of Delft under Prof. Hanjalic.

Akino, N. and Kunugi, T., *ASME HTD,* Vol. 112, 1989.

4.7   Mass Transfer

Anthony F. Mills

Introduction

Mass transfer may occur in a gas mixture, a liquid solution, or a solid solution. There are several physical mechanisms that can transport a chemical species through a phase and transfer it across phase boundaries. The two most important mechanisms are ordinary diffusion and convection. Mass diffusion is analogous to heat conduction and occurs whenever there is a gradient in the concentration of a species. Mass convection is essentially identical to heat convection: a fluid flow that transports heat may also transport a chemical species. The similarity of mechanisms of heat transfer and mass transfer results in the mathematics often being identical, a fact that can be exploited to advantage. But there are some significant differences between the subjects of heat and mass transfer. One difference is the much greater variety of physical and chemical processes that require mass transfer analysis. Another difference is the extent to which the essential details of a given process may depend on the particular chemical system involved, and on temperature and pressure.

   In the next subsection, concentrations, velocities, and fluxes are defined, and special attention is paid to phase interfaces where the concentration of a chemical species is almost always discontinuous. Fick's law of ordinary diffusion is introduced in the third section, where other diffusion phenomena are also discussed. The fourth section presents various forms of the species conservation equation. Results for diffusion in a stationary medium are given in the fifth section, and include steady diffusion across a plane wall, transient diffusion in a semi-infinite solid, and diffusion in a porous catalyst. Results for diffusion in a moving medium are given in the sixth section, and the Stefan flow is introduced for diffusion with one component stationary. Also considered are particle combustion, droplet evaporation, and combustion of a volatile liquid hydrocarbon fuel droplet. The last section deals with mass convection. Low mass transfer rate theory is presented and how to exploit the analogy between convective heat and mass transfer is shown. Particular attention is given to situations involving simultaneous heat and mass transfer associated with evaporation or condensation. The section closes by presenting high mass transfer rate theory for convection, and gives engineering calculation methods for boundary layer flows that account for variable property effects.

Concentrations, Velocities, and Fluxes

Definitions of Concentrations

In a gas mixture, or liquid or solid solution, the local *concentration* of a mass species can be expressed in a number of ways. The *number density* of species i in a mixture or solution of n species is defined as

$$\text{Number density of species } i \equiv \text{Number of molecules of } i \text{ per unit volume}$$
$$\equiv \mathcal{N}_i \text{ molecules}/\text{m}^3 \tag{4.7.1}$$

Alternatively, if the total number of molecules of all species per unit volume is denoted as $\mathcal{N}$, then we define the *number fraction* of species i as

$$n_i \equiv \frac{\mathcal{N}_i}{\mathcal{N}}; \qquad \mathcal{N} = \sum \mathcal{N}_i \tag{4.7.2}$$

where the summation is over all species present, $i = 1,2,\ldots,n$. Equations (4.7.1) and (4.7.2) describe *microscopic* concepts and are used, for example, when the kinetic theory of gases is used to describe transfer processes.

Whenever possible, it is more convenient to treat matter as a continuum. Then the smallest volume considered is sufficiently large for macroscopic properties such as pressure and temperature to have their usual meanings. For this purpose we also require *macroscopic* definitions of concentration. First, on a mass basis,

$$\textit{Mass concentration of species } i \equiv \text{partial density of species } i$$
$$\equiv \rho_i \; kg/m^3 \tag{4.7.3}$$

The total mass concentration is the total mass per unit volume, that is, the density $\rho = \Sigma\rho_i$. The *mass fraction* of species i is defined as

$$m_i = \frac{\rho_i}{\rho} \tag{4.7.4}$$

Second, on a molar basis,

$$\textit{Molar concentration of species } i \equiv \text{number of moles of } i \text{ per unit volume}$$
$$\equiv c_i \; kmol/m^3 \tag{4.7.5}$$

If M_i (kg/kmol) is the molecular weight of species i, then

$$c_i = \frac{\rho_i}{M_i} \tag{4.7.6}$$

The total molar concentration is the molar density $c = \Sigma c_i$. The *mole fraction* of species i is defined as

$$x_i \equiv \frac{c_i}{c} \tag{4.7.7}$$

A number of important relations follow directly from these definitions. The mean molecular weight of the mixture of solution is denoted M and may be expressed as

$$M = \frac{\rho}{c} = \sum x_i M_i \tag{4.7.8a}$$

or

$$\frac{1}{M} = \sum \frac{m_i}{M_i} \tag{4.7.8b}$$

There are summation rules

$$\sum m_i = 1 \tag{4.7.9a}$$

$$\sum x_i = 1 \tag{4.7.9b}$$

It is often necessary to have the mass fraction of species i expressed explicitly in terms of mole fractions and molecular weights; this relation is

$$m_i = \frac{x_i M_i}{\sum_i x_j M_j} = x_i \frac{M_i}{M} \tag{4.7.10a}$$

and the corresponding relation for the mole fraction is

$$x_i = \frac{m_i / M_i}{\sum_i m_j / M_j} = m_i \frac{M}{M_i} \tag{4.7.10b}$$

Dalton's law of partial pressures for an ideal gas mixture states that

$$P = \sum_i P_i, \quad \text{where} \quad P_i = \rho_i R_i T \tag{4.7.11}$$

Dividing partial pressure by total pressure and substituting $R_i = \mathcal{R}/M_i$ gives

$$\frac{P_i}{P} = \frac{\rho_i}{M_i} \frac{\mathcal{R} T}{P} = c_i \frac{\mathcal{R} T}{P} = x_i \frac{c\mathcal{R} T}{P} = x_i \tag{4.7.12}$$

Thus, for an ideal gas mixture, the mole fraction and partial pressure are equivalent measures of concentration (as also is the number fraction).

A commonly used specification of the composition of dry air is 78.1% N_2, 20.9% O_2, and 0.9% Ar, by volume. (The next largest component is CO_2, at 0.3%.) Since equal volumes of gases contain the same number of moles, specifying composition on a volume basis is equivalent to specifying mole fractions, namely,

$$x_{N_2} = 0.781; \qquad x_{O_2} = 0.209; \qquad x_{Ar} = 0.009$$

The corresponding mass fractions are calculated to be

$$m_{N_2} = 0.755; \qquad m_{O_2} = 0.231; \qquad m_{Ar} = 0.014$$

Concentrations at Interfaces

Although temperature is continuous across a phase interface, concentrations are usually discontinuous. In order to define clearly concentrations at interfaces, we introduce imaginary surfaces, denoted u and s, on both sides of the real interface, each indefinitely close to the interface, as shown in Figure 4.7.1 for water evaporating into an airstream. Thus, the liquid-phase quantities at the interface are subscripted u, and gas-phase quantities are subscripted s. If we ignore the small amount of air dissolved in the water, $x_{H_2O,u} = 1$. Notice that the subscript preceding the comma denotes the chemical species, and the subscript following the comma denotes location. To determine $x_{H_2O,s}$ we make use of the fact that, except in extreme circumstances, the water vapor and air mixture at the s-surface must be in thermodynamic equilibrium with water at the u-surface. Equilibrium data for this system are found in conventional steam tables: the saturation vapor pressure of steam at the water temperature, T_s, ($T_s = T_u$), is the required partial pressure $P_{H_2O,s}$. With the total pressure P known, $x_{H_2O,s}$ is calculated as $P_{H_2O,s}/P$. If $m_{H_2O,s}$ is required, Equation (4.7.10a) is used.
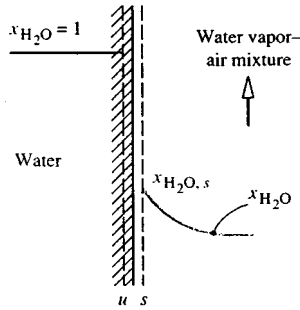
FIGURE 4.7.1 Concentrations at a water-air interface.

For example, at T_s = 320 K, the saturation vapor pressure is obtained from steam tables as 0.10535 × 10⁵ Pa. If the total pressure is 1 atm = 1.0133 × 10⁵,

$$x_{H_2O,s} = \frac{0.10535 \times 10^5}{1.0133 \times 10^5} = 0.1040$$

$$m_{H_2O,s} = \frac{(0.1040)(18)}{(0.1040)(18) + (1 - 0.1040)(29)} = 0.06720$$

For a gas or solid dissolving in a liquid, equilibrium data are often referred to simply as solubility data, found in chemistry handbooks. Many gases are only sparingly soluble, and for such dilute solutions solubility data are conveniently represented by *Henry's law*, which states that the mole fraction of the gas at the *s*-surface is proportional to its mole fraction in solution at the *u*-surface, the constant of proportionality being the *Henry number*, He. For species *i*,

$$x_{i,s} = \text{He}_i x_{i,u} \tag{4.7.13}$$

The Henry number is inversely proportional to total pressure and is also a function of temperature. The product of Henry number and total pressure is the *Henry constant*, C_{He}, and for a given species is a function of temperature only:

$$\text{He}_i P = C_{He_i}(T) \tag{4.7.14}$$

Solubility data are given in Table 4.7.1.

TABLE 4.7.1   Henry Constants C_{He} for Dilute Aqueous Solutions at Moderate Pressures ($P_{i,s}/x_{i,u}$ in atm, or in bar = 10⁵ Pa, within the accuracy of the data).

Solute	290 K	300 K	310 K	320 K	330 K	340 K
H_2S	440	560	700	830	980	1,140
CO_2	1,280	1,710	2,170	2,720	3,220	—
O_2	38,000	45,000	52,000	57,000	61,000	65,000
H_2	67,000	72,000	75,000	76,000	77,000	76,000
CO	51,000	60,000	67,000	74,000	80,000	84,000
Air	62,000	74,000	84,000	92,000	99,000	104,000
N_2	16,000	89,000	101,000	110,000	118,000	124,000

For example, consider absorption of carbon dioxide from a stream of pure CO_2 at 2 bar pressure into water at 310 K. From Table 4.7.1, $C_{He} = 2170$ bar; thus

$$\text{He}_{CO_2} = \frac{2170}{2} = 1085; \qquad x_{CO_{2,u}} = \frac{1}{1085} = 9.22 \times 10^{-4}$$

Dissolution of gases into metals is characterized by varied and rather complex interface conditions. Provided temperatures are sufficiently high, hydrogen dissolution is reversible (similar to CO_2 absorption into water); hence, for example, titanium-hydrogen solutions can exist only in contact with a gaseous hydrogen atmosphere. As a result of hydrogen going into solution in atomic form, there is a characteristic square root relation

$$m_{H_2,u} \alpha P_{H_2,s}^{1/2}$$

The constant of proportionality is strongly dependent on temperature, as well as on the particular titanium alloy: for Ti-6Al-4V alloy it is twice that for pure titanium. In contrast to hydrogen, oxygen dissolution in titanium is irreversible and is complicated by the simultaneous formation of a rutile (TiO_2) scale on the surface. Provided some oxygen is present in the gas phase, the titanium-oxygen *phase diagram* (found in a metallurgy handbook) shows that $m_{O_2,u}$ in alpha-titanium is 0.143, a value essentially independent of temperature and O_2 partial pressure. Dissolution of oxygen in zirconium alloys has similar characteristics to those discussed above for titanium.

All the preceding examples of interface concentrations are situations where thermodynamic equilibrium can be assumed to exist at the interface. Sometimes thermodynamic equilibrium does not exist at an interface: a very common example is when a chemical reaction occurs at the interface, and temperatures are not high enough for equilibrium to be attained. Then the concentrations of the reactants and products at the *s*-surface are dependent both on the rate at which the reaction proceeds — that is, the *chemical kinetics* — as well as on mass transfer considerations.

Definitions of Fluxes and Velocities

The mass (or molar) flux of species i is a vector quantity giving the mass (or moles) of species i that pass per unit time through a unit area perpendicular to the vector (Figure 4.7.2). We denote the absolute mass and molar fluxes of species i, that is, relative to stationary coordinate axes, as n_i (kg/m²sec) and N_i (kmol/m²sec), respectively. The absolute mass flux of the mixture (mass velocity) is

$$n = \sum n_i \tag{4.7.15}$$

and the local mass-average velocity is
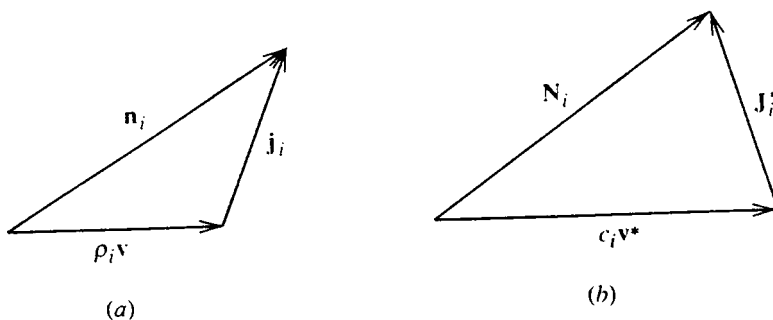
FIGURE 4.7.2 Flux vectors: (a) mass basis, (b) molar basis.

$$v = \frac{n}{\rho} \, \text{m/sec} \tag{4.7.16}$$

The velocity v is the velocity that would be measure by a Pitot tube and corresponds to the velocity used in considering pure fluids. On a molar basis, the absolute molar flux of the mixture is

$$N = \sum N_i \tag{4.7.17}$$

and the local molar-average velocity is

$$v^* = \frac{N}{c} \, \text{m/sec} \tag{4.7.18}$$

The absolute fluxes at species i have two components. On a mass basis we write

$$n_i = \rho_i v + j_i \tag{4.7.19}$$

where $\rho_i n$ is transport of species i by bulk motion of the fluid at velocity v and is the *convective* component. Thus, j_i is transport of species i relative to the mass average velocity; it is called the *diffusive* component because most commonly it is due to ordinary (concentration) diffusion of the species. On a molar basis the corresponding relation is

$$N_i = c_i v^* + J_i^* \tag{4.7.20}$$

Some important relations follow from these definitions:

$$\sum j_i = \sum J_i^* = 0 \tag{4.7.21}$$

$$N_i = \frac{n_i}{M_i} \tag{4.7.22}$$

$$n_i = \rho_i v + j_i = m_i \sum n_i + j_i \tag{4.7.23a}$$

$$N_i = c_i v^* + J_i^* = x_i \sum N_i + J_i^* \tag{4.7.23b}$$

Mechanisms of Diffusion

Ordinary Diffusion

Fick's law of ordinary diffusion is a linear relation between the rate of diffusion of a chemical species and the local concentration gradient of that species. It is exact for a binary gas mixture, for which the kinetic theory of gases gives

$$j_1 = -\rho \mathcal{D}_{12} \nabla m_1 \, \text{kg/m}^2 \, \text{sec} \tag{4.7.24a}$$

on a mass basis, and

$$\boldsymbol{J}_1^* = -c\mathcal{D}_{12}\nabla x_1 \text{ kg/m}^2 \text{ sec} \tag{4.7.24b}$$

on a molar basis; $\mathcal{D}_{12}$ (m²/sec) is the binary diffusion coefficient (or mass diffusivity), and $\mathcal{D}_{21} = \mathcal{D}_{21}$. Equations (4.7.24a) and (4.7.24b) are mathematically equivalent; however, notice that it is incorrect to write

$$\boldsymbol{j}_i = -\mathcal{D}_{12}\nabla\rho_1 \tag{4.7.25}$$

since $\nabla\rho_1 \neq \rho \nabla m_1$ in general. Fick's law in the form of Equations (4.7.24a) and (4.7.24b) is also valid for dilute liquid and solid solutions, for which it is often possible to assume ρ (or c) constant, and then Equation (4.7.25) or its molar equivalent are good approximations.

Ordinary diffusion in multicomponent systems is described by the Stefan–Maxwell equations (Hirschfelder et al., 1954). These equations are difficult to use for engineering analysis. In gas mixtures containing species that do not have widely varying molecular weights, it is possible to model approximately the diffusion process by using an effective binary diffusion coefficient in Fick's law. This coefficient is a suitable average over the species in the mixture, and may be calculated from

$$\mathcal{D}_{1m} = \frac{\left(1 - x_1\right)}{\displaystyle\sum_{i=2}^{n}\left(x_i/\mathcal{D}_{1i}\right)}; \qquad x_1 \ll 1 \tag{4.7.26}$$

This equation works well for most mixtures of combustion gases (except those containing appreciable concentrations of H or H_2).

Binary diffusion coefficients at 300 K are of the order of 10^{-5} m²/sec in gases at 1 atm, 10^{-9} m²/sec in aqueous solutions, and 10^{-10} to 10^{-13} m²/sec in solids. However, the product $\rho\mathcal{D}$ or $(c\mathcal{D})$ is, at most, one order of magnitude different for gases and liquids. Data for diffusion coefficients may be found in Tables 4.7.2 through 4.7.5.

Molecules in a gas mixture, and in a liquid or solid solution, can diffuse by mechanisms other than ordinary diffusion governed by Fick's law. *Thermal diffusion* is diffusion due to a temperature gradient and is often called the *Soret effect*. Thermal diffusion is usually negligible compared with ordinary diffusion, unless the temperature gradient is very large. However, there are some important processes that depend on thermal diffusion, the most well known being the large-scale separation of uranium isotopes. *Pressure diffusion* is diffusion due to a pressure gradient and is also usually negligible unless the pressure gradient is very large. Pressure diffusion is the principle underlying the operation of a centrifuge. Centrifuges are used to separate liquid solutions and are increasingly being used to separate gaseous isotopes as well. *Forced diffusion* results from an external force field acting on a molecule. Gravitational force fields do not cause separation since the force per unit mass of a molecule is constant. Forced diffusion occurs when an electrical field is imposed on an electrolyte (for example, in charging an automobile battery), on a semiconductor, or on an ionized gas (for example, in a neon tube or metal-ion laser). Depending on the strength of the electric field, rates of forced diffusion can be very large.

Some interesting diffusion phenomena occur in porous solids. When a gas mixture is in a porous solid, such as a catalyst pellet or silica–gel particle, the pores can be smaller than the mean free path of the molecules. Then, the molecules collide with the wall more often than with other molecules. In the limit of negligible molecule collisions we have *Knudsen diffusion*, also called *free molecule flow* in the fluid mechanics literature. If the pore size approaches the size of a molecule, then Knudsen diffusion becomes negligible and *surface diffusion*, in which adsorbed molecules move along the pore walls, becomes the dominant diffusion mechanism.

TABLE 4.7.2   Diffusion Coefficients in Air at 1 atm (1.013×10^5 Pa)[a]

T(K)	Binary Diffusion Coefficient (m²/sec $\times 10^4$)							
	O_2	CO_2	CO	C_7H_6	H_2	NO	SO_2	He
200	0.095	0.074	0.098	0.036	0.375	0.088	0.058	0.363
300	0.188	0.157	0.202	0.075	0.777	0.180	0.126	0.713
400	0.325	0.263	0.332	0.128	1.25	0.303	0.214	1.14
500	0.475	0.385	0.485	0.194	1.71	0.443	0.326	1.66
600	0.646	0.537	0.659	0.270	2.44	0.603	0.440	2.26
700	0.838	0.684	0.854	0.364	3.17	0.782	0.576	2.91
800	1.05	0.857	1.06	0.442	3.93	0.978	0.724	3.64
900	1.26	1.05	1.28	0.538	4.77	1.18	0.887	4.42
1000	1.52	1.24	1.54	0.641	5.69	1.41	1.060	5.26
1200	2.06	1.69	2.09	0.881	7.77	1.92	1.440	7.12
1400	2.66	2.17	2.70	1.13	9.90	2.45	1.870	9.20
1600	3.32	2.75	3.37	1.41	12.5	3.04	2.340	11.5
1800	4.03	3.28	4.10	1.72	15.2	3.70	2.850	13.9
2000	4.80	3.94	4.87	2.06	18.0	4.48	3.360	16.6

[a]   Owing to the practical importance of water vapor-air mixtures, engineers have used convenient empirical formulas for $\mathscr{D}_{H_2O\ air}$. A formula that has been widely used for many years is

$$\mathscr{D}_{H_2O\ air} = 1.97 \times 10^{-5} \left(\frac{P_0}{P} \right) \left(\frac{T}{T_0} \right)^{1.685} \quad m^2 / sec; \quad 273\ K < T < 373\ K$$

where $P_0 = 1$ atm; $T_0 = 256$ K. More recently, the following formula has found increasing use. (Marrero, T.R. and Mason, E.A. 1992. Gaseous diffusion coefficients, *J. Phys. Chem. Ref. Data*, 1, 3–118):

$$\mathscr{D}_{H_2O\ air} = 1.87 \times 10^{-10} \frac{T^{2.072}}{P}; \quad 280\ K < T < 450\ K$$

$$= 2.75 \times 10^{-9} \frac{T^{1.632}}{P}; \quad 450\ K < T < 1070\ K$$

for P in atmospheres and T in kelvins. Over the temperature range 290 to 330 K, the discrepancy between the two formulas is less than 2.5%. For small concentrations of water vapor in air, the older formula gives a constant value of $Sc_{H_2O\ air} = 0.61$ over the temperature range 273 to 373 K. On the other hand, the Marrero and Mason formula gives values of $Sc_{H_2O\ air}$ that vary from 0.63 at 280 K to 0.57 at 373 K.

Very small particles of 10^{-3} to 10^{-1} μm size — for example, smoke, soot, and mist — behave much like large molecules. Ordinary diffusion of such particles is called *Brownian motion* and is described in most elementary physics texts. Diffusion of particles due to a temperature gradient is called *thermophoresis* and plays an important role for larger particles, typically in the size range 10^{-1} to 1 μm. Diffusion of particles in a gas mixture due to concentration gradients of molecular species is called *diffusiophoresis*. *Forced diffusion* of a charged particle in an electrical field is similar to that for an ionized molecular species. Thermal and electrostatic precipitators are used to remove particles from power plant and incinerator stack gases, and depend on thermophoresis and forced diffusion, respectively, for their operation. Diffusion phenomena are unimportant for particles of size greater than about 1 μm in air at 1 atm; the motion of such particles is governed by the laws of Newtonian mechanics. Transport of particles is dealt with in the *aerosol science* literature.

Species Conservation Equation

The principle of conservation of a chemical species is used to derive the *species conservation equation.* On a mass basis this equation is

TABLE 4.7.3   Schmidt Number for Vapors in Dilute Mixture in Air at Normal Temperature, Enthalpy of Vaporization, and Boiling Point at 1 atm[a]

Vapor	Chemical Formula	Sc[b]	h_{fg}, J/kg × 10⁻⁶	T_{BP}, K
Acetone	CH_3COCH_3	1.42	0.527	329
Ammonia	NH_3	0.61	1.370	240
Benzene	C_6H_6	1.79	0.395	354
Carbon dioxide	CO_2	1.00	0.398	194
Carbon monoxide	CO	0.77	0.217	81
Chlorine	Cl_2	1.42	0.288	238
Ethanol	CH_3CH_2OH	1.32	0.854	352
Helium	He	0.22	—	4.3
Heptane	C_7H_{16}	2.0	0.340	372
Hydrogen	H_2	0.20	0.454	20.3
Hydrogen sulfide	H_2S	0.94	0.548	213
Methanol	CH_3OH	0.98	1.110	338
Naphthalene	$C_{10}H_8$	2.35[c]	—	491
Nitric oxide	NO	0.87	0.465	121
Octane	C_8H_{18}	2.66	0.303	399
Oxygen	O_2	0.83	0.214	90.6
Pentane	C_5H_{12}	1.49	0.357	309
Sulfur dioxide	SO_2	1.24	0.398	263
Water vapor	H_2O	0.61	2.257	373

[a]   With the Clausius-Clapeyron relation, one may estimate vapor pressure as

$$P_{sat} \simeq \exp\left\{-\frac{Mh_{fg}}{\mathcal{R}}\left(\frac{1}{T} - \frac{1}{T_{BP}}\right)\right\} \text{ atm } \text{ for } T \sim T_{BP}$$

[b]   The Schmidt number is defined as Sc = $\mu/\rho\mathcal{D}$ = $\nu/\mathcal{D}$. Since the vapors are in small concentrations, values for μ, ρ, and ν can be taken as pure air values.

[c]   From a recent study by Cho, C., Irvine, T.F., Jr., and Karni, J. 1992. Measurement of the diffusion coefficient of naphthalene into air, *Int. J. Heat Mass Transfer*, 35, 957–966. Also, h_{sg} = 0.567 × 10⁶ J/kg at 300 K.

$$\frac{\partial \rho_i}{\partial t} + \nabla \cdot \boldsymbol{n}_i = \dot{r}_i''' \tag{4.7.27}$$

and on a molar basis

$$\frac{\partial c_i}{\partial t} + \nabla \cdot \boldsymbol{N}_i = \dot{R}_i''' \tag{4.7.28}$$

where $\dot{r}_i'''$ and $\dot{R}_i'''$ are the mass and molar rates of production of species i due to chemical reactions. Summing Equation 4.7.27 over all species gives the mass conservation or continuity equation,

$$\frac{\partial \rho}{\partial t} + \nabla \cdot \rho \boldsymbol{v} = 0 \tag{4.7.29}$$

The molar form is

$$\frac{\partial c}{\partial t} + \nabla \cdot c\boldsymbol{v}^* = \sum_i \dot{R}_i''' \tag{4.7.30}$$

since, in general, moles are not conserved in chemical reactions. A useful alternative form to Equation 4.7.27 can be obtained using Equations (4.7.23a) and (4.7.29) and is

TABLE 4.7.4   Schmidt Numbers for Dilute Solution in Water at 300 K[a]

Solute	Sc	M
Helium	120	4.003
Hydrogen	190	2.016
Nitrogen	280	28.02
Water	340	18.016
Nitric oxide	350	30.01
Carbon monoxide	360	28.01
Oxygen	400	32.00
Ammonia	410	17.03
Carbon dioxide	420	44.01
Hydrogen sulfide	430	34.08
Ethylene	450	28.05
Methane	490	16.04
Nitrous oxide	490	44.02
Sulfur dioxide	520	64.06
Sodium chloride	540	58.45
Sodium hydroxide	490	40.00
Acetic acid	620	60.05
Acetone	630	58.08
Methanol	640	32.04
Ethanol	640	46.07
Chlorine	670	70.90
Benzene	720	78.11
Ethylene glycol	720	62.07
n-Propanol	730	60.09
i-Propanol	730	60.09
Propane	750	44.09
Aniline	800	93.13
Benzoic acid	830	122.12
Glycerol	1040	92.09
Sucrose	1670	342.3

[a] Schmidt number $Sc = \mu/\rho\mathcal{D}$; since the solutions are dilute, μ and ρ can be taken as pure water values. For other temperatures use $Sc/Sc_{300\,K} \simeq (\mu^2/\rho T)/(\mu^2\rho T)_{300\,K}$, where μ and ρ are for water, and T is absolute temperature. For chemically similar solutes of different molecular weights use $Sc_2/Sc_1 \simeq (M_2/M_1)^{0.4}$. A table of $(\mu^2/\rho T)/(\mu^2\rho T)_{300\,K}$ for water follows.

T(K)	$(\mu^2/\rho T)/(\mu^2/\rho T)_{300\,K}$
290	1.66
300	1.00
310	0.623
320	0.429
330	0.296
340	0.221
350	0.167
360	0.123
370	0.097

From Spalding, D.B. 1963. *Convective Mass Transfer*, McGraw-Hill, New York. With permission.

$$\rho\frac{Dm_i}{Dt} = \nabla \cdot \boldsymbol{j}_i + \dot{r}_i''' \tag{4.7.31}$$

where *D/Dt* is the substantial derivative operator.

If we consider a binary system of species 1 and 2 and introduce Fick's law, Equation (4.7.24a) into Equation (4.7.31), then

TABLE 4.7.5 Diffusion Coefficients in Solids, $\mathcal{D} = \mathcal{D}_o \exp(-E_a/\mathcal{R}T)$

System	$\mathcal{D}_o$, m²/sec	E_a, kJ/kmol
Oxygen-Pyrex glass	6.19×10^{-8}	4.69×10^4
Oxygen-fused silica glass	2.61×10^{-9}	3.77×10^4
Oxygen-titanium	5.0×10^{-3}	2.13×10^5
Oxygen-titanium alloy (Ti-6Al-4V)	5.82×10^{-2}	2.59×10^5
Oxygen-zirconium	4.68×10^{-5}	7.06×10^5
Hydrogen-iron	7.60×10^{-8}	5.60×10^3
Hydrogen-α-titanium	1.80×10^{-6}	5.18×10^4
Hydrogen-β-titanium	1.95×10^{-7}	2.78×10^4
Hydrogen-zirconium	1.09×10^{-7}	4.81×10^4
Hydrogen-Zircaloy^{-4}	1.27×10^{-5}	6.05×10^5
Deuterium-Pyrex glass	6.19×10^{-8}	4.69×10^4
Deuterium-fused silica glass	2.61×10^{-9}	3.77×10^4
Helium-Pyrex glass	4.76×10^{-8}	2.72×10^4
Helium-fused silica glass	5.29×10^{-8}	2.55×10^4
Helium-borosilicate glass	1.94×10^{-9}	2.34×10^4
Neon-borosilicate glass	1.02×10^{-10}	3.77×10^4
Carbon-FCC iron	2.3×10^{-5}	1.378×10^5
Carbon-BCC iron	1.1×10^{-6}	8.75×10^4

Various sources.

$$\rho \frac{Dm_i}{Dt} = \nabla \cdot \left(\rho \mathcal{D}_{12} \nabla m_1 \right) + \dot{r}_1''' \qquad (4.7.32)$$

When working on a mass basis we define a stationary medium as one in which the mass average velocity v is zero everywhere. Substituting in Equation (4.7.32) with no chemical reactions and assuming constant properties,

$$\frac{\partial m_1}{\partial t} = \mathcal{D}_{12} \nabla^2 m_1 \qquad (4.7.33)$$

which is the *diffusion* equation, and is the mass transfer analog to Fourier's equation for heat conduction. For steady diffusion, Equation (4.7.33) reduces to Laplace's equation

$$\nabla^2 m_1 = 0 \qquad (4.7.34)$$

Notice that since properties have been assumed constant, any measure of concentration can be used in Equations (4.7.33) and (4.7.34), for example ρ_1, c_1, and x_1.

Diffusion in a Stationary Medium

Many problems involving diffusion in a stationary medium are governed by the diffusion equation (Equation 4.7.33). Often solutions may be obtained from their heat conduction analogs. Some important cases follow.

Steady Diffusion through a Plane Wall

The mass flow of species 1 across a plane wall of thickness L and cross-sectional area A is

$$\dot{m}_1 = \frac{\rho \mathcal{D}_{12} A}{L} \left(m_{1,u} - m_{1,u'} \right) \text{kg/m}^2 \text{ sec} \qquad (4.7.35)$$
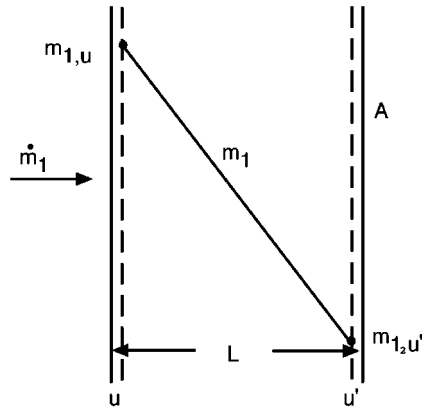
FIGURE 4.7.3 Steady diffusion across a plane wall.

where the u- and u'-surfaces are shown in Figure 4.7.3. Solubility data are required to relate the u- and u'-surface concentrations to s- and s'-surface concentrations. Alternatively for systems that obey Henry's law, a solubility $\mathscr{S}$ can be defined as the volume of solute gas (at STP of 0°C and 1 atm) dissolved in unit volume when the gas is at a partial pressure of 1 atm. Then, defining permeability $\mathscr{P}_{12}$ as the product $\mathscr{D}_{12}\mathscr{S}$, the volume flow of species 1 is

$$\dot{V}_1 = \frac{\mathscr{P}_{12}A}{L}\left(P_{1,s} - P_{1,s'}\right) \text{ m}^3 \text{ (STP)/sec} \tag{4.7.36}$$

where the partial pressures P_1 are in atmospheres. The SI units for permeability are m³ (STP)/m²sec(atm/m). Permeability and solubility data are given in Table 4.7.6. For example, consider helium at 10^5 Pa contained in a 7056-glass vessel with a 1-mm-thick wall at 680 K. For a surface area of 0.01 m², the leakage rate into ambient air is

$$\dot{V} = \frac{\left(1.0 \times 10^{-12}\right)(0.01)}{(0.001)}\left(10^5 - 0\right) = 1.0 \times 10^{-6} \text{ m}^3 \text{ (STP)/sec}$$

where the value $\mathscr{P}_{12}$ was obtained from Table 4.7.6.

In general, mass fractions are discontinuous across phase interfaces. Hence, Equation (4.7.35) cannot be generalized to a number of walls in series by simply adding diffusion resistances. However, equilibrium partial pressures P_1 are continuous, and for two walls A and B, Equation 4.7.36 becomes

$$\dot{V}_1 = \frac{P_{1,s} - P_{1,s'}}{\dfrac{L_A}{\mathscr{P}_{1A}A} + \dfrac{L_B}{\mathscr{P}_{1B}A}} \text{ m}^3 \text{ (STP)/sec} \tag{4.7.37}$$

Transient Diffusion in a Semi-Infinite Solid

The typically low diffusion coefficients characterizing solids result in many situations where concentration changes are limited to a thin region near the surface (of thickness $\delta_c \sim (\mathscr{D}_{12}t)^{1/2}$). Examples include case-hardening of mild steel and coloring of clear sapphires. Details of the geometry are then unimportant

TABLE 4.7.6   Solubility and Permeability of Gases in Solids

| Gas	Solid	Temperature, K	$\mathcal{S}$ (m³(STP)/m³ atm) or $\mathcal{S'}$[a]	Permeability[b] m³(STP)/m² sec (atm/m)
H₂	Vulcanized rubber	300	$\mathcal{S}$ = 0.040	0.34×10^{-10}
	Vulcanized neoprene	290	$\mathcal{S}$ = 0.051	0.053×10^{-10}
	Silicone rubber	300		4.2×10^{-10}
	Natural rubber	300		0.37×10^{-10}
	Polyethylene	300		0.065×10^{-10}
	Polycarbonate	300		0.091×10^{-10}
	Fused silica	400	$\mathcal{S'} \simeq 0\,035$	
		800	$\mathcal{S'} \simeq 0.030$	
	Nickel	360	$\mathcal{S'}$ = 0.202	
		440	$\mathcal{S'}$ = 0.192	
He	Silicone rubber	300		2.3×10^{-10}
	Natural rubber	300		0.24×10^{-10}
	Polycarbonate	300		0.11×10^{-10}
	Nylon 66	300		0.0076×10^{-10}
	Teflon	300		0.047×10^{-10}
	Fused silica	300	$\mathcal{S'} \simeq 0.018$	
		800	$\mathcal{S'} \simeq 0.026$	
	Pyrex glass	300	$\mathcal{S'} \simeq 0.006$	
		800	$\mathcal{S'} \simeq 0.024$	
	7740 glass	470	$\mathcal{S}$ = 0.0084	4.6×10^{-13}
	(94% SiO₂ + B₂O₃ + P₂O₅,	580	$\mathcal{S}$ = 0.0038	1.6×10^{-12}
	5% Na₂O + Li₂ + K₂O,	720	$\mathcal{S}$ = 0.0046	6.4×10^{-12}
	1% other oxides)			
	7056 glass	390	$\mathcal{S'}$ = 0.0039	1.2×10^{-14}
	(90% SiO₂ + B₂O₃ + P₂O₅,	680	$\mathcal{S'}$ = 0.0059	1.0×10^{-12}
	8% Na₂O + Li₂ + K₂O,			
	1% PbO, 5% other oxides)			
O₂	Vulcanized rubber	300	$\mathcal{S}$ = 0.070	0.15×10^{-10}
	Silicone rubber	300		3.8×10^{-10}
	Natural rubber	300		0.18×10^{-10}
	Polyethylene	300		4.2×10^{-12}
	Polycarbonate	300		0.011×10^{-10}
	Silicone-polycarbonate copolymer (57% silicone)	300		1.2×10^{-10}
	Ethyl cellulose	300		0.09×10^{-10}
N₂	Vulcanized rubber	300	$\mathcal{S}$ = 0.035	0.054×10^{-10}
	Silicone rubber	300		1.9×10^{-12}
	Natural rubber	300		0.062×10^{-10}
	Silicone-polycarbonate copolymer (57% silicone)	300		0.53×10^{-10}
	Teflon	300		0.019×10^{-10}
CO₂	Vulcanized rubber	300	$\mathcal{S}$ = 0.090	1.0×10^{-10}
	Silicone rubber	290		21×10^{-10}
	Natural rubber	300		1.0×10^{-10}
	Silicone-polycarbonate copolymer (57% silicone)	300		7.4×10^{-10}
	Nylon 66	300		0.0013×10^{-10}
H₂O	Silicone rubber	310		$0.91–1.8 \times 10^{-10}$
Ne	Fused silica	300–1200	$\mathcal{S} \simeq 0.002$	
Ar	Fused silica	900–1200	$\mathcal{S} \simeq 0.01$	

TABLE 4.7.6   Solubility and Permeability of Gases in Solids

Gas	Solid	Temperature, K	$\mathscr{S}$ (m³(STP)/m³ atm) or $\mathscr{S}'^{a}$	Permeability[b] m³(STP)/m² sec (atm/m)

[a] Solubility $\mathscr{S}$ = volume of solute gas (0°C, 1 atm) dissolved in unit volume of solid when the gas is at 1 atm partial pressure. Solubility coefficient $\mathscr{S}' = c_{1,u}/c_{1,s}$.

[b] Permeability $\mathcal{P}_{12} = \mathcal{D}_{12}\mathscr{S}$.

From various sources, including Geankoplis, C.J. 1993. *Transport Processes and Unit Operations*, 3rd ed., Prentice-Hall; Englewood Cliffs, N.J.; Doremus, R.H. 1973. *Glass Science,* Wiley, New York; Altemose, V.O. 1961. Helium diffusion through glass, *J. Appl. Phys.*, 32, 1309–1316. With permission.
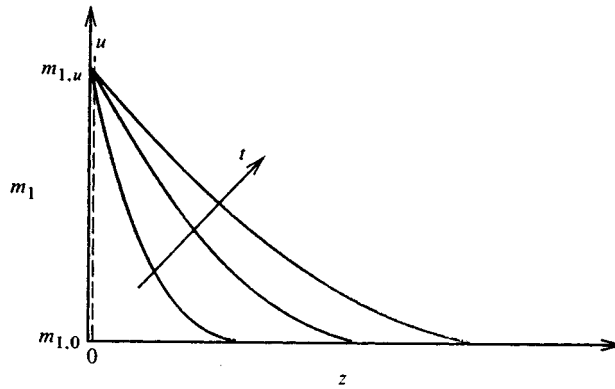
FIGURE 4.7.4 Transient diffusion in a plane slab.

and semi-infinite solid model can be used (Figure 4.7.4). For an initial concentration $m_{1,0}$ and a u-surface concentration suddenly changed to $m_{1,u}$ at time $t = 0$, the concentration distribution $m_1(z,t)$ is

$$\frac{m_1 - m_{1,0}}{m_{1,u} - m_{1,0}} = erfc\,\frac{z}{\left(4\mathcal{D}_{12}t\right)^{1/2}} \tag{4.7.38}$$

and the dissolution rate is

$$\dot{m}_1 = j_{1,u}A = \rho A\left(\frac{\mathcal{D}_{12}}{\pi t}\right)^{1/2}\left(m_{1,u} - m_{1,0}\right)\,\text{kg/sec} \tag{4.7.39}$$

For example, consider a Pyrex glass slab at 800 K suddenly exposed to helium at 10^4 Pa. The molar equivalent to Equation (4.7.39) for an assumed constant solid phase molar concentration c is

$$\frac{\dot{M}_1}{A} = \left(\frac{\mathcal{D}_{12}}{\pi t}\right)^{1/2}\left(c_{1,u} - c_{1,0}\right)$$

From Table 4.7.6, $\mathscr{S}' = c_{1,u}/c_{1,s} \cong 0.024$; hence, $c_{1,u} = (0.024)(10^4)/(8314)(800) = 3.61 \times 10^{-5}$ kmol/m³. From Table 4.7.4, $\mathcal{D}_{12} = 4.76 \times 10^{-8}\,\exp[-(2.72 \times 10^4)(10^3)/(8314)(800)] = 7.97 \times 10^{-10}$ m²/sec. Hence,

$$\frac{\dot{M}_1}{A} = \left(\frac{7.97 \times 10^{-10}}{\pi t}\right)^{1/2}\left(3.61 \times 10^{-5} - 0\right) = 5.75 \times 10^{-10}/t\,\text{kmol/sec}$$

Transient Diffusion in Slabs, Cylinders, and Spheres

Transient heat conduction in slates, cylinders, and spheres with surface convection is dealt with in Section 4.1. The analogous mass diffusion problem for the slab $-L < z < L$ is now considered. On a molar basis the governing differential equation is

$$\frac{\partial x_1}{\partial t} = \mathcal{D}_{12} \frac{\partial^2 x_1}{\partial z^2} \tag{4.7.40}$$

with initial condition $x_1 = x_{1,0}$ at $t = 0$. Boundary conditions are $\partial x_1/\partial z = 0$ at $z = 0$, and at the surface $z = L$,

$$-c\mathcal{D}_{12} \frac{\partial x_1}{\partial z}\bigg|_{z=L} = \mathcal{G}_{m1}\left(y_{1,s} - y_{1,e}\right) \tag{4.7.41}$$

The convective boundary condition is of the same form as Newton's law of cooling, and defines the mole transfer conductance $\mathcal{G}_{m1}$ (kmol/m²sec) (see also the section on mass and mole transfer conductances). Also, we have followed chemical engineering practice and denoted mole fraction x in the solid (or liquid) phase and y in the liquid (or gas) phase, to emphasize that generally mole fraction is not continuous across a phase interface. For example, consider absorption of a sparingly soluble gas into a liquid for which Henry's law, Equation (4.7.13), applies: then $y_{1,s} = \text{He}x_{1,u}$.

In using heat conduction charts for mass diffusion problems, particular care must be taken with the evaluation of the Biot number. For heat conduction $\text{Bi} = h_c L/k$, where k is the solid conductivity. For mass diffusion the Biot number accounts for the discontinuity in concentration across the phase interface. Using gas absorption into a plane layer of liquid, for example, when Equation (4.7.41) is put into an appropriate dimensionless form, the mass transfer Biot number is seen to be

$$\text{Bi}_m = \frac{\mathcal{G}_{m1}\text{He}L}{c\mathcal{D}_{12}} \tag{4.7.42}$$

For sparingly soluble gases, e.g., O_2 or CO_2 in water, He, and hence Bi_m, are very large, and the absorption process is liquid-side controlled; that is, a uniform gas-phase composition can be assumed. Often interface equilibrium data are in graphical or tabular form; then an effective Biot number at the concentration of concern must be used.

For example, consider a 2-mm-diameter droplet of water at 300 K entrained in an air flow at 1 atm pressure containing 1% by volume CO_2. From Table 4.7.5, $\text{He} = C_{\text{He}} = 1710$. The liquid phase molar density can be approximated by the pure water value of $c = \rho/M = 996/18 = 55.3$ kmol/m³. The liquid phase diffusion coefficient is obtained from Table 4.7.4 as $\mathcal{D}_{12} = v_{\text{H}_2\text{O}}/Sc_{12} = 0.87 \times 10^{-6}/420 = 2.07 \times 10^{-9}$ m²/sec. For negligible relative motion between the droplet and gas, the Sherwood number (see the section on dimensionless groups) is approximately 2.0, and hence the gas phase mole transfer conductance is $\mathcal{G}_{m1} = 2c\mathcal{D}_{12}/\mathcal{D}$. For the gas phase, the molar density $c = \mathcal{P}/\mathcal{R}T = (1.0133 \times 10^5)/(8314)(300) = 0.0406$ kmol/m³ and $\mathcal{D}_{12} = 0.157 \times 10^{-4}$ m²/sec from Table 4.7.2. Thus,

$$\mathcal{G}_{m1} = \frac{(2)(0.0406)\left(0.157 \times 10^{-4}\right)}{(0.002)} = 6.37 \times 10^{-4} \ \text{kmol/m}^2 \ \text{sec}$$

From Equation 4.7.42 with $L = R$ the droplet radius, the mass transfer Biot number is

$$\text{Bi}_m = \frac{\left(6.37 \times 10^{-4}\right)(1710)(0.001)}{(55.3)\left(2.07 \times 10^{-9}\right)} = 9520$$

Thus, even for a small droplet with a relatively large gas-side mole transfer conductance, the absorption process is liquid-side controlled.

Diffusion in a Porous Catalyst

Porous catalysts are used to give a large surface area per unit volume of catalyst surface. Current practice for automobile catalytic convertors is to use a ceramic matrix as a support for a thin porous alumina layer that is impregnated with the catalyst (called a *washcoat*). A typical matrix has passages of hydraulic diameter 1 mm, and the washcoat may be about 20 μm thick. Pore sizes are of the order of 1 μm for which ordinary and Knudsen diffusion resistances are important. A simple model for diffusion in a porous catalyst is

$$J_1 = -c\mathcal{D}_{1,\text{eff}} \nabla x_1 \text{ kmol}/\text{m}^2 \text{ sec} \tag{4.7.43}$$

where the subscript eff denotes an effective diffusivity that accounts for the presence of the solid material. Assuming additive resistances,

$$\frac{1}{\mathcal{D}_{1,\text{eff}}} = \frac{1}{\mathcal{D}_{12,\text{eff}}} + \frac{1}{\mathcal{D}_{K1,\text{eff}}} \tag{4.7.44}$$

and

$$\mathcal{D}_{12,\text{eff}} = \frac{\varepsilon_v}{\tau}\mathcal{D}_{12}; \qquad \mathcal{D}_{K1,\text{eff}} = \frac{\varepsilon_v}{\tau}\mathcal{D}_{K1,\text{eff}} \tag{4.7.45}$$

where ε_v is the volume void fraction and τ is the tortuosity factor (usually between 4 and 8). From the kinetic theory of gases the Knudsen diffusion coefficient is

$$\mathcal{D}_{K1} = 97 r_e \left(T/M_1\right)^{1/2} \text{ m}^2/\text{sec} \tag{4.7.46}$$

for effective pore radius r_e in meters and T in kelvins.

When a chemical reaction takes place within a porous layer, a concentration gradient is set up, and surfaces on pores deep within the pellet are exposed to lower reactant concentrations than surfaces near the pore openings. For a first-order reaction it is straightforward to obtain the concentration distribution. The results of such an analysis are conveniently given in the form of an effectiveness η_p, which is defined as the actual consumption rate of the reactant divided by that for an infinite diffusion coefficient. For a layer of thickness L exposed to reactants on one side, as shown in Figure 4.7.5.

$$\eta_p = \frac{\tanh bL}{bL}; \qquad b = \left(\frac{k''\text{a}_P}{\mathcal{D}_{1,\text{eff}}}\right)^{1/2} \tag{4.7.47}$$

where k'' (m/sec) is the rate constant for a first-order reaction and a_p (m^{-1}) is the catalyst area per unit volume. Notice that this effectiveness is analogous to the efficiency of a heat transfer fin.

For example, consider a 30-μm-thick porous alumina washcoat with a volume void fraction $\varepsilon_v = 0.8$, a tortuosity factor $\tau = 4.0$, average pore radius $r_e = 1$ μm, and catalytic surface area per unit volume $a_p = 7.1 \times 10^5$ cm^2/cm^3. For carbon monoxide oxidation by copper oxide at 800 K, 1 atm, the rate constant is approximately 4.2×10^{-4} m^2/sec. To calculate the effectiveness of the washcoat, we first need to calculate the effective diffusion coefficient $\mathcal{D}_{1,\text{eff}}$:
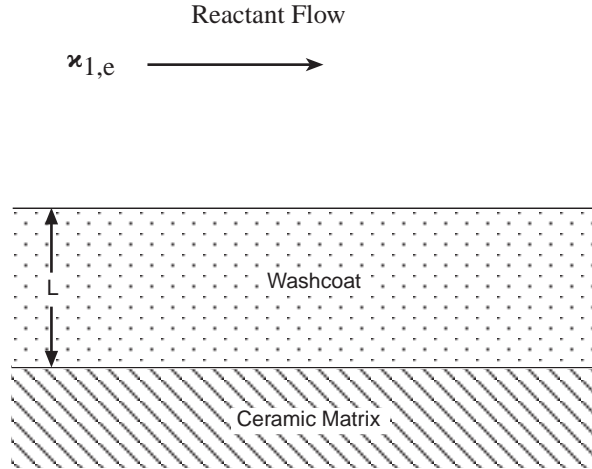

Reactant Flow

$\varkappa_{1,e}$ $\longrightarrow$

FIGURE 4.7.5 A catalyst layer.

$$\mathcal{D}_{12,\text{eff}} = \frac{\varepsilon_v}{\tau}\mathcal{D}_{12} = \frac{0.8}{4.0}\left(1.06\times10^{-4}\right) = 2.12\times10^{-5}\ \text{m}^2/\text{sec}$$

where $\mathcal{D}_{12}$ is approximated as the CO-air value from Table 4.7.2.

$$\mathcal{D}_{K1,\text{eff}} = \frac{\varepsilon_v}{\tau}\mathcal{D}_{12} = \frac{0.8}{4.0}(97)\left(1\times10^{-6}\right)\left(800/28\right)^{1/2} = 1.04\times10^{-4}\ \text{m}^2/\text{sec}$$

$$\frac{1}{\mathcal{D}_{1,\text{eff}}} = \frac{1}{2.12\times10^{-5}} + \frac{1}{1.04\times10^{-4}}; \qquad \mathcal{D}_{1,\text{eff}} = 1.76\times10^{-5}\ \text{m}^2/\text{sec}$$

$$b = \left[\frac{\left(4.2\times10^{-4}\right)\left(7.1\times10^{5}\right)\left(10^{2}\right)}{1.76\times10^{-5}}\right]^{1/2} = 4.2\times10^{4}\ \text{m}^{-1}; \qquad bL = \left(4.2\times10^{4}\right)\left(30\times10^{-6}\right) = 1.236$$

$$\eta_P = \frac{\tanh 1.236}{1.236} = 68.3\%$$

In an automobile catalytic convertor, Equation 4.7.47 applies to the catalyst washcoat. However, the mass transfer problem also involves a convective process for transport of reactants from the bulk flow. Referring to Figure 4.7.6 there are two mass transfer resistances in series, and the consumption rate of species 1 per unit surface area of the washcoat is

$$J_{1,s} = \frac{-x_{1,e}}{\dfrac{1}{L\eta_p k''c} + \dfrac{1}{\mathcal{G}_{m1}}}\ \text{kmol}/\text{m}^2\ \text{sec} \tag{4.7.48}$$

where $\mathcal{G}_{m1}$ is the mole transfer conductance describing convective transport to the washcoat surface (see the section on mass and mole transfer conductances). Notice that when $\mathcal{G}_{m1} \ll L\eta_p k''c$ the reaction rate is controlled by mass transfer from the gas stream to the washcoat surface; when $L\eta_p k''c \ll \mathcal{G}_{m1}$, the reaction rate is controlled by diffusion within the washcoat and the kinetics of the reaction.
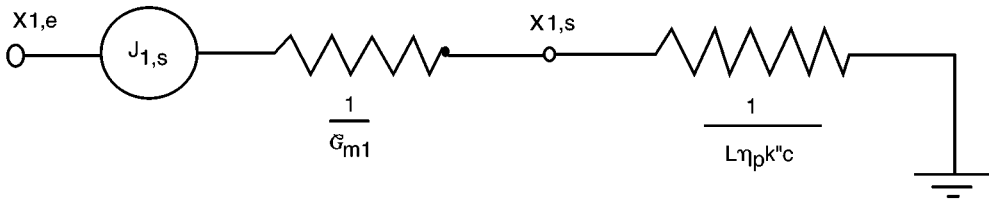
FIGURE 4.7.6 Equivalent circuit for mass transfer in an automobile catalytic convertor.

Diffusion in a Moving Medium

Net mass transfer across a surface results in a velocity component normal to the surface, and an associated convective flux in the direction of mass transfer. This convective flow is called a *Stefan flow*. The solutions of a number of mass transfer problems, involving a Stefan flow induced by the mass transfer process itself, follow. When necessary to obtain an analytical result, properties are assumed constant. Thus, use of these results requires evaluation of properties at a suitable reference state.

Diffusion with One Component Stationary

As an example, consider the simple heat pipe shown in Figure 4.7.7 with the evaporator and condenser located at the ends only (a bad design!). Then, if the working fluid is species 1, and a noncondensable gas is species 2, the concentration distribution is

$$\left(\frac{1-x_1}{1-x_{1,s}}\right) = \left(\frac{1-x_{1,e}}{1-x_{1,s}}\right)^{z/L} \tag{4.7.49}$$

and the vapor flux along the heat pipe is

$$N_1 = \frac{c\mathcal{D}_{12}}{L}\ln\frac{1-x_{1,e}}{1-x_{1,s}} \; \text{kmol/m}^2 \; \text{sec} \tag{4.7.50}$$
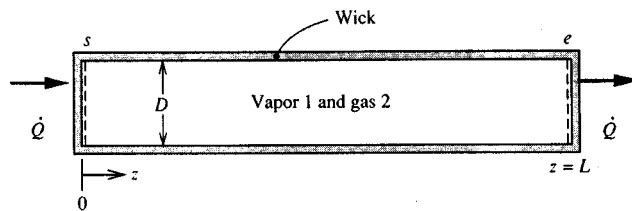

FIGURE 4.7.7 A simple heat pipe with the evaporator and condenser located at its ends.

Notice that $N_2 = 0$; that is, the gas is stationary. The rate of heat flow for a heat pipe of cross-sectional area of A_c is $\dot{Q} = N_1 M_1 h_{fg} A_c$. Evaluation of the $c\mathcal{D}$ product at a reference temperature $T_r = (1/2)(T_s + T_e)$ is adequate for most applications. Equation (4.7.50) applies to any situation where a one-dimensional model of mass transport is appropriate.

Heterogeneous Combustion

As an example, consider a small carbon particle entrained in a high-temperature airstream, as shown in Figure 4.7.8. The surface reaction is $2C + O_2 \rightarrow 2CO$ and there are no reactions in the gas phase. The stoichiometric ratio for the reaction is $r = 4/3$ kg oxygen/kg carbon. The reaction is diffusion controlled at the temperatures under consideration, that is, $m_{O_2,s} \simeq 0$. The mass transfer rate is n_s, which we give

the distinctive symbol $\dot{m}''$ since it is usually the desired result of an analysis; in this situation $\dot{m}'' = n_{C,u}$ is the combustion rate of carbon, and for a spherical particle of radius R is given by

$$\dot{m}'' = \frac{\rho\mathcal{D}_{O_2,m}}{R}\ln\left[1 + \frac{m_{O_2,e} - m_{O_2,s}}{m_{O_2,s} + 4/3}\right] = 0.160\frac{\rho\mathcal{D}_{O_2,m}}{R}\ \text{kg/m}^2\ \text{sec} \tag{4.7.51}$$
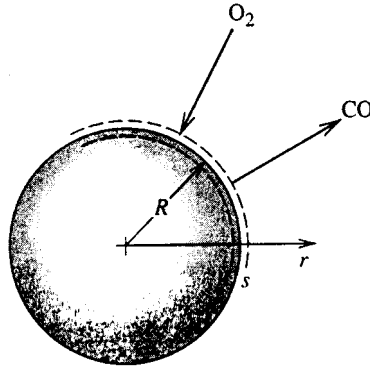

FIGURE 4.7.8 Combusion of a carbon particle in high-temperature air. The surface reaction is $2C + O_2 \rightarrow 2CO$.

The carbon particle temperature depends on its radius, and it is required to evaluate the property product $\rho\mathcal{D}$ at an appropriate reference temperature: an energy balance on the particle should be performed by this purpose. The resulting particle lifetime τ is

$$\tau = \frac{\rho_{\text{solid}}D_O^2}{1.28\left(\rho\mathcal{D}_{O_2,m}\right)_r}\ \text{sec} \tag{4.7.52}$$

for an initial particle diameter of D_0. Air properties at an average mean film temperature can be used to evaluate $\rho\mathcal{D}_{O_2,m}$.

　　Consider a 10-μm-diameter carbon particle ignited in an airstream at 1500 K and 1 atm. An energy balance on the particle (including radiation to surroundings at 1500 K) shows that the average temperature of the particle is approximately 2550 K, and, thus, $T_r = (1/2)(1500 + 2550) = 2025$ K or $\rho \simeq \rho_{\text{air}} = 0.175$ kg/m³ and $\mathcal{D}_{O_2,m} \simeq \mathcal{D}_{O_2,\text{air}} = 4.89 \times$ m²/sec (from Table 4.7.1). Then

$$\tau = \frac{(1810)(10\times10^{-6})^2}{(1.28)(0.175)(4.89\times10^{-4})} = 1.65\times10^{-3}\ \text{sec}$$

Droplet Evaporation

Consider a small droplet of species 1 entrained in a gas stream, species 2 (Figure 4.7.9). This is a simultaneous heat and mass transfer problem, and the mass transfer rate can be obtained by solving simultaneously

$$\dot{m}'' = \frac{\rho\mathcal{D}_{12}}{R}\ln\left(1 + \frac{m_{1,e} - m_{1,s}}{m_{1,s} - 1}\right) = \frac{k/c_{p1}}{R}\ln\left(1 + \frac{c_{p1}\left(T_e - T_s\right)}{h_{fg}}\right)\ \text{kg/m}^2\ \text{sec} \tag{4.7.53a}$$

$$m_{1,s} = m_{1,s}(T,P)\quad\left(\text{from vapor-pressure data}\right) \tag{4.7.53b}$$
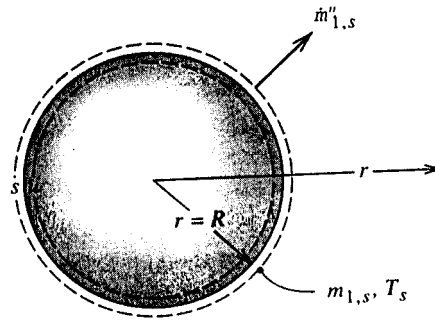
FIGURE 4.7.9 Evaporation of a droplet.

Temperature T_s is the adiabatic vaporization temperature and is essentially the psychrometric wet-bulb temperature. Properties can be evaluated at mean film temperature and composition; alternatively, c_{p1} can be set equal to the reference specific heat and all properties evaluated using Hubbard's $^1/_3$ rule, namely,

$$m_{1,r} = m_{1,s} + (1/3)\left(m_{1,e} - m_{1,s}\right) \tag{4.7.54a}$$

$$T_r = T_s + (1/3)\left(T_e - T_s\right) \tag{4.7.54b}$$

Droplet Combustion

Figure 4.7.10 shows a schematic of a volatile liquid hydrocarbon fuel droplet burning in air at zero gravity. The flame diameter is typically four to six times the droplet diameter. Heat is transferred from the flame to the droplet and serves to vaporize the fuel. In the flame the vapor reacts with oxygen to form gaseous products, primarily CO_2 and H_2O. When a fuel droplet ignites, there is a short initial transient during which the droplet heats up, until further conduction into the droplet is negligible and the droplet attains a steady temperature (approximately the wet-bulb temperature, which is very close to the boiling point for a typical hydrocarbon fuel). The reaction in the flame can be modeled as a single-step reaction with a constant stoichiometric ratio, r, and heat of combustion Δh_c J/kg of fuel.

The burning (mass transfer) rate of the droplet is given by the Godsave–Spalding formula,

$$\dot{m}'' = \frac{k/c_p}{R} \ln[1 + \mathcal{B}] \text{ kg/m}^2 \text{ sec} \tag{4.7.55}$$

where

$$\mathcal{B} = \frac{m_{ox,e}\, \Delta h_c / r + c_p\left(T_e - T_s\right)}{h_{fg}}$$

is the *mass transfer driving force* (or *transfer number*). The droplet lifetime is then

$$\tau = \frac{\rho_l D_O^2}{8\left(k/c_p\right)\ln(1 + \mathcal{B})} \text{ sec} \tag{4.7.56}$$

Based on experimental data for alkane droplets burning in air, Law and Williams (1972) recommend that properties be evaluated at a reference temperature $T_r = (1/2)(T_{BP} + T_{flame})$ where T_{flame} is the adiabatic flame temperature. The reference specific heat is $c_{pr} = c_{pfu}$, and the reference thermal conductivity is k_r
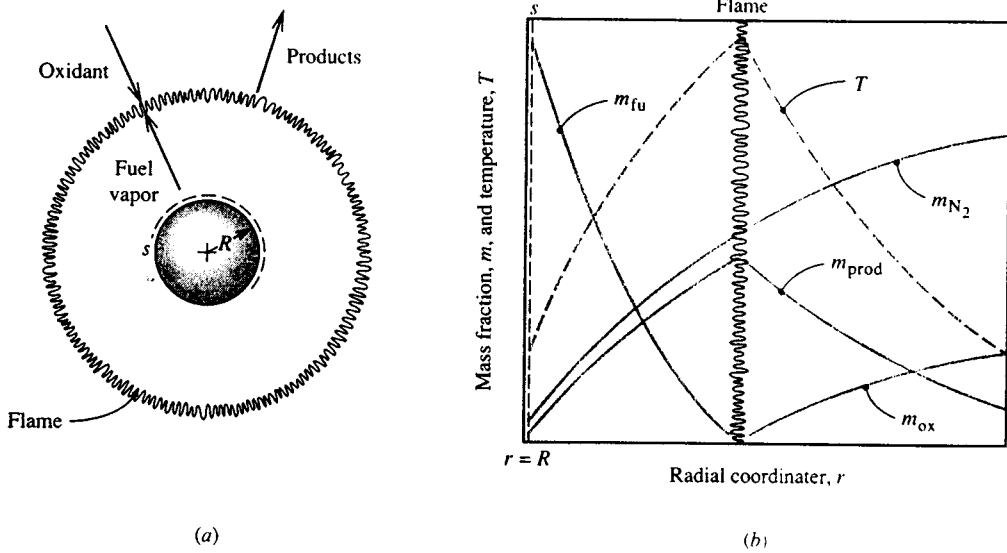
FIGURE 4.7.10 Combustion of a volatile fuel droplet burning in air: (a) schematic showing the flame, (b) concentration and temperature profiles.

$= 0.4k_{fu} + 0.6k_{air}$. Radiation has been ignored in the analysis leading to Equation (4.7.55) but is accounted for in using the Law and Williams reference-property scheme.

For example, consider a 1-mm-diameter *n*-octane droplet burning in air at 1 atm and 300 K, at near zero gravity. For *n*-octane (n-C_8H_{18}), $\rho_l = 611$ kg/m³, $h_{fg} = 3.03 \times 10^5$ J/kg, $\Delta h_c = 4.44 \times 10^7$ J/kg, and $T_{BP} = 399$ K. The flame temperature is $T_{flame} = 2320$ K. At a reference temperature of $(1/2)$ $(T_{flame} + T_{BP}) = 1360$ K, property values of *n*-octane vapor include $k = 0.113$ W/m K, $c_p = 4280$ J/kg K. The reaction is

$$C_8H_{18} + 12.5O_2 \rightarrow 8CO_2 + 9H_2O$$
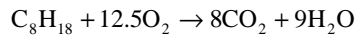
Hence, the stoichiometric ratio $r = 400/114.2 = 3.50$. Also $m_{ox,e} = 0.231$ and $T_s \cong T_{BP} = 399$ K. Thus, the transfer number is

$$\mathcal{B} = \frac{(0.231)(4.44 \times 10^7)/(3.50) + 4280(300 - 399)}{3.03 \times 10^5} = 8.27$$

At $T_r = 1360$ K, $k_{air} = 0.085$ W/m K. Hence,

$$k_r = 0.4k_{fu} + 0.6k_{air} = (0.4)(0.113) + (0.6)(0.085) = 0.096 \text{ W/m K}$$

and the droplet lifetime is

$$\tau = \frac{(611)(1 \times 10^{-3})^2}{(8)(0.096/4280)\ln(1 + 8.27)} = 1.53 \text{ sec}$$

Mass Convection

The terms *mass convection* or *convective mass transfer* are generally used to describe the process of mass transfer between a surface and a moving fluid, as shown in Figure 4.7.11. The surface may be that
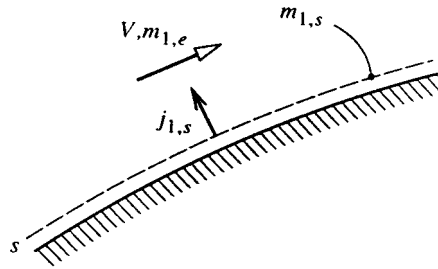
FIGURE 4.7.11 Notation for convective mass transfer into an external flow.

of a falling water film in an air humidifier, of a coke particle in a gasifier, or of a silica-phenolic heat shield protecting a reentry vehicle. As is the case for heat convection, the flow can be *forced* or *natural, internal* or *external,* and *laminar* or *turbulent*. In addition, the concept of whether the mass transfer rate is *low* or *high* plays an important role: when mass transfer rates are low, there is a simple analogy between heat transfer and mass transfer that can be efficiently exploited in the solution of engineering problems.

Mass and Mole Transfer Conductances

Analogous to convective heat transfer, the rate of mass transfer by convection is usually a complicated function of surface geometry and *s*-surface composition, the fluid composition and velocity, and fluid physical properties. For simplicity, we will restrict our attention to fluids that are either binary mixtures or solutions, or situations in which, although more than two species are present, diffusion can be adequately described using effective binary diffusion coefficients, as was discussed in the section on ordinary diffusion. Referring to Figure 4.7.11, we define the *mass transfer conductance* of species 1, g_{m1}, by the relation

$$j_{1,s} = g_{m1}\,\Delta m_1; \qquad \Delta m_1 = m_{1,s} - m_{1,e} \qquad (4.7.57)$$

and the units of g_{m1} are seen to be the same as for mass flux (kg/m²sec). Equation (4.7.57) is of a similar form to Newton's law of cooling, which defines the heat transfer coefficient h_c. Why we should not use a similar name and notation (e.g., mass transfer coefficient and h_m) will become clear later. On a molar basis, we define the *mole transfer conductance* of species 1, G_{m1}, by a corresponding relation,

$$J_{1,s} = G_{m1}\,\Delta x_1; \qquad \Delta x_1 = x_{1,s} - x_{1,e} \qquad (4.7.58)$$

where G_{m1} has units (kmol/m²sec).

Low Mass Transfer Rate Theory

Consider, as an example, the evaporation of water into air, as shown in Figure 4.7.12. The water–air interface might be the surface of a water reservoir, or the surface of a falling water film in a cooling tower or humidifier. In such situations the mass fraction of water vapor in the air is relatively small; the highest value is at the *s*-surface, but even if the water temperature is as high as 50°C, the corresponding value of $m_{H_2O,s}$ at 1 atm total pressure is only 0.077. From Equation 4.7.54 the driving potential for diffusion of water vapor away from the interface is $\Delta m_1 = m_{1,s} - m_{1,e}$, and is small compared to unity, even if the free-stream air is very dry such that $m_{1,e} \simeq 0$. We then say that the mass transfer rate is *low* and the rate of evaporation of the water can be approximated as $j_{1,s}$; for a surface area A,

$$\dot{m}_1 = \left(m_{1,s} n_s + j_{1,s}\right)A \simeq j_{1,s} A \ \text{kg/sec} \qquad (4.7.59)$$
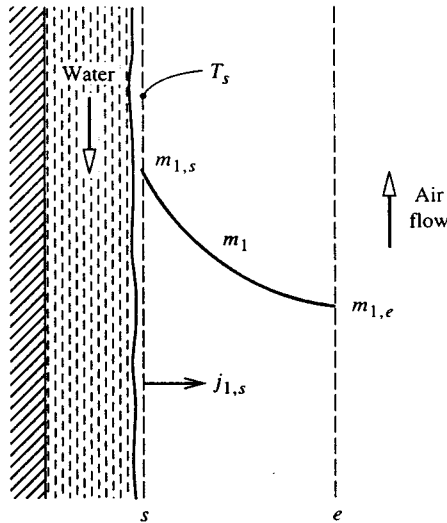
FIGURE 4.7.12 Evaporation of water into an air flow.

In contrast, if the water temperature approaches its boiling point, $m_{1,s}$ is no longer small, and of course, in the limit of $T_s = T_{BP}$, $m_{1,s} = 1$. The resulting driving potential for diffusion Δm_1 is then large, and we say that the mass transfer rate is *high*. Then, the evaporation rate cannot be calculated from Equation 4.7.59, as will be explained in the section on high mass transfer rate theory. For water evaporation into air, the error incurred in using low mass transfer rate theory is approximately $(^1\!/_2)\,\Delta m_1$, and a suitable criterion for application of the theory to engineering problems is $\Delta m_1 < 0.1$ or 0.2.

A large range of engineering problems can be adequately analyzed assuming low mass transfer rates. These problems include cooling towers and humidifiers as mentioned above, gas absorbers for sparingly soluble gases, and catalysis. In the case of catalysis, the *net* mass transfer rate is actually zero. Reactants diffuse toward the catalyst surface and the products diffuse away, but the catalyst only promotes the reaction and is not consumed. On the other hand, problems that are characterized by high mass transfer rates include condensation of steam containing a small amount of noncondensable gas, as occurs in most power plant condensers; combustion of volatile liquid hydrocarbon fuel droplets in diesel engines and oil-fired power plants, and ablation of phenolic-based heat shields on reentry vehicles.

Dimensionless Groups

Dimensional analysis of convective mass transfer yields a number of pertinent dimensionless groups that are, in general, analogous to dimensionless groups for convective heat transfer. The most important groups are as follows.

1. The Schmidt number, $\mathrm{Sc}_{12} = \mu/\rho\mathcal{D}_{12},$ which is a properties group analogous to the Prandtl number. For gas mixtures, $\mathrm{Sc}_{12} = O(1)$, and for liquid solutions, $\mathrm{Sc}_{12} = O(100)$ to $O(1000)$. There are not fluids for which $\mathrm{Sc}_{12} \ll 1$, as is the case of Prandtl number for liquid metals.
2. The Sherwood number (or mass transfer Nusselt number). $\mathrm{Sh} = g_{m1}L/\rho\mathcal{D}_{12}$ $(= G_{m1}L/c\mathcal{D}_{12})$ is a dimensionless conductance.
3. The mass transfer Stanton number $\mathrm{St}_m = g_{m1}/\rho V$ $(= G_{m1}/cV)$ is an alternative dimensionless conductance.

As for convective heat transfer, forced convection flows are characterized by a Reynolds number, and natural convection flows are characterized by a Grashof or Rayleigh number. In the case of Gr or Ra it is not possible to replace $\Delta\rho$ by $\beta\Delta T$ since density differences can result from concentration differences (and both concentration and temperature differences for simultaneous heat and mass transfer problems).

Analogy between Convective Heat and Mass Transfer

A close analogy exists between convective heat and convective mass transfer owing to the fact that conduction and diffusion in a fluid are governed by physical laws of identical form, that is, Fourier's and Fick's laws, respectively. As a result, in many circumstances the Sherwood or mass transfer Stanton number can be obtained in a simple manner from the Nusselt number or heat transfer Stanton number for the same flow conditions. Indeed, in most gas mixtures Sh and St_m are nearly equal to their heat transfer counterparts. For dilute mixtures and solutions and low mass transfer rates, the rule for exploiting the analogy is simple: The *Sherwood or Stanton number is obtained by replacing the Prandtl number by the Schmidt number in the appropriate heat transfer correlation*. For example, in the case of fully developed turbulent flow in a smooth pipe

$$Nu_D = 0.023 Re_D^{0.8} Pr^{0.4}; \qquad Pr > 0.5 \tag{4.7.60a}$$

which for mass transfer becomes

$$Sh_D = 0.023 Re_D^{0.8} Sc^{0.4}; \qquad Sc > 0.5 \tag{4.7.60b}$$

Also, for natural convection from a heated horizontal surface facing upward,

$$\overline{Nu} = 0.54 \left(Gr_L Pr\right)^{1/4}; \qquad 10^5 < Gr_L Pr < 2 \times 10^7 \quad \text{(laminar)} \tag{4.7.61a}$$

$$\overline{Nu} = 0.14 \left(Gr_L Pr\right)^{1/3}; \qquad 2 \times 10^7 < Gr_L Pr < 3 \times 10^{10} \quad \text{(turbulent)} \tag{4.7.61b}$$

which for isothermal mass transfer with $\rho_s < \rho_e$ become

$$\overline{Sh} = 0.54 \left(Gr_L Sc\right)^{1/4}; \qquad 10^5 < Gr_L Sc < 2 \times 10^7 \quad \text{(laminar)} \tag{4.7.62a}$$

$$\overline{Sh} = 0.14 \left(Gr_L Sc\right)^{1/3}; \qquad 2 \times 10^7 < Gr_L Sc < 3 \times 10^{10} \quad \text{(turbulent)} \tag{4.7.62b}$$

With evaporation, the condition, $\rho_s < \rho_e$ will be met when the evaporating species has a smaller molecular weight than the ambient species, for example, water evaporating into air. Mass transfer correlations can be written down in a similar manner for almost all the heat transfer correlations given in Section 4.2. There are some exceptions: for example, there are no fluids with a Schmidt number much less than unity, and thus there are no mass transfer correlations corresponding to those given for heat transfer to liquid metals with $Pr \ll 1$. In most cases it is important for the wall boundary conditions to be of analogous form, for example, laminar flow in ducts. A uniform wall temperature corresponds to a uniform concentration $m_{1,s}$ along the *s*-surface, whereas a uniform heat flux corresponds to a uniform diffusive flux $j_{1,s}$. In chemical engineering practice, the analogy between convective heat and mass transfer is widely used in a form recommended by Chilton and Colburn in 1934, namely, $St_m/St = (Sc/Pr)^{-2/3}$. The Chilton-Colburn form is of adequate accuracy for most external forced flows but is inappropriate for fully developed laminar duct flows.

For example, air at 1 atm and 300 K flows inside a 3-cm-inside-diameter tube at 10 m/sec. Using pure-air properties the Reynolds number is $VD/\nu = (10)(0.03)/15.7 \times 10^{-6} = 1.911 \times 10^4$. The flow is turbulent. Using Equation (4.7.60b) with $Sc_{12} = 0.61$ for small concentrations of H_2O in air,

$$Sh_D = (0.023)\left(1.911 \times 10^4\right)^{0.8}(0.61)^{0.4} = 50.2$$

$$g_{m1} = \rho \mathcal{D}_{12} \mathrm{Sh}/D = \rho v \mathrm{Sh}/\mathrm{Sc}_{12} D = \frac{(1.177)(15.7 \times 10^{-6})(50.2)}{(0.61)(0.03)} = 5.07 \times 10^{-2} \ \mathrm{kg/m^2 \ sec}$$

Further insight into this analogy between convective heat and mass transfer can be seen by writing out Equations (4.7.60a) and (4.7.60b) as, respectively,

$$\frac{(h_c/c_p)D}{k/c_p} = 0.023 \mathrm{Re}_D^{0.8} \left(\frac{\mu}{k/c_p} \right)^{0.4} \tag{4.7.63a}$$

$$\frac{g_m D}{\rho \mathcal{D}_{12}} = 0.023 \mathrm{Re}_D^{0.8} \left(\frac{\mu}{\rho \mathcal{D}_{12}} \right)^{0.4} \tag{4.7.63b}$$

When cast in this form, the correlations show that the property combinations k/c_p and $\rho \mathcal{D}_{12}$ play analogous roles; these are *exchange coefficients* for heat and mass, respectively, both having units kg/m sec, which are the same as those for dynamic viscosity μ. Also, it is seen that the ratio of heat transfer coefficient to specific heat plays an analogous role to the mass transfer conductance, and has the same units (kg/m² sec). Thus, it is appropriate to refer to the ratio h_c/c_p as the *heat transfer conductance*, g_h, and for this reason we should not refer to g_m as the mass transfer *coefficient*.

Simultaneous Heat and Mass Transfer

Often problems involve simultaneous convective heat and mass transfer, for which the surface energy balance must be carefully formulated. Consider, for example, evaporation of water into air, as shown in Figure 4.7.13. With H_2O denoted as species 1, the steady-flow energy equation applied to a control volume located between the *u*- and *s*-surfaces requires that

$$\dot{m}(h_{1,s} - h_{1,u}) = A(q''_{\mathrm{cond}} - q''_{\mathrm{conv}} - q''_{\mathrm{rad}}) \ \mathrm{W} \tag{4.7.64}$$

where it has been recognized that only species 1 crosses the *u*- and *s*-surfaces. Also, the water has been assumed to be perfectly opaque so that all radiation is emitted or absorbed between the *u*-surface and the interface.

If we restrict our attention to conditions for which low mass transfer rate theory is valid, we can write $\dot{m}/A \simeq j_{1,s} = g_{m1}(m_{1,s} - m_{1,e})$. Also, we can then calculate the convective heat transfer as if there were no mass transfer, and write $q_{\mathrm{conv}} = h_c(T_s - T_e)$. Substituting in Equation (4.7.64) with $q_{\mathrm{conv}} = -k\partial T/\partial y|_u$, $h_{1,s} - h_{1,u} = h_{fg}$, and rearranging, gives

$$-k \frac{\partial T}{\partial y}\bigg|_u = h_c(T_s - T_e) + g_{m1}(m_{1,s} - m_{1,e})h_{fg} + q''_{\mathrm{rad}} \ \mathrm{W/m^2} \tag{4.7.65}$$

It is common practice to refer to the convective heat flux $h_c(T_s - T_e)$ as the *sensible* heat flux, whereas the term $g_{m1}(m_{1,s} - m_{1,e})h_{fg}$ is called the *evaporative* or *latent* heat flux. Each of the terms in Equation 4.7.65 can be positive or negative, depending on the particular situation. Also, the evaluation of the conduction heat flux at the *u*-surface, $-k\partial T/\partial y|_u$, depends on the particular situation. Four examples are shown in Figure 4.7.13. For a water film flowing down a packing in a cooling tower (Figure 4.7.13b), this heat flux can be expressed in terms of convective heat transfer from the bulk water at temperature T_L to the surface of the film, $-k\partial T/\partial y|_u = h_{cL}(T_L - T_s)$. If the liquid-side heat transfer coefficient h_{cL} is large enough, we can simply set $T_s \simeq T_L$, which eliminates the need to estimate h_{cL}. The evaporation process is then *gas-side controlled*. Figure 4.7.13c shows film condensation from a steam-air mixture on the outside of a vertical tube. In this case we can write $k\partial T/\partial y|_u = U(T_s - T_c)$, where T_c is the coolant
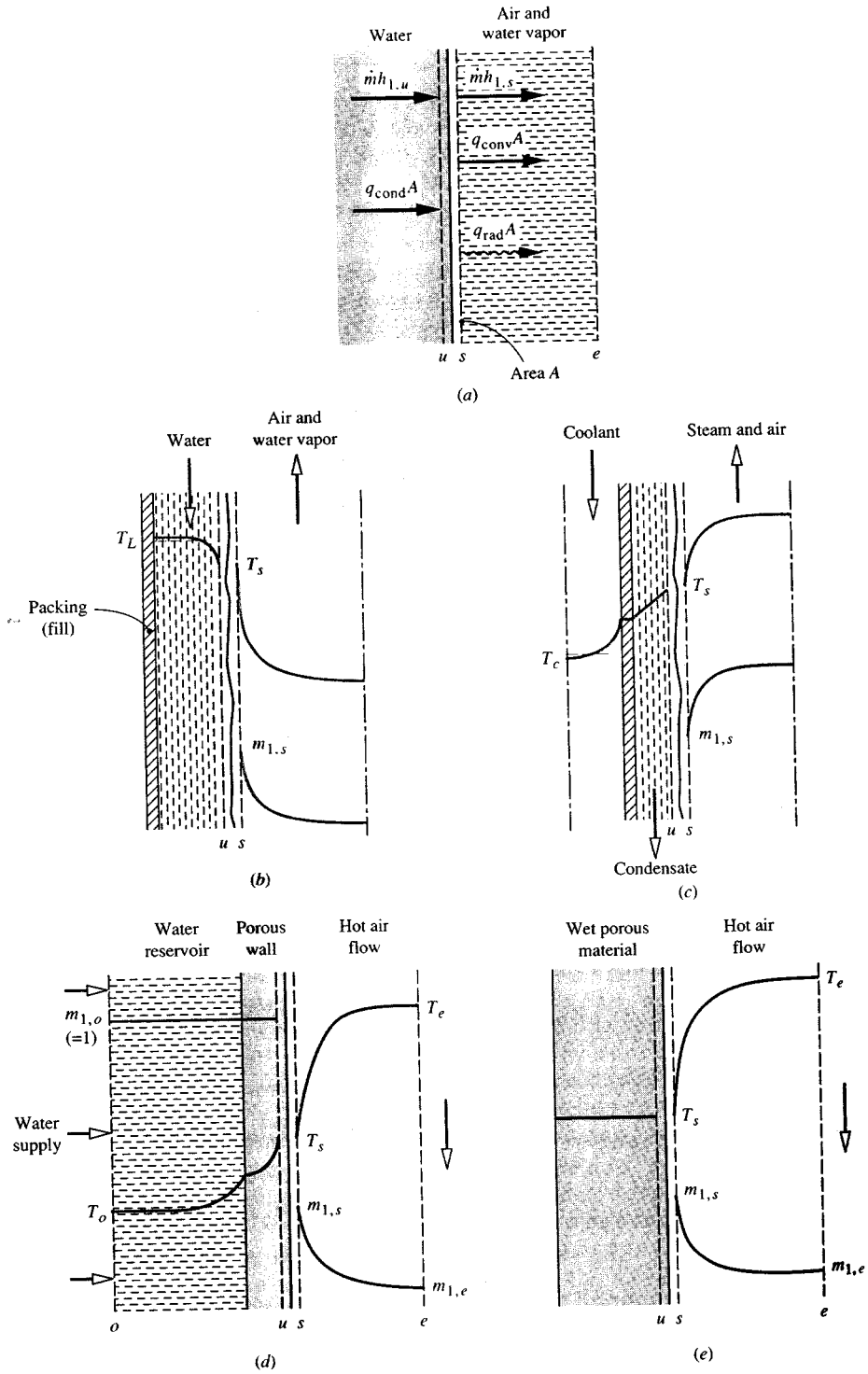
FIGURE 4.7.13 The surface energy balance for evaporation of water into an air stream.

bulk temperature. The overall heat transfer coefficient U includes the resistances of the condensate film, the tube wall, and the coolant. Sweat cooling is shown in Figure 4.7.13d, with water from a reservoir (or *plenum chamber*) injected through a porous wall at a rate just sufficient to keep the wall surface wet. In this case, the conduction across the *u*-surface can be related to the reservoir conditions by application of the steady-flow energy equation to a control volume located between the *o*- and *u*-surfaces. Finally, Figure 4.7.13e shows drying of a wet porous material (e.g., a textile or wood). During the constant-rate period of the process, evaporation takes place from the surface with negligible heat conduction into the solid; then $-k\partial T/\partial y|_u \simeq 0$. The term *adiabatic vaporization* is used to describe evaporation when $q_{cond} = 0$; constant-rate drying is one example, and the wet-bulb psychrometer is another.

Consider a 1-m-square wet towel on a washline on a day when there is a low overcast and no wind. The ambient air is at 21°C, 1 atm, and 50.5% RH. In the constant-rate drying period the towel temperature is constant, and $q_{cond} = 0$. An iterative calculation is required to obtain the towel temperature using correlations for natural convection on a vertical surface to obtain h_c and g_{m1}; q_{rad} is obtained as $q_{rad} = \sigma\varepsilon(T_s^4 - T_e^4)$ with $\varepsilon = 0.90$. The results are $T_s = 17.8°C$, $h_c = 1.69$ W/m²K, $g_{m1} = 1.82 \times 10^{-3}$ kg/m²sec, and the energy balance is

$$q_{cond} = h_c\left(T_s - T_e\right) + g_{m1}\left(m_{1,s} - m_{1,e}\right)h_{fg} + q_{rad}$$

$$0 = -5.4 + 21.7 - 16.3 \text{ W/m}^2$$

Evaluation of composition-dependent properties, in particular the mixture specific heat and Prandtl number, poses a problem. In general, low mass transfer rates imply small composition variations across a boundary layer, and properties can be evaluated for a mixture of the free-stream composition at the mean film temperature. In fact, when dealing with evaporation of water into air, use of the properties of dry air at the mean film temperature gives results of adequate engineering accuracy. If there are large composition variations across the boundary layer, as can occur in some catalysis problems, properties should be evaluated at the mean film composition and temperature.

The Wet- and Dry-Bulb Psychrometer

The wet- and dry-bulb psychrometer is used to measure the moisture content of air. In its simplest form, the air is made to flow over a pair of thermometers, one of which has its bulb covered by a wick whose other end is immersed in a small water reservoir. Evaporation of water from the wick causes the wet bulb to cool and its steady-state temperature is a function of the air temperature measured by the dry bulb and the air humidity. The wet bulb is shown in Figure 4.7.14. In order to determine the water vapor mass fraction $m_{1,e}$, the surface energy balance Equation (4.7.66) is used with conduction into the wick and q''_{rad} set equal to zero. The result is

$$m_{1,e} = m_{1,s} - \frac{c_p}{h_{fg}}\left(\frac{\text{Pr}}{\text{Sc}_{12}}\right)^{-2/3}\left(T_e - T_s\right) \tag{4.7.66}$$

Usually $m_{1,e}$ is small and we can approximate $c_p = c_{p\text{ air}}$ and $(\text{Pr}/\text{Sc}_{12})^{-2/3} = 1/1.08$. Temperatures T_s and T_e are the known measured wet- and dry-bulb temperatures. With T_s known, $m_{1,s}$ can be obtained using steam tables in the usual way. For example, consider an air flow at 1000 mbar with measured wet- and dry-bulb temperatures of 305.0 and 310.0 K, respectively. Then $P_{1,s} = P_{sat}(T_s) = P_{sat}(305.0 \text{ K}) = 4714$ Pa from steam tables. Hence, $x_{1,s} = P_{1,s}/P = 4714/10^5 = 0.04714$, and

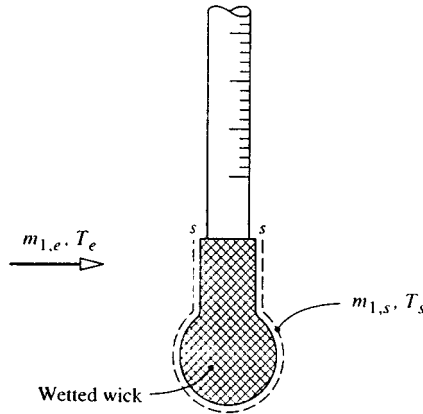$$m_{1,s} = \frac{0.04714}{0.04714 + (29/18)(1 - 0.04714)} = 0.02979$$

FIGURE 4.7.14 Wet bulb of a wet- and dry-bulb psychrometer.

Also, h_{fg} (305 K) = 2.425×10^6 J/kg, and $c_{p\ air}$ = 1005 J/kg K; thus

$$m_{1,e} = 0.02979 - \frac{1005}{(1.08)\left(2.425 \times 10^6\right)}(310 - 305) = 0.02787$$

$$x_{1,e} = \frac{0.02787}{0.02787 + (18/29)(1 - 0.02787)} = 0.04415$$

$$P_{1,e} = x_{1,e}P = (0.04415)\left(10^5\right) = 4412 \text{ Pa}$$

By definition, the relative humidity is RH = $P_{1,e}/P_{sat}(T_e)$; RH = 4415/6224 = 70.9%.

In the case of other adiabatic vaporization processes, such as constant-rate drying or evaporation of a water droplet, $m_{1,e}$ and T_e are usually known and Equation (4.7.66) must be solved for T_s. However, the thermodynamic wet-bulb temperature obtained from psychrometric charts or software is accurate enough for engineering purposes.

High Mass Transfer Rate Theory

When there is net mass transfer across a phase interface, there is a convective component of the absolute flux of a species across the *s*-surface. From Equation (4.7.23a) for species 1,

$$n_{1,s} = \rho_{1,s} v_s + j_{1,s} \ \text{kg/m}^2 \text{ sec} \qquad (4.7.67)$$

During evaporation the convection is directed in the gas phase, with a velocity normal to the surface v_s. When the convective component cannot be neglected, we say that the mass transfer rate is *high*. There are two issues to consider when mass transfer rates are high. First, the rate at which species 1 is transferred across the *s*-surface is not simply the diffusive component $j_{1,s}$ as assumed in low mass transfer rate theory, but is the sum of the convective and diffusive components shown in Equation 4.7.67. Second, the normal velocity component v_s has a *blowing* effect on the concentration profiles, and hence on the Sherwood number. The Sherwood number is no longer analogous to the Nusselt number of conventional heat transfer correlations, because those Nusselt numbers are for situations involving impermeable surfaces, e.g., a metal wall, for which $v_s = 0$.

Substituting for $j_{1,s}$ from Equation (4.7.57) into Equation (4.7.67) gives

$$\dot{m}'' = g_{m1} \frac{m_{1,e} - m_{1,s}}{m_{1,s} - n_{1,s}/\dot{m}''} = g_{m1} \mathcal{B}_{m1} \qquad (4.7.68)$$

where $\dot{m}'' = n_s$ is the mass transfer rate introduced in the section on heterogeneous combustion and $\mathcal{B}_{m1}$ is the *mass transfer driving force*. In the special case where only species 1 is transferred, $n_{1,s}/\dot{m}''$ = 1, for example, when water evaporates into air, and dissolution of air in the water is neglected. It is convenient to rewrite Equation (4.7.68) as

$$\dot{m}'' = g_{m1}^* \left(g_{m1}/g_{m1}^* \right) \mathcal{B}_{m1} \ \text{kg/m}^2 \ \text{sec} \qquad (4.7.69a)$$

where

$$g_{m1}^* = \lim_{\mathcal{B}_m \to 0} g_{m1} \qquad (4.7.69b)$$

Now g_{m1}^* is the limit value of g_{m1} for zero mass transfer (i.e., $v_s = 0$), and Sh* can be obtained from conventional heat transfer Nusselt number correlations for impermeable surfaces. The ratio (g_{m1}/g_{m1}^*) is termed a *blowing factor* and accounts for the effect of v_s on the concentration profiles. Use of Equation (4.7.69) requires appropriate data for the blowing factor. For the constant-property laminar boundary layer on a flat plate, Figure 4.7.15 shows the effect of the Schmidt number on the blowing factor. The abscissa is a *blowing parameter* $B_m = \dot{m}''/g_m^*$.

The blowing velocity also affects the velocity and temperature profiles, and hence the wall shear stress and heat transfer. The curve for Sc = 1 in Figure 4.7.15 also gives the effect of blowing on shear stress as τ_s/τ_s^*, and the curve for Sc = 0.7 gives the effect of blowing on heat transfer for air injection into air as h_c/h_c^* (since Pr = 0.7 for air).

Variable Property Effects of High Mass Transfer Rates

High mass transfer rate situations are usually characterized by large property variations across the flow, and hence property evaluation for calculating g_m and h_c is not straightforward. An often-encountered situation is transfer of a single species into an inert laminar or turbulent boundary layer flow. The effect of variable properties can be very large as shown in Figure 4.7.16 for laminar boundary layers, and Figure 4.7.17 for turbulent boundary layers.

A simple procedure for correlating the effects of flow type and variable properties is to use weighting factors in the exponential functions suggested by a constant-property Couette-flow model (Mills, 1995). Denoting the injected species as species *i*, we have

$$\frac{g_{m1}}{g_{m1}^*} = \frac{a_{mi} B_{mi}}{\exp(a_{mi} B_{mi}) - 1}; \qquad B_{mi} = \frac{\dot{m}''}{g_{mi}^*} \qquad (4.7.70a)$$

or

$$\frac{g_{m1}}{g_{mi}^*} = \frac{\ln(1 + a_{mi} \mathcal{B}_{mi})}{a_{mi} \mathcal{B}_{mi}}; \qquad \mathcal{B}_{mi} = \frac{\dot{m}''}{g_{mi}} = \frac{m_{i,e} - m_{i,e}}{m_{i,s} - 1}$$

$$\frac{\tau_s}{\tau_s^*} = \frac{a_{fi} B_f}{\exp(a_{fi} B_f) - 1}; \qquad B_f = \frac{\dot{m}'' u_e}{\tau_s^*} \qquad (4.7.70b)$$
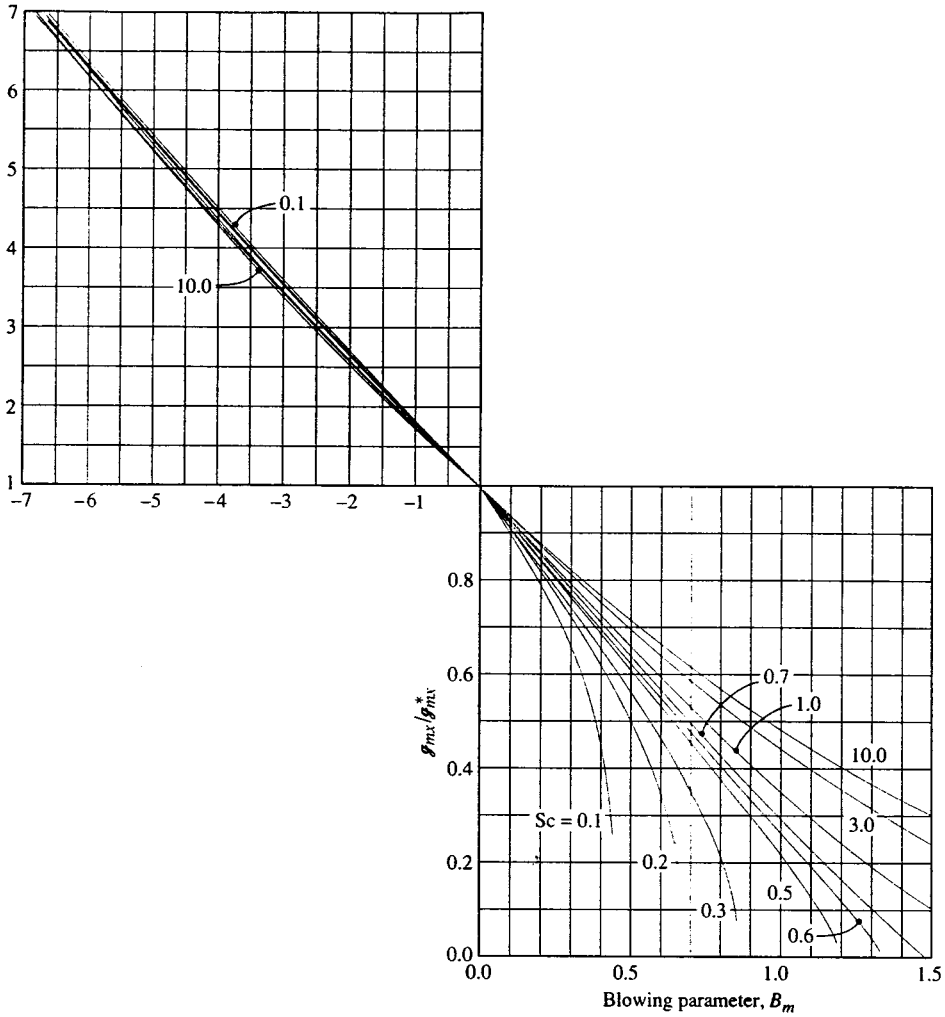
FIGURE 4.7.15 Effect of mass transfer on the mass transfer conductance for a laminar boundary layer on a flat plate: g_m/g_m^* vs. blowing parameter $B_m = \dot{m}''/g_m^*$.

$$\frac{h_c}{h_c^*} = \frac{a_{hi}B_h}{\exp(a_{hi}B_h)-1}; \qquad B_h = \frac{\dot{m}''c_{pe}}{h_c^*} \qquad (4.7.70c)$$

Notice that $g_{mi}^*, \tau_s^*, h_c^*$, and c_{pe} are evaluated using properties of the free-stream gas at the mean film temperature. The weighting factor a may be found from exact numerical solutions of boundary layer equations or from experimental data. Some results for laminar and turbulent boundary layers follow.

1. *Laminar Boundary Layers*. We will restrict our attention to low-speed air flows, for which viscous dissipation and compressibility effects are negligible, and use exact numerical solutions of the self-similar laminar boundary layer equations (Wortman, 1969). Least-squares curve fits of the numerical data were obtained using Equations (4.7.70a) to (4.7.70c). Then, the weighting factors for axisymmetric stagnation-point flow with a cold wall ($T_s/T_e = 0.1$) were correlated as

$$a_{mi} = 1.65\left(M_{\text{air}}/M_i\right)^{10/12} \qquad (4.7.71a)$$
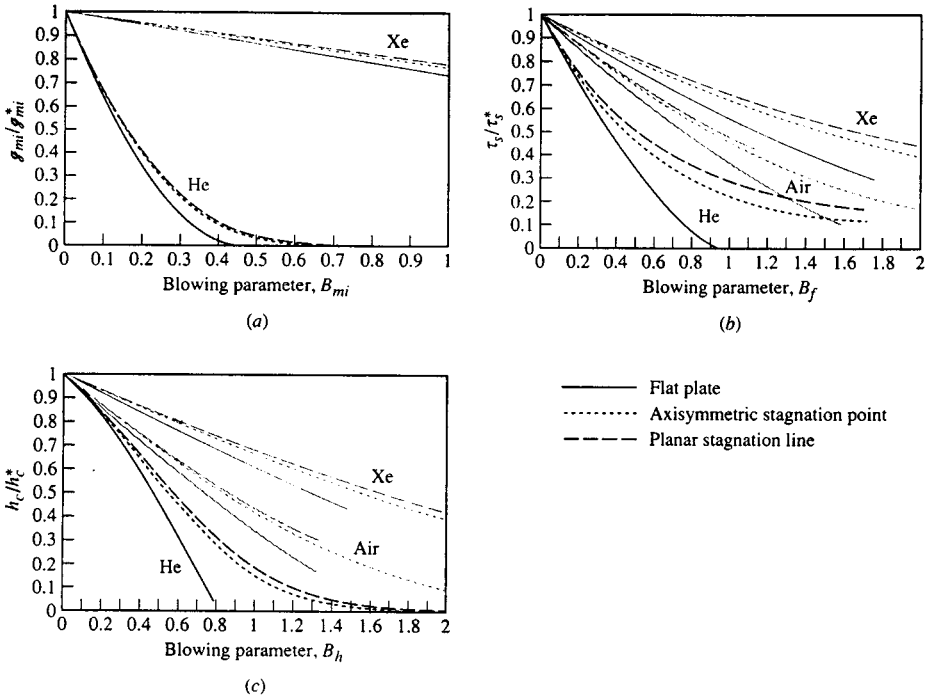
FIGURE 4.7.16 Numerical results for the effect of pressure gradient and variable properties on blowing factors for laminar boundary layers: low-speed air flow over a cold wall ($T_s/T_e = 0.1$) with foreign gas injection: (a) mass transfer conductance, (b) wall shear stress, (c) heat transfer coefficient. (From Wortman, A., Ph.D. dissertation, University of California, Los Angeles, 1969. With permission.)

$$a_{fi} = 1.38\left(M_{air}/M_i\right)^{5/12} \tag{4.7.71b}$$

$$a_{hi} = 1.30\left(M_{air}/M_i\right)^{3/12}\left[c_{pi}/\left(2.5\mathcal{R}/M_i\right)\right] \tag{4.7.71c}$$

Notice that $c_{pi}/2.5\mathcal{R}/M_i)$ is unity for a monatomic species. For the planar stagnation line and the flat plate, and other values of the temperature ratio T_s/T_e, the values of the species weighting factors are divided by the values given by Equations (4.7.71a,b,c) to give correction factors G_{mi}, G_{fi}, and G_{hi}, respectively. The correction factors are listed in

The exponential relation blowing factors cannot accurately represent some of the more anomalous effects of blowing. For example, when a light gas such as H_2 is injected, Equation (4.7.70c) indicates that the effect of blowing is always to reduce heat transfer, due to both the low density and high specific heat of hydrogen. However, at very low injection rates, the heat transfer is actually increased, as a result of the high thermal conductivity of H_2. For a mixture, $k \approx \sum x_i k_i$ whereas $c_p = \sum m_i c_{pi}$. At low rates of injection, the mole fraction of H_2 near the wall is much larger than its mass fraction; thus, there is a substantial increase in the mixture conductivity near the wall, but only a small change in the mixture specific heat. An increase in heat transfer results. At higher injection rates, the mass fraction of H_2 is also large, and the effect of high mixture specific heat dominates to cause a decrease in heat transfer.

2. *Turbulent Boundary Layers.* Here we restrict our attention to air flow along a flat plate for Mach numbers up to 6, and use numerical solutions of boundary layer equations with a mixing length turbulence model (Landis, 1971). Appropriate species weighting factors for $0.2 < T_s/T_e < 2$ are
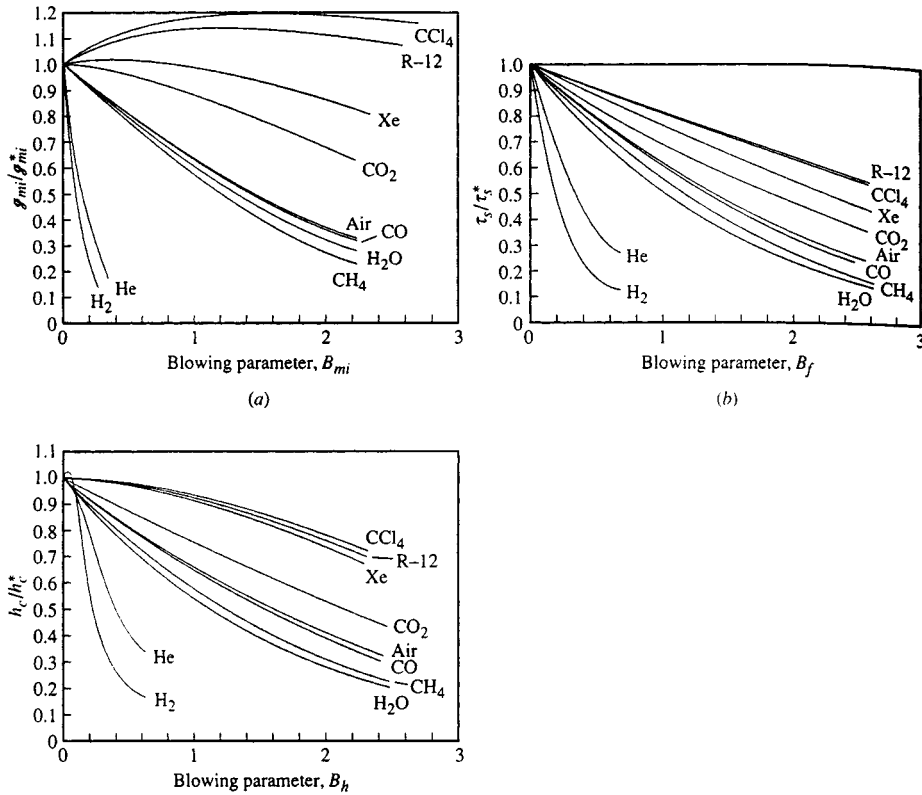
FIGURE 4.7.17 Numerical results for the effect of variable properties on blowing factors for a low-speed turbulent air boundary layer on a cold flat plate ($T_s/T_e = 0.2$) with foreign gas injection: (a) mass transfer conductance, (b) wall shear stress, (c) heat transfer coefficient. (From Landis, R.B., Ph.D. dissertation, University of California, Los Angeles, 1971. With permission.)

$$a_{mi} = 0.79\left(M_{\text{air}}/M_i\right)^{1.33} \qquad (4.7.72a)$$

$$a_{fi} = 0.91\left(M_{\text{air}}/M_i\right)^{0.76} \qquad (4.7.72b)$$

$$a_{hi} = 0.86\left(M_{\text{air}}/M_i\right)^{0.73} \qquad (4.7.72c)$$

In using Equation (4.7.70), the limit values for $\dot{m}'' = 0$ are elevated at the same location along the plate. Whether the injection rate is constant along the plate or varies as $x^{-0.2}$ to give a self-similar boundary layer has little effect on the blowing factors. Thus, Equation (4.7.72) has quite general applicability. Notice that the effects of injectant molecular weight are greater for turbulent boundary layers than for laminar ones, which is due to the effect of fluid density on turbulent transport. Also, the injectant specific heat does not appear in a_{hi} as it did for laminar flows. In general, c_{pi} decreases with increasing M_i and is adequately accounted for in the molecular weight ratio.

Reference State Schemes. The reference state approach, in which constant-property data are used with properties evaluated at some reference state, is an alternative method for handling variable-property effects. In principle, the reference state is independent of the precise property data used and of the

TABLE 4.7.7   Correction Factors for Foreign Gas Injection into Laminar Air Boundary Layers

Geometry	Species	$G_{mi}\,T_s/T_e$ 0.1	0.5	0.9	$G_{fi}\,T_s/T_e$ 0.1	0.5	0.9	$G_{hi}\,T_s/T_e$ 0.1	0.5	0.9
	H	1.14	1.36	1.47	1.30	1.64	1.79	1.15	1.32	—
	H_2	1.03	1.25	1.36	1.19	1.44	1.49	1.56	1.17	1.32
	He	1.05	1.18	1.25	1.34	1.49	1.56	1.18	1.32	—
	Air	—	—	—	1.21	1.27	1.27	1.17	1.21	—
	Xe	1.21	1.13	1.15	1.38	1.34	1.34	1.19	1.18	—
	CCl_4	1.03	0.95	1.00	1.00	1.03	1.03	1.04	1.04	—
Axisymmetric	H	1.00	1.04	1.09	1.00	0.62	0.45	1.00	0.94	0.54
stagnation point	H_2	1.00	1.06	1.06	1.00	0.70	0.62	1.00	1.00	1.01
	He	1.00	1.04	1.03	1.00	0.66	0.56	1.00	1.00	0.95
	C	1.00	1.01	1.00	1.00	0.79	0.69	1.00	0.99	0.87
	CH_4	1.00	1.01	1.00	1.00	0.88	0.84	1.00	1.00	1.00
	O	1.00	0.98	0.97	1.00	0.79	0.70	1.00	0.98	0.95
	H_2O	1.00	1.01	1.00	1.00	0.82	0.73	1.00	1.00	0.99
	Ne	1.00	1.00	0.98	1.00	0.83	0.75	1.00	0.97	0.95
	Air	—	—	—	1.00	0.87	0.82	1.00	0.99	0.97
	A	1.00	0.97	0.94	1.00	0.93	0.91	1.00	0.96	0.95
	CO_2	1.00	0.97	0.95	1.00	0.96	0.94	1.00	0.99	0.97
	Xe	1.00	0.98	0.96	1.00	0.96	1.05	1.00	1.06	0.99
	CCl_4	1.00	0.90	0.83	1.00	1.03	1.07	1.00	0.96	0.93
	I_2	1.00	0.91	0.85	1.00	1.02	1.05	1.00	0.97	0.94
Planar stagnation line	He	0.96	0.98	0.98	0.85	0.53	0.47	0.93	0.91	0.92
	Air	—	—	—	0.94	0.84	0.81	0.94	0.94	—
	Xe	0.92	0.87	0.83	0.90	0.93	0.95	0.93	0.93	—

Based on numerical data of Wortman (1969). Correlations developed by Dr. D.W. Hatfield.

combination of injectant and free-stream species. A reference state for a boundary layer on a flat plate that can be used in conjunction with Figure 4.7.14 is (Knuth, 1963)

$$m_{1,r} = 1 - \frac{M_2}{M_2 - M_1}\frac{\ln(M_e/M_s)}{\ln(m_{2,e}M_e/m_{2,s}M_s)} \tag{4.7.73}$$

$$T_r = 0.5(T_e + T_s) + 0.2r^*\left(u_e^2/2c_{pr}\right) + 0.1\left[B_{hr} + \left(B_{hr} + B_{mr}\right)\frac{c_{p1} - c_{pr}}{c_{pr}}\right](T_s - T_e) \tag{4.7.74}$$

where species 1 is injected into species 2 and r^* is the recovery factor for an impermeable wall. Use of the reference state method is impractical for hand calculations: a computer program should be used to evaluate the required mixture properties.

References

Hirschfelder, J.O., Curtiss, C.F., and Bird, R.B. 1954. *Molecular Theory of Gases and Liquids*, John Wiley & Sons, New York.

Knuth, E.L. 1963. Use of reference states and constant property solutions in predicting mass-, momentum-, and energy-transfer rates in high speed laminar flows, *Int. J. Heat Mass Transfer*, 6, 1–22.

Landis, R.B. 1972. Numerical solution of variable property turbulent boundary layers with foreign gas injection, Ph.D. dissertation, School of Engineering and Applied Science, University of California, Los Angeles.

Law, C.K. and Williams, F.A. 1972. Kinetics and convection in the combustion of alkane droplets, *Combustion and Flame*, 19, 393–405.

Mills, A.F. 1995. *Heat and Mass Transfer*, Richard D. Irwin, Chicago.

Wortman, A. 1969. Mass transfer in self-similar boundary-layer flows, Ph.D. dissertation, School of Engineering and Applied Science, University of California, Los Angeles.

Further Information

Geankoplis, C.J. 1993. *Transport Processes and Unit Operations*, 3rd ed., Prentice-Hall, Englewood Cliffs, NJ. This text gives a chemical engineering perspective on mass transfer.

Mills, A.F. 1995. *Heat and Mass Transfer*, Richard D. Irwin, Chicago. Chapter 11 treats mass transfer equipment relevant to mechanical engineering.

Strumillo, C. and Kudra, T. 1986. *Drying: Principles, Applications and Design*, Gordon and Breach, New York.

Mujamdar, A.S.. Ed. 1987. *Handbook of Industrial Drying*, Marcel Dekker, New York.

4.8   Applications

Enhancement

Arthur E. Bergles

Introduction

Energy- and materials-saving considerations, as well as economic incentives, have led to efforts to produce more efficient heat exchange equipment. Common thermal-hydraulic goals are to reduce the size of a heat exchanger required for a specified heat duty, to upgrade the capacity of an existing heat exchanger, to reduce the approach temperature difference for the process streams, or to reduce the pumping power.

The study of improved heat transfer performance is referred to as heat transfer *enhancement*, *augmentation*, or *intensification*. In general, this means an increase in heat transfer coefficient. Attempts to increase "normal" heat transfer coefficients have been recorded for more than a century, and there is a large store of information. A survey (Bergles et al., 1991) cites 4345 technical publications, excluding patents and manufacturers' literature. The literature has expanded rapidly since 1955.

Enhancement techniques can be classified either as passive methods, which require no direct application of external power (Figure 4.8.1), or as active methods, which require external power. The effectiveness of both types of techniques is strongly dependent on the mode of heat transfer, which may range from single-phase free convection to dispersed-flow film boiling. Brief descriptions of these methods follow.

Treated surfaces involve fine-scale alternation of the surface finish or coating (continuous or discontinuous). They are used for boiling and condensing; the roughness height is below that which affects single-phase heat transfer.

Rough surfaces are produced in many configurations ranging from random sand-grain-type roughness to discrete protuberances. See Figure 4.8.1a. The configuration is generally chosen to disturb the viscous sublayer rather than to increase the heat transfer surface area. Application of rough surfaces is directed primarily toward single-phase flow.

Extended surfaces are routinely employed in many heat exchangers. See Figure 4.8.1a to d. Work of special interest to enhancement is directed toward improvement of heat transfer coefficients on extended surfaces by shaping or perforating the surfaces.

Displaced enhancement devices are inserted into the flow channel so as indirectly to improve energy transport at the heated surface. They are used with forced flow. See Figure 4.8.1e and f.

Swirl-flow devices include a number of geometric arrangements or tube inserts for forced flow that create rotating and/or secondary flow: coiled tubes, inlet vortex generators, twisted-tape inserts, and axial-core inserts with a screw-type winding.

Surface-tension devices consist of wicking or grooved surfaces to direct the flow of liquid in boiling and condensing.

Additives for liquids include solid particles and gas bubbles in single-phase flows and liquid trace additives for boiling systems.

Additives for gases are liquid droplets or solid particles, either dilute-phase (gas-solid suspensions) or dense-phase (fluidized beds).

Mechanical aids involve stirring the fluid by mechanical means or by rotating the surface. Surface "scraping," widely used for batch processing of viscous liquids in the chemical process industry, is applied to the flow of such diverse fluids as high-viscosity plastics and air. Equipment with rotating heat exchanger ducts is found in commercial practice.

Surface vibration at either low or high frequency has been used primarily to improve single-phase heat transfer.
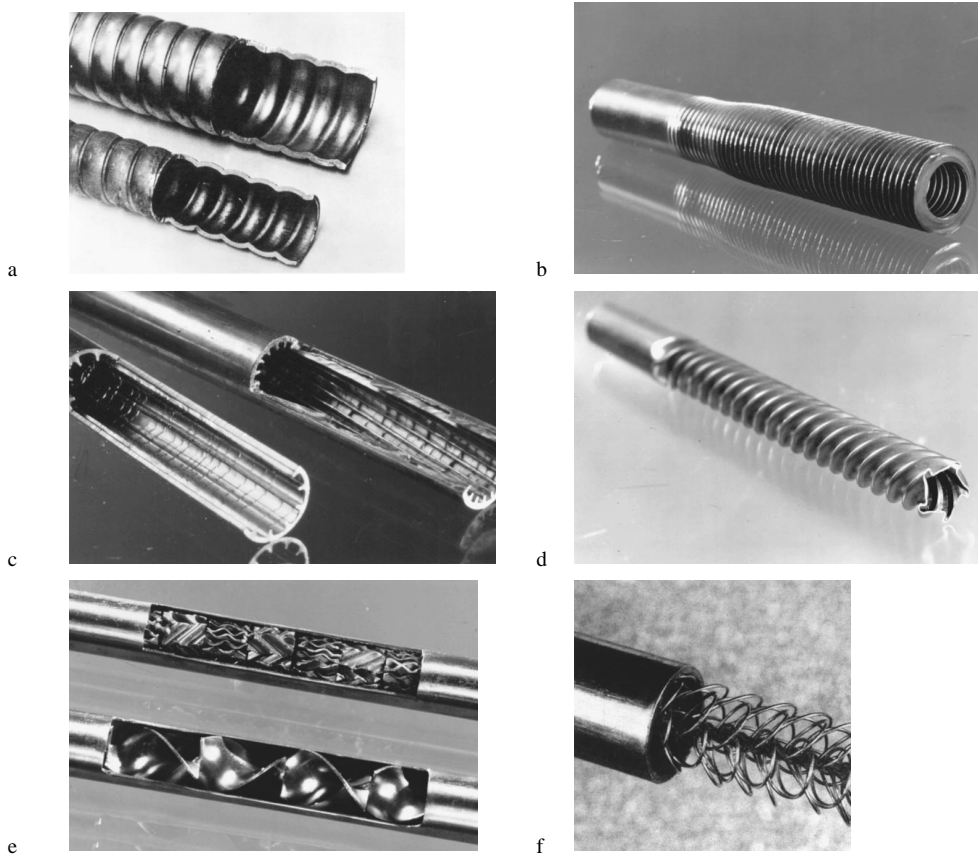
FIGURE 4.8.1 Enhanced tubes for augmentation of single-phase heat transfer. (a) Corrugated or spirally indented tube with internal protuberances. (b) Integral external fins. (c) Integral internal fins. (d) Deep spirally fluted tube. (e) Static mixer inserts. (f) Wire-wound insert.

Fluid vibration is the practical type of vibration enhancement because of the mass of most heat exchangers. The vibrations range from pulsations of about 1 Hz to ultrasound. Single-phase fluids are of primary concern.

Electrostatic fields (DC or AC) are applied in many different ways to dielectric fluids. Generally speaking, electrostatic fields can be directed to cause greater bulk mixing or fluid or disruption of fluid flow in the vicinity of the heat transfer surface, which enhances heat transfer.

Injection is utilized by supplying gas to a stagnant or flowing liquid through a porous heat transfer surface or by injecting similar fluid upstream of the heat transfer section. Surface degassing of liquids can produce enhancement similar to gas injection. Only single-phase flow is of interest.

Suction involves vapor removal, in nucleate or film boiling, or fluid withdrawal, in single-phase flow, through a porous heated surface.

Two or more of the above techniques may be utilized simultaneously to produce an enhancement that is larger than either of the techniques operating separately. This is termed *compound enhancement*.

It should be emphasized that one of the motivations for studying enhanced heat transfer is to assess the effect of an inherent condition on heat transfer. Some practical examples include roughness produced by standard manufacturing, degassing of liquids with high gas content, surface vibration resulting from rotating machinery or flow oscillations, fluid vibration resulting from pumping pulsation, and electrical fields present in electrical equipment.

The surfaces in Figure 4.8.1 have been used for both single-phase and two-phase heat transfer enhancement. The emphasis is on effective and cost-competitive (proved or potential) techniques that have made the transition from the laboratory to commercial heat exchangers.

Single-Phase Free Convection

With the exception of the familiar technique of providing extended surfaces, the passive techniques have little to offer in the way of enhanced heat transfer for free convection. This is because the velocities are usually too low to cause flow separation or secondary flow.

The restarting of thermal boundary layers in interrupted extended surfaces increases heat transfer so as to more than compensate for the lost area.

Mechanically aided heat transfer is a standard technique in the chemical and food industries when viscous liquids are involved. The predominant geometry for surface vibration has been the horizontal cylinder, vibrated either horizontally or vertically. Heat transfer coefficients can be increased tenfold for both low-frequency/high-amplitude and high-frequency/low-amplitude situations. It is, of course, equally effective and more practical to provide steady forced flow. Furthermore, the mechanical designer is concerned that such intense vibrations could result in equipment failures.

Since it is usually difficult to apply surface vibrations to practical equipment, an alternative technique is utilized whereby vibrations are applied to the fluid and focused toward the heated surface. With proper transducer design, it is also possible to improve heat transfer to simple heaters immersed in gases or liquids by several hundred percent.

Electric fields are particularly effective in increasing heat transfer coefficients in free convection. Dielectrophoretic or electrophoretic (especially with ionization of gases) forces cause greater bulk mixing in the vicinity of the heat transfer surface. Heat transfer coefficients may be improved by as much as a factor of 40 with electrostatic fields up to 100,000 V. Again, the equivalent effect could be produced at lower capital cost and without the voltage hazard by simply providing forced convection with a blower or fan.

Single-Phase Forced Convection

The present discussion emphasizes enhancement of heat transfer *inside* ducts that are primarily of circular cross section. Typical data for turbulence promoters inserted inside tubes are shown in Figure 4.8.2. As shown in Figure 4.8.2a, the promoters produce a sizable elevation in the Nusselt number, or heat transfer coefficient, at constant Reynolds number, or velocity. However, as shown in Figure 4.8.2b, there is an accompanying large increase in the friction factor.

Surface roughness has been used extensively to enhance forced convection heat transfer. Integral roughness may be produced by the traditional manufacturing processes of machining, forming, casting, or welding. Various inserts can also provide surface protuberances. In view of the infinite number of possible geometric variations, it is not surprising that, even after more than 300 studies, no completely satisfactory unified treatment is available.

In general, the maximum enhancement of laminar flow with many of the techniques is the same order of magnitude, and seems to be independent of the wall boundary condition. The enhancement with some rough tubes, corrugated tubes, inner-fin tubes, various static mixers, and twisted-type inserts is about 200%. The improvements in heat transfer coefficient with turbulent flow in rough tubes (based on nominal surface area) are as much as 250%. Analogy solutions for sand-grain-type roughness and for square-repeated-rib roughness have been proposed. A statistical correlation is also available for heat transfer coefficient and friction factor.

The following correlations are recommended for tubes with transverse or helical repeated ribs (Figure 4.8.1a) with turbulent flow (Ravigururajan and Bergles, 1985):

$$\mathrm{Nu}_{D_i,a}/\mathrm{Nu}_{D_i,s} = \left\{ 1 + \left[2.64\,\mathrm{Re}^{0.036}\left(e/D_i\right)^{0.212}\left(\left(p/D_i\right)^{-0.21}\right)\left(\alpha/90\right)^{0.29}\left(\mathrm{Pr}\right)^{-0.024} \right]^7 \right\}^{1/7} \qquad (4.8.1)$$
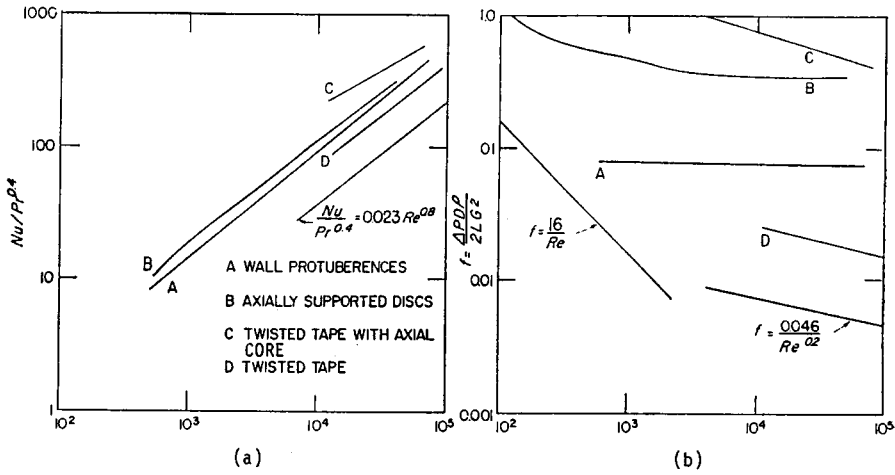
FIGURE 4.8.2 Typical data for turbulence promoters inserted inside tubes: (a) heat transfer data, (b) friction data. (From Bergles, 1969. With permission.)

$$f_a/f_s = \left\{1 + \left[29.1\text{Re}_{D_i}^{\left(0.67-0.06p/D_i-0.49a/90\right)} \times \left(e/D_i\right)^{\left(0.37-0.157p/D_i\right)} \times \left(p/D_i\right)^{\left(-1.66\times10^{-6}\text{Re}_{D_i}-0.33\alpha/90\right)}\right.\right.$$

$$\left.\left.\times \left(\alpha/90\right)^{\left(4.59+4.11\times10^{-6}\text{Re}_{D_i}-0.15p/D_i\right)} \times \left(1+\frac{2.94}{n}\right)\sin\beta\right]^{15/16}\right\}^{16/15}$$

(4.8.2)

where the subscript a refers to the enhanced tube and the subscript s refers to the smooth tube. The special symbols are given as follows: e = protuberance height; p = repeated-rib pitch; α = spiral angle for helical ribs, °; n = number of sharp corners facing the flow; and β = contact angle of rib profile, °.

Also,

$$\text{Nu}_s = 0.125f\,\text{Re}_{D_i}\text{Pr}\Big/\left(1+12.7\left(0.125f\right)^{0.5}\text{Pr}^{0.667}-1\right)$$

and

$$f_s = \left(1.82\log_{10}\text{Re}_{D_i}-1.64\right)^{-2}{}^{*}$$

Much work has been done to obtain the enhanced heat transfer of parallel angled ribs in short rectangular channels, simulating the interior of gas turbine blades. Jets are frequently used for heating, cooling, and drying in a variety of industrial applications. A number of studies have reported that roughness elements of the transverse-repeated-rib type mitigate the deterioration in heat transfer downstream of stagnation.

Extended surfaces can be considered "old technology" as far as most applications are concerned. The real interest now is in increasing heat transfer coefficients on the extended surface. Compact heat exchangers of the plate-fin or tube-and-center variety use several enhancement techniques: offset strip fins, louvered fins, perforated fins, or corrugated fins. Coefficients are several hundred percent above the

---

* The Fanning friction factor is used throughout this section.

smooth-tube values; however, the pressure drop is also substantially increased, and there may be vibration and noise problems.

For the case of offset strip fins the following correlations are recommended for calculating the *j* and *f* characteristics (Manglik and Bergles, 1990)

$$j_h = 0.6522 \text{Re}_h^{-0.5403} \, \alpha^{-0.1541} \, \delta^{0.1499} \, \gamma^{-0.0678} \times \left[1 + 5.269 \times 10^{-5} \text{Re}_h^{1.340} \, \alpha^{0.504} \, \delta^{0.456} \, \gamma^{-1.055}\right]^{0.1} \quad (4.8.3)$$

$$f_h = 9.6243 \text{Re}_h^{-0.7422} \, \alpha^{-0.1856} \, \delta^{0.3053} \, \gamma^{-0.2659} \times \left[1 + 7.669 \times 10^{-8} \text{Re}_h^{4.429} \, \alpha^{0.920} \, \delta^{3.767} \, \gamma^{0.236}\right]^{0.1} \quad (4.8.4)$$

where j_H (the heat transfer *j*-factor $\text{Nu}_H/\text{Re}_H\text{Pr}^{1/3}$), and f_h, and Re_h are based on the hydraulic diameter given by

$$D_h = 4shl\big/\left[2(sl + hl + th) + ts\right] \quad (4.8.5)$$

Special symbols are α = aspect ratio s/h, δ = ratio t/l, γ = ratio t/s, s = lateral spacing of strip fin, h = strip fin height, l = length of one offset module of strip fins, and t = fin thickness.

These equations are based on experimental data for 18 different offset strip-fin geometries, and they represent the data continuously in the laminar, transition, and turbulent flow regions.

Internally finned circular tubes are available in aluminum and copper (or copper alloys). Correlations (for heat transfer coefficient and friction factor) are available for laminar flow, for both straight and spiral continuous fins.

Turbulent flow in tubes with straight or helical fins (Figure 4.8.1c) was correlated by (Carnavos, 1979)

$$\text{Nu}_h = 0.023 \text{Pr}^{0.4} \text{Re}_h^{0.8} \left[\frac{A_c}{A_{ci}}\right]^{0.1} \left[\frac{A_{s,i}}{A_s}\right]^{0.5} (\sec \alpha)^3 \quad (4.8.6)$$

$$f_h = 0.046 \text{Re}_h^{-0.2} \left[\frac{A_c}{A_{c,i}}\right]^{0.5} (\sec \alpha)^{0.75} \quad (4.8.7)$$

where $A_{c,i}$ is based on the maximum inside (envelope) flow area, $A_{s,i}$ is based on the maximum inside (envelope) surface area, and α the spiral angle for helical fins, °.

A numerical analysis of turbulent flow in tubes with idealized straight fins was reported. The necessary constant for the turbulence model was obtained from experimental data for air. Further improvements in numerical techniques are expected, so that a wider range of geometries and fluids can be handled without resort to extensive experimental programs.

Many proprietary surface configurations have been produced by deforming the basic tube. The "convoluted," "corrugated," "spiral," or "spirally fluted" tubes (Figure 4.8.1a) have multiple-start spiral corrugations, which add area, along the tube length. A systematic survey of the single-tube performance of condenser tubes indicates up to 400% increase in the nominal inside heat transfer coefficient (based on diameter of a smooth tube of the same maximum inside diameter); however, pressure drops on the water side are about 20 times higher.

Displaced enhancement devices are typically in the form of inserts, within elements arranged to promote transverse mixing (static mixers, Figure 4.8.1e). They are used primarily for viscous liquids, to promote either heat transfer or mass transfer. Displaced promoters are also used to enhance the radiant heat transfer in high-temperature applications. In the flue-tube of a hot-gas-fired hot water heater, there is a trade-off between radiation and convection. Another type of displaced insert generates vortices, which enhance the downstream flow. Delta-wing and rectangular wing promoters, both co-rotating and

counterrotating, have been studied. Wire-loop inserts (Figure 4.8.1f) have also been used for enhancement of laminar and turbulent flow.

Twisted-tape inserts have been widely used to improve heat transfer in both laminar and turbulent flow. Correlations are available for laminar flow, for both uniform heat flux and uniform wall temperature conditions. Turbulent flow in tubes with twisted-tape inserts has also been correlated. Several studies have considered the heat transfer enhancement of a decaying swirl flow, generated, say, by a short twisted-tape insert.

Performance Evaluation Criteria for Single-Phase Forced Convection in Tubes

Numerous, and sometimes conflicting, factors enter into the ultimate decision to use an enhancement technique: heat duty increase or area reduction that can be obtained, initial cost, pumping power or operating cost, maintenance cost (especially cleaning), safety, and reliability, among others. These factors are difficult to quantitize, and a generally acceptable selection criterion may not exist. It is possible, however, to suggest some performance criteria for preliminary design guidance. As an example, consider the basic geometry and the pumping power fixed, with the objective of increasing the heat transfer. The following ratio is then of interest

$$R_3 = \left(\frac{h_a}{h_s}\right)_{D_i, L, N, P, T_{\text{in}}, \Delta T} = \frac{\left(\text{Nu}/\text{Pr}^{0.4}\right)_a}{\left(\text{Nu}/\text{Pr}^{0.4}\right)_s} = \frac{q_a}{q_s} \qquad (4.8.8)$$

where P = pumping power, T_{in} = inlet bulk temperature of fluid, and ΔT = average wall-fluid temperature difference.

With the pumping power (neglecting entrance and exit losses) given as

$$P = NV A_c 4f(L/D)\rho V^2/2 \qquad (4.8.9)$$

and

$$f_s = 0.046/\text{Re}_s^{0.2} \qquad (4.8.10)$$

$$A_{c,a} f_a \text{Re}_a^3 = {}^{0.046} A_{c,s} \text{Re}_s^{2.8} \qquad (4.8.11)$$

The calculation best proceeds by picking $\text{Re}_{D_i,a}$, and reading $\text{Nu}_{D_i,a}/\text{Pr}^{0.4}$ and f_a. $\text{Re}_{D_i,s}$ is then obtained from Equation (4.8.11) and $\text{Nu}_{D_i,s}/\text{Pr}^{0.4}$ obtained from a conventional, empty-tube correlation. The desired ratio of Equation (4.8.8) is then obtained. Typical results are presented in Figure 4.8.3 for a repeated-rib roughness (Bergles et al., 1974).

Active and Compound Techniques for Single-Phase Forced Convection

Under active techniques, mechanically aided heat transfer in the form of surface scraping can increase forced convection heat transfer. Surface vibration has been demonstrated to improve heat transfer to both laminar and turbulent duct flow of liquids. Fluid vibration has been extensively studied for both air (loudspeakers and sirens) and liquids (flow interrupters, pulsators, and ultrasonic transducers). Pulsations are relatively simple to apply to low-velocity liquid flows, and improvements of several hundred percent can be realized.

Some very impressive enhancements have been recorded with electrical fields, particularly in the laminar-flow region. Improvements of at least 100% were obtained when voltages in the 10-kV range were applied to transformer oil. It is found that even with intense electrostatic fields, the heat transfer enhancement disappears as turbulent flow is approached in a circular tube with a concentric inner electrode.
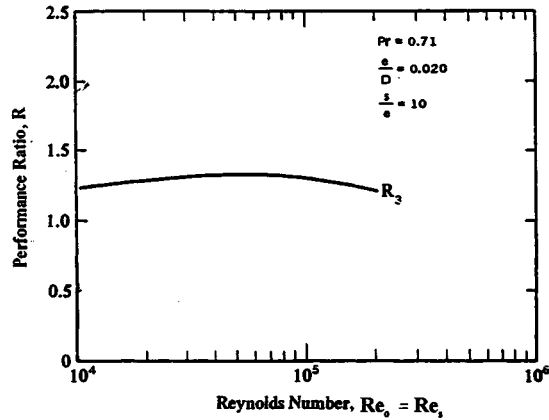
FIGURE 4.8.3 Constant pumping power performance criterion applied to repeated rib roughness.

Compound techniques are a slowly emerging area of enhancement that holds promise for practical applications, since heat transfer coefficients can usually be increased above each of the several techniques acting along. Some examples that have been studied are as follows: rough tube wall with twisted-tape inserts, rough cylinder with acoustic vibrations, internally finned tube with twisted-tape inserts, finned tubes in fluidized beds, externally finned tubes subjected to vibrations, rib-roughened passage being rotated, gas-solid suspension with an electrical field, fluidized bed with pulsations of air, and a rib-roughened channel with longitudinal vortex generation.

Pool Boiling

Selected passive and active enhancement techniques have been shown to be effective for pool boiling and flow boiling/evaporation. Most techniques apply to nucleate boiling; however, some techniques are applicable to transition and film boiling.

It should be noted that phase-change heat transfer coefficients are relatively high. The main thermal resistance in a two-fluid heat exchanger often lies on the non-phase-change side. (Fouling of either side can, of course, represent the dominant thermal resistance.) For this reason, the emphasis is often on enhancement of single-phase flow. On the other hand, the overall thermal resistance may then be reduced to the point where significant improvement in the overall performance can be achieved by enhancing the two-phase flow. Two-phase enhancement would also be important in double-phase-change (boiling/condensing) heat exchangers.

As discussed elsewhere, surface material and finish have a strong effect on nucleate and transition pool boiling. However, reliable control of nucleation on plain surfaces is not easily accomplished. Accordingly, since the earliest days of boiling research, there have been attempts to relocate the boiling curve through use of relatively gross modification of the surface. For many years, this was accomplished simply by area increase in the form of low helical fins. The subsequent tendency was to structure surfaces to improve the nucleate boiling characteristics by a fundamental change in the boiling process. Many of these advanced surfaces are being used in commercial shell-and-tube boilers.

Several manufacturing processes have been employed: machining, forming, layering, and coating. In Figure 4.8.4a standard low-fin tubing is shown. Figure 4.8.4c depicts a tunnel-and-pore arrangement produced by rolling, upsetting, and brushing. An alternative modification of the low fins is shown in Figure 4.8.4d, where the rolled fins have been split and rolled to a T shape. Further modification of the internal, Figure 4.8.4e, or external, Figure 4.8.4f, surface is possible. Knurling and rolling are involved in producing the surface shown in Figure 4.8.4g. The earliest example of a commercial structured surface, shown in Figure 4.8.4b is the porous metallic matrix produced by sintering or brazing small particles. Wall superheat reductions of up to a factor of ten are common with these surfaces. The advantage is not
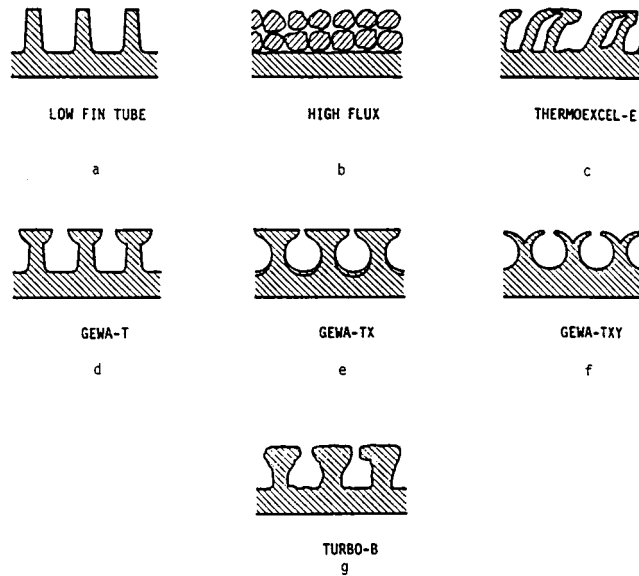
FIGURE 4.8.4 Examples of commercial structured boiling surfaces. (From Pate, M.B. et al., in *Compact Heat Exchangers*, Hemisphere Publishing, New York, 1990. With permission.)

only a high nucleate boiling heat transfer coefficient, but the fact that boiling can take place at very low temperature differences.

These structured boiling surfaces, developed for refrigeration and process applications, have been used as "heat sinks" for immersion-cooled microelectronic chips.

The behavior of tube bundles is often different with structured-surface tubes. The enhanced nucleate boiling dominates, and the convective boiling enhancement, found in plain tube bundles, does not occur.

Active enhancement techniques include heated surface rotation, surface wiping, surface vibration, fluid vibration, electrostatic fields, and suction at the heated surface. Although active techniques are effective in reducing the wall superheat and/or increasing the critical heat flux, the practical applications are very limited, largely because of the difficulty of reliably providing the mechanical or electrical effect.

Compound enhancement, which involves two or more techniques applied simultaneously, has also been studied. Electrohydrodynamic enhancement was applied to a finned tube bundle, resulting in nearly a 200% increase in the average boiling heat transfer coefficient of the bundle, with a small power consumption for the field.

Convective Boiling/Evaporation

The structured surfaces described in the previous section are generally not used for in-tube vaporization, because of the difficulty of manufacture. One notable exception is the high-flux surface in a vertical thermosiphon reboiler. The considerable increase in the low-quality, nucleate boiling coefficient is desirable, but it is also important that more vapor is generated to promote circulation.

Helical repeated ribs and helically coiled wire inserts have been used to increase vaporization coefficients and the dry-out heat flux in once-through boilers.

Numerous tubes with internal fins, either integral or attached, are available for refrigerant evaporators. Original configurations were tightly packed, copper, offset strip fin inserts soldered to the copper tube or aluminum, star-shaped inserts secured by drawing the tube over the insert. Examples are shown in Figure 4.8.5. Average heat transfer coefficients (based on surface area of smooth tube of the same diameter) for typical evaporator conditions are increased by as much as 200%. A cross-sectional view of a typical "microfin" tube is included in Figure 4.8.5. The average evaporation boiling coefficient is
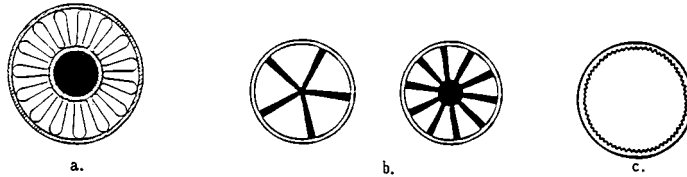
FIGURE 4.8.5 Inner-fin tubes for refrigerant evaporators: (a) Strip-fin inserts, (b) Star-shaped inserts, (c) Microfin.

increased 30 to 80%. The pressure drop penalties are less; that is, lower percentage increases in pressure drop are frequently observed.

Twisted-tape inserts are generally used to increase the burnout heat flux for subcooled boiling at high imposed heat fluxes $10^7 – 10^8$ W/m^2, as might be encountered in the cooling of fusion reactor components. Increases in burnout heat flux of up to 200% were obtained at near atmospheric pressure.

Vapor-Space Condensation

As discussed elsewhere, condensation can be either filmwise or dropwise. In a sense, dropwise condensation is enhancement of the normally occurring film condensation by surface treatment. The only real application is for steam condensers, because nonwetting coatings are not available for most other working fluids. Even after much study, little progress has been made in developing permanently hydrophobic coatings for practical steam condensers. The enhancement of dropwise condensation is pointless, because the heat transfer coefficients are already so high.

Surface extensions are widely employed for enhancement of condensation. The integral low fin tubing (Figure 4.8.4a), used for kettle boilers, is also used for horizontal tube condensers. With proper spacing of the fins to provide adequate condensate drainage, the average coefficients can be several times those of a plain tube with the same base diameter. These fins are normally used with refrigerants and other organic fluids that have low condensing coefficients, but which drain effectively, because of low surface tension.

The fin profile can be altered according to mathematical analysis to take full advantage of the Gregorig effect, whereby condensation occurs mainly at the tops of convex ridges. Surface tension forces then pull the condensate into concave grooves, where it runs off. The average heat transfer coefficient is greater than that for an axially uniform film thickness. The initial application was for condensation of steam on vertical tubes used for reboilers and in desalination. According to numerical solutions, the optimum geometry is characterized by a sharp fin tip, gradually changing curvature of the fin surface from tip to root, wide grooves between fins to collect condensate, and periodic condensate strippers. Figure 4.8.6 schematically presents the configuration.
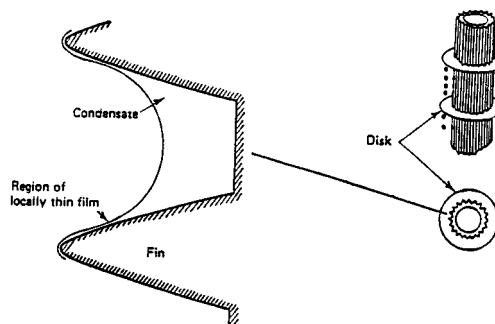

FIGURE 4.8.6 Recommended flute profile and schematic of condensate strippers.

Recent interest has centered on three-dimensional surfaces for horizontal-tube condensers. The considerable improvement relative to low fins or other two-dimensional profiles is apparently due to multidimensional drainage at the fin tips. Other three-dimensional shapes include circular pin fins, square pins, and small metal particles that are bonded randomly to the surface.

Convective Condensation

This final section on enhancement of the various modes of heat transfer focuses on in-tube condensation. The applications include horizontal kettle-type reboilers, moisture separator reheaters for nuclear power plants, and air-conditioner condensers.

Internally grooved or knurled tubes, deep spirally fluted tubes, random roughness, conventional inner-fin tubes have been shown to be effective for condensation of steam and other fluids.

The microfin tubes mentioned earlier have also been applied successfully to in-tube condensing. As in the case of evaporation, the substantial heat transfer improvement is achieved at the expense of a lesser percentage increase in pressure drop. By testing a wide variety of tubes, it has been possible to suggest some guidelines for the geometry, e.g., more fins, longer fins, and sharper tips; however, general correlations are not yet available. Fortunately for heat-pump operation, the tube that performs best for evaporation also performs best for condensation.

Twisted-tape inserts result in rather modest increases in heat transfer coefficient for complete condensation of either steam or refrigerant. The pressure drop increases are large because of the large wetted surface. Coiled tubular condensers provide a modest improvement in average heat transfer coefficient.

References

Bergles, A.E. 1969. Survey and evaluation of techniques to augment convective heat and mass transfer, in *Progress in Heat and Mass Transfer*, Vol. 1, Pergamon, Oxford, England.

Bergles, A.E. 1985. Techniques to augment heat transfer, in *Handbook of Heat Transfer Applications*, W.M. Rohsenow, J.P. Hartnett, and E.N. Ganic, Eds., McGraw-Hill, New York, 3-1–3-80.

Bergles, A.E. 1988. Some perspectives on enhanced heat transfer — second generation heat transfer technology, *J. Heat Transfer*, 110, 1082–1096.

Bergles, A.E. 1997. Heat transfer enhancement — the encouragement and accommodation of high heat fluxes. *J. Heat Transfer*, 119, 8–19.

Bergles, A.E., Blumenkrantz, A.R., and Taborek, J. 1974. Performance evaluation criteria for enhanced heat transfer surfaces, in *Heat Transfer 1974*, The Japan Society of Mechanical Engineers, Tokyo, Vol. II, 234–238.

Bergles, A.E., Jensen, M.K., Somerscales, E.F.C., and Manglik, R.M. 1991. Literature Review of Heat Transfer Enhancement Technology for Heat Exchangers in Gas-Fired Applications, Gas Research Institute Report, GR191-0146.

Carnavos, T.C. 1979. Heat transfer performance of internally finned tubes in turbulent flow, in *Advances in Advanced Heat Transfer*, ASME, New York, 61–67.

Manglik, R.M. and Bergles, A.E. 1990. The thermal-hydraulic design of the rectangular offset-strip-fin compact heat exchanger, in *Compact Heat Exchangers*, Hemisphere Publishing, New York, 123–149.

Pate, M.B., Ayub, Z.H., and Kohler, J. 1990. Heat exchangers for the air-conditioning and refrigeration industry: state-of-the-art design and technology, in *Compact Heat Exchangers*, Hemisphere Publishing, New York, 567–590.

Ravigururajan, S. and Bergles, A.E. 1985. General Correlations for Pressure Drop and Heat Transfer for Single-Phase Turbulent Flow in Internally Ribbed Tubes, in *Augmentation of Heat Transfer in Energy Systems*, HTD-Vol. 52, ASME, New York, 9–20.

Thome, J.R. 1990. *Enhanced Boiling Heat Transfer*, Hemisphere Publishing, New York.

Webb, R.L. 1994. *Principles of Enhanced Heat Transfer*, John Wiley & Sons, New York.

Further Information

This section gives some indication as to why heat transfer enhancement is one of the fastest growing areas of heat transfer. Many techniques are available for improvement of the various modes of heat transfer. Fundamental understanding of the transport mechanism is growing, but, more importantly, design correlations are being established. Many effective and cost-competitive enhancement techniques have made the transition from the laboratory to commercial heat exchangers.

Broad reviews of developments in enhanced heat transfer are available (Bergles, 1985; Bergles, 1988; Thome, 1990; Webb, 1994, Bergles, 1997). Also, several journals, especially *Heat Transfer Engineering, Enhanced Heat Transfer,* and *International Journal of Heating, Ventilating, Air-Conditioning and Refrigerating Research*, feature this technology.

Cooling Towers

Anthony F. Mills

Introduction

In a wet cooling tower, water is evaporated into air with the objective of cooling the water stream. Both natural- and mechanical-draft towers are popular, and examples are shown in Figure 4.8.7. Large natural-draft cooling towers are used in power plants for cooling the water supply to the condenser. Smaller mechanical-draft towers are preferred for oil refineries and other process industries, as well as for central air-conditioning systems and refrigeration plant. Figure 4.8.7a shows a natural draft *counterflow* unit in which the water flows as thin films down over a suitable packing, and air flows upward. In a natural-draft tower the air flows upward due to the buoyancy of the warm, moist air leaving the top of the packing. In a mechanical-draft tower, the flow is forced or induced by a fan. Since the air inlet temperature is usually lower than the water inlet temperature, the water is cooled both by evaporation and by sensible heat loss. For usual operating conditions the evaporative heat loss is considerably larger than the sensible heat loss. Figure 4.8.7b shows a mechanical draft cross-flow unit. Figure 4.8.8 shows a natural-draft cross-flow tower for a power plant.

Packing Thermal Performance

Counterflow units. Merkel's method (Merkel, 1925) for calculating the number of transfer units required to cool the water stream, for specified inlet and outlet water temperatures and inlet air condition is (Mills, 1995)

$$N_{tu} = \frac{g_m S}{\dot{m}_L} = \int_{h_{L,\text{in}}}^{h_{L,\text{out}}} \frac{dh_L}{h_s - h_G} \qquad (4.8.12)$$

$$h_G = h_{G,\text{in}} + \left(\dot{m}_L / \dot{m}_G\right)\left(h_L - h_{L,\text{out}}\right) \qquad (4.8.13)$$

$$h_s\left(P, T_s\right) = h_s\left(P, T_L\right) \qquad (4.8.14)$$

It is imperative that the usual enthalpy datum states be used, namely, zero enthalpy for dry air and liquid water at 0°C. Table 4.8.1 gives enthalpy data for 1 atm pressure. The important assumptions required to obtain this result include

1. A Lewis number of unity;
2. Low mass transfer rate theory is valid;
3. The liquid-side heat transfer resistance is negligible, that is, $T_s \simeq T_L$;
4. The amount of water evaporated is small compared with the water and air flow rates.
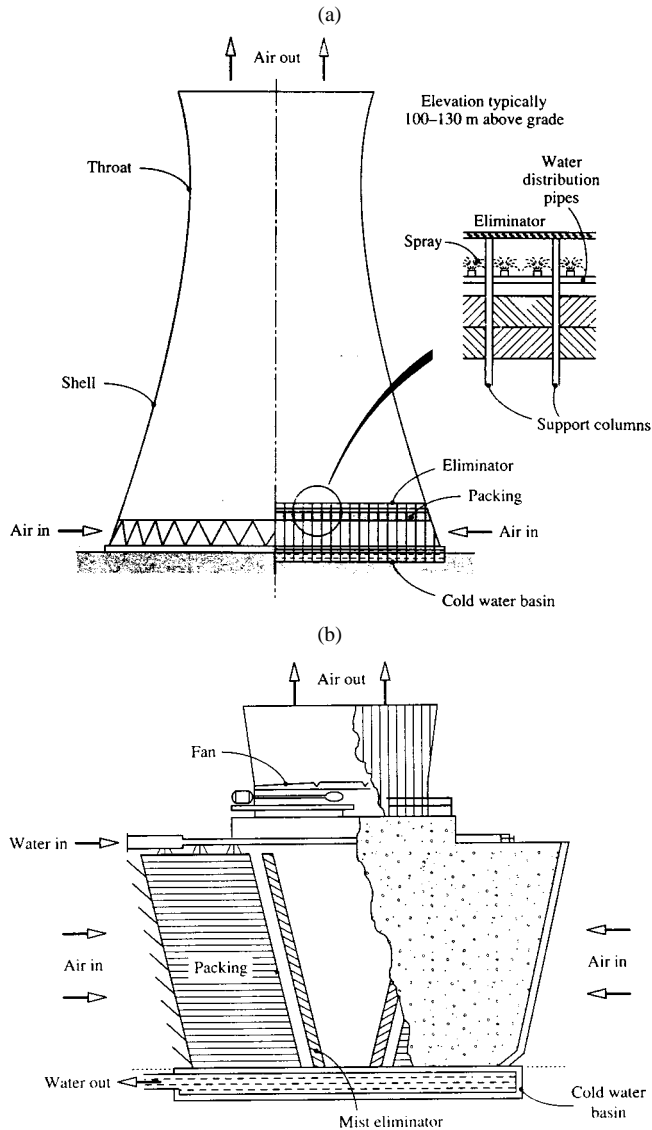
FIGURE 4.8.7 (a) A natural-draft counterflow cooling tower for a power plant. (b) A cross-flow cooling tower for an air-conditioning system.

The method is accurate up to temperatures of about 60°C; comparisons with more exact results are usually within 3 to 5%, and seldom show errors greater than 10%. Notice that the method does not give the outlet state of the air; however, in situations encountered in practice, the outlet air can be assumed to be saturated for the purposes of calculating its density. It is possible to extend Merkel's method to include a finite liquid-side heat transfer resistance, but such refinement is seldom warranted. For typical operating conditions the bulk liquid temperature is seldom more than 0.3 K above the interface temperature.

Cross-flow units. Figure 4.8.9 shows a schematic of a cross-flow packing. If we assume that both the liquid and gas streams are unidirectional, and that there is no mixing in either stream, then use of Merkel's assumptions leads to the following pair of differential equations (Mills, 1995):

FIGURE 4.8.8 A natural-draft cross-flow cooling tower for a power plant.

$$\frac{\partial h_G}{\partial x} = \frac{g_m a}{G}\left(h_s - h_G\right) \tag{4.8.15}$$

$$\frac{\partial h_L}{\partial y} = -\frac{g_m a}{L}\left(h_s - h_G\right) \tag{4.8.16}$$

Also $h_s = h_s(h_L)$ for a negligible liquid-side heat transfer resistance and the required boundary conditions are the inlet enthalpies of both streams. Equations (4.8.15) and (4.8.16) are solved numerically and the solution used to evaluate the average enthalpy of the outlet liquid,

$$\bar{h}_{L,\text{out}} = \frac{1}{X}\int_0^X h_{L,\text{out}}\ dx \tag{4.8.17}$$

Substituting in an exchanger energy balance on the liquid stream gives the heat transfer as

$$q = \dot{m}_L\left(h_{L,\text{in}} - h_{L,\text{out}}\right) \tag{4.8.18}$$

TABLE 4.8.1   Thermodynamic Properties of Water Vapor-Air Mixtures at 1 atm

Temp., °C	Saturation Mass Fraction	Specific Volume, m³/kg		Enthalpy[a,b] kJ/kg		
		Dry Air	Saturated Air	Liquid Water	Dry Air	Saturated Air
10	0.007608	0.8018	0.8054	42.13	10.059	29.145
11	0.008136	0.8046	0.8086	46.32	11.065	31.481
12	0.008696	0.8075	0.8117	50.52	12.071	33.898
13	0.009289	0.8103	0.8148	54.71	13.077	36.401
14	0.009918	0.8131	0.8180	58.90	14.083	38.995
15	0.01058	0.8160	0.8212	63.08	15.089	41.684
16	0.01129	0.8188	0.8244	67.27	16.095	44.473
17	0 01204	0.8217	0.8276	71.45	17.101	47.367
18	0 01283	0.8245	0.8309	75.64	18.107	50.372
19	0.01366	0.8273	0.8341	79.82	19.113	53.493
20	0.01455	0.8302	0.8374	83.99	20.120	56.736
21	0.01548	0.8330	0.8408	88.17	21.128	60.107
22	0.01647	0.8359	0.8441	92.35	22.134	63.612
23	0.01751	0.8387	0.8475	96.53	23.140	67.259
24	0.01861	0.8415	0.8510	100.71	24.147	71.054
25	0.01978	0.8444	0.8544	104.89	25.153	75.004
26	0.02100	0.8472	0.8579	109.07	26.159	79.116
27	0.02229	0.8500	0.8615	113.25	27.166	83.400
28	0.02366	0.8529	0.8650	117.43	28.172	87.862
29	0.02509	0.8557	0.8686	121.61	29.178	92.511
30	0.02660	0.8586	0.8723	125.79	30.185	97.357
31	0.02820	0.8614	0.8760	129.97	31.191	102.408
32	0.02987	0.8642	0.8798	134.15	32.198	107.674
33	0.03164	0.8671	0.8836	138.32	33.204	113.166
34	0.03350	0.8699	0.8874	142.50	34.211	118.893
35	0.03545	0.8728	0.8914	146.68	35.218	124.868
36	0.03751	0.8756	0.8953	150.86	36.224	131.100
37	0.03967	0.8784	0.8994	155.04	37.231	137.604
38	0.04194	0.8813	0.9035	159.22	38.238	144.389
39	0.04432	0.8841	0.9077	163.40	39.245	151.471
40	0.04683	0.8870	0.9119	167.58	40.252	158.862
41	0.04946	0.8898	0.9162	171.76	41.259	166.577
42	0.05222	0.8926	0.9206	175.94	42.266	174.630
43	0.05512	0.8955	0.9251	180.12	43.273	183.037
44	0.05817	0.8983	0.9297	184.29	44.280	191.815
45	0.06137	0.9012	0.9343	188.47	45.287	200.980
46	0.06472	0.9040	0.9391	192.65	46.294	210.550
47	0.06842	0.9068	0.9439	196.83	47.301	220.543
48	0.07193	0.9097	0.9489	201.01	48.308	230.980
49	0.07580	0.9125	0.9539	205.19	49.316	241.881

[a]   The enthalpies of dry air and liquid water are set equal to zero at a datum temperature of 0°C.

[b]   The enthalpy of an unsaturated water vapor-air mixture can be calculated as $h = h_{\text{dry air}} + (m_1/m_{1,\text{sat}})(h_{\text{sat}} - h_{\text{dry air}})$.

Sample calculation. Consider a counterflow unit that is required to cool water from 40 to 26°C when the inlet air is at 10°C, 1 atm, and saturated. We will calculate the number of transfer units required for balanced flow, that is, $\dot{m}_G/\dot{m}_L = 1$. Equation (4.8.12) is to be integrated numerically, with h_G obtained from Equation 4.8.13. The required thermodynamic properties can be obtained from Table 4.8.1. Using Table 4.8.1, $h_{G,\text{in}} = h_{\text{sat}}$ (10°C) = 29.15 kJ/kg, $h_{L,\text{out}} = h_L$(26°C) = 109.07 kJ/kg. Substituting in Equation (4.8.13),

$$h_G = 29.15 + \left(h_L - 109.07\right)$$

T_L, °C	h_L, kJ/kg	h_G, kJ/kg	h_s, kJ/kg	$h_s - h_g$, kJ/kg	$\dfrac{1}{h_s - h_g}$
26	109.07	29.15	79.12	49.97	0.02001
28	117.43	37.51	87.86	50.35	0.01986
30	125.79	45.87	97.36	51.49	0.01942
32	134.15	54.23	107.67	53.44	0.01871
34	142.50	62.58	118.89	56.31	0.01776
36	150.86	70.94	131.10	60.16	0.01662
38	159.22	79.30	144.39	65.09	0.01536
40	167.58	87.66	158.86	71.20	0.01404

Choosing 2°C intervals for convenient numerical integration, the above table is constructed, with h_L and $h_s = h_s(T_L)$ also obtained from Table 4.8.1.
Using the trapezoidal rule,

$$\int_{h_{L,\text{out}}}^{h_{L,\text{in}}} \frac{dh_L}{h_s - h_G} = \frac{8.36}{2}\big[0.02001 + 2(0.01986 + 0.01942 + 0.01871 + 0.01776$$

$$+ 0.01662 + 0.01536) + 0.01404\big]$$

$$= 1.043$$

From Equation (4.8.12), $N_{tu} = 1.043$. Also, by using Table 4.8.1, $T_{G,\text{out}} = 27.9°$ for saturated outlet air.
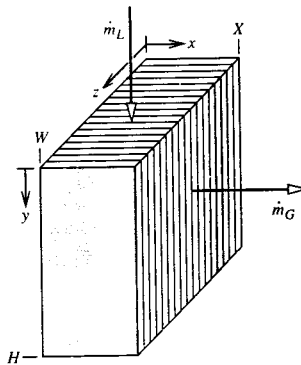

FIGURE 4.8.9 Schematic of a cross-flow cooling tower packing showing the coordinate system.

Thermal-Hydraulic Design of Cooling Towers

The thermal-hydraulic design of a mechanical-draft cooling tower is relatively straightforward. The flow rate ratio $\dot{m}_L / \dot{m}_G$ can be specified and varied parametrically to obtain an optimal design, for which the size and cost of the packing is balanced against fan power requirements and operating cost. Data are required for mass transfer conductances and friction for candidate packings. Tables 4.8.2a and b give correlations for a selection of packings. In Table 4.8.2b, the mass transfer conductance is correlated as $g_m a/L$, where a is the transfer area per unit volume and $L = \dot{m}_L / A_{fr}$ is the superficial mass velocity of the water flow (also called the *water loading* on the packing). Similarly, we define $G = \dot{m}_G / A_{fr}$. Typical water loadings are 1.8 to 2.7 kg/m² sec, and superficial air velocities fall in the range 1.5 to 4 m/sec. No attempt is made to correlate g_m and a separately. The number of transfer units of a packing of height H is then

$$N_{tu} = \frac{\mathcal{g}_m S}{\dot{m}_L} = \frac{\mathcal{g}_m a H}{L} \tag{4.8.19}$$

TABLE 4.8.2a Packings for Counterflow and Cross-Flow Cooling Towers: Designations and Descriptions

Counterflow Packings

1. Flat asbestos sheets, pitch 4.45 cm
2. Flat asbestos sheets, pitch 3.81 cm
3. Flat asbestos sheets, pitch 3.18 cm
4. Flat asbestos sheets, pitch 2.54 cm
5. 60° angle corrugated plastic, Munters M12060, pitch 1.17 in.
6. 60° angle corrugated plastic, Munters M19060, pitch 1.8 in.
7. Vertical corrugated plastic, American Tower Plastics Coolfilm, pitch 1.63 in.
8. Horizontal plastic screen, American Tower Plastics Cooldrop, pitch 8 in. 2 in. grid
9. Horizontal plastic grid, Ecodyne shape 10, pitch 12 in.
10. Angled corrugated plastic, Marley MC67, pitch 1.88 in.
11. Dimpled sheets, Toschi Asbestos-Free Cement, pitch 0.72 in.
12. Vertical plastic honeycomb, Brentwood Industries Accu-Pack, pitch 1.75 in.

Cross-Flow Packings

1. Doron V-bar, 4 × 8 in. spacing
2. Doron V-bar, 8 × 8 in. spacing
3. Ecodyne T-bar, 4 × 8 in. spacing
4. Ecodyne T-bar, 8 × 8 in. spacing
5. Wood lath, parallel to air flow, 4 × 4 in. spacing
6. Wood lath, perpendicular to air flow, 4 × 4 in. spacing
7. Marley α-bar, parallel to air flow, 16 × 4 in. spacing
8. Marley ladder, parallel to air flow, 8 × 2 in. spacing

The correlations are in terms of dimensionless mass velocities L^+ and G^+, and a *hot water correction* T_{HW}^+. The hot water correction accounts for a number of factors, such as errors associated with Merkel's method, deviations from low mass transfer rate theory at higher values of T_s, and fluid property dependence on temperature. Frictional resistance to air flow through the packings is correlated as a *loss coefficient* $N = \Delta P/(\rho V^2/2)$ per unit height or depth of packing, as a function of L^+ and G^+. The velocity V is superficial gas velocity. No hot water correction is required.

In a natural-draft tower, the thermal and hydraulic performance of the tower are coupled, and the flow rate ratio $\dot{m}_L / \dot{m}_G$ cannot be specified *a priori*. The buoyancy force producing the air flow depends on the state of the air leaving the packing which in turn depends on $\dot{m}_L / \dot{m}_G$ and the inlet air and water states. An iterative solution is required to find the operating point of the tower. The buoyancy force available to overcome the shell and packing pressure drops is

$$\Delta P^B = g\left(\rho_a - \rho_{G,\text{out}}\right) H \tag{4.8.20}$$

where ρ_a is the ambient air density and H is usually taken as the distance from the bottom of the packing to the top of the shell. The various pressure drops are conveniently expressed as

$$\Delta P_i = N_i \frac{\rho_{Gi} V_i^2}{2} \tag{4.8.21}$$

TABLE 4.8.2b Mass Transfer and Pressure Drop Correlations for Cooling Towers

Packing Number	C_1, m^{-1}	n_1	n_2	n_3	C_2, m^{-1}	n_4	n_5
Counterflow Packings: $L_0 = G_0 = 3.391$ kg/m^2 sec							
1	0.289	–0.70	0.70	0.00	2.72	0.35	–0.35
2	0.361	–0.72	0.72	0.00	3.13	0.42	–0.42
3	0.394	–0.76	0.76	0.00	3.38	0.36	–0.36
4	0.459	–0.73	0.73	0.00	3.87	0.52	–0.36
5	2.723	–0.61	0.50	–0.34	19.22	0.34	0.19
6	1.575	–0.50	0.58	–0.40	9.55	0.31	0.05
7	1.378	–0.49	0.56	–0.35	10.10	0.23	–0.04
8	0.558	–0.38	0.48	–0.54	4.33	0.85	–0.60
9	0.525	–0.26	0.58	–0.45	2.36	1.10	–0.64
10	1.312	–0.60	0.62	–0.60	8.33	0.27	–0.14
11	0.755	–0.51	0.93	–0.52	1.51	0.99	0.04
12	1.476	–0.56	0.60	–0.38	6.27	0.31	0.10
Cross-Flow Packings: $L_0 = 8.135$ kg/m^2 sec, $G_0 = 2.715$ kg/m^2 sec							
1	0.161	–0.58	0.52	–0.44	1.44	0.66	–0.73
2	0.171	–0.34	0.32	–0.43	1.97	0.72	–0.82
3	0.184	–0.51	0.28	–0.31	1.38	1.30	0.22
4	0.167	–0.48	0.20	–0.29	1.25	0.89	0.07
5	0.171	–0.58	0.28	–0.29	3.18	0.76	–0.80
6	0.217	–0.51	0.47	–0.34	4.49	0.71	–0.59
7	0.213	–0.41	0.50	–0.42	3.44	0.71	–0.85
8	0.233	–0.45	0.45	–0.48	4.89	0.59	0.16

Correlations (SI units)

Mass transfer: $\dfrac{g_m a}{L\left[\text{kg/m}^2\ \text{sec}\right]} = C_1\left(L^+\right)^{n_1}\left(G^+\right)^{n_2}\left(T_{HW}^+\right)^{n_3}$; Pressure drop: $\dfrac{N}{H\ \text{or}\ X} = C_2\left(L^+\right)^{n} + \left(G^+\right)^{n_s}$

where $L^+ = \dfrac{L}{L_0}$, $G^+ = \dfrac{G}{G_0}$, $T_{HW}^+ = \dfrac{1.8 T_{L,\text{in}}[\text{°C}] + 32}{110}$

Sources: Lowe, H.J. and Christie, D.G. 1961. "Heat transfer and pressure drop data on cooling tower packings, and model studies of the resistance of natural draft towers to airflow" Paper 113, *International Developments in Heat Transfer, Proc. of the International Heat Transfer Conference*, Boulder, CO, ASME, New York; Johnson, B.M., Ed. 1990. *Cooling Tower Performance Prediction and Improvement*, Vols. 1 and 2, EPRI GS-6370, Electric Power Research Institute, Palo Alto, CA. With permission.

Where N_i is the loss coefficient and V_i is the air velocity at the corresponding location. The pressure drops are associated with the shell, the packing, the mist eliminators, supports and pipes, and the water spray below the packing. Some sample correlations are given in Table 4.8.3.

Water loadings in counterflow natural-draft towers typically range from 0.8 to 2.4 kg/m^2 sec, and superficial air velocities range from 1 to 2 m/sec. The ratio of base diameter to height may be 0.75 to 0.85, and the ratio of throat to base diameter 0.55 to 0.65. The height of the air inlet is usually 0.10 to 0.12 times the base diameter to facilitate air flow into the tower. In practice the air flow distribution in natural-draft towers is not very uniform. However, the assumption of uniform air and water flows in our model of counterflow packing is adequate for most design purposes.

Cost-optimal design of cooling towers requires consideration of the complete power or refrigeration system. For refrigeration, the economics are determined mainly by the operating cost of the chiller (Kintner-Meyer and Emery, 1955).

TABLE 4.8.3   Pressure Drop Correlations for Cooling Tower Shells, Sprays, Supports, and Mist Eliminators

1.   Shell (natural draft counterflow):

$$N = 0.167 \left(\frac{D_B}{b} \right)^2$$

       where D_B is the diameter of the shell base and b is the height of the air inlet.

2.   Spray (natural-draft counterflow):

       $N = 0.526(Z_p[\text{m}] + 1.22)\ (\dot{m}_L / \dot{m}_G)^{1.32}$

3.   Mist eliminators:

       $N = 2\text{–}4$

4.   Support columns, pipes, etc. (natural-draft counterflow):

       $N = 2\text{–}6$

5.   Fan exit losses for mechanical-draft towers (velocity based on fan exit area):

       $N = 1.0,\ \text{forced draft}$

       $\simeq 0.5,\ \text{induced draft, depending on diffuser design}$

6.   Miscellaneous losses for mechanical-draft towers (velocity based on packing crosssectional area):

       $N \simeq 3$

Note: N is the loss coefficient defined by Equation 4.8.21, with velocity based on cross-sectional area for air flow underneath the packing in items 1 through 4.

Sources: Lowe, H.J. and Christie, D.G. 1961. Heat transfer and pressure drop data on cooling tower packings, and model studies of the resistance of natural draft towers to airflow. Paper 113, *International Developments in Heat Transfer Proc. of the International Heat Transfer Conference*, Boulder, CO, ASME, New York; Singham, J.R. 1990. Natural draft towers, in *Hemisphere Handbook of Heat Exchanger Design,* Sec. 3.12.3, Hewitt, G.E., Coord. Ed., Hemisphere, New York. With permission.

Cooling Tower Behavior

There are a number of computer programs available that use variations of Merkel's method to calculate the cooling tower performance, for example, TEFRI (Bourillot, 1983), VERA2D-84 (Mujamdar et al., 1985), CTOWER (Mills, 1995). These programs can be used to perform parametric studies to obtain the response of cooling towers to environmental, duty, and design changes. However, before using such programs, some thought should be given to the important characteristics of cooling tower behavior. For this purpose, it is useful to consider a graphical representation of Merkel's theory for a counterflow tower. Figure 4.8.10 shows a chart with moist air enthalpy plotted vs. water enthalpy (or, equivalently, water temperature) at 1 atm pressure. The *saturation curve* $h_s(T_s)$ is the enthalpy of saturated air. The *operating lines* $h_G(h_L)$ are given by Equation (4.8.13) and relate the air enthalpy to the water enthalpy at each location in the packing. The slope of an operating line is L/G. Since the assumption $T_s = T_L$ is made in Merkel's method, vertical lines on the chart connect h_s and h_G at each location in the packing. The driving force for enthalpy transfer, $(h_s - h_G)$, is the vertical distance between the saturation curve and the operating line. The integral in Equation (4.8.12) averages the reciprocal of this distance. By using this chart, a number of observations about cooling tower behavior can be made.

1. Figure 4.8.10 shows the effect of *L/G* for fixed water inlet and outlet temperatures, and fixed inlet air temperature and humidity. If we imagine *L* to be fixed as well, we see that as *G* decreases, the driving forces decrease, and so a larger NTU is required.
2. The minimum NTU required corresponds to *L/G* = 0, that is, an infinite air flow rate, for which the operating line is horizontal.
3. Due to the curvature of the operating line, it is possible for the operating line to be tangent to the saturation curve. The indicated NTU is then infinite, which tells us that the air flow rate must be increased in order to achieve the desired water cooling range.
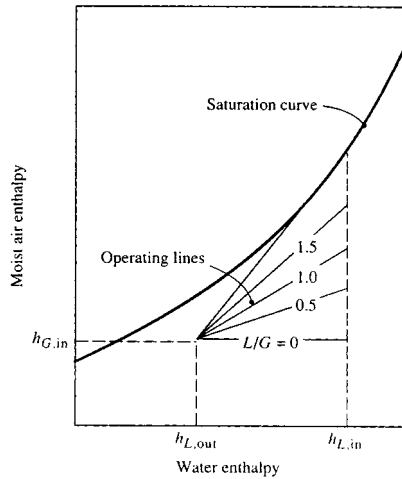
FIGURE 4.8.10 Counterflow cooling tower operating lines for various water-to-air flow-rate ratios shown on an enthalpy chart.

4. For a mechanical-draft tower, the optimal value of *L/G* lies between the two limits described in items 2 and 3 above. If *L/G* is large, the required height of packing is large, and the capital cost will be excessive. If *L/G* is small, the fan power will be excessive (since fan power is proportional to air volume flow rate times pressure drop).

Range and Approach

Cooling tower designers and utility engineers have traditionally used two temperature differences to characterize cooling tower operation. The *range* is the difference between the water inlet and outlet temperatures (also called simply the hot and cold water temperatures). The *approach* is the difference between the outlet water temperature and the wet-bulb temperature of the entering (ambient) air. The approach characterizes cooling tower performance; for a given inlet condition, a larger packing will produce a smaller approach to the ambient wet-bulb temperature, and hence a lower water outlet temperature. (The water cannot be cooled below the ambient wet-bulb temperature.) The approach concept is useful because the ambient dry-bulb temperature has little effect on performance at usual operating conditions (for a specified wet-bulb temperature).

Cooling Demand Curves

Electrical utility engineers have found it convenient to use charts of *cooling demand curves* to evaluate packing specifications. Figure 4.8.11 is an example of such a chart, on which the required NTU, for a given inlet air wet-bulb temperature and range, is plotted vs. *L/G* with the approach as a parameter. Such a plot is possible since the inlet air dry-bulb temperature has only a small effect under usual operating conditions. Now, if it is possible to correlate the mass transfer conductance as

$$\frac{g_m a}{L} = C\left(\frac{L}{G}\right)^{-n} \tag{4.8.22}$$

the NTU of a packing of height *H* is

$$\frac{g_m S}{\dot{m}_L} = \frac{g_m a H}{L} = C\left(\frac{L}{G}\right)^{-n} H \tag{4.8.23}$$
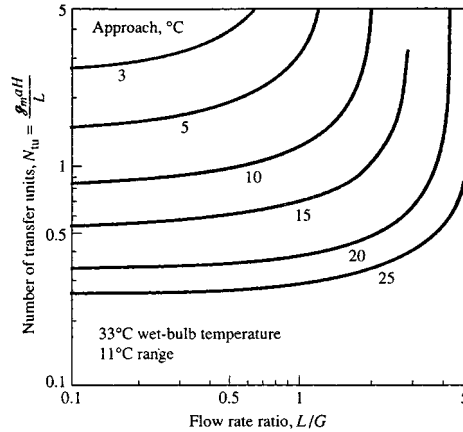
FIGURE 4.8.11 Example of cooling demand curves for a specified wet-bulb temperature and range: NTU vs. flow rate ratio for a fixed approach.

Equation (4.8.23) can also be plotted on the chart to give the *packing capability line*. For a required approach, the *operating point* of the tower is the intersection of the cooling demand curve and packing capability line. Charts of cooling demand curves are available (Cooling Tower Institute, 1967; Kelly, 1976). Correlations of the form of Equation (4.8.22) do not necessarily fit experimental data well. A dependence $g_m a \propto L^{1-n} G^n$ is implied and, in the past, experimental data were often forced to fit such a relation. If the $g_m a$ correlation does not have the form of Equation (4.8.22), the NTU cannot be plotted as a line on a cooling demand chart.

With the almost universal use of computers and the availability of suitable computer programs, one can expect less use of cooling demand charts in the future. The major sources of error in the predictions made by these programs are related to nonuniform air and water flow, and the correlations of packing mass transfer and pressure drop experimental data. The experimental data are obtained in small-scale test rigs, in which it is impossible to simulate many features of full-size towers — for example, nonuniform flow due to entrance configuration, nonuniform wetting of the packing, and, in the case of counterflow towers, the effect of spray above the packing and rain below the packing. Furthermore, since testing of packings in small-scale test rigs is itself not easy, considerable scatter is seen in such test data. Correlations of the data typically have root mean square errors of 10 to 20%.

Legionnaires' Disease

Legionnaires' disease is a form of pneumonia caused by a strain of legionnella bacteria (sero group I). Smokers and sick people are particularly vulnerable to the disease. Major outbreaks have occurred at conventions and in hospitals, for which the source of the bacteria has been traced to cooling towers of air-conditioning systems. The bacteria require nutrients such as algae or dead bacteria in sludge, and thrive if iron oxides are present. However, properly designed, installed, and maintained cooling towers have never been implicated in an outbreak of the disease. Key requirements to be met include the following:

1. Mist (drift) eliminators should be effective.
2. The tower should be located so as to minimize the possibility of mist entering a ventilation system.
3. Corrosion in the tower and water lines should be minimized by use of glass fiber, stainless steel, and coated steel.
4. The design should facilitate inspection and cleaning, to allow early detection and remedy of sludge buildup.
5. Water treatment and filtration procedures should meet recommended standards.

References

Bourillot, C. 1983. *TEFRI: Numerical Model for Calculating the Performance of an Evaporative Cooling Tower*, EPRI CS-3212-SR, Electric Power Research Institute, Palo Alto, CA.

Cooling Tower Institute, 1967. *Cooling Tower Performance Curves*, the Institute, Houston.

Kelly, N.W. 1976. *Kelly's Handbook of Cross-Flow Cooling Tower Performance*, Neil W. Kelly and Associates, Kansas City, MO.

Kintner-Meyer, M. and Emery, A.F. 1995. Cost-optimal design of cooling towers, *ASHRAE J.*, April, 46–55.

Merkel, F. 1925. Verdunstungskühlung, *Forschungsarb. Ing. Wes.*, no. 275.

Mills, A.F. 1995. *Heat and Mass Transfer*, Richard D. Irwin, Chicago.

Majumdar, A.K., Singhal, A.K., and Spalding, D.B. 1985. *VERA2D-84: A Computer Program for 2-D Analysis of Flow, Heat and Mass Transfer in Evaporative Cooling Towers*, EPRI CS-4073, Electric Power Research Institute, Palo Alto, CA.

Further Information

Baker, D. 1984. *Cooling Tower Performance*, Chemical Publishing Company, New York.

Johnson, B.M. Ed. 1990. *Cooling Tower Performance Prediction and Improvement*, Vols. 1 and 2, EPRI GS-6370, Electric Power Research Institute, Palo Alto, CA.

Singham, J.R. 1990. Natural draft towers, in *Hemisphere Handbook of Heat Exchanger Design*, Section 3.12.3, Hewitt, G.E., Coord Ed., Hemisphere Publishing, New York.

Stoeker, W.F. and Jones, J.W. 1982. *Refrigeration and Air Conditioning*, 2nd ed., McGraw-Hill, New York.

Webb, R.L. 1988. A critical review of cooling tower design methods, in *Heat Transfer Equipment Design*, Shah, R.K., Subba Rao, E.C., and Mashelkar, R.A., Eds., Hemisphere Publishing, Washington, D.C.

Heat Pipes

Larry W. Swanson

Introduction

The heat pipe is a vapor-liquid phase-change device that transfers heat from a hot reservoir to a cold reservoir using **capillary forces** generated by a **wick** or porous material and a working fluid. Originally conceived by Gaugler in 1944, the operational characteristics of heat pipes were not widely publicized until 1963 when Grover and his colleagues at Los Alamos Scientific Laboratory independently reinvented the concept. Since then many types of heat pipes have been developed and used by a wide variety of industries.

Figure 4.8.12 shows a schematic of a heat pipe aligned at angle ψ relative to the vertical axis (gravity vector). The heat pipe is composed of a container lined with a wick that is filled with liquid near its saturation temperature. The vapor-liquid interface, usually found near the inner edge of the wick, separates the liquid in the wick from an open vapor core. Heat flowing into the evaporator is transferred through the container to the liquid-filled wicking material, causing the liquid to evaporate and vapor to flow into the open core portion of the evaporator. The capillary forces generated by the evaporating interface increase the pressure difference between the vapor and liquid. The vapor in the open core flows out of the evaporator through the adiabatic region (insulated region) and into the condenser. The vapor then condenses, generating capillary forces similar, although much less in magnitude, to those in the evaporator. The heat released in the condenser passes through the wet wicking material and container out into the cold reservoir. The condensed liquid is then pumped, by the liquid pressure difference due to the net capillary force between the evaporator and condenser, out of the condenser back into the
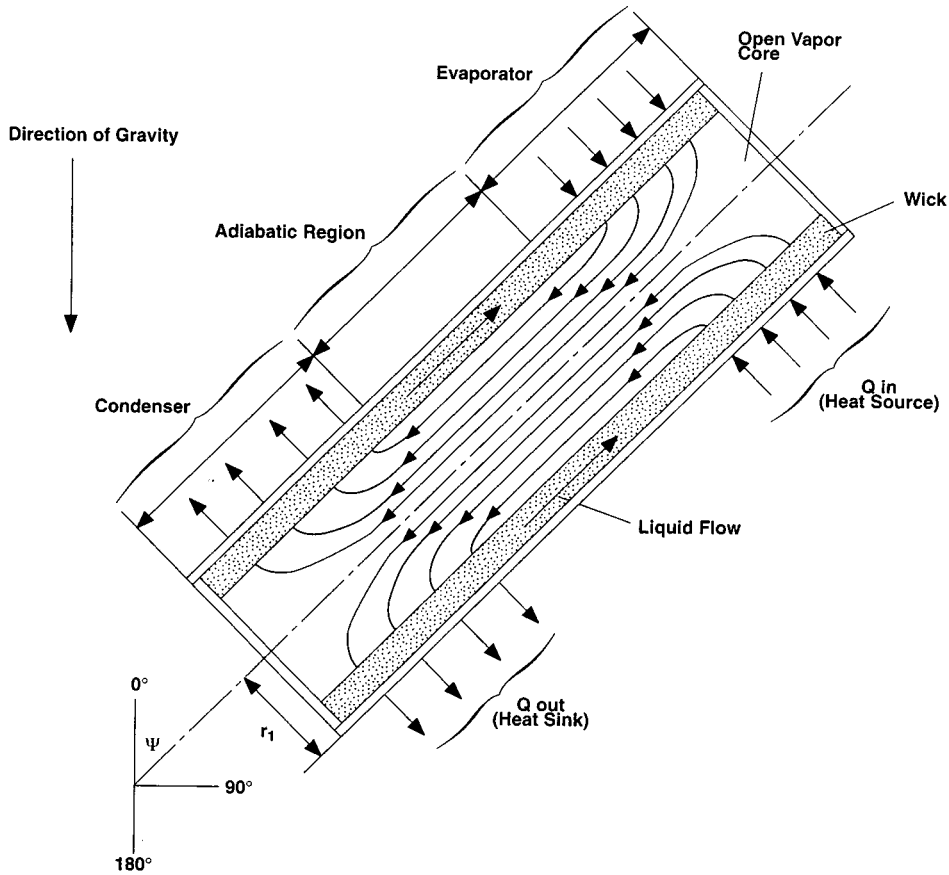
FIGURE 4.8.12 Schematic of a typical heat pipe.

evaporator. Proper selection and design of the pipe container, working fluid, and wick structure are essential to the successful operation of a heat pipe. The **heat transfer limitations, effective thermal conductivity**, and axial temperature difference define the operational characteristics of the heat pipe.

Heat Pipe Container, Working Fluid, and Wick Structures

The container, working fluid, and wick structure of a heat pipe determine its operational characteristics. One of the most important considerations in choosing the material for the heat pipe container and wick is its compatibility with the working fluid. Degradation of the container or wick and contamination of the working fluid due to chemical reaction can seriously impair heat pipe performance. For example, noncondensable gas created during a chemical reaction eventually can accumulate near the end of the condenser, decreasing the condensation surface area. This reduces the ability of the heat pipe to transfer heat to the external heat sink. The material and geometry of the heat pipe container also must have a high burst strength, low weight, high thermal conductivity, and low porosity.

Using the proper working fluid for a given application is another critical element of proper heat pipe operation. The working fluid must have good thermal stability properties at the specified operational temperature and pressure. The operational temperature range of the working fluid has to lie between its triple point and its critical point for liquid to exist in the wicking material. The **wettability** of the working fluid contributes to its capillary pumping and priming capability. High-surface-tension fluids are commonly used in heat pipes because they provide the capillary pumping and wetting characteristics necessary for proper operation. Other desirable thermophysical properties include a high liquid thermal

TABLE 4.8.4   Thermophysical Properties of Some Heat-Pipe Fluids

Temper- ature (°C)	Latent Heat (kJ /kg)	Liquid Density (kg/m³)	Vapor Density (kg/m³)	Liquid Thermal Conduc- tivity (W/m°C)	Liquid Viscosity (cP)	Vapor Viscosity (cP,× 10²)	Vapor Pressure (bars)	Vapor Specific Heat (kJ/kg°C)	Liquid Surface Tension (N/m× 10²)
Methanol									
−50	1194	843.5	0.01	0.210	1.700	0.72	0.01	1.20	3.26
−30	1187	833.5	0.01	0.208	1.300	0.78	0.02	1.27	2.95
−10	1182	818.7	0.04	0.206	0.945	0.85	0.04	1.34	2.63
10	1175	800.5	0.12	0.204	0.701	0.91	0.10	1.40	2.36
30	1155	782.0	0.31	0.203	0.521	0.98	0.25	1.47	2.18
50	1125	764.1	0.77	0.202	0.399	1.04	0.55	1.54	2.01
70	1085	746.2	1.47	0.201	0.314	1.11	1.31	1.61	1.85
90	1035	724.4	3.01	0.199	0.259	1.19	2.69	1.79	1.66
110	980	703.6	5.64	0.197	0.211	1.26	4.98	1.92	1.46
130	920	685.2	9.81	0.195	0.166	1.31	7.86	1.92	1.25
150	850	653.2	15.90	0.193	0.138	1.38	8.94	1.92	1.04
Water									
20	2448	998.0	0.02	0.603	1.00	0.96	0.02	1.81	7.28
40	2402	992.1	0.05	0.630	0.65	1.04	0.07	1.89	7.00
60	2359	983.3	0.13	0.649	0.47	1.12	0.20	1.91	6.66
80	2309	972.0	0.29	0.668	0.36	1.19	0.47	1.95	6.26
100	2258	958.0	0.60	0.680	0.28	1.27	1.01	2.01	5.89
120	2200	945.0	1.12	0.682	0.23	1.34	2.02	2.09	5.50
140	2139	928.0	1.99	0.683	0.20	1.41	3.90	2.21	5.06
160	2074	909.0	3.27	0.679	0.17	1.49	6.44	2.38	4.66
180	2003	888.0	5.16	0.669	0.15	1.57	10.04	2.62	4.29
200	1967	865.0	7.87	0.659	0.14	1.65	16.19	2.91	3.89
Potassium									
350	2093	763.1	0.002	51.08	0.21	0.15	0.01	5.32	9.50
400	2078	748.1	0.006	49.08	0.19	0.16	0.01	5.32	9.04
450	2060	735.4	0.015	47.08	0.18	0.16	0.02	5.32	8.69
500	2040	725.4	0.031	45.08	0.17	0.17	0.05	5.32	8.44
550	2020	715.4	0.062	43.31	0.15	0.17	0.10	5.32	8.16
600	2000	705.4	0.111	41.81	0.14	0.18	0.19	5.32	7.86
650	1980	695.4	0.193	40.08	0.13	0.19	0.35	5.32	7.51
700	1960	685.4	0.314	38.08	0.12	0.19	0.61	5.32	7.12
750	1938	675.4	0.486	36.31	0.12	0.20	0.99	5.32	6.72
800	1913	665.4	0.716	34.81	0.11	0.20	1.55	5.32	6.32
850	1883	653.1	1.054	33.31	0.10	0.21	2.34	5.32	5.92

conductivity, high latent heat of vaporization, low liquid viscosity, and a low vapor viscosity. Table 4.8.4 gives the thermophysical properties for three typical heat pipe working fluids that span a fairly wide operating temperature range. The thermophysical properties for other heat pipe working fluids can be obtained from Dunn and Reay (1982) and Peterson (1994).

The wick structure and working fluid generate the capillary forces required to (1) pump liquid from the condenser to the evaporator and (2) keep liquid evenly distributed in the wicking material. Heat pipe wicks can be classified as either homogeneous wicks or composite wicks. Homogeneous wicks are composed of a single material and configuration. The most common types of homogeneous wicks include wrapped screen, sintered metal, axial groove, annular, crescent, and arterial. Composite wicks are composed of two or more materials and configurations. The most common types of composite wicks include variable screen mesh, screen-covered groove, screen slab with grooves, and screen tunnel with

grooves. Regardless of the wick configuration, the desired material properties and structural character- istics of heat pipe wick structures are a high thermal conductivity, high wick porosity, small capillary radius, and high wick permeability. Table 4.8.2 gives the geometric properties of some commonly used homogeneous wicks. The properties of other wick structures, including nonhomogenous types, can be obtained from Peterson (1994). The container, wick structure, and working fluid are used to determine the heat transfer limitations of heat pipes.

Heat Transfer Limitations

Heat pipes undergo various heat transfer limitations depending on the working fluid, the wick structure, the dimensions of the heat pipe, and the heat pipe operational temperature. Figure 4.8.13 gives a qualitative description of the various heat transfer limitations, which include vapor-pressure, sonic, entrainment, capillary, and boiling limitations. The composite curve enclosing the shaded region in Figure 4.8.13 gives the maximum heat transfer rate of the heat pipe as a function of the operational temperature. The figure shows that as the operational temperature increases, the maximum heat transfer rate of the heat pipe is limited by different physical phenomena. As long as the operational heat transfer rate falls within the shaded region, the heat pipe will function properly.
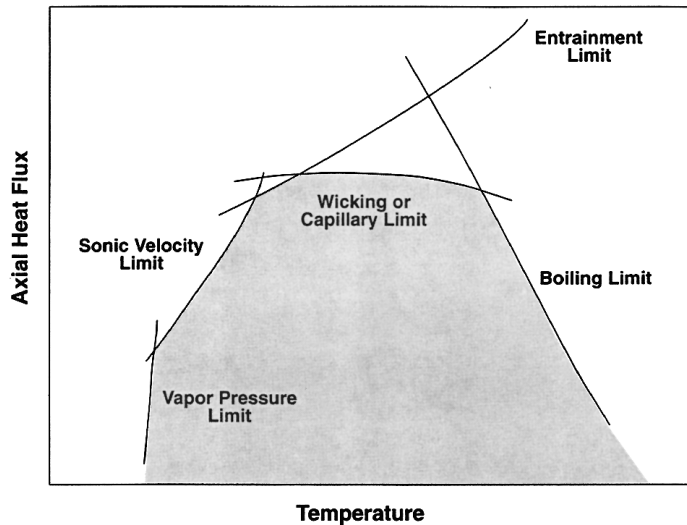

FIGURE 4.8.13 Heat transfer limitations in heat pipes.

The vapor-pressure limitation (or viscous limitation) in heat pipes develops when the pressure drop in the vapor core reaches the same order of magnitude as the vapor pressure in the evaporator. Under these conditions, the pressure drop due to flow through the vapor core creates an extremely low vapor pressure in the condenser preventing vapor from flowing in the condenser. A general expression for the vapor-pressure limitation is (Dunn and Reay, 1982)

$$Q_{vp,\max} = \frac{\pi r_v^4 h_{fg} \rho_{v,e} P_{v,e}}{12 \mu_{v,e} l_{\text{eff}}} \tag{4.8.24}$$

where r_v is the cross-sectional radius of the vapor core (m), h_{fg} is the latent heat of vaporization (J/kg), $\rho_{v,e}$ is the vapor density in the evaporator (kg/m^3), P_{ve} is the vapor pressure in the evaporator (Pa), and μ_{ve} is the vapor viscosity in the evaporator (N sec/m^2). l_{eff} is the effective length of the heat pipe (m) equal to $l_{\text{eff}} = 0.5(l_e + 2l_a + l_c)$. The vapor-pressure limitation can occur during the start-up of heat pipes at the lower end of the working-fluid-temperature range.

The sonic limitation also can occur in heat pipes during start-up at low temperatures. The low temperature produces a low vapor density, thereby reducing the speed of sound in the vapor core. Thus, a sufficiently high mass flow rate in the vapor core can cause sonic flow conditions and generate a shock wave that chokes the flow and restricts the pipes ability to transfer heat to the condenser. Dunn and Reay (1982) give an expression for the sonic limitation that agrees very well with experimental data,

$$Q_{s,\max} = 0.474 A_v h_{fg} \left(\rho_v P_v \right)^{1/2}$$

(4.8.25)

where A_v is the cross-sectional area of the vapor core (m²). The sonic limitation should be avoided because large temperature gradients occur in heat pipes under choked-flow conditions.

The entrainment limitation in heat pipes develops when the vapor mass flow rate is large enough to shear droplets of liquid off the wick surface causing dry-out in the evaporator. A conservative estimate of the maximum heat transfer rate due to entrainment of liquid droplets has been given by Dunn and Reay (1982) as

$$Q_{e,\max} = A_v h_{fg} \left[\frac{\rho_v \sigma_l}{2 r_{c,\text{ave}}} \right]^{1/2}$$

(4.8.26)

where σ_l is the surface tension (N/m) and $r_{c,\text{ave}}$ is the average capillary radius of the wick. Note that for many applications $r_{c,\text{ave}}$ is often approximated by $r_{c,e}$.

The capillary limitation in heat pipes occurs when the net capillary forces generated by the vapor-liquid interfaces in the evaporator and condenser are not large enough to overcome the frictional pressure losses due to fluid motion. This causes the heat pipe evaporator to dry out and shuts down the transfer of heat from the evaporator to the condenser. For most heat pipes, the maximum heat transfer rate due to the capillary limitation can be expressed as (Chi, 1976).

$$Q_{c,\max} = \left[\frac{\rho_l \sigma_l h_{fg}}{\mu_l} \right] \left[\frac{A_w K}{l_{\text{eff}}} \right] \left(\frac{2}{r_{c,e}} - \left[\frac{\rho_l}{\sigma_l} \right] g L_t \cos \Psi \right)$$

(4.8.27)

where K is the wick permeability (m²), A_w is the wick cross-sectional area (m²), ρ_l is the liquid density (m³), μ_l is the liquid viscosity (N sec/m²), $r_{c,e}$ is the wick capillary radius in the evaporator (m), g is the acceleration due to gravity (9.8 m/sec²), and L_t is the total length of the pipe (m). For most practical operating conditions, this limitation can be used to determine maximum heat transfer rate in heat pipes.

The boiling limitation in heat pipes occurs when the degree of liquid superheat in the evaporator is large enough to cause the nucleation of vapor bubbles on the surface of the wick or the container. Boiling is usually undesirable in heat pipes because local hot spots can develop in the wick, obstructing the flow of liquid in the evaporator. An expression for the boiling limitation is (Chi, 1976)

$$Q_{b,\max} = \frac{4\pi l_{\text{eff}} k_{\text{eff}} T_v \sigma_v}{h_{fg} \rho_l \ln(r_i / r_v)} \left(\frac{1}{r_n} - \frac{1}{r_{c,e}} \right)$$

(4.8.28)

where k_{eff} is the effective thermal conductivity of the composite wick and working fluid (W/m K), T_v is the vapor saturation temperature (K), r_i is the inner container radius (m), r_n is the nucleation radius (equal to 2.00×10^{-6} m in the absence of noncondensable gas).

Effective Thermal Conductivity and Heat Pipe Temperature Difference

One key attribute of the heat pipe is that it can transfer a large amount of heat while maintaining nearly isothermal conditions. The temperature difference between the external surfaces of the evaporator and the condenser can be determined from the following expression

$$\Delta T = R_t Q \tag{4.8.29}$$

where R_t is the total thermal resistance (K/W) and Q is the heat transfer rate (W). Figure 4.8.14 shows the thermal resistance network for a typical heat pipe and the associated thermal resistances. In most cases, the total thermal resistance can be approximated by

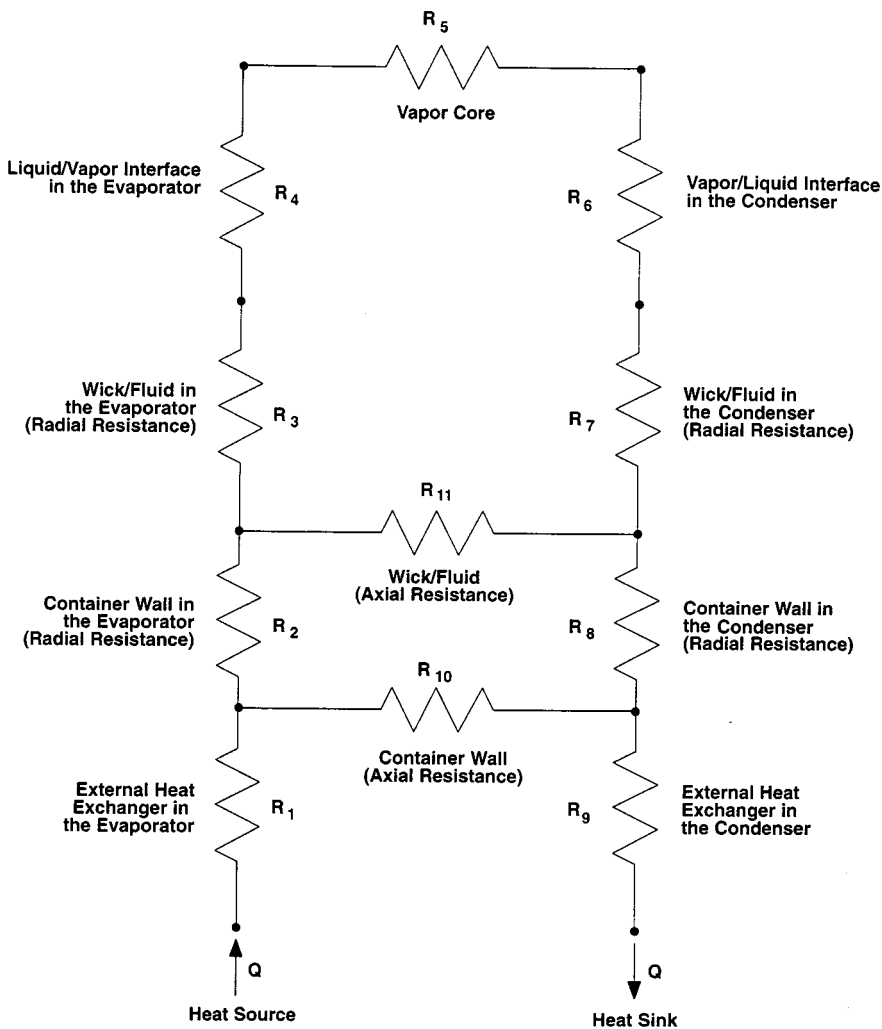$$R_t = R_1 + R_2 + R_3 + R_5 + R_7 + R_8 + R_9 \tag{4.8.30}$$

FIGURE 4.8.14 Thermal resistance network in a heat pipe.

The reader is referred to Peterson (1994) for the specific mathematical relationships used to calculate each thermal resistance. The effective thermal conductivity of the heat pipe is defined as the heat transfer rate divided by the temperature difference between the heat source and heat sink,

$$k_{\text{eff}} = \frac{L_t}{R_t A_t} \qquad (4.8.31)$$

where A_t is the overall cross-sectional area of the pipe (m²). Under normal operating conditions, the total thermal resistance is relatively small, making the external surface temperature in the evaporator approximately equal to that in the condenser. Thus, the effective thermal conductivity in a heat pipe can be very large (at least an order of magnitude larger than that of aluminum).

Design Example

Design a water heat pipe to transport 80 W of waste heat from an electronics package to cooling water. The heat pipe specifications are

1. Axial orientation — complete gravity-assisted operation (condenser above the evaporator; $\psi = 180°$)
2. Maximum heat transfer rate — 80 W
3. Nominal operating temperature — 40°C
4. Inner pipe diameter — 3 cm
5. Pipe length — 25 cm evaporator length, 50 cm adiabatic section, and 25 cm condenser length

The simplest type of wick structure to use is the single-layer wire mesh screen wick shown in Table 4.8.5. The geometric and thermophysical properties of the wick have been selected as (this takes some forethought)

$d = 2.0 \times 10^{-5}$ m

$w = 6.0 \times 10^{-5}$ m

$\dfrac{1}{2N} = r_c = \frac{1}{2}(2.0 \times 10^{-5} + 6 \times 10^{-5}) = 4.0 \times 10^{-5}$ m

$\varepsilon = 1$

$k_{\text{eff}} = k_1 = 0.630 \ \dfrac{\text{W}}{\text{mK}}$

$t_w = 1.0 \times 10^{-3}$ m

$K = \dfrac{t_w^2}{12} = \dfrac{\left(1 \times 10^{-3}\right)^2}{12} = 8.33 \times 10^{-8} \text{ m}^2$

The other heat pipe geometric properties are

$r_v = r_i - t_w = 0.015 - 0.001 = 0.014$ m

$l_{\text{eff}} = \dfrac{0.25 + 0.25}{2} + 0.5 = 0.75$ m

$L_t = 0.25 + 0.50 + 0.25 + 1.0$ m

$A_w = \pi(r_i^2 - r_v^2) = \pi[(0.015)^2 - (0.014)^2] = 9.11 \times 10^{-5} \text{ m}^2$

$A_v = \pi r_v^2 = \pi(0.014)^2 = 6.16 \times 10^{-4} \text{ m}^2$

The thermophysical properties of water at 40°C are (see Table 4.8.4):

$\rho_l = 992.1$ kg/m³

$\rho_v = 0.05$ kg/m³

$\sigma_l = 2.402 \times 10^6$ J/kg

$\mu_l = 6.5 \times 10^{-3}$ kg/m sec

$\mu_v = 1.04 \times 10^{-4}$ kg/m sec

$P_v = 7000$ Pa

The various heat transfer limitations can now be determined to ensure the heat pipe meets the 80 W heat transfer rate specification. The vapor-pressure limitation is

$$Q_{vp,\max} = \frac{\pi(0.014)^4 \left(2.402 \times 10^6\right)(0.05)(7000)}{12\left(1.04 \times 10^{-4}\right)(0.75)} = 1.08 \times 10^5 \text{ W} \tag{4.8.32}$$

The sonic limitation is

$$Q_{s,\max} = 0.474\left(6.16 \times 10^{-4}\right)\left(2.402 \times 10^6\right)\left[(0.05)(7000)\right]^{1/2}$$
$$= 1.31 \times 10^4 \text{ W} \tag{4.8.33}$$

The entrainment limitation is

$$Q_{e,\max} = \left(6.16 \times 10^{-4}\right)\left(2.402 \times 10^6\right)\left[\frac{(0.05)(0.07)}{2\left(4.0 \times 10^{-5}\right)}\right]^{1/2}$$
$$= 9.79 \times 10^3 \text{ W} \tag{4.8.34}$$

Noting that $\cos \psi = -1$, the capillary limitation is

$$Q_{c,\max} = \left[\frac{(992.1)(0.07)\left(2.402 \times 10^6\right)}{6.5 \times 10^{-3}}\right]\left[\frac{\left(9.11 \times 10^{-5}\right)\left(8.33 \times 10^{-8}\right)}{0.75}\right]\left[\frac{2}{4.0 \times 10^{-5}} + \frac{992.1}{0.07}9.8(1.0)\right]$$
$$= 4.90 \times 10^4 \text{ W} \tag{4.8.35}$$

Finally, the boiling limitation is

$$Q_{b,\max} = \frac{4\pi(0.75)(0.63)(313)(0.07)}{\left(2.402 \times 10^6\right)(992.1)\ln\left(\frac{0.015}{0.014}\right)}\left[\frac{1}{2.0 \times 10^{-6}} - \frac{1}{4.0 \times 10^{-5}}\right]$$
$$= 0.376 \text{ W} \tag{4.8.36}$$

All of the heat transfer limitations, with the exception of the boiling limitation, exceed the specified heat transfer rate of 80 W. The low value of 0.376 W for the boiling limitation strongly suggests that the liquid will boil in the evaporator and possibly cause local dry spots to develop. The reason the liquid boils is because the effective thermal conductivity of the wick is equal to the conductivity of the liquid, which is very low in this case. Because the liquid is saturated at the vapor-liquid interface, a low effective thermal conductivity requires a large amount of wall superheat which, in turn, causes the liquid to boil. This problem can be circumvented by using a high conductivity wire mesh or sintered metal wick, which greatly increases the effective conductivity. It should be noted, however, that because porous wicks have

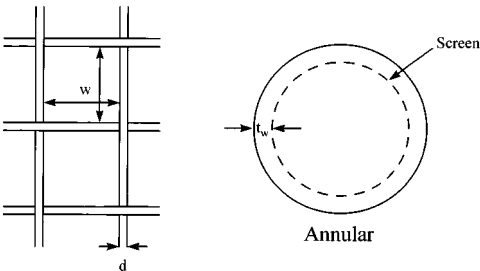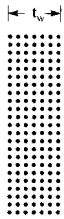**TABLE 4.8.5   Physical Properties of Wick Structures**

Wick Type[a]	Thermal Conductivity	Porosity	Minimum Capillary Radius	Permeability
Single-layer wire mesh screens (heat-pipe axis in the plane of the paper in this sketch) Screen / Annular $1/N = d + w$ N = number of apertures per unit length	$k_{\mathrm{eff}} = k_e$	$\varepsilon = 1$	$r_c = {}^1\!/_{(2N)}$	$K = t_w^2/12$
Multiple wire mesh screens,[b] plain or sintered (screen dimensions as for single layers illustrated above)	$k_{\mathrm{eff}} = \dfrac{k_e\left[k_e + k_s - (1-\varepsilon)(k_e - k_s)\right]}{k_e + k_s + (1-\varepsilon)(k_e - k_s)}$	Estimated from $\varepsilon = 1 - (\pi N d)/4$	$r_c = {}^1\!/_{(2N)}$	$k = \dfrac{d^2\varepsilon^2}{122(1-\varepsilon)^2}$

TABLE 4.8.5   Physical Properties of Wick Structures (continued)

	Wick Type[a]		Thermal Conductivity	Porosity	Minimum Capillary Radius	Permeability
	Unconsolid-ated packed spherical particles (d = average particle diameter)	Plain	$k_{\text{eff}} = \dfrac{k_e\left[2k_e + k_s - 2(1-\varepsilon)(k_e - k_s)\right]}{2k_e + k_s + (1-\varepsilon)(k_e - k_s)}$	Estimated from (assuming cubic packing) $\varepsilon = 0.48$	$r_c = 0.21d$	$k = \dfrac{d^2\varepsilon^2}{150(1-\varepsilon)^2}$
		Sintered	$k_{\text{eff}} = \dfrac{k_e\left[2k_s + k_e - 2\varepsilon(k_s - k_e)\right]}{2k_s + k_e + \varepsilon(k_s - k_e)}$			
	Sintered metal fibers (d = fiber diameter)		$k_{\text{eff}} = \varepsilon^2 k_e (1-\varepsilon)^2 k_s$ $+ \dfrac{4\varepsilon(1-\varepsilon)k_e k_s}{k_e + k_s}$	Use manufacturers data	$r_c = \dfrac{d}{2(1-\varepsilon)}$	$k = C_1\dfrac{y^2 - 1}{y^2 - 1}$ where $y = 1 + \dfrac{C_2 d^2 \varepsilon^3}{(1-\varepsilon)^2}$ $C_1 = 6.0 \times 10^{-10}\ \text{m}^2$ $C_2 = 3.3 \times 10^7\ 1/\text{m}^2$

[a] The axis of the pipe and direction of fluid flow are normal to the paper.

[b] These wicks are positioned so that the layers follow the contours of the iner surface of the pipe wall.

Revised from Peterson, G.P., *An Introduction to Heat Pipes Modeling, Testing, and Applications*, John Wiley & Sons, New York, 1994.

lower permeabilities, the capillary limitation should be lower as well. Let's try a sintered particle wick made of copper with the following properties (see Table 4.8.5):

$$d = 1.91 \times 10^{-4} \text{ m}$$

$$r_{c,3} = 0.21d = 4.0 \times 10^{-5} \text{ m (same as before)}$$

$$\varepsilon = 0.48$$

$$K = \frac{\left(1.91 \times 10^{-4}\right)^2 (0.48)}{150(1 - 0.48)^2} = 2.07 \times 10^{-10} \text{ m}^2$$

$$k_s = 400 \; \frac{\text{W}}{\text{mK}} \text{ (copper)}$$

$$k_1 = 0.630 \; \frac{\text{W}}{\text{mK}} \text{ (water)}$$

$$k_{\text{eff}} = \frac{400\left[2(400) + 0.63 - 2(0.48)(400 - 0.63)\right]}{2(400) + 0.63 + 0.48(400 - 0.63)} = 168 \text{ W/mK}$$

All other geometric and thermophysical properties are the same. The heat transfer limitations affected by the change in wick structure are the capillary and boiling limitations. The sintered metal wick produces a capillary limitation of

$$Q_{c,\max} = \left[\frac{(992.1)(0.07)\left(2.402 \times 10^6\right)}{6.5 \times 10^{-3}}\right]\left[\frac{\left(9.11 \times 10^{-5}\right)\left(2.07 \times 10^{-10}\right)}{0.75}\right]\left[\frac{2}{4.0 \times 10^{-5}} + \frac{992.1}{0.07} 9.8(1.0)\right] \qquad (4.8.37)$$

$$= 122 \text{ W}$$

The boiling limitation for the sintered wick is

$$Q_{b,\max} = \frac{4\pi(0.75)(168)(313)(0.07)}{\left(2.402 \times 10^6\right)(992.1)\ln\left(\dfrac{0.015}{0.014}\right)}\left[\frac{1}{2.0 \times 10^{-6}} - \frac{1}{4.0 \times 10^{-5}}\right] \qquad (4.8.38)$$

$$= 100 \text{ W}$$

This design now meets all the specifications defined in the problem statement.

Application of Heat Pipes

Heat pipes have been applied to a wide variety of thermal processes and technologies. It would be an impossible task to list all the applications of heat pipes; therefore, only a few important industrial applications are given in this section. In the aerospace industry, heat pipes have been used successfully in controlling the temperature of vehicles, instruments, and space suits. Cryogenic heat pipes have been applied in (1) the electronics industry for cooling various devices (e.g., infrared sensors, parametric amplifiers) and (2) the medical field for cryogenic eye and tumor surgery. Heat pipes have been employed to keep the Alaskan tundra frozen below the Alaskan pipeline. Other cooling applications include (1) turbine blades, generators, and motors; (2) nuclear and isotope reactors; and (3) heat collection from exhaust gases, solar and geothermal energy.

In general, heat pipes have advantages over many traditional heat-exchange devices when (1) heat has to be transferred isothermally over relatively short distances, (2) low weight is essential (the heat pipe is a passive pumping device and therefore does not require a pump), (3) fast thermal-response times are required, and (4) low maintenance is mandatory.

Defining Terms

Capillary force: The force caused by a curved vapor-liquid interface. The interfacial curvature is dependent on the surface tension of the liquid, the contact angle between the liquid wick structure, the vapor pressure, and the liquid pressure.

Effective thermal conductivity: The heat transfer rate divided by the temperature difference between the evaporator and condenser outer surfaces.

Heat transfer limitations: Limitations on the axial heat transfer capacity imposed by different physical phenomena (i.e., vapor pressure, sonic, entrainment, capillary, and boiling limitations).

Wettability: The ability of a liquid to spread itself over a surface. A wetting liquid spreads over a surface whereas a nonwetting liquid forms droplets on a surface.

Wick: A porous material used to generate the capillary forces that circulate fluid in a heat pipe.

References

Chi, S.W. 1976. *Heat Pipe Theory and Practice*, Hemisphere Publishing, Washington, D.C.

Dunn, P.D. and Reay, D.A. 1982. *Heat Pipes*, 3rd ed., Pergamon Press, Oxford, U.K.

Gaugler, R.S. 1944. Heat Transfer Device. U.S. Patent No. 2350348.

Grover, G.M. 1963. Evaporation-Condensation Heat Transfer Device. U.S. Patent No. 3229759.

Peterson, G.P. 1994. *An Introduction to Heat Pipes Modeling, Testing, and Applications*, John Wiley & Sons, New York.

Further Information

Recent developments in heat pipe research and technology can be found in the proceedings from a number of technical conferences: (1) The International Heat Pipe Conference (2) The National Heat Transfer Conference, (3) The ASME Winter Annual Meeting, (4) The AIAA Thermophysics Conference.

Books particularly useful for the design of heat pipes include (1) *Heat Pipe Design Handbook* by Brennan and Kroliczek available from B&K Engineering in Baltimore, M.D. (2) *The Heat Pipe* by Chisholm available from Mills and Boon Limited in London, England, and (3) *Heat Pipes: Construction and Application* by Terpstra and Van Veen available from Elsevier Applied Science in New York, N.Y.

An additional book particularly strong in heat pipe theory is *The Principles of Heat Pipes* by Ivanovskii, Sorokin, and Yagodkin available from Clarendon Press in Oxford, England.

Cooling Electronic Equipment

Vincent W. Antonetti

Introduction

In electronic packages, the thermal resistances to heat transfer from heat source to heat sink are often grouped into an internal resistance and an external resistance. The **internal thermal resistance** R_{int} is conductive and exists between the chip and the module case:

$$R_{int} = \frac{T_{chip} - T_{case}}{P_{chip}} \tag{4.8.39}$$

where P_{chip} is the chip power.

The **external thermal resistance** R_{ext} is primarily convective and exists between the surface of the case of the module and some reference point, typically the temperature of the cooling fluid near the module. In a multichip module, the module power P_m is the sum of the individual chip powers, and the external resistance is

$$R_{\text{ext}} = \frac{T_{\text{case}} - T_{\text{coolant}}}{P_m} \tag{4.8.40}$$

The internal and external resistances are related to the chip junction temperature T_j through the following expression:

$$T_j = \Delta T_{j-\text{chip}} + P_{\text{chip}} R_{\text{int}} + P_m R_{\text{ext}} + \Delta T_{\text{coolant}} + T_{\text{coolant in}} \tag{4.8.41}$$

Many factors are involved in determining the appropriate cooling mode to be used. If the component junction temperature is constrained to approximately 85°C, Table 4.8.6 may be used to make a preliminary selection of the cooling mode. Extended surfaces can often be used to increase the allowable heat fluxes.

TABLE 4.8.6   Maximum Component Heat Flux for Various Cooling Modes

Cooling Mode	W/cm²
Free convection air	0.05
Forced convection air	0.5
Impingement air	1.0
Free convection immersion	1.0
Forced convection immersion	50
Pool boiling	20
Forced convection boiling	100
Jet immersion (single phase)	40
Boiling jet immersion	90

Free Convection Air Cooling of Vertical Printed Circuit Boards

Data have been collected from rack-mounted simulated printed circuit boards (PCBs) (see Figure 4.8.15) and from several actual electronic systems at AT&T Bell Laboratories. Results indicated that existing parallel plate correlations for symmetric isoflux plates (separated by distance "b") could be adapted to PCB conditions. Specifically, for $\text{Ra}_b < 10$ use the equation corresponding to the fully developed laminar boundary layer condition:

$$\text{Nu}_b = 0.144 \text{Ra}_b^{0.5} \tag{4.8.42}$$

For $10 < \text{Ra}_b < 1000$, use

$$\text{Nu}_b = \left[\frac{48}{\text{Ra}_b} + \frac{2.5}{\text{Ra}_b^{0.4}} \right]^{-0.5} \tag{4.8.43}$$

where

$$\text{Ra}_b = \frac{g \beta c_p \rho^2 b^5 q''}{\mu k L}$$

For $\text{Ra} > 1000$, the expression for an isolated plate in infinite media is recommended:

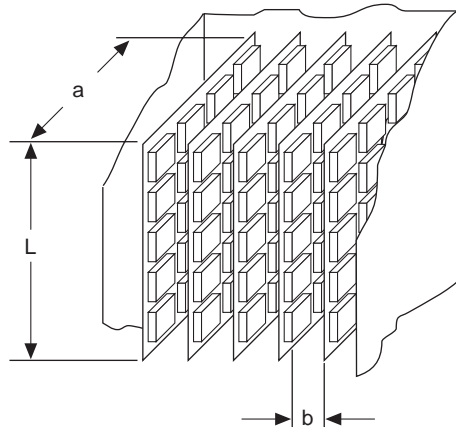$$\text{Nu}_b = 0.524 \text{Ra}_b^{0.2} \tag{4.8.44}$$

FIGURE 4.8.15 Typical PCB array.

In the previous three expressions air properties are evaluated at the average of the module case and ambient temperatures.

The PCB spacing b_{max} for a given power dissipation which yields the lowest PCB component case temperatures (or which maximizes the rate of heat transfer while maintaining PCB temperatures below the maximum allowable) occurs when the developing boundary layers from adjacent PCBs do not interfere, i.e., so the isolated plate condition is approached as follows: If heat is transferred from both sides of the PCB, let $Ra_{ab} = 17,000$ and the recommended PCB spacing is $b_{max} = 7.02\xi^{-0.2}$. If heat is transferred from only one side of the PCB, let $Ra_{ab} = 5400$ and the recommended PCB spacing is $b_{max} = 5.58\xi^{-0.2}$. In both cases

$$\xi = \frac{g\beta\rho^2 Pr q''}{\mu^2 kL} \tag{4.8.45}$$

Forced Convection Air Cooling of Vertical PCBs

Sparrow et al. (1982, 1984) studied vertical arrays with simulated modules of uniform size, which was 4 modules wide by 17 module rows deep in the flow direction; the modules were 26.7 mm square and 10 mm high; the space between modules was 6.67 mm, and the distance from the top of the module to the adjoining card $Hc = 16.7$ mm. The Nusselt number as a function of module row position for a fully populated array may be determined from Figure 4.8.16. Correction factors to the fully developed Nusselt numbers for the effect of missing modules and the presence of modules whose height differs from others in the array are presented in the cited references.

In actual electronic packages, conditions differ from the relatively ideal setups in laboratories because in real packages the flow is disturbed by the PCB supporting hardware and may extend the entry region effect.

Data from actual computer hardware with PCBs containing a 6×4 array of 28 mm modules (4 in the flow direction) were used to develop the following expressions:

$$Nu_x = C\left\{Re_{D_h}\left[1 + x/(D_h)^{-0.836}\right]\right\}^m \tag{4.8.46}$$
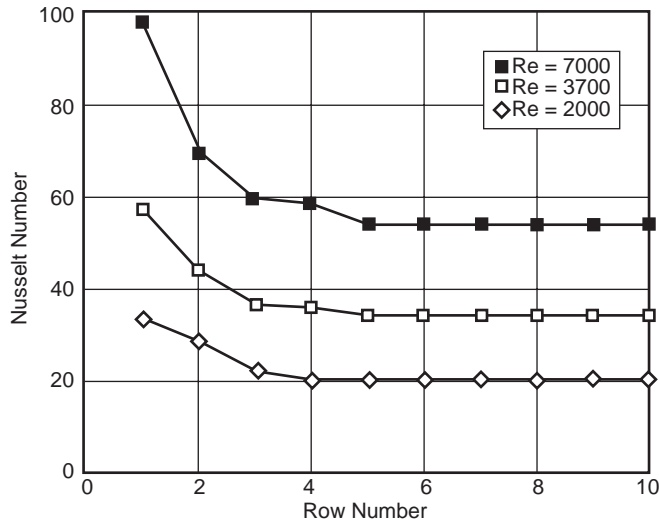
FIGURE 4.8.16 Nusselt number for fully populated array of modules.

For Re < 2000, $C = 0.072$ and $m = 0.70$, and for $2000 < $ Re $ < 10,000$, $C = 0.056$ and $m = 1.02$, where x is the distance in the flow direction. Because the array was only 4 modules deep, all the modules on the PCB were in the entry region.

Tests have been conducted on a 9×7 array of 25-mm-square by 6.4-mm-high blocks cooled by a 3×3 array of air jets directed normal to the face of each block. The spent flow exited along the channel formed by the orifice plate and the heat transfer surfaces. Test results were correlated by the relation:

$$N_d = 0.213(z/d)^{-0.376} \mathrm{Re}_d^{0.743} \tag{4.8.47}$$

where d is the jet orifice diameter, s is the orifice-to-orifice spacing, and z is the distance from the orifice outlet to the face of the module.

Immersion Cooling

The highly inert perfluorinated liquids, called FC coolants by the 3M Company, are frequently used in **immersion cooling** applications. FC coolants are available with boiling points from 30 to 172°C at atmospheric pressure. FC-75 are FC-77 with boiling points of 100°C are often used in single-phase applications, while FC-72 and FC-87, with boiling points of 56 and 30°C, respectively, are used in systems involving phase change.

Data exist for free convection immersion cooling of a 3×3 array of simulated chips mounted on a vertical wall in an enclosure filled with FC-75. Each heat source was 8 mm high by 24 mm wide by 6 mm thick. With the Nusselt and modified Rayleigh numbers based on the heater height, L, the best fit to the data is

$$\mathrm{Nu}_L = 0.279 \mathrm{Ra}_b^{0.224} \tag{4.8.48}$$

Air cooling expressions have been modified to make them applicable to free convection immersion cooling of vertical PCB arrays with FC coolants. The Nusselt number (based on PCB spacing "b") at the top of the PCB is

$$\text{Nu}_L = \left[\frac{C}{\text{Ra}_b} + \frac{2.78}{\text{Ra}_b^{0.4}} \right]^{-0.5} \tag{4.8.49}$$

$C = 24$ when heat transfer is from one side of the PCB, and $C = 48$ when from both sides.

Nucleate Pool Boiling

A number of investigators have tested small flush heat sources boiling in a pool of dielectric liquid. The heaters ranged from 4×4 mm to 12.7×12.7 mm. Typical saturated pool boiling data for FC-72 and FC-87 are shown in Figure 4.8.17. Note that a temperature overshoot up to 25°C has been regularly observed for silicon chips in dielectric liquid pools. To estimate the temperature excursion at boiling incipience (q_i''), the following approximation is recommended

$$\Delta T_{\text{ex}} = T_{\text{sat}}\left(p - \frac{2\sigma}{r_b} - p_g \right) - T_{\text{sat}} - C\left(q_i''\right)^n \tag{4.8.50}$$

where

$$C = \mu h_{fg}\left[\frac{c_p}{h_{fg}\text{Pr}^b C_{sf}} \right]^{1/a} \left[\frac{\alpha}{g(\rho - \rho_g)} \right]^{0.5} \tag{4.8.51}$$

with $r_b = 0.25$ μm, $C_{sf} = 0.003$, $a = 0.33$, and $b = 1.7$. (Note that $n = 1/a = 3$.)

Park and Bergles (1988) determined the critical heat flux (CHF) as a function of size for flush heaters operating in a saturated pool of R-113. For a 5-mm-wide heater, and for heater heights from 5 to 80 mm, use

$$\frac{q_{c_{\text{sat}}}''}{q_{c_z}''} = 0.86\left[1 + \frac{152}{L^{*3.29}} \right]^{0.14} \tag{4.8.52}$$

where the CHF prediction of Zuber, $q_{c_z}'' = \rho_g^{0.5} h_{fg}[\sigma g(\rho_f - \rho_g)]^{0.5}$, and $L^* = L[g(\rho_f - \rho_g)/\sigma]^{0.5}$.

For a 5-mm-high heater, and for heater widths from 2.5 to 70 mm, use

$$\frac{q_{c_{\text{sat}}}''}{q_{c_z}''} = 0.93\left[1 + \frac{52}{I^{1.02}} \right]^{0.14} \tag{4.8.53}$$

where the induced convection parameter is $I = (\rho_f W\sigma/\mu^2)^{0.5}$.

For flush 12.7×12.7 mm heaters in FC-72, test data yield $q_{c_{\text{sat}}}'' / q_{c_z}'' \approx 1.45$. These subcooling data were correlated by

$$\frac{q_{c_{\text{sub}}}''}{q_{c_{\text{sat}}}''} = 1 + \frac{0.0643\rho_f c_{p,f}}{\rho_g h_{fg}}\left[\frac{\rho_g}{\rho_f} \right]^{1/4} \Delta T_{\text{sub}} \tag{4.8.54}$$

Single-Phase and Boiling Forced Convection in Channel Flow

The average Nusselt numbers for 12 flush 12.7×12.7 mm heaters (4 rows of 3 sources per row) operating in FC-77 has been correlated by the following expression:
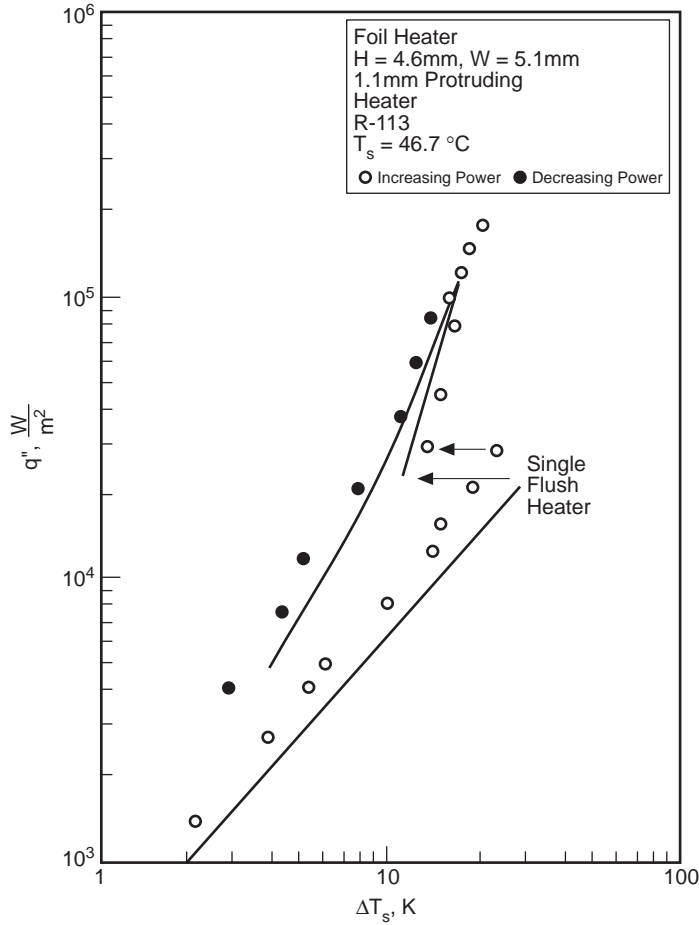
FIGURE 4.8.17 Typical pool boiling curve for small heater.

$$\overline{\mathrm{Nu}_L} = C\left(\mathrm{Re}_{D_h}\right)^m \mathrm{Pr}^{0.11} \qquad (4.8.55)$$

For row 1: $C = 0.194$ and $m = 0.60$; for row 2: $C = 0.069$ and $m = 0.69$; for row 3: $C = 0.041$ and $m = 0.74$; and for row 4: $C = 0.029$ and $m = 0.78$. All properties are determined at the inlet temperature except for μ_h, which is evaluated at the heater temperature. Note that when heat sinks are employed, forced convection immersion cooling can support a heat flux of approximately 50 W/cm^2.

Test data have been obtained for a vertical column of ten 6.4 mm × 6.4 mm heaters, with subcooled R-113 flowing in the upward direction. In general, CHF occurred first at the last downstream element in the array, and that CHF values of 100 W/cm^2 were easily attained. The CHF data yielded the following equation:

$$q_c'' = C_5 \mathrm{We}^n V \rho_f h_{fg}\left(\frac{\rho_f}{\rho_g}\right)^{15/23}\left(\frac{L}{D_h}\right)^{1/23}\left[1 + \frac{c_{pf}\Delta T_{\mathrm{sub}}}{h_{fg}}\right]^{7/23}\left[1 + \frac{0.021\rho_f c_{pf}\Delta T_{\mathrm{sub}}}{\rho_g h_{fg}}\right] \qquad (4.8.56)$$

where the Weber number, $\mathrm{We} = \rho_f V^2 L/\sigma$. Note that for We > 100, $C_5 = 0.125$ and $n = -8/23$, and for We < 10, $C_5 = 0.254$ and $n = -\frac{1}{2}$.

Immersion Cooling Using Jets

Two modes have been studied. In the first, a dielectric liquid jet discharges into a miscible liquid and is said to be submerged; in the second, a liquid jet discharges into an immiscible gas (air) and is said to be free. In general, the average Nusselt number can be expressed as

$$\overline{\text{Nu}} = f\left(\text{Re}^m, \text{Pr}^n, L/d, z/d\right) \tag{4.8.57}$$

where L/d is the ratio of the chip length to orifice diameter, and z/d is the ratio of the jet to heat source distance to the orifice diameter. A free jet is virtually unaffected by the orifice-to-chip distance, and as a consequence the (z/d) term drops out.

Data for single-phase forced convection cooling with free jets are available for 2×2 and 3×3 heat source arrays. The heat sources were 12.7×12.7 mm and the cooling fluid was FC-77. Each heat source was cooled either by a single jet or by a 2×2 or 3×3 array of jets per source. For all the configurations tested, the average Nusselt number was correlated by a single expression:

$$\overline{\text{Nu}_L} = 3.84\left(0.008\frac{L}{d}n + 1\right)\text{Re}^{1/2}\text{Pr}^{1/3} \tag{4.8.58}$$

where fluid properties are to be evaluated at an average of the heat source and jet inlet temperatures.

Data for single-phase forced convection using submerged jets are available for a 5×5 mm vertical heat source cooled by a 1.0-mm-diameter submerged jet of R-113. The Nusselt number at the stagnation point was correlated by

$$\text{Nu}_d = 1.29\text{Re}_d^{1/2}\text{Pr}^{0.4} \tag{4.8.59}$$

Also note that the performance of a submerged liquid jet should be approximately equivalent to gas jet impingement.

Data for two-phase forced convection using free jets have been collected for a single 12.7×12.7 mm heat source cooled by either a single jet or a 2×2 or 3×3 array of jets. The jet diameter, velocity, and jet-to-source distance were varied. The CHF data was correlated by

$$q_c'' = 0.0742\text{We}^{-0.365}V\rho_f h_{fg}\left(\frac{\rho_g}{\rho_f}\right)^{0.239}\left[1 + 0.952\left(\frac{\rho_f}{\rho_g}\right)^{0.118}\left(\frac{c_{pf}\Delta T_{\text{sub}}}{h_{fg}}\right)\right]^{1.414} \tag{4.8.60}$$

Experimental evidence in two-phase forced convection using submerged jets indicates that (1) the temperature overshoot at incipient boiling was very small compared with pool or forced boiling; (2) the boiling curves at various velocities merge to a single curve and that this curve coincides approximately with an upward extrapolation of the pool boiling curve; (3) the CHF varies as the cube of the jet velocity; (4) the CHF is greatly improved by increasing the subcooling; and (5) powers in excess of 20 W (5×5-mm chip) could be accommodated within a 85°C chip temperature.

Defining Terms

External thermal resistance: The thermal resistance from a convenient reference point on the outside of the electronic package to the local ambient.

Internal thermal resistance: The thermal resistance from the device junction inside an electronic package to a convenient reference point on the outside surface of the package.

Immersion cooling: Concerns applications where the coolant is in direct physical contact with the electronic components.

References

Antonetti, V.W. 1993. Cooling electronic equipment — section 517, *Heat Transfer and Fluid Flow Data Books*, Kreith, F., Ed., Genium Publishing, Schenectady, NY.

Antonetti, V.W. and Simons, R.E. 1985. Bibliography of heat transfer in electronic equipment, *IEEE Trans. Components, Hybrids, Manuf. Tech.*, CHMT-8(2), 289–295.

Park, K.A. and Bergles, A.E. 1988. Effects of size of simulated microelectron chips on boiling and critical heat flux, *J. Heat Transfer*, 110, 728–734.

Simons, R.E. 1988. Bibliography of heat transfer in electronic equipment, in *Advances in Thermal Modeling of Electronic Components and Systems*, Vol. 1, Bar-Cohen, A. and Kraus, A.D., Eds., Hemisphere Publishing, New York, 413–441.

Simons, R.E. 1990. Bibliography of heat transfer in electronic equipment, in *Advances in Thermal Modeling of Electronic Components and Systems*, Vol. 2, Bar-Cohen, A. and Kraus, A.D., Eds., ASME Press, New York, 343–412.

Sparrow, E.M., Niethammer, J.E., and Chaboki, A. 1982. Heat transfer and pressure-drop characteristics of arrays of rectangular modules in electronic equipment, *Int. J. Heat Mass Transfer*, 25, 961–973.

Sparrow, E.M., Yanezmoreno, A.A., and Otis, D.R. 1984. Convective heat transfer response to height differences in an array of block-like electronic components, *Int. J. Heat Mass Transfer*, 27, 469–473.

4.9 Non-Newtonian Fluids — Heat Transfer

Thomas F. Irvine, Jr., and Massimo Capobianchi

Introduction

The general characteristics of non-Newtonian fluids are described in Section 3.9 and will not be repeated here. Topics to be included in this section are laminar and turbulent heat transfer in fully developed duct flow, and laminar free convection heat transfer in vertical channels and plates and several other common geometries.

For non-Newtonian flows, except for certain classes of fluids which exhibit a slip phenomenon at solid boundaries, the boundary condition is taken as no-slip or zero velocity at all solid surfaces. For heat transfer analyses, however, the situation is more complicated because there are many different ways to heat a wall, which in turn affects the type of thermal boundary conditions.

In general, the rate of heat transfer from a surface, or the temperature difference between the wall and the fluid, is calculated using the equation $q_c = h_c A_q \Delta T$. Since the heat transfer coefficient can vary considerably for different thermal boundary conditions, it is important that the boundary conditions be specified correctly. Although the number of thermal boundary conditions is in principle infinite, several classical types have been identified and are in common use. They are usually identified in terms of the Nusselt number, Nu = $h_c L / k$, with a particular subscript. For example, for duct flow, the symbol Nu_T is used to specify the Nusselt number when the wall temperature is constant in both the flow and peripheral directions. Other thermal boundary conditions are described in Table 4.9.1 for duct heat transfer and will be used throughout this section.

TABLE 4.9.1   Thermal Boundary Conditions for Duct Heat Transfer

1.	Constant wall temperature in both the flow and circumferential direction	Nu_T
2.	Constant heat flux in the flow direction and constant temperature in the circumferential direction	Nu_{H1}
3.	Constant heat flux in the flow and circumferential directions	Nu_{H2}
4.	Constant heat flux per unit volume in the wall with circumferential wall heat conduction	Nu_{H4}

It should be noted that because of the symmetry in circular and parallel plate ducts, Nu_{H1} and Nu_{H2} are identical and are referred to simply as Nu_H. Nu_{H4} with wall conduction is a more-complicated problem where the energy equations must be solved simultaneously in both the wall and the fluid. Such problems are called conjugated. In the Nu_{H4} situation, the designer has the flexibility of affecting the heat transfer by varying either or both the characteristics of the duct wall or the convective fluid. In the heat transfer relations to be considered later, care will be taken to identify the proper thermal boundary conditions using the nomenclature in Table 4.9.1.

Laminar Duct Heat Transfer — Purely Viscous, Time-Independent Non-Newtonian Fluids

As discussed in Section 3.9, a convenient and comprehensive constitutive equation for pseudoplastic fluids (flow index, $n < 1$) is the modified power law equation:

$$\mu_a = \frac{\mu_o}{1 + \dfrac{\mu_o}{K}(\dot{\gamma})^{1-n}} \tag{4.9.1}$$

Equation (4.9.1) has the characteristic that at low shear rates, the equation approaches that for a Newtonian fluid while at large shear rates it describes a power law fluid. In addition, solutions using

Equation (4.9.1) generate a shear rate parameter, β, which describes whether any particular system is in the Newtonian, transitional, or power law region. For duct flow, β is given by

$$\beta = \frac{\mu_o}{K}\left(\frac{\bar{u}}{D_H}\right)^{1-n} \qquad (4.9.2)$$

If $\log_{10}\beta > 2$: Power law region
If $\log_{10}\beta < -2$: Newtonian region
If $-2 \le \log_{10}\beta \le 2$: Transition region

For fully developed flow, the characteristic length is the hydraulic diameter, D_H, and the fluid temperature is the "bulk" temperature defined as

$$T_b = \frac{1}{A_c\bar{u}}\int_{A_c} uTdA_c \qquad (4.9.3)$$

Figure 4.9.1 illustrates the values of Nu_T vs. β for a circular duct with the flow index, n, as a parameter. It is seen from the figure that the effect of β on Nu_T is only moderate, but for some applications it may be important to know at what value of β the system is operating. The situation is similar for boundary condition Nu_H.

Although Figure 4.9.1 shows the Nusselt number relation graphically, it is convenient to have simple correlation equations to represent the solutions for both boundary conditions. For fully developed Nusselt numbers with values of $0.5 \le n \le 1.0$ and $10^{-4} \le \beta \le 10^4$, Irvine et al. (1988) present the following equation which represents both solutions with a maximum difference of 1.5%:

$$\mathrm{Nu} = \frac{\mathrm{Nu}_N(1+\beta)}{1+\dfrac{\mathrm{Nu}_N\beta}{\mathrm{Nu}_P}} \qquad (4.9.4)$$

The Newtonian Nusselt numbers are $\mathrm{Nu}_N = 3.6568$ for Nu_T, and $\mathrm{Nu}_N = 4.3638$ for Nu_H. In addition, Table 4.9.2 lists the power law Nusselt numbers, Nu_{TP} and Nu_{HP}, for $\log_{10}\beta = 4$.

Graetz solutions for the thermal entrance lengths are also available. They assume that the velocity profile is fully developed at the duct entrance and present the duct lengths required for the Nusselt numbers to reach within 1% of the fully developed values. Figure 4.9.2 shows these thermal entrance lengths for Nu_T thermal boundary condition. The situation is similar for boundary condition Nu_H.

A correlation equation for the thermal entrance lengths for both the Nu_T and Nu_H boundary conditions by Irvine et al. (1988) represents the numerical solutions within 0.5% for $0.5 \le n \le 1.0$ and $-4 \le \log_{10}\beta \le 4$. Table 4.9.3 lists the power law thermal entrance lengths which are needed to evaluate the following correlation equation:

$$x_{\mathrm{ent},\beta,n}^+ = \frac{x_{\mathrm{ent},N}^+(1+\beta)}{1+\dfrac{x_{\mathrm{ent},N}^+(\beta)}{x_{\mathrm{ent},P}^+}} \qquad (4.9.5)$$

where $x_{\mathrm{ent},\beta,n}^+$ is the modified power law dimensionless entrance length defined as $x_{\mathrm{ent},\beta,n}^+ = (x_{\mathrm{ent},\beta,n}/D_H)/Pe$, and $x_{\mathrm{ent},N}^+$ and $x_{\mathrm{ent},P}^+$ are the Newtonian and power law values, respectively. The Newtonian dimensionless entrance lengths are $x_{\mathrm{ent},N}^+ = 0.03347$ for Nu_T and $x_{\mathrm{ent},N}^+ = 0.04309$ for Nu_H.
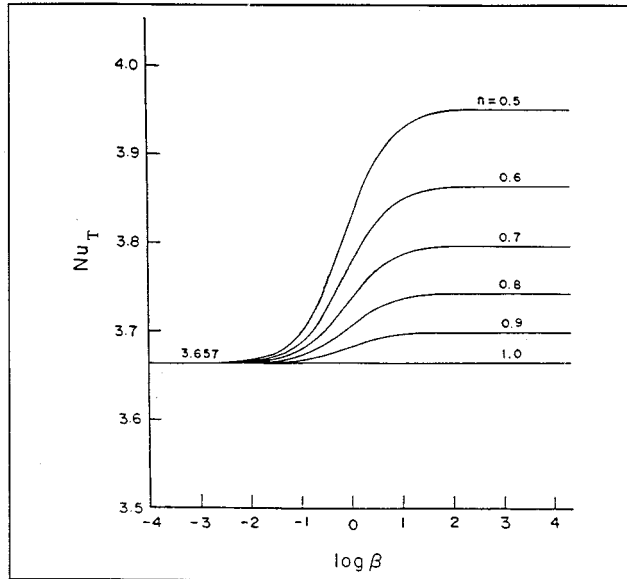
FIGURE 4.9.1 Variation of the fully developed circular duct Nusselt numbers, Nu_T, with the shear rate parameter β and n. (From Irvine, T.F., Jr. et al., in *ASME Symposium on Fundamentals of Forced Convection Heat Transfer*, ASME publ. HTD 101, 1988, 123–127. With permission.)

TABLE 4.9.2 Power Law Nu_T and Nu_H Solutions for a Circular Duct ($\log_{10} \beta = 4$)

n	Nu_{TP}	Nu_{HP}
1.0 (Newtonian)	3.6568	4.3638
0.9	3.6934	4.4109
0.8	3.7377	4.4679
0.7	3.7921	4.5385
0.6	3.8605	4.6281
0.5	3.9494	4.7456

Source: Irvine, T.F., Jr. et al., in *ASME Symposium on Fundamentals of Forced Convection Heat Transfer*, ASME publ. HTD 101, 1988, 123–127.

Only one noncircular geometry using the modified power law equation has been published in the archival literature for laminar fully developed heat transfer (Capobianchi and Irvine, 1992). A correlation equation for Nu_{H1} for annuli with constant heat flux at the inner wall and the outer wall insulated is

$$n < 1 \qquad Nu_{H1} = \frac{1+\beta}{\dfrac{1}{Nu_{H1,N}} + \dfrac{\beta}{Nu_{H1,P}}} \qquad (4.9.6)$$

Nusselt numbers for square ducts and power law fluids can be found in Chandrupatla and Sastri (1977) and, for isosceles triangular ducts, in Cheng (1984). Thermally developing and thermally developed laminar heat transfer in rectangular channels has been studied by Hartnett and Kostic (1989).

For other cross-sectional shapes, a power law approximate correlation has been proposed by Cheng (1984):
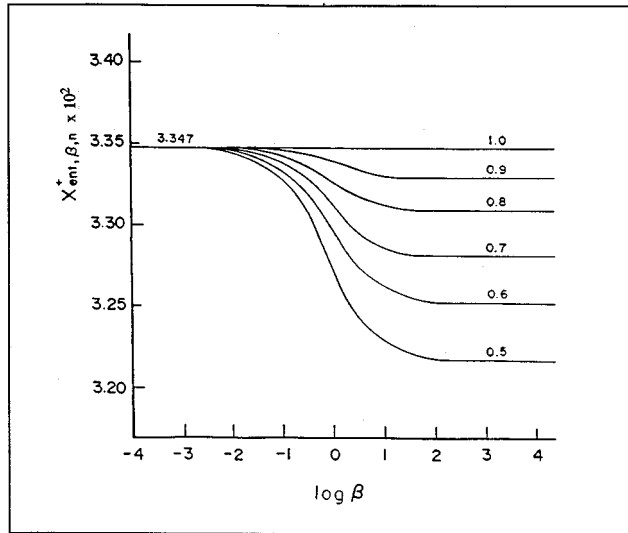
FIGURE 4.9.2 Thermal entrance lengths vs. shear rate parameter β and n for Nu_T in circular ducts. (From Irvine, T.F., Jr. et al., in *ASME Symposium on Fundamentals of Forced Convection Heat Transfer*, ASME publ. HTD 101, 1988, 123–127. With permission.)

TABLE 4.9.3   Values of Circular Duct Thermal Entrance Lengths for Nu_T and Nu_H for Use in Equation 4.9.5

n	Nu_T, $x^+_{\text{ent},P} \times 10^2$	Nu_H, $x^+_{\text{ent},P} \times 10^2$
1.0 (Newtonian)	3.347	4.309
0.9	3.326	4.281
0.8	3.306	4.248
0.7	3.279	4.210
0.6	3.250	4.166
0.5	3.213	4.114

Source: Irvine, T.F., Jr., et al., in *ASME Symposium on Fundamentals of Forced Convection Heat Transfer*, ASME publ. HTD 101, 1988, 123–127.

$$Nu_P = Nu_N \left[\frac{(a+bn)}{(a+b)n} \right]^{1/3} \tag{4.9.7}$$

where a and b are the Kozicki geometric constants listed in Table 3.9.3 in the section on non-Newtonian flows. Equation (4.9.7) applies to any thermal boundary condition. For circular ducts, Equation 4.9.7 predicts the correct solution for both Nu_T and Nu_H.

Turbulent Duct Flow for Purely Viscous Time-Independent Non-Newtonian Fluids

It is known that in turbulent flow, the type of thermal boundary conditions has much less effect than in laminar flow. Therefore, turbulent flow heat transfer investigations are often reported without specifying the thermal boundary conditions. Yoo (1974) has presented an empirical correlation for turbulent heat transfer in circular ducts for purely viscous time-independent power law fluids.

$$\text{StPr}_a^{2/3} = 0.0152\text{Re}_a^{-0.155} \tag{4.9.8}$$

Equation (4.9.8) describes all of the experimental data available in the literature at the time with a mean deviation of 2.3%. Equation (4.9.8) is recommended in order to predict the turbulent fully developed heat transfer in the ranges $0.2 \le n \le 0.9$ and $3000 \le \text{Re}_a \le 90{,}000$. The Reynolds number and Prandtl numbers in Equation (4.9.8) are based on the apparent viscosity at the wall, μ_a, i.e.,

$$\text{Re}_a = \frac{\rho \bar{u} D_H}{\mu_a} \tag{4.9.9}$$

$$\text{Pr}_a = \frac{\mu_a c_p}{k} \tag{4.9.10}$$

In order to evaluate Equations (4.9.9) and (4.9.10) in terms of the rheological properties and operating parameters, an expression must be obtained for μ_a in terms of these quantities. The value of μ_a is evaluated by considering that μ_a is determined from fully developed laminar circular tube power law fluid flow for which it can be shown that (Irvine and Karni, 1987)

$$\mu_a = K \left(\frac{3n+1}{4n} \right)^{n-1} \left(\frac{8\bar{u}}{D_H} \right)^{n-1} \tag{4.9.11}$$

assuming that the quantities K, n, c_p, and k are constant. It is also of interest that the Prandtl number is no longer a thermophysical property for power law fluids but depends upon the average velocity, $\bar{u}$, and the hydraulic diameter, D_H.

Hartnett and Rao (1987) have investigated fully developed turbulent heat transfer for a rectangular duct with a 2:1 aspect ratio and propose the following equation which generally agreed with their experimental data within $\pm 20\%$:

$$\text{Nu} = (0.0081 + 0.0149n)\text{Re}_a^{0.8}\text{Pr}_a^{0.4} \tag{4.9.12}$$

Viscoelastic Fluids

An important characteristic of viscoelastic fluids is their large hydrodynamic and thermal entrance lengths. Cho and Hartnett (1982) have reported hydrodynamic entrance lengths of up to 100 diameters and thermal entrance lengths up to 200 to 800 diameters depending upon the Reynolds and Prandtl numbers. These can be compared with Newtonian fluids entrance lengths which are of the order of 10 to 15 diameters. Therefore, care must be used in applying fully developed relations to practical situations.

Cho et al. (1980) reported heat transfer measurements in the thermal entrance region and recommend the following empirical equation for saturated aqueous polymer solutions for $6000 \le \text{Re}_a$ and x/D_H values up to 450:

$$J_H = 0.13 \left(x/D_H \right)^{-0.24} \text{Re}_a^{-0.45} \tag{4.9.13}$$

where $J_H = \text{St Pr}_a^{2/3}$ and St - $h_c/\rho c_p \bar{u}$.

All of the reported fully developed turbulent flow heat transfer measurements have been plagued by solute and solvent, thermal entrance, and degradation effects, and thus there is considerable scatter in the results. Degradation effects can be reduced or eliminated by using large amounts of polymer (500

to 10,000 wppm) so that the solution becomes saturated. Cho and Hartnett (1982) attempted to eliminate these effects by using a thermal entrance length of 430 diameters and saturated polymer solutions which should yield maximum heat transfer reductions. Their experimental results for fully developed heat transfer were correlated for a Reynolds number range $3500 \leq \mathrm{Re}_a \leq 40{,}000$ and concentration solutions of 500 to 5000 wppm of polyacrylamide and polyethylene oxide by

$$J_H = 0.03\mathrm{Re}_a^{-0.45} \tag{4.9.14}$$

For viscoelastic fluids in fully developed (hydrodynamically and thermally) *laminar flow in circular ducts* there is no apparent viscoelastic effect. Thus, the heat transfer relations are the same as those for time-independent fluids such as power law or modified power law fluids. The same situation holds for thermal entrance region heat transfer (Graetz problem). Relations for laminar Nusselt numbers in thermal entrance regions are presented by Cho and Hartnett (1982).

Free Convection Flows and Heat Transfer

Free convection information available in the heat transfer literature up to the present time is concentrated on heat transfer to power law fluids for vertical plates and parallel plate channels. For free convection flows, however, the velocities and thus the shear rates are low and care must be taken that the flow for a particular fluid is in the power law shear rate region before using power law solutions or correlations. Comprehensive review articles on free convection with non-Newtonian fluids have been presented by Shenoy and Mashelkar (1982) and Irvine and Karni (1987).

For a single vertical plate with a modified power law fluid and a thermal boundary condition $\overline{Nu}_T$, in laminar flow, the following relation is recommended by Shenoy and Mashelkar (1982):

$$\overline{Nu}_{TL} = T(n)\,Gr_{TL}^{1/(2n+2)}\mathrm{Pr}_{TL}^{n/(3n+1)} \tag{4.9.15}$$

where $\overline{Nu}_{TL}$ is the average Nusselt number and

$$\mathrm{Gr}_{TL} = \frac{\rho^2 L^{n+2}}{K^2}\Big[g\alpha\big(T_s - T_\infty\big)\Big]^{2-n} \tag{4.9.16}$$

$$\mathrm{Pr}_{TL} = \frac{\rho c_p}{k}\left(\frac{K}{\rho}\right)^{2/(n+1)} L^{(n-1)/(2n+2)}\Big[g\alpha\big(T_s - T_\infty\big)\Big]^{(3n-3)/(2n+2)} \tag{4.9.17}$$

where α is the isobaric thermal expansion coefficient.

In the range $0.5 \leq n \leq 1$, $T(n)$ can be approximated by

$$T(n) = 0.1636n + 0.5139 \tag{4.9.18}$$

The characteristic dimension in the Nusselt and Grashof numbers is the plate height, *L*.

For thermal boundary conditions Nu_H, the following relation is also recommended by Shenoy and Mashelkar (1982). Since the heat flux, q_w is specified in this case, the local plate temperature at any x (measured from the bottom of the plate) can be obtained from the local Nusselt number Nu_{Hx}. The heat transfer coefficient is defined in terms of the difference between the wall and free-stream temperatures.

$$\mathrm{Nu}_{Hx} = 0.619\Big[\mathrm{Gr}_{Hx}^{(3n+2)/(n+4)}\mathrm{Pr}_{Hx}^{n}\Big]^{0.213} \tag{4.9.19}$$

where

$$\text{Gr}_{Hx} = \frac{\rho^2 x^4}{k^2} \left(\frac{g\alpha q_w}{k} \right)^{2-n} \tag{4.9.20}$$

$$\text{Pr}_{Hx} = \frac{\rho c_p}{K} \left(\frac{K}{\rho} \right)^{5/(n+4)} x^{(2n-2)/(n+4)} \left(\frac{g\alpha q_w}{k} \right)^{(3n-3)/(n+4)} \tag{4.9.21}$$

Vertical Parallel Plates

For *power law fluids* and laminar flow, Figure 4.9.3 presents the graphical results of a numerical solution. Of interest are the average Nusselt number $\overline{Nu}_{Tb}$ and the dimensionless average flow velocity between the plates, U_o^+. These are shown on the left and right ordinates respectively in Figure 4.9.3 (Irvine et al., 1982). The characteristic dimension in the Nusselt and Grashof numbers is the plate spacing, *b*. The dimensionless quantities used in Figure 4.9.3 are defined as follows:

$$\overline{Nu}_{Tb} = \frac{\overline{h}_c b}{k} \qquad U_o^+ = \frac{b u_o}{L u^*}$$

$$\text{Pr}_g = \frac{\rho c_p}{k} \left[\frac{v_k^{1/(2-n)}}{\left(\dfrac{L}{b} \right)^{(1-n)/(2-n)} b^{(2n-2)/(2-n)}} \right] \qquad v_K = \frac{K}{\rho}$$

$$\text{Gr}_g = \frac{g\alpha \left(T_s - T_\infty \right) b^{(n+2)/(2-n)}}{v_K^{2/(2-n)} \left(\dfrac{L}{b} \right)^{n/(2-n)}} \qquad u^* = \frac{v_K^{1/(2-n)} b^{(1-2n)/(2-n)}}{L^{(1-n)/(2-n)}}$$

For vertical parallel plates for the average Nusselt number, $\overline{Nu}_{Hb}$, and the between plate average velocity, Schneider and Irvine (1984) have presented graphical results similar to Figure 4.9.3.

Lee (1992) has presented a numerical solution for laminar flow of a *modified power law fluid* between vertical plates. Lee has also calculated thermal entrance regions and shown that if a parallel plate system is actually operating in the transition region and if the power law solution is used, both the total heat transfer and the velocity between plates can differ by over an order of magnitude. It is important to consider the shear rate parameter in order to determine which free convection solution to use.

Sphere and Horizontal Cylinder — Power Law Fluids

For flow over a sphere, the correlation for power law fluids by Amato and Tien (1976) is

$$\overline{Nu}_{Tr} = CZ^D \tag{4.9.22}$$

where

$$Z = \text{Gr}_{Tr}^{1/(2n+2)} \, \text{Pr}_{Tr}^{n/(3n+1)} \tag{4.9.23}$$

and

$$C = 0.996 \pm 0.120, \quad D = 0.682 \qquad \text{for } Z < 10$$

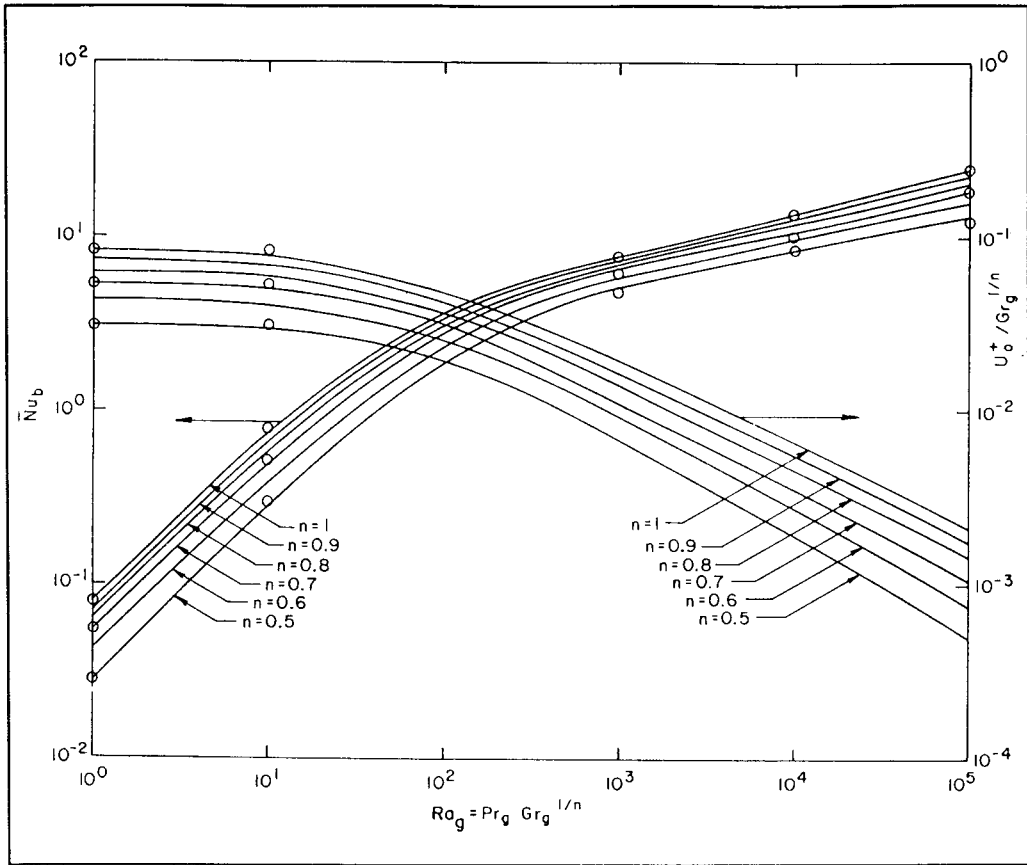$$C = 0.489 \pm 0.005, \quad D = 1.10 \qquad \text{for } 10 \le Z \le 40$$

FIGURE 4.9.3 Free convection average Nusselt number, $\overline{Nu}_b$ and dimensionless average velocity U_o^+ between vertical plates for a power law fluid vs. generalized Raleigh number for the Nu_T boundary condition. (From Irvine, T.F., Jr. et al., ASME Paper 82-WA/HT-69, 1982. With permission.)

where the characteristic dimension in all dimensionless variables is the sphere radius, r, and Gr_{Tr} and Pr_{Tr} are defined in Equations (4.9.16) and (4.9.17).

For pseudoplastic fluids flowing over a cylinder, an experimental correlation proposed by Gentry and Worllersheim (1974) for the average Nusselt number, $\overline{Nu}_{TD}$, is

$$\overline{Nu}_{TD} = \frac{\overline{h}_c D}{k} = 1.19 \left(Gr_{TD} \, Pr_{TD} \right)^{0.2} \tag{4.9.24}$$

where Gr_{TD} and Pr_{TD} are defined as in Equations (4.9.16) and (4.9.17) with the cylinder diameter, D, being used instead of L.

References

Acrivos, A. 1960. A theoretical analysis of laminar natural convection heat transfer to non-Newtonian fluids, *AIChE J.*, 6, 584–590.

Amato, W.S. and Tien, C. 1976. Free convection heat transfer from isothermal spheres in polymer solutions, *Int. J. Heat Mass Transfer*, 19, 1257–1266.

Capobianchi, M. and Irvine, T.F., Jr. 1992. Predictions of pressure drop and heat transfer in concentric annular ducts with modified power law fluids, *Wärme Stoffübertragung*, 27, 209–215.

Chandrupatla, A.R. and Sastri, V.M. 1977. Laminar forced convection heat transfer of a non-Newtonian fluid in a square duct, *Int. J. Heat Mass Transfer*, 20, 1315–1324.

Cheng, J.A. 1984. Laminar Forced Convection Heat Transfer of Power Law Fluids in Isosceles Triangular Ducts, Ph.D. Thesis, Mechanical Engineering Department, State University of New York at Stony Brook.

Cho, Y.I. and Hartnett, J.P. 1982. Non-Newtonian fluids in circular pipe flow, *Adv. Heat Transfer*, 15, 59–141.

Cho, Y.I., Ng, K.S., and Hartnett, J.P. 1980. Viscoelastic fluids in turbulent pipe flow — a new heat transfer correlation, *Lett. Heat Mass Transfer*, 7, 347.

Gentry, C.C. and Wollersheim, D.E. 1974. Local free convection to non-Newtonian fluids from a horizontal isothermal cylinder, *ASME J. Heat Transfer*, 96, 3–8.

Hartnett, J.P. and Kostic, M. 1989. Heat transfer to Newtonian and non-Newtonian fluids in rectangular ducts, *Adv. Heat Transfer*, 19, 247–356.

Hartnett, J.P. and Rao, B.K. 1987. Heat transfer and pressure drop for purely viscous non-Newtonian fluids in turbulent flow through rectangular passages, *Wärme Stoffüberetragung*, 21, 261.

Irvine, T.F., Jr. and Karni, J. 1987. Non-Newtonian flow and heat transfer, in *Handbook of Single Phase Convective Heat Transfer*, John Wiley & Sons, New York, 20-1–20-57.

Irvine, T.F., Jr., Wu, K.C., and Schneider, W.J. 1982. Vertical Channel Free Convection to a Power Law Fluid, ASME Paper 82-WA/HT-69.

Irvine, T.F., Jr., Kim, S.C., and Gui, F.L. 1988. Graetz problem solutions for a modified power law fluid, in *ASME Symposium on Fundamentals of Forced Convection Heat Transfer*, ASME publ. HTD 101, pp. 123–127.

Lee, S.R. 1992, A Computational Analysis of Natural Convection in a Vertical Channel with a Modified Power Law Fluid, Ph.D. Thesis, Mechanical Engineering Department, State University of New York at Stony Brook.

Schneider, W.J. and Irvine, T.F., Jr. 1984. Vertical Channel Free Convection for a Power Law Fluid with Constant Heat Flux, ASME Paper 84-HT-16.

Shenoy, A.V. and Mashelkar, R.A. 1982 Thermal convection in non-Newtonian fluids, *Adv. Heat Transfer*, 15, 143–225.

Yoo, S.S. 1974. Heat Transfer and Friction Factors for Non-Newtonian Fluids in Turbulent Pipe Flow, Ph.D. Thesis, University of Illinois at Chicago Circle.

Further Information

Other sources which may be consulted for more detailed information are Cho and Hartnett (1982), Shenoy and Mashelkar (1982), Irvine and Karni (1987), and Hartnett and Kostic (1989).